

4-22-2014

# Understanding the Impact of Iron Availability on *Bacillus anthracis* Metabolism

Eddy Johana Bautista Bautista

*University of Connecticut - Storrs*, eddyb2@gmail.com

Follow this and additional works at: <https://opencommons.uconn.edu/dissertations>

---

## Recommended Citation

Bautista Bautista, Eddy Johana, "Understanding the Impact of Iron Availability on *Bacillus anthracis* Metabolism" (2014). *Doctoral Dissertations*. 336.

<https://opencommons.uconn.edu/dissertations/336>

# **Understanding the Impact of Iron Availability on *Bacillus anthracis* Metabolism**

**Eddy Johana Bautista Bautista, PhD**

University of Connecticut, 2014

*Bacillus anthracis*, the causative agent of anthrax, has to be able to adapt to different physical conditions encountered during the beginning and establishment of the infection process inside the host. One of these conditions is the availability of nutrients like iron. *B. anthracis* secretes siderophores capable of competing with the iron transport/storage proteins of the host. Previous studies have been dedicated to the analysis of these systems. However, the impact of iron availability on *B. anthracis* metabolism from a global perspective remains as unclear. In this dissertation, I combined an *in silico* genome-scale metabolic analysis with experimental studies for *B. anthracis* grown under different iron conditions in order to study the impact of iron availability on the metabolism of the bacterium.

To develop the first genome-scale metabolic model for *B. anthracis*, I designed and implemented a new methodology for the curation of genome scale metabolic models that combined a genetic algorithm and flux balance analysis (GAFBA). GAFBA finds metabolites whose mass balance constraints cannot be satisfied, because the metabolite is participating in additional reactions that were not taken into account during the reconstruction process. This resulted in an unfeasible solution to the optimization



Eddy Johana Bautista Bautista, University of Connecticut, 2014

problem. GAFBA facilitates the curation of genome-scale metabolic networks, and aids in fundamental studies in metabolism.

During the experimental studies of the growth of *B. anthracis* under iron-poor/rich conditions, the carbon metabolism increased under iron-poor conditions, although this did not directly support growth. Thus, the *B. anthracis* model was used to characterize the metabolic response of the bacteria under iron-poor/rich conditions. Under iron-poor conditions, a down regulation in the TCA cycle reactions resulted in the reduced uptake of some amino acids. Also, the production of siderophores increased. A higher glucose uptake rate was found to fulfill amino acids requirements for siderophore biosynthesis and growth. For the first time, I found a correlation between the biosynthesis of autoinducer-2, a quorum sensing signal molecule, and the growth of *B. anthracis* under iron-poor conditions.

**Understanding the Impact of Iron Availability on *Bacillus anthracis* Metabolism**

**Eddy Johana Bautista Bautista**

B.S. Universidad Industrial de Santander, 2007

M.S. University of Connecticut, 2012

A Dissertation

Submitted in Partial Fulfillment of the  
Requirements for the Degree of Doctor of Philosophy  
at the University of Connecticut

2014

Copyright by  
Eddy Johana Bautista Bautista

**APPROVAL PAGE**

**Doctor of Philosophy Dissertation**

**Understanding the Impact of Iron Availability on *Bacillus anthracis* Metabolism**

Presented by

Eddy Johana Bautista Bautista, B.S., M.S.

Major Advisor \_\_\_\_\_  
Ranjan Srivastava

Associate Advisor \_\_\_\_\_  
Richard Parnas

Associate Advisor \_\_\_\_\_  
Yu Lei

(Associate Advisor) \_\_\_\_\_  
Kenneth Noll

(Associate Advisor) \_\_\_\_\_  
Peter Karp

University of Connecticut

2014

## **Dedication**

To my family,  
Gratiniano, Maria Emma, Diana y Elizabeth.

To my dear husband,  
Diego

## Acknowledgements

I want to thank to all the people that were part of this journey through my PhD program. Specially thanks to:

- My major advisor, Dr. Ranjan Srivastava, for his guidance and support. Thanks for teaching me about biology and Lisp programing. His positive aptitude towards my research always incentive me to continue.
- I thank to my associate advisor, Dr. Peter Karp, for taking time of his schedule to teach me about Pathway tools and bioinformatics. For wonderful discussions and suggestion.
- Thanks to my committee members Dr. Kenneth Noll, Dr. Richard Parnas, and Dr. Yu Lei for your invaluable comments and suggestion during my dissertation process.
- My former advisor, Dr. Jorge Seminario, whom gave me the opportunity to start my research career. I really appreciate all your confidence and your support, even when I am away from Texas.
- My labmates Jason White, Si-Yu Li, Erik Johnson, Joseph Zinski, Abe Friedman, Andrea DiVenere. It was a pleasure to work with you and thanks for your help and support.
- My friends, Tatiana, Richard, Yenny, Frank y Tami. It is hard to be away home, but it was easier having you. Thanks for your friendship and love.
- I thank to my family, Gratiniano, Maria Emma, Diana y Licha for their support and for encouraging me to follow my dreams. You have been always with me and have believed in me. For their support, understanding, and for give me joy when I need it.
- Last but not least, to my love. Diego, thanks for bringing to our life such a wonderful energy and happiness. Thanks to be with me during that late nights and early mornings at the lab, and for the discussions about programming and optimization. I thank you for believe in me and for encouraging me to go further.

## Table of Contents

Acknowledgements .....	iv
Table of Contents .....	v
List of Tables .....	xii
List of Figures .....	xv
<b>1. INTRODUCTION</b>	<b>20</b>
1.1. Overview .....	20
1.2. Motivation .....	23
1.3. Research significance and novelty .....	24
1.4. Dissertation organization .....	27
<b>2. LITERATURE REVIEW</b>	<b>28</b>
2.1. Genome-scale metabolic models (GEMs) .....	28
2.1.1. Constraint-based modeling .....	29
2.1.1.1. Flux balance analysis (FBA) .....	30
2.2. Genetic algorithm (GA) .....	33
2.2.1. Selection strategy .....	34
2.2.2. Crossover operation .....	34
2.2.3. Mutation operation .....	35
2.3. Pathogenic microorganisms .....	36
2.3.1. <i>Mycoplasma gallisepticum</i> .....	36
2.3.2. <i>Bacillus anthracis</i> .....	39
2.3.2.1. History .....	39
2.3.2.2. Microbiology and pathogenesis .....	40

<b>3. A GENETIC ALGORITHM/FLUX BALANCE ANALYSIS (GAFBA) METHODOLOGY FOR CURATION OF GENOME-SCALE METABOLIC MODELS</b>	<b>42</b>
3.1. Chapter Synopsis .....	42
3.2. Introduction .....	43
3.3. Material and Methods .....	47
3.3.1. Genetic algorithm parameters .....	47
3.3.2. Flux balance analysis .....	48
3.3.3. Experimental protocols .....	49
3.4. Results .....	49
3.4.1. Hybrid Genetic Algorithm/Flux Balance Analysis (GAFBA).....	49
3.4.2. Initial reconstruction of the <i>M. gallisepticum</i> metabolic model .....	54
3.4.3. Refinement of the initial reconstruction .....	59
3.4.4. Final model .....	68
3.4.5. Comparison of <i>M. gallisepticum</i> model and <i>M. genitalium</i> iPS189 model.....	70
3.4.6. <i>M. gallisepticum</i> model created with Model SEED.....	72
3.5. Discussion .....	73
<b>4. GAFBA v1.0 IMPROVEMENT</b>	<b>78</b>
4.1. Leveraging Ensemble Information of Evolving Populations in Genetic Algorithms to Identify Incomplete Metabolic Pathways .....	79
4.1.1. Introduction .....	79
4.1.2. Methods.....	80
4.1.2.1. Frequency analysis of relaxed metabolic constraints.....	80
4.1.3. Results .....	82
4.1.4. Impact .....	85
4.2. MassChecker, a mass balance constraint consistency checker tool for GAFBA .....	86
4.2.1 Methods.....	87



4.2.1.1	Genetic algorithm parameters .....	87
4.2.1.2	Flux Balance analysis parameters .....	88
4.2.1.3	Mass balance constraint consistency checker (MassChecker) .....	89
4.2.2	Results .....	91
4.2.3.	Impact .....	94
4.3.	GAFBA v1.1 Software: a tool for the semi-automated curation of genome scale metabolic reconstruction. ....	95
4.3.1.	Introduction .....	95
4.3.2.	Methods.....	96
4.3.3.	Implementation .....	100
4.3.4.	impact.....	100
<b>5</b>	<b>IMPACT OF IRON AVAILABILITY ON <i>BACILLUS ANTHRACIS</i> METABOLISM</b>	<b>101</b>
5.1	Chapter Synopsis .....	101
5.2	Introduction .....	102
5.3	Materials and Methods .....	105
5.4	Results .....	110
5.5	Discussion .....	127
<b>6.</b>	<b>GENOME-SCALE METABOLIC RECONSTRUCTION FOR <i>BACILLUS ANTHRACIS</i> STERNE AND ANALYSIS OF ITS METABOLIC ADAPTATION TO DIFFERENT IRON CONDITIONS.</b>	<b>131</b>
6.1.	Chapter Synopsis .....	131
6.2.	Introduction .....	132
6.3.	Methods.....	135
6.3.1.	Genetic algorithm/Flux balance analysis approach (GAFBA v1.1) .....	135
6.3.2	Flux Balance analysis .....	136

6.3.3.	Flux variability analysis (FVA) .....	137
6.4.	Results .....	138
6.4.1.	Metabolic Network reconstruction .....	138
6.4.2.	Siderophores biosynthesis, secretion, and uptake pathways .....	143
6.4.3.	Model application: metabolic adaptation to iron-poor conditions by <i>B. anthracis</i> .....	147
6.4.3.1.	Comparison of the iron-poor and iron-rich cell metabolomes at Phase I. ....	147
6.4.3.2.	Comparison of the iron-poor and iron-rich cells metabolomes at Phase II. ....	152
6.5.	Discussion .....	165
<b>7.</b>	<b>AUTOINDUCER-2 CORRELATION THE GROWTH OF <i>BACILLUS ANTHRACIS</i> UNDER IRON-POOR CONDITIONS</b>	<b>169</b>
7.1.	Background .....	169
7.2	Materials and Methods .....	171
7.2.1	Flux Balance analysis constraints .....	171
7.2.2.	Flux variability analysis (FVA) .....	172
7.3	Results and Discussion .....	172
7.3.1	<i>luxS</i> mutation affects <i>in silico</i> growth .....	173
7.3.2	AI-2 production increases AMP and ADP pool .....	174

7.4. Impact .....	176
<b>8 CONCLUSIONS</b>	<b>178</b>
<b>9 FUTURE WORK</b>	<b>180</b>
<b>APPENDIX 1. EXAMPLES OF METHODOLOGIES FOR RESOLVING INFEASIBLE MODELS.</b>	<b>183</b>
<b>APPENDIX 2. EXPERIMENTAL PROTOCOLS FOR <i>M. GALLISEPTICUM</i> MODEL</b>	<b>187</b>
A2.1. Strains, Culture Conditions .....	187
A2.2. Determining Dry Cell Weight and CFU/ml .....	187
A2.3. Metabolism Experimental Design.....	188
A2.4. Sampling and Cell Growth Assay .....	189
A2.5. Glucose and Lactate Assays.....	189
A2.6. Dry Weight Measurement.....	190
A.2.7. Determination of biomass equation .....	191
<b>APPENDIX 3. GENOME-SCALE METABOLIC MODEL OF <i>M. GALLISEPTICUM</i></b>	<b>197</b>
A3.1. Metabolites located in the cytosol space.....	197
A3.2. Metabolites located in the extracellular space .....	208
A3.3. Intracellular reactions.....	210
A3.4. Exchanges fluxes .....	230
A3.5. Biomass reaction .....	233
A3.6. Experimentally measured fluxes .....	235
<b>APPENDIX 4. GAFBA v1.1 USER MANUAL</b>	<b>236</b>
A4.1. Introduction .....	236
A4.2. Development. ....	236

A4.3. Getting Started .....	237
A4.4. Quick tour through GAFBA v1.1 .....	237
A4.5. Creating the model .....	239
A4.6. Saving input information in a file. ....	253
A4.7. Load a previous input file. ....	254
A4.8. Start GAFBA. ....	255
A4.9. Results files. ....	255
A4.10. Possible solutions to fill gaps.....	259
A.4.11. Running a new simulation.....	259
A.4.12. Input file .....	260
A.4.13. Frequency analysis .....	260
<b>APPENDIX 5. ADDITIONAL EXPERIMENTAL METHODS</b>	<b>263</b>
<b>APPENDIX 6. TRIPLICATED EXPERIMENTAL DATA</b>	<b>268</b>
<b>APPENDIX 7. SUPPLEMENTARY FIGURES</b>	<b>273</b>
<b>APPENDIX 8. GENOME-SCALE METABOLIC MODEL FOR <i>BACILLUS ANTHRACIS</i> STERNE</b>	<b>280</b>
A8.1. Extracellular metabolites .....	280
A8.2. Intracellular metabolites.....	282
A8.3. Reactions .....	314
A8.4. Exchange fluxes .....	425
A8.5. Biomass for iron-poor media phase I.....	427
A8.6. Biomass for iron-rich media phase I.....	430
A8.7. Biomass for iron-poor media Phase II .....	433

A8.8. Biomass for iron-rich media Phase II .....	436
A8.9. Additional constraints .....	440
<b>10 REFERENCE</b>	<b>443</b>

## List of Tables

Table 1. Summary of reactions added to the metabolic model based on experimental data in the literature. ....	56
Table 2. Summary of reactions added based on BLASTP analysis. ....	57
Table 3. Reactions removed based on experimental studies. ....	57
Table 4. Enzymes added based on Pathway Tools analysis. ....	58
Table 5. Initial model modifications. ....	61
Table 6. Remaining changes made to model. ....	62
Table 7. Comparison of the <i>Mycoplasma genitalium</i> model (iPS189) and the model presented in this paper for <i>Mycoplasma gallisepticum</i> . ....	71
Table 8. Result of the analysis of relaxed mass balance constraints for select simulations. ....	83
Table 9. Iron reduced media (IRDM) media composition. ....	89
Table 10. Experimentally measured fluxes used as constraints for the FBA model. ....	89
Table 11. Experimentally measured fluxes for the growth of <i>B. anthracis</i> under iron-poor media and iron-rich media. ....	139
Table 12. NGAM, GAM, <i>in silico</i> growth rate, and experimental growth rate comparison for the four cases. ....	142
Table 13. Experimentally measured fluxes for the growth of <i>B. anthracis</i> under iron-reduced media (IRDM) and iron-replete media (IRM). ....	171
Table 14. Substrate level phosphorylation reactions and oxidative phosphorylation reactions for <i>B. anthracis</i> grown under iron-poor/rich conditions. ....	176
Table S1. OD/(g/cfu) Correlation .....	191
Table S2. Lipid Fraction Estimation. ....	194

Table S3. Average Fatty Acid Molecular Weight. ....	195
Table S4. Estimation of molecular weights for major lipid components making up biomass.. ....	195
Table S5. Metabolites in the cytosol space for <i>M. gallisepticum</i> model.....	197
Table S6. Metabolites in the extracellular space for <i>M. gallisepticum</i> model. ....	208
Table S7. Intracellular reactions for <i>M. gallisepticum</i> model. ....	210
Table S8. Exchange fluxes for nutrients and secretion in the <i>M. gallisepticum</i> model. ....	230
Table S9. Reactants of Biomass reactions for <i>M. gallisepticum</i> model. ....	233
Table S10. Products of Biomass reactions for <i>M. gallisepticum</i> model. ....	234
Table S11. Measured fluxes for <i>M. gallisepticum</i> model. ....	235
Table S12. Calculation of Hydrogen carbonate activity for iron-reduced media. ....	266
Table S13. Calculation of Hydrogen carbonate activity for iron-replete media. ....	267
Table S14. Metabolites in the extracellular space for <i>B. anthracis</i> . ....	280
Table S15. Metabolites in the cytosol space for <i>B. anthracis</i> . ....	282
Table S16. Reaction of the model for <i>B. anthracis</i> . T.....	314
Table S17. List of exchange fluxes for nutrients and secretion for the model for <i>B. anthracis</i> . ....	425
Table S18. List of biomass's reactants for <i>B. anthracis</i> model under iron-poor conditions Phase I. ....	427
Table S19. List of biomass's products for <i>B. anthracis</i> model under iron-poor conditions Phase I. ....	429

<b>Table S20. List of biomass's reactants for <i>B. anthracis</i> model under iron-rich conditions Phase I.</b>	430
<b>Table S21. List of biomass's products for <i>B. anthracis</i> model under iron-rich conditions Phase I.</b>	432
<b>Table S22. List of biomass's reactants for <i>B. anthracis</i> model under iron-poor conditions Phase II.</b>	433
<b>Table S23. List of biomass's products for <i>B. anthracis</i> model under iron-poor conditions Phase II.</b>	435
<b>Table S24. List of biomass's reactants for <i>B. anthracis</i> model under iron-rich conditions Phase II.</b>	436
<b>Table S25. List of biomass's products for <i>B. anthracis</i> model under iron-rich conditions Phase II.</b>	439
<b>Table S26. List of biomass's products for <i>B. anthracis</i> model under iron-rich conditions Phase II.</b>	440



## List of Figures

<b>Figure 1. Schematic representation of the integration of various data types for the reconstruction of metabolic models. ....</b>	<b>21</b>
<b>Figure 2. The conceptual basis of constraint-based modeling. ....</b>	<b>29</b>
<b>Figure 3. One point crossover operation.....</b>	<b>35</b>
<b>Figure 4. Mutation operation. ....</b>	<b>36</b>
<b>Figure 5. Comparison of normal (A) and infected (B) tracheal tissue.. ....</b>	<b>38</b>
<b>Figure 6. Forms of anthrax .....</b>	<b>41</b>
<b>Figure 7. Flowchart for the GAFBA v1.0 algorithm. ....</b>	<b>50</b>
<b>Figure 8. An example of relaxed and enforced mass balance constraints for a metabolite.....</b>	<b>52</b>
<b>Figure 9. Choline Subnetwork. ....</b>	<b>65</b>
<b>Figure 10. Predicted growth rate over the course of model evolution .....</b>	<b>69</b>
<b>Figure 11. Metabolic constraints relaxed over the course of model evolution. ....</b>	<b>70</b>
<b>Figure 12. Frequency Analysis of Relaxed Metabolic Constraints. ....</b>	<b>81</b>
<b>Figure 13. GAFBA v1.1. ....</b>	<b>91</b>
<b>Figure 14. Comparison of the evolution of mass balance constraints on GAFBA v1.0 and GAFBA v1.1.. ....</b>	<b>92</b>
<b>Figure 15. Evolution of the number of false positives in the elite pool for the first run using GAFBA v1.1. ....</b>	<b>94</b>
<b>Figure 16. Four stages of the curation process. ....</b>	<b>98</b>
<b>Figure 17. Levels of extracellular metabolites and growth rate under iron-poor conditions.. ....</b>	<b>111</b>

<b>Figure 18. Levels of extracellular metabolites and growth rate under iron-rich conditions. ....</b>	<b>112</b>
<b>Figure 19. Growth rate for both phases. ....</b>	<b>115</b>
<b>Figure 20. (A) Lactate secretion rate during Phase I and (B) lactate uptake rate during Phase II. ....</b>	<b>116</b>
<b>Figure 21. Carbon dioxide secretion rate during Phases I and II. ....</b>	<b>119</b>
<b>Figure 22. Glutamic acid uptake in Phases I and II. ....</b>	<b>120</b>
<b>Figure 23. Glucose uptake rate at Phase I and Phase II. ....</b>	<b>121</b>
<b>Figure 24. Oxygen uptake rate during Phases I and II. ....</b>	<b>122</b>
<b>Figure 25. Siderophore secretion rate for Phase II. ....</b>	<b>123</b>
<b>Figure 26. Iron uptake rate during Phases I and II. ....</b>	<b>125</b>
<b>Figure 27. Western blot analysis of Protective Antigen protein. ....</b>	<b>127</b>
<b>Figure 28. Representation of the siderophore secretion, iron loading, ferric-siderophore complex uptake, and iron release from ferric-siderophore complex. ....</b>	<b>144</b>
<b>Figure 29. Comparison of the amino acid uptake and biosynthesis in <i>B. anthracis</i> under iron-poor/rich conditions at Phase I. ....</b>	<b>149</b>
<b>Figure 30. Comparison of the TCA cycle pathway under iron-poor and iron-rich conditions at Phase I. ....</b>	<b>152</b>
<b>Figure 31. Comparison of the bacillibactin biosynthesis pathway under iron-poor and iron-rich conditions during Phase II. ....</b>	<b>153</b>
<b>Figure 32. Comparison of the protocatechuate and the petrobactin biosynthesis pathway under iron-poor and iron-rich conditions during Phase II. ....</b>	<b>154</b>
<b>Figure 33. Comparison of the amino acid uptake and biosynthesis in <i>B. anthracis</i> under iron-poor/rich conditions at Phase II. ....</b>	<b>157</b>

<b>Figure 34. Comparison of the pentose phosphate pathway under iron-poor and iron-rich conditions during Phase II. ....</b>	<b>160</b>
<b>Figure 35. Comparison of the autoinducer-2 (AI-2) biosynthesis pathway under iron-poor and iron-rich conditions during Phase II. ....</b>	<b>162</b>
<b>Figure 36. Comparison of the TCA cycle pathway under iron-poor and iron-rich conditions during Phase II. ....</b>	<b>164</b>
<b>Figure 37. Autoinducer-2 biosynthesis pathway connected to adenine salvage pathway and adenosine de novo biosynthesis pathway. ....</b>	<b>173</b>
<b>Figure 38. Autoinducer-2 biosynthesis pathway connected to adenine salvage pathway and adenosine de novo biosynthesis pathway under iron-reduced/replete iron conditions. ....</b>	<b>175</b>
<b>Figure S1. Case 1. Change directionality of reactions. ....</b>	<b>184</b>
<b>Figure S2. Case 2. Add exchange flux. ....</b>	<b>185</b>
<b>Figure S3. Case 3. Add reaction. ....</b>	<b>186</b>
<b>Figure S4. GAFBA v1.1 structure. ....</b>	<b>238</b>
<b>Figure S5. Choosing a SBML file ....</b>	<b>240</b>
<b>Figure S6. Creating a biomass reaction. ....</b>	<b>241</b>
<b>Figure S7. Choose an objective function ....</b>	<b>243</b>
<b>Figure S8. Existing reaction in the model ....</b>	<b>244</b>
<b>Figure S9. Create a new reaction ....</b>	<b>245</b>
<b>Figure S10. Defining reactants and products of the new reaction. ....</b>	<b>245</b>
<b>Figure S11. Defining the exchange fluxes. ....</b>	<b>246</b>
<b>Figure S12. Measured fluxes. ....</b>	<b>248</b>
<b>Figure S13. Medium composition. ....</b>	<b>249</b>

<b>Figure S14. Regulatory constraints.</b>	250
<b>Figure S15. Genetic algorithm preferences.</b>	251
<b>Figure S16. Loading a saved input file.</b>	254
<b>Figure S17. FBA solution file</b>	257
<b>Figure S18. Frequency analysis input information.</b>	261
<b>Figure S19. Levels of biomass under iron-reduced conditions (IRDM) for triplicated experiments.</b>	268
<b>Figure S20. Levels of glucose under iron-reduced conditions (IRDM) for triplicated experiments.</b>	268
<b>Figure S21. Levels of lactate under iron-reduced conditions (IRDM) for triplicated experiments.</b>	269
<b>Figure S22. Levels of carbon dioxide under iron-reduced conditions (IRDM) for triplicated experiments.</b>	269
<b>Figure S23. Levels of oxygen under iron-reduced conditions (IRDM) for triplicated experiments.</b>	270
<b>Figure S24. Levels of biomass under iron-replete conditions (IRM) for triplicated experiments.</b>	270
<b>Figure S25. Levels of glucose under iron-replete conditions (IRM) for triplicated experiments.</b>	271
<b>Figure S26. Levels of lactate under iron-replete conditions (IRM) for triplicated experiments.</b>	271
<b>Figure S27. Levels of carbon dioxide under iron-replete conditions (IRM) for triplicated experiments.</b>	272
<b>Figure S28. Levels of oxygen under iron-replete conditions (IRM) for triplicated experiments.</b>	272
<b>Figure S29. Biosynthesis pathway of petrobactin and protocatechaute.</b>	273

<b>Figure S30. Biosynthesis pathway of bacillibactin.....</b>	<b>274</b>
<b>Figure S31. Comparison of the glycolysis pathway under iron-poor/rich at Phase I. ....</b>	<b>275</b>
<b>Figure S32. Comparison of the pentose phosphate pathway under iron-poor and iron-rich conditions at Phase I.....</b>	<b>276</b>
<b>Figure S33. Comparison of the by-product secretion in <i>B. anthracis</i> under iron-poor/rich conditions at Phase I. ....</b>	<b>277</b>
<b>Figure S34. Comparison of the glycolytic pathway under iron-poor/rich conditions at Phase II.....</b>	<b>278</b>
<b>Figure S35. Comparison of the by-product secretion and L-lactate uptake in <i>B. anthracis</i> under iron poor/rich conditions at Phase I. ....</b>	<b>279</b>
<b>Figure S36. Lactate metabolism at Phase II. ....</b>	<b>279</b>

# 1. INTRODUCTION

## 1.1. Overview

The development of high-throughput experimental technologies, computational biology, and bioinformatics has allowed the study of cells as a system, as opposed to the traditional reductionist approach that studies complex systems as individual elements working in isolation. This field of scientific research, which takes a global approach, is known as systems biology. Here, theoretical, experimental, and computational approaches are integrated in order to establish connections between genes, proteins, metabolites, and other cellular/subcellular entities. This global approach aids in the explanation and prediction of the complex cellular behaviors of biological systems.

Systems biology has been extensively used for the elucidation of metabolic models [1,2], because it allows the collection and integration of various data types in a form suitable for mathematical analysis, as is schematically represented in Figure 1. The establishment of a quantitative model allows for the compact and integrated analysis of complex metabolic networks, and their associated and often non-intuitive behavior. These models can be used to analyze phenotypes, guide strain design, and investigate fundamental metabolic questions.

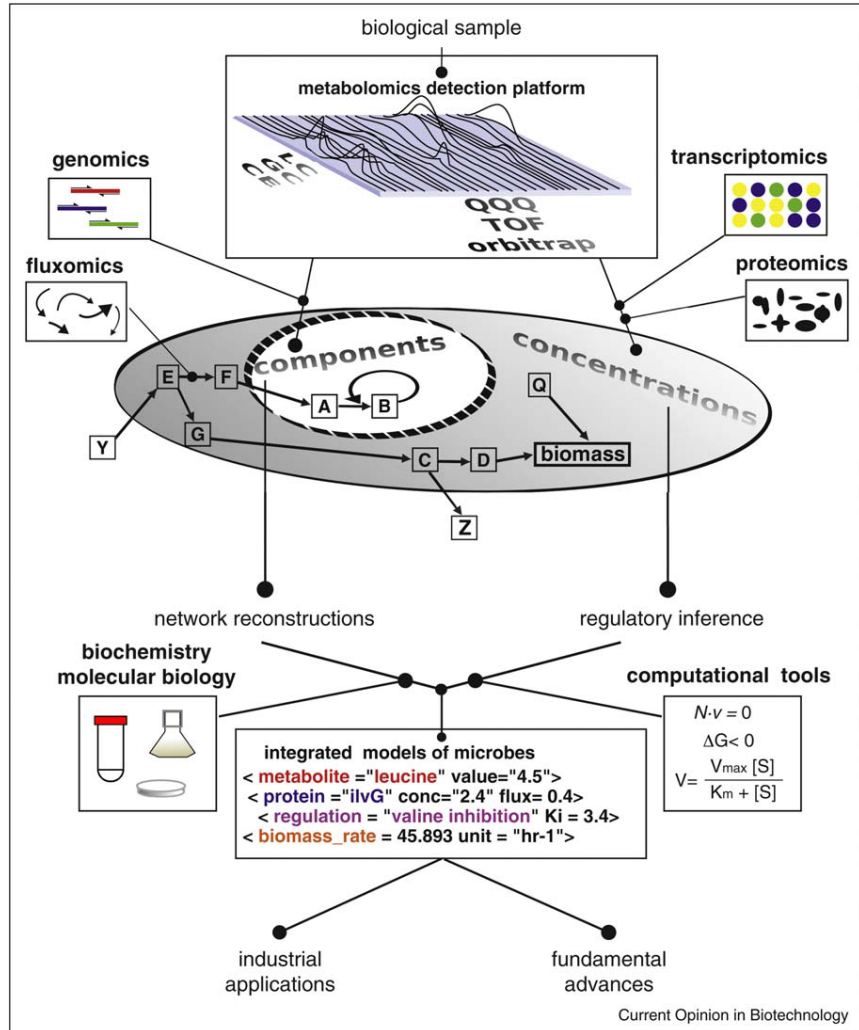


**Figure 1. Schematic representation of the integration of various data types for the reconstruction of metabolic models.** Figure taken from Reaves *et al.* [1]

The research reported herein applies systems biology to the reconstruction and analysis of the metabolic networks of *Mycoplasma gallisepticum*, and *Bacillus anthracis*. It takes advantage of the use of genome-scale metabolic models to investigate fundamental metabolic questions, and combines experimental and computational work. Through experiments, a microorganism's behavior can be

characterized. Nonetheless, metabolic interactions can be difficult to understand through experimentation alone.. On the other hand, metabolic models give a complete description of cellular functions. Therefore, this thesis will bring together these two tools, and demonstrate how the reconstruction and analysis of metabolic models help to explain the impact of iron availability on the *Bacillus anthracis* metabolism.

The reconstruction of genome-scale metabolic modeling is a time consuming process. Thiele *et al.* [3] have mentioned that the reconstruction could take anywhere from six months to two years depending on the knowledge of the organism, genome size, and the complexity of the metabolism. I hypothesized that the reconstruction time could be reduced through the use of a new methodology that combines a genetic algorithm (GA), and flux balance analysis (FBA), named GAFBA. I developed and tested GAFBA with the reconstruction of the genome-scale metabolic model of *M. gallisepticum* and *B. anthracis*. The reconstruction time using GAFBA ranged between 1-4 months. Moreover, it provided additional help throughout the curation process. It is a powerful tool for fundamental advances in biology. For instance, during the curation process of the *M. gallisepticum* genome-scale metabolic model, many logical hypotheses arose that have yet to be experimentally confirmed, such as the presence of formate dehydrogenase, NAD<sup>+</sup> synthetase, and Na-ATPase enzymes.

Based on the transcriptional profiles [6-8] of *Bacillus anthracis* under iron deprivation conditions, I hypothesized that the following changes would be likely to occur under iron-poor conditions: an increase in the flux of reactions involved in the



biosynthesis, secretion and re-uptake of siderophores, a decrease in some amino acid uptake, and a reduced growth rate under iron-poor conditions. All these conditions were observed during the experiments and in the results of the model when the iron concentration of the media was reduced.

## **1.2.Motivation**

The overall motivation behind the research presented here was to understand the cellular behavior of *M. gallisepticum* and *B. anthracis* from a metabolic perspective. This was achieved by combining an *in silico* genome scale metabolic analysis with experimental studies. Through the GAFBA methodology, two models were created: *M. gallisepticum* and *B. anthracis*.

A model of *M. gallisepticum* was reconstructed and curated in order to prove the principle of the GAFBA v1.0 methodology. Genome-scale metabolic models are generally under-determined. To solve these models, optimization theory is used where an objective function for the cell is postulated in order to determine the optimal distribution of metabolic resources. However, genome-scale metabolic models often result in an unfeasible solution when the model is constrained to experimental information. It was hypothesized that this was because some metabolites' mass balance constraints could not be satisfied due to missing/incorrect reactions, incorrect directionality of reactions, and missing/incorrect metabolites. This was the result of an incomplete or erroneous genomic annotation. Identifying the metabolites that violate the mass balance constraints is a non-trivial problem. GAFBA v1.0 determines these

problematic metabolites. To resolve the problematic metabolites, it is generally necessary to add some reactions, or to adjust their metabolic networks in a way that will solve the optimization problem. Furthermore, GAFBA v1.0 helped to identify minimal media growth components, which is the main issue during the growth of fastidious microorganisms such as *M. gallisepticum*.

The motivation behind the *B. anthracis* was to gain a better understanding of its metabolism. This information could ultimately lead to the development of strategies that will better protect people from anthrax. There are many studies on *B. anthracis* that have focused on virulence factors, elucidating and understanding the biosynthetic pathway, and the secretion and uptake of siderophores as individual elements. Very few studies however, have looked at the global metabolism of *B. anthracis* under conditions similar to the ones found in the alveolar macrophage (iron starvation and oxidative stress), a primary infection target for *B. anthracis*. These studies are based on transcriptomic and proteomic analysis [4-6], but based on the literature review, no metabolomic studies have been carried out.

### **1.3. Research significance and novelty**

This research helped me develop and test GAFBA, the new methodology for the curation process. GAFBA was used in the reconstruction of a small, and a large genome-scale metabolic network. *M. gallisepticum* has a small genome (~1 MB) compared to that of *B. anthracis* Sterne (~5.2 MB). GAFBA reduces the time required

for the reconstruction process, and is a powerful tool for fundamental biological studies.

GAFBA compiled all previously generated metabolic data into the *M. gallisepticum* genome-scale metabolic model, which is the first model for this pathogenic microorganism. Through the curation process, many logical hypotheses arose that have yet to be experimentally confirmed. The study of *M. gallisepticum*'s metabolism improves the understanding of its inner workings.

The genome-scale metabolic network analysis of the global metabolism of *B. anthracis*' vegetative cells elucidates of how *B. anthracis* survives within the alveolar macrophage, and establishes a productive infection. This is an initial approximation of how the host and *B. anthracis* interact during the infection process. Ultimately, it can help in the development of improved treatment options and vaccines.

The host/pathogen interaction was ranked as number seven out of the top ten biotechnologies for improving health in developing countries [7]. As a consequence, some have started to use models in order to study these interactions, such as the model developed using an MS2-infected *Escherichia coli* [8], and the model for the human alveolar macrophage and *Mycoplasma tuberculosis* [9]. The known host-pathogen interactions for *B. anthracis* have been partially determined by experimental observation of the bacteria. But, there is no mechanistic model that provides a deeper insight of the infection process. Therefore, this research attempts to start this process

of reconstruction of the interaction between the human alveolar macrophage (HM) and *Bacillus anthracis*, by generating a metabolic model for the bacteria.

This *B. anthracis* model is the first one for the bacterium. Additionally, it is the first one to include the siderophore biosynthetic, secretion, and uptake pathways in gram-positive bacteria. The existing metabolic models for gram-positive bacteria do not take into account the siderophore sub-pathway. Therefore, this *B. anthracis* model is expected to can be used as a guide for other gram-positive bacteria models, and it is anticipated that some of the knowledge discovered in this work can be applied to related species.

The analysis of the genome-scale model of *B. anthracis* under different iron conditions allows one to identify a down-regulation in the TCA cycle reactions from 2-oxoglutarate to oxaloacetate, which resulted in the reduced uptake of some amino acids under iron-poor conditions. This situation produced an increase in the glycolysis pathway to synthesize some of the amino acids required for siderophore production and for growth. Finally, I found a possible correlation of the growth between *B. anthracis*' metabolism under iron-poor conditions and the production of autoinducer-2, a quorum sensing signal molecule. This correlation has not been experimentally reported yet, however I was able to find it by using the genome-scale metabolic modeling of the bacterium. This outcome highlights the importance of studying bacterial metabolism from a global perspective, rather than as individual elements working in isolation.

## 1.4. Dissertation organization

The dissertation is divided into nine chapters. The background is presented in Chapter 2. Meanwhile, Chapter 3 introduces a genetic algorithm/flux balance analysis (GAFBA v1.0) methodology for reconstructing genome scale metabolic models. In this chapter, GAFBA v1.0 is developed and validated by reconstructing a genome-scale metabolic network of *Mycoplasma gallisepticum*. Chapter 4 is dedicated to enhancing GAFBA v1.0. A user-friendly interface is presented, as well as additional algorithms to speed up the curation process. This chapter is pure computational work. On the contrary, Chapter 5 explains the *in vivo* experiments of *B. anthracis* growing under two different iron conditions: a media treated with a resin to decrease the iron concentration (iron-poor media), and a media supplemented with ferrous sulfate solution (iron-rich media). Next, Chapter 6 introduces the first genome-scale metabolic network for *B. anthracis*. In this chapter, the experimentally measured fluxes reported in Chapter 5 are applied as constraints to the model. Thus, *in silico* analysis gives insight into the metabolic adaptation of the bacterium under different iron conditions (poor/rich). Then, Chapter 7 inquires about the possible connection between the secretion of a quorum sensing signal molecule and the growth of *B. anthracis* under iron reduced conditions. Finally, Chapters 8 and 9 conclude this work and present possible future work.

## 2. LITERATURE REVIEW

Below is a summary of the background for the research presented in the following chapters.

### 2.1. Genome-scale metabolic models (GEMs)

A GEM is a fully mechanistic model that represents the relationship between the genotype and phenotype of an organism's metabolism. These models have been used in biomedical and biological research such as the contextualization of high-throughput data [10], guidance of metabolic engineering [11], directing hypothesis-driven discovery [12], representation of multi-species relationships [13], and network property discovery [14], as was summarized by Oberhardt *et al.* [15].

GEMs compile the available genomic, biochemical, and physiological information on an organism, creating a draft reconstruction. It then goes through a curation process to fill the gaps, and remove any possible errors by examining the literature, experimental data, and databases. Finally, the reconstruction is converted into a mathematical model. The mathematical models can be quantitative, analyzed using a dynamic modeling approach, or a constraint-based modeling approach [15,16]. The dynamic modeling of metabolic networks consisting of thousands of reactions is often difficult, because of the necessity for a large number of experimentally determined parameters and the computational complexity. To overcome these issues, the constraint-based modeling approach was used [17].

### 2.1.1. CONSTRAINT-BASED MODELING

In constraint-based modeling, the solution space of all possible metabolic phenotypes is narrowed by imposing mass balance constraints and cellular limitations to the reconstructed metabolic network, as is shown in Figure 2. Constraints such as cellular limitations are based on enzyme capacity, reaction stoichiometry, directionality of the reaction, gene regulatory constraints, and environmental factors. The allowable solution space contains all the possible flux distributions that a metabolic network could have [18]. Then, linear programming (LP) is used to calculate an optimal flux distribution that satisfies a relevant objective function. Flux Balance Analysis (FBA) was used to calculate the optimal states in this research.

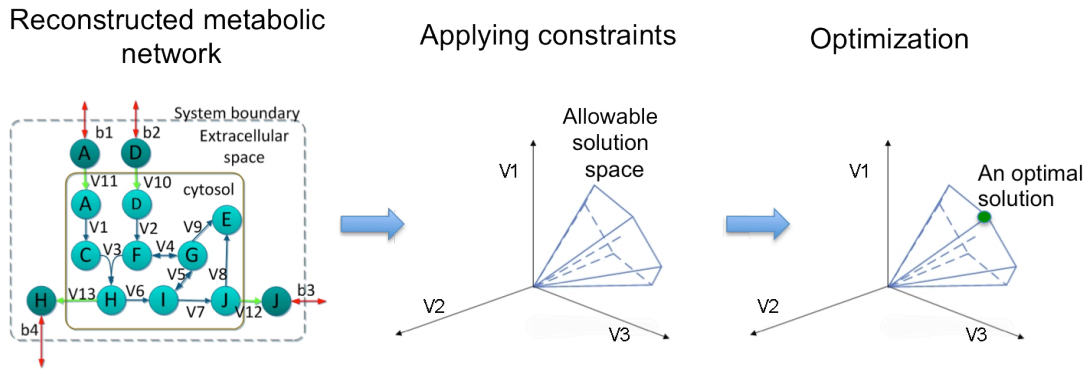


**Figure 2. The conceptual basis of constraint-based modeling.** This figure is an adaptation of Figure 1 from Orth, *et al.* [19], and Box 1 from Papp, *et al.* [20]. Mass balance constraints and capacity constraints are imposed to a reconstructed metabolic network leading to a allowable solution space. The network can have any flux distribution within this space. Linear programming can be applied to optimize a defined objective function.

### 2.1.1.1. Flux balance analysis (FBA)

FBA starts with a mathematical representation of the reaction network stoichiometries, and describes how substrates are converted to metabolite products and biomass constituents [21]. Thus, a dynamic mass balance for each of the metabolites presented in the network is written:

$$\frac{dx_i}{dt} = \sum_j S_{ij}v_j - \mu x_i \quad \text{Eq. (2.1)}$$

where  $x_i$  is the concentration (moles/ cell mass) of metabolite  $i$ ,  $S_{ij}$  is the stoichiometric coefficient of metabolite  $i$  in reaction  $j$ ,  $v_j$  is the flux (moles/cell mass/time) of reaction  $j$ , and  $\mu$  is the cellular growth rate ( $\text{time}^{-1}$ ).

It is generally accepted that metabolism operates on a much faster time scale than changes in cellular phenotype, for instance cell division [16,21,22]. Therefore, the transient mass balance can be simplified to only consider the steady state. As a result, there is no accumulation of metabolites, or:

$$0 = \sum_j S_{ij}v_j - \mu x_i \quad \text{Eq. (2.2)}$$

In Equation 2.2, the first term on the right-hand side represents the net synthesis rate of metabolite  $i$  over all the reactions. The second term is the dilution of



the metabolite  $i$  pool due to biomass growth. The dilution term can be neglected, because the effect of this term on the metabolite concentration is generally small compared to the fluxes for each reaction in which the metabolite participates [21,23,24]. Thus, the Equation 2.2 is reduced to a simpler linear mass balance:

$$\bar{\bar{S}} \cdot \bar{v} = 0 \quad \text{Eq. (2.3)}$$

where  $\bar{\bar{S}}$  represents the matrix of stoichiometric coefficients, and  $\bar{v}$  is the vector of fluxes through all the reactions. Each row from the matrix  $\bar{\bar{S}}$  corresponds to a unique metabolite in the network. Some of them are intracellular, and some are extracellular. Each column from the matrix represents one reaction. The fluxes can be classified as intracellular reactions, transport fluxes, and exchange fluxes. The last one represents the flow of nutrients/products into, or out of the biochemical system. Transport reactions define the flow of metabolites occurring across cell and subcellular compartment membranes.

Additional constraints are added to the system in order to reduce the space of the allowable flux distribution. The set of constraints are represented as:

$$\alpha_j \leq v_j \leq \beta_j \quad \text{Eq. (2.4)}$$

where  $\alpha_j$  and  $\beta_j$  are the lower and upper bound respectively of the  $j$  fluxes. The constraints can be of the physicochemical kind, based on the reversibility/irreversibility

of the reaction. For irreversible reactions, the lower boundary  $\alpha_j$  is set to zero. On the contrary, for reversible reactions, the lower boundary is defined as negatively infinite. The upper boundary for reversible and irreversible reactions is set to infinity. Furthermore, any experimental information can be added into the model by assigning values to  $\alpha_j$  and  $\beta_j$ , such as experimentally measured uptake/secretion rates. It is also possible to add regulatory constraints by using Equation 2.4. For instance, setting  $a_j$  and  $B_j$  to zero can represent the repression of certain enzymes under specific environmental conditions.

Typically, in genome-scale metabolic networks, the number of metabolites is less than the number of fluxes. This results in an under-determined system, for which there exists a range of possible solutions to the network fluxes [22]. Each solution represents a specific metabolic phenotype under particular conditions. Because the objective function and constraints are linear in nature, FBA employs linear programming (LP) to choose the flux distribution that is most optimal for a given objective [23]. It should be noted that the flux distribution is not necessarily unique, and there can be more than one flux distribution that reaches the optimal value of the objective function [16].

In LP, the constraints and the objective function are all linear with respect to the fluxes. The LP problem is formulated as;

Minimize/Maximize Z

$$\text{where } Z = \sum c_i \cdot v_i = \langle \mathbf{c} \cdot \mathbf{v} \rangle \quad \text{Eq. (2.5)}$$

Where Z is the objective function to be maximized. This is represented as linear combination of fluxes  $v_i$ . The term  $c_i$  is a biologically determined coefficient that exhibits the contribution of  $v_i$  to the objective function Z.

Different objective functions can be applied, such as the maximization of biomass, maximization/minimization of ATP production, and the minimization of redox potential [23,25,26]. In the past, the FBA approach combined with the maximization of biomass formation as an objective function has successfully predicted the growth rate [16]. Moreover, it has been argued that the growth of microorganisms over a long period of time in laboratory conditions confers an optimal growth phenotype on commonly used substrates in growth media [27]. For that reason, the objective function used for this research is the maximization of biomass formation.

## 2.2. Genetic algorithm (GA)

Genetic algorithms (GAs) were invented by John Holland in the 1960s at the University of Michigan [28]. GAs are adaptive heuristic search algorithms based on the evolutionary theories of natural selection and genetic. GAs identify solutions to optimization problems by searching a set of candidate solutions referred to as the *population*. The candidate solutions are encoded on simple data structures referred to as *chromosomes*. Each of the encoded parameters in a chromosome is referred to as a

*gene*. The genes are either single bits or small blocks of neighboring bits. They usually have a value of 0 or 1.

The GA process starts with the random generation of an initial population. Then the chromosomes in the current population are evaluated and assigned a fitness value that depends on how well that chromosome solves the problem. The next step is the formation of a new population to be used in the following iteration, or *generation* of the algorithm. The new population is formed using a specific selection strategy, operations such as crossover and/or mutation resulting in the generation of new solutions to the problem being solved [29].

#### **2.2.1. SELECTION STRATEGY**

There are many ways to accomplish selection, including roulette wheel selection, tournament selection, elite selection, and linear-rank selection [28]. Elite selection guarantees that the fittest members of each generation are selected. Specifically, a limited number of chromosomes with the best fitness values are copied to the next generation, avoiding the crossover and mutation operators.

#### **2.2.2. Crossover OPERATION**

Crossover operation is the primary genetic operator. It exchanges the information between two parent chromosomes. First, random segments of the parent chromosomes are selected. Then, those segments are exchanged to form two new

chromosomes with the same length as the parents. A schematic representation is shown in Figure 3.

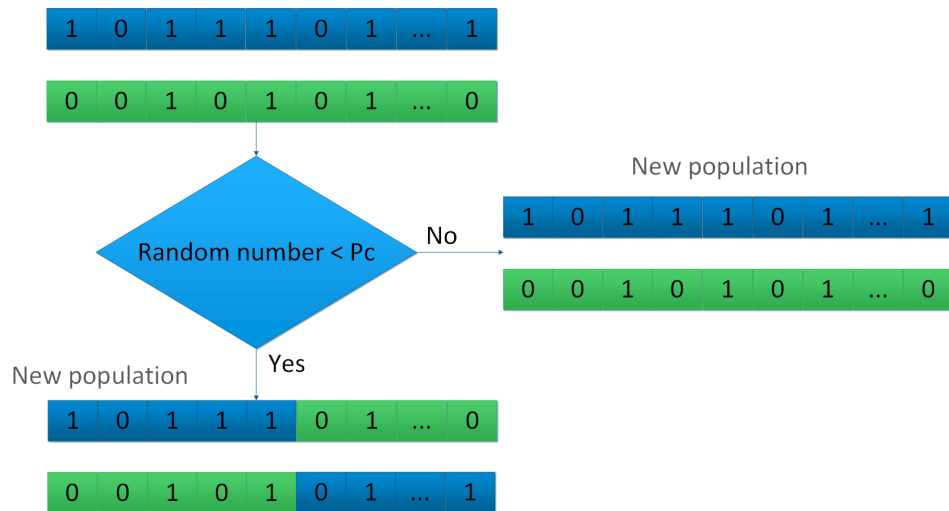


**Figure 3. One point crossover operation.** A crossover operation is performed in two parental chromosomes if a random number is lower than the probability of crossover ( $P_c$ ).

### 2.2.3. MUTATION OPERATION

Mutation operation replaces a randomly chosen gene on a chromosome with its opposite value. For instance, if the value of the gene were zero, it would be changed to one. Randomly sampling new points within the search space helps prevent premature convergence.. Mutation occurs randomly and very rarely with a probability ( $P_m$ ). Typically, this mutation rate is less than ten percent [30]. Figure 4 has an example of mutation operation.

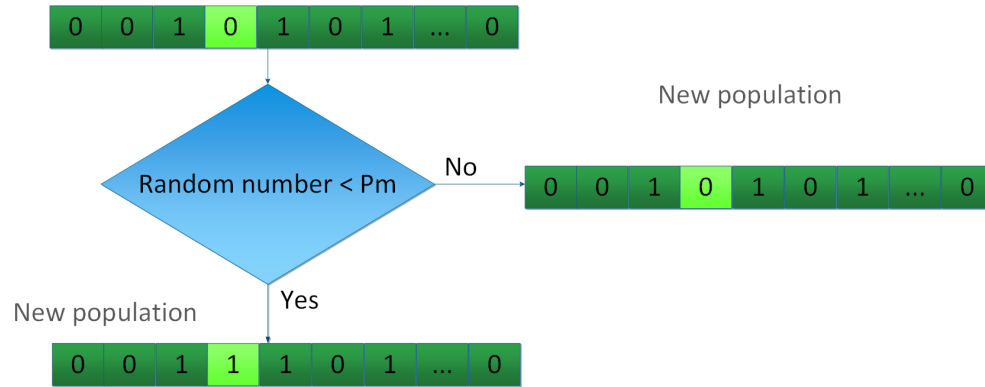


**Figure 4. Mutation operation.**  $P_m$  is the probability of mutation.

The process of going from the evaluation of fitness to the formation of a new population constitutes one generation in the execution of a genetic algorithm. Genetic algorithms cannot guarantee convergence. Therefore, termination is commonly triggered when either a maximum number of generations has been reached, or a satisfactory fitness level has been achieved [30].

## 2.3. Pathogenic microorganisms

This sub-section presents a general review of the pathogenesis and microbiological characteristics of the two microorganisms studied in this dissertation.

### 2.3.1. *MYCOPLASMA GALLISEPTICUM*

*M. gallisepticum* is an avian pathogen that results in chronic respiratory disease (CRD) in poultry. It lacks a cell wall, has a flask-shaped appearance, and can survive from a few days to months depending on the environmental conditions.

Conventionally, *Mycoplasma* have a small genome. Therefore, they have been considered model systems for defining the minimal set of genes required for survival. *M. gallisepticum*'s genome size is 996,422 bp long, with a G+C content of 31% [31].

*M. gallisepticum* infections are the source of significant economic losses in poultry production annually. Worldwide, the yearly losses have been estimated to exceed \$780 million, and in the United States the annual losses in egg production have been estimated to be about \$150 million. As a consequence, the National Poultry Improvement Plan has requested regular surveillance and the development of strategies to control and prevent the *M. gallisepticum* infection [32].

In the United States, a great deal of attention has been given to the eradication of this organism from most commercial chickens and turkey breeding flocks. However, it remains present in other poultry operations, mainly because the *M. gallisepticum* infection is difficult to diagnose. Current techniques are laborious, depend upon special expertise, and typically have false results [32]. Furthermore, the infection is easily spread via by aerosol exposure and egg transmission. Outbreaks are hard to control with antimicrobial therapy. Antibiotics can alleviate clinical signs, but they cannot eliminate the infection. In the U.S., there are three live vaccines available for use during the growing phase (F strain, ts-11, and 6/85), but they can be used only with permission of the state veterinarian. Some virulence is retained in the F strain, and ts-11 and 6/85 are less virulent than the F strain, but they are also less effective [33].

The infection starts when the bacteria colonize the mucosal surface of the respiratory tract. Figure 5 compares normal and infected tracheal tissue in birds. One important step in the colonization process is the cytoadherence of the tip-like structures of *M. gallisepticum* to the tracheal lumen epithelial cells. Once the bacterium is attached to the epithelial cell, the fusion of the cell membrane with *M. gallisepticum* can occur. This can happen within 5 minutes after infection, and the number of intracellular mycoplasmas increase in 24 hours. Then, the disease may progress through systemic infection [34,35].

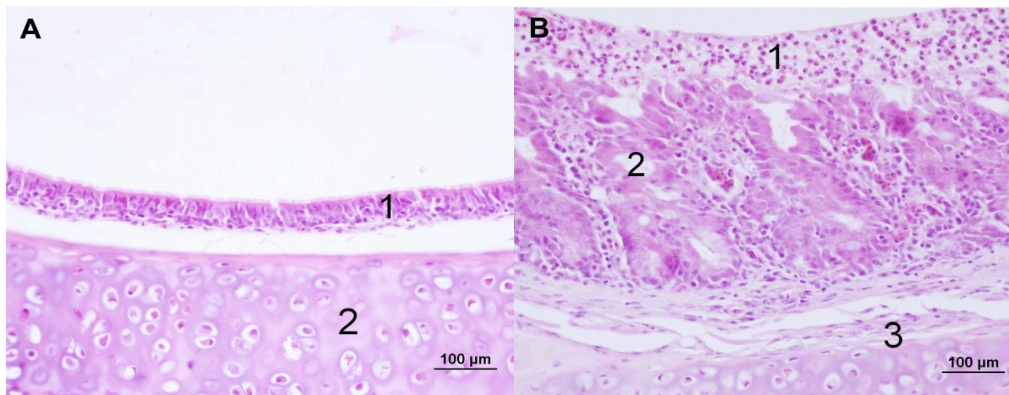


**Figure 5. Comparison of normal (A) and infected (B) tracheal tissue.** This figure was taken from Figure 2 from Vitula, *et al* [36]. Figure 2A: Normal mucosa lined with a pseudo-stratified columnar epithelium with knocilia(1), and a fibrocartilaginous layer (2]) Figure 2B: Trachea of a bird infected with *M. gallisepticum*. The inflammatory exudate is adhered to the epithelium (1). The trachea is moderately infiltrated by lymphocytes and plasma cells (2) and (3).



### **2.3.2. *BACILLUS ANTHRACIS***

#### **2.3.2.1. History**

In 1850, Pierre Rayer and Casimir-Joseph Davaine observed rod-like organisms present in the blood of anthrax-infected animals and humans. Davaine suggested that those microorganisms were probably causing the disease. In 1876, Robert Koch studied the complete life cycle of the bacteria, and stated that anthrax could only be transmitted from one host to another by transfer of the *Bacilli* [37]. Louis Pasteur created the first vaccine against anthrax containing live attenuated organisms in 1881. During the last century, anthrax infections decreased significantly.. However, during World War I and World War II, countries such as Germany, England, France, Russia, and Japan developed programs in order to produce *B. anthracis* for biological warfare. In 1979, an accidental anthrax outbreak occurred near Moscow. This case is known as the Sverdlovsk Epidemic. Many individuals suffered gastrointestinal, cutaneous, and inhalation anthrax. After many investigations, the incident was linked to a secret biological weapons program at a nearby military compound. In 2001, anthrax attacks occurred in the U.S with spores in powder form. The spores were sent to several news media offices and two U.S. Senators. Five people died, including one in Connecticut, and 17 others were infected [38]. Taking these events and the potential harm anthrax may cause into consideration, it is necessary to develop better strategies to protect people from anthrax infections.

### 2.3.2.2. Microbiology and pathogenesis

*B. anthracis* is a facultative anaerobic, gram-positive, non-motile, large rod and spore forming bacteria. *Bacilli* will form spores when local nutrients in the environment are exhausted, as happens after host death and exposure to air. The spores are highly resistant and can survive for decades.

*B. anthracis* has two plasmids, pXO1 and pXO2, that encode the major virulence factors. The pXO1 plasmid codes for three toxins: the lethal factor, the edema factor, and the protective antigen. These proteins are individually nontoxic, but in binary combinations, they result in hemorrhages, edema, and necrosis. The pXO2 plasmid encodes the genes involved in the synthesis of the polyglutamyl capsule that inhibits host phagocytosis of the vegetative form of *B. anthracis*. Both plasmids are necessary for full virulence; the loss of either results in an attenuated strain, such as the Sterne strain, which only has the pXO1 plasmid. Therefore, *B. anthracis* Sterne can synthesize exotoxins, but not the capsule [39]. It is known that the capsule does not have an important role in the first stages of the infection process, but it facilitates the systemic spread of the *Bacilli* through the bloodstream, and its escape from the lungs [40].

Anthrax can be manifested in three forms: cutaneous, inhalation or gastrointestinal. A picture of cutaneous and inhalation anthrax is shown in Figure 6. Inhalation and gastrointestinal anthrax result in higher incidences of fatality. The infection process begins when spores enter the body through the skin or mucosa. Then,

local macrophages phagocytose the spores and transport them to the regional lymph nodes. The spores germinate inside the macrophage during the intracellular step of the life cycle of *B. anthracis*. It is believed that spore germination may be triggered by signals such as elevated temperature ( $\geq 37\text{ }^{\circ}\text{C}$ ), elevated  $\text{CO}_2$  concentrations ( $\geq 5\%$ ), and serum components, which are typical conditions inside the host. After the vegetative cells are released from the macrophage, they continue to multiply and enter the lymphatic system and bloodstream, where they spread to the body and produce septicemia [41].

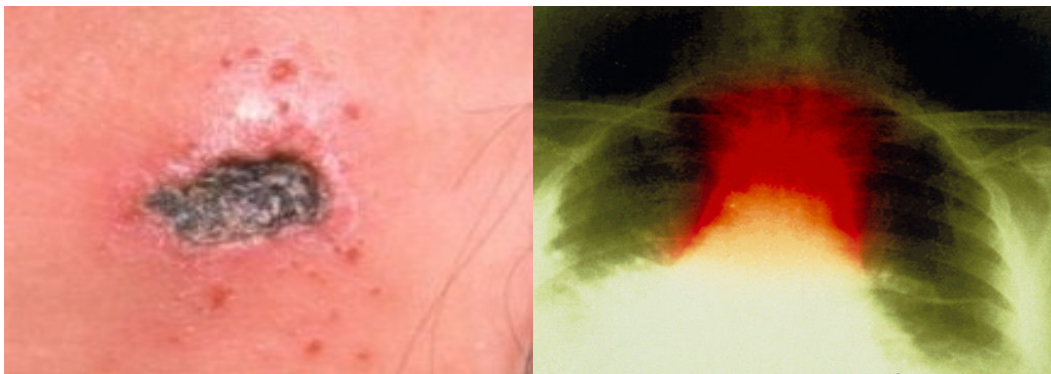


**Figure 6. Forms of anthrax,** a picture of cutaneous anthrax is on the left, and a picture of inhalation anthrax is on the right panel [42], The dark space at the upper right and upper left of the colored chest x-ray are the lungs, and the red region represents the *B. anthracis* infection. [43]

### **3. A GENETIC ALGORITHM/FLUX BALANCE ANALYSIS (GAFBA) METHODOLOGY FOR CURATION OF GENOME-SCALE METABOLIC MODELS**

This chapter is a modified version of the paper: “Semi-automated curation of metabolic models via flux balance analysis: a case study with *Mycoplasma gallisepticum*,” by Eddy J. Bautista, Joseph Zinski, Steven M. Szczepanek, Erik L. Johnson, Edan R. Tulman, Wei-Mei Ching, Steven J. Geary, Ranjan Srivastava. The author’s contribution to this research included model development, curation, and all of the computational work.

#### **3.1. Chapter Synopsis**

Genome-scale metabolic modeling, a technique primarily used for metabolic engineering and synthetic biology, shows tremendous potential as a tool for fundamental research, and the curation of metabolism. Through a novel integration of flux balance analysis and genetic algorithms, a strategy to curate metabolic networks and facilitate the identification of metabolic pathways that may not be directly inferable solely from genome annotation was developed. Specifically, metabolites involved in unknown reactions can be determined, and potentially erroneous pathways can be identified. The procedure developed allows for a new fundamental insight into metabolism, as well as acting as a semi-automated curation methodology for genome-scale metabolic modeling. To validate the methodology, a genome-scale metabolic model for the bacterium *Mycoplasma gallisepticum* was created. Several reactions not

predicted by genome annotation were postulated by the curator and validated via the literature. The model predicted an average growth rate of  $0.358 \pm 0.12 h^{-1}$ , closely matching the experimentally determined growth rate of *M. gallisepticum*, which is  $0.244 \pm 0.03 h^{-1}$ . This work presents a powerful algorithm for facilitating the identification and curation of previously known and new metabolic pathways, as well as presenting the first genome-scale reconstruction of *M. gallisepticum*.

### 3.2. Introduction

Metabolic network modeling is an iterative process that starts with the generation of a genome-scale reconstruction of metabolism, utilizing all current annotations and literature information. Next, an expert manually curates the draft reconstruction, and the computational model is generated. Finally, a comparison of the *in silico* results relative to the experimental information is assessed. The iterative process stops when the results from the model are nearly the same as the experimental results. In the future, as more information becomes available, the model can be updated in order to fill all possible gaps and achieve better results [3,44,45]. Most genome annotations are carried out using automated techniques, many of which rely on pairwise similarity scoring of the predicted proteins to those in databases [45-48]. Such a process is imperfect, as the ability to reliably annotate a given protein with a specific function can be greatly impacted by sequence divergence, lack of reliable functional knowledge, or annotation for sequence matches. This currently results in genome annotations that may not accurately or completely reflect the organism's metabolic functions. The use of metabolic network modeling provides an additional

and powerful methodology to help compensate for these gaps in knowledge, leading to a more accurate reconstruction of an organism's metabolism.

The model curation process improves the draft reconstruction by identifying and filling the gaps present in the network, removing reactions that are not likely present in the organism, and enforcing overall consistency across the network. Some automatic computational strategies for identifying missing reactions and filling the gaps have been developed previously, such as GapFind [47], GapFill [47], the Pathway Tools Hole Filler [49], the “metabolic expression placement” [50,51], MetaFlux [52], and Model SEED [53]. GapFind is an optimization-based procedure to identify missing reactions in the network. Gaps can be filled with GapFill by adjusting the existing metabolic network through reversing the directionality of existing reactions; adding transport reactions between compartments; adding exchange fluxes; or by adding a minimum number of reactions from a reference database [54]. MetaFlux is part of the Pathway Tools software for generating FBA models. It uses a multiple gap filling approach based on mixed integer linear programming (MILP), which suggests reactions to be added from the MetaCyc database, identifies biomass metabolites which are required but can not be produced, and chooses nutrient and secretion fluxes to be added to the model from a “try set” defined by the user. Model SEED is a web-based resource for the creation of new metabolic models. After a preliminary reconstruction model is created in Model SEED, an auto-completion step is performed by using an MILP algorithm that identifies the minimal set of reactions from the SEED reaction database needed to fill the gaps present in the network.

However, all these approaches are dependent upon an existing reference database of information to resolve these curation issues. Here, a new algorithm for facilitating the curation of models is presented. The approach integrates a genetic algorithm (GA) with flux balance analysis. The novelty and strength of this GA/Flux Balance Analysis (GAFBA v1.0) strategy lies in its ability to both aid in fundamental studies of metabolism, and to facilitate the curation of genome-scale metabolic networks, rather than functioning solely as a predictive tool. Furthermore, the strategy is independent of a reference database, allowing the researcher to investigate other avenues of curation. However, this approach does not preclude the use of existing databases as one of those sources of information. Rather it provides increased flexibility in evaluating the system of interest.

The premise of the GAFBA v1.0 method is based upon the observation that the optimization of an initial genome-scale metabolic model often results in no feasible solution when experimental information is incorporated. This result indicates that some of the constraints cannot be satisfied, because they are mutually contradictory. The GAFBA v1.0 method identifies the mass balanced constraints that may be relaxed to solve the FBA optimization problem. If relaxing a selected constraint allows the problem to be solved, it is likely that the associated metabolite was participating in a metabolic reaction that, due to lack of information during the reconstruction process, was not taken into account in the model. As a result, the metabolite and the potential reactions in which it may participate should be reviewed. The approach developed here employs a genetic algorithm to identify the minimum number of constraints that

could be relaxed in order to achieve a feasible solution to the FBA optimization problem.

To develop and evaluate this strategy, *Mycoplasma gallisepticum* was chosen as the model organism. The choice of *M. gallisepticum* for the validation of the GAFBA v1.0 methodology was driven by our expertise on the organism, and the organism's importance to the poultry industry. *M. gallisepticum* causes chronic respiratory disease in chickens and infectious sinusitis in turkeys [55]. The disease can be easily propagated by direct or indirect means. *M. gallisepticum* has been a concern to the poultry industry because of the resultant increase in chick and poultry mortality, reduced egg production, and increased costs related to medication, prevention and control programs. For example, in 1994, the layer industry alone lost between \$118 and \$150 million in the United States [56] due to *M. gallisepticum* infections. A better understanding of *M. gallisepticum* biology, including virulence, genomics, and metabolic processes has the potential to allow for the development and improvement of the vaccines and control strategies for this disease.

In this work, the metabolic network of *M. gallisepticum* was developed by using the organism's annotated genome sequence, compiling existing enzymatic data, employing genome-scale bioinformatics-driven homology searches, referencing the metabolism of other closely related *Mycoplasma* strains, generating a comprehensive biomass equation, and finally analyzing how all the metabolites in the system interacted with each other using the GAFBA v1.0 algorithm.



### 3.3. Material and Methods

#### 3.3.1. GENETIC ALGORITHM PARAMETERS

The genetic algorithm (GA) maintained a population of chromosomes where each one of them represented a potential metabolic model for *M. gallisepticum*. The chromosomes were encoded in such a way that each gene symbolized a mass balance constraint. If the mass balance constraint for a metabolite was relaxed, the gene was assigned a value of zero. If it was enforced, the gene was assigned a value of one. The population was evolved using the genetic operations of reproduction, crossover, and mutation. In the reproduction operation (elite selection), the best chromosomes were copied unchanged into the new population. Meanwhile, the crossover operation swapped information between two parent chromosomes. Finally, the mutation operation randomly selected one or more mass balance constraints to alter the gene value from its initial value. For instance, if the initial gene value was one, it was changed to zero and vice versa.

GA was implemented using an *elite selection* strategy [28]. The population consisted of 30 chromosomes. The crossover probability was set to 70%. The mutation probability was set to 1%. The GAFBA v1.0 algorithm was run for 2,000 generations per simulation. The choice of 2,000 generations as the termination criteria was based on empirical observation. It was found that by 2,000 generations, the system generally reached a plateau, and no further changes in biomass and constraints were observed. Each simulation took around seven hours on a 3.33 GHz Intel Core 2 Duo CPU/ 4 GB workstation. Thus, the total time for the 40 simulations was approximately 12 days.

### 3.3.2. FLUX BALANCE ANALYSIS

The theory behind the development of FBA was discussed in chapter 2. However, in this subsection the constraints applied to the specific case of *M.gallisepticum* are defined. Since the media was undefined, the exchange fluxes had to be determined from literature information on relative species [57-59]. The boundaries for the exchange fluxes were defined for metabolites in the media as  $-\infty \leq v_j \leq \infty$ , and for secretion of metabolites the following constraint was implemented:  $0 \leq v_j \leq \infty$  [58]. The list of nutrients and secretions are provided in appendix A3.4. The lower boundary of the non-growth associate maintenance (NGAM) value was set to  $8.4 \text{ mmol gDW}^{-1}\text{h}^{-1}$ , based on the value for the *M. genitalium* iPS189 model [58]. The NGAM value represents the energy consumed for processes such as turnover of macromolecules, maintenance of concentration gradients, and electrical potential gradients when the cells do not grow [60]. The upper and lower boundaries of the glucose uptake rate and lactate secretion rate were set to the experimentally determined values, which were  $-16.53 \text{ mmol gDW}^{-1}\text{h}^{-1}$  for glucose, and  $10.29 \text{ mmol gDW}^{-1}\text{h}^{-1}$  for lactate. The lower boundary value of the oxygen uptake rate was constrained to  $-43 \text{ mmol gDW}^{-1}\text{h}^{-1}$  to avoid reaction-looping behavior [3,52]. The objective function to be maximized was the biomass equation for *M. gallisepticum*.

### **3.3.3. EXPERIMENTAL PROTOCOLS**

All the relevant information on the experimental methodology can be found in appendix 2.

## **3.4. Results**

### **3.4.1. HYBRID GENETIC ALGORITHM/FLUX BALANCE ANALYSIS (GAFBA)**

The hybrid Genetic Algorithm/Flux Balance Analysis Algorithm (GAFBA v1.0) algorithm embeds the Flux Balance Analysis (FBA) optimization problem within a genetic algorithm to identify problematic metabolic constraints, and is schematically depicted in Figure 7. The optimization problem was resolved through a hierarchical approach, with the minimization of the number of relaxed constraints being given primary importance. The pool of models that had the same number of constraints relaxed were then further discriminated against by determining which individual models had the highest growth rate values, a frequently used objective function for FBA [61-64]. After each simulation, a list of problematic metabolites, whose mass balance constraints were forced to be relaxed, was generated to elucidate potential errors or missing information. Based on these data, it was possible to decide the best manner by which to fill in the missing information if possible. A revised version of the mechanisms for solving gaps previously presented by Maranas' group was manually applied [47]. The options were: 1) change the directionality of a reaction, 2) add an exchange flux for the metabolite, 3) add a transport or intracellular reaction, 4) remove a reaction or metabolite from the model, or 5) no change.

Examples for each case are presented in the appendix 1. The option chosen was based on experimental data, literature data or information from related organisms.

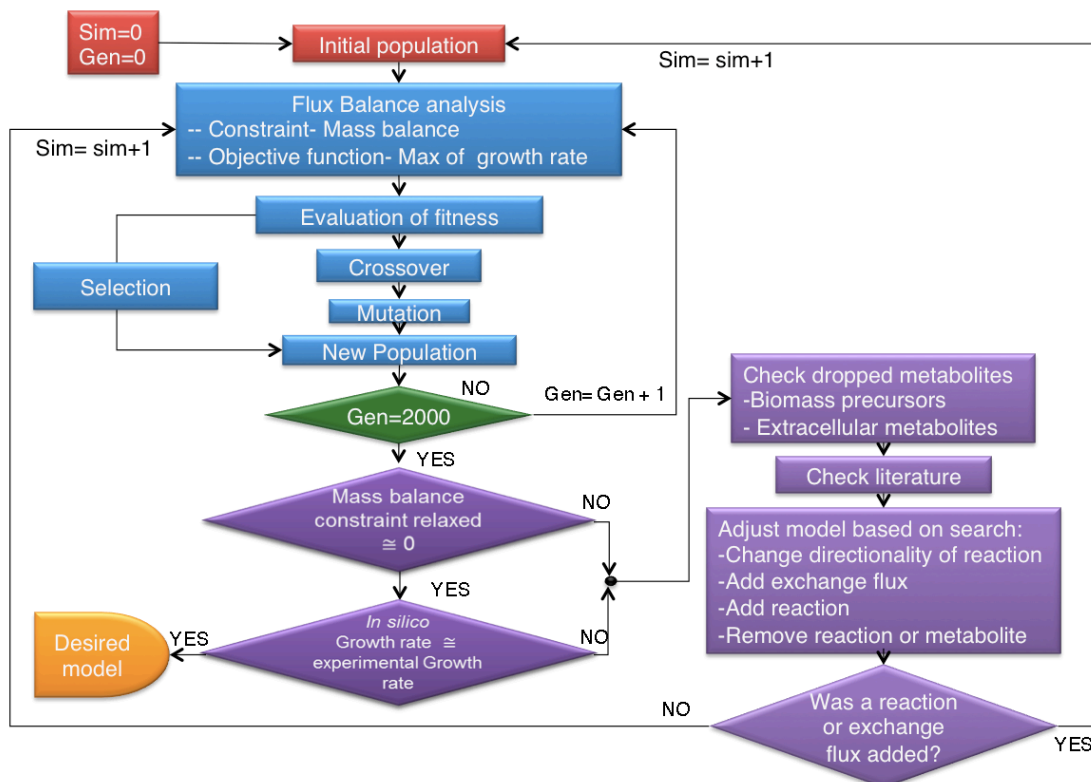


**Figure 7. Flowchart for the GAFBA v1.0 algorithm.** A schematic depiction of the GAFBA v1.0 algorithm used to determine the genome-scale metabolic model for *M. gallisepticum*. The steps in purple are operations performed by the user.

The initial genome-scale metabolic model was based upon an updated annotation of the *M. gallisepticum* genome [65]. Using the Pathway tools software platform [66], a Pathway Genome Database was constructed that accounted for all metabolic pathways, as determined from the genome annotation.

The GA started with the random generation of an initial population of data structures referred to as “chromosomes”, per the GA parlance [28,67]. Each chromosome represented a potential metabolic model of the microorganism. The chromosomes were binary encoded where each of the genes represented a mass balance constraint. If the mass balance constraint for a metabolite was relaxed, the gene was assigned a value of zero. If it was enforced, the gene was assigned a value of one. The number of mass balance constraints that were relaxed in the initial population was determined randomly. Examples of the mass balance constraints enforced and relaxed are shown in Figure 8. A feasible solution to the optimization problem is found when the mass balance constraints of metabolite E and A are allowed to be relaxed. By relaxing the mass balance constraint of metabolite A, the flux through V1 can be different than zero, allowing the production of metabolite D required to fulfill the experimentally observed secretion of metabolite H. Something similar happens when the mass balance constraint of metabolite E is relaxed. V5 can be carried out with a flux different than zero, allowing the experimentally observed uptake of metabolite C.

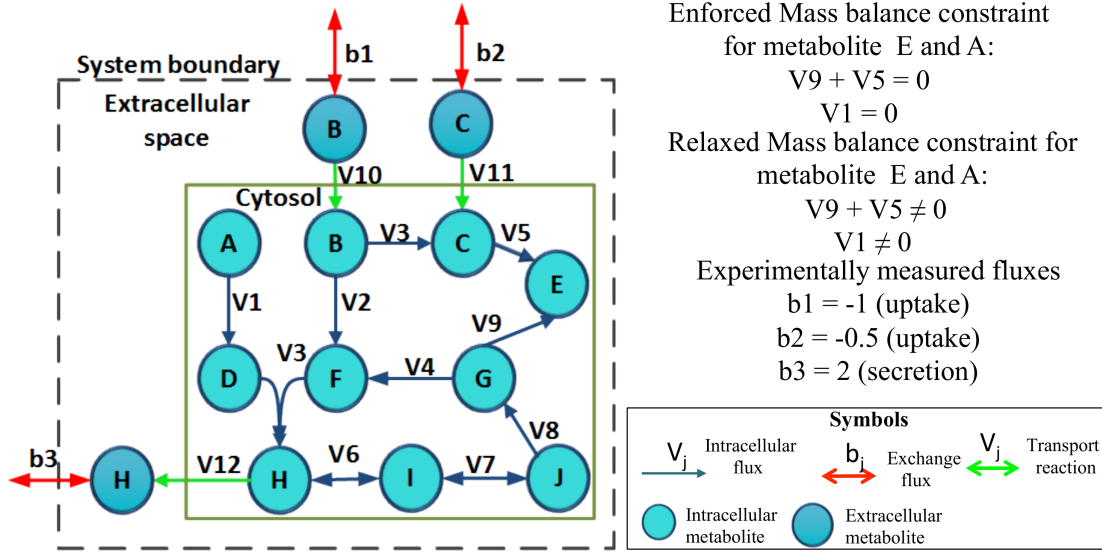


**Figure 8. An example of relaxed and enforced mass balance constraints for a metabolite.**

The population was then allowed to evolve using the genetic operations of reproduction, crossover, and mutation in order to achieve a fitter population, and ultimately an accurate metabolic model. The objective function for GAFBA v1.0 was to minimize the number of mass balance constraints relaxed. The problem is formulated as follows,

$$\text{Minimize } F = l - \sum_{i=0}^l g_i \quad \text{Eq. (3.1)}$$

where  $F$  is the number of mass balance constraints relaxed,  $l$  is the length of the chromosome or total number of mass balance constraints,  $i$  is the number of genes, and  $g$  is the gene value (0 or 1).

The objective function of GAFBA was subject to the requirement that the FBA model return a feasible solution. If the FBA optimization of a chromosome resulted in an unfeasible solution, a negative one (-1) was assigned to its  $F$  value. Moreover, if two chromosomes had the same number of mass balance constraints relaxed ( $F$  value), the best one was the chromosome with the higher growth rate.

The FBA problem is presented in the set of Equations 3.2,

$$\begin{aligned}
 &\text{Maximize } Z = \sum c_i \cdot v_i \\
 &\text{Subject to } \overline{\overline{S}}_E \cdot \overline{v}_E = 0 \\
 &\quad \text{and } \overline{\overline{S}}_R \cdot \overline{v}_R \neq 0 \\
 &\quad \text{and } \alpha_j \leq v_j \leq \beta_j
 \end{aligned}
 \tag{Eq. (3.2)}$$

where  $Z$  is the growth rate, the subscript  $E$  refers to the mass balance constraints enforced, and the subscript  $R$  indicates the mass balance constraints relaxed. All the other variables have been defined in the previous chapter.

A list of the problematic metabolites was generated upon completion of the run. Problematic metabolites were defined as those that were unable to fulfill the mass balance under the given conditions; manual review of each of the metabolites, as well as some of the upstream and/or downstream metabolites in the associated pathway was required. The analysis of the metabolites upstream and/or downstream in the pathway helped to determine if the problem could be corrected by adjusting the mass balance of a closely connected metabolite instead of the problematic metabolite directly. For

example in Figure 8, the problematic metabolite could be C because one of the downstream reactions (V5) responsible for consuming the metabolite (C) is blocked, since it is producing a dead end metabolite (E). Thus, it is necessary to adjust the mass balance of the dead end metabolite (E) and not the mass balance of the so-called problematic metabolite (C). An example of an upstream issue in Figure 8 could be the problematic metabolite D. V1 is the reaction responsible for producing metabolite D, however it has no flux due to the lack of a reactant (A). Under such conditions, the mass balance for the reactant (A) has to be adjusted rather than the mass balance of the initially identified “problematic” metabolite (D).

After updating the model, a new simulation was started. If a metabolite was added or removed, a new initial population was generated randomly and evolution was allowed to proceed. If no metabolite was added or removed, GAFBA v1.0 could either be continued from where it left off using the final population from the previous run as the seed population, or an entirely new population could be generated. The evolutionary process was then re-started. The ultimate termination criterion was when none of the mass balances constraints needed to be relaxed.

### **3.4.2. INITIAL RECONSTRUCTION OF THE *M. GALLISEPTICUM* METABOLIC MODEL**

The first step in the reconstruction of a genome-scale metabolic model of *M. gallisepticum*, was to analyze the published annotation of Strain R Clone 2 [65] using the Pathway Tools Pathologic automated metabolic network generation platform [68]. Pathway Tools Pathologic compiled reactions associated with Enzyme Commission



(EC) numbers and enzymes listed in the annotation [66]. Next, an in-depth literature review focusing on previously elucidated enzymatic activity was performed. Reactions shown to be active in *M. gallisepticum* were subsequently added. Reactions shown to be inactive were removed. A total of 23 reactions were added due to supporting experimental data and are listed in Table 1. Five total reactions, shown in Table 2, were added based on BLASTP homology results. Two reactions catalyzed by annotated enzymes that were found in previous studies were not present in *M. gallisepticum*. These reactions were subsequently removed and are listed in Table 3.

Once the pool of published enzymatic data had been exhausted, the Pathway Tools Hole Filler was used to generate a list of gene candidates to potentially fill gaps in various metabolic pathways. Any candidate reaction from Pathway Hole Filler with a probability assignment over 0.9 was selected for further evaluation in order to eliminate false positives, and about two thirds of the candidates were accepted. Supporting evidence for the additional function of the genes selected by the Pathway Hole Filler, along with the reactions catalyzed are shown in Table 4. In total, 12 high confidence enzymes were assigned due to the results of the Pathway Hole Filler analysis. Taking these modifications into account, the initial model consisted of 446 metabolites involved in 380 reactions.

**Table 1. Summary of reactions added to the metabolic model based on experimental data in the literature.** Enzyme names normally catalyzing reactions described in the literature and corresponding E.C. assignments are listed. All EC numbers were determined via Pathway Tools v14. *M. gallisepticum* genes potentially associated with these activities are noted, and enzymes/activities lacking gene associations of confidence are indicated with question marks.

Enzyme Name	EC #	Associated Gene	Citation
HMG-CoA Synthase	2.3.3.10	?	[69]
CoA transphorase	2.8.3.8	?	[69]
Membrane DNAases and RNAases	None	?	[70]
Succinyl CoA: Acetoacetate CoA-transferase	2.8.3.5	?	[69]
HMG-CoA Reductase	1.1.1.34	?	[69]
Malate synthase	2.3.3.9	?	[71]
Pyruvate Carboxylase	6.4.1.1	?	[71]
AMP phosphatase	3.1.3.5	?	[72,73]
GMP phosphatase	3.1.3.5	?	[72-74]
dAMP	3.1.3.5	?	[75]
Adenylosuccinate synthetase	6.3.4.4	?	[76]
Adenylosuccinate lyase	4.3.2.2	?	[76]
Deoxyadenosine kinase (ATP-dependent)	2.7.1.76	MGA_0174, MGA_0175	[74]
Deoxyguanosine kinase (ATP-dependent)	2.7.1.133	MGA_0174, MGA_0175	[74]
Deoxycytidine deaminase	3.5.4.14	MGA_0361	[49,77]
Uridine phosphorylase	2.4.2.3	?	[49,73,77]
Deoxyuridine phosphorylase	2.4.2.23	?	[73]
Uracil phosphorylase	None	MGA_0362	[49,73]
Malate dehydrogenase	1.1.1.37	MGA_0746	[71,78,79]
Ribose-5-phosphate isomerase	5.3.1.6	MGA_0886	[74,80]
Asparate aminotransferase	2.6.1.1	?	[81]
Serine hydroxymethyltransferase	None	MGA_1146	[82]
Phospholipase A1	3.1.1.32	?	[83]

**Table 2. Summary of reactions added based on BLASTP analysis.** Listed here are *M. gallisepticum* genes found by forward and reverse BLASTP [84,85] searches to be significantly similar to genes in related mycoplasmas that catalyze the corresponding listed reactions. These reactions were added to the model. All EC numbers were determined via Pathway Tools v14.

Enzyme name	EC #	M. gal Locus	Organism	Locus	Forward E value	Reverse E Value	Citation
1,2 diacylglycerol 3-B-galactosyltransferase	2.4.1.46	MGA_0001	<i>M. pneumoniae</i>	mpn483	3.E-15	7E-13	[86,87]
Galactolipid galactosyltransferase	2.4.1.184	MGA_0001	<i>M. pneumoniae</i>	mpn483	3.E-15	7.E-13	[86,87]
Phosphoglycerate kinase (dGTP)	2.7.2.3	MGA_1187	<i>M. pneumoniae</i>	mpn429	1.E-128	1.E-128	[88,89]
Phosphoglycerate kinase (GTP)	2.7.2.10	MGA_1187	<i>M. pneumoniae</i>	mpn429	1.E-128	1.E-128	[88,89]
Phosphopentomutase	5.4.2.7	MGA_0358	<i>M. pneumoniae</i>	mpn066	6.E-120	7.E-120	[89]

**Table 3. Reactions removed based on experimental studies.** Here, the reactions and associated enzymes that were shown to be absent in *M. gallisepticum* based on previous experimental studies, and were therefore not incorporated into the model are listed.

Removed due to experimental evidence			
Enzyme name	EC #	Associated gene	Citation
Deoxyribose-5-phosphate aldolase	4.1.2.4	MGA_0363	[80]
dUTPase	3.6.1.23	MGA_0994	[75,90]

**Table 4. Enzymes added based on Pathway Tools analysis.** This table shows the genes, previously annotated functions, newly annotated functions, reaction EC numbers, and HF probability, along with the rationale for why they were added. All EC numbers were determined via Pathway Tools v14. It should be noted that the functionalities listed here are in addition to the original functionality of the given gene.

Gene	Annotated Gene Function	New HF Gene Function	Hole EC#	Ptools HF Probability	Additional Citation/Rationale
MGA_0008	Putative Glycerol-3-phosphate acyltransferase	Glycerol-3-phosphate O-acyltransferase	2.3.1.15	0.98	Needed for glycerol incorporation for phospholipid biosynthesis
MGA_0161	Dihydrolipoamide dehydrogenase (E3) component of PDH complex	Glycine Decarboxylase	None	1.00	Folate interconversion
MGA_0161	Dihydrolipoamide dehydrogenase (E3) component of PDH complex	NAD(P)(+) Transhydrogenase (B-specific)	1.6.1.1	0.99	Needed for NADP charging
MGA_0181	Fatty acid /phospholipid synthesis protein Plsx	Acyl-Phosphate Synthase	None	0.99	Needed to provide an acyl carrier protein for lipid metabolism
MGA_0291	Inorganic polyphosphate /ATP-NAD kinase	NADH Kinase	2.7.1.86	0.96	Needed for NADH metabolism
MGA_0364	Purine nucleoside phosphorylase deoD-type	Deoxyinosine phosphatase	None	0.99	[73]
MGA_0594	Glutamyl-tRNA synthetase (Glutamate—tRNA ligase) (GluRS)	Glutamine tRNA ligase	6.1.1.18	1.00	Necessary tRNA charging pathway
MGA_0594	Glutamyl-tRNA synthetase (Glutamate—tRNA ligase) (GluRS)	Glutamine tRNA ligase	None	0.92	Necessary to the glutaminytRNA charging pathway

Gene	Annotated Gene Function	New HF Gene Function	Hole EC#	Ptools HF Probability	Additional Citation/ Rationale
MGA_0596	Bifunctional protein fold	Methylenetetrahydrofolate dehydrogenase (NAD+)	1.5.1.15	1.00	Homology to <i>E. Coli</i> 's FOLD which catalyzes this reaction
MGA_0833	Acetyl-CoA hydrolase	Acetate CoA transferase	2.8.3.8	0.98	[69]
MGA_0950	Guanosine polyphosphate pyrophosphohydrolases/synthetase	GTP-pyrophosphokinase	2.7.6.5	1.00	Needed for ppGpp Biosynthesis
MGA_1065	Asparaginyl-tRNA synthetase	Aspartate tRNA ligase	6.1.1.-	1.00	Needed for L-asparaginyl tRNA charging pathway

### 3.4.3. REFINEMENT OF THE INITIAL RECONSTRUCTION

FBA of the initial *M. gallisepticum* model resulted in no feasible solution. Thus, the model was analyzed using GAFBA v1.0 to identify reaction holes, unproduced but necessary biomass components, and metabolites with no membrane transporter or degradation pathway. The biomass equation was meticulously investigated. A large number of citations were accumulated for many metabolites that were known to be biosynthesized by *M. gallisepticum*, but were not accounted for based on the genome annotation. For example, phosphatidylcholine, cardiolipin, and sphingomyelin are all phospholipids known to have working biosynthesis pathways in *M. gallisepticum* based on previously conducted fatty acid radioactive labeling assays [91]. Nevertheless, there are a number of reactions necessary to biosynthesize these components that are absent in *M. gallisepticum*. Therefore, logical reactions were

assigned to complete these biosynthesis pathways, usually by referencing similar pathways in other *Mycoplasma* genomes. A total of 16 reactions were added. A list of all of these added reactions, along with a brief description of the rationale for the additions and all relevant citations are shown in Table 5. However, it is critical to note that the rationale for including these pathways was to complete the model. It does not constitute as proof of the existence of these pathway. That being said, the requirement of such pathways for the model does open up interesting experimental questions and new hypotheses.

Despite the application of the changes shown in Table 5, some mass balances remained inconsistent. Using GAFBA v1.0, additional changes were needed in order to fulfill the mass balance and additional runs continued to require refinement of the model. The remaining modifications are presented in Table 6 with the details described below.

Through the use of GAFBA v1.0, it was found that the mass balance on the charged tRNA's and uncharged tRNA's could not be enforced under the given metabolic description. The discrepancy was due to uncharged tRNA's being converted to charged tRNA's by tRNA ligase reactions without participating in other reactions. This ultimately resulted in the depletion of uncharged tRNA's if the mass balance was enforced without modifications. To rectify this imbalance, another reaction was added representing a recycling process to convert the charged tRNA's to uncharged tRNA's, thereby completing the cycle. These reactions were added to the biomass equation.

This was similar to the approach taken for *M. genitalium* model *iPS189* [58], which also includes charged and uncharged tRNA molecules in the biomass equation.

**Table 5. Initial model modifications.** The first set of changes made to the preliminary model based on GAFBA v1.0 results is provided. Rationale and relevant citations are listed for each.

Enzyme Name	EC #	Needed Product/ Un-degraded Metabolite	Rationale	Citation
Pyruvate kinase	2.7.4.6	DNA	Needed for DNA synthesis. 7 reactions total of this EC# added.	[88]
Phosphatidate phosphatase	3.1.3.4	A phosphatidylcholine	Needed to synthesize a lipid experimentally proven to be biosynthesized	[91]
Phosphatidylglycerophosphatase	3.1.3.27	Cardiolipin	Needed to synthesize a lipid experimentally proven to be biosynthesized	[91]
Unnamed	2.7.8.-	Cardiolipin	Needed to synthesize a lipid experimentally proven to be biosynthesized	[91]
Chlorinephosphate cytidyltransferase	2.7.7.15	A phosphatidylcholine	Needed to synthesize a lipid experimentally proven to be biosynthesized	[91]
Diacylglycerol chlorinephosphotransferase	2.7.8.2	A phosphatidylcholine	Needed to synthesize a lipid experimentally proven to be biosynthesized	[91]
Sphingomyelin Synthase	2.7.8.27	A sphingomyelin	Needed to synthesize a lipid experimentally proven to be biosynthesized	[83,91]
PNPase	3.1.3.7	Adenosine 3',5'-biphosphate	Biphosphate, the byproduct of the acyl carrier protein charging reaction necessary for fatty acid utilization	[91-93]
Fatty acid acyl group creator	6.2.1.20	Acyl-fatty acid	Needed for fatty acid assimilation	[91-93]

Enzyme Name	EC #	Needed Product/ Un-degraded Metabolite	Rationale	Citation
Maltose phosphorylase	2.4.1.8	B-D-glucose-6-phosphate	Needed for maltose degradation	[94]
Serine hydromethyl transferase	None	5-methyl-tetrahydrofolate	Tetrahydrofolate	[82]
Pyridoxamine kinase	2.7.1.35	Pyridozyl 5'-phosphate	Needed for vitamin B6 production	[89]
Fructose-1-phosphate kinase	2.7.1.89	Fructose-1,6-biphosphate	Fructose degradation essential	[94]
Thiamine kinase	2.7.1.89	Thiamine diphosphate	From thiamine	[89]
Thiamine-monophosphate kinase	2.7.4.16	Thiamine diphosphate	Needed to complete vitamin b1 biosynthesis from thiamine	[89]
Adenosylhomocysteine	3.3.1.1	S-adenosyl-L-homocysteine	Needed to degrade the S-adenosyl-L-homocysteine formed from tRNA methylation	none

**Table 6. Remaining changes made to model.** The cumulative changes from the second and succeeding rounds of analysis done with the GAFBA v1.0 algorithm are presented.

Metabolite	compartment	change	reference
Charged tRNA's	cytosol	added recycling rxn to biomass	[51]
Uncharged tRNA's	cytosol	added recycling rxn to biomass	[51]
Oxygen	cytosol	added exchange flux	Experimental conditions
Cytidine	cytosol	added exchange flux	[57]
Hydrogen peroxide	cytosol	added exchange flux	
Carbon dioxide	cytosol	added exchange flux	
Chloride	cytosol	added exchange flux	[57]
L-alpha-alanine	cytosol	added exchange flux	[57]
L-cysteine	cytosol	added exchange flux	[57]
L-threonine	Cytosol	added exchange flux	[57]
L-glutamine	Cytosol	added exchange flux	[95]
L-aspartate	Cytosol	added exchange flux	[57]



Metabolite	compartment	change	reference
Glycine	Cytosol	added exchange flux	[57]
all the rest of amino acids	Extracellular	added exchange flux	[57]
Ceramides	Extracellular	added exchange flux	
Biomass	Cytosol	GAM was calculated and added to biomass equation	[3]
Ribose-5-phosphate	Cytosol	changed the directionality of E.C. 5.3.1.6	KEGG [96]
Ribose-5-phosphate	Cytosol	changed the directionality of E.C. 5.1.3.1	KEGG [96]
Thymidine	Cytosol	changed the directionality of E.C. 2.4.2.4	KEGG [96]
Sodium ion	Extracellular	added exchange flux	[57,97]
Formate	Cytosol	added E.C. 1.2.1.2 rxn	[89]
a protein L-methionine	cytosol	remove general rxn RXN-8668	
Choline	Cytosol	added E.C. 3.6.3.7	[98]
dCTP	Cytosol	Changed the direction of E.C. 1.8.1.9	KEGG [96]
NAD <sup>+</sup>	Cytosol	Added E.C. 6.3.5.1	[57,58]

Because the growth medium used experimentally was undefined, many of the necessary exchange fluxes for the model could not be explicitly resolved. The decision to add an exchange flux to the model was based on experimental information and on the composition of defined media for relative species, such as *M. genitalium* [58] and *M. laidlawii* [57]. All added exchange fluxes are listed in Table 6.

The experimental data was insufficient to directly calculate the value of growth associated maintenance (GAM) and non-growth associated maintenance (NGAM) for *M. gallisepticum*. Thus, the GAM of *M. pneumonia* [89] was added to the biomass

equation, and the value for NGAM was taken from the *M. genitalium* iPS189 model [58].

GAFBA v1.0 selected formate as a problematic metabolite, since formate was produced by the peptide deformylase enzyme (E.C. 3.5.1.88) and the biomass reaction, as is shown in Figure S3. However, no reaction consuming formate was present. Therefore, the reaction catalyzed by the enzyme formate dehydrogenase (E.C. 1.2.1.2) was added to the model in order to complete the mass balance of formate. This reaction is present in other *Mycoplasmas* [89], and based on the GAFBA v1.0 results. It was hypothesized that this reaction was also part of *M. gallisepticum*'s metabolic network.

Another problematic metabolite identified by GAFBA v1.0 that was hindering the successful simulation of the metabolic network, was choline. The *M. gallisepticum* model required choline for the production of phosphatidyl choline, which was ultimately necessary for biomass. Although the reaction for the consumption of choline was present, no choline was predicted to enter the cell. Based on the reconstruction, the transport reaction for choline, represented by flux V21 in Figure 9, was coupled with sodium ion transport. When choline was transported from the extracellular space to the cytosol, it co-transported a sodium ion. The problem was that the sodium ion in the cytosol was not used in any other reaction. To avoid the accumulation of unused sodium in the cell, the model predicted that the flux through the transport reaction (V21) was zero. A possible solution for this problem was to add

a reaction that used sodium ions. In reviewing the literature, it was found that sodium is used for volume regulation in *Mycoplasma* [98-103] via translocation from the cytosol to the extracellular environment by Na-ATPase (E.C. 3.6.3.7). Searching the *M. gallisepticum* proteome for Na-ATPase using BLASTP [84,85], and the *Aspergillus fumigatus* Af293 sodium P-type ATPase (GenBank Accession no. XP\_751881.1) as a probe, the best match (82% percentage coverage, score of 306, and E-producing value of 5.E-91) was identified at locus NP\_853020.2, the previously annotated cation that transported ATPase MGA\_1061.

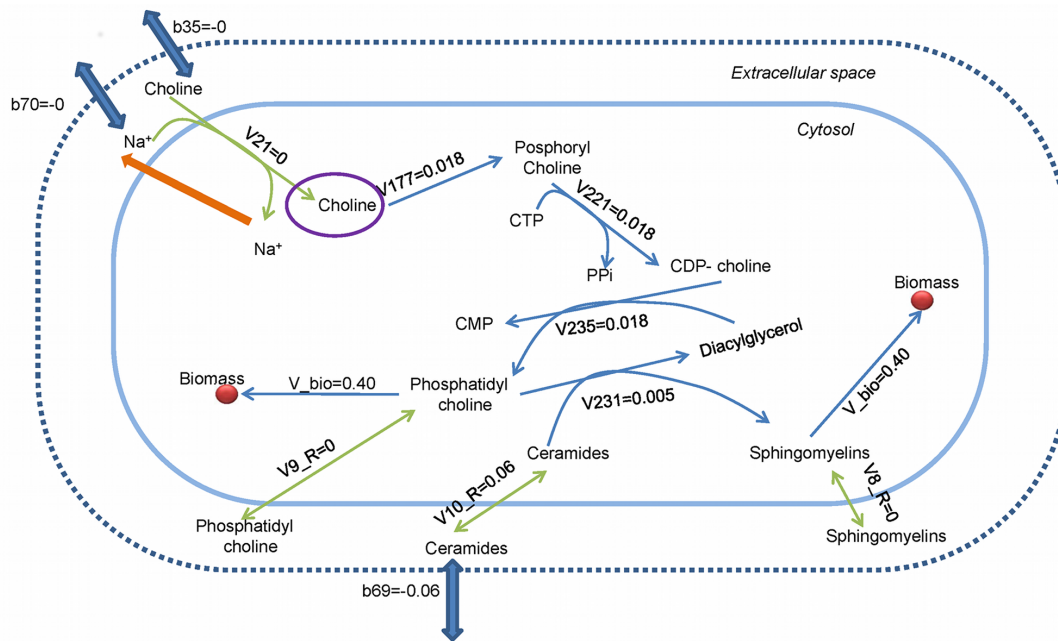


**Figure 9. Choline Subnetwork.** The purple circle shows the unconstrained metabolite. The thin blue arrows are the standard fluxes, while the thick blue arrows are the exchange fluxes. The orange arrow represents the proposed solution. The solid blue line is the plasma membrane and the dashed blue line is the system boundary. The red circle is an abstraction of the biomass pool.

The mass balance for dCTP was also required to be unconstrained, based on GAFBA v1.0 results. This was because more dCTP was produced from dCDP than was consumed by the biomass reaction. The dCDP was produced from CDP coupled with reduced thioredoxin, and oxidized NrdH glutaredoxin-like protein. When the metabolic networks of these metabolites were checked, the thioredoxin reductase reaction (E.C. 1.8.1.9) was found to be reversed [96]. Correcting E.C. 1.8.1.9 directionality resolved the dCTP problem.

The last two metabolites for which the mass balance constraints were relaxed were 2-phospho-4-{cytidine 5'-diphospho}-2-C-methyl-D-erythritol, and nicotinamide adenine dinucleotide (NAD<sup>+</sup>).

2-phospho-4-{cytidine 5'-diphospho}-2-C-methyl-D-erythritol is a metabolite in the methylerythritol phosphate pathway (MEP). It is used for the production of isopentenyl diphosphate (IPP) and dimethylallyl diphosphate (DMAPP), the two precursors of isoprenoid. For many years, it was assumed that all organisms produced IPP from acetyl-CoA through the mevalonic acid pathway (MVA), and that IPP was isomerized to DMAPP [104-106]. However, an alternative pathway was reported for the production of the building blocks of isoprenoid in bacteria and plants [107-110]. Although this has been studied in a variety of mycoplasmas, results regarding the presence or even partial presence of the MEP pathway have yet to be resolved. Some labs have reported not finding any of the genes encoding for the MEP pathway [111-113], while other labs found that mycoplasmas have portions of the MEP pathway

[106], including *M. penetrans* [114] and *M. gallisepticum* [115]. The MEP pathway in the *M. gallisepticum* model ended in the production of (E)-4-hydroxy-3-methyl-but-2-enyl pyrophosphate (HMB-PP), a dead-end metabolite in the model. No gene was associated with the HMB-PP reductase reaction (E.C. 1.17.1.2) responsible for converting HMB-PP to IPP. Two things that remain unclear are whether or not *M. gallisepticum* has a complete MEP pathway, and the purpose of the HMB-PP metabolite.

The second constraint that required relaxing was that of the NAD<sup>+</sup> mass balance. NAD<sup>+</sup> is recovered by passing the electrons from NADH to oxygen and lactate, but these mechanisms did not provide enough NAD<sup>+</sup> in the model. Thus, a reaction to synthesize NAD<sup>+</sup> was required. *M. gallisepticum* had a partial NAD<sup>+</sup> salvage pathway. The partial pathway starts with the conversion of nicotinate to nicotinate mononucleotide, catalyzed by the enzyme nicotinate phosphoribosyltransferase (E.C. 2.4.2.11). Then, nicotinate mononucleotide is converted to nicotinate adenine dinucleotide through the reaction catalyzed by nicotinate-nucleotide adenylyltransferase (E.C. 2.7.7.18). Next, nicotinate adenine dinucleotide is converted to NAD<sup>+</sup> by NAD<sup>+</sup> synthetase (E.C. 6.3.5.1), but no gene was found for this enzyme in *M. gallisepticum*. Interestingly, *M. pneumonia* uses NAD<sup>+</sup> synthetase reaction to synthesize NAD<sup>+</sup>, but blasting this gene against *M. gallisepticum* shows no close homology. One more possibility was that NAD<sup>+</sup> was taken from the media, but no literature evidence was found concerning the requirements of NAD<sup>+</sup> [116]. Instead, the media composition of *M. genitalium* [58]

and *M. laidlawii* [57] had nicotinate, the starting component of the partial NAD salvage pathway. Based on the observation that *M. gallisepticum* had two reactions of the partial pathway and the requirement of the starting component in other relatives, it was hypothesized that the NAD<sup>+</sup> synthetase reaction was present in *M. gallisepticum*. However, more experimental and computational work is clearly required to validate this theory.

Interestingly, when the NAD<sup>+</sup> synthetase reaction was added to the model, it was possible to enforce all the mass balance constraints. The mass balance of 2-phospho-4-{cytidine 5'-diphospho}-2-C-methyl-D-erythritol was consistent after adding NAD<sup>+</sup> synthetase, because the MEP pathway no longer had any flux going through it.

#### **3.4.4. FINAL MODEL**

The final model was obtained after 40 runs of GAFBA v1.0, with each run consisting of 2,000 generations. Figure 10 shows the results for each of the simulations and the corresponding growth rate values, and Figure 11 shows the number of mass balance constraints that were relaxed. The best model, represented by simulation 40, was able to close all the mass balance constraints and had a growth rate value of  $0.358 \pm 0.12 \text{ h}^{-1}$ , compared to the experimental value of  $0.244 \pm 0.03 \text{ h}^{-1}$ . The final *M. gallisepticum* model accounted for 441 metabolites and 395 reactions. The model had 234 intracellular reactions; 86 transport reactions for the transfer of metabolites between the extracellular space and the cytosolic compartment; and 73

exchange reactions that allowed the uptake or secretion of metabolites either to or from the system boundary. A complete description of the model is provided in appendix 3.

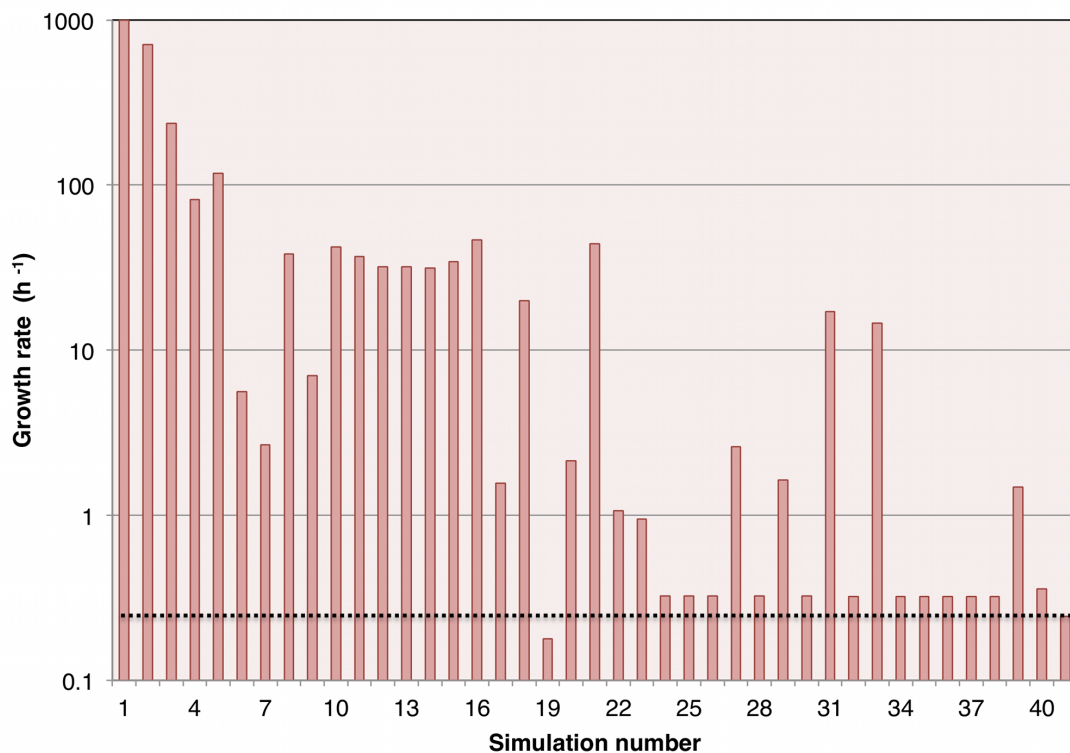


**Figure 10. Predicted growth rate over the course of model evolution.** 40 simulations were carried out for 2,000 generations each. The columns represent the growth rate values. Result 41 is the average value of the experimentally measured *M. gallisepticum* growth rate. The dashed line running the length of the graph also indicates the average experimentally measured growth rate, and is shown as a reference to facilitate comparison with the simulation results.

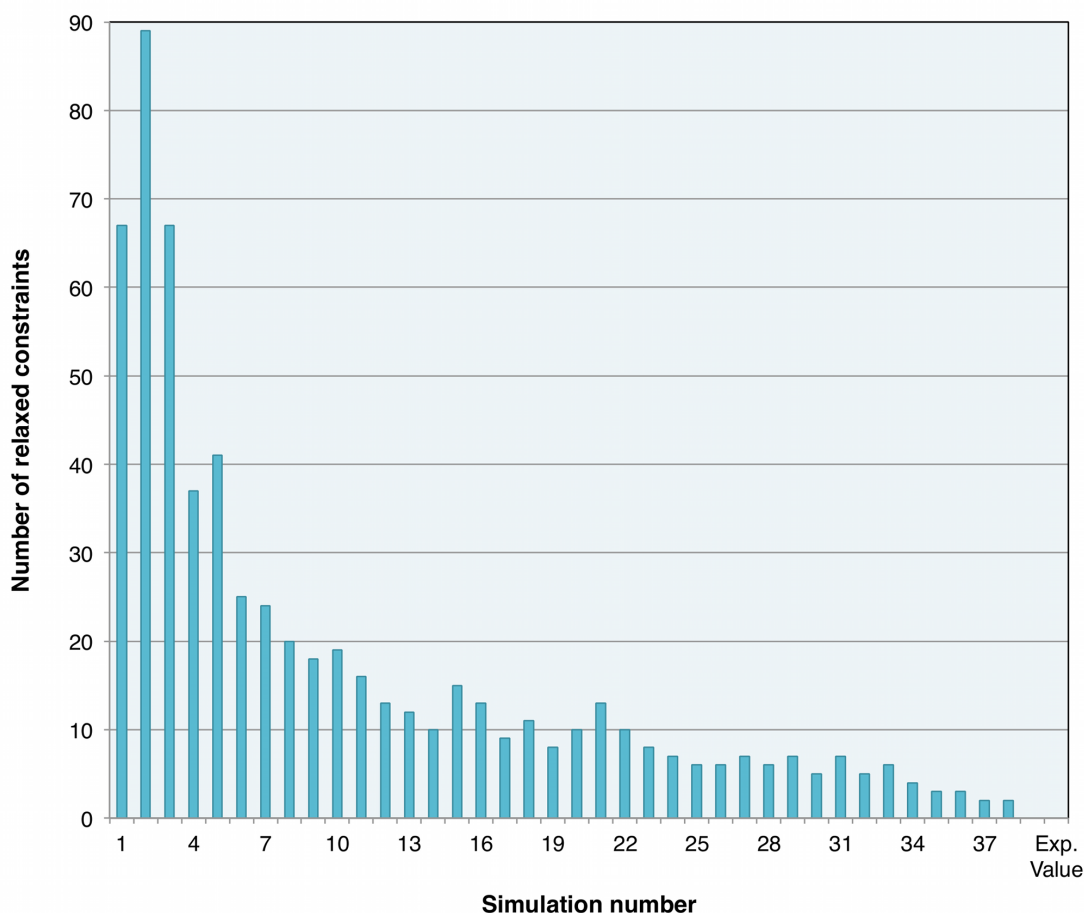


**Figure 11. Metabolic constraints relaxed over the course of model evolution.** 40 simulations were carried out for 2,000 generations each. The columns represent the number of mass balances for which the constraints were relaxed.

#### 3.4.5. COMPARISON OF *M. GALLISEPTICUM* MODEL AND *M. GENITALIUM* iPS189 MODEL

To provide a better context for the *M.gallisepticum* model, it is compared to the iPS189 of *M.genitalium* [58]. A summary of the comparison is provided in Table 7.



The *M. gallisepticum* model was larger than the *M. genitalium* model, as was expected since the genome size of *M.genitalium* is 0.58 Mb compared to 1.01 Mb for *M.gallisepticum*. The genome of *M. gallisepticum* had 817 genes that encoded for 763 proteins [31]; in contrast, *M.genitalium* had 524 genes that codified for 475 proteins [117]. The G+C content of *M.gallisepticum* is 31.5%, while the G+C content of *M. genitalium* is 32% [31].

**Table 7. Comparison of the *Mycoplasma genitalium* model (iPS189) [58] and the model presented in this paper for *Mycoplasma gallisepticum*.**

	<i>Mycoplasma genitalium</i> (iPS189)	<i>Mycoplasma gallisepticum</i>
Metabolites	276	362
Cytoplasmic	261	359
Extracellular	85	82
Reactions	349	395
Intracellular Rxn	178	234
Transport Rxn	84	86
Exchange Flux	87	73

The *M.genitalium* model had 46 fewer reactions than the *M.gallisepticum* model. However, it turns out that the iPS189 model had more exchange fluxes. The additional exchange fluxes in the *M. genitalium* model were required to account for the exchange of amino acids as a combination of dipeptides. *M.gallisepticum*, only had fluxes for the amino acid exchange as mono peptides. The exchange of dipeptides in the *M. gallisepticum* model was represented as a general reaction (trans-rxn7tv-3945), due to a lack of information about the specificity of this transporter.

Additionally, the *M.gallisepticum* model had 86 more metabolites than the *iPS189* model. These metabolites were mainly located in the cytosol space and included lipids. The *iPS189* model did not have fully specified lipids in the biomass reaction, or the associated lipid reactions. The *M. gallisepticum* model included cardiolipin, sphingomyelin, phosphatidylcholine, cholesterol, etc; and a set of reactions related to lipid metabolism, such as phosphatidate phosphatase (E.C.3.1.3.40); phosphatidylglycerophosphatase (E.C.3.1.3.27); diacylglycerol chlorophosphotransferase (E.C. 2.7.8.2); sphingomyelin synthase (E.C. 2.7.8.27); etc.

#### **3.4.6. *M. GALLISEPTICUM* MODEL CREATED WITH MODEL SEED**

The RAST annotation server [118] was used to develop an annotated genome for SEED. Then, Model SEED [53] was used to generate a preliminary reconstruction of the *M. gallisepticum* model via the web-based resource (<http://iris.kbase.us>). During this process, Model SEED created a biomass reaction. The media chosen was a defined media already present in Model SEED. After running the auto-completion tool in Model SEED, a growth rate of  $2.02\ h^{-1}$  was predicted. The model had 358 reactions and 389 metabolites. When the *M. gallisepticum* model from SEED was constrained to the experimentally measured glucose uptake rate and lactate production rate, the model predicted no growth. It was not possible to use the model optimization tools of Model SEED, as they were not available on the website at that time. As a result, a better fitting model incorporating the experimental growth data could not be created. Instead, GAFBA v1.0 was used to perform a 2,000 generation

run, resulting in a growth rate value of  $2.5 \text{ h}^{-1}$ . However, the mass balances constraints of acetaldehyde, and dCMP had to be relaxed.

One more trial was done using the *M.gallisepticum* model from Model SEED, and adding the biomass reaction and media composition defined in this work without adding any of the lipid metabolites and tRNA charged/uncharged, since the *M.gallisepticum* model from Model SEED did not have them. The model generated had 354 reactions and 391 metabolites. The glucose uptake rate and lactate production rate were constrained to the experimental values, and again; no growth was predicted. GAFBA v1.0 was used to evaluate the potential gaps of Model SEED. A 2,000 generation run was performed, resulting in a growth rate of  $1.32 \text{ h}^{-1}$  with 12 mass balance constraints being relaxed. These results indicate that GAFBA v1.0 may be used with Model SEED to identify problematic metabolites.

### 3.5. Discussion

The goal of this work was to develop an approach that could be used to curate metabolic networks, facilitating a fundamental understanding and the discovery of metabolism. To test this idea, a strategy was applied to the reconstruction of a genome-scale metabolic network for *M. gallisepticum*. By using GAFBA v1.0, it was possible to find gaps and inconsistencies present in the network that went beyond genome annotation. It was generally possible to fill these gaps based on the described heuristics, and/or searching through the literature. Even when the process was not automated, time spent at the curation level was minimized because problematic

metabolites were identified, allowing one to focus only on the significant issues remaining.

An argument could be made for using optimization strategies other than a genetic algorithm, such as a mixed integer linear programming (MILP) approach, like MetaFlux, Model SEED, and GapFill. Although the MILP approach is a powerful one, the GA method provides certain advantages such as scaling more effectively for the study of large networks, and generating a population of solutions that, as a whole, provide further insight into the problem domain.

A factor in favor of MILP, is that it could potentially be faster than using GA. This is especially true for smaller models. However, even when the GA running time is greater than MILP, the computational time is not the rate-limiting step in the overall curation process. Rather the manual portion of the curation, such as the literature review and the assembly of the preliminary model, are the most time consuming..

In general, a GA based method may be seen as unnecessary for a small model such as the one developed in this work. However, it is anticipated that in the future, systems to be analyzed will grow significantly. Such growth may be due to organism complexity, or dealing with microbial consortia. Under such circumstances, it is expected that GAFBA v1.0 will be comparable or faster than MILP based methods, since the computational complexity of GA falls within a range of  $O(n^{1.5})$  to  $O(n^2)$ , where  $n$  is the number of metabolites in the model [119]. In contrast, MILP

computational complexity grows exponentially with system size [120,121]. It should be further pointed out that GA's fall into the class of algorithms known as "embarrassingly parallel." Although the approach presented does not currently take advantage of this feature, work is currently underway to parallelize the algorithm. With the advent of massively multi-core systems and especially GPU based computing, it is anticipated that significant gains in speed may be realized.

Additionally, the GAFBA v1.0 approach provides some important advantages over existing curation strategies. The most significant advantage is the possibility to identify problems without relying on a database for reference. For example, MetaFlux requires MetaCyc, Model SEED requires the SEED reaction database, and GapFill requires a customized multi-organism database. GAFBA v1.0 provides flexibility by allowing the identification and potential resolution of metabolic inconsistencies without requiring access to any type of database. It is important to realize, however, that GAFBA v1.0 may be used in conjunction with the other approaches described, as was illustrated earlier with Model SEED. Thus, the information from these databases is not lost. Rather, GAFBA v1.0 may be used to complement existing approaches, or it may be used on its own.

MetaFlux requests that the user set the values for the weights of the objective function in the MILP objective function. This step necessitates the proper understanding of the meaning of each weight. The weights can be selected to create models for different scenarios. The GAFBA v1.0 methodology does not need the user

to define any weights. Thus, the set of metabolites to be studied will not depend on values defined by the user. In addition, MetaFlux does not have the ability to add reactions between compartments (e.g. transport reaction), resulting in an additional level of complexity for curation purposes. GAFBA v1.0, however, does permit the addition of reactions between compartments. Interestingly, MetaFlux does not give information about the metabolites that may be problematic; instead it provides a set of reactions to add in order to resolve metabolic inconsistencies. Conversely, GAFBA v1.0 does not provide a list of reactions to add, but rather points out problematic metabolites that may be used to direct further research. These complementary approaches suggest that some synergy may be possible.

When comparing Model SEED with GAFBA v1.0, Model SEED provides a significant advantage in that it generates a biomass reaction and defined media for an organism. However, when the *M. gallisepticum* model created by Model SEED was used with the experimentally determined glucose and lactate constraints, the model predicted no growth, suggesting that more curation was needed. By applying GAFBA v1.0 to the Model SEED generated model incorporating the experimental data, it was possible to identify the two problematic metabolic constraints inhibiting the viability of the model. This result serves to highlight GAFBA v1.0's role as a curation tool and its ability to complementarity the existing model development software.

In general, GAFBA v1.0 provides an alternative and complementary curation and modeling strategies to existing approaches. GAFBA v1.0 could help improve the

quality of existing metabolic networks, and generate new and more complete networks. Furthermore, because the approach used by GAFBA v1.0 is complementary to existing approaches, it can be used after a model is created with Model SEED or MetaFlux.

With respect to *M. gallisepticum* specifically, the new genome-scale model generated using GAFBA v1.0 replicated the experimentally observed data well. It is likely that the predicted growth rate was higher than the experimental value observed, because the NGAM value and the GAM used in the model were based on the *M. genitalium* iPS189 model [58] and *M. pneumoniae* [89]. Further experiments are required to determine the appropriate NGAM value and GAM value for *M. gallisepticum*.

The results of GAFBA v1.0 have highlighted a number of pursuable experimental avenues. For example, while GAFBA v1.0 predicts the presence of formate dehydrogenase, NAD<sup>+</sup> synthetase, and Na-ATPase enzymes for *M. gallisepticum*, their presence still needs to be experimentally verified. The elucidation of the MEP pathway's role in *M. gallisepticum* metabolism may ultimately provide a fundamental understanding of the organism's metabolism. It is also important to determine if the MEP pathway is essential to the survival of *M. gallisepticum*, since it could elucidate possible drug targets, as was recently illustrated in research for control of the *Mycobacterium tuberculosis* [122,123], *Haemophilus influenzae* [124], and in the treatment against malaria [125,126].

#### **4. GAFBA v1.0 IMPROVEMENT**

This chapter introduces three important tools developed to build a more robust, user-friendly, and faster curation tool. The chapter is divided into three subsections.

The first one introduces the frequency analysis tool, which identifies unique problematic metabolites across the population of the chromosomes. This subsection is a modified version of the proceedings paper published as “Leveraging ensemble information of evolving populations in genetic algorithms to identify incomplete metabolic pathways,” [127] by Eddy J Bautista and Ranjan Srivastava. In Proceeding of the fifteenth annual conference companion on Genetic and evolutionary computation. Amsterdam, The Netherlands: ACM; 2013. p. 39-40.

In subsection two, the consistency checker tool (MassChecker) is developed. MassChecker finds metabolites that are taken as “problematic” ones as a result of the random generation of the initial population in the first step of GAFBA v1.1, but are already fulfilling their mass balance constraint.

The last subsection describes the graphic user-friendly interface for GAFBA v1.1.



## **4.1. Leveraging Ensemble Information of Evolving Populations in Genetic Algorithms to Identify Incomplete Metabolic Pathways**

### **4.1.1. INTRODUCTION**

The genome-scale metabolic model is a powerful tool for modeling metabolism. The constraint-based approach known as flux balance analysis (FBA) has been particularly fruitful [128]. FBA has been successfully used for fundamental research [129], recombinant protein and metabolite production [130], and for biomedical development [131], with applications in drug target identification [132], understanding host/pathogen interactions [8], and the investigation of human metabolic diseases. FBA models are constructed through an iterative process where reactions are assigned to the annotated genes in a genome sequence; the biomass composition and energy requirements are determined; and additional constraints such as mass balance, thermodynamic, environmental and other physico-chemicals are specified. Gaps in the metabolic network are identified and filled using literature information and databases, resulting in a quantitative stoichiometric model of the system. Because the model is underdetermined, an objective function is postulated, such as the maximization of the biomass reaction, to determine the optimal distribution of metabolic resources or fluxes.

The most time-consuming part of the reconstruction process is identifying and resolving the gaps in the metabolic network. In Chapter 3, GAFBA v1.0, which integrates a genetic algorithm (GA) with FBA, was introduced to identify and resolve ill-formed mass balance constraints resulting in erroneous models. In the process, it is

possible to take advantage of the ensemble of information inherent to the evolving population. Specifically, it is possible to identify and focus on the analysis of metabolites with relaxed mass balance constraints, which appear in most of the chromosomes across a population. Here, an algorithm is presented to help identify these metabolites. The algorithm should be used after a considerable number of simulations has been accumulated, or when the number of mass balance constraints relaxed is overwhelming. Thus, an additional criteria or tool is necessary to identify the most problematic metabolites. It was applied during the development of a genome-scale metabolic model for *Mycoplasma gallisepticum* using GAFBA v1.0. The methodology and results were discussed in chapter 3.

#### **4.1.2. METHODS**

##### **4.1.2.1.Frequency analysis of relaxed metabolic constraints**

When minimizing the number of relaxed constraints, the GA generates a population of models represented by chromosomes from which one can determine the metabolic restraints that need to be relaxed.. It is possible to determine the frequency with which a metabolic constraint is relaxed across the population of the chromosomes. The metabolic constraints that have the highest frequency of relaxation are likely to be the most problematic to the generation of a feasible metabolic model. As the populations evolved, frequencies were tracked across generations This provided additional information regarding the importance of a particular metabolic constraint to the viability of the model. The specific details regarding the implementation of the frequency analysis for the relaxed metabolic constraints are depicted in Figure 12.

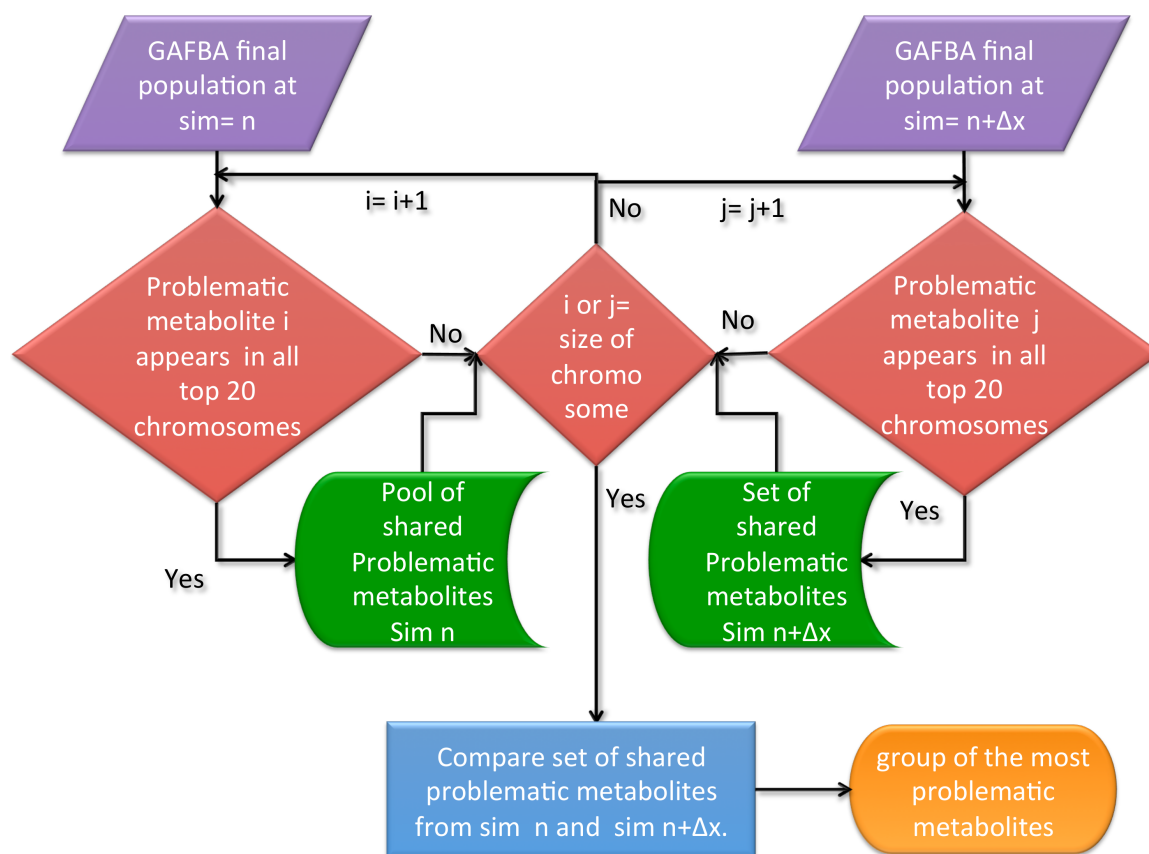


**Figure 12. Frequency Analysis of Relaxed Metabolic Constraints.** The frequency of relaxed metabolic constraints across chromosomes in a population, as well as across simulations, provides insight into which metabolites are truly critical to the development of a viable genome-scale metabolic model. Each simulation consisted of 30 chromosomes that were evolved for 2,000 generations. The frequency of relaxed metabolic constraints across the top 20 chromosomes and across different simulations was monitored. The most frequently relaxed constraints were targeted for curation to resolve the inconsistencies in the model. The step in blue is an operation performed by the user.

The process started by selecting the final populations of two different GAFBA simulations for comparison, as is shown in Figure 12. For instance, simulation  $n$  and simulation  $n+\Delta x$ , where  $n$  is any number of simulations and  $\Delta x$  is an incremental interval defined by the user. Each simulation consisted of evolving model populations for 2,000

generations. Then in each simulation, the metabolites with relaxed mass balance constraints that appeared in all the top 20 chromosomes of the population were selected. These metabolites formed the set of shared problematic metabolites at simulation  $n$ , and simulation  $n+\Delta x$  respectively. Finally, the sets of shared problematic metabolites from simulation  $n$  and  $n+\Delta x$  were compared, and the metabolites that arose in both sets formed the group of the most problematic metabolites. Therefore, the most problematic metabolites were studied first, and then the rest of problematic metabolites were analyzed.

#### **4.1.3. RESULTS**

The initial model of *M. gallisepticum* consisted of 446 metabolites and 380 reactions. Implementing the model resulted in no feasible solution to the optimization problem due to inconsistent constraints. The model was then analyzed using GAFBA v1.0 to identify problematic metabolites. Randomly selected simulations were used for carrying out frequency analysis. The analysis was done at simulations 3, 5, 17, 27, 36, and the results are presented in Table 8. At simulation number three, 23 metabolites were shared among the pool of the best 20 chromosomes. The best model only had one more metabolite dropped.

**Table 8. Result of the analysis of relaxed mass balance constraints for select simulations.**

<b>Simulation number</b>	<b>Number of shared relaxed metabolic constraints in the best 20 chromosomes</b>	<b>Number of relaxed metabolic constraints in the best individual</b>	<b>Number of shared relaxed metabolic constraints already present in a previous simulation</b>
3	23	24	NA
5	16	24	9
17	9	12	6
27	5	5	4
36	1	1	1

At simulation number five, 16 metabolites with relaxed mass balance constraints were common in the pool of the best 20 chromosomes. While reviewing the list of metabolites, it was observed that nine metabolites were already dropped in simulation number 3, and four of them were charged/uncharged tRNAs. Thus, a recycling reaction for the charged/uncharged metabolites was added to the biomass equation [58].

Nine common metabolites were found at simulation number 17 among the best 20 chromosomes. Six of them already appeared in either simulation number 3 or 5. One of them was ribose-5-phosphate. By checking the metabolic pathway around this metabolite, the directionality of two reactions, Ribulp3epim-Rxn (E.C. 5.1.3.1) and Rib5pisom-Rxn, were changed to reversible (E.C. 5.3.1.6).

At simulation number 27, five metabolites were found to be common in all the best 20 chromosomes. Four of them appeared in previous simulations. At this point, sodium ion and L-phosphatidate were selected for analysis. It was observed that by

solving the mass balance of sodium ion, the mass balance of L-phosphatidate could be closed, since the metabolites were connected through the choline pathway. The problem with the sodium ion was that its transport was coupled with the transport of choline. Choline was one of the precursors of phosphatidyl choline, which is a component of the biomass of *M. gallisepticum*. Thus, the transportation of choline was required, but it was set to zero to avoid the accumulation of sodium ions in the cytosol. The solution was to add a reaction that used sodium ions in the cytosol. A Na-ATPase transport reaction that regulates volume in *Mycoplasma* was added [103].

NAD<sup>+</sup> was the only problematic metabolite in the best chromosome at simulation number 36. It was present in all the top 20 chromosomes, and it had already appeared in a previous simulation. The model had a partial biosynthesis pathway for NAD<sup>+</sup>. It was hypothesized that NAD<sup>+</sup> synthase reaction was present in *M. gallisepticum*, based on the observation of two reactions of the partial pathway, and the requirement of the starting component in other relatives [57,58],

At simulation 40, the best and final model was obtained. This model was able to close all the mass balance constraints, and had a growth rate value of  $0.3258 \pm 0.12 \text{ h}^{-1}$ , compared to the experimental value of  $0.244 \pm 0.03 \text{ h}^{-1}$ . The final *M. gallisepticum* model accounted for 441 metabolites and 395 reactions.

#### **4.1.4. IMPACT**

The importance of the development, curation, and implementation of high quality genome-scale metabolic models will continue to grow in the biotechnological and biomedical arenas. As a result, the development of strategies to facilitate this process will be of extraordinary value. Of particular interest will be strategies that reduce the amount of experimental work required, as experiments are costly, time consuming, and often tedious. The use of GAs for optimization purposes is well established. In this case, the ensemble of information on the population being evolved turns out to be biologically relevant.

A significant advantage to GAFBA v1.0, is its ability to carry out a population frequency analysis in order to determine the most problematic metabolites. By observing the most frequently occurring relaxed constraints in that population, it was possible to identify candidate metabolites that were most likely to be problematic. These results are extraordinarily valuable, as they provide the researcher with a starting point regarding which metabolites are most likely causing the model to fail. It allows the researcher to focus on the most critical metabolites whose resolution will likely give the greatest return on the investment of time, effort, and money.

#### **4.2. MassChecker, a mass balance constraint consistency checker tool for GAFBA.**

The composition of the initial population in GAs has been reported to affect their convergence, performance, and their ability to find the best possible solution [133-136]. If the initial population is good, the possibility of finding good solutions increases. Random generation of the initial population is useful, because it increases the diversity of the population and can represent any region within the search space [136].

In GAFBA v1.0, during the generation of the initial population of solutions for use with the GA, whether a mass balance constraint is enforced or relaxed is determined randomly. As a result, some metabolites with an already closed mass balance are inaccurately labeled as “problematic”. These metabolites will be referred to as “false positives.” As new solutions evolve over the course of generations, the number of false positives decreases. However, these situations slow down the evolution of the model through the curation process. Moreover, the number of “false positives” at the end of a simulation increases with the size of the model. Therefore, a mass balance constraint consistency checker tool, MassChecker, is introduced. MassChecker was developed to find these false positives and adjust the chromosomes to keep them in the model as enforced mass balance constraints. MassChecker enhances the performance of GAFBA v1.0, while reducing the number of simulations required during the curation process, as well as the total running time.

MassChecker was implemented in GAFBA v1.1, and tested during the development of the genome-scale metabolic model for *Bacillus anthracis*. Here, a



comparison of the evolution of the model using GAFBA v1.0 and GAFBA v1.1, which includes the MassChecker tool, is presented.

#### **4.2.1 METHODS**

##### **4.2.1.1 Genetic algorithm parameters**

The genetic algorithm parameters used were: a population size of 30 chromosomes, crossover probability of 30%, and mutation probability of 1%. Elite selection was chosen as a selection strategy, with an elite fraction of 20%. Two-point crossover was performed, and bottom re-seed was not allowed. The GAFBA v1.1 algorithm was run for 2,000 generations per simulation, and 10 simulations in total were carried out. All simulations were implemented on a 2.7 GHz Intel Core i5 computer. For the GAFBA v1.0 algorithm, each simulation (2,000 generations) took approximately 4 hours. Meanwhile, the running time for one simulation with GAFBA v1.1 was 3 hours. Thus, the total time for the 10 simulations was 40 hours with GAFBA v1.0, and 30 hours with GAFBA v1.1.

GAFBA v1.1 is a new version of the GAFBA algorithm that includes a MassChecker tool, and the bottom re-seed operation. The bottom re-seed operation replaces the chromosomes of the bottom part of the population with new randomly generated chromosomes.

#### 4.2.1.2 Flux Balance analysis parameters

The Pathway Tools v16.0 software platform [68] was used to generate the initial model for *B. anthracis* from an existing pathway genome database (bant260899 version15.5), which accounted for all metabolic pathways as determined from the genome annotation. The model had 1,104 reactions and 1,094 metabolites. More information on the *B. anthracis* model is presented in Chapter 6.

The bounds for the reversible reactions were  $-\infty \leq v_j \leq \infty$ , whereas for the irreversible reactions, they were  $0 \leq v_j \leq \infty$ . The boundaries for the exchange fluxes were defined for metabolites in the media as  $-\infty \leq v_j \leq \infty$ , and for the secretion of metabolites the following constraint was implemented:  $0 \leq v_j \leq \infty$ . The media composition used was the one from the iron reduced media (IRDM) [137] shown in Table 9. The lower boundary of the NGAM value was set to  $6.75 \text{ mmol gDW}^{-1}\text{h}^{-1}$ , based on the experimentally measured value for *Bacillus subtilis* [138]. The upper and lower boundaries of the experimentally measured fluxes are presented in Table 10. The objective function chosen for the optimization problem was the maximization of the biomass equation for *B. anthracis*, which is provided in appendix A8.7.

**Table 9. Iron reduced media (IRDM) media composition.**

IRDM media composition		
glucose	aspartate	Fe3+
arginine	proline	K+
leucine	serine	Mg2+
methionine	thiamine	Mn2+
cysteine	threonine	Na+
phenylalanine	tryptophan	sulfate
histidine	glutamate	phosphate
isoleucine	Ca2+	water
valine	Cl-	proton

**Table 10. Experimentally measured fluxes used as constraints for the FBA model.**

Rate	Upper/Lower boundary (mmol gDW <sup>-1</sup> h <sup>-1</sup> )
Glucose uptake rate	-13.157
Carbon dioxide production rate	6.29
Oxygen uptake rate	-6.737
Lactate uptake rate	-0.973
Glutamic acid uptake rate	-0.266
Iron uptake rate	-0.00075
Bacillibactin production rate	0.0023
Petrobactin production rate	0.0163
Protocatechuate production rate	0.0241

#### 4.2.1.3 Mass balance constraint consistency checker (MassChecker)

The GAFBA v1.1 algorithm is presented in Figure 13. After the initial population was randomly generated, an optimal flux distribution was determined by FBA for each of the chromosomes in the population.. The fitness of each chromosome was scored based on the minimum number of mass balance constraints relaxed, and the value of the biomass reaction. Next, the elite pool was selected based on the predetermined elite

fraction, and MassChecker was applied to each of the chromosomes in the elite pool. MassChecker inspected each of the mass balances of the metabolites with relaxed constraints in the chromosome. It took the flux distribution from FBA, and calculated the summation of the fluxes through the reactions in which the metabolite participated. If the summation was equal to zero, by definition the mass balance constraint was fulfilled. Thus, the gene on the corresponding chromosome was changed to one that enforced the mass balance constraints.

Subsequently, MassChecker analyzed all the chromosomes from the elite pool. They were then copied to the new population. Applying the genetic operations of crossover and mutation, the remainder of the population was bred. Next, if the bottom re-seed operation was allowed, and the generation number was equal to the desired bottom re-seed frequency, then the bottom part of the population determined by the bottom re-seed fraction was replaced with randomly generated chromosomes. This prevents premature convergence of the population, and also increases the searching space. This process kept running until the number of generations was equal to 2,000, at which point GAFBA v1.1 stopped and the list of problematic metabolites was generated. After the changes were made in the model, GAFBA v1.1 could be initialized from the random generation of the initial population, or by using the last population from the previous simulation. This process was continued until the number of mass balance constraints relaxed was equal to zero and the growth rate was near the experimental one.

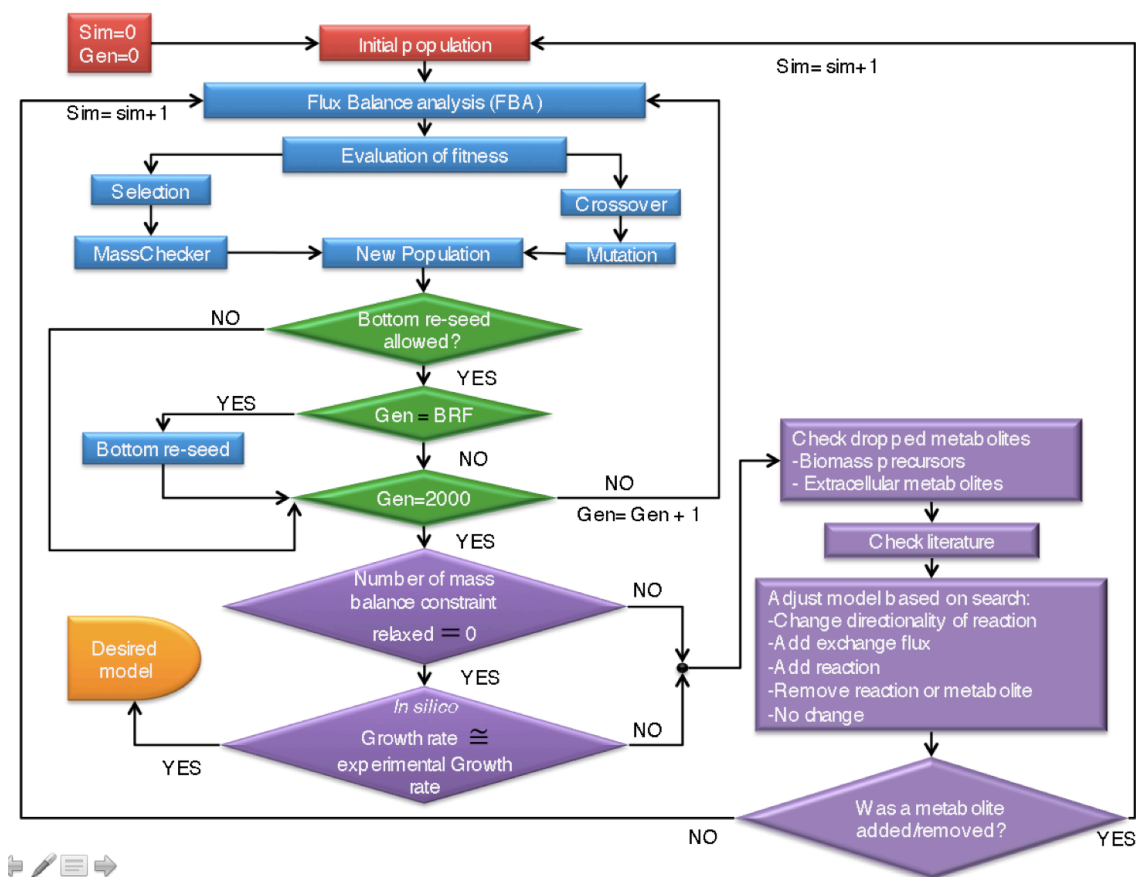


**Figure 13. GAFBA v1.1.** This new version of the GAFBA algorithm includes a MassChecker tool and the bottom re-seed operation. BRF refers to the bottom reseed frequency. The steps in purple are operations performed by the user.

## 4.2.2 RESULTS

The evolution of the number of mass balance constraints relaxed is presented in Figure 14 for the GAFBA v1.0 algorithm without MassChecker. Three trials were run with the same initial conditions, and with the random generation of the initial population. The number of mass balance constraints relaxed at generation zero was 323 for the first run, 314 for the second run, and 263 for the third run. The relaxed constraints were slowly decreased to a final value of around 60 for the first run, 63 for the second run, and

69 for the third run. After 20,000 generations, the number of mass balance constraints relaxed had not stabilized for any of the runs. This means that more generations are needed for it to reach a stable value.

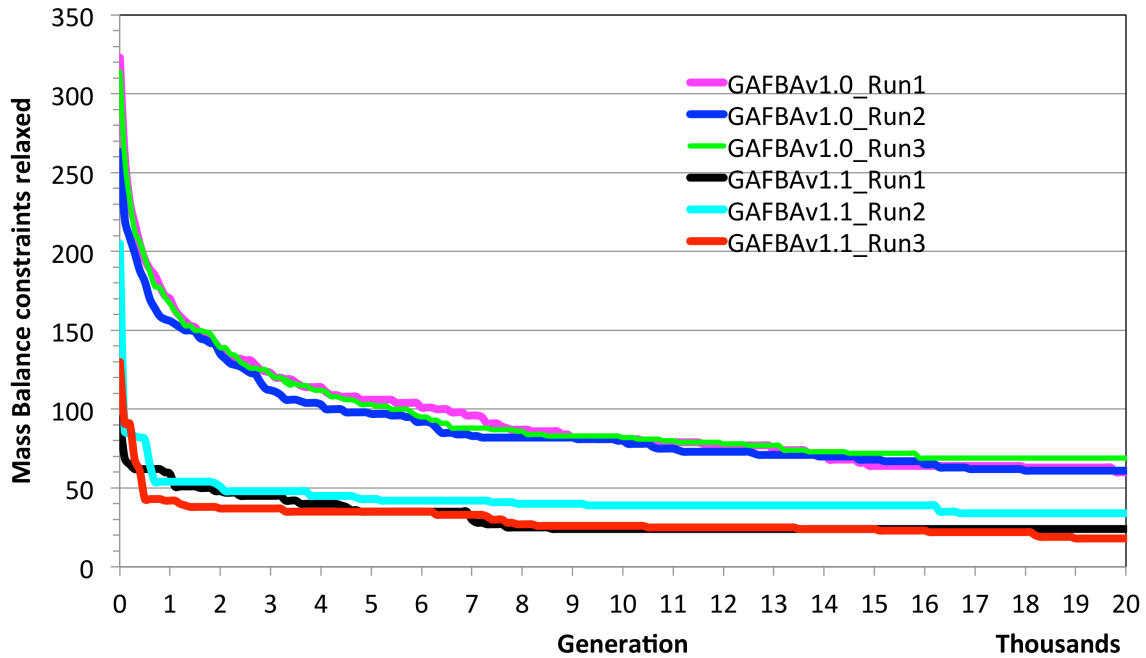


**Figure 14. Comparison of the evolution of mass balance constraints on GAFBA v1.0 and GAFBA v1.1.** For each algorithm three runs were made. The magenta (run 1), blue (run 2), and light green (run 3) lines are the runs for GAFBA v1.0. The black (run 1), light blue (run 2), and red (run 3) lines are the results for GAFBA v1.1.

Figure 14 shows the evolution of the mass balance constraints relaxed for GAFBA v1.1, which includes the MassChecker tool. The same conditions were used as the ones for the GAFBA v1.0 trials. The number of mass balance constraints relaxed at simulation zero were 94 for the first run, 205 for the second run, and 130 for the third run. It is evident that MassChecker sped up the minimization of the number of problematic mass balances. After only 2,000 generations, it had fallen below 50 for all

three trials. Moreover, the stabilization of the number of mass balance constraints dropped was reached around 9,000 generations for the first and third runs. The second run was stable for some generations, until generation 16,000 when the number of mass balance constraints relaxed decreased from 39 to 34. Thus, only nine simulations were needed to start the analysis of the problematic metabolites. More importantly, only 24 (run 1), 34 (run 2), and 18 (run 3) metabolites needed to be analyzed with GAFBA v1.1, compared to the 60 (run 1), 61 (run 2), and 69 (run 3) metabolites from GAFBA v1.0 without MassChecker.

The number of false positives found in the chromosomes from the elite pool is established in Figure 15. The values are only for the first run of GAFBA v1.0 with MassChecker. Since the elite fraction was set to 20%, six chromosomes formed the elite pool. At generation zero, MassChecker found 212 false positives for chromosome one, 284 for chromosome two, 332 for chromosome three, 459 for chromosome four, 487 for chromosome five, and zero false positives for chromosome six. As the number of generations increased, the number of false positives decreased substantially. This result was mainly because the effects of the random population generation had dissipated.

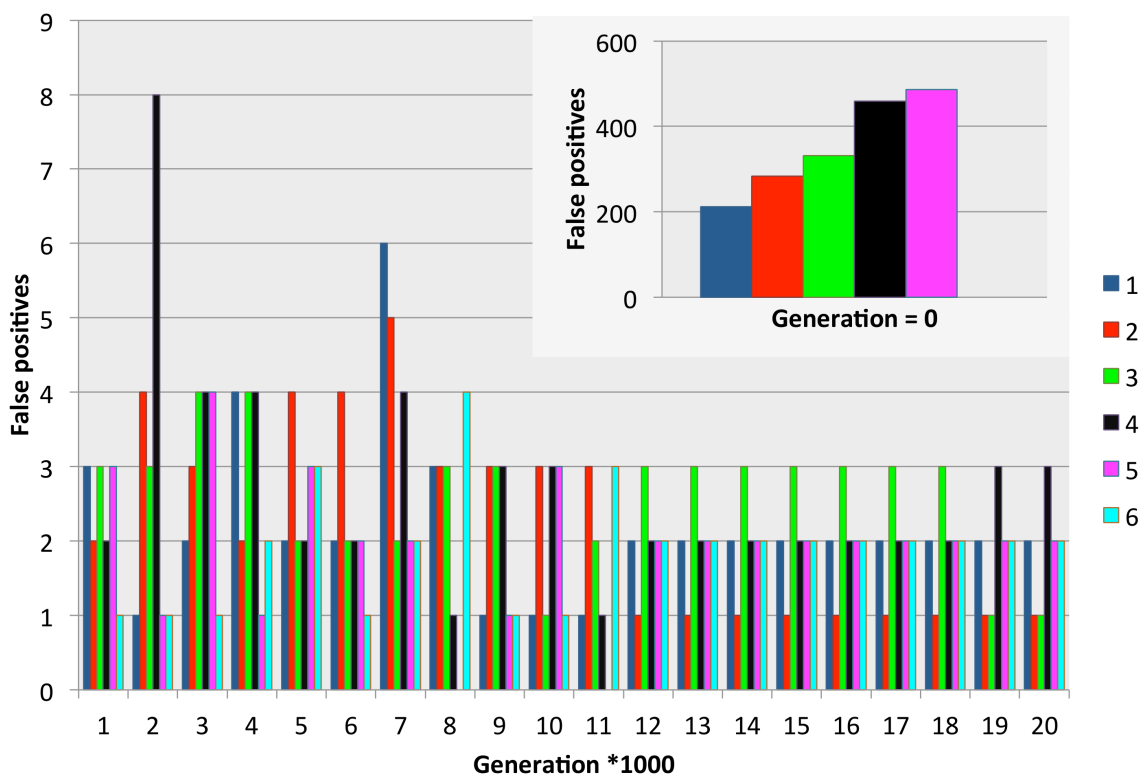


**Figure 15. Evolution of the number of false positives in the elite pool for the first run using GAFBA v1.1.** The embedded chart presents the number of false positives found in the top elite chromosomes at generation number zero.

#### 4.2.3. IMPACT

The random generation of the initial population for the GA part of the GAFBA v1.0 methodology caused some metabolites with an already closed mass balance to be considered problematic. MassChecker was developed to find these false positives, and adjust the chromosomes to keep them in the model as enforced mass balance constraints.

MassChecker was developed as a consequence of the overwhelming number of false positives that appeared in the first runs of GAFBA v1.0. The main concern was the



curation of large models, where the number of mass balance constraints dropped from the beginning of the reconstruction could confuse the curator. Furthermore, toward the end of the reconstruction process, the number of mass balance constraints relaxed in GAFBA v1.0 could hit a plateau before reaching the ideal scenario of all mass balance constraints being enforceable. As a result, the curator might think that something was wrong with the model when there really was no problem at all.

MassChecker was merged with GAFBA v1.0 in GAFBA v1.1. It randomly generates an initial population while simultaneously removing the debilitating effects of false positives.. GAFBA v1.1 is faster and more efficient than the old version. The MassChecker tool speeds up the curation process by decreasing the number of simulations needed to achieve stability. Most importantly, the number of mass balance constraints relaxed was reduced by 60%, which permits one to focus only on the metabolites that really have problems.

#### **4.3.GAFBA v1.1 Software: a tool for the semi-automated curation of genome scale metabolic reconstruction.**

##### **4.3.1. INTRODUCTION**

The capability of emulating the experimental behavior of a microorganism *in silico* depends on the quality of the genome-scale metabolic network [3,139]. For that reason, an outstanding curation process during the reconstruction of the network is

required. The curation process helps to solve issues such as erroneous metabolite names or reaction names, localization of metabolites within the cell, directionality of the reaction to proceed and filling the gaps present in the network [47]. Several tools have been developed such as the Pathway tools hole filler [49]. Here, a Bayesian classifier is used to determine the probability that a candidate protein will be able to fill the hole. With metabolic expression placement (MEP), the algorithm searches for possible enzymes to fill the gaps using gene expression data, and the local structure of the partially reconstructed metabolic network [51]. Satish Kumar et al. [47] developed an optimization based procedure (GapFind) to find the gaps present in the network, which can then be filled with an optimization based procedure (GapFill) using four specific mechanisms [47]. MetaFlux [52] uses a multiple gap filling approach based on mixed integer linear programming (MILP), which suggests reactions to be added from the MetaCyc database. Model SEED [53] identifies the minimum set of reactions from the SEED reaction database that must be added in order to fill the gaps present in the network.

GAFBA v1.1 [127] is complementary to previously developed software platforms. It uses a genetic algorithm (GA) to help the user identify metabolites preventing the optimization problem from being solved.

#### **4.3.2. METHODS**

The process of curating the metabolic network involves four stages illustrated in Figure 16. The first stage involves collecting the requisite information. In the second

stage, the GA is run. Results are evaluated during the third stage. In the fourth stage, the final model is generated.

The first stage requires an SBML file of the metabolic information as input. The SBML file may be generated from the Pathway Tools bioinformatics suite [66]. Additionally, the specific biomass reaction, the exchange fluxes, and the environmental conditions, such as measured fluxes and medium composition need to be specified. Finally, an objective function must be chosen. It can be the maximization or minimization of biomass, a specific reaction present in the data, or users can create their own objective functions. At this stage, the parameters for the GA should be specified, such as crossover probability, number of points for the crossover operation, the mutation rate, the elite fraction, the bottom re-seed fraction, the frequency of bottom re-seed, the population size of the potential solutions, the number of generations, and the number of simulations.. If the user is unfamiliar with these parameters, reasonable default values are provided. It is recommended that the population size be smaller ( $<50$ ), and that multi-point crossover ( $> 2$ ) and lower elite fractions ( $< 0.2$ ) should be used. If the user observes that the population is becoming uniform too quickly, the bottom re-seed fraction and the frequency of the bottom re-seed should be defined. Typically, values are 0.2 for the bottom re-seed fraction, while the suggested frequency for carrying out bottom re-seed is once every 100 generations.

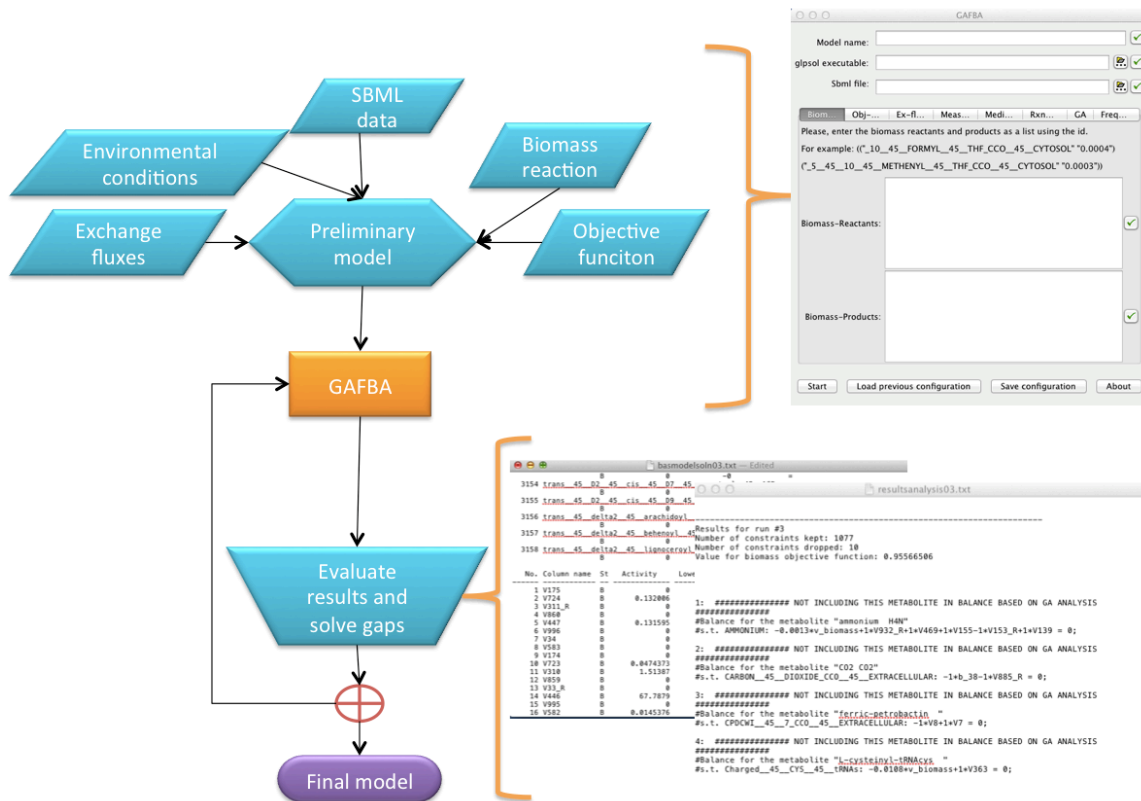


**Figure 16. Four stages of the curation process.** The parallelograms indicate the first stage. Also shown is the corresponding GUI window for this stage. The second stage is represented by the hexagon and the rectangle. The third stage is the trapezoid, and two of the files generated are shown. The fourth stage is indicated by the oval. The steps in blue are operations performed by the user.

For the second stage, all of the information is integrated to generate an initial population of solutions for GAFBA v1.1. Then GAFBA v1.1 evolves the initial population into a new population by applying all the genetic operations, including reproduction, crossover, mutation, and bottom re-seed, as well as the MassChecker tool. When the program reaches the number of desired generations, five files are generated. The first one has the model of the best chromosome from the GA population, which is the

one with the minimum number of mass balance constraints relaxed. It is the input file for running the linear programming solver, glpsol. This file has all the variables associated with each of the reactions, the constraints and the objective functions. The second file has the flux distribution of this model. The lists of the problematic metabolites, whose mass balances were left open, are generated in another file. The fourth file has the best chromosome identified every 100 generations throughout the entire simulation. The final file has the last population of the current simulation.

The third stage involves identifying the potential missing reactions in the network, whether through literature review, experiments, or re-evaluation of the metabolic network for potential errors in the preliminary model. Additionally, the user should review the problematic metabolites and determine whether the mass balance constraints may be kept by either removing or adding exchange fluxes or intracellular reactions, changing the directionality of reactions, and/or removing metabolites. To help the user, GAFBA v1.1 has a tool that analyzes the frequency of relaxed metabolic constraints. This tool finds the metabolites with the highest frequency of relaxation throughout the population. These metabolites are the most likely to be pathological to the generation of a feasible metabolic model, since they must consistently be relaxed in most models to generate a feasible solution [127].

The first three stages are repeated until the *in silico* results closely match the experimental ones, or until all the mass balance constraints are kept. At this point, the fourth stage has been reached and the result is the final model.

#### **4.3.3. IMPLEMENTATION**

The software platform was developed in Common Lisp, and compiled using the LispWorks 6.0.1 Professional Edition compiler. The software is available under the BSD Open Source License. The software package carries out linear programming by calling the GNU Linear Programming Kit (<http://www.gnu.org/software/glpk/>). The software is available for Windows, OS X, and Linux. More information can be found in the comprehensive manual, which is provided in appendix 4.

#### **4.3.4. IMPACT**

A software platform capable of facilitating the curation and implementation of a genome-scale metabolic model for flux balance analysis has been developed. Using a genetic algorithm, it is capable of finding metabolites that may be participating in unspecified reactions. With this software platform, it is anticipated that novel reactions or pathways may be identified, and curation may be simplified and streamlined.

## **5      IMPACT OF IRON AVAILABILITY ON *BACILLUS ANTHRACIS***

### **METABOLISM**

This chapter has been submitted with minor modification as “Impact of iron availability on *Bacillus anthracis* metabolism.” Eddy J. Bautista, Andrea M. DiVenere, and Ranjan Srivastava. 2013, *Journal of Bacteriology*.

#### **5.1 Chapter Synopsis**

To establish a successful infection, *Bacillus anthracis* must be able to adapt to a variety of different physico-chemical conditions encountered when infecting a host, including the presence or scarcity of nutrients. One such critical nutrient is iron, which is generally sequestered by a variety of iron transport/storage protein systems. For *B. anthracis* to effectively compete with these host systems for iron, it secretes high-affinity metal chelators. Previous studies have been dedicated to the analysis of these systems. However, it is still unclear how the availability of iron impacts bacterial metabolism.. In this work, the results of fermentation studies on the Sterne strain of *B. anthracis* grown under iron-poor/rich conditions are reported, and a comparative metabolic analysis is presented. During the exponential phase, the growth rate and six production/uptake rates were measured: glucose uptake rate, lactate production rate, siderophore production rate, iron uptake rate, carbon dioxide production rate, and oxygen uptake rate. It was observed that in iron-poor conditions the glucose uptake rate, oxygen uptake rate, and carbon

dioxide production rate were higher than in iron-rich conditions. Furthermore, it was noted that in both cases, a metabolic shift was observed. The first phase was characterized by lactate secretion (Phase I); during the second phase (Phase II), lactate was consumed. Other observations when going from Phase I to Phase II in both iron-rich and iron-poor conditions included a marked decrease in growth rate, and a decreased iron uptake rate. Also, no siderophore production was detected in Phase I.

## **5.2 Introduction**

During the bacterial pathogen infection process, bacteria go through a series of metabolic adaptations in order to germinate and grow within a host. The bacteria have to be able to adjust to different physical conditions, such as pH, oxygen availability, osmotic pressure, and the availability of nutrients like iron. In fact, host-imposed iron availability is one of the initial barriers to infection [140].

Iron is an essential nutrient for almost all microorganisms. However, free iron damages biological macromolecules as a result of the oxidative stress caused by the metal-catalyzed generation of superoxides, hydrogen peroxide, hydroxyl radicals, ferryl and perferryl radicals [141]. As a result, practically no iron exists in serum that is not bound to heme, sequestered in iron-storage and iron-transport proteins (ferritin, transferrin, lactoferrin), or incorporated as cofactors for various enzymes [142].



*Bacillus anthracis*, a gram-positive bacterium, is the causative agent of anthrax. In order to survive and grow, it has to be able to capture iron from its host. To fulfill this goal, the bacteria produce compounds referred to as siderophores and hemophores. Hemophores scavenge heme from various hemoproteins. Siderophores are high affinity metal chelators that are able to compete with the iron-transport proteins and iron-storage proteins. It has been reported in an *in vitro* study that *B. anthracis* can acquire iron from hemoglobin and transferrin, but not from lactoferrin [143]. Siderophores are produced when *B. anthracis* is inside the alveolar macrophage, where the environment allows the germination of spores and the rapid out-growth of vegetative cells during the intracellular phase of the anthrax lifecycle. This stage is very important in establishing the infection. *B. anthracis* produces two known catechol siderophores: bacillibactin and petrobactin.

Recently, attention has been given to the study of iron acquisition systems in gram-positive bacteria [144,145]. *B. anthracis* contains more iron acquisition systems than non-pathogenic members of the genus *Bacillus* [140]. It has been argued that the number and efficiency of these systems in *B. anthracis* are linked to bacterial pathogenicity [146-148].

Many studies have focused on elucidating and understanding the biosynthetic pathway, as well as the secretion and uptake of siderophores in *B. anthracis* [142,148-152]. However, there have not been any studies to date investigating the metabolism of the bacterium by studying key metabolites of the exo-metabolome under conditions

similar to the ones found in the alveolar macrophage (iron starvation and oxidative stress).

The metabolic response of *B. anthracis* to different iron conditions is reported here. The experiments were carried out under two conditions. The first was an iron-rich condition with concentrations of iron at 20  $\mu\text{M}$ , while the second condition, referred to as an iron-poor condition, involved treating media with a chelating agent to reduce the iron concentration to 2.24  $\mu\text{M}$ .

During the course of the experiment, a shift from lactate production to lactate consumption was observed under both iron conditions. Based on this shift, two phases were defined. The period in which lactate was produced was referred to as Phase I, while the period in which lactate was consumed was referred to as Phase II. The growth rate and concentrations of eight key metabolites were measured in both phases. The uptake rates were calculated for glucose, iron, glutamic acid, lactate, and oxygen. The secretion rates were determined for carbon dioxide, lactate and the siderophores. A clear increase in the carbon metabolism of *B. anthracis* during iron-poor conditions was observed when compared to iron-rich conditions in both phases.

### 5.3 Materials and Methods

**Pre-treatment of glassware, fermentor vessel, and tubing.** All glassware used in the experiments was washed with 9 M nitric acid solution for three hours and rinsed with copious amounts of distilled water [148]. The tubing, the carbon dioxide probe, and the oxygen probe from the fermentor vessel were treated with 1% sodium carbonate and 1 mM ethylenediaminetetra-acetic acid (EDTA), following the procedure described previously [153]. The fermentor vessel was cleaned with a 15% potassium hydroxide-ethanol saturated solution for 24 hours. Then, the potassium hydroxide-ethanol solution was removed, and a 0.5 M phosphoric acid solution was added to the vessel for one more hour. Finally, the vessel was washed with an abundant amount of distilled water. The vessel was assembled; the tubing was put in place and covered with aluminum foil, along with any open port. The entire apparatus was then autoclaved.

**Media preparation.** Two types of media were used for the experiments. The first was *reduced iron media* (IRDM), representing an iron-poor environment. The second media used was *replete iron media* (IRM), representing an iron-rich environment. IRDM was based on a previously described formulation [137]. Stock solutions of defined medium, salts, 10% casamino acids (Fisher), and 20% dextrose were made with distilled-deionized water (MilliQ), and they were treated separately with CHELEX 100 resin following the manufacture's batch chelatin method (BioRad). The resin was removed by filtration. The defined medium composition (g/l) was as follows: 0.53 serine, 1.5 threonine, 1.5 valine,

3.28 leucine, 1.66 aspartic acid, 4.05 glutamic acid, 2.18 arginine hydrochloride, 1.94 histidine monohydrochloride monohydrate, 0.22 cystine, 0.75 methionine, 0.72 proline, 1.65 phenylalanine, 1.28 tryptophan, 0.03 thiamine hydrochloride, and 2% hydrochloric acid. Salts included (g/l): 0.25  $\text{MgSO}_4 \cdot 7\text{H}_2\text{O}$ , 0.025  $\text{MnSO}_4 \cdot \text{H}_2\text{O}$ , 17  $\text{KH}_2\text{PO}_4$ , 21.8  $\text{K}_2\text{HPO}_4$ , and 2% hydrochloric acid. Since the CHELEX resin has a moderate affinity for  $\text{Mg}^+$  ions,  $\text{MgSO}_4 \cdot 7\text{H}_2\text{O}$  was added to the salts after the resin treatment [148]. The defined medium, salt stock solution, and glucose stock solutions were sterilized by filtration. The casamino acids stock solution was autoclaved for 20 min. IRDM was composed of 4% of the defined medium and salts, 12% of casamino acids, 1% of dextrose solution, and 0.3% PIPES buffer. 10 N NaOH solution was added to adjust the pH to 7.5. The iron concentration of IRDM was determined by ion-coupled plasma mass spectrometry, and was found to be 2.24  $\mu\text{M}$ . The formulation of IRM was the same as IRMD, except that IRMD was supplemented with a freshly prepared ferrous sulfate solution to a final concentration of 20  $\mu\text{M}$ .

**Bacterial strains and growth conditions.** *Bacillus anthracis* Sterne 34F<sub>2</sub> (pXO1<sup>+</sup> pXO2<sup>-</sup>) was used in all the work described here. *B. anthracis* stock cultures were prepared from vegetative cells grown to late exponential phase in IRDM at 37 °C and shaken at 300 rpm in an incubator-shaker (New Brunswick Scientific, Edison, NJ, Classic Series C24 incubator shaker). The stock cultures were prepared by mixing 0.5 ml of bacterial cultures with 0.5 ml of 30% glycerol. These stocks were stored at -70 °C. For the IRDM experiments, fresh media were inoculated to 1.5% (v/v) stock cultures, and

grown overnight (17 h) in IRDM at 37 °C at 300 rpm. The bacteria were then diluted in IRDM media to a ratio of 1:3, and allowed to recover for 1.5 hours. Cells were collected by centrifugation, and washed three times with phosphate-buffered saline and a final wash in IRDM [150]. The pellet was re-suspended in 10 ml of IRDM. Then, the bacteria were diluted to an OD<sub>600</sub> of 0.05 in 1.4 L of IRDM in the fermentor vessel. For the IRM experiments, the protocol was the same as the IRDM experiments, except that the media used was IRM for the final wash prior to inoculation of the fermentation vessel.

**Fermentation conditions.** The fermentation experiments were done using a New Brunswick Bio-Flo 3000 Bioreactor with a 3.0 L working volume vessel. 1.4 L of IRDM media were added to the sterilized vessel. For the IRDM experiments, the media was supplemented with ferrous sulfate 30 minutes prior to inoculum addition. For each condition, triplicate experiments were carried out on different days. The OxyProbe dissolved oxygen sensor (Broadley James) and the InPro 5000i carbon dioxide sensor (Mettler-toledo) were sterilized with 70% ethanol solution and UV light. The probes were inserted into the vessel, which were connected to the fermentor unit. The OxyProbe was calibrated following the two point calibration method as described in the Bio-Flo 3000 fermentor manual, and the InPro 5000i carbon dioxide sensor was calibrated using a one point calibration methodology as described in the Mettler-Toledo M400 transmitter manual. The temperature was measured with a resistance temperature detector submerged into the thermowell of the vessel. The temperature set point was fixed at 37 °C, and was controlled by the BioFlo 3000 microprocessor-based built-in controller. Agitation was set

to 400 rpm. Air was allowed to enter the system through a 0.2  $\mu\text{m}$  PTFE filter, and aeration was adjusted to 2.0 SLPM. The dissolved oxygen ( $\text{dO}_2$ ) was not allowed to decrease below 75% of saturation. Oxygen control was accomplished by increasing agitation from the initial 400 rpm to 500 rpm using an agitation/ $\text{dO}_2$  cascade control system as described in the Bio-Flo 3000 fermentor manual. The pH was measured offline using an Accumet pH/temperature electrode (Fisher Scientific). It was adjusted to approximately 7.5 before the addition of the inoculum with 10N NaOH solution and/or 10 N HCl.

Then, the inoculum was added to the fermentor vessel through the addition port of the headplate. The initial carbon dioxide concentration and  $\text{dO}_2$  were recorded. A sample from the fermentation liquor was taken to measure the initial  $\text{OD}_{600}$ , pH, glucose concentration, lactate concentration, glutamic acid concentration, siderophore concentration, and iron concentration. Cells were allowed to enter the exponential phase, and three samples were taken during this time.

**Analytical techniques.** Cell density was measured at 600 nm using a BioMate™ 3 spectrophotometer (Thermo Spectronic, USA). Samples were first filtered through a 0.2  $\mu\text{m}$  syringe filter. Glucose concentration, lactate concentration, and glutamic acid concentration were measured using a YSI 2700 Biochemistry Analyzer. The Arnov Assay was used to measure the levels of extracellular catechol siderophores as described elsewhere [137,152,154]. A standard curve was established using 2,3-dihydroxybenzoate

(2,3-dhb). Iron concentration was measured using a Perkin Elmer Optima 7300DV Inductively Coupled Plasma Optical Emission Spectrometer (ICP/OES).

The dry weight correlation for the bacteria in each media was determined by taking 100 ml of fermentation broth three times during the exponential phase. The cells were collected by centrifugation at 4000 rpm at 4 °C for ten minutes. Then, the pellet was washed twice with PBS, re-centrifuged, and transferred to dry pre-weighed 2 ml centrifuge tubes. The pellets were dried at 75 °C for 7 days, or to a constant volume [23].

**Metabolite uptake and secretion rate calculation.** For all the metabolites, the solution for the dynamic equation of the mass balance was fit to the experimental data using nonlinear fitting algorithms [8,23,155] from Matlab (MathWorks, USA). Appendix five describes the calculations in detail.

**Western blot analysis.** Samples for western blot were taken from the fermentor broth at an OD<sub>600</sub> of 0.8. Cells were collected by centrifugation, and washed three times with PBS buffer [156]. The pellets were stored at -70 °C. To analyze samples via western blotting, 48 µL of pellet were solubilized by boiling in 32 µL of 5X sodium dodecyl sulfate-polyacrylamide gel electrophoresis (SDS-PAGE) sample buffer at 95 °C for 10 minutes. Blanks were prepared in the same way with IRMD and IRM without bacteria. An equal amount of samples, and blanks were loaded into 4-15% Mini-PROTEAN TGX Precast Gels (Biorad). They were blotted to a nitrocellulose membrane. Protein blots were

blocked in 5% nonfat milk in TBS-T buffer for one hour at room temperature under gentle agitation. Next, the membranes were exposed to 1 µg/ml of *B. anthracis* mouse anti-PA monoclonal serum (Thermo scientific) in TBS-T with 5% nonfat milk for two hours at room temperature under gentle agitation. The membranes were washed three times with TBS-T for 5 minutes. The membranes were incubated with anti-mouse IgG-alkaline phosphatase (Sigma) dilute 1:15,000 in TBS-T with 5% nonfat milk for one hour at room temperature with gentle agitation. Next, the membrane was washed three times with TBS-T for 5 minutes, and rinsed with TBS. Finally, the blot was developed using SIGMAFAST BCIP/NBT (Sigma) tablets. All western blot experiments were run in duplicate using samples from two different cultures [157,158].

## 5.4 Results

**Two metabolic states observed during growth under iron-poor/rich conditions.** *B. anthracis* Sterne was grown aerobically under iron-poor and iron-rich conditions. During the experiments, two phases were observed. The first phase was characterized by the production of L-lactate, and is referred to as *Phase I*. It was then observed that L-lactate was re-assimilated in the second phase, which is referred to as *Phase II*. This behavior was observed independently of the iron concentration, as is shown in Figures 17a and 18a. It was further noted that the consumption of L-lactate occurred before glucose exhaustion, and started when the dissolved oxygen concentration reached 75% of



saturation. At this point, the agitation/dO<sub>2</sub> cascade control system of the fermentor oscillated the agitation speed between 400 rpm to 500 rpm to maintain control of the dO<sub>2</sub>.

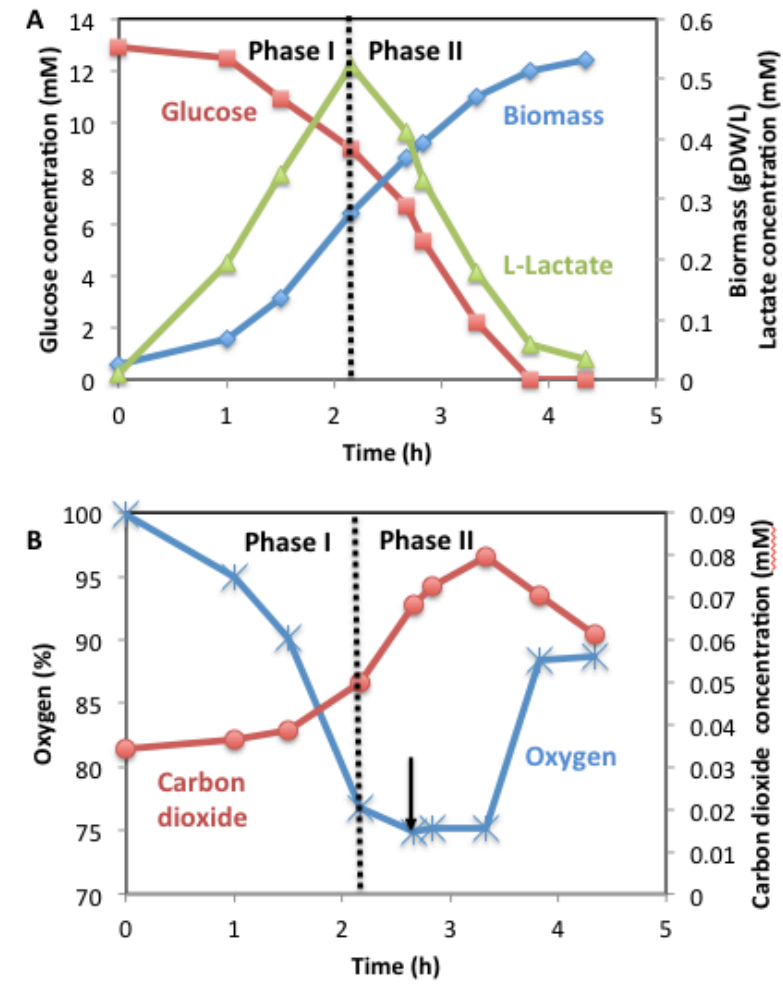


**Figure 17. Levels of extracellular metabolites and growth rate under iron-poor conditions.** A. L-lactate (green triangles), glucose (red squares), and biomass (Blue diamonds). B. Oxygen (blue stars), and carbon dioxide (red dots). The dotted vertical line represents the point of transition between Phase I and Phase II. The black arrow in the B panel indicates the point that oxygen concentration reached 75%, and the control of the dissolved oxygen concentration started by changing the speed of the agitator. The data corresponds to one of the experiments carried out in triplicate. The data points for the other experiments are provided in Appendix 6.

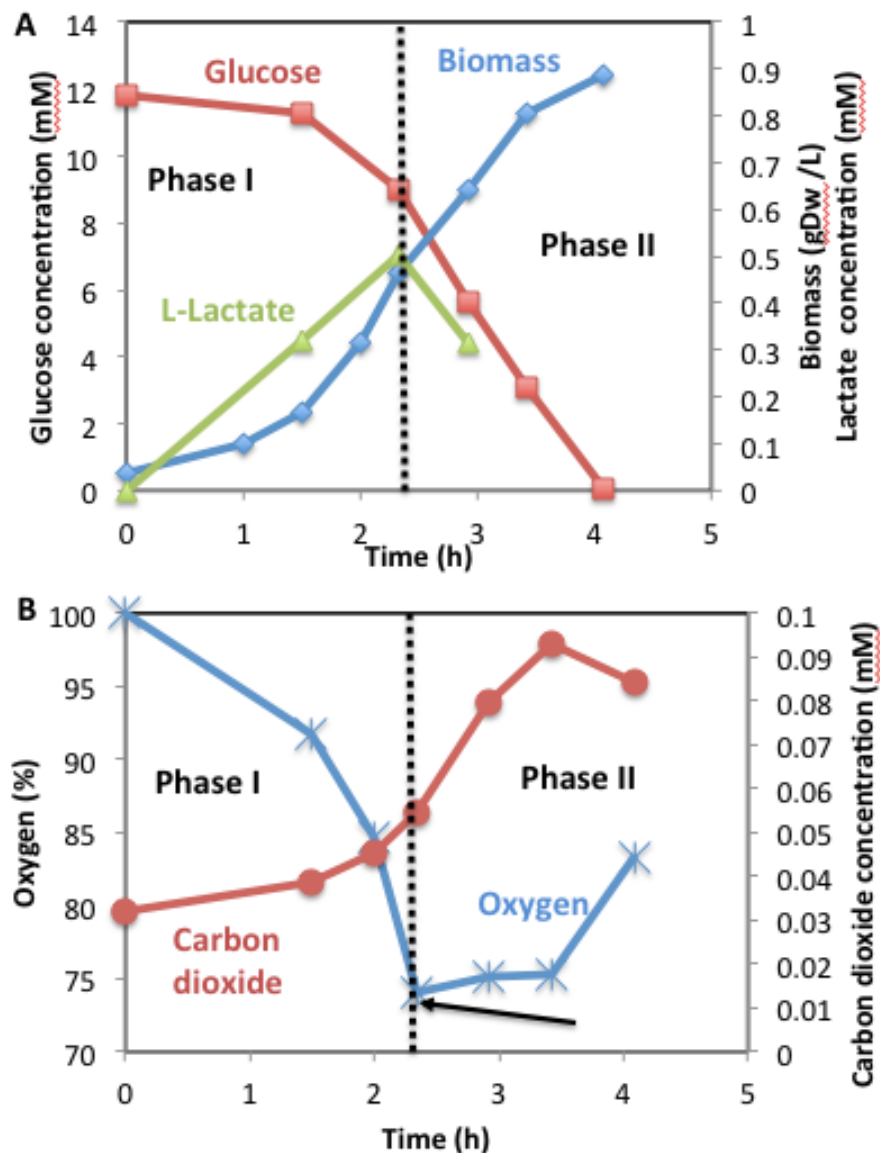


**Figure 18. Levels of extracellular metabolites and growth rate under iron-rich conditions.** A. L-lactate (green triangles), glucose (red squares), and biomass (blue diamonds). B. Oxygen (blue stars), and carbon dioxide (red dots). The dotted line represents the point of transition between Phase I and Phase II. The black arrow in the B panel indicates the point that oxygen concentration reached 75% and the control of the dissolved oxygen concentration started by changing the speed of the agitator. The data corresponds to one of the triplicated experiments. The data points for the other experiments are provided in Appendix 6.

During the lactate production stage, *B. anthracis* produced lactic acid via the lactate dehydrogenase enzyme (*ldh*). The production of lactate under aerobic conditions was likely an indication of overflow metabolism, as has been reported for *Bacillus subtilis* when growing in a medium containing an excess of glucose [159-161]. Under such conditions, lactate production eliminates excess carbon from the cell. Meanwhile, the lactate dehydrogenase reaction helped the electron transfer chain keep the redox balance by regenerating  $\text{NAD}^+$ , which is required in the earlier steps of glycolysis [162]. In the second stage observed, *B. anthracis* started to consume the lactate that was accumulated in the media. Lactate likely provided additional energy for siderophore biosynthesis, since siderophore production started at nearly the same time as lactate consumption (data not shown). Also, lactate could contribute to carbon structure through phosphoenolpyruvate, which is needed for siderophore biosynthesis.

Two reactions could be responsible for the consumption of lactate in Phase II; they are lactate dehydrogenases, or lactate oxidoreductase. In *Lactobacillus plantarum*, lactate utilization has been reported to be carried out through  $\text{NAD}^+$ -dependent lactate dehydrogenases [163]. However, in *B. subtilis* [164,165] and *Staphylococcus aureus* [166], lactate consumption is achieved with the enzyme lactate oxidoreductase encoded by the *lutABC* operon. Chai *et al.* [164] found homologs of *B. subtilis* *lutABC* in different bacteria, including *B. anthracis*, by doing chromosomal alignment. Moreover, Pohl *et al.* [5] reported the induction of BA1315 (LutA protein), BA1316 (LutB protein), BA1317 (LutC protein), and BA1314 (LutR protein) genes in *B. anthracis* when hydrogen

peroxide was added to the media to cause oxidative stress to the bacterium. LutR is a GntR-like repressor, which mediates the induction of *lutABC* when lactate is present in the media. Therefore, it was hypothesized that the lactate consumption in *B. anthracis* was carried out through the lactate oxidoreductase reaction rather than using the lactate dehydrogenase enzyme.

**Growth rate decreased under iron-poor conditions.** The effect of iron on the growth rate was quantified during fermentation runs under iron-poor/rich conditions. The growth was monitored spectrophotometrically. The results are shown in Figure 19 for Phases I and II. The growth rate was lower in iron-poor conditions compared to iron-rich conditions in both phases. However, the effect of iron depletion in the media was more detrimental to the growth rate in Phase II. The growth rate decreased by 30% in Phase II under iron-poor conditions relative to iron-rich conditions, as compared to a reduced growth rate of only 8% during Phase I. These results are in agreement with previously described behavior for *B. anthracis* under iron-poor conditions [6,137,167]. Carlos *et al.* [6] reported a noticeable decrease in growth rate during the middle of the exponential phase, and an early on-set of stationary phase under iron-poor conditions.

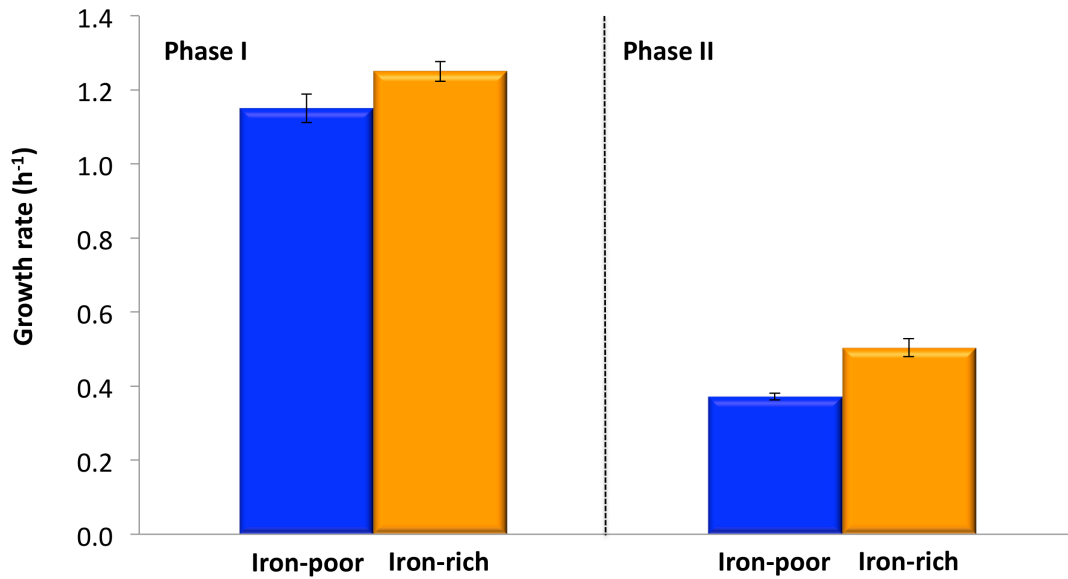


**Figure 19. Growth rate for both phases.** Blue columns indicate iron-poor conditions, and orange columns are the iron-rich conditions. The columns denote the mean of the independently triplicated experiments, and the error bars are the standard error of the mean.

**Lactate secretion/uptake rates.** During Phase I, no significant difference in lactate secretion was observed under the iron-poor versus iron-rich conditions, as indicated in Figure 20A. In Phase II however, a more than two-fold increase in the lactate uptake rate under iron-poor conditions was seen, as indicated in Figure 20B.

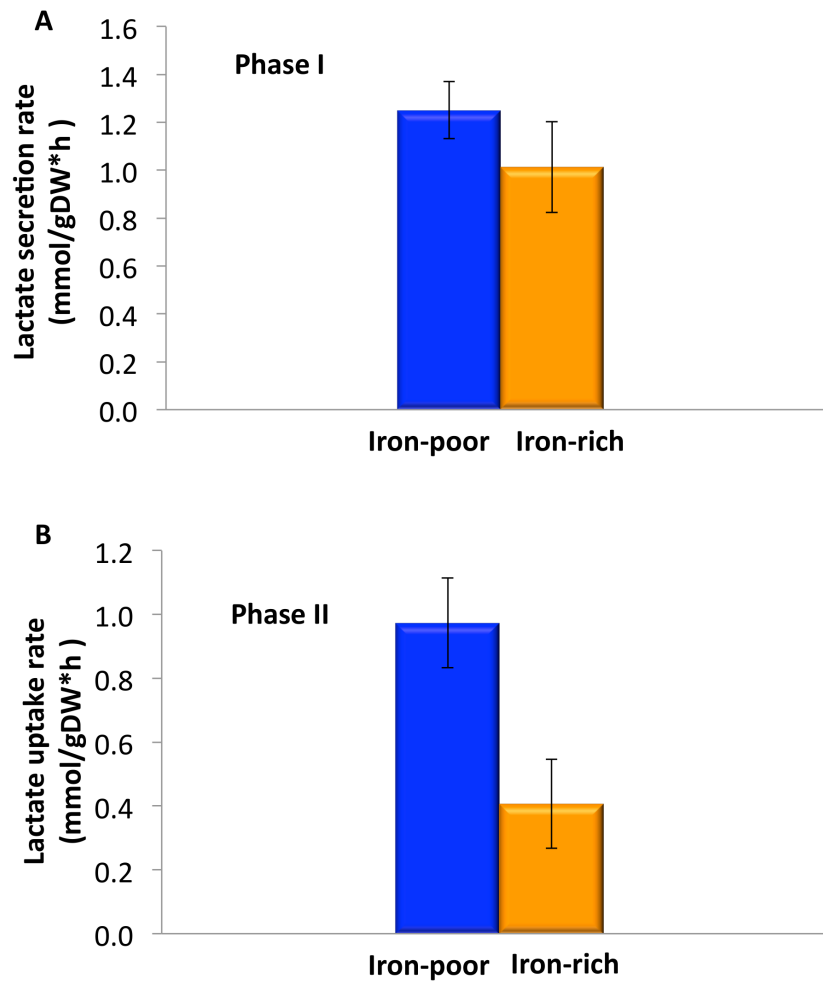


**Figure 20. (A) Lactate secretion rate during Phase I and (B) lactate uptake rate during Phase II.** Blue columns indicate iron-poor conditions, and orange columns are the iron-rich conditions. The columns denote the mean of the independently triplicated experiments, and the error bars are the standard error of the mean.

Interestingly, the shift to lactate consumption in Phase II was different than what has been reported in other studies. For instance, *Staphylococcus aureus* increases the production of lactate in order to decrease the local pH, which facilitates the release of host iron-sequestering proteins under iron deprivation conditions [168]. Also, *B.*

*anthracis* transcriptomic analysis shows an up-regulation of lactate dehydrogenase and lactate permease under iron depletion conditions [6]. Furthermore, *B. subtilis* studies of the iron-sparing response identify a repression in the synthesis of the LutABC lactate oxidoreductase enzyme [165,169], which is responsible for lactate utilization under iron deprivation conditions.

In the current study, no large reduction in the pH value under iron-poor conditions was observed relative to iron-rich conditions. This result is contrary to the pH behavior reported for *S. aureus* growing under iron-poor conditions. Indeed, the pH in *B. anthracis* under iron-poor and iron-rich condition showed similar behavior, and they finished near the same values. In iron-poor conditions, the pH started at 7.50 and dropped to 7.02 by the end of Phase I. By the end of Phase II, the pH was approximately 6.53. In iron-rich conditions, the pH started at 7.55 and finished at 6.92 by the end of Phase I. It decreased slightly to 6.45 by the end of Phase II.

The difference between the lactate secretion results reported here and elsewhere [6,165,168,169] could be caused by differences in the experimental conditions. Specifically, none of the other studies controlled the  $dO_2$ . Additionally, in *S. aureus* experiments iron was depleted by either adding an iron chelator (2,2'-dipyridyl) to the media, or by mutating the *fur* gene, which is a ferric uptake global transcriptional repressor. These two approaches could result in a more severe reduction in iron concentration than in the experiments described here.

As a part of the iron sparing response of *B. subtilis*, Smaldone *et al.* reported that under limited iron conditions, sRNAs regulated by the *fur* gene repressed the translation of the LutABC proteins [165,169]. However, the consumption of lactate during Phase II suggests that the genes encoding for lactate oxidoreductase were not repressed under the current experimental conditions. These contradictory results could be caused by the severe iron reduction imposed by the mutation of the *fur* gene in the *B. subtilis* study, as compared to the current study. Another possibility is that, under the experimental conditions studied, the LutABC proteins in *anthracis* are not translationally regulated by the *fur* gene.

**Reduction in iron concentration increases the carbon dioxide secretion rate.** The carbon dioxide secretion rate was found to be higher under iron-poor conditions than in iron-rich conditions for both phases. These results are depicted in Figure 21. The secretion rate was found to be 27% lower in iron-rich conditions than in iron-poor conditions during Phase I. During Phase II, the secretion rate was 21% lower in iron-rich conditions. Similar ratios between iron-poor/rich values were kept for both phases.



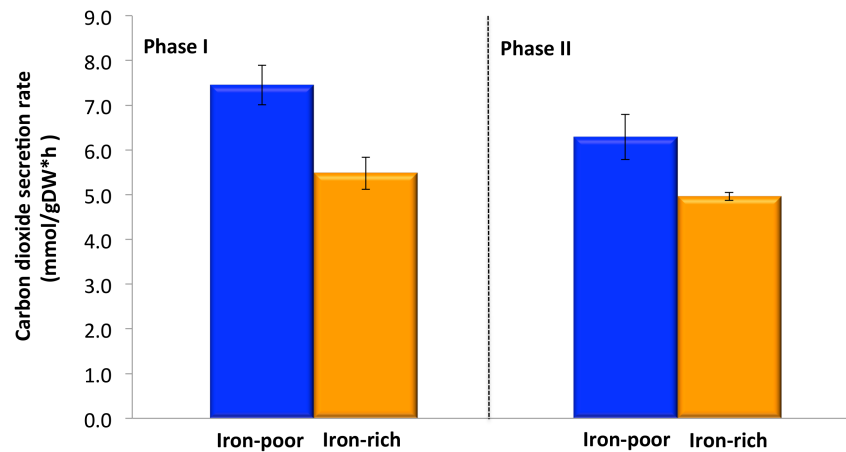


**Figure 21. Carbon dioxide secretion rate during Phases I and II.** The blue columns indicate iron-poor conditions, and the orange columns are the iron-rich conditions. The columns denote the mean of the independently triplicated experiments, and the error bars are the standard error of the mean.

**Glutamic acid uptake rate.** No statistically significant difference was found between the iron-poor and iron-rich conditions for the glutamic acid uptake rate during Phase I, as is shown in Figure 22. During Phase II, the consumption of glutamic acid was five-fold lower during growth in iron-poor conditions. This reduction in the glutamic acid uptake rate under iron-poor conditions could be caused by a down-regulation of the proton/glutamic acid transport gene, as was reported by analyzing the data from the transcriptional profiling of *B. anthracis* during iron starvation [6].

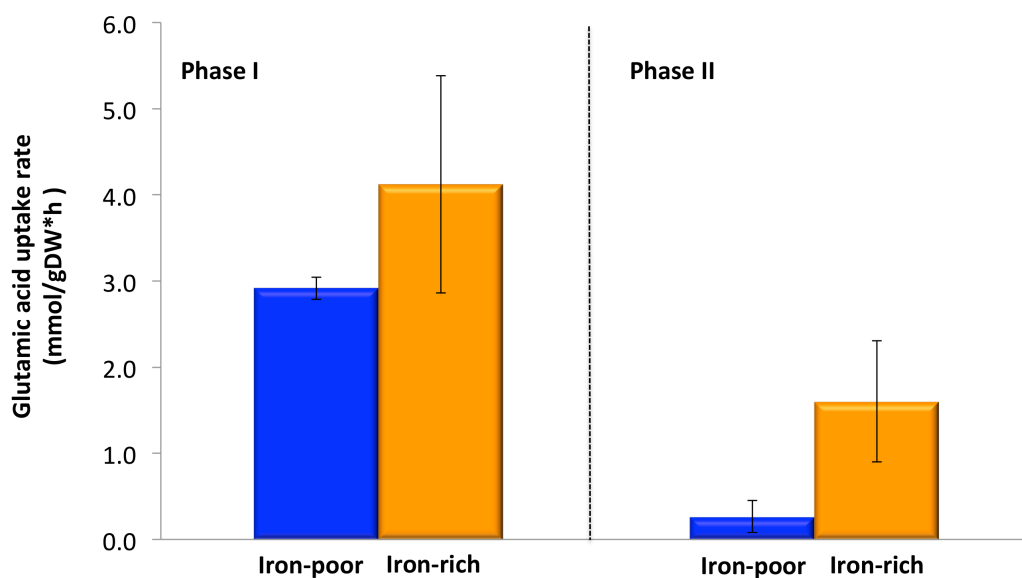


**Figure 22. Glutamic acid uptake in Phases I and II.** The blue columns indicate iron-poor conditions, and the orange columns are the iron-rich conditions. The columns denote the mean of the independently triplicated experiments, and the error bars are the standard error of the mean.

**Glucose uptake rate was higher under iron-poor conditions.** It was found that *B. anthracis* consumed less glucose during iron-rich conditions than in iron-poor conditions in both phases, as is shown in Figure 23. During Phase I, the glucose uptake rate in iron-rich conditions was 20% lower than in iron-poor cultures. During Phase II, the glucose uptake rate under iron-rich conditions was 35% lower as compared to the iron-poor cultures. A slight incremental increase in the glucose uptake rate under lower iron concentrations was observed at Phase II compared to Phase I.

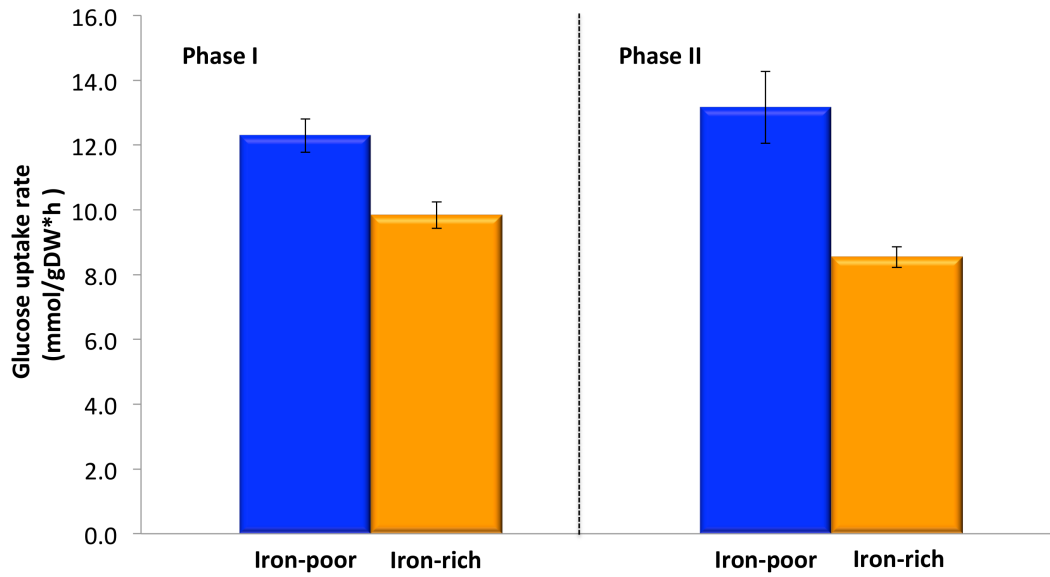


**Figure 23. Glucose uptake rate at Phase I and Phase II.** The blue columns indicate iron-poor conditions, and the orange columns are the iron-rich conditions. The columns denote the mean of the independently triplicated experiments, and the error bars are the standard error of the mean.

**Oxygen uptake rate decreased as iron concentration increased.** The oxygen uptake rate (OUR) was found to be higher in iron-poor conditions than in iron-rich conditions during Phase I and Phase II, as is shown in Figure 24. During Phase I, OUR was 21% higher in iron-poor conditions than in iron-rich conditions. However in Phase II, OUR was 44% higher in iron-poor conditions than in iron-rich conditions.

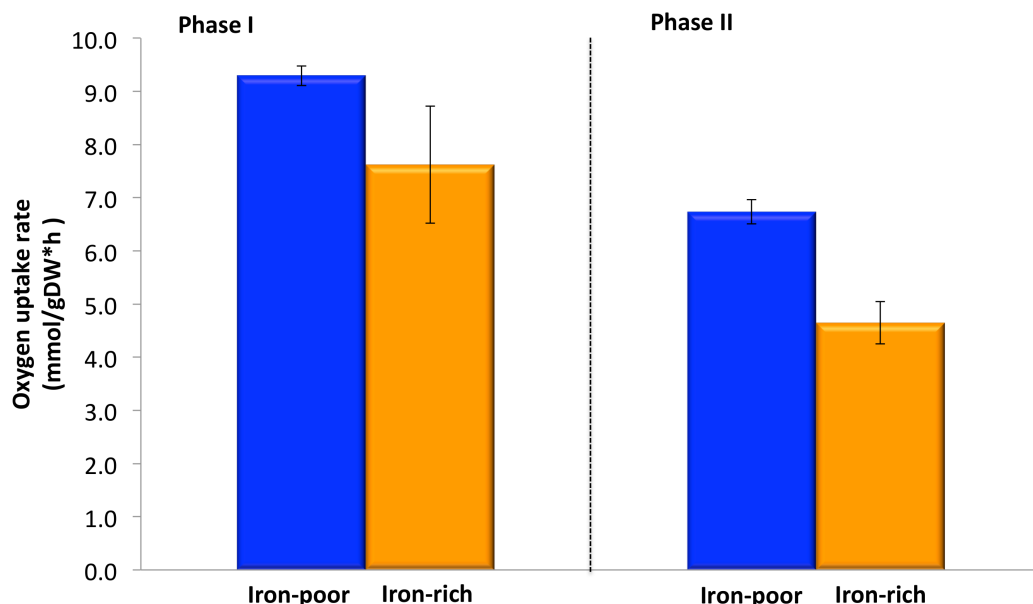


**Figure 24. Oxygen uptake rate during Phases I and II.** The blue columns indicate iron-poor conditions, and the orange columns are the iron-rich conditions. The columns denote the mean of the independently triplicated experiments, and the error bars are the standard error of the mean.

**Siderophores were produced only during Phase II.** Siderophores were not detected in either iron-rich or iron-poor cultures during Phase I. These results are in agreement with previously reported findings, stating that the production of siderophores begins in the middle of exponential phase, and peaks in the stationary phase [149,167].

Siderophores were secreted 3.3 times faster in iron-poor conditions than in iron-rich conditions, as is shown in Figure 25. This is not surprising, since studies have shown that iron deprivation up-regulates the biosynthesis pathway and secretion of siderophores, as well as other iron transport mechanisms [6,170]. *B. anthracis* secretes two known

siderophores: bacillibactin and petrobactin. Both have higher affinity for iron ( $K_f^{bac} = 10^{47.6}$  and  $K_f^{pet} = 10^{23}$ ) as compared to transferrin  $K_f = 10^{21}$  [142]. This property allows the bacteria to compete more efficiently for iron during the infection process.

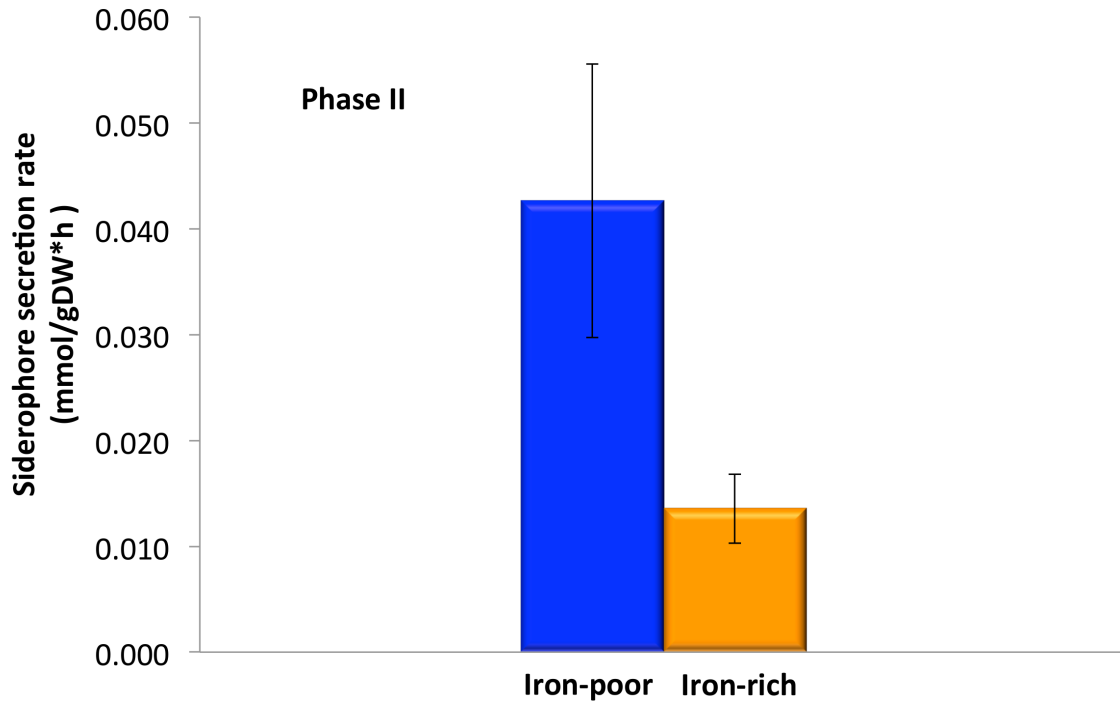


**Figure 25. Siderophore secretion rate for Phase II.** No siderophores were detected in Phase I. The blue columns indicate iron-poor conditions, and the orange columns are the iron-rich conditions. The columns denote the mean of the independently triplicated experiments, and the error bars are the standard error of the mean.

Supplementation of the media with iron did not abolish siderophore secretion. The secretion of siderophores at high iron concentrations has been reported in previous experiments [149,171]. Lee *et al.* [171] suggest that the *bac* locus encoding the

biosynthesis of bacillibactin is highly regulated at the transcriptional level by iron concentration. However, under iron rich conditions, small amounts of bacillibactin could be produced [148]. Meanwhile, the transcriptional regulation of the petrobactin biosynthesis pathway at the *asb* locus is less effective under iron rich conditions. In addition to the iron regulation of the siderophore biosynthetic pathway, it has been found that temperature [143,148,149], aeration rates [171], and CO<sub>2</sub>/bicarbonate levels [148,149] also have an impact on petrobactin and bacillibactin production. Nonetheless, under any combination of these conditions, petrobactin has always been detected, suggesting constitutive production. In this study, petrobactin and bacillibactin concentrations were not measured directly; rather the total siderophore concentration was measured. However, based on the previous evidence, it was hypothesized that the main siderophore detected under iron rich condition was likely to be petrobactin.

**Iron was primarily consumed during Phase I.** The iron uptake rate was 1.72-fold higher in Phase I under iron-rich conditions than in iron-poor conditions. In Phase II, the iron uptake-rate was 3.8 times faster in iron-rich conditions than in iron-poor conditions, although absolute uptake rates in both conditions were slower than observed for Phase I. The results are illustrated in Figure 26. It is likely that during Phase I, the iron concentration in the iron-poor cultures was adequate to facilitate the passive/active transport of iron into the bacteria. As a consequence, the relative difference in the iron uptake rate between the iron-rich and iron-poor conditions was not as high as seen in Phase II.

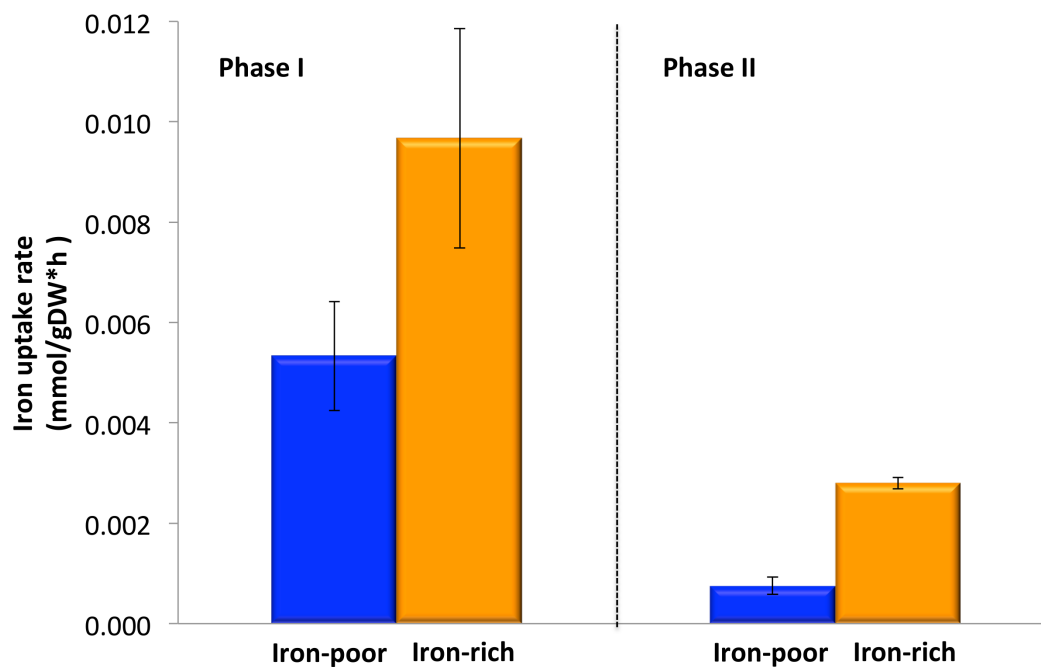


**Figure 26. Iron uptake rate during Phases I and II.** The blue columns indicate iron-poor conditions, and the orange columns are the iron-rich conditions. The columns denote the mean of the independently triplicated experiments, and the error bars are the standard error of the mean.

During Phase II, the iron in the IRDM media was nearly depleted. As a result, the uptake of iron was lower under these conditions. Even with the production of siderophores, the bacteria were unable to collect significant levels of iron due to the lack of iron in the environment.

**Carbon metabolism was more active under iron-poor conditions.** As was shown, more glucose and oxygen were consumed under iron-poor conditions in both phases.

Additionally, more carbon dioxide was produced during iron-poor conditions in both phases. Nonetheless, this increased carbon metabolism did not reflect in higher growth rates under iron-poor conditions. On the contrary, the growth rates were slower in iron-poor cultures than in iron-rich cultures in both phases. These results suggest that an increased carbon metabolism does not necessarily support growth.

**Impact of iron concentration on protective antigen production.** To determine the effect of iron on the production of toxins, the presence of the protective antigen (PA) protein was monitored via western blot. Additionally, it was hypothesized that if toxins were detected in the cell, they could explain the increased carbon metabolism observed under iron-poor conditions. Samples were taken at the end of the exponential growth phase, since accumulations of toxins are highest at this time [172].

Figure 27 shows the western blot results for PA detection in IRDM, representing iron-poor conditions, and IRM, representing iron-rich conditions. The results were compared to cells growing under IRDM/IRM with bicarbonate. It is known that bicarbonate induces the production of toxins [173]; thus it was used to establish a positive control. Experiments showed that unless bicarbonate was in the media, PA was not produced, which was expected and consistent with previous reports [173]. These results suggest that the observed increase in carbon metabolism under iron-poor conditions is not caused by toxin production.



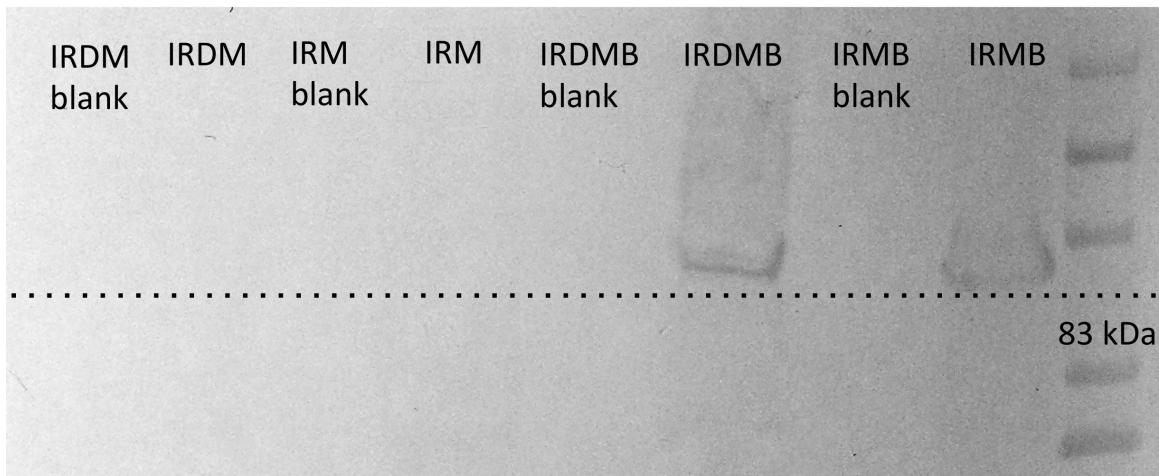


**Figure 27. Western blot analysis of Protective Antigen protein.** Western blot results for the four conditions and their blanks. “Blanks” were media before the inoculation of bacteria. IRDM is iron-reduced media, IRM is iron-replete media, IRDMB is iron reduced media with bicarbonate, and IRMB is iron replete media with bicarbonate. The black-dashed line shows the approximate position of the protective antigen at 83 kDa.

## 5.5 Discussion

For years, the importance of iron to the growth and development of pathogenic bacteria has been recognized. As a mechanism of defense, the host organisms sequester their iron in iron storage/transport proteins. Meanwhile, *B. anthracis* secretes two siderophores, bacillibactin and petrobactin in order to battle for iron under iron deplete conditions. Bacillibactin is deactivated by siderocalin, a protein that is part of the host’s immune response. Petrobactin, however, is able to evade siderocalin, and it has been shown that a mutation in its biosynthesis pathway attenuates *B. anthracis* pathogenesis in mice [137]. In *B. anthracis*, siderophore metabolism has been well studied [142,148-

152]. Despite these studies, the impact of iron availability on the metabolism of *B. anthracis* remains unclear. Over the course of the current studies, an increase in the production of siderophores under iron-poor condition in Phase II was observed, as has been reported in the previous studies [149,150]. During Phase I, the concentration of iron in iron-poor conditions was initially enough to support almost normal bacteria growth. However, as the number of cells increased, the continuing depletion of iron in the iron-poor environment during Phase II activated components of the iron-sparing response, such as the biosynthesis of siderophores [169,170].

During Phase II, the energy requirements for growth and siderophore production were fulfilled by an increase in glucose uptake and by the consumption of lactate accumulated in the media during Phase I. *B. anthracis* not only needs energy for siderophore biosynthesis, but also for recapturing the ferric-siderophore complexes secreted into the media [142,150,152,174-176]. Additionally, the bacteria require sufficient reducing power to free the iron from the ferric-siderophore complexes, which also increases the energy demand [174,177].

It was surprising to observe an increase in the glucose uptake rate, carbon dioxide secretion rate, and oxygen uptake rate during iron-poor conditions, especially in conditions where the growth rates decreased. There are two potential explanations for this phenomenon. The first possibility is that *B. anthracis* may have an up-regulated glycolysis pathway during iron-poor conditions to produce fermentation by-products for

energy, and to regenerate  $\text{NAD}^+$ . A similar behavior has been observed in *S. aureus*, albeit for a different purpose. In *S. aureus*, the glycolysis pathway is up-regulated to produce lactate for media acidification purposes [168]. The second possibility is that the biosynthesis of amino acids may be up-regulated for the production of siderophores during Phase II, as has been seen in *B. subtilis*. Here, it can be argued that under the media condition used, amino acid biosynthesis is not required, since casamino acids should provide them. However, the transcriptional profiling of *B. anthracis* under iron starvation conditions reported a downregulation of amino acid permease family proteins and oligopeptide ABC transporters [6]. This is in agreement with the reduction of the glutamic acid uptake rate observed in these studies during the iron-poor conditions in Phase II. Thus, in response to the reduction of amino acids uptake, the bacteria may increase the biosynthesis of some amino acids, and many of the precursors to the amino acids' biosynthesis pathways come from the glycolysis pathway.

The higher glucose uptake rate and oxygen uptake rate did not result in a higher growth rate in *B. anthracis* under iron-poor conditions. Thus, it is hypothesized that *B. anthracis* conserves energy less efficiently under iron-poor conditions, which is similar to what has been reported for *Escherichia coli* growing in succinate under iron-deficient conditions [178]. It is possible that there are other energy consuming process occurring in the bacteria not related to biomass production. These could include processes such as maintenance, energy loss due to leaks, and/or production of signaling molecules, regulatory proteins, or small RNAs. Small RNAs such as RyhB, have been reported to

mediate the repression of iron-containing proteins under iron starvation conditions in *B. subtilis* [169] and other bacteria [179,180].

## **6. GENOME-SCALE METABOLIC RECONSTRUCTION FOR *BACILLUS ANTHRACIS* STERNE AND ANALYSIS OF ITS METABOLIC ADAPTATION TO DIFFERENT IRON CONDITIONS.**

### **6.1.Chapter Synopsis**

The infection process for *Bacillus anthracis*, the causative agent of anthrax, begins when spores enter the body through the skin or mucosa. Then, local macrophages phagocytose the spores, where they germinate. After the vegetative cells are released from the macrophage, they enter the lymphatic system and bloodstream where they spread through the body and produce septicemia, shock, and finally death. When *B. anthracis* are living inside macrophages, the bacteria have to compete for iron with host iron transport/storage proteins. To effectively compete, the bacteria secrete siderophores, which are powerful iron chelators. The biology of siderophores has been well studied. However, the impact of iron availability to *B. anthracis* metabolism from a global perspective remains unknown. Genome-scale metabolic models allow for the compact and integrated analysis of complex metabolic networks and their associated, often non-intuitive, behavior. In this work, the metabolic model of *B. anthracis* was developed using GAFBA v1.1 which compiled all the available information for the bacteria and other closely related *Bacillus* strains to generate a comprehensive biomass equation, and analyzed how all of the metabolites in the system interacted with each other. Then the *B. anthracis* model was used to analyze the metabolic response to iron-poor/rich conditions.

During iron deprivation, a down regulation of some of the reactions of the TCA cycle, and a reduction on the uptake of amino acids were observed. For the first time, a correlation between the biosynthesis of autoinducer-2, a quorum sensing signal molecule, and the growth of *B. anthracis* under iron-poor conditions was reported.

## **6.2. Introduction**

*B. anthracis* is a gram positive, spore forming, and facultative anaerobe bacterium. *Bacilli* will form spores when local nutrients in the environment are exhausted, which happens after host death and exposure to air. The spores are highly resistant and can survive in soil for decades. *B. anthracis* has been recognized as a bioterrorism agent because of its ability to produce anthrax. The Center for Disease Control and Prevention has created three levels of classification for biological agents using three categories, A, B, and C, depending upon threat level. *B. anthracis* is part of category A, the highest priority agents. Considering that anthrax can be easily transmitted from person to person, an anthrax attack could result in a high mortality rate [181,182].

During the 20th century, anthrax was part of military programs for developing of biological agents for warfare in countries such as Germany, England, France, Russia and Japan. In 1979, an accidental anthrax occurred outbreak near Moscow. This case is known as the Sverdlovsk epidemic. Many individuals suffered gastrointestinal, cutaneous, and inhalation anthrax. After many investigations, the incident was linked to a

secret biological weapons program at a nearby military compound. In 2001, anthrax attacks occurred in the U.S with spores in powder form. Five people were killed, and 17 others were infected [38,183].

Anthrax can be treated with antibiotics, if it is diagnosed early enough in the infection process. However, the diagnosis is very difficult to make [184]. Furthermore, the existing vaccines are not completely effective.. Therefore, a better understanding of the bacteria's metabolism during the infection process, and its interaction with the host will provide an exceptional insight into the anthrax disease.

During the different stages of infection, *B. anthracis* has to be able to adapt to the availability of nutrients such as iron. Iron is important for numerous cellular processes. Nevertheless, it is highly toxic because it is insoluble at physiological pH. As a consequence, host molecules with very high binding affinities such as transferrin, ferritin and hemoglobin sequester iron. This mechanism protects the host from bacterial infection, since the iron concentration is kept below the level required to support bacterial growth and virulence.

*B. anthracis* secretes siderophores and hemophores in order to compete with the host's iron transport and iron storage proteins for iron. Hemophores are useful after the escape from the macrophage, since they extract heme groups from hemoglobin. On the contrary, siderophores are important during the intracellular life cycle of *B. anthracis*

inside the macrophage. There are two known biosynthesis systems for siderophores encoded within the genome of *B. anthracis*: petrobactin and bacillibactin. Petrobactin confers an important advantage to the bacteria, because petrobactin can escape from the action of host-produced siderocalin. Siderocalin binds to bacterial siderophores, preventing iron delivery to the bacteria [140].

The influence of *B. anthracis*'s iron acquisition systems on its pathogenicity has been previously studied. For instance, when the genome of *B. anthracis* was compared with the genome of non-pathogenic members of the genus *Bacillus*, it was found that *B. anthracis* contains more iron acquisition systems [140]. In another study, a mutation in the petrobactin biosynthesis pathway of *B. anthracis* ( $\Delta asbA$ ) reduced the growth in iron-depleted media and in macrophages. Moreover, the *B. anthracis* virulence in mice was attenuated with this mutation. However, the mutation ( $\Delta bacCEBF$ ) in the bacillibactin biosynthesis pathway did not show any impact on the growth of iron-depleted media or in macrophages. Additionally, no effect on the virulence in mice was observed [137].

The biosynthesis pathway, secretion, and uptake of siderophores in *B. anthracis* have been well studied [142,148-152]. However, there are few studies [5,6,185,186] about the global metabolism of *B. anthracis* during conditions similar to the ones found in the alveolar macrophage (iron starvation and oxidative stress). Existing studies are based on transcriptomic and proteomic analysis. Based upon a survey of the literature, no metabolomic studies have been carried out. For that reason, the goal of this study is to



understand the cellular behavior of the bacteria as a whole from a metabolic perspective. An *in silico* genome scale metabolic model was used to simulate the growth of the bacteria under different iron conditions.

This chapter presents the analyses of the metabolic adaptation of *B. anthracis* to different iron conditions. As a part of the study, the first genome-scale reconstruction of the metabolic network of *B. anthracis* Sterne 34F<sub>2</sub> was developed. It contains fully functional biosynthesis, secretion and uptake pathways for siderophores. The model was validated against experimental data for the growth of *B. anthracis*. The bacteria were grown in iron-poor media that had an iron concentration of 2.24  $\mu\text{M}$ , and in iron-rich media with a concentration of 20  $\mu\text{M}$ . During the experiments on both iron conditions, two metabolic states or phases were observed. The first phase, Phase I, was characterized by lactate production. In the second phase, referred to as Phase II, lactate was consumed. Thus, in total four models were analyzed: two models for Phase I under iron-poor/rich conditions, and two more for Phase II in iron-poor/rich cultures.

## **6.3.Methods**

### **6.3.1. GENETIC ALGORITHM/FLUX BALANCE ANALYSIS APPROACH (GAFBA v1.1)**

GAFBA v1.1 methodology has been explained in detailed in Chapter 3 and Chapter 4. However, in this subsection, the parameters for the genetic algorithm are

defined. The population size used was 30 chromosomes. The crossover probability was set to 70%, and the mutation probability was 1%. Elite selection was chosen as the selection strategy, with an elite fraction of 20%. Seven-point crossover was performed, and bottom re-seed was allowed, with a bottom re-seed frequency of every 100 generations. The GAFBA v1.1 algorithm was run for 2,000 generations per simulation, and 169 simulations in total were carried out. All simulations were implemented on a 2.7 GHz Intel Core i5 computer. Each simulation (2,000 generations) took about three hours. Thus, the total time for the 169 simulations was 28 days.

### **6.3.2 FLUX BALANCE ANALYSIS**

Flux Balance analysis was introduced in Chapter 2. However, in this subsection, the constraints applied to the specific case of *B. anthracis* are described. The media composition used was the one from the iron-poor/iron-reduced media (IRDM), or iron-rich/iron-replete media (IRM) [137]. The nutrient and secretion fluxes are defined in appendix A8.4. The upper and lower boundaries of the experimentally measured fluxes are presented in Table 11 for each of the four conditions. For the siderophores' experimental constraints, the Arnor Assay only allows for the measurement of total catechol siderophore. To get the specific values for petrobactin, bacillibactin, and protocatechuate, a ratio was calculated using experimental information [149,171]. Additional constraints to the model were defined based on the available experimental information. The upper boundaries for transport of the ferric-siderophore complexes were calculated using the maximum transport velocity based on the kinetic experiments for *B.*

*cereus* [187]. Furthermore, some regulatory constraints were applied to the model based on the experimental conditions and information from the literature. These constraints are defined in Appendix A8.9, along with a brief description of the rationale for the regulation, and all relevant citations. In all four models, 17 reactions were down-regulated based on media composition. The reaction responsible for iron transport was only down-regulated under iron-poor conditions in Phase II. It was hypothesized that under low iron concentrations, the iron was only taken up through the ferric-siderophore complex. The objective function chosen for the optimization problem was the maximization of the biomass reaction for *B. anthracis*. The biomass equations for each case are defined in Appendix A8.5-A8.8.

### **6.3.3. FLUX VARIABILITY ANALYSIS (FVA)**

FVA is a method that helps to investigate the metabolic network flexibility and redundancy [188]. FVA determines the range of values where the fluxes can change without affecting the value of the objective function [189]. The process starts by calculating the value of the objective function for the base type FBA problem. Then, FVA applies a series of optimization problems to maximize and minimize each of the fluxes of the metabolic network while keeping the value of the objective function fixed to the one found for the base type FBA solution [190].

FVA analysis was applied for each of the *in silico* simulations reported in here. It was found that the model of *B. anthracis* under iron-poor conditions during Phase II was

more flexible than in any of the other conditions. The number of fluxes with variable ranges was higher in iron-poor conditions at Phase II; meaning that *B. anthracis* metabolism under iron-poor conditions in Phase II had more alternative pathways and was more adaptable to changes in the environment.

## **6.4.Results**

### **6.4.1. METABOLIC NETWORK RECONSTRUCTION**

An existing pathway genome database (PGDB) from Pathways tools (PT) version 16.0 [68] was refined using Pathologic from PT. Then MetaFlux through the instantiation code [52] was used to create the specific reactions for the lipid biosynthesis pathway of the major fatty acids of *B. anthracis*, such as palmitic and stearic acids [191]. Later, GAFBA v1.1 [192] was used for evolving the initial model for *B. anthracis* under iron-poor condition Phase II (IRDM2). The following exchange fluxes were constrained to their experimentally calculated values: glucose uptake rate, carbon dioxide secretion rate, oxygen uptake rate, glutamic acid uptake rate, ferric iron uptake rate, petrobactin secretion rate, bacillibactin secretion rate and 3-4-dihydroxybenzoate (protocatechuate) secretion rate. The experimentally measured fluxes are presented in Table 11. GAFBA v1.1 was run for 169 simulations to evolve only the model of *B. anthracis* under iron-poor condition at Phase II. The gotten model was used to study the metabolism of the bacteria under the other three conditions by applying the experimentally measured fluxes

for each condition as presented in Table 11. Thus, only one model was created and it was evaluated under four experimental conditions. The model accounted for 1,003 metabolites and 1,049 reactions. All 1,003 metabolites could be found in the intracellular space, while 87 of them were also found in the extracellular space. Additionally, 1,007 (96%) reactions were intracellular, and 87 (4%) were exchange fluxes. The full model is presented in Appendix 8.

**Table 11. Experimentally measured fluxes for the growth of *B. anthracis* under iron-poor media and iron-rich media.** The secretion/uptake rates for nine metabolites were measured experimentally in all the conditions. IRDM1, iron reduced media Phase I. IRM1, iron-replete media Phase 1. IRDM2, iron-reduced media Phase 2. IRM2, iron-replete media Phase 2. Positives values are production rates. Negative values are uptake rates.

rates (mmol/gDW*h)	IRDM1	IRM1	IRDM2	IRM2
Glucose uptake rate	-12.29	-9.84	-13.16	-8.54
Carbon dioxide production rate	7.45	5.48	6.29	4.96
Lactate production/secretion rate	1.25	1.01	-0.97	-0.41
Oxygen uptake rate	-9.29	-7.62	-6.74	-4.65
Glutamate uptake rate	-2.92	-4.12	-0.27	-1.6
Iron uptake rate	-0.005	-0.01	-0.00075	-0.0028
Protocatechuate secretion rate	0	0	0.0241	0.008
Petrobactin secretion rate	0	0	0.0163	0.0055
Bacillibactin secretion rate	0	0	0.0023	0.00004

The biomass equation contained all the available published information for *B. anthracis* and other similar *Bacillus* such as *Bacillus cereus* and *Bacillus subtilis*. The ratios between the major biochemical components were adjusted based on data described

in the literature. Protein values were determined experimentally using the Biuret method [193,194]. RNA, DNA, and lipid values were taken from those determined for *B. cereus* [191,195,196]. The cell wall, ions, and cofactors were calculated using the available values for *B. subtilis* [197-199].

Lipids were classified as phospholipids and neutral lipids, and the relative ratios were taken from published information for *B. cereus* [196]. Then, the phospholipids were divided into cardiolipin, phosphatidylglycerol, phosphatidylserine, and phosphatidylethanolamine following the compositions presented by Koga *et al.* [200] for *B. cereus*. Neutral lipids were just represented as diglycerides [198]. The fatty acid compositions were determined using information for *B. anthracis*, and only the major fatty acids, stearic acid and palmitic acid, were included [191,201].

The biomass equation did not include lipoteichoic acids (LTA) since experimentally they have not been detected [202,203] in *B. anthracis* preparations. In *Staphylococcus aureus*, the product of the *ltaS* gene catalyzes the LTA synthesis. Although Garufi *et al.* [204] reported homologues of *ltaS* gene in the genome of *B. anthracis*, the LTA biosynthesis has not been fully characterized and the stoichiometric composition of LTA in the biomass has not been quantified.

Teichoic acids were not included in the biomass equation since the low phosphate content of the bacteria cell wall does not allow its presence in the cell [202,205].

Furthermore, no gene associated with the teichoic acid biosynthesis pathway has been characterized [204,206]. Finally, the teichoic acid constituents have not been found in *B. anthracis* envelope preparations [207].

The stoichiometric coefficient of iron in the biomass equation was taken from *B. subtilis* growing in iron-rich conditions. No problems were found with this coefficient during Phase I under both iron conditions or in iron-rich conditions during Phase II. Nevertheless, in iron-poor conditions during Phase II (IRDM2), the experimentally measured iron uptake rate was not enough to fulfill the requirements of iron for biomass production using the *B. subtilis* coefficient. Thus, the stoichiometric coefficient was adjusted using the experimentally measured growth rate and iron uptake rate under the assumption that all the iron consumed was only for biomass production. This assumption is based on the observation that many bacteria under iron starvation conditions redistributed the intracellular iron for the most critical cellular functions such as production of nucleic acids and amino acids, which are critical components for biomass production [169,179,208,209]. The resulted biomass equations for each condition are presented in Appendix 8.

The non-growth associated maintenance (NGAM) was set to  $5.47 \text{ mmol gDW}^{-1}\text{h}^{-1}$  based upon the average of the experimentally measured values for different *Bacilli* [138,210,211]. The growth-associated maintenance (GAM) was initially calculated using the protocol from Thieles *et al.* [3]. However, the *in silico* calculations

of the growth rate were higher than the experimentally determined growth rate for each of the four cases. A likely explanation for this observation is that *B. anthracis* may be expending energy in other processes not accounted for in the model. Furthermore, the effect of the changes in GAM on the *in silico* growth rate was determined following Puchalka *et al.*'s approach [189] of keeping NGAM as a constant. From these analyses, it was clear that the GAM needed to be increased. Through the Thieles *et al.* [3] methodology, only the energy required for macromolecular synthesis was taken into account. Thus, an increase in GAM would include additional processes that require ATP such as re-polymerization of degraded molecules, ATP consumption due to leaks, futile cycles, and ATP consumed for maintenance of concentration gradients and electrical potential [21,212]. As a consequence, the values selected for GAM were those that led to a better match between *in silico* growth rate and the experimental growth rate values. The NGAM, GAM, *in silico* growth rate, and experimental growth rate for each case is presented in Table 12. Interestingly, the GAM values were of the same order of magnitude as the reported value for *Bacillus megaterium* of 56.82 mmol /gDW\*h [211].

**Table 12. NGAM, GAM, *in silico* growth rate, and experimental growth rate comparison for the four cases.** IRDM1 – iron-reduced media (iron-poor) Phase I. IRM1 – iron-replete media (iron-rich) Phase 1. IRDM2 – iron-reduced media (iron-poor) Phase 2. IRM2, iron-replete media (iron-rich) Phase 2.

	IRDM1	IRM1	IRDM2	IRM2
NGAM (mmol/gDW*h)	5.47	5.47	5.47	5.47
GAM (mmol/gDW)	43.5	26.5	64.2	56.6
<i>In silico</i> growth rate (h <sup>-1</sup> )	1.149	1.252	0.359	0.498
Experimental growth rate (h <sup>-1</sup> )	1.15	1.25	0.372	0.504



#### 6.4.2. SIDEROPHORES BIOSYNTHESIS, SECRETION, AND UPTAKE PATHWAYS

*B. anthracis* produces two known siderophores: bacillibactin and petrobactin. Additionally, protocatechuate (3,4-DHB), one of the precursors of petrobactin, has been detected in the broth of *B. anthracis* [149,167,213]. However, its function as a siderophore is not well studied. Zawadzka *et al.* [187] reports that 3,4-DHB can serve as a siderophore in *B. cereus*. They calculated the stoichiometry ratio of ferric-siderophore complex formation with 3,4-DHB, which equals 1:3 iron to ligand. Furthermore, they characterized the membrane-associated substrate-binding proteins (SBPs) for transport of ferric-3,4-DHB. As a consequence, protocatechuate was added to the model as a potential siderophore for *B. anthracis*.

A schematic representation of protocatechuate, petrobactin, and bacillibactin biosynthesis, secretion, uptake of ferric-siderophore complex, and release of iron from ferric-siderophore complex is presented in Figure 28. Additionally, the biosynthesis pathways, specifically for petrobactin, protocatechuate and bacillibactin, are shown in Appendix 7 at Figure S29 and S30. The pathways included the associated gene for each reaction if it had been characterized.

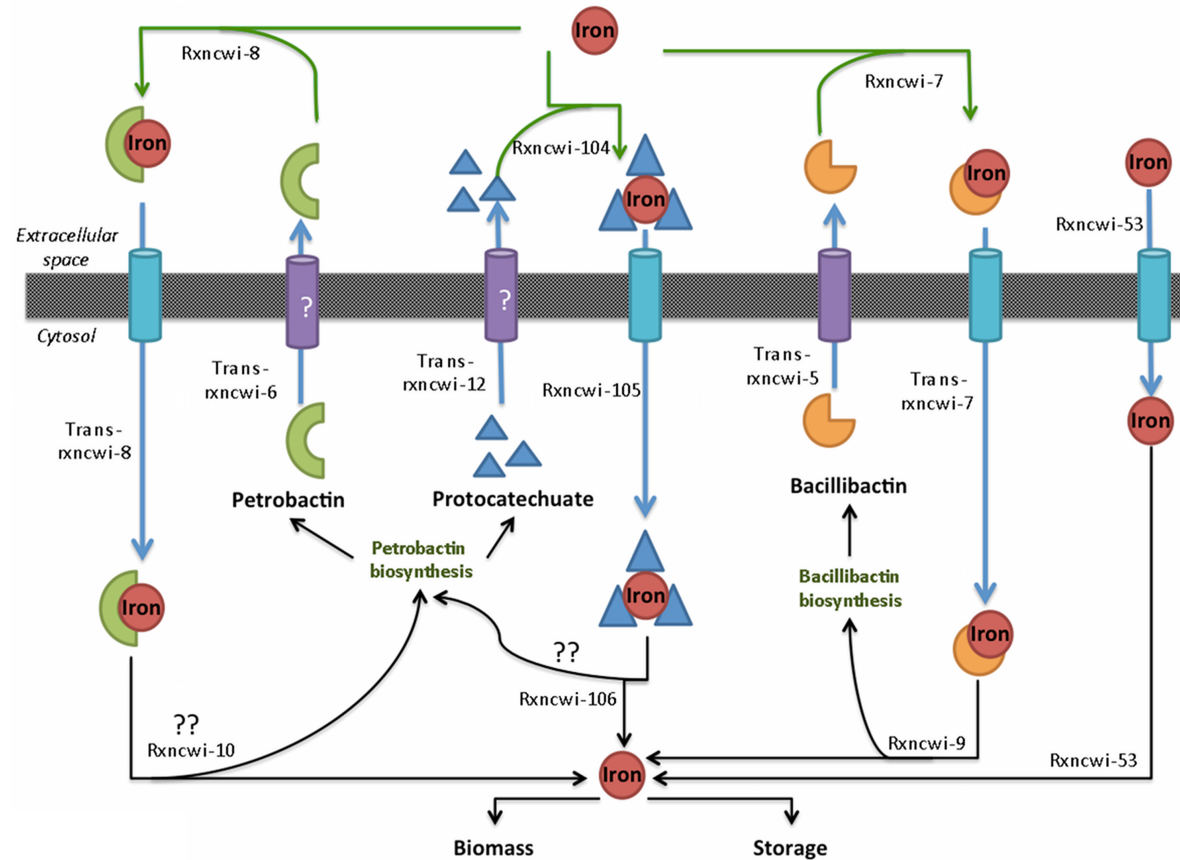


**Figure 28. Representation of the siderophore secretion, iron loading, ferric-siderophore complex uptake, and iron release from ferric-siderophore complex.** The name of each reaction in the model appears next to the schematic reaction. The question marks represent reactions without an assigned gene. Green arrows are extracellular reactions, blue arrows are transport reactions, and black arrows are intracellular reactions. Blue cylinders are uptake transporters and purple cylinders are secretion transporters.

The gene cluster *asb*ABCDEF has been determined to be responsible for the biosynthesis of petrobactin from spermidine, 3,4-dihydroxybenzoic acid, and citrate [150,151]. Once petrobactin is synthesized, it is exported out of the cell. The mechanism of the secretion of petrobactin has not been characterized. However, a simple reaction was added to the model because petrobactin has been detected outside the cell in different experiments [137,148,149,167,213]. Then, petrobactin is loaded with iron ion through a spontaneous reaction. Next, the ferric-petrobactin complex is imported into the cell through an ATP-binding cassette (ABC), which was identified in previous works [142,152,175,187]. Finally, the iron is released from the ferric-siderophore complex. There was no available information for ferric-petrobactin iron release. Thus, the mechanism for iron release was chosen using the characteristic of aerobactin, a similar siderophore of petrobactin as a guide [150]. The Ferric-siderophore formation constants are similar for both siderophores:  $K_f^{petrobactin} = 10^{23}$  [142], and  $K_f^{aerobactin} = 10^{22.93}$  [214]. As a result, they should have similar redox potentials, which for aerobactin is -336 mV [214]. This redox potential falls in the range of physiological reductants. Therefore, iron is likely released from the ferric-petrobactin complex through a reduction of ferric ion to ferrous ion using flavins such as FMN, followed by a dissociation of the siderophore [177,215-217]. Finally, petrobactin is recycled to its precursors because no evidence has been found that *B. anthracis* accumulates or secretes the isomeric precursor (3,4-DHB attached to the 4-carbon end of spermidine) [150].

Protocatechuate is synthesized in the first step of petrobactin biosynthesis (Figure S29) from 3-dehydroshikimate. Then, protocatechuate is secreted out of the cell through an unknown mechanism, represented as a simple diffusion reaction in the model. Protocatechuate spontaneously loads itself with iron following the stoichiometric experimentally-determined ratio of 1:3 iron to ligand [187]. Next, an ATP-binding cassette (ABC) transports the ferric-protocatechuate complex into the cell. It has been reported that FatB enzyme is responsible for this transport [142,187]. Then, a binding site protonation and/or conformational change releases the iron from the ferric-protocatechuate complex [177]. Finally, protocatechuate is recycled into its metabolism.

The *dhb* operon encodes the bacillibactin biosynthesis pathway [142] as shown in supplementary Figure S30. An MFS-type transporter exports bacillibactin as it is reported for *B. subtilis* [174,218] and *B. anthracis* [142]. Next the ferric-bacillibactin complex spontaneously forms. Then the FeuABC system is responsible for the uptake of the iron-loaded siderophore through an ABC type porter [142,174,218]. The iron release from the ferric-siderophore complex is more difficult than in petrobactin because of its high formation constants,  $K_f^{bacillibactin} = 10^{47.6}$  [142], which results in a lower redox potential that is out of the range of physiological reductants [219]. However, it has been reported that for *B. subtilis*, an esterase, BesA encoded in the gene locus *yuiI*, carries out the enzymatic hydrolysis of the ferric-bacillibactin complex [174,220]. Homologues of this gene were found in *B. anthracis* [142]. As a consequence, the model included the release of iron from the ferric-bacillibactin complex as an enzymatic hydrolysis. Finally, bacillibactin is recycled to its precursors.

Iron ions are then transported into the cell through the ferric-siderophore complex or through the iron-ABC transport system. The iron may be used for biomass synthesis, or it could be stored as shown in Figure 24. The iron storage in the model was represented through a hypothetical metabolite, which represents ferritin or the miniferritin DpS2. Both iron storage proteins have been found in *B. anthracis* [147,221].

#### **6.4.3. MODEL APPLICATION: METABOLIC ADAPTATION TO IRON-POOR CONDITIONS BY *B. ANTHRACIS***

The model of *B. anthracis* was used to study the behavior of the bacteria under different iron conditions. The experimentally measured fluxes were used as constraints on the model. A total of four models were studied: iron-poor Phase I, iron-rich Phase I, iron-poor Phase II, and iron-rich Phase II. The flux distributions from the models were compared to find possible variations in the metabolism.

##### **6.4.3.1. Comparison of the iron-poor and iron-rich cell metabolomes at Phase I.**

A comparison of the major pathways in *B. anthracis* under iron-poor conditions was made with those in iron-rich conditions. During the Phase I experiments, no siderophores were detected in either of the two iron conditions. These results are in agreement with the reported information that the production of siderophores starts in the middle of the exponential phase and reaches a maximum in the stationary phase

[149,167]. As a consequence, the biosyntheses of petrobactin, bacillibactin, and protocatechuate were down-regulated in iron-poor and iron-rich conditions.

Figures 29a-29b show the amino acid uptake rates. The amino acids found in the media, only three were not taken up in either of the two conditions: isoleucine (I), methionine (M), and proline (P). Aspartate (D) uptake was up-regulated in iron-poor conditions, and valine (V) uptake was up-regulated in iron-rich conditions. Meanwhile, for the rest of the amino acids, the uptake rates showed minor changes between the two iron conditions. Serine (S) was the exception since its uptake was three-folds higher in iron-rich than in iron-poor conditions. Pyruvate and ammonia were produced from the degradation of serine. The fluxes through the biosynthesis reactions for most of the amino acid were the same at both conditions, as shown in Figure 29c, excluding aspartic acid (D) and valine (V). The flux through aspartate biosynthesis reaction was higher by 3.5-fold in iron-rich conditions. Meanwhile, the flux through valine biosynthesis reaction was five-fold higher in iron-poor conditions compared to iron-rich conditions.

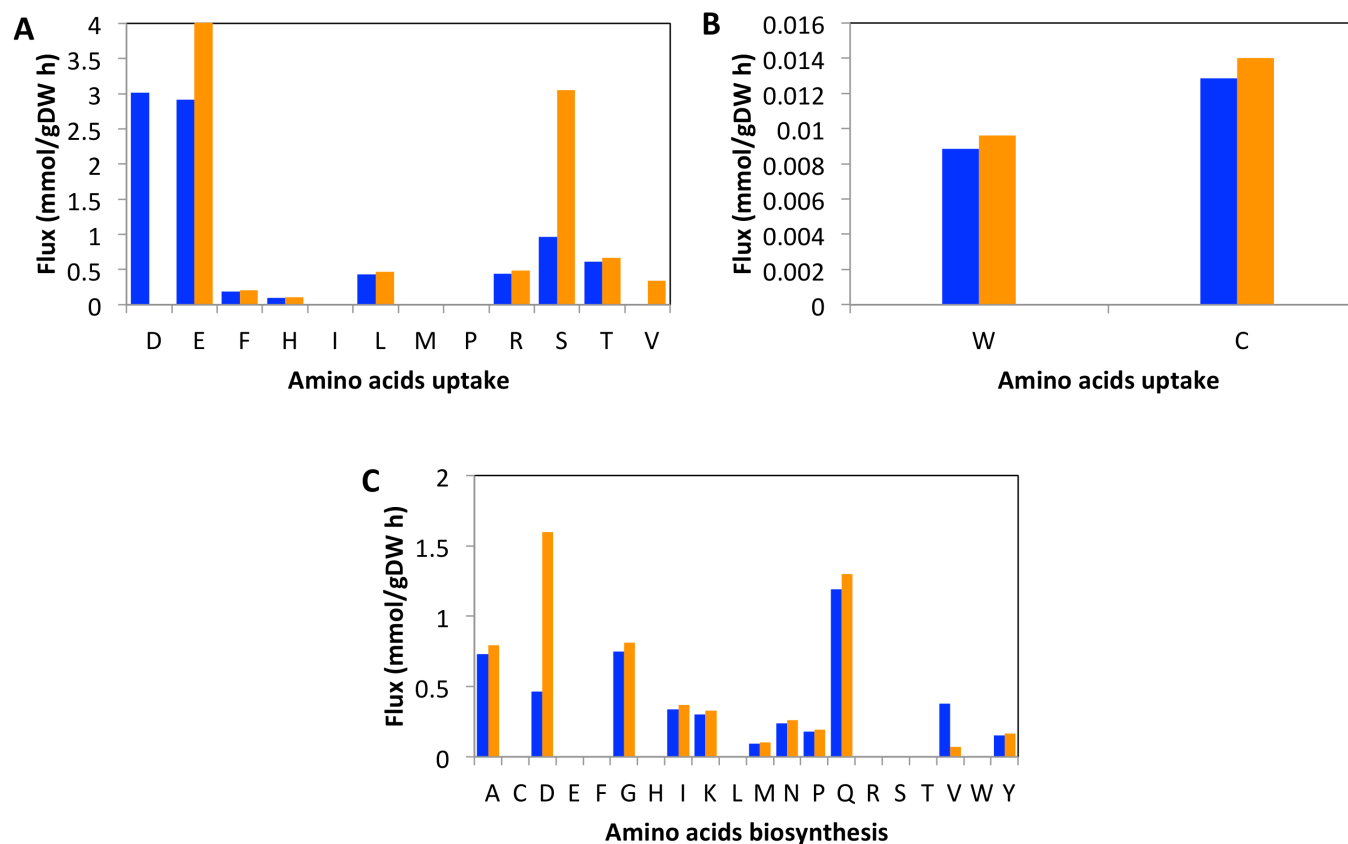


**Figure 29. Comparison of the amino acid uptake and biosynthesis in *B. anthracis* under iron-poor/rich conditions at Phase I.** The blue columns are iron-poor conditions, and orange columns are iron-rich conditions. The x-axis labels represent the single letter amino acid abbreviations. Only the amino acids in the defined media were allowed to be taken up. (A) and (B) Amino acids uptake. (C) Amino acid biosynthesis.

The glycolysis pathway and the pentose phosphate pathway had only slight changes in the flux distribution in both conditions. These pathways are shown in Appendix 7 at Figures S31 and S32. However, the fluxes through glycolysis were higher in iron-poor conditions than in iron-rich conditions, because more glucose was feeding into the system in iron-poor conditions. Furthermore, it was observed that most of the flux that entered the glycolysis pathway went to the final step into pyruvate without diverging to any other pathways in both iron conditions. The oxidative branch of the pentose phosphate pathway was inactive under both iron conditions. Meanwhile, the non-oxidative branch had similar fluxes in both conditions.

The TCA cycle was active under the two iron conditions, with similar fluxes at the four initial reactions from oxaloacetate to 2-oxoglutarate as shown in Figure 30. Beyond that, the fluxes were 1.6-fold higher in iron-rich conditions compared to iron-poor conditions until fumarate. This increase was a result of the assimilation of the glutamic acid taken from the media since its uptake rate was higher in iron-rich conditions. Next, at the fumarate hydratase reaction (E.C. 4.2.1.2), the flux in iron-poor conditions was higher than in iron-rich conditions. This observation can be explained with the assimilation of aspartate through the aspartase reaction (E.C. 4.3.1.1). This reaction consumed the aspartate taken from the media and produced ammonia and fumarate. At (S)-malate the flux was divided, going back to oxaloacetate through the malate dehydrogenase reaction (E.C. 1.1.1.37) or to pyruvate through the malate dehydrogenase-decarboxylating reaction (E.C. 1.1.1.40). The fluxes were similar under



both conditions for the malate dehydrogenase reaction. However, for the malate dehydrogenase-decarboxylating reaction, the fluxes were higher in iron-poor conditions. The explanation for this phenomenon was that the assimilation of the amino acids through the TCA cycle was incorporated into oxaloacetate and pyruvate metabolism equitably in iron-rich conditions. On the contrary, pyruvate metabolism was preferred as the final step of the TCA cycle under iron-poor conditions.

The secretion of byproducts was similar under both conditions. Acetate and formate secretions were higher in iron-poor conditions. Meanwhile, a slight difference was observed between the values at iron-poor and iron-rich conditions in the ethanol secretion and lactate secretion fluxes. The comparison of the fluxes is presented in Appendix 7 at Figure S33.

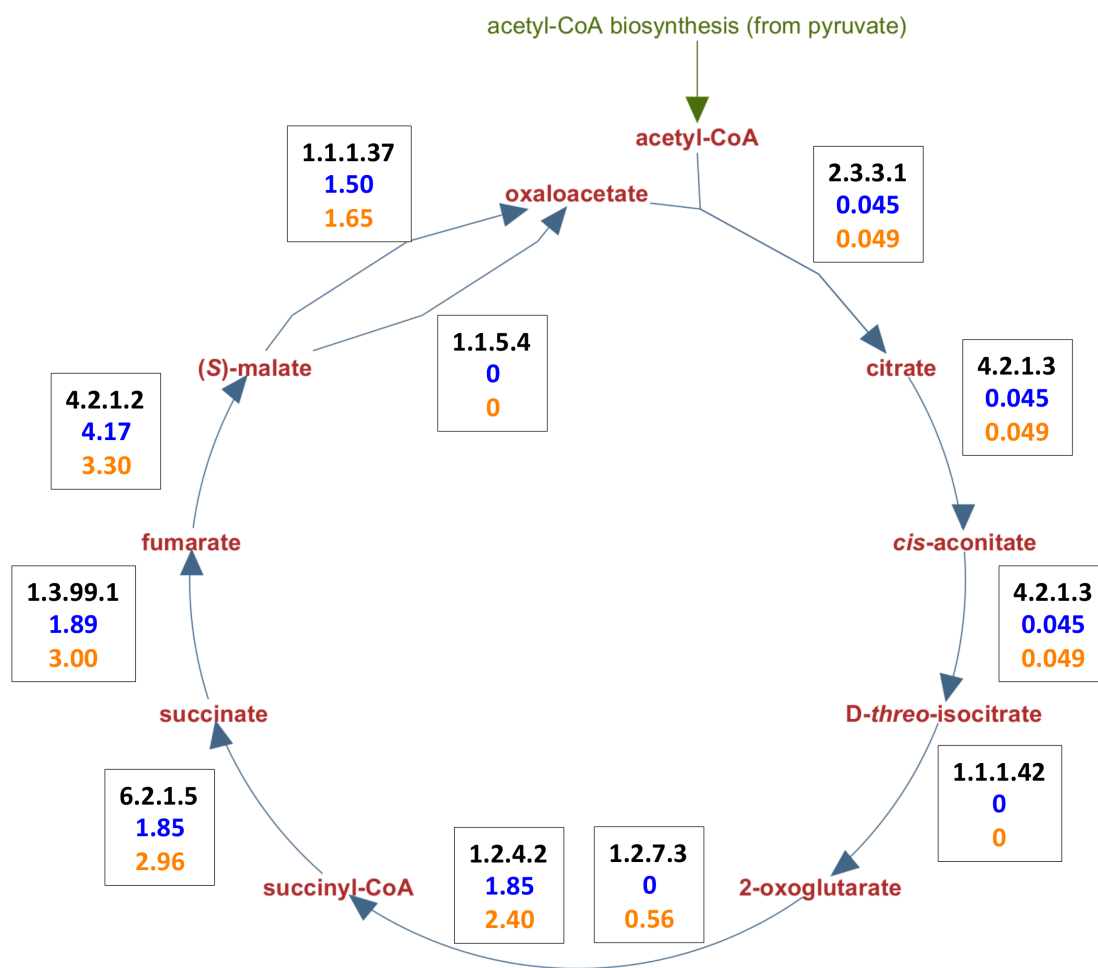


**Figure 30. Comparison of the TCA cycle pathway under iron-poor and iron-rich conditions at Phase I.** The words in red represent metabolites. The rectangular boxes have at the top line the E.C. number for each reaction; the blue numbers correspond to the flux values under iron-poor conditions, and the numbers in orange are the flux values under iron-rich conditions.

#### 6.4.3.2. Comparison of the iron-poor and iron-rich cells metabolomes at Phase II.

The biosynthesis pathways of the siderophore were active under both iron conditions during Phase II. The fluxes through the bacillibactin production were two

orders of magnitude higher in iron-poor conditions than those in iron-rich conditions, as shown in Figure 31. Meanwhile, the fluxes through the petrobactin and protocatechuate biosynthesis pathway were three-fold higher in iron-poor than in iron-rich conditions. Figure 32 provides a schematic representation of the petrobactin and protocatechuate biosynthesis pathways.

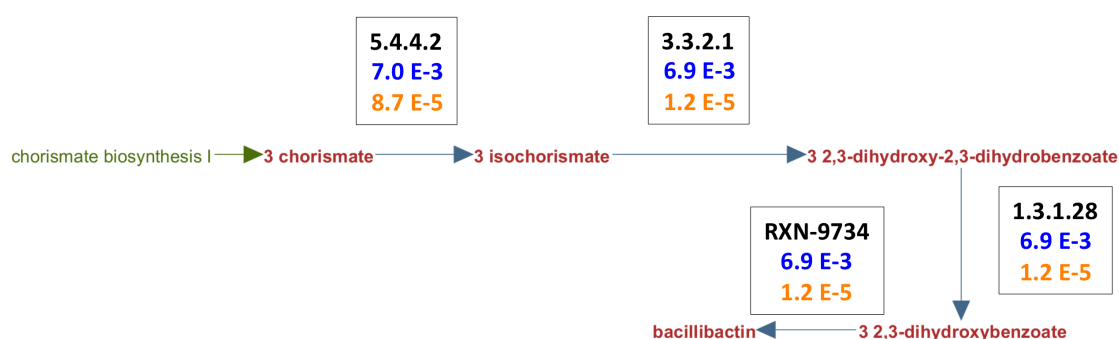


**Figure 31. Comparison of the bacillibactin biosynthesis pathway under iron-poor and iron-rich conditions during Phase II.** The words in red represent metabolites. The rectangular boxes have at the top line the E.C. number for each reaction. If no E.C. has been assigned to the reaction; the corresponding reaction's name is shown instead. The blue numbers correspond to the flux values at iron-poor conditions, and the numbers in orange are the flux values at iron-rich conditions.

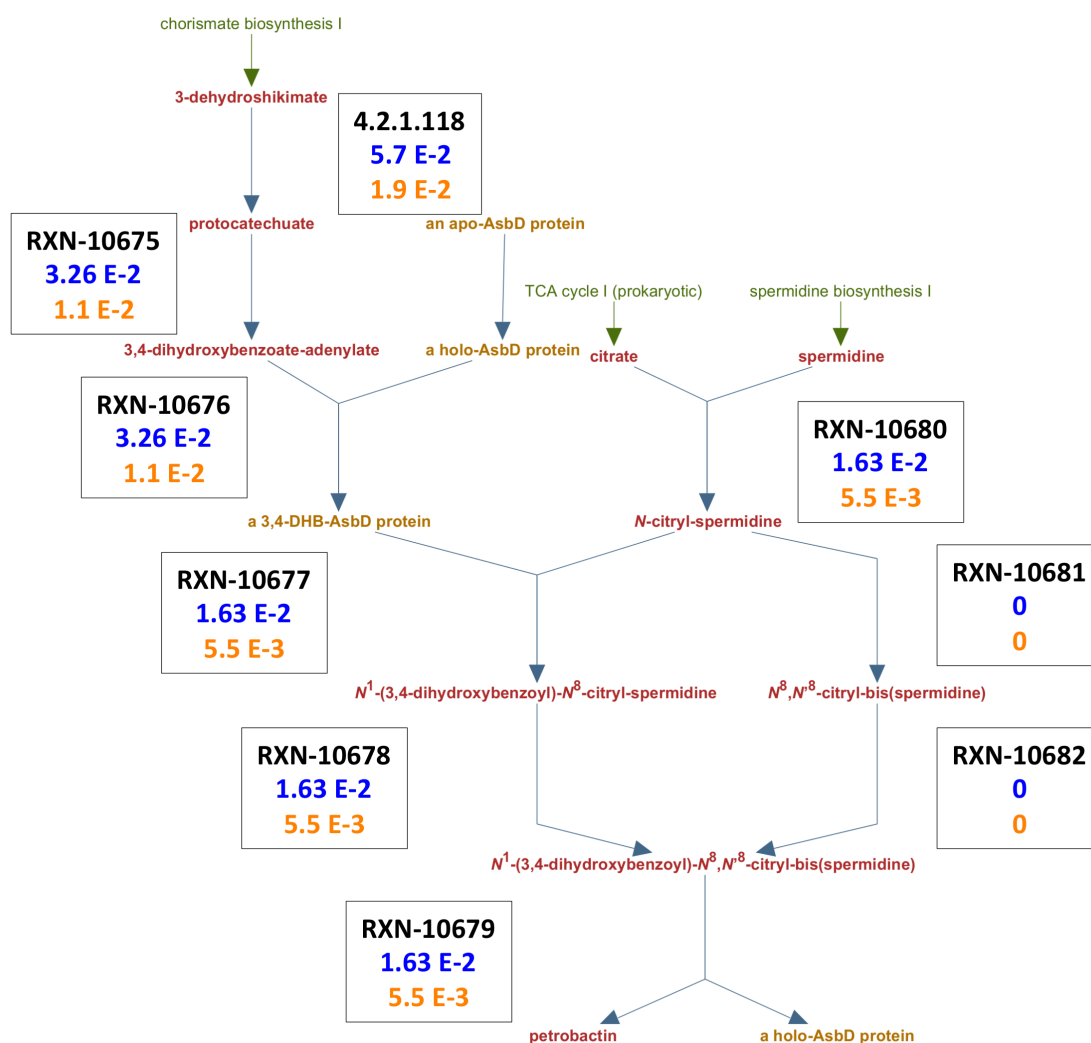


**Figure 32. Comparison of the protocatechuate and the petrobactin biosynthesis pathway under iron-poor and iron-rich conditions during Phase II.** The words in red represent metabolites. The rectangular boxes have at the top line the E.C. number for each reaction. If not E.C. has been assigned to the reaction; the corresponding reaction's name is shown instead. The blue numbers correspond to the flux values at iron-poor conditions, and the numbers in orange are the flux values at iron-rich conditions.

The effect of iron on the petrobactin biosynthesis pathway was not as marked as the changes in the bacillibactin biosynthesis pathway between iron-poor/rich conditions.

The bacillibactin pathway was severely affected by the presence of iron in the media. Under iron-rich conditions, the fluxes were down-regulated to values near zero. This is in agreement with Carlson *et. al.* [6], who observed in their transcriptional profiling that the genes of the petrobactin biosynthesis pathway were not significantly up-regulated during iron deprivation. On the contrary, genes from bacillibactin appeared to be most strongly induced during iron starvation. Furthermore, previous studies have reported that petrobactin production is not repressed by an increase in iron concentration [148,149,171]. Additionally, bacillibactin biosynthesis is highly regulated at the transcriptional level by iron concentration [171].

The model included protocatechuate (3,4-dihydroxybenzoate) as a siderophore. Under iron-rich conditions, iron was transported into the bacteria primarily through active transport. A small amount was also transported via the ferric-protocatechuate complex. Meanwhile, in iron-poor conditions, the transport of iron into the bacteria was mainly through the ferric-protocatechuate complex transport and ferric-bacillibactin complex transport. It was surprising that petrobactin did not contribute to iron transport. To explain this situation, it is necessary to take into account three factors. First, Zawadzka *et al.* [187] reported common transporter routes for the uptake of ferric-petrobactin and ferric-protocatechuate complexes in *B. cereus*, which had a higher affinity for ferric-protocatechuate than for ferric-petrobactin. Second, the dissociation of ferric-protocatechuate complex is through a protonation and/or conformational change within the complex, which is easier than the reduction of ferric ion to ferrous ion using flavins.

Third, the rate of transport for ferric-petrobactin is higher than ferric-protocatechuate, Thus, it is hypothesized that petrobactin is functional as an iron transporter under severely reduced iron concentrations, which were not reached under the experimental conditions used throughout the analysis in this work. Under severely reduced iron concentrations, the faster ferric-petrobactin transport rate will overcome the difficulty of releasing the iron from the ferric-petrobactin complex.

More amino acids were consumed under iron-rich conditions than in iron-poor conditions, as is shown in Figures 33a and 33b. Cysteine (C) and threonine (T) were only taken up under iron-rich conditions. Meanwhile, aspartate (D) and serine (S) uptake were 1.6-fold higher in iron-poor conditions than in iron-poor conditions. In contrast, the uptake of glutamate (E) and histidine (H) were five-fold higher and four fold higher respectively in iron-rich conditions versus iron-poor conditions.

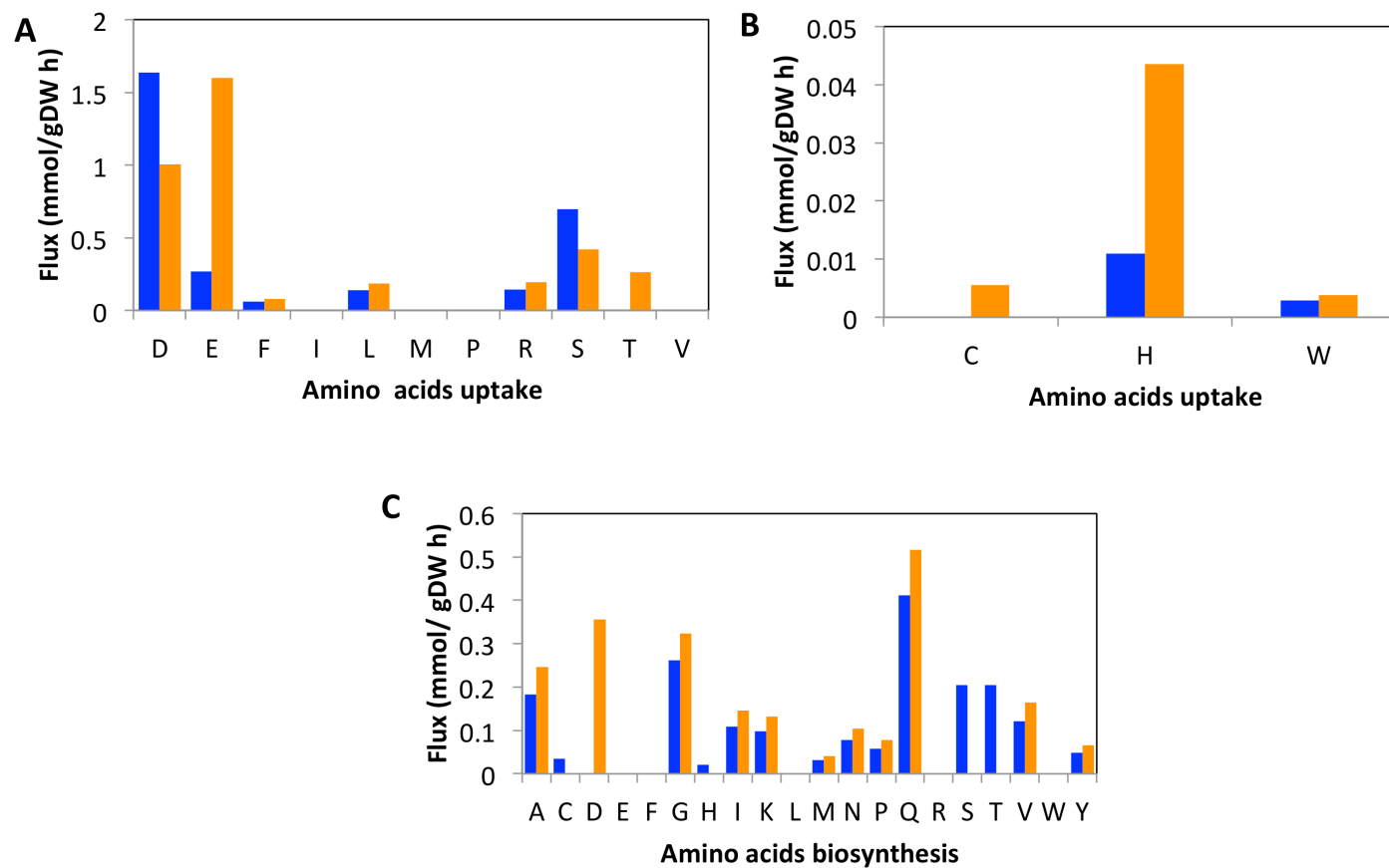


**Figure 33. Comparison of the amino acid uptake and biosynthesis in *B. anthracis* under iron-poor/rich conditions at Phase II.** The blue columns are iron-poor conditions, and orange columns are iron-rich conditions. The x-axis labels represent the single letter amino acid abbreviations. Only the amino acids in the defined media were allowed to be taken up. (A) and (B) Amino acids uptake. (C) Amino acid biosynthesis.

The comparison of the fluxes through the biosynthesis reactions of amino acids under the two conditions is presented in Figure 33c. Cysteine (C), histidine (H), serine (S), and threonine (T) were produced only in iron-poor conditions. Meanwhile, the flux through the biosynthesis reaction of aspartate (D) was only active in iron-rich conditions.

Clearly, the iron status of the cell affected the transport of amino acids, which resulted in an up-regulation of the biosynthesis of some amino acids in iron-poor conditions. Many amino acid permease family proteins have been reported as down-regulated during iron starvation in the transcriptional profile of *B. anthracis* [6]. Furthermore, Friedman *et al.* [168] reported an up-regulation of cysteine synthetase in *S. aureus* under iron-poor conditions. Moreover, in the transcriptional profile of *B. anthracis* [6], the gene associated with histidinol phosphate aminotransferase was up-regulated under iron-poor conditions. This reaction is part of the histidine biosynthesis pathway.

The Glycolysis pathway schematic is represented in Appendix 7 at Figure S34. The differences between the fluxes through the glycolysis pathway under iron-poor/rich conditions were not significant. Similarly to Phase I, the fluxes through glycolysis in the iron-poor condition were slightly higher than in the iron-rich condition, as a result of the higher glucose uptake rate. Additionally, two bifurcation points along the glycolysis pathway were found: one from D-fructose-6-phosphate into the pentose phosphate pathway; and a second one from 3-phospho-D-glycerate into the serine biosynthesis.



The non-oxidative branch of the pentose phosphate pathway was higher in iron-poor conditions by as much as six to eight times as is presented in Figure 34. This pathway resulted in a net production of ribose-5-phosphate (R5P) and erythrose-4-phosphate (E4P). E4P was used in the synthesis of 3-dehydroshikimate, which is part of the biosynthesis of petrobactin and bacillibactin.. Meanwhile, R5P was the precursor of 5-phosphoribosyl diphosphate (PRPP). PRPP is a key component in histidine biosynthesis, which was up-regulated under iron-poor conditions. Furthermore, PRPP is part of the adenine salvage pathway, which is connected with the autoinducer-2 (AI-2) biosynthesis pathway.

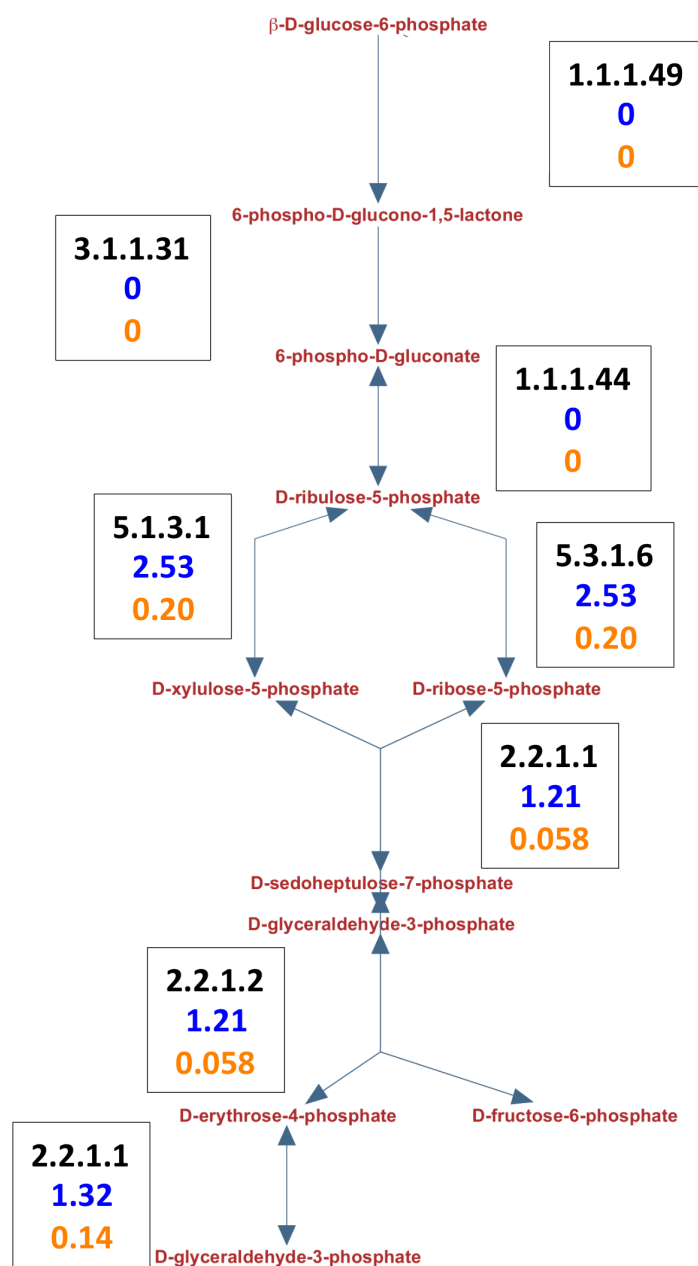


**Figure 34. Comparison of the pentose phosphate pathway under iron-poor and iron-rich conditions during Phase II.** The words in red represent metabolites. The rectangular boxes have at the top line the E.C. number for each reaction. The blue numbers correspond to the flux values at iron-poor conditions, and the numbers in orange are the flux values at iron-rich conditions.

AI-2 biosynthesis pathways were more active under iron-poor conditions than in iron-rich conditions. A schematic of this pathway is shown in Figure 35. AI-2 is not directly linked to iron metabolism. It is known to be a signaling molecule used in quorum sensing. Nevertheless, in a proteomic analysis of *Yersenia pestis*, the S-ribosylhomocysteinase lyase (LuxS) enzyme which is required for AI-2 synthesis, was found to be moderately increased in iron depleted conditions [222]. In other bacteria such as *Actinobacillu actinomycetemcomitans* [223,224], *Vibrio vulnificus* [225], and *Pophyromonas gingivalis* [223] it has been suggested that the *luxS* gene may regulate aspects of iron acquisition. Further, in *A. actinomycetemcomitans* [224] and *A. pleuropneumoniae* [226], it has been shown that growth under iron depletion could be regulated by LuxS through AI-2 production. From this result and the available information, it is hypothesized that AI-2 may help *B. anthracis* during growth in iron-poor conditions. It was not possible through the modeling analysis to determine its relation to the regulation of iron acquisition systems. This should be further investigated experimentally.

One of the byproducts of AI-2 biosynthesis is adenine, which was recycled into the adenine nucleotide pool through adenine phosphoribosyltransferase (E.C. 2.4.2.7). It consumed PRPP and adenine in order to produce AMP. In this way, more AMP is available for the production of adenosine nucleotides through the *de novo* biosynthesis pathway.

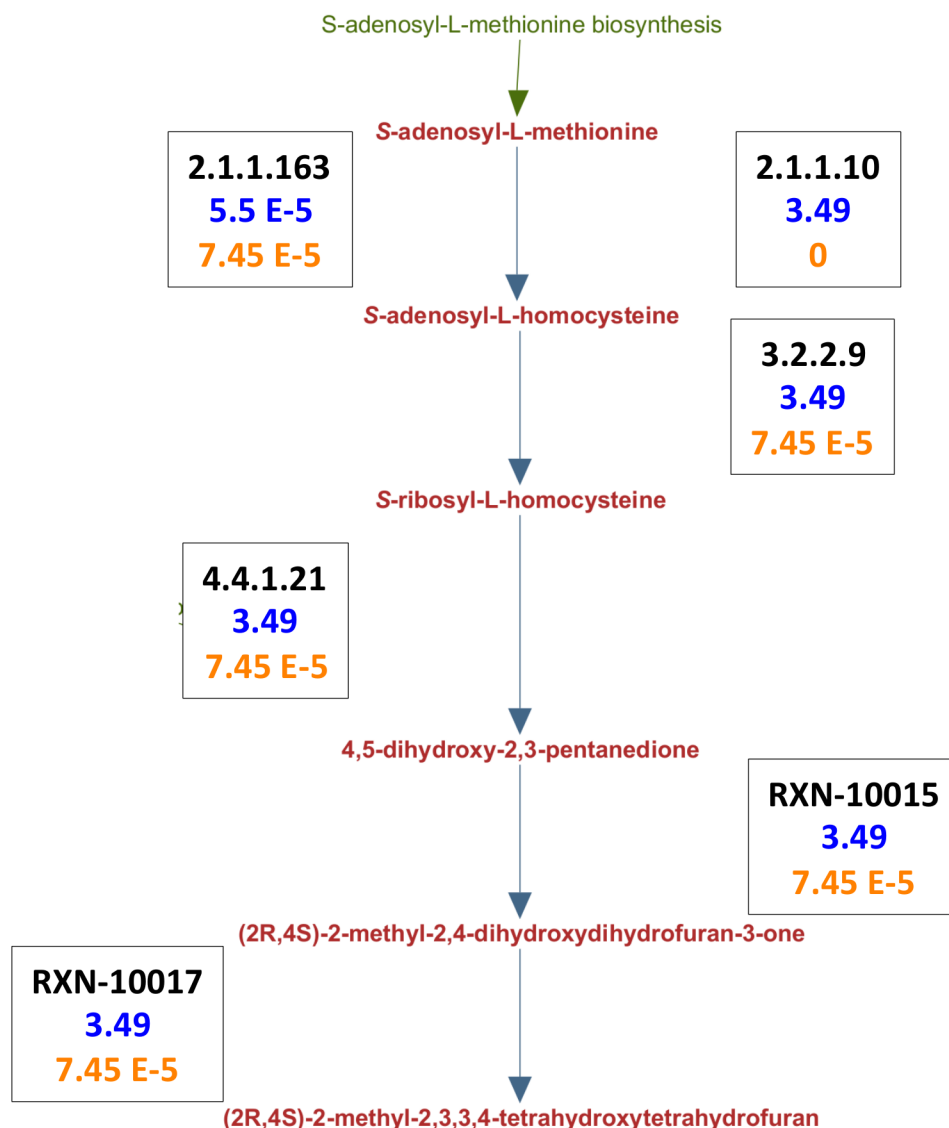


**Figure 35. Comparison of the autoinducer-2 (AI-2) biosynthesis pathway under iron-poor and iron-rich conditions during Phase II.** The words in red represent metabolites. Rectangular boxes have at the top line the E.C. number for each reaction. If no E.C. has been assigned to the reaction; the corresponding reaction's name is shown instead. The blue numbers correspond to the flux values at iron-poor conditions, and the numbers in orange are the flux values at iron-rich conditions.

The flux through the TCA cycle from oxaloacetate to 2-oxoglutarate was five-fold higher in iron-poor than in iron-rich conditions, as is presented in Figure 36. The TCA cycle was down-regulated in iron-poor conditions from 2-oxoglutarate to fumarate. The fumarate hydratase reaction (E.C. 4.2.1.2) was 8.6-fold higher in iron-rich cultures than in iron-poor cultures. The malate dehydrogenase reaction (E.C. 1.1.1.37) went in the opposite direction under each condition. Specifically, in iron-poor conditions, the malate dehydrogenase reaction consumed oxaloacetate to produce (S)-malate. The opposite happened under iron-rich conditions. This behavior resulted from the inactivation of the phosphoenolpyruvate carboxykinase reaction (E.C. 4.1.1.49) under iron-poor conditions. Thus, the oxaloacetate produced from side reactions was converted to (S)-malate, and then pyruvate. However, in iron-rich conditions, oxaloacetate was consumed to produce phosphoenolpyruvate through the phosphoenolpyruvate carboxykinase reaction. Friedman *et al.* [168] reported a decrease in the activity of phosphoenolpyruvate carboxykinase under iron-poor conditions in *S. aureus*. Three more reactions from the TCA cycle have been reported to decrease under iron starvation conditions in *S. aureus* [168] and *B. subtilis* [169,208]: succinate dehydrogenase, fumarate hydratase, and aconitate hydratase.. The model predicted the inactivation of succinate dehydrogenase and the downregulation of fumarate hydratase. However, aconitate hydratase was up-regulated.

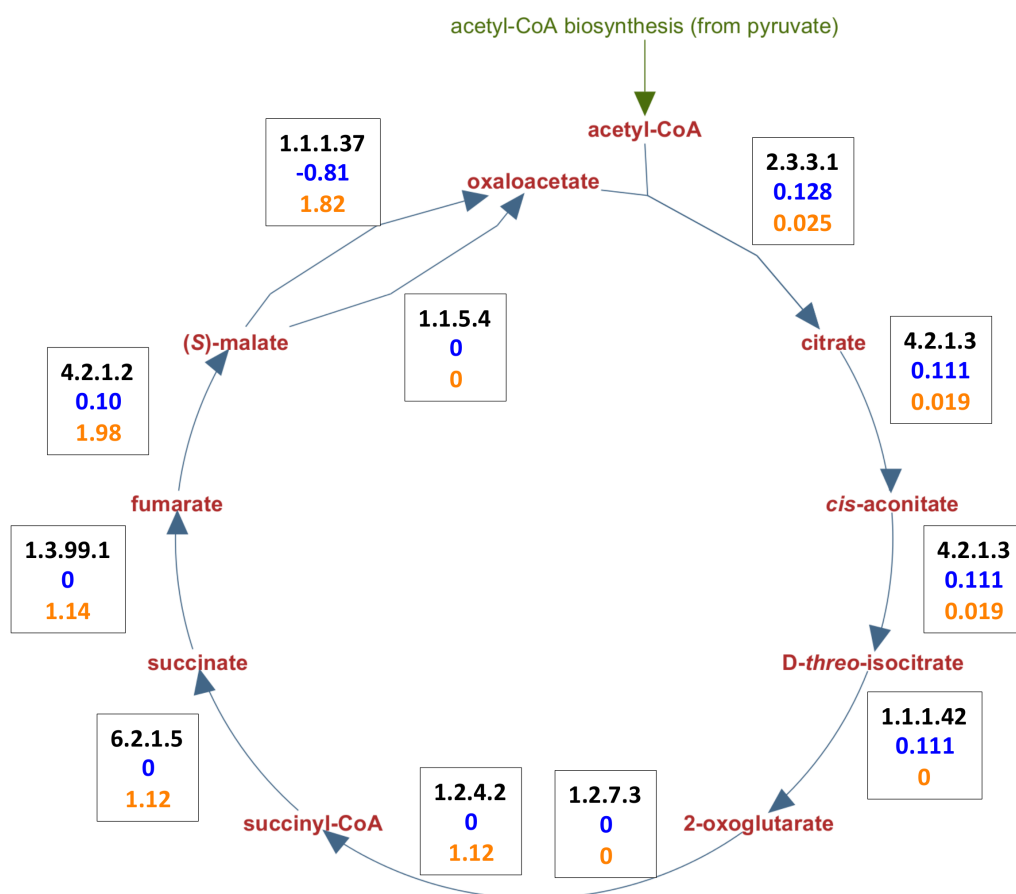


**Figure 36. Comparison of the TCA cycle pathway under iron-poor and iron-rich conditions during Phase II.** The words in red represent metabolites. The rectangular boxes have at the top line the E.C. number for each reaction, the blue numbers correspond to the flux values at iron-poor conditions, and the numbers in orange are the flux values at iron-rich conditions. The negative flux value indicates that the flux is going in the other direction than the one displayed on the diagram.

The differences in the byproduct secretion between the iron-poor/rich conditions were not significant, as is shown in Appendix 7 at Figure S35. Formate and ethanol secretion were almost the same under both conditions, and acetate was only 0.85-fold higher in iron-poor conditions than in iron-rich conditions. During Phase II, lactate was

consumed. This behavior was independent of the iron status of the cell. It was not possible to explain this shift with the available experimental information. However, the model predicted that during Phase II, the two enzymes involved in lactate metabolism would be active, as is shown in Appendix 7 at Figure S36. Lactate dehydrogenase produced lactate from pyruvate. Then, lactate was converted back to pyruvate through lactate oxidoreductase. Similar cycling behavior between lactate dehydrogenase and lactate oxidoreductase was reported in *S. aureus* under nitric oxide stress [166].

Additionally, lactate metabolism was up-regulated under iron-poor conditions. The lactate permease increased 2.5-fold. Meanwhile, the lactate dehydrogenase and lactate oxidoreductase increased 1.4-fold. The transcriptional profile of *B. anthracis* [6] reported an up-regulation of lactate permease and lactate dehydrogenase under iron deprivation conditions. However, lactate oxidoreductase was not reported, probably because the gene has not been experimentally characterized and has only been found through bioinformatic approaches [164].

## **6.5. Discussion**

In this study, I have presented a genome scale metabolic model for the causative agent of anthrax, *B. anthracis*. The model was constructed with all available information from the literature concerning the bacteria, and has been well curated. A comprehensive biomass equation was constructed using information from related *Bacillus* species, as

well as from directly measured experimental components. Although it was not possible to find information regarding the energy requirements of the bacteria, a methodology was applied to get an estimation [189].

The analysis of metabolism under different iron conditions proved the predictive capability of the model. Many of the reactions and behavior observed during the analysis have been reported before for *B. anthracis* and other bacteria under similar study conditions, such as the down-regulation of some of the reactions during the TCA cycle in Phase II under iron-poor conditions [168,169,208], as well as a reduction in the uptake of amino acids in the iron-poor conditions during Phase II [6].

The model included a fully functional pathway for petrobactin and bacillibactin, two well-known siderophores of *B. anthracis*. Further, protocatechuate, one of the precursors of petrobactin, was included as a siderophore based on the reported information regarding its presence in the culture of *B. anthracis* [149,167,213]. Protocatechuate was the preferred siderophore for the uptake of iron under iron-rich/poor conditions. As a result, more experimental studies are required to confirm the potential of protocatechuate as a siderophore in *B. anthracis*.

The major pathways of *B. anthracis* exhibited similar behavior under iron-poor/rich conditions during Phase I. Thus, the levels of iron during the iron-poor conditions were enough to support almost normal growth of the bacteria. Some



differences were observed in the preferred uptake of amino acids, such as the up-regulation of the uptake of aspartic acid in iron-poor conditions. Most of the glucose consumed was used for production of acetate, formate, ethanol, and lactate in both conditions. Even when the glucose uptake rate was higher in iron-poor conditions, only a slight difference in the profile of acetate and formate was observed. Ethanol and lactate secretion were also similar. This was because the degradation of amino acids (glutamate and serine) taken from the media in iron-rich conditions provided enough pyruvate to get similar fermentation profiles.

The metabolism of *B. anthracis* under iron-poor conditions was more affected during Phase II, as was observed by the changes in the main pathways. It was not a surprise to see an increase in siderophore biosynthesis pathways with the reduction of iron concentrations due to the siderophores' ability to sequester iron.

The higher glucose uptake rates under iron-poor conditions as compared to iron-rich conditions in Phase II were not correlated with an increase in byproduct secretion, since similar profiles for byproducts were found. Instead, glucose was used for the production of PRPP and amino acids, as was observed from the divergence of the glycolysis pathway from D-fructose-6-phosphate into the pentose phosphate pathway, and from the divergence at 3-phospho-D-glycerate into the serine biosynthesis.

The depletion of iron at Phase II disturbed the TCA cycle by reducing some of the fluxes through it. As a consequence, the amino acid uptake from the media was reduced, since the catabolism of amino acids enter into different intermediates of the TCA cycle. For instance, glutamate and histidine are assimilated through 2-oxoglutarate. To replenish the amino acids, the biosynthesis pathways of some of them were upregulated, which resulted in a higher glucose uptake rate.

Genome-scale metabolic models are useful to formulate hypotheses that lead to biological discoveries. This study revealed an apparent correlation between AI-2 and the growth of *B. anthracis* under iron-poor conditions. Previous works reported this correlation only in Gram-negative bacteria. Thus, experimental studies are required to elucidate the role of AI-2 during iron starvation in *B. anthracis*. Furthermore, the model helped to explain the lactate shift observed during the experimental studies. However, proof of the hypothesized cycling behavior in the lactate metabolism of *B. anthracis* based upon modeling results needs to be determined in the laboratory.

## 7. AUTOINDUCER-2 CORRELATION THE GROWTH OF *BACILLUS ANTHRACIS* UNDER IRON-POOR CONDITIONS

### 7.1. Background

Genome scale metabolic models are constructed by compiling genomic, biochemical, and physiological information on the desired organism [227]. Different tools are available for the reconstruction process; most of them follow a protocol well described in Thieles *et al.* [3]. These models are useful for connecting the organism's genotype and phenotype [139,228]. Furthermore, they provide a fundamental understanding of global bacterial metabolism under diverse experimental conditions [139]. It has been shown that siderophore biosynthesis is up-regulated at the transcriptional level when *B. anthracis* grows inside the macrophages as compared to bacterial growing under iron-rich conditions [140]. As a result, the *in silico* analysis of the global metabolism under conditions similar to the one encountered inside the macrophage allows for the analysis and discovery of interactions not easily deduced experimentally, such as the up-regulation of the AI-2 biosynthesis pathway.

AI-2 is part of the signaling molecules used in quorum sensing [229,230]. Quorum sensing is a cell-to-cell communication system that activates the control of bacterial gene expression in response to cell density [231]. As the number of bacteria

increases, the number of signaling molecules accumulated in the environment does as well. When a certain threshold is reached, changes in gene expression occur [232]. Some of the processes controlled by AI-2 are the synthesis of pathogenicity factors in *Streptococcus pyogenes*, toxin production in *Clostridium perfringens*, biofilm formation by *Streptococcus gordonii*, *Porphyromonas gingivalis*, and *Bacillus cereus* [233], and bioluminescence in *Vibrio harveyi* [234]. AI-2 is synthesized when the enzyme encoded by the *luxS* gene cleaves S-ribosylhomocysteine to produce homocysteine, and 4,5-dihydroxy-2,3-pentanedione (DPD) [232,235]. Then, DPD spontaneously cyclizes to form furanone. Finally, furanone is complexed with borate to form AI-2 [236]. Jones *et al.* [237] reported an ortholog of *luxS* in *B. anthracis*, which allows for the synthesis of AI-2. Furthermore, the mutation of *luxS* in *B. anthracis* resulted in slow growth compared to the wild type [237].

Previous works reported a possible connection between AI-2 and iron acquisition systems in gram-negative bacteria such as *Actinobacillus actinomycetemcomitans* [223,224], *Vibrio vulnificus* [225], and *Porphyromonas gingivalis* [232]. Furthermore, in experiments with *A. actinomycetemcomitans* [224] and *A. pleuropneumoniae* [226] growing under iron deplete conditions, it was observed that growth could be regulated by LuxS through AI-2 production. It was additionally reported that ferric iron uptake and ferric-hydroxamate transport by *luxS* were both up-regulated in *Escherichia coli* growing in LB media supplemented with glucose [238].

The goal of this study is the *in silico* analysis of the metabolic response to different AI-2 conditions. It is an attempt to elucidate the role of AI-2 in the metabolism of *B. anthracis* under different iron-poor conditions.

## 7.2 Materials and Methods

### 7.2.1 FLUX BALANCE ANALYSIS CONSTRAINTS

The constraints used for FBA in this chapter correspond to the iron-poor and iron-rich conditions at Phase 2 in Chapter 6. They are shown in Table 13. The objective function chosen for the optimization problem was the maximization of the biomass reaction for *B. anthracis*.

**Table 13. Experimentally measured fluxes for the growth of *B. anthracis* under iron-reduced media (IRDM) and iron-replete media (IRM).** Positive values are production rates, negative values are uptake rates.

<b>Rates (mmol/gDW*h)</b>	<b>IRDM</b>	<b>IRM</b>
Glucose uptake rate	-13.16	-8.54
Carbon dioxide production rate	6.29	4.96
Lactate production/secretion rate	-0.97	-0.41
Oxygen uptake rate	-6.74	-4.65
Glutamate uptake rate	-0.27	-1.6
Iron uptake rate	-0.00075	-0.0028
Protocatechuate secretion rate	0.0241	0.008
Petrobactin secretion rate	0.0163	0.0055
Bacillibactin secretion rate	0.0023	0.00004

### **7.2.2. FLUX VARIABILITY ANALYSIS (FVA)**

FVA is a method that helps to investigate the metabolic network flexibility and redundancy [188]. FVA determines the range of values where the fluxes can change without affecting the value of the objective function [189]. As in Chapter 6, FVA analysis was applied for each of the *in silico* simulations reported here.

## **7.3 Results and Discussion**

One of the byproducts of the AI-2 biosynthesis pathway shown in Figure 37 is adenine. S-adenosylhomocysteine nucleosidase (E.C. 3.2.2.9) converts S-adenosyl-l-homocysteine into adenine and S-ribosylhomocysteine. S-ribosylhomocysteine goes to methionine recycle through the S-adenosyl-methionine (SAM) cycle [239]. Meanwhile, adenine is also recycled through the adenine salvage pathway to go into adenosine nucleotides de novo biosynthesis pathway. As a consequence, the role of the production of AI-2 in adenosine de novo biosynthesis and growth rate were studied.

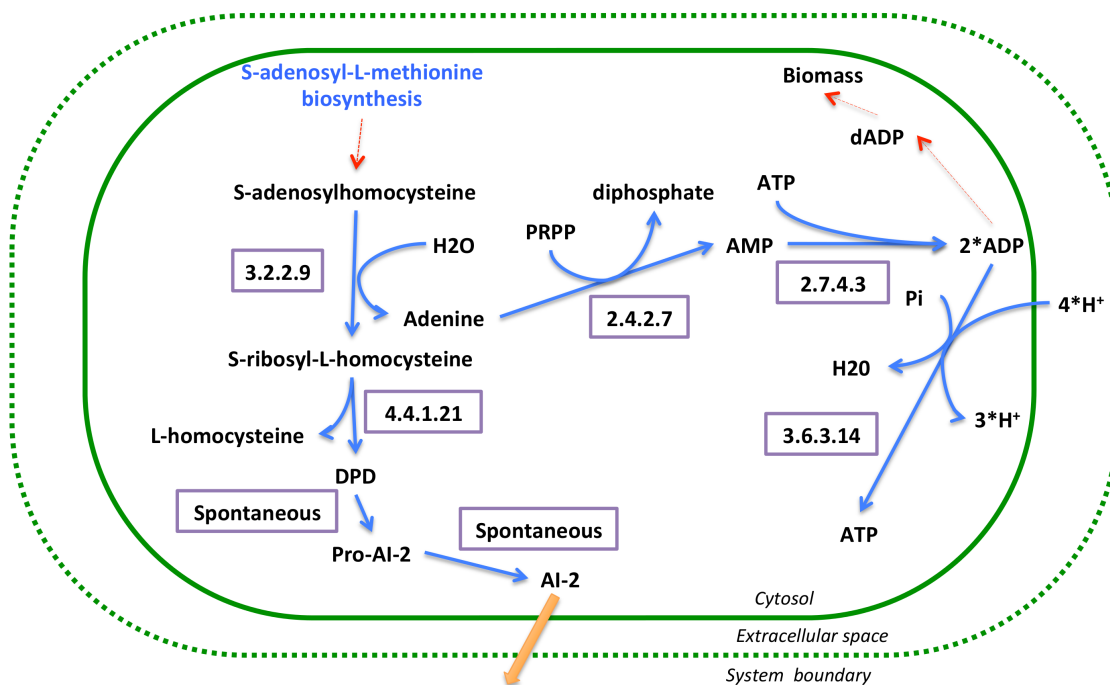


**Figure 37. Autoinducer-2 biosynthesis pathway connected to adenine salvage pathway and adenosine de novo biosynthesis pathway.** Intracellular fluxes are the blue arrows, exchange flux is the yellow arrow, and the red-dot arrows are connection reactions with other pathways. Metabolites are in black. The E.C. number for each reaction is provided in the box near each reaction.

### 7.3.1 *LUXS* MUTATION AFFECTS *IN SILICO* GROWTH

Fong *et al.* [224] and Li *et al.* [226] show that the growth of *A. actinomycetemcomitans* and *A. pleuropneumoniae* under iron restricted conditions was reduced in strains with a mutation in the *luxS* gene. Nonetheless, the growth returned to normal values when DPD was added to the media [226], or by complementation of the strain with a functional plasmid-borne copy of *luxS* [224]. These results provided the impetus for studying the effect of *luxS* gene on the growth rate of *B. anthracis* with an *in*

*in silico* mutation of *luxS* under iron restricted conditions. To simulate the *luxS* mutation, the flux through the S-ribosylhomocysteinase reaction (E.C. 4.4.1.21) catalyzed by the *luxS* product was constrained to zero. This mutation was lethal for *B. anthracis*, since an *in silico* growth rate of zero was found. The discrepancy between the experimental results of *A. pleuropneumoniae* and *A. actinomycetemcomitans*, and the *in silico* results could be due to the fact that they are different bacteria. Furthermore, *A. pleuropneumoniae* and *A. actinomycetemcomitans* were grown in nutritionally rich media. The *in silico* media for *B. anthracis* was an iron-reduced media [137] composed of a defined media and casamino acids.

### 7.3.2 AI-2 PRODUCTION INCREASES AMP AND ADP POOL

The AI-2 pathway is connected to energy metabolism through the production of adenine from the S-adenosylhomocysteine nucleosidase (E.C. 3.2.2.9) reaction, as is shown in Figure 38. Under iron-reduced conditions, the up-regulation of AI-2 resulted in more adenine being utilized through the adenine phosphoribosyltransferase (E.C. 2.4.2.7). Then, AMP was converted to ADP through adenylate kinase (E.C. 2.7.4.3), which was almost 3.5 times higher in iron-reduced than in iron-replete conditions. This enzyme has also been reported to be up-regulated in iron-poor conditions in *S. aureus* [168]. Finally, ADP could be used for ATP production through F<sub>0</sub>F<sub>1</sub>-ATPase (E.C. 3.6.3.14), or substrate level phosphorylation. The reactions that are part of these pathways are shown in Table 14. The fluxes through the reaction under iron-poor



conditions are higher than in iron-rich conditions, with a 2.2 times higher change through the PEPDEPHOS-RXN.

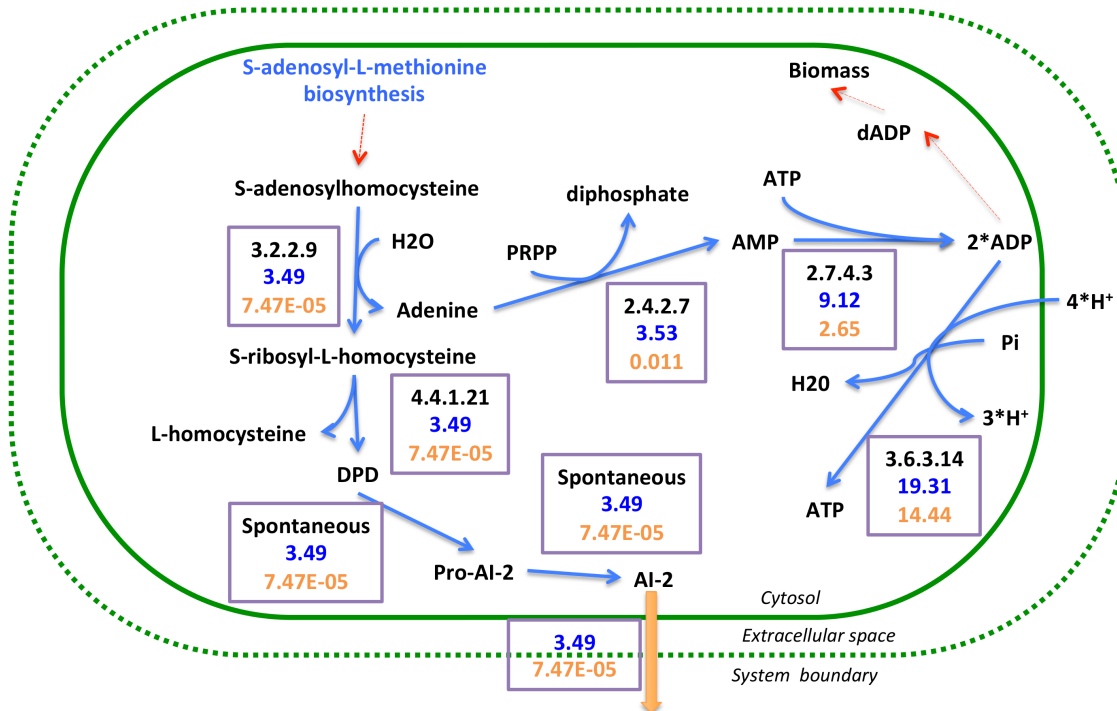


**Figure 38. Autoinducer-2 biosynthesis pathway connected to adenine salvage pathway and adenosine de novo biosynthesis pathway under iron-reduced/replete iron conditions.** Intracellular fluxes are the blue arrows, exchange fluxes are the yellow arrows, and the red-dot arrows are connection reactions with other pathways. Metabolites are in black. The boxes near each reaction have in the first line the E.C. number for the enzyme, the second line in blue is the flux under iron-reduced conditions, and the third line in orange is the flux under iron-replete conditions.

**Table 14. Substrate level phosphorylation reactions and oxidative phosphorylation reactions for *B. anthracis* grown under iron-poor/rich conditions.** Iron-poor/iron-reduced (IRDM) and iron-rich/iron-replete (IRM).

Name	E.C.	IRDM	IRM	Fold change (IRDM/IRM)
PEPDEPHOS-RXN	2.7.1.40	19.437	9.108	-2.187
ACETATEKIN-RXN	2.7.2.1	15.102	11.160	-0.873
ATPSYN-RXN	3.6.3.14	19.310	14.437	-0.839
PHOSGLYPHOS-RXN	2.7.2.3	19.830	16.387	-0.550
SUCCCOASYN-RXN	6.2.1.5	0	1.120	

#### 7.4. Impact

LuxS has two roles in metabolism. One is the synthesis of the precursor of AI-2. The second is as part of the S-adenosyl-methionine (SAM) cycle. These double functions have led to much debate about the real role of AI-2 – whether it is a quorum sensing signal molecule, or a metabolic by-product [229,235,240]. In this chapter, the effect of the synthesis of AI-2 on the metabolism of *B. anthracis* under different iron conditions was analyzed through an *in silico* approach. As shown, the AI-2 production resulted in an increase of the AMP and ADP pools under iron-reduced conditions through adenine recycling, which resulted in an increase in the production of ATP through substrate level phosphorylation reactions and oxidative phosphorylation reactions.

The mutation of the *luxS* gene was lethal for the growth of *B. anthracis* under iron-reduced conditions. However, this mutation has been reported to not be lethal for other bacteria. As was pointed out, the discrepancies could result from differences in the media used, as well as the species of bacteria. This mutation resulted in the disruption of the SAM cycle, which is important to the production of the major methyl donor S-adenosyl-L-methionine, and for the recycling of methionine. This result highlights the importance of the *luxS* gene's product in the metabolism.

This work represents the first time that the relationship between AI-2 and the growth and metabolism of *B. anthracis* under iron-reduced conditions has been studied. The *in silico* analysis indicated a possible correlation between AI-2 and the growth of the bacteria under iron deprivation conditions. Experimental studies are needed to confirm these results, as well as to analyze the role of AI-2 as a signal molecule or as a metabolic by-product.

## 8 CONCLUSIONS

The work presented in this dissertation integrates genome-scale metabolic modeling with experiments to study the microorganism's metabolism and understand the impact of varying iron levels on *B. anthracis*' metabolism. This integration allowed for predictions to determine metabolic interactions not easily observed experimentally, and for the analysis of metabolic adaptations of bacteria to changes in the environment.

In this thesis, not only were genome-scale metabolic models created, but additionally a novel methodology that facilitates the curation of genome-scale metabolic networks was developed. Moreover, it was shown that GAFBA methodology aids in fundamental studies of metabolism. Different tools were added to GAFBA v1.1 to speed up, facilitate the curation process, and make it more user-friendly. I believe that in the future, GAFBA v1.1 could evolve into a much faster methodology, which would result in more models created through this approach.

The experimental growth of *B. anthracis* under different iron conditions suggested a more active carbon metabolism during iron-poor conditions. Higher uptake rates of glucose, oxygen, and lactate, as well as higher secretion rates for carbon dioxide were all noted. This observation was difficult to reconcile at the beginning of these studies given that under iron-poor conditions, lower growth rates were found. At this

point, it was clear that either more experiments were required to measure additional metabolites, or an *in silico* global metabolism analysis was needed. Given financial, time, and expertise constraints, the second option was chosen.

The comparison of the global metabolism of *B. anthracis* under iron-poor/rich conditions revealed the purpose of the higher carbon metabolism under iron poor conditions. It was shown that reduced iron concentration had a negative impact on some reactions of the TCA cycle, which resulted in the reduced catabolism of amino acids. Thus, some amino acid biosynthesis pathways were up-regulated to supply the required amino acids for growth and for siderophore biosynthesis. Additionally, under iron-reduced conditions it is possible that other energy consuming processes in addition to growth are likely occurring, such as maintenance, production of signaling molecules, and biosynthesis of regulatory proteins or small RNAs.

Finally, a correlation between AI-2 and the growth of *B. anthracis* under iron-poor conditions was discovered for the first time. However, it is required to investigate the real role of AI-2 as a signal molecule or as a metabolic byproduct.

## 9 FUTURE WORK

Many hypotheses and a number of pursuable experimental avenues have arisen from the work presented in this dissertation. This chapter highlights the most important of them.

In Chapter 3, from the reconstruction and analysis of the metabolism of *M. gallisepticum*, it was hypothesized that formate dehydrogenase (E.C. 1.2.1.2), NAD<sup>+</sup> synthetase (E.C. 6.3.5.1), and Na-ATPase (E.C. 3.6.3.7) would be present in the bacteria. This still needs to be experimentally verified. Furthermore, the role of the methylerythritol phosphate pathway (MEP) in *M. gallisepticum*'s metabolism requires further study, and its potential as a drug target should be considered.

GAFBA v1.1 could be further improved. The parallelization of the algorithm should be considered a priority. Even with the run time efficiencies recently implemented, the parallelism of the code has the potential to take advantage of massively multi-core systems, and especially GPU based computing systems housed in the UConn School of Engineering and the BECAT HPC cluster. This could be achieved using Symmetric Multiprocessing LispWorks (SMP LispWorks). Another tool that would enhance the user experience, is a text-mining tool based on K-means clustering to search abstracts in Pubmed (<http://pubmed.nih.org>) and correlate metabolites and reactions that

GAFBA v1.1 lists as problematic. It will provide more information for users to solve the problems present in the metabolic network being analyzed. It could use the name of the bacteria and the problematic metabolite as keywords to identify any relevant compounds that are not currently linked to the metabolite in question. Thus, the user will look for possible solutions in this set of generated documents. Work has already begun on this text-mining tool; it needs to be optimized and connect its graphic user interface (GUI) with GAFBA v1.1 GUI.

During the experiments presented in Chapter 5 for the growth of *B. anthracis* under iron-reduced/replete conditions, a significant challenge that arose was how to reduce the iron concentration to levels of starvation in the fermentor. It was observed that the iron concentration of the media increased when transferred to the fermentor from a value of 0.77  $\mu\text{M}$  to 2.24  $\mu\text{M}$ . It is possible that the stainless material retains some traces of iron even after the cleaning process. There are two potential alternatives to overcome this situation. One is to employ a Teflon vessel such as the one used in the study of trace metal metabolism in *Streptococcus mutans* [241]. The second possibility is to use single-use bioreactors (Applikon Biotechnolog, New Brunswick).

On the modeling front, the *B. anthracis* model could be integrated with the existing human alveolar macrophage (HM) model iAB-AMØ-1410 created by Bordbar *et al* [9]. The reconstruction process would allow GAFBA v1.1 to be evaluated in multispecies cases. Moreover, this host/pathogen model may be used to identify new

drug targets, characterize the mechanism of the action of drugs, optimize treatment strategies, and enhance the early diagnosis and prompt treatment of the disease, since the progression of anthrax is typically quite rapid once the systemic phase of infection begins.

During the analysis of the metabolism of *B. anthracis* under different iron conditions, the possibility of a connection between autoinducer-2 (AI-2) and the growth of the bacteria under iron-reduced conditions arose. It is necessary to experimentally measure the production of AI-2 in *B. anthracis* under iron-reduced/replete conditions. The AI-2 concentrations could be monitored using the *Vibrio harveyi* MM32 reporter strain [242,243]. This strain is an ideal reporter, since it cannot synthesize AI-2, and it does not respond to N-Acyl homoserine lactone (AHL) signal molecules. Moreover, the impact of AI-2 production in the growth of the bacteria under rich/poor conditions may be evaluated by doing a mutation on the *luxS* gene in *B. anthracis* and growing the mutant with/without the addition of exogenous AI-2 or the AI-2 precursor DPP.

The *B. anthracis* model may be improved by adding more experimentally measured fluxes, such as the byproduct secretion rates of acetate, formic acid, ethanol, and amino acid uptake rate. The uptake/secretion rates could be measured using high performance liquid chromatography, and/or gas chromatography. Moreover, carbon-13 measurements would also help to further verify the model [244,245].



## **APPENDIX 1. EXAMPLES OF METHODOLOGIES FOR RESOLVING INFEASIBLE MODELS.**

Generally, four types of solution for the unbalanced metabolites can resolve curation issues.

**Case 1:** The change of the directionality of a reaction may solve the problem. Figure S1 has an example of this case. The ribulose-5 phosphate did not have a reaction to be produced and the mass balance of ribose- 5 phosphate was dropped, because any of the possible reactions to consume it were inactivated. If the reaction v278 catalyzed by the enzyme ribose-5-phosphate isomerase (E.C. 5.3.1.6) was changed to reversible, it could consume the ribose-5-phosphate.

From the Kyoto Encyclopedia of Genes and Genomes (KEGG) [96], this reaction does indeed appear to be reversible, along with reaction v274 catalyzed by the enzyme ribulose-phosphate 3-epimerase (E.C. 5.1.3.1).

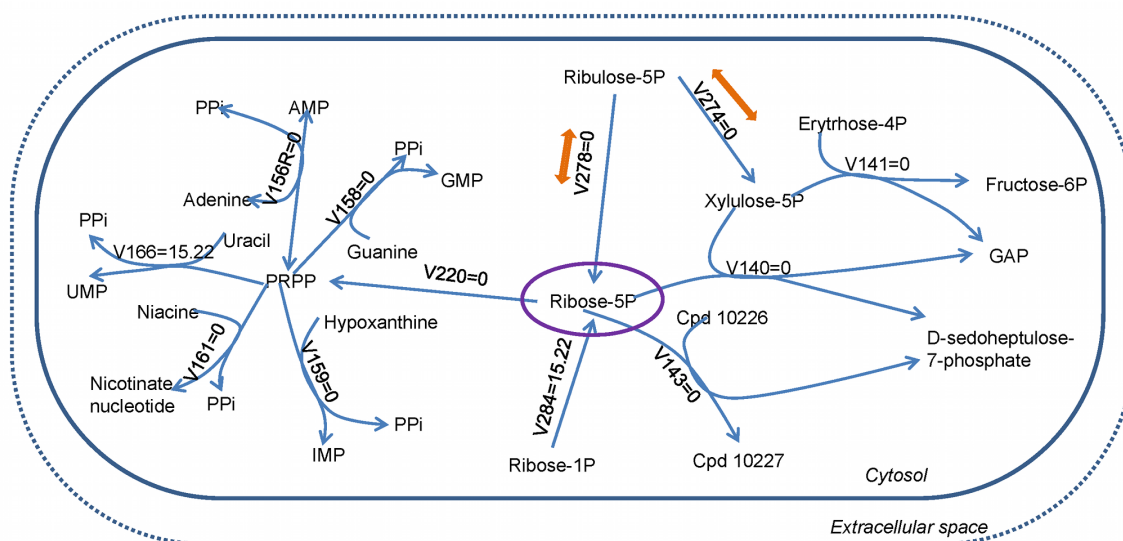


**Figure S1. Case 1. Change directionality of reactions.** The purple circle showed the dropped metabolite. The blue arrows are the fluxes and the orange arrows are the proposed solutions. The solid blue line is the plasma membrane and the dashed blue line is the system boundary.

**Case 2.** The addition of an exchange flux may resolve the issue. In the case highlighted in Figure S2, glycine was produced by two reactions involved in folate transformations: V140 (GLYOHMETRANS-RXN E.C. 2.1.2.1) and V\_95R (GCVMULTI-RXN in Pathway tools nomenclature). However, these reactions were unable to produce all the glycine required for the tRNA charging reaction, thus the additional glycine had to be taken from the media. The literature reported the presence of glycine in the media of the *Mycoplasma laidlawii* and the *Mycoplasma genitalium*, related species to the *M. gallisepticum* (Suthers, et al., 2009; Tourtellotte, et al., 1964).

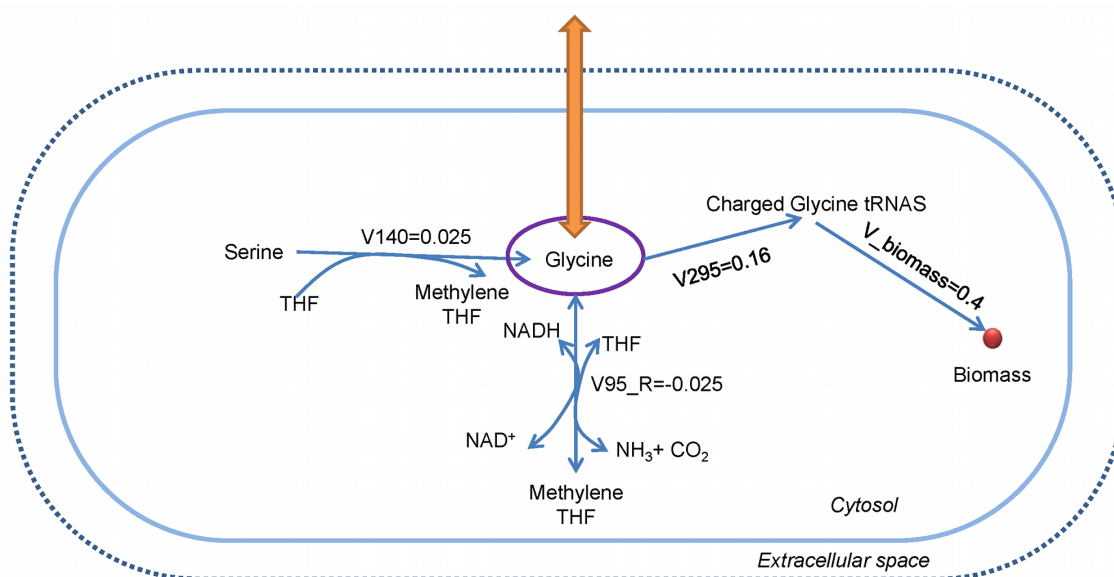


**Figure S2. Case 2. Add exchange flux.** The purple circle showed the dropped metabolite. The blue arrows are the intracellular fluxes and the orange arrow is the proposed solutions. The solid blue line is the plasma membrane and the dashed blue line is the system boundary. The red circle represents the Biomass pool.

**Case 3:** Figure S3 shows an example for the case when the addition of a reaction could help to complete the mass balance of the metabolite. Here, the formate was produced via reaction V256. The peptide deformylase enzyme (E.C. 3.5.1.88) catalyzed this reaction and the biomass reaction. However, no reaction consuming formate was present. Therefore, a simple degradation pathway present in other Mycoplasmas [89] was added to the model.

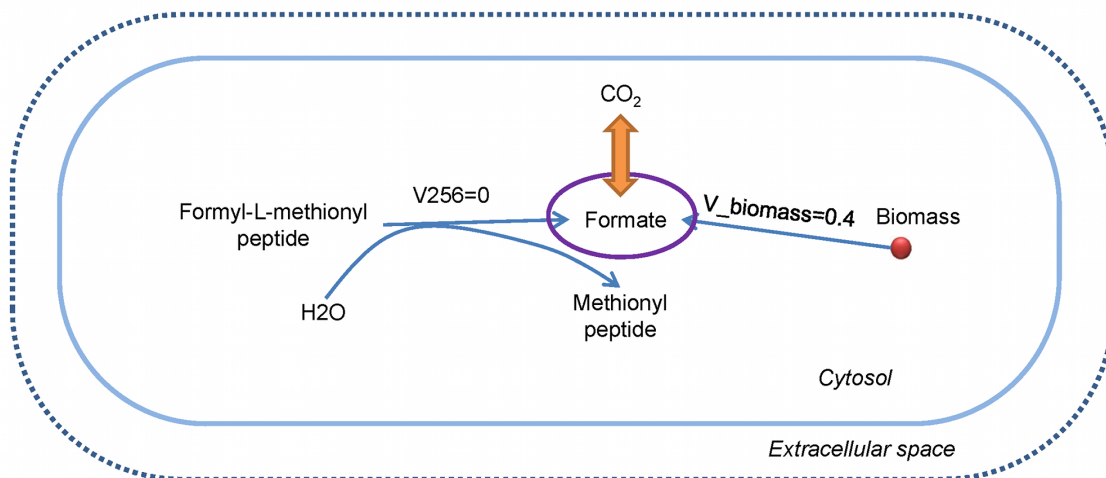


**Figure S3. Case 3. Add reaction.** (formate case). The purple circle showed the dropped metabolite. The blue arrows are the fluxes, the blue thick arrows are the exchange fluxes, and the orange arrow is the proposed solutions. The solid blue line is the plasma membrane and the dashed blue line is the system boundary. The red circle represents the Biomass pool.

**Case 4:** Finally, removing a reaction or metabolite from model may resolve the issue. On some occasions, the deletion of a general reaction or general metabolite from the model was required to fulfill the mass balance. These general reactions and metabolites were present in the model based on some of the software tools used to generate the initial model from the genome annotation. Usually, a general reaction is first created, and as the experimental data and information are available to confirm the presence of the specific reactions, the general reaction is expanded to the specific ones. Occasionally this may require the manual intervention of the curator.

## **APPENDIX 2. EXPERIMENTAL PROTOCOLS FOR *M. GALLISEPTICUM***

### **MODEL**

#### **A2.1. Strains, Culture Conditions**

A previously sequenced clonal isolate of *M. gallisepticum* R<sub>low</sub>, R<sub>low</sub> Clone 2 (RLC2) [31] was used. The bacteria were grown in complete Hayflick's medium [246] with an initial concentration 3.5 g/L glucose .

#### **A2.2. Determining Dry Cell Weight and CFU/ml**

The CFU/ml concentrations for all experiments were calculated using a previously determined correlation [247] between CFUs/ml and the absorbance of cell culture at 620 nm. A correlation between dry cell weight and absorbance was generated by directly measuring the weight of dried cell pellet, volume of the supernatant, and OD<sub>620</sub> of the culture. To accomplish this, 500 ml of RLC2 was grown in Hayflick's media [246] at 37°C to mid-log phase. The absorbance of the culture was measured at 620 nm. The culture was then quickly chilled to 4°C. 30 ml of the culture was placed in a 50 ml Falcon Tube and centrifuged at 15,000 x g at 4°C for 15 mins. The supernatant was transferred to a graduated cylinder for measurement without disturbing the pellet, and another 30 ml of culture was added to the same tube and centrifuged at the conditions mentioned above. This was repeated until all 500 ml of culture had been centrifuged into

one large pellet. The pellet in the 50 ml centrifuge tube was dried for two weeks at 37°C. The tube was then capped stored at 23°C for two months. The dried flaking pellet was then scraped off and measured using a scale accurate to the nearest mg. This protocol was repeated for four different cell concentrations in mid-log phase growth and one control using only medium.

### **A2.3. Metabolism Experimental Design**

100 ml aliquots of Hayflick's media with 3.5 g/L of glucose in 250 ml plastic flat-bottom centrifuge tubes were inoculated with mid-log cultures of RLC2 and incubated at 37°C. Sampling of these vessels was initiated approximately 15-19 hours post-inoculation, when the dry cell density in each vessel reached 46.89 mg/L ( $7.27 \times 10^7$  CFU/ml) and ended once the dry cell density exceeded 125 mg/L. Samples of culture were taken at nearly one-hour intervals over the aforementioned period during late log-growth. This allowed for four to five individual sample points to be taken during this late log-phase growth for each run. From these samples, cell dry weight concentration, glucose concentration, and lactate concentration were determined by the assays described below. Seven runs were completed for RLC2. Three sets of runs were performed on separate days. Each set included approximately three RLC2 runs.

#### **A2.4. Sampling and Cell Growth Assay**

$10^6$  CFUs of RLC2 (growing in late log-phase) was added to 100 ml of media in a 250 ml plastic flat bottom centrifuge tube. This tube was incubated at 37°C while being shaken at 140 rpm for 15-19 hrs. 1 ml samples from each flat bottom centrifuge tube were then placed into 1.5 ml microfuge tubes. A 700  $\mu$ L volume of each sample was immediately centrifuged at 20,000 x g for 15 minutes at 4°C in an Eppendorf 5417 microfuge using a fixed-angle aerosol-tight rotor (FA-45-30-11) for 1.5-2.0 ml tubes.

The supernatant was transferred into new 1.5 ml microfuge tubes and placed in a -80°C freezer for storage until further analysis. The OD<sub>620</sub> of the remaining 300  $\mu$ L of each sample was measured while the other 700  $\mu$ L was being centrifuged. This OD<sub>620</sub> reading was used to determine the biomass concentration using the experimentally determined correlation between cell dry weight and OD<sub>620</sub>. This sampling process was repeated until the dry cell density in each vessel reached 125 mg/L. At this point, sampling ended and the remaining culture was allowed to grow overnight and was checked 24 hours later for visible signs of contamination. No contamination occurred.

#### **A2.5. Glucose and Lactate Assays**

After two to five days of storage at -80°C, the 700  $\mu$ L supernatant samples were thawed and prepared for analysis using a YSI 2700 SELECT single-channel Biochemistry Analyzer. Supernatant samples were filtered with 13mm GHP 0.2 micron

syringe filters (WAT097962) to remove any remaining cellular debris. The supernatant samples were then placed in a -80°C freezer for another 1-7 days.

To assay for lactate, the standard YSI 2700 SELECT protocol for measuring L-lactate concentration using a L-lactate membrane (part # 2329) was followed. Standard buffer (part # 2357) and L-lactate calibration standard (part # 2776) were used. 25 µL of sample was taken and analyzed for a 30 second period before being flushed. Two readings were performed for each supernatant sample. Six supernatant samples at a time were thawed, assayed, and then refrozen to -80°C.

To assay for glucose, the standard YSI 2700 SELECT protocol for measuring glucose concentration using a glucose membrane (part # 2365) was followed. Standard buffer (part # 2357) and glucose calibration standard (part # 2776) were used. 25 µL of sample was taken and analyzed for a 30 second period before flush. For each supernatant sample, three replicates were performed and averaged. Six supernatant samples at a time were thawed, assayed, and then refrozen to -80°C.

#### **A2.6. Dry Weight Measurement**

The correlation between optical density and dry cell weight per ml is shown in Table S1. Consistent readings were achieved for four points within the range of optical densities covered by the metabolism experiment.



**Table S1. OD/(g/cfu) Correlation.** Calculations of the g/cfu conversion.

Run	OD <sub>620</sub>	Pellet Weight (g)	Supernatant Volume (ml)	Concentration (g/ml)	cfu/ml	g/cfu
Control	0	0	432	0.000E+00	N/A	N/A
1	0.089	0.051	478	1.067E-04	1.66E+08	6.44E-13
2	0.084	0.05	480	1.042E-04	1.56E+08	6.68E-13
3	0.098	0.053	480	1.146E-04	1.83E+08	6.26E-13
4	0.094	0.052	482	1.120E-04	1.75E+08	6.39E-13
					average:	6.45E-13
					std:	1.75E-14

#### A.2.7. Determination of biomass equation

The biomass equation was determined by incorporating all available published information about the makeup of *M. gallisepticum* and other similar mycoplasmas. The starting equation was taken from a metabolic reconstruction of *M. genitalium*, one of *M. gallisepticum*'s closest relatives [58]. Metabolites added in by the GrowMatch portion of that reconstruction were discarded due to lack of supporting evidence. Other cofactors not conducive with *Mycoplasma* metabolism that did not possess any cited synthesis or absorption pathways, such as Menaquinol 7, were modified or removed. The relative ratios of the various components of DNA, RNA, and amino acids reported in the *M. genitalium* reconstruction were kept due to the similar GC content and large number of shared proteins between the two organisms [248]. However, the ratios between the major biochemical components, consisting of DNA, RNA, amino acids, cofactors, ions, and lipids, were adjusted to reflecting a previously reported chemical composition analysis of *M. gallisepticum* [249].

The composition of the lipid fraction was calculated from published data on the lipid fractions of *M. gallisepticum* and other related *Mycoplasmas*. First, the ratios of the classes phospholipid, sterol, and triglyceride were determined relative to each other from previously published work [91,249]. Though recent studies suggest that *M. gallisepticum* may possess a capsule, it has not been directly shown that its capsule or *M. gallisepticum* itself contains glycolipids [250]. Because of this uncertainty, and due to the small amounts of carbohydrates found in *M. gallisepticum*'s chemical composition relative to other related glycolipid possessing species, glycolipids were not included in the biomass composition [249].

The ratios of the subclasses of sterol and phospholipid groups relative to each other were then analyzed. First, sterols were analyzed. The amount of cholesterol and cholesterol ester was calculated using published ratios of cholesterol to cholesterol ester [83,91].

Next, phospholipids were analyzed. The amount of sphingomyelin present in *M. gallisepticum*'s membrane was estimated from previously reported values [83,91]. The percent of the phospholipid fraction made up of phosphatidylcholine was estimated by using a reported ratio between phosphatidylcholine and sphingomyelin in *M. gallisepticum*'s membrane along with the reported sphingomyelin membrane fraction [83,91]. The phosphatidic acid (1,2-diacylglycerol-3-phosphate) percent was estimated

using a lipid percent reported by Tourtellotte *et al.* The amount of phosphatidic acid was decreased by 25% before incorporation into the biomass equation due to an author statement suggesting the value was higher than it should have been [91]. No conclusive assays of the existence or membrane percent of phosphatidylethanolamine have been published. Phosphatidyl-ethanolamine was shown to be absent by a complement fixing antigen assay of the membrane of *Mycoplasma pneumoniae* [251]. Because of the similarity between these two organisms, it was assumed that *M. gallisepticum* lacked this phospholipid as well. Tourtellotte *et al.* reported that phosphatidylglycerol likely made up less than 10% of the phospholipids. Since no definitive quantitative assay of phosphatidyl-glycerol have been performed on *M. gallisepticum* or any of its close relatives, the phospholipid percent of phosphatidyl-glycerol was estimated from a published value in *A. ladwarii* [252]. Cardiolipin's composition or existence in *M. gallisepticum* has yet to be studied. However, cardiolipin has been shown to be present in *Mycoplasma pneumoniae*'s membrane [253]. In a recent study, *M. pneumoniae* was shown to have the metabolic reactions necessary to biosynthesize cardiolipin from fatty acids and glycerol [89]. Cardiolipin is speculated to be the dominant phospholipid in other more distantly related *Mycoplasma* such as *M. mycoides* and *M. hyopneumoniae* [254]. Therefore, the remaining phospholipid fraction was assumed to be comprised primarily of cardiolipin. Table S2 summarizes the calculated composition of the lipid fraction used in the biomass equation.

**Table S2. Lipid Fraction Estimation.** Percent composition of the lipid fraction of *M. gallisepticum*, the estimated molecular weights, and the relevant references used to generate these percentages.

Lipid Type	%of Total Lipid Mass	Lipid Name	MW	Mass % of Lipid Type	g/gDW	Citations
phospholipid	70.3					[91]
		cardiolipin	1524.7	49.5	0.0546	[83,89,253,254]
		1,2-diacylglycerol-3-phosphate	651.3	7.5	0.0083	[91]
		phosphatidylcholine	819.5	23.8	0.0283	[83,91]
		sphingo-myelin	771.8	9.2	0.0102	[91]
		phosphatidylethanolamine	776.4	0	0.0000	[91,251]
		phosphatidylglycerol	807.4	10	0.0110	[91,252]
Sterols	21.9					[91,249]
		cholesterol	386.7	90.6	0.0312	[83,255]
		cholesterol ester	643.7	9.3	0.0032	[255]
triglycerides	7.7					[91]
		triacylglyceride	794.1	100	0.0121	[83,91]
glycolipids	0					[250]

The average molecular weight of *M. gallisepticum*'s phospholipids, sterols, and triglycerides R groups were by weighted averaging the molecular weights of the constituent fatty acids (Table S3). The fatty acid compositions of each of the three lipid types were taken from a previously reported study [91]. Using these R group molecular weight estimations, the full lipid molecular weights were calculated using the chemical structures of the major lipid components (Table S4). Using these molecular weights, the mmol/gDW values for each of the major lipid components were calculated from the mass

percents shown in supplementary Table S2. The final biomass reaction is presented in the appendix A3.5

**Table S3. Average Fatty Acid Molecular Weight.** The calculation of the average fatty acid molecular weight from the fatty acid composition of *Mycoplasma gallisepticum* as reported by Tourtelloute et al. [91]

	MW (g/mol)	Phospholipids %	cholesterol esters %	triglycerides %
Caproic	116.16	0	0	0.6
Caprylic	144.22	0	0	0.9
Capric	172.27	0	0	6.1
Unidentified	172.27	0	0	0.6
Lauric	200.32	0.7	0	6.3
Myristic	228.36	3.3	1.2	14.3
Myrisroleic	240.4	2.2	0.3	1.4
Pentadecanoic	242.4	0	0.3	1.1
Palmitic	256.43	24.8	23.4	32.2
Palmitoleic	256.43	2.9	6.3	1.1
Heptadecanoic	270.45	2.4	1.2	0.5
Stearic	284.48	36	13.1	10.1
Oleic	282.47	20.4	54.2	21.9
Linoleic	278.43	7.3	0	3.9
Average Fatty Acid MW		272.1	274	251

**Table S4. Estimation of molecular weights for major lipid components making up biomass.** Using the chemical structure, the molecular weights of each molecule, and the estimated molecular weights of the R group, whose calculations are shown in Table S3, the molecular weight of each major lipid component was estimated.

Component	MW	a 1,2- diacylglycerol- 3-phosphate	a phosphotidyl- choline	cardiolipin
O	16	8	8	17
C	12.01	5	10	13
H	1.01	7	19	20
P	82	1	1	2
N	14	0	1	0
R groups	228.1	2	2	4

<b>Component</b>	<b>MW</b>	<b>a 1,2- diacylglycerol- 3-phosphate</b>	<b>a phosphatidyl- choline</b>	<b>cardiolipin</b>	
Estimated Total MW		733.32	819.49	1524.73	
<b>Component</b>	<b>MW</b>	<b>a sphingomyelin</b>	<b>an L-1- Phosphatidyl- ethanolamine</b>	<b>an L-1- phosphatidylglycerol</b>	
O	16	6	8	10	
C	12.01	24	7	8	
H	1.01	49	12	13	
P	82	1	1	1	
N	14	2	1	0	
R groups	228.1	1	2	2	
Estimated Total MW		771.83	776.39	807.41	
<b>Component</b>	<b>MW</b>	<b>cholesterol</b>	<b>a cholesterol ester</b>	<b>MW</b>	<b>a triacylglycerol</b>
O	16	1	2	169	6
C	12.01	27	28	12.01	6
H	1.01	46	45	1.01	5
P	82	0	0	82	0
N	14	0	0	14	0
R groups	230	0	1	207	3
Estimated Total MW		386.73	643.73		794.11

### APPENDIX 3. GENOME-SCALE METABOLIC MODEL OF *M.*

#### *GALLISEPTICUM*

##### A3.1. Metabolites located in the cytosol space

**Table S5. Metabolites in the cytosol space for *M. gallisepticum* model.** The name, id, and formula for each species are provided.

Species id	Species name	Formula
10-FORMYL-THF[c]	10-formyl-tetrahydrofolate	C20H23N7O7
2-3-4-Saturated-L-Phosphatidates[c]	a 2,3,4-saturated L-phosphatidate	C11H17O8RR2P
2-C-METHYL-D-ERYTHRITOL-4-PHOSPHATE[c]	2-C-methyl-D-erythritol-4-phosphate	C5H11O7P
2-KETOGLUTARATE[c]	2-oxoglutarate	C5H4O5
2-PG[c]	2-phospho-D-glycerate	C3H4O7P
2-PHOSPHO-4-CYTIDINE-5-DIPHOSPHO-2-C-MET[c]	2-phospho-4-{cytidine 5'-diphospho}-2-C-methyl-D-erythritol	C14H22N3O17P3
2C-METH-D-ERYTHRITOL-CYCLODIPHOSPHATE[c]	2-C-methyl-D-erythritol-2,4-cyclodiphosphate	C5H10O9P2
3-5-ADP[c]	adenosine 3',5'-bisphosphate	C10H11N5O10P2
3-HYDROXY-3-METHYL-GLUTARYL-COA[c]	{S}-3-hydroxy-3-methylglutaryl-CoA	C27H39N7O20P3S
3-KETOBUTYRATE[c]	acetoacetate	C4H5O3
3-Prime-Ribonucleoside-Monophosphates[c]	a nucleoside 3'-phosphate	C5H10O7RP
3-terminal-unsaturated-sugars[c]	a 3'-terminal unsaturated sugar	
4-AMINO-BUTYRALDEHYDE[c]	4-aminobutanal	C4H10NO
4-AMINO-BUTYRATE[c]	4-aminobutyrate	C4H9NO2
4-CYTIDINE-5-DIPHOSPHO-2-C[c]	4-{cytidine 5'-diphospho}-2-C-methyl-D-erythritol	C14H23N3O14P2
5-10-METHENYL-THF[c]	5,10-methenyltetrahydrofolate	C20H22N7O6
5-FORMYL-THF[c]	5-formyl-tetrahydrofolate	C20H21N7O7
5-Phosphopolynucleotides[c]	a 5'-phosphopolynucleotide	
Acceptor[c]	an oxidized electron acceptor	
ACET[c]	acetate	C2H3O2
ACETOACETYL-COA[c]	acetoacetyl-CoA	C25H36N7O18P3S
ACETYL-COA[c]	acetyl-CoA	C23H34N7O17P

Species id	Species name	Formula
		3S
ACETYL-P[c]	acetylphosphate	C2H3O5P
ACP[c]	a holo-[acp]	C14H25N3O8a holo-[acp]2PS
ACYL-ACP[c]	an acyl-[acp] Coavholo-[acp]R	
ACYL-COA[c]	an acyl-CoA	C22H35N7O17R P3S
Acyl-Phosphates[c]	an acyl phosphate	CH2O5RP
ACYL-SN-GLYCEROL-3P[c]	a 1-acyl-sn-glycerol-3-phosphate	C4H8O7RP
ADENINE[c]	adenine	C5H5N5
ADENOSINE[c]	adenosine	C10H13N5O4
ADENOSYL-HOMO-CYS[c]	S-adenosyl-L-homocysteine	C14H20N6O5S
ADENYLOSUCC[c]	adenylo-succinate	C14H14N5O11P
ADP[c]	ADP	C10H12N5O10P 2
ALA-tRNAs[c]	tRNAala	
ALPHA-GLC-6-P[c]	alpha-D-glucose 6-phosphate	C6H11O9P
Amino-Acids-20[c]	a standard alpha amino acid	C2H4NO2R
AMMONIA[c]	ammonia	NH3
AMMONIUM[c]	NH4+	NH4
AMP[c]	AMP	C10H12N5O7P
ANTHRANILATE[c]	anthranilate	C7H6NO2
AP-Site-Created[c]	an AP {apurinic or apyrimidinic} site created by glycosylic bond cleavage	
apo-ACP[c]	an apo-[acp]	
ARG-tRNAs[c]	tRNAarg	
ARG[c]	L-arginine	C6H15N4O2
ARSENATE[c]	arsenate	HO4As
ASN-tRNAs[c]	tRNAasn	
ASN[c]	L-asparagine	C4H8N2O3
ASP-tRNAs[c]	tRNAasp	
ATP[c]	ATP	C10H13N5O13P 3
BCAA-dehydrogenase-DH-lipoyl[c]	lipoamide acyltransferase N6- {dihydrolipoyl} lysine	
BCAA-dehydrogenase-lipoyl[c]	lipoamide acyltransferase N6- {lipoyl} lysine	
BIOMASS[c]	biomass	
BUTYRIC_ACID[c]	butyrate	C4H7O2
BUTYRYL-COA[c]	butyryl-CoA	C25H38N7O17P 3S
CA-2[c]	Ca2+	Ca2+



Species id	Species name	Formula
CARBON-DIOXIDE[c]	CO2	CO2
CARDIOLIPIN[c]	cardiolipin	C13H20O17R4P 2
Cations[c]	a cation	
CDP-2-3-4-Saturated-Diacylglycerols[c]	a CDP-2,3,4-saturated-diacylglycerol	C20H29N3O15R 2RP2
CDP-CHOLINE[c]	CDP-choline	C14H27N4O11P 2
CDP[c]	CDP	C9H12N3O11P2
CDPDIACYLGLYCEROL[c]	a CDP-diacylglycerol	C14H19N3O15R 1R2P2
Ceramides[c]	a ceramide	C19H36NO3R
Charged-ALA-tRNAs[c]	L-alanyl-tRNAala	
Charged-ARG-tRNAs[c]	L-arginyl-tRNAarg	
Charged-ASN-tRNAs[c]	L-asparaginyl-tRNAasn	
Charged-ASP-tRNAs[c]	L-aspartyl-tRNAasp	
Charged-CYS-tRNAs[c]	L-cysteinyl-tRNAcys	
Charged-GLN-tRNAs[c]	L-glutaminyt-tRNAgln	
Charged-GLT-tRNAs[c]	L-glutamyl-tRNAGlu	C5H8NO3tRNA Glu
Charged-GLY-tRNAs[c]	glycyl-tRNAgly	
Charged-HIS-tRNAs[c]	L-histidyl-tRNAhis	
Charged-ILE-tRNAs[c]	L-isoleucyl-tRNAile	
Charged-LEU-tRNAs[c]	L-leucyl-tRNAleu	
Charged-LYS-tRNAs[c]	L-lysyl-tRNAlys	
Charged-MET-tRNAs[c]	L-methionyl-tRNAmet	
Charged-PHE-tRNAs[c]	L-phenylalanyl-tRNAphe	
Charged-PRO-tRNAs[c]	L-prolyl-tRNApro	
Charged-SER-tRNAs[c]	L-seryl-tRNAser	
Charged-THR-tRNAs[c]	L-threonyl-tRNAthr	
Charged-TRP-tRNAs[c]	L-tryptophanyl-tRNAtrp	
Charged-TYR-tRNAs[c]	L-tyrosyl-tRNAtyr	
Charged-VAL-tRNAs[c]	L-valyl-tRNAval	
Cholesterol-esters[c]	a cholesterol ester	C28H45O2R
CHOLESTEROL[c]	cholesterol	C27H46O
CHOLINE[c]	choline	C5H14NO
CL[c]	chloride	Cl
CMP[c]	CMP	C9H12N3O8P
CO-2[c]	Co2+	Co2+
CO-A[c]	coenzyme A	C21H32N7O16P 3S

Species id	Species name	Formula
CPD-10226[c]	3-amino-3-deoxy-D-fructose 6-phosphate	C6H13NO8P
CPD-10227[c]	1-deoxy-1-imino-D-erythrose 4-phosphate	C4H9NO6P
CPD-10363[c]	a beta,beta digalactosyldiacylglycerol	C17H26O15R1R 2
CPD-1181[c]	salicin-6-phosphate	C13H19O10P
CPD-1241[c]	D-galactose 6-phosphate	C6H11O9P
CPD-3[c]	molybdate	O4Mo
CPD-4211[c]	dimethylallyl diphosphate	C5H9O7P2
CPD-448[c]	beta-D-glucose 1-phosphate	C6H11O9P
CPD-5727[c]	5,10-methenyl-tetrahydropteroyl-[gamma-Glu]{n}	C8H10N6OR
CPD-6124[c]	1-pyrroline	C4H8N
CPD-678[c]	hydrogen selenide	Se
CPD-8532[c]	AP site removed form DNA	
CPD-8533[c]	AP site on created by glycosylase in repair process	
CPD-8537[c]	tRNA pseudouridine	C37H49N13O32 R2P5
CPD-8538[c]	tRNA uridine	C37H49N13O32 R1P5
CPD-8989[c]	L-methionine-{S}-S-oxide	C5H11NO3S
CPD0-1147[c]	methyl red	C15H14N3O2
CPD0-1148[c]	N,N'-dimethyl-p-phenylenediamine	C8H12N2
CTP[c]	CTP	C9H12N3O14P3
CU-2[c]	Cu2+	Cu2+
Cyclic-2-3-Ribonucleoside-Monophosphates[c]	a nucleoside 2',3'-cyclic phosphate	C5H8O6RP
CYS-tRNAs[c]	tRNAcys	
CYS[c]	L-cysteine	C3H7NO2S
CYTIDINE[c]	cytidine	C9H13N3O5
CYTOSINE[c]	cytosine	C4H5N3O
D-Galactosyl-12-diacyl-glycerols[c]	a monogalactosyldiacylglycerol	C11H16O10R1R 2
D-SEDOHEPTULOSE-7-P[c]	D-sedoheptulose-7-phosphate	C7H13O10P
DADP[c]	2'-deoxyadenosine-5'-diphosphate	C10H12N5O9P2
Damaged-DNA-Pyrimidine[c]	a damaged DNA pyrimidine	
DAMP[c]	dAMP	C10H12N5O6P
DATP[c]	dATP	C10H13N5O12P 3
DCDP[c]	dCDP	C9H12N3O10P2
DCMP[c]	dCMP	C9H12N3O7P

Species id	Species name	Formula
DCTP[c]	dCTP	C9H12N3O13P3
DEAMIDO-NAD[c]	nicotinate adenine dinucleotide	C21H24N6O15P 2
DEOXY-D-RIBOSE-1-PHOSPHATE[c]	deoxy-D-ribose 1-phosphate	C5H9O7P
Deoxy-Ribonucleoside-Diphosphates[c]	a 2'-deoxyribonucleoside diphosphate	C5H11O9R1P2
Deoxy-Ribonucleoside-Monophosphates[c]	a 2'-deoxyribonucleoside monophosphate	C5H10O6RP
Deoxy-Ribonucleoside-Triphosphates[c]	a 2'-deoxyribonucleoside triphosphate	C5H12O12R1P3
Deoxy-Ribonucleosides[c]	a deoxynucleoside	C5H9O3R
DEOXY-RIBOSE-1P[c]	deoxyribose-1-phosphate	C5H9O7P
DEOXYADENOSINE[c]	2'-deoxyadenosine	C10H13N5O3
DEOXYCYTIDINE[c]	deoxycytidine	C9H13N3O4
DEOXYGUANOSINE[c]	deoxyguanosine	C10H13N5O4
DEOXYINOSINE[c]	deoxyinosine	C10H12N4O4
Deoxynucleotides[c]	a deoxynucleotide	
DEOXYNUCLEOTIDESM[c]	{deoxynucleotides} {m}	C15H25O13RR1 R2P2
DEOXYURIDINE[c]	deoxyuridine	C9H12N2O5
DEOXYXYLULOSE-5P[c]	1-deoxy-D-xylulose 5-phosphate	C5H9O7P
DEPHOSPHO-COA[c]	dephospho-CoA	C21H33N7O13P 2S
DGDP[c]	2'-deoxyguanosine-5'-diphosphate	C10H12N5O10P 2
DGMP[c]	dGMP	C10H12N5O7P
DGTP[c]	dGTP	C10H12N5O13P 3
DIACYLGLYCEROL[c]	a 1,2-diacylglycerol	C5H6O5R1R2
Dihydro-Lipoyl-Proteins[c]	protein N6-{dihydrolipoyl} lysine	
DIHYDROFOLATE[c]	7,8-dihydrofolate	C19H21N7O6
DIHYDROLIPOAMIDE[c]	dihydrolipoamide	C8H17NOS2
DIHYDROLIPOYL-GCVH[c]	H-Gcv-protein-{dihydrolipoyl} lysine	C8H15OS2Apo-GcvH
DIHYDROXY-ACETONE-PHOSPHATE[c]	dihydroxyacetone phosphate	C3H5O6P
DIPEPTIDES[c]	a dipeptide	C4H6N2O3R1R 2
DNA-containing-a-Apyrimidinic-Sites[c]	a DNA containing a apyrimidinic site	
DNA-containing-abasic-Sites[c]	a DNA containing abasic site	
DNA-N[c]	DNA <sub>n</sub>	

Species id	Species name	Formula
DNA-with-Uracils[c]	a DNA with uracil	
Donor-H2[c]	a reduced electron acceptor	
DPG[c]	1,3-diphosphateglycerate	C3H4O10P2
DUDP[c]	dUDP	C9H11N2O11P2
DUMP[c]	dUMP	C9H11N2O8P
DUTP[c]	dUTP	C9H11N2O14P3
ENZYME-S-SULFANYLCYSTEINE[c]	a protein-S-sulfanylcysteine	C3H5NOProtein 2S2
ERYTHROSE-4P[c]	D-erythrose-4-phosphate	C4H7O7P
FAD[c]	FAD	C27H30N9O15P 2
Fatty-Acids[c]	a fatty acid	C4H6O2R
Fatty-Acyl-CoA[c]	a fatty acyl CoA	C22H35N7O17R P3S
FE-2[c]	Fe2+	Fe2+
FE-3[c]	Fe3+	Fe3+
FMN[c]	FMN	C17H18N4O9P
FORMATE[c]	formate	CHO2
FORMYL-L-METHIONYL-PEPTIDE[c]	formyl-L-methionyl peptide	C12H17N4O6R3 S
FORMYL-THF-GLU-N[c]	an N10-formyl-tetrahydrofolate	C20H23N7O6R1
FRU[c]	D-fructose	C6H12O6
FRU1P[c]	fructose-1-phosphate	C6H11O9P
FRUCTOSE-16-DIPHOSPHATE[c]	fructose-1,6-bisphosphate	C6H10O12P2
FRUCTOSE-6P[c]	D-fructose-6-phosphate	C6H11O9P
FUM[c]	fumarate	C4H2O4
G3P[c]	3-phospho-D-glycerate	C3H4O7P
GAP[c]	D-glyceraldehyde-3-phosphate	C3H5O6P
GDP[c]	GDP	C10H12N5O11P 2
General-Phos-Protein-Substrates[c]	a phosphoprotein	
General-Protein-Substrates[c]	a protein	
GLC-6-P[c]	beta-D-glucose-6-phosphate	C6H11O9P
GLC[c]	beta-D-glucose	C6H12O6
GLN-tRNAs[c]	tRNA <sub>Gln</sub>	
GLN[c]	L-glutamine	C5H10N2O3
GLT-tRNAs[c]	tRNA <sub>Glu</sub>	
GLT[c]	L-glutamate	C5H8NO4
GLUTAMINYL-TRNA-GLN[c]	L-glutaminyL-tRNA <sub>Gln</sub>	
GLUTAMYL-TRNA-GLN[c]	L-glutamyl-tRNA <sub>Gln</sub>	

Species id	Species name	Formula
GLY-tRNAs[c]	tRNAgly	
GLY[c]	glycine	C2H5NO2
GLYCERALD[c]	D-glyceraldehyde	C3H6O3
GLYCEROL-3P[c]	sn-glycerol-3-phosphate	C3H7O6P
GLYCEROL[c]	glycerol	C3H8O3
GLYOX[c]	glyoxylate	C2HO3
GMP[c]	guanosine-5'-phosphate	C10H12N5O8P
GTP[c]	GTP	C10H12N5O14P 3
GUANINE[c]	guanine	C5H5N5O
GUANOSINE-5DP-3DP[c]	ppGpp	C10H11N5O17P 4
GUANOSINE[c]	guanosine	C10H13N5O5
HCO3[c]	bicarbonate	CHO3
HIS-tRNAs[c]	tRNAhis	
HIS[c]	L-histidine	C6H9N3O2
HYDROGEN-PEROXIDE[c]	hydrogen peroxide	H2O2
HYDROXY-METHYL-BUTENYL-DIP[c]	1-hydroxy-2-methyl-2-{E}-butenyl 4-diphosphate	C5H9O8P2
HYPOXANTHINE[c]	hypoxanthine	C5H4N4O
ILE-tRNAs[c]	tRNAile	
ILE[c]	L-isoleucine	C6H13NO2
IMP[c]	inosine-5'-phosphate	C10H11N4O8P
INOSINE[c]	inosine	C10H12N4O5
K[c]	K+	K+
L-1-PHOSPHATIDYL-GLYCEROL-P[c]	an L-1-phosphatidylglycerol-phosphate	C8H14O13R2P2
L-1-PHOSPHATIDYL-GLYCEROL[c]	an L-1-phosphatidyl-glycerol	C8H13O10R12P
L-ALPHA-ALANINE[c]	L-alanine	C3H7NO2
L-ASPARTATE[c]	L-aspartate	C4H6NO4
L-aspartyl-tRNAAsn[c]	L-aspartyl-tRNAasn	
L-CITRULLINE[c]	L-citrulline	C6H13N3O3
L-LACTATE[c]	L-lactate	C3H5O3
L-PHOSPHATIDATE[c]	a 1,2-diacylglycerol-3-phosphate	C5H7O8R1R2P
L-SELENOCYSTEINE[c]	L-selenocysteine	C3H6NO2Se
L-seryl-SEC-tRNAs[c]	L-seryl-tRNAsec	
LACTOSE-6P[c]	lactose 6-phosphate	C12H21O14P
LACTOSE[c]	lactose	C12H22O11
Leader-Sequences[c]	a leader sequence	
LEU-tRNAs[c]	tRNAleu	

Species id	Species name	Formula
LEU[c]	L-leucine	C <sub>6</sub> H <sub>13</sub> NO <sub>2</sub>
LIPID[c]	lipid	
LIPOAMIDE[c]	lipoamide	C <sub>8</sub> H <sub>15</sub> NOS <sub>2</sub>
LIPOIC-ACID[c]	lipoate	C <sub>8</sub> H <sub>13</sub> O <sub>2</sub> S <sub>2</sub>
LIPOYL-AMP[c]	lipoyl-AMP	C <sub>18</sub> H <sub>25</sub> N <sub>5</sub> O <sub>8</sub> PS <sub>2</sub>
Lipoyl-Protein[c]	protein N6- {lipoyl} lysine	
Long-Chain-Polyphosphate[c]	long chain polyphosphate	H <sub>7</sub> O <sub>16</sub> P <sub>5</sub>
LYS-tRNAs[c]	tRNA <sub>lys</sub>	
LYS[c]	L-lysine	C <sub>6</sub> H <sub>15</sub> N <sub>2</sub> O <sub>2</sub>
MAL[c]	{S}-malate	C <sub>4</sub> H <sub>4</sub> O <sub>5</sub>
MALTOSE[c]	maltose	C <sub>12</sub> H <sub>22</sub> O <sub>11</sub>
MANNITOL-1P[c]	mannitol-1-phosphate	C <sub>6</sub> H <sub>15</sub> O <sub>9</sub> P
MANNOSE-1P[c]	alpha-D-mannose 1-phosphate	C <sub>6</sub> H <sub>11</sub> O <sub>9</sub> P
MANNOSE-6P[c]	D-mannose-6-phosphate	C <sub>6</sub> H <sub>11</sub> O <sub>9</sub> P
MET-tRNAs[c]	tRNA <sub>met</sub>	
MET[c]	L-methionine	C <sub>5</sub> H <sub>11</sub> NO <sub>2</sub> S
METHIONYL-PEPTIDE[c]	methionyl peptide	C <sub>11</sub> H <sub>17</sub> N <sub>4</sub> O <sub>5</sub> R <sub>3</sub> S
METHYLENE-THF[c]	5,10-methylene-THF	C <sub>20</sub> H <sub>23</sub> N <sub>7</sub> O <sub>6</sub>
MEVALONATE[c]	{R}-mevalonate	C <sub>6</sub> H <sub>11</sub> O <sub>4</sub>
Mg-2[c]	Mg <sup>2+</sup>	Mg <sup>2+</sup>
Mn-2[c]	Mn <sup>2+</sup>	Mn <sup>2+</sup>
Multidrug[c]	multidrug	
N-formyl-L-methionyl-tRNA <sub>met</sub> [c]	N-formyl-L-methionyl-tRNA <sub>met</sub>	
N-Substituted-Amino-Acids[c]	an N-substituted amino acid	C <sub>2</sub> H <sub>4</sub> NO <sub>2</sub> R <sub>1</sub>
N-Substituted-Aminoacyl-tRNA[c]	N-substituted aminoacyl-tRNA	
NAD(P)[c]	NAD{P}+	
NAD(P)H[c]	NAD{P}H	
NA[c]	Na <sup>+</sup>	Na <sup>+</sup>
NAD[c]	NAD <sup>+</sup>	C <sub>21</sub> H <sub>26</sub> N <sub>7</sub> O <sub>14</sub> P <sub>2</sub>
NADH[c]	NADH	C <sub>21</sub> H <sub>27</sub> N <sub>7</sub> O <sub>14</sub> P <sub>2</sub>
NADP[c]	NADP <sup>+</sup>	C <sub>21</sub> H <sub>25</sub> N <sub>7</sub> O <sub>17</sub> P <sub>3</sub>
NADPH[c]	NADPH	C <sub>21</sub> H <sub>26</sub> N <sub>7</sub> O <sub>17</sub> P <sub>3</sub>
Ni-2[c]	Ni <sup>2+</sup>	Ni <sup>2+</sup>
NIACINE[c]	nicotinate	C <sub>6</sub> H <sub>4</sub> NO <sub>2</sub>

Species id	Species name	Formula
NICOTINAMIDE_NUCLEOTIDE[c]	nicotinamide mononucleotide	C11H14N2O8P
NICOTINATE_NUCLEOTIDE[c]	nicotinate mononucleotide	C11H12NO9P
Nucleoside-Triphosphates[c]	a nucleoside triphosphate	C5H12O13RP3
OLIGOPEPTIDE[c]	oligopeptide	
Ox-Thioredoxin[c]	an oxidized thioredoxin	
OXALACETIC_ACID[c]	oxaloacetate	C4H2O5
Oxidized-ferredoxins[c]	an oxidized ferredoxin	
Oxidized-NrdH-Proteins[c]	an oxidized NrdH glutaredoxin-like protein	
Oxo-glutarate-dehydrogenase-DH-lipoyl[c]	dihydrolipoyltranssuccinylase N6-{dihydrolipoyl}lysine	
Oxo-glutarate-dehydrogenase-lipoyl[c]	dihydrolipoyltranssuccinylase	N6-{lipoyl}lysine
OXYGEN-MOLECULE[c]	oxygen	O2
Peptides-with-Leader-Sequence[c]	a peptide with a leader sequence	
Peptides[c]	a peptide	
PHE-tRNAs[c]	tRNAphe	
PHE[c]	L-phenylalanine	C9H11NO2
PHOSPHATIDYLCHOLINE[c]	a phosphatidylcholine	C10H19NO8R2R1P
PHOSPHO-ENOL-PYRUVATE[c]	phosphoenolpyruvate	C3H2O6P
PHOSPHORYL-CHOLINE[c]	phosphoryl-choline	C5H13NO4P
Pi[c]	phosphate	HO4P
PPI[c]	diphosphate	HO7P2
Prenyl-tRNAs[c]	prenyl-tRNA	
PRO-tRNAs[c]	tRNApro	
PRO[c]	L-proline	C5H9NO2
PROPIONATE[c]	propionate	C3H5O2
PROPIONYL-P[c]	propionyl-P	C3H5O5P
PROT-CYS[c]	a protein L-cysteine	C3H6N2OProtein2S
Protein-3-phospho-L-histidines[c]	a protein-Npi-phospho-L-histidine	C6H8N3O5Protein2P
Protein-6-N-lipoyl-lysine[c]	a protein 6-N-{lipoyl}lysine	
Protein-Histidines[c]	a protein histidine	C6H7N3OProtein2
Protein-L-methionine-R-S-oxides[c]	a protein-L-methionine-{R}-S-oxide	
Protein-L-methionine[c]	a protein L-methionine	

Species id	Species name	Formula
PROTEIN-LIPOYLLYSINE[c]	H-Gcv-protein-{lipoyl}lysine	C8H13OS2Apo-GcvH
PROTON[c]	H <sup>+</sup>	H <sup>+</sup>
PRPP[c]	5-phosphoribosyl 1-pyrophosphate	C5H8O14P3
Purine-Bases[c]	a purine base	
Purine-Ribonucleosides[c]	a purine ribonucleoside	
PUTRESCINE[c]	putrescine	C4H14N2
PYRIDOXAL[c]	pyridoxal	C8H9NO3
PYRIDOXAL_PHOSPHATE[c]	pyridoxal 5'-phosphate	C8H8NO6P
Pyruvate-dehydrogenase-acetylDHlipoyl[c]	lipoate acetyltransferase N6-{S-acetyldihydrolipoyl}lysine	
Pyruvate-dehydrogenase-dihydrolipoate[c]	lipoate acetyltransferase N6-{dihydrolipoyl}lysine	
Pyruvate-dehydrogenase-lipoate[c]	lipoate acetyltransferase N6-{lipoyl}lysine	
PYRUVATE[c]	pyruvate	C3H3O3
Red-Thioredoxin[c]	a reduced thioredoxin	
Reduced-ferredoxins[c]	a reduced ferredoxin	
Reduced-NrdH-Proteins[c]	a reduced NrdH glutaredoxin-like protein	
RIBOFLAVIN[c]	riboflavin	C17H19N4O6
Ribonucleoside-Diphosphates[c]	a ribonucleoside diphosphate	
RIBOSE-1-ARSENATE[c]	ribose-1-arsenate	C5H9O8As
RIBOSE-1P[c]	alpha-D-ribose-1-phosphate	C5H9O8P
RIBOSE-5P[c]	D-ribose-5-phosphate	C5H9O8P
RIBULOSE-5P[c]	D-ribulose-5-phosphate	C5H9O8P
RNA-N[c]	RNA {n}	
S-ACETYLDIHYDROLIPOAMIDE[c]	S-acetyldihydrolipoamide	C10H19NO2S2
S-ADENOSYLMETHIONINE[c]	S-adenosyl-L-methionine	C15H23N6O5S
Saturated-2-Lysophosphatidates[c]	a 2,3,4-saturated 2-lysophosphatidate	C7H12O7RP
Saturated-Fatty-Acyl-ACPs[c]	a 2,3,4-saturated fatty acyl-[acp]	C4H6Oa holo-[acp]R
SEC-tRNAs[c]	tRNA <sup>sec</sup>	
SER-tRNAs[c]	tRNA <sup>ser</sup>	
SER[c]	L-serine	C3H7NO3
Some-tRNA[c]	a tRNA	
SPERMIDINE[c]	spermidine	C7H22N3
Sphingomyelins[c]	a sphingomyelin	C24H49N2O6R1P



Species id	Species name	Formula
SUC-CoA[c]	succinyl-CoA	C25H35N7O19P 3S
SUC[c]	succinate	C4H4O4
Sugar-Phosphate[c]	a sugar phosphate	
Sugar[c]	a sugar	
SULFATE[c]	sulfate	SO4
TAGATOSE-6-PHOSPHATE[c]	tagatose-6-phosphate	C6H11O9P
TDP[c]	dTDP	C10H13N2O11P 2
THF[c]	tetrahydrofolate	C19H23N7O6
THIAMINE-P[c]	thiamine-phosphate	C12H16N4O4PS
THIAMINE-PYROPHOSPHATE[c]	thiamine diphosphate	C12H16N4O7P2 S
THIAMINE[c]	thiamin	C12H17N4OS
THR-tRNAs[c]	tRNA <sup>thr</sup>	
THR[c]	L-threonine	C4H9NO3
THYMIDINE[c]	thymidine	C10H14N2O5
THYMINE[c]	thymine	C5H6N2O2
TMP[c]	dTMP	C10H13N2O8P
Triacylglycerols[c]	a triacylglycerol	C6H5O6R1R2R 3
tRNA-Containing-6Isopentenyladenosine[c]	tRNA containing N6-dimethylallyl-adenosine	
tRNA-Containing-N1-Methylguanine[c]	tRNA containing N1-methylguanine	
tRNA-precursors[c]	a tRNA precursor	
tRNAs-with-N7-methyl-guanine[c]	a tRNA containing N7-methylguanine	
TRP-tRNAs[c]	tRNA <sup>trp</sup>	
TRP[c]	L-tryptophan	C11H12N2O2
TTP[c]	dTTP	C10H13N2O14P 3
TYR-tRNAs[c]	tRNA <sup>tyr</sup>	
TYR[c]	L-tyrosine	C9H11NO3
UDP-GALACTOSE[c]	UDP-D-galactose	C15H22N2O17P 2
UDP[c]	uridine-5'-diphosphate	C9H11N2O12P2
UMP[c]	uridine-5'-phosphate	C9H11N2O9P
URACIL[c]	uracil	C4H4N2O2
URIDINE[c]	uridine	C9H12N2O6
UTP[c]	UTP	C9H11N2O15P3
VAL-tRNAs[c]	tRNA <sup>val</sup>	

Species id	Species name	Formula
VAL[c]	L-valine	C5H11NO2
WATER[c]	H2O	H2O
XANTHOSINE-5-PHOSPHATE[c]	xanthosine-5-phosphate	C10H11N4O9P
XYLULOSE-5-PHOSPHATE[c]	D-xylulose-5-phosphate	C5H9O8P
ZN-2[c]	Zn2+	Zn2+

### A3.2. Metabolites located in the extracellular space

**Table S6. Metabolites in the extracellular space for *M. gallisepticum* model.** The name, id, and formula for each species are provided

Species name	Species id	Formula
2-KETOGLUTARATE[e]	2-ketoglutarate	C5H6O5
ACET[e]	acetate	C2H3O2
ACYL-COA[e]	acyl-CoA	C22H35N7O17RP3 S
ADENINE[e]	adenine	C5H5N5
Amino-Acids-20[e]	a standard alpha amino acid	C2H4NO2R
AMMONIUM[e]	NH4+	H4N
AMP[e]	AMP	C10H14N5O7P
ARG[e]	L-arginine	C6H14N4O2
ASN[e]	L-asparagine	C4H8N2O3
CA-2[e]	Ca2+	Ca2+
Cations[e]	a cation	
Ceramides[e]	a ceramide	
Cholesterol-esters[e]	a cholesterol ester	C28H45O2R
CHOLESTEROL[e]	cholesterol	C27H46O
CHOLINE[e]	choline	C5H14NO
CMP[e]	CMP	C9H14N3O8P
CO-2[e]	Co2+	Co2+
CO-A[e]	coenzyme	C21H36N7O16P3S
CPD-1142[e]	salicin	C13H18O7
CPD-3[e]	molybdate	O4Mo
CU-2[e]	Cu2+	Cu2+
CYTOSINE[e]	cytosine	C4H5N3O
DATP[e]	dATP	C10H16N5O12P3
Deoxy-Ribonucleosides[e]	a deoxynucleoside	C5H9O3R
DGTP[e]	dGTP	C10H16N5O13P3
DIHYDROFOLATE[e]	7,8-dihydrofolate	C19H22N7O6
DIPEPTIDES[e]	a dipeptide	C4H6N2O3R1R2

Species name	Species id	Formula
Fatty-Acids[e]	a fatty acid	C4H7O2R
FE-2[e]	Fe2+	Fe2+
FE-3[e]	Fe3+	Fe3+
FRU[e]	D-fructose	C6H12O6
GLC[e]	beta-D-glucose	C6H12O6
GLT[e]	L-glutamate	C5H9NO4
GLYCEROL-3P[e]	sn-glycerol-3-phosphate	C3H7O6P
GLYCEROL[e]	glycerol	C3H8O3
GMP[e]	GMP	C10H14N5O8P
GTP[e]	GTP	C10H16N5O14P3
GUANINE[e]	guanine	C5H5N5O
HIS[e]	L-histidine	C6H9N3O2
ILE[e]	L-isoleucine	C6H13NO2
K[e]	K+	K+
L-1-PHOSPHATIDYL-GLYCEROL[e]	an L-1-phosphatidyl-glycerol	C8H13O10R12P
L-LACTATE[e]	L-lactate	C3H5O3
L-PHOSPHATIDATE[e]	a 1,2-diacylglycerol-3-phosphate	C5H7O8R1R2P
LEU[e]	L-leucine	C6H13NO2
LIPID[e]	lipid	
LYS[e]	L-lysine	C6H14N2O2
MALTOSE[e]	maltose	C12H22O11
MANNITOL[e]	D-mannitol	C6H14O6
MANNOSE[e]	D-mannose	C6H12O6
MET[e]	L-methionine	C5H11NO2S
MG-2[e]	Mg2+	Mg2+
MN-2[e]	Mn2+	Mn2+
Multidrug[e]	multidrug	
NA[e]	Na+	Na+
NI-2[e]	Ni2+	Ni2+
NIACINE[e]	nicotinate	C6H5NO2
OLIGOPEPTIDE[e]	oligopeptide	
PHE[e]	L-phenylalanine	C9H11NO2
PHOSPHATIDYLCHOLINE[e]	a phosphatidylcholine	C10H19NO8R2R1P
Pi[e]	phosphate	HO4P
PRO[e]	L-proline	C5H9NO2
PROPIONATE[e]	propionate	C3H6O2
PROTON[e]	H+	H+

Species name	Species id	Formula
PUTRESCINE[e]	putrescine	C4H14N2
PYRIDOXAL[e]	pyridoxal	C8H9NO3
RIBOFLAVIN[e]	riboflavin	C17H20N4O6
SER[e]	L-serine	C3H7NO3
SPERMIDINE[e]	spermidine	C7H22N3
Sphingomyelins[e]	a sphingomyelin	C24H49N2O6R1P
Sugar[e]	a sugar	
SULFATE[e]	sulfate	O4S
THIAMINE[e]	thiamin	C12H17N4OS
THYMIDINE[e]	thymidine	C10H14N2O5
THYMINE[e]	thymine	C5H6N2O2
Triacylglycerols[e]	a triacylglycerol	C6H5O6R1R2R3
TRP[e]	L-tryptophan	C11H12N2O2
TYR[e]	L-tyrosine	C9H11NO3
UMP[e]	UMP	C9H13N2O9P
URACIL[e]	uracil	C4H4N2O2
VAL[e]	L-valine	C5H11NO2
ZN-2[e]	Zn2+	Zn2+

### A3.3. Intracellular reactions

**Table S7. Intracellular reactions for *M. gallisepticum* model.** The name and gene(s) locus for each reaction are provided. \*Monomer97n-#### refers to genes created by the curator which could not be found associated with a gene, but were inferred from literature review.

Name	Reaction	Locus*
FHLMULTI-RXN	1*FORMATE[c]+1*NAD[c] --> 1*NADH[c]+1*CARBON-DIOXIDE[c]	
TRANS-RXN7TV-7128	1*GLC[c] --> 1*GLC[e]	
DXPREDISOM-RXN	1*PROTON[c]+1*NADPH[c]+1*DEOXYXYLULOSE-5P[c] --> 1*NADP[c]+1*2-C-METHYL-D-ERYTHRITOL-4-PHOSPHATE[c]	MGA-0787
GLYC3PDEHYDROGBIOSYN-RXN	1*PROTON[c]+1*NAD(P)H[c]+1*DIHYDROXY-ACETONE-PHOSPHATE[c] <--> 1*NAD(P)[c]+1*GLYCEROL-3P[c]	MGA-1133
L-LACTATE-DEHYDROGE	1*PYRUVATE[c]+1*NADH[c]+1*PROTON[c] --> 1*L-LACTATE[c]+1*NAD[c]	MGA-0746

Name	Reaction	Locus*
NASE-RXN		
MALATE-DEH-RXN	1*NAD[c]+1*MAL[c] <--> 1*NADH[c]+1*OXALACETIC_ACID[c]+1*PROTON[c]	MGA-0746
GLYCEROL-3-PHOSPHATE-OXIDASE-RXN	1*GLYCEROL-3P[c]+1*OXYGEN-MOLECULE[c] --> 1*DIHYDROXY-ACETONE-PHOSPHATE[c]+1*HYDROGEN-PEROXIDE[c]	MGA-0646
ADPREDUCT-RXN	1*Red-Thioredoxin[c]+1*ADP[c] --> 1*WATER[c]+1*Ox-Thioredoxin[c]+1*DADP[c]	MGA-0695,MGA-0698
CDPREDUCT-RXN	1*Red-Thioredoxin[c]+1*CDP[c] --> 1*WATER[c]+1*Ox-Thioredoxin[c]+1*DCDP[c]	MGA-0695,MGA-0698
GDPREDUCT-RXN	1*Red-Thioredoxin[c]+1*GDP[c] --> 1*WATER[c]+1*Ox-Thioredoxin[c]+1*DGDP[c]	MGA-0695,MGA-0698
RIBONUCLEOSIDE-DIP-REDUCTI-RXN	1*WATER[c]+1*Ox-Thioredoxin[c]+1*Deoxy-Ribonucleoside-Diphosphates[c] --> 1*Red-Thioredoxin[c]+1*Ribonucleoside-Diphosphates[c]	MGA-0698,MGA-0695
RIBONUCLEOSIDE-DIP-REDUCTII-RXN	1*Oxidized-NrdH-Proteins[c]+1*CDP[c] --> 1*WATER[c]+1*Reduced-NrdH-Proteins[c]+1*DCDP[c]	MGA-0695
TRANS-RXN7TV-3819	1*L-1-PHOSPHATIDYL-GLYCEROL[e] <-> 1*L-1-PHOSPHATIDYL-GLYCEROL[c]	
RXN0-722	1*Reduced-NrdH-Proteins[c]+1*UDP[c] --> 1*WATER[c]+1*Oxidized-NrdH-Proteins[c]+1*DUDP[c]	MGA-0695
RXN0-747	1*Reduced-NrdH-Proteins[c]+1*ADP[c] --> 1*WATER[c]+1*Oxidized-NrdH-Proteins[c]+1*DADP[c]	MGA-0695
RXN0-748	1*Reduced-NrdH-Proteins[c]+1*GDP[c] --> 1*WATER[c]+1*Oxidized-NrdH-Proteins[c]+1*DGDP[c]	MGA-0695
UDPREDUCT-RXN	1*Red-Thioredoxin[c]+1*UDP[c] --> 1*WATER[c]+1*Ox-Thioredoxin[c]+1*DUDP[c]	MGA-0695,MGA-0698
RXN0-882	2*Reduced-ferredoxins[c]+1*2C-METH-D-ERYTHRITOL-CYCLODIPHOSPHATE[c] -> 1*WATER[c]+2*Oxidized-ferredoxins[c]+1*HYDROXY-METHYL-	MGA-1156

Name	Reaction	Locus*
	BUTENYL-DIP[c]	
1.2.1.9-RXN	1*WATER[c]+1*NADP[c]+1*GAP[c] --> 1*NADPH[c]+1*G3P[c]+2*PROTON[c]	MGA-0860
1.5.1.35-RXN	2*WATER[c]+1*NAD[c]+1*CPD-6124[c] -- > 2*PROTON[c]+1*NADH[c]+1*4- AMINO-BUTYRATE[c]	MGA-0590
AMINOBU TDEHYDROG- RXN	1*WATER[c]+1*NAD[c]+1*4-AMINO- BUTYRALDEHYDE[c] --> 2*PROTON[c]+1*NADH[c]+1*4-AMINO- BUTYRATE[c]	MGA-0590
GAPOXNPHO SPHN-RXN	1*NAD[c]+1*Pi[c]+1*GAP[c] <--> 1*NADH[c]+1*DPG[c]+1*PROTON[c]	MGA-0330,MGA-1184
TRANS- RXN7TV-3818	1*Sphingomyelins[e] <--> 1*Sphingomyelins[c]	
PYRUVDEH- RXN	1*NAD[c]+1*CO-A[c]+1*PYRUVATE[c] -- > 1*NADH[c]+1*CARBON- DIOXIDE[c]+1*ACETYL-COA[c]	MGA-0161
PYRUVATED ECARB-RXN	1*LIPOAMIDE[c]+1*PYRUVATE[c]+1*PR OTON[c] --> 1*CARBON- DIOXIDE[c]+1*S- ACETYLDIHYDROLIPOAMIDE[c]	MGA-0165,MGA-0164
RXN0-1134	1*Pyruvate-dehydrogenase- lipoate[c]+1*PYRUVATE[c] --> 1*CARBON-DIOXIDE[c]+1*Pyruvate- dehydrogenase-acetylDhlipoyl[c]	MGA-0165,MGA-0164
1.5.1.15-RXN	1*NAD[c]+1*METHYLENE-THF[c] --> 1*NADH[c]+1*5-10-METHENYL-THF[c]	MGA-0596
DIHYDROFO LATEREDUC T-RXN	1*DIHYDROFOLATE[c]+1*NADPH[c]+1* PROTON[c] --> 1*THF[c]+1*NADP[c]	MGA-0701
METHYLENE THFDEHYDR OG-NADP- RXN	1*NADP[c]+1*METHYLENE-THF[c] --> 1*5-10-METHENYL-THF[c]+1*NADPH[c]	MGA-0596
PYRNUTRAN SHYDROGEN -RXN	1*NADPH[c]+1*NAD[c] --> 1*NADP[c]+1*NADH[c]	MGA-0161
RXN0-5375	2*NADH[c]+1*CPD0- 1147[c]+2*PROTON[c] --> 2*NAD[c]+1*CPD0- 1148[c]+1*ANTHRAATE[c]	MGA-0243
1.8.1.4-RXN	1*NAD[c]+1*Dihydro-Lipoyl-Proteins[c] --> 1*PROTON[c]+1*NADH[c]+1*Lipoyl- Protein[c]	MGA-0161
DIHYDLIPOX	1*NAD[c]+1*DIHYDROLIPOAMIDE[c] --	MGA-0161

Name	Reaction	Locus*
N-RXN	> 1*NADH[c]+1*LIPOAMIDE[c]+1*PROTON[c]	
TRANS-RXN7TV-3817	1*PHOSPHATIDYLCHOLINE[e] <--> 1*PHOSPHATIDYLCHOLINE[c]	
RXN-7716	1*NAD[c]+1*Oxo-glutarate-dehydrogenase-DH-lipoyl[c] --> 1*PROTON[c]+1*NADH[c]+1*Oxo-glutarate-dehydrogenase-lipoyl[c]	MGA-0161
RXN-7719	1*NAD[c]+1*BCAA-dehydrogenase-DH-lipoyl[c] --> 1*PROTON[c]+1*NADH[c]+1*BCAA-dehydrogenase-lipoyl[c]	MGA-0161
RXN-8629	1*NAD[c]+1*DIHYDROLIPOYL-GCVH[c] --> 1*PROTON[c]+1*NADH[c]+1*PROTEIN-LIPOYLLYSINE[c]	MGA-0161
RXN0-1132	1*NAD[c]+1*Pyruvate-dehydrogenase-dihydrolipoate[c] --> 1*PROTON[c]+1*NADH[c]+1*Pyruvate-dehydrogenase-lipoate[c]	MGA-0161
THIOREDOXIN-REDUCT-NADPH-RXN	1*PROTON[c]+1*NADPH[c]+1*Ox-Thioredoxin[c] --> 1*NADP[c]+1*Red-Thioredoxin[c]	MGA-0124,MGA-1221
1.8.4.12-RXN	1*WATER[c]+1*Ox-Thioredoxin[c]+1*Protein-L-methionine[c] --> 1*Red-Thioredoxin[c]+1*Protein-L-methionine-R-S-oxides[c]	MGA-0149
RXN-8669	1*WATER[c]+1*Ox-Thioredoxin[c]+1*MET[c] --> 1*Red-Thioredoxin[c]+1*CPD-8989[c]	MGA-0571
THYMIDYLATESYN-RXN	1*DUMP[c]+1*METHYLENE-THF[c] <--> 1*DIHYDROFOLATE[c]+1*TMP[c]	MGA-0699
TRNA-GUANINE-N1--METHYLTRANSFERASE-RXN	1*S-ADENOSYLMETHIONINE[c]+1*Some-tRNA[c] --> 1*tRNA-Containing-N1-Methylguanine[c]+1*ADENOSYL-HOMO-CYS[c]	MGA-0439
TRNA-GUANINE-N7--METHYLTRANSFERASE-RXN	1*S-ADENOSYLMETHIONINE[c]+1*Some-tRNA[c] --> 1*tRNAs-with-N7-methyl-guanine[c]+1*ADENOSYL-HOMO-CYS[c]	MGA-1194

Name	Reaction	Locus*
TRANS-RXN7TV-3816	1*Ceramides[e] <--> 1*Ceramides[c]	
GLYOHMETRANS-RXN	1*THF[c]+1*SER[c] --> 1*WATER[c]+1*GLY[c]+1*METHYLENE-THF[c]	MGA-1146
METHIONYL-TRNA-FORMYLTRANSFERASE-RXN	1*WATER[c]+1*Charged-MET-tRNAs[c]+1*10-FORMYL-THF[c] --> 1*N-formyl-L-methionyl-tRNA <sup>met</sup> [c]+1*THF[c]	MGA-0846
1TRANSKETO-RXN	1*XYLULOSE-5-PHOSPHATE[c]+1*RIBOSE-5P[c] <--> 1*GAP[c]+1*D-SEDOHEPTULOSE-7-P[c]	MGA-0342,MGA-0666
2TRANSKETO-RXN	1*XYLULOSE-5-PHOSPHATE[c]+1*ERYTHROSE-4P[c] <--> 1*GAP[c]+1*FRUCTOSE-6P[c]	MGA-0342,MGA-0666
DXS-RXN	1*GAP[c]+1*PYRUVATE[c]+1*PROTON[c] --> 1*CARBON-DIOXIDE[c]+1*DEOXYXYLULOSE-5P[c]	MGA-1267
RXN-9583	1*RIBOSE-5P[c]+1*CPD-10226[c] --> 1*D-SEDOHEPTULOSE-7-P[c]+1*CPD-10227[c]	MGA-0342,MGA-0666
1-ACYLGLYCEROL-3-P-ACYLTRANSFER-RXN	1*ACYL-ACP[c]+1*ACYL-SN-GLYCEROL-3P[c] --> 1*ACP[c]+1*L-PHOSPHATIDATE[c]	MGA-0039
DIHYDLIPACETRANS-RXN	1*DIHYDROLIPOAMIDE[c]+1*ACETYL-COA[c] --> 1*S-ACETYLDIHYDROLIPOAMIDE[c]+1*CO-A[c]	MGA-0162
PHOSACETYLTRANS-RXN	1*ACETYL-COA[c]+1*Pi[c] --> 1*CO-A[c]+1*ACETYL-P[c]	MGA-0432
RXN-1623	1*ACYL-SN-GLYCEROL-3P[c]+1*Fatty-Acyl-CoA[c] --> 1*CO-A[c]+1*L-PHOSPHATIDATE[c]	MGA-0039
TRANS-RXN7TV-3815	1*L-PHOSPHATIDATE[e] <--> 1*L-PHOSPHATIDATE[c]	
RXN0-1133	1*Pyruvate-dehydrogenase-acetylDHlipoyl[c]+1*CO-A[c] --> 1*Pyruvate-dehydrogenase-dihydrolipoate[c]+1*ACETYL-COA[c]	MGA-0162
RXN0-5514	1*Saturated-Fatty-Acyl-ACPs[c]+1*Saturated-2-	MGA-0039



Name	Reaction	Locus*
	Lysophosphatidates[c] --> 1*ACP[c]+1*2-3-4-Saturated-L-Phosphatidates[c]	
HYDROXYMETHYLGLUTARYL-COA-SYNTHASE-RXN	1*ACETYL-COA[c]+1*WATER[c]+1*ACETOACETYL-COA[c] --> 1*3-HYDROXY-3-METHYL-GLUTARYL-COA[c]+1*CO-A[c]+1*PROTON[c]	MONOMER97N-9 HMG-CoA Synthase
MALSYN-RXN	1*GLYOX[c]+1*WATER[c]+1*ACETYL-COA[c] --> 1*CO-A[c]+1*MAL[c]+1*PROTON[c]	MONOMER97N-294 Malate Synthase
2.4.1.46-RXN	1*UDP-GALACTOSE[c]+1*DIACYLGLYCEROL[c] --> 1*UDP[c]+1*D-Galactosyl-12-diacyl-glycerols[c]	MGA-1315
MALTOSE-PHOSPHORYLASE-RXN	1*MALTOSE[c]+1*Pi[c] --> 1*GLC[c]+1*CPD-448[c]	MGA-1265
RXN-1226	2*D-Galactosyl-12-diacyl-glycerols[c] --> 1*DIACYLGLYCEROL[c]+1*CPD-10363[c]	MGA-1315
ADENPHOSPHOR-RXN	1*Pi[c]+1*ADENOSINE[c] <--> 1*ADENINE[c]+1*RIBOSE-1P[c]	MGA-0364
ADENPRIBOSYLTRAN-RXN	1*PPI[c]+1*AMP[c] <--> 1*ADENINE[c]+1*PRPP[c]	MGA-0955
DEOXYURIDINE-PHOSPHORYLASE-RXN	1*Pi[c]+1*DEOXYURIDINE[c] --> 1*DEOXY-D-RIBOSE-1-PHOSPHATE[c]+1*URACIL[c]	MONOMER97N-556 (deoxyuridine phosphorylase )
TRANS-RXN7TV-3814	1*Cholesterol-esters[e] <--> 1*Cholesterol-esters[c]	
GUANPRIBOSYLTRAN-RXN	1*GUANINE[c]+1*PRPP[c] --> 1*GMP[c]+1*PPI[c]	MGA-0658
HYPOXANPRIBOSYLTRAN-RXN	1*HYPOXANTHINE[c]+1*PRPP[c] --> 1*IMP[c]+1*PPI[c]	MGA-0658
INOPHOSPHOR-RXN	1*Pi[c]+1*INOSINE[c] --> 1*HYPOXANTHINE[c]+1*RIBOSE-1P[c]	MGA-0364
NICOTINATEPRIBOSYLTRANS-RXN	1*PRPP[c]+1*NIACINE[c]+1*PROTON[c] -> 1*PPI[c]+1*NICOTINATE_NUCLEOTIDE[c]	MGA-0428
PNP-RXN	1*Pi[c]+1*Purine-Ribonucleosides[c] --> 1*RIBOSE-1P[c]+1*Purine-Bases[c]	MGA-0364

Name	Reaction	Locus*
RXN-7001	1*ARSENATE[c]+1*Purine-Ribonucleosides[c] --> 1*Purine-Bases[c]+1*RIBOSE-1-ARSENATE[c]	MGA-0364
RXN0-5199	1*Pi[c]+1*GUANOSINE[c] <--> 1*GUANINE[c]+1*RIBOSE-1P[c]	MGA-0364
THYM-PHOSPH-RXN	1*THYMIDINE[c]+1*Pi[c] --> 1*THYMINE[c]+1*DEOXY-RIBOSE-1P[c]	MGA-0362
URACIL-PRIBOSYLTRANS-RXN	1*URACIL[c]+1*PRPP[c] --> 1*UMP[c]+1*PPI[c]	MGA-1159
URPHOS-RXN	1*URIDINE[c]+1*Pi[c] --> 1*URACIL[c]+1*RIBOSE-1P[c]	MONOMER97N-546 (uridine phosphorylase)
TRANS-RXN7TV-3813	1*CHOLESTEROL[e] <--> 1*CHOLESTEROL[c]	
RXN-4543	1*CPD-4211[c]+1*Some-tRNA[c] --> 1*PPI[c]+1*Prenyl-tRNAs[c]	MGA-0914
S-ADENMETSYN-RXN	1*WATER[c]+1*MET[c]+1*ATP[c] --> 1*S-ADENOSYLMETHIONINE[c]+1*PPI[c]+1*Pi[c]+1*PROTON[c]	MGA-0128
TRNA-ISOPENTENYLTRANSFERASE-RXN	1*CPD-4211[c]+1*Some-tRNA[c] --> 1*PPI[c]+1*tRNA-Containing-6Isopentenyladenosine[c]	MGA-0914
ASPAMINOTRANS-RXN	1*2-KETOGLUTARATE[c]+1*L-ASPARTATE[c] <--> 1*OXALACETIC ACID[c]+1*GLT[c]	MONOMER97N-539 (Asparate aminotransferase)
1PFRUCTPHOSN-RXN	1*FRU1P[c]+1*ATP[c] --> 1*FRUCTOSE-16-DIPHOSPHATE[c]+1*ADP[c]+2*PROTON[c]	MONOMER97N-1269 (Fructose-1-phosphate kinase)
2.7.1.145-RXN	1*ATP[c]+1*Deoxy-Ribonucleosides[c] --> 1*ADP[c]+1*Deoxy-Ribonucleoside-Monophosphates[c]	MGA-0175,MGA-0174
2.7.1.148-RXN	1*ATP[c]+1*4-CYTIDINE-5-DIPHOSPHO-2-C[c] --> 1*ADP[c]+1*2-PHOSPHO-4-CYTIDINE-5-DIPHOSPHO-2-C-MET[c]+2*PROTON[c]	MGA-0635
2.7.1.69-RXN	1*Sugar[c]+1*Protein-3-phospho-L-histidines[c] --> 1*Sugar-Phosphate[c]+1*Protein-Histidines[c]	MGA-0508,MGA-0855
6PFRUCTPHOS-RXN	1*FRUCTOSE-6P[c]+1*ATP[c] --> 1*FRUCTOSE-16-DIPHOSPHATE[c]+1*ADP[c]+2*PROTON[c]	MGA-0157

Name	Reaction	Locus*
CHOLINE-KINASE-RXN	1*ATP[c]+1*CHOLINE[c] --> 1*ADP[c]+1*PHOSPHORYL- CHOLINE[c]+2*PROTON[c]	MGA-0931
TRANS-RXN7TV-3812	1*Triacylglycerols[e] <--> 1*Triacylglycerols[c]	
CYTIDINEKIN-RXN	1*GTP[c]+1*CYTIDINE[c] --> 1*GDP[c]+1*CMP[c]+1*PROTON[c]	MGA-0106
CYTIKIN-RXN	1*ATP[c]+1*CYTIDINE[c] --> 1*ADP[c]+1*CMP[c]+2*PROTON[c]	MGA-0106
DEOXYADENOSINE-KINASE-RXN	1*ATP[c]+1*DEOXYADENOSINE[c] --> 1*ADP[c]+1*DAMP[c]+2*PROTON[c]	MGA-0174
DEOXYGUANOSINE-KINASE-RXN	1*ATP[c]+1*DEOXYGUANOSINE[c] --> 1*ADP[c]+1*DGMP[c]+2*PROTON[c]	MGA-0174
DEPHOSPHOCOAKIN-RXN	1*ATP[c]+1*DEPHOSPHO-COA[c] --> 1*ADP[c]+1*CO-A[c]+2*PROTON[c]	MGA-1054N
DURIDKI-RXN	1*ATP[c]+1*DEOXYURIDINE[c] --> 1*ADP[c]+1*DUMP[c]+2*PROTON[c]	MGA-0502
FRUCTOSEPHOSPHO-RXN	1*Protein-3-phospho-L-histidines[c]+1*FRU[c] --> 1*WATER[c]+1*FRU1P[c]+1*Protein-Histidines[c]	MGA-0508,MGA-0855
GLYCEROL-KIN-RXN	1*ATP[c]+1*GLYCEROL[c] --> 1*ADP[c]+1*GLYCEROL-3P[c]+2*PROTON[c]	MGA-0644
LACTOSEPHOSPHO-RXN	1*LACTOSE[c]+1*Protein-3-phospho-L-histidines[c] --> 1*LACTOSE-6P[c]+1*Protein-Histidines[c]	MGA-0508,MGA-0855
NAD-KIN-RXN	1*ATP[c]+1*NAD[c] --> 1*ADP[c]+1*NADP[c]+2*PROTON[c]	MGA-0291
TRANS-RXN7TV-3811	1*Fatty-Acids[e] <--> 1*Fatty-Acids[c]	
NADH-KINASE-RXN	1*ATP[c]+1*NADH[c] --> 1*ADP[c]+1*NADPH[c]+2*PROTON[c]	MGA-0291
PEPDEPHOS-RXN	1*PHOSPHO-ENOL-PYRUVATE[c]+1*ADP[c]+2*PROTON[c] -> 1*PYRUVATE[c]+1*ATP[c]	MGA-0156
PYRIDOXKIN-RXN	1*PYRIDOXAL[c]+1*ATP[c] --> 1*PYRIDOXAL_PHOSPHATE[c]+1*ADP[c]+2*PROTON[c]	MONOMER97N-1194 (Pyridoxamine kinase)
RIBOFLAVIN KIN-RXN	1*ATP[c]+1*RIBOFLAVIN[c] --> 1*ADP[c]+1*FMN[c]+2*PROTON[c]	MGA-0832
THIKIN-RXN	1*ATP[c]+1*THIAMINE[c] -->	MONOMER97N-5510

Name	Reaction	Locus*
	1*ADP[c]+1*THIAMINE-P[c]+2*PROTON[c]	(Thiamin kinase)
THYKI-RXN	1*ATP[c]+1*THYMIDINE[c] --> 1*ADP[c]+1*TMP[c]+2*PROTON[c]	MGA-0502
URIDINEKIN-RXN	1*ADP[c]+1*UMP[c]+2*PROTON[c] --> 1*ATP[c]+1*URIDINE[c]	MGA-0106
URKI-RXN	1*GTP[c]+1*URIDINE[c] --> 1*GDP[c]+1*UMP[c]+1*PROTON[c]	MGA-0106
PROTEIN-KINASE-RXN	1*ATP[c]+1*General-Protein-Substrates[c] --> 1*ADP[c]+1*General-Phos-Protein-Substrates[c]	MGA-0459
ACETATEKIN-RXN	1*ACETYL-P[c]+1*ADP[c]+1*PROTON[c] --> 1*ACET[c]+1*ATP[c]	MGA-0169
3.6.3.2-RXN	1*ATP[c]+1*WATER[c]+1*MG-2[e] --> 1*ADP[c]+1*Pi[c]+1*MG-2[c]	MGA-1061
PHOSGLYPHOS-RXN	1*ATP[c]+1*G3P[c] <--> 1*ADP[c]+1*DPG[c]+1*PROTON[c]	MGA-1187
RXN-7958	1*PROPIONATE[c]+1*ATP[c] --> 1*PROPIONYL-P[c]+1*ADP[c]+1*PROTON[c]	MGA-0169
2.7.3.9-RXN	1*Protein-Histidines[c]+1*PHOSPHO-ENOL-PYRUVATE[c] --> 1*Protein-3-phospho-L-histidines[c]+1*PYRUVATE[c]	MGA-0763
2.7.4.22-RXN	1*UMP[c]+1*ATP[c] --> 1*UDP[c]+1*ADP[c]+1*PROTON[c]	MGA-0783
ADENYLKIN-RXN	1*ATP[c]+1*AMP[c] --> 2*ADP[c]+1*PROTON[c]	MGA-0743
CDPKIN-RXN	1*ATP[c]+1*CDP[c] <--> 1*ADP[c]+1*CTP[c]+1*PROTON[c]	MGA-0156
CMPKI-RXN	1*CMP[c]+1*ATP[c] --> 1*CDP[c]+1*ADP[c]+1*PROTON[c]	MGA-0900
DADPKIN-RXN	1*ATP[c]+1*DADP[c] --> 1*ADP[c]+1*DATP[c]	MGA-0156
3.6.3.27-RXN	1*Pi[e]+1*WATER[c]+1*ATP[c] --> 2*Pi[c]+1*ADP[c]	MGA-0693
DCDPKIN-RXN	1*ATP[c]+1*DCDP[c] --> 1*ADP[c]+1*DCTP[c]+1*PROTON[c]	MGA-0156
DGDPKIN-RXN	1*ATP[c]+1*DGDP[c] --> 1*ADP[c]+1*DGTP[c]+1*PROTON[c]	MGA-0156
DTDPKIN-RXN	1*ATP[c]+1*TDP[c] --> 1*ADP[c]+1*TTTP[c]+1*PROTON[c]	MGA-0156
DTMPKI-RXN	1*TMP[c]+1*ATP[c] --> 1*TDP[c]+1*ADP[c]+1*PROTON[c]	MGA-0606
DUDPKIN-RXN	1*ATP[c]+1*DUDP[c] --> 1*ADP[c]+1*DUTP[c]+1*PROTON[c]	MGA-0156

Name	Reaction	Locus*
GDPKIN-RXN	1*ATP[c]+1*GDP[c] --> 1*ADP[c]+1*GTP[c]+1*PROTON[c]	MGA-0156
GUANYL-KIN-RXN	1*ATP[c]+1*GMP[c] --> 1*ADP[c]+1*GDP[c]+1*PROTON[c]	MGA-0462
RXN-7913	1*DCMP[c]+1*ATP[c] --> 1*DCDP[c]+1*ADP[c]+1*PROTON[c]	MGA-0900
THI-P-KIN-RXN	1*ATP[c]+1*THIAMINE-P[c] --> 1*ADP[c]+1*THIAMINE-PYROPHOSPHATE[c]+1*PROTON[c]	MONOMER97N-5666 (Thiamine-monophosphate kinase)
UDPKIN-RXN	1*ATP[c]+1*UDP[c] --> 1*ADP[c]+1*UTP[c]+1*PROTON[c]	MGA-0156
3.6.3.29-RXN	1*ATP[c]+1*WATER[c]+1*CPD-3[e] --> 1*ADP[c]+1*Pi[c]+1*CPD-3[c]	MONOMER7TV-43 (molybdate-transporting atpase)
UMPKI-RXN	1*UMP[c]+1*ATP[c] --> 1*UDP[c]+1*ADP[c]+1*PROTON[c]	MGA-0900
GDPPYPHOS KIN-RXN	1*GDP[c]+1*ATP[c] --> 1*GUANOSINE-5DP-3DP[c]+1*AMP[c]+2*PROTON[c]	MGA-0950
PRPPSYN-RXN	1*RIBOSE-5P[c]+1*ATP[c] --> 1*AMP[c]+1*PRPP[c]+2*PROTON[c]	MGA-0348
2.7.7.15-RXN	1*CTP[c]+1*PHOSPHORYL-CHOLINE[c] -> 1*PPI[c]+1*CDP-CHOLINE[c]	MONOMER97N-1669 (Phosphorylcholine transferase)
2.7.7.60-RXN	1*CTP[c]+1*2-C-METHYL-D-ERYTHRITOL-4-PHOSPHATE[c]+1*PROTON[c] --> 1*PPI[c]+1*4-CYTIDINE-5-DIPHOSPHO-2-C[c]	MGA-1069
CDPDIGLYSYN-RXN	1*L-PHOSPHATIDATE[c]+1*CTP[c] --> 1*PPI[c]+1*CDPDIACYLGLYCEROL[c]	MGA-0785
DNA-DIRECTED-DNA-POLYMERASE-RXN	1*DNA-N[c]+1*Deoxy-Ribonucleoside-Triphosphates[c] --> 1*DNA-N[c]+1*PPI[c]	MGA-0618,MGA-0605,MGA-0401,MGA-1048,MGA-0791,MGA-0344,MGA-0336
DNA-DIRECTED-RNA-POLYMERASE-RXN	1*RNA-N[c]+1*Nucleoside-Triphosphates[c] --> 1*RNA-N[c]+1*PPI[c]	MGA-0443,MGA-1005,MGA-1000,MGA-0497
FADSYN-RXN	1*ATP[c]+1*FMN[c] --> 1*PPI[c]+1*FAD[c]	MGA-0832
NICONUCADENYLYLTRAN-RXN	1*NICOTINATE_NUCLEOTIDE[c]+1*ATP[c] --> 1*DEAMIDO-NAD[c]+1*PPI[c]	MGA-0052

Name	Reaction	Locus*
3.6.3.35-RXN	1*ATP[c]+1*WATER[c]+1*MN-2[e] --> 1*ADP[c]+1*Pi[c]+1*MN-2[c]	MGA-1061
RXN-8654	1*LIPOIC-ACID[c]+1*ATP[c] --> 1*LIPOYL-AMP[c]+1*PPI[c]	MGA-0158
RXN-8655	1*General-Protein-Substrates[c]+1*LIPOYL- AMP[c] --> 1*AMP[c]+1*Protein-6-N- lipoyl-lysine[c]	MGA-0158
RXN0-5515	1*2-3-4-Saturated-L- Phosphatidates[c]+1*CTP[c] --> 1*CDP-2-3- 4-Saturated-Diacylglycerols[c]+1*PPI[c]	MGA-0785
2.7.8.27-RXN	1*PHOSPHATIDYLCHOLINE[c]+1*Ceram ides[c] --> 1*DIACYLGLYCEROL[c]+1*Sphingomyeli ns[c]	MONOMER97N-5687 (Sphingomyelin synthase)
CARDIOLIPS YN-RXN	2*L-1-PHOSPHATIDYL-GLYCEROL[c] -- > 1*GLYCEROL[c]+1*CARDIOLIPIN[c]	MONOMER97N-1654 (Cardiolipin synthase)
HOLO-ACP- SYNTH-RXN	1*CO-A[c]+1*apo-ACP[c] --> 1*ACP[c]+1*3-5-ADP[c]	MGA-0041
PHOSPHAGL YPSYN-RXN	1*GLYCEROL- 3P[c]+1*CDPDIACYLGLYCEROL[c] --> 1*CMP[c]+1*L-1-PHOSPHATIDYL- GLYCEROL-P[c]	MGA-1067
GAPDHSYNE C-RXN	1*Pi[c]+1*GAP[c]+1*NAD(P)[c] <--> 1*DPG[c]+1*NAD(P)H[c]	MGA-0860
RXN-5781	1*CDP- CHOLINE[c]+1*DIACYLGLYCEROL[c] -- > 1*CMP[c]+1*PHOSPHATIDYLCHOLINE[c ]	MONOMER97N-1677 (Diacylglycerol cholinephosphotransferase)
PEPSYNTH- RXN	1*ATP[c]+1*PYRUVATE[c]+1*WATER[c] --> 1*AMP[c]+1*PHOSPHO-ENOL- PYRUVATE[c]+1*Pi[c]+3*PROTON[c]	MGA-0763
RXN0-308	1*CYS[c]+1*PROT-CYS[c] --> 1*L- ALPHA-ALANINE[c]+1*ENZYME-S- SULFANYLCYSTEINE[c]	MGA-1128
3.6.3.4-RXN	1*ATP[c]+1*WATER[c]+1*CU-2[e] --> 1*ADP[c]+1*Pi[c]+1*CU-2[c]	MGA-1061
R11-RXN	1*ACET[c]+1*BUTYRYL-COA[c] --> 1*ACETYL-COA[c]+1*BUTYRIC_ACID[c]	MONOMER97N-35 (Coenzyme A Transphorase), MGA-0833
RXNI-2	1*3-KETOBUTYRATE[c]+1*SUC-COA[c] --> 1*ACETOACETYL-COA[c]+1*SUC[c]	MONOMER97N-50 (Coenzyme A Transphorase)
AMINOCYL- TRNA- HYDROLASE	1*N-Substituted-Aminoacyl- tRNA[c]+1*WATER[c] --> 1*N-Substituted- Amino-Acids[c]+1*Some-tRNA[c]	MGA-0506

Name	Reaction	Locus*
-RXN		
ACETYL-COA-HYDROLASE-RXN	1*ACETYL-COA[c]+1*WATER[c] --> 1*CO-A[c]+1*ACET[c]+1*PROTON[c]	MGA-0833
3.1.21.2-RXN	1*AP-Site-Created[c] --> 1*CPD-8532[c]	MGA-1293
RXN0-2582	1*CPD-8533[c] --> 1*CPD-8532[c]	MGA-1293
3.1.26.5-RXN	1*tRNA-precursors[c] --> 1*Some-tRNA[c]	MGA-0630
325-BISPHOSPHATE-NUCLEOTIDASE-RXN	1*WATER[c]+1*3-5-ADP[c] --> 1*AMP[c]+1*Pi[c]	MONOMER97N-7997
AMP-DEPHOSPHORYLATION-RXN	1*WATER[c]+1*AMP[c] --> 1*Pi[c]+1*ADENOSINE[c]	MONOMER97N-384
PGPPHOSPHATE-RXN	1*WATER[c]+1*L-1-PHOSPHATIDYL-GLYCEROL-P[c] --> 1*Pi[c]+1*L-1-PHOSPHATIDYL-GLYCEROL[c]	MONOMER97N-525
ACH1-RXN	1*NA[e]+1*CHOLINE[e] --> 1*NA[c]+1*CHOLINE[c]	MONOMER7TV-185
PHOSPHATIDATE-PHOSPHATASE-RXN	1*WATER[c]+1*L-PHOSPHATIDATE[c] --> 1*Pi[c]+1*DIACYLGLYCEROL[c]	MONOMER97N-2
RXN-7609	1*WATER[c]+1*GMP[c] --> 1*Pi[c]+1*GUANOSINE[c]	MONOMER97N-392
RXN7TV-27	1*WATER[c]+1*DAMP[c] --> 1*PROTON[c]+1*Pi[c]+1*DEOXYADENOSINE[c]	MONOMER97N-417
CYCPHOSDIESTER-RXN	1*WATER[c]+1*Cyclic-2-3-Ribonucleoside-Monophosphates[c] --> 1*3-Prime-Ribonucleoside-Monophosphates[c]	MGA-0141
PPGPPSYN-RXN	1*WATER[c]+1*GUANOSINE-5DP-3DP[c] --> 1*GDP[c]+1*PPI[c]	MGA-0950
RXN0-2584	1*DNA-with-Uracils[c] --> 1*URACIL[c]+1*AP-Site-Created[c]	MGA-0415
3.4.11.1-RXN	1*WATER[c]+1*Peptides[c] --> 1*Peptides[c]+1*Amino-Acids-20[c]	MGA-0114
3.4.21.89-RXN	1*Peptides-with-Leader-Sequence[c] --> 1*Leader-Sequences[c]+1*Peptides[c]	MGA-1091
3.5.1.88-RXN	1*FORMYL-L-METHIONYL-PEPTIDE[c]+1*WATER[c] --> 1*FORMATE[c]+1*METHIONYL-	MGA-0463

Name	Reaction	Locus*
	PEPTIDE[c]+1*PROTON[c]	
ARGININE-DEIMINASE-RXN	1*ARG[c]+1*WATER[c] --> 1*L-CITRULLINE[c]+1*AMMONIA[c]+1*PROTON[c]	MGA-0105,MGA-1220
TRANS-RXN-185	1*K[e] --> 1*K[c]	MGA-0171
CYTIDEAM-RXN	1*DEOXYCYTIDINE[c]+1*WATER[c] --> 1*AMMONIA[c]+1*DEOXYURIDINE[c]	G97N-539, MGA-0361
CYTIDEAM2-RXN	1*CYTIDINE[c]+1*WATER[c] <--> 1*AMMONIA[c]+1*URIDINE[c]	MGA-0361
DCMP-DEAMINASE-RXN	1*WATER[c]+1*DCMP[c] --> 1*DUMP[c]+1*AMMONIA[c]	MGA-0701
METHENYLT HFCYCLOHYDRO-RXN	1*5-10-METHENYL-THF[c]+1*WATER[c] <--> 1*10-FORMYL-THF[c]+1*PROTON[c]	MGA-0596
RXN-6282	1*WATER[c]+1*CPD-5727[c] --> 1*FORMYL-THF-GLU-N[c]	MGA-0596
EXOPOLYPHOSPHATASE-RXN	1*WATER[c]+1*Long-Chain-Polyphosphate[c] --> 1*Pi[c]+1*Long-Chain-Polyphosphate[c]	MGA-0683
INORGPYROPHOSPHAT-RXN	1*PPI[c]+1*WATER[c] --> 2*Pi[c]+1*PROTON[c]	MGA-1121
RXN0-5462	1*WATER[c]+1*GTP[c] --> 1*Pi[c]+1*GDP[c]+1*PROTON[c]	MGA-0339,MGA-0110,MGA-0053,MGA-0898
F16ALDOLASE-RXN	1*FRUCTOSE-16-DIPHOSPHATE[c] <--> 1*GAP[c]+1*DIHYDROXY-ACETONE-PHOSPHATE[c]	MGA-0498
RXN-8631	1*FRU1P[c] --> 1*GLYCERALD[c]+1*DIHYDROXY-ACETONE-PHOSPHATE[c]	MGA-0498
TRANS-RXN7TV-0	1*PROTON[e]+1*RIBOFLAVIN[e] --> 1*PROTON[c]+1*RIBOFLAVIN[c]	MONOMER7TV-1
2PGADEHYDRAT-RXN	1*2-PG[c] <--> 1*WATER[c]+1*PHOSPHO-ENOL-PYRUVATE[c]	MGA-0209
4.2.99.18-RXN	1*DNA-containing-abasic-Sites[c] --> 1*3-terminal-unsaturated-sugars[c]+1*5-Phosphopolynucleotides[c]	MGA-1053
RXN0-2601	1*Damaged-DNA-Pyrimidine[c] --> 1*DNA-containing-a-Apyrimidinic-Sites[c]	MGA-1053
AMPSYN-RXN	1*ADENYLOSUCC[c] --> 1*AMP[c]+1*FUM[c]	MONOMER97N-503
SELENOCYC	1*L-SELENOCYSTEINE[c]+1*Donor-H2[c]	MGA-1128



Name	Reaction	Locus*
TEINE-LYASE-RXN	--> 1*CPD-678[c]+1*L-ALPHA-ALANINE[c]+1*Acceptor[c]	
RXN0-302	1*2-PHOSPHO-4-CYTIDINE-5-DIPHOSPHO-2-C-MET[c] --> 1*CMP[c]+1*2C-METH-D-ERYTHRITOL-CYCLODIPHOSPHATE[c]	MGA-0657
RIBULP3EPI M-RXN	1*RIBULOSE-5P[c] <--> 1*XYLULOSE-5-PHOSPHATE[c]	MGA-0455
LACTOSE-6-PHOSPHATE-ISOMERASE-RXN	1*CPD-1241[c] --> 1*TAGATOSE-6-PHOSPHATE[c]	MGA-0866
MANNPISOM-RXN	1*MANNOSE-6P[c] <--> 1*FRUCTOSE-6P[c]	MGA-0514
PGLUCISOM-RXN	1*GLC-6-P[c] <--> 1*FRUCTOSE-6P[c]	MGA-0457
TRANS-RXN7TV-102	1*FE-2[e] --> 1*FE-2[c]	MGA-0171
RIB5PISOM-RXN	1*RIBULOSE-5P[c] <--> 1*RIBOSE-5P[c]	MGA-0886
RXN-6182	1*ALPHA-GLC-6-P[c] --> 1*FRUCTOSE-6P[c]	MGA-0457
TRIOSEISO MERIZATION-RXN	1*DIHYDROXY-ACETONE-PHOSPHATE[c] <--> 1*GAP[c]	MGA-0357
3PGAREARR-RXN	1*G3P[c] <--> 1*2-PG[c]	MGA-0356
BETA-PHOSPHOGLUCOMUTASE-RXN	1*CPD-448[c] --> 1*GLC-6-P[c]	MGA-1263
PHOSMANMUT-RXN	1*MANNOSE-6P[c] --> 1*MANNOSE-1P[c]	MGA-0358
PPENTOMUT-RXN	1*RIBOSE-1P[c] --> 1*RIBOSE-5P[c]	MGA-0358
TRNA-PSEUDOURIDINE-SYNTHASE-I-RXN	1*CPD-8538[c] --> 1*CPD-8537[c]+1*PROTON[c]	MGA-1331D,MGA-0831
ALANINE--TRNA-LIGASE-RXN	1*ATP[c]+1*L-ALPHA-ALANINE[c]+1*ALA-tRNAs[c] --> 1*AMP[c]+1*PPI[c]+1*Charged-ALA-tRNAs[c]	MGA-0834
ARGININE--	1*ATP[c]+1*ARG[c]+1*ARG-tRNAs[c] -->	MGA-0636

Name	Reaction	Locus*
TRNA-LIGASE-RXN	1*AMP[c]+1*PPI[c]+1*Charged-ARG-tRNAs[c]	
TRANS-RXN7TV-104	1*FE-3[e] --> 1*FE-3[c]	MGA-0171
ASPARAGINE--TRNA-LIGASE-RXN	1*ATP[c]+1*ASN[c]+1*ASN-tRNAs[c] --> 1*AMP[c]+1*PPI[c]+1*Charged-ASN-tRNAs[c]	MGA-1065,MGA-1100
ASPARTATE--TRNA-LIGASE-RXN	1*ATP[c]+1*L-ASPARTATE[c]+1*ASP-tRNAs[c] --> 1*AMP[c]+1*PPI[c]+1*Charged-ASP-tRNAs[c]	MGA-0948
CYSTEINE--TRNA-LIGASE-RXN	1*ATP[c]+1*CYC[c]+1*CYC-tRNAs[c] --> 1*AMP[c]+1*PPI[c]+1*Charged-CYC-tRNAs[c]	MGA-0533
GLURS-RXN	1*ATP[c]+1*GLT[c]+1*GLT-tRNAs[c] --> 1*AMP[c]+1*PPI[c]+1*Charged-GLT-tRNAs[c]	MGA-0594
GLUTAMINE--TRNA-LIGASE-RXN	1*ATP[c]+1*GLN[c]+1*GLN-tRNAs[c] --> 1*AMP[c]+1*PPI[c]+1*Charged-GLN-tRNAs[c]	MGA-0594
GLYCINE--TRNA-LIGASE-RXN	1*ATP[c]+1*GLY[c]+1*GLY-tRNAs[c] --> 1*AMP[c]+1*PPI[c]+1*Charged-GLY-tRNAs[c]	MGA-0015
HISTIDINE--TRNA-LIGASE-RXN	1*ATP[c]+1*HIS[c]+1*HIS-tRNAs[c] --> 1*AMP[c]+1*PPI[c]+1*Charged-HIS-tRNAs[c]	MGA-0947
ISOLEUCINE--TRNA-LIGASE-RXN	1*ATP[c]+1*ILE[c]+1*ILE-tRNAs[c] --> 1*AMP[c]+1*PPI[c]+1*Charged-ILE-tRNAs[c]	MGA-1196
LEUCINE--TRNA-LIGASE-RXN	1*ATP[c]+1*LEU[c]+1*LEU-tRNAs[c] --> 1*AMP[c]+1*PPI[c]+1*Charged-LEU-tRNAs[c]	MGA-0087
LYSINE--TRNA-LIGASE-RXN	1*ATP[c]+1*LYS[c]+1*LYS-tRNAs[c] --> 1*AMP[c]+1*PPI[c]+1*Charged-LYS-tRNAs[c]	MGA-0753
TRANS-RXN7TV-109	1*PROTON[e]+1*THYMINE[e] --> 1*PROTON[c]+1*THYMINE[c]	MONOMER7TV-110
METHIONINE--TRNA-LIGASE-RXN	1*ATP[c]+1*MET[c]+1*MET-tRNAs[c] --> 1*AMP[c]+1*PPI[c]+1*Charged-MET-tRNAs[c]	MGA-0893,MGA-0884
PHENYLALANINE--TRNA-LIGASE-RXN	1*ATP[c]+1*PHE[c]+1*PHE-tRNAs[c] --> 1*AMP[c]+1*PPI[c]+1*Charged-PHE-tRNAs[c]	MGA-1281,MGA-1278
PROLINE--TRNA-	1*ATP[c]+1*PRO[c]+1*PRO-tRNAs[c] --> 1*AMP[c]+1*PPI[c]+1*Charged-PRO-	MGA-1022

Name	Reaction	Locus*
LIGASE-RXN	tRNAs[c]	
RXN0-2161	1*ATP[c]+1*SER[c]+1*SEC-tRNAs[c] --> 1*AMP[c]+1*PPI[c]+1*L-seryl-SEC- tRNAs[c]	MGA-0608
RXN490-3616	1*ATP[c]+1*L-ASPARTATE[c]+1*ASN- tRNAs[c] --> 1*AMP[c]+1*PPI[c]+1*L- aspartyl-tRNAAsn[c]	MGA-1065
SERINE-- TRNA- LIGASE-RXN	1*ATP[c]+1*SER[c]+1*SER-tRNAs[c] --> 1*AMP[c]+1*PPI[c]+1*Charged-SER- tRNAs[c]	MGA-0608
THREONINE- -TRNA- LIGASE-RXN	1*ATP[c]+1*THR[c]+1*THR-tRNAs[c] --> 1*AMP[c]+1*PPI[c]+1*Charged-THR- tRNAs[c]	MGA-0925
TRYPTOPHA N--TRNA- LIGASE-RXN	1*TRP[c]+1*TRP-tRNAs[c]+1*ATP[c] --> 1*Charged-TRP- tRNAs[c]+1*PPI[c]+1*AMP[c]	MGA-0293
TYROSINE-- TRNA- LIGASE-RXN	1*ATP[c]+1*TYR-tRNAs[c]+1*TYR[c] --> 1*AMP[c]+1*PPI[c]+1*Charged-TYR- tRNAs[c]	MGA-1144
VALINE-- TRNA- LIGASE-RXN	1*ATP[c]+1*VAL[c]+1*VAL-tRNAs[c] --> 1*AMP[c]+1*PPI[c]+1*Charged-VAL- tRNAs[c]	MGA-0338
TRANS- RXN7TV-11	1*ACYL-COA[e] --> 1*ACYL-COA[c]	MONOMER7TV-12
ACYLACPSY NTH-RXN	1*ATP[c]+1*ACP[c]+1*Fatty-Acids[c] --> 1*PPI[c]+1*AMP[c]+1*ACYL-ACP[c]	MONOMER97N-5692
ASNSYNA- RXN	1*ATP[c]+1*L- ASPARTATE[c]+1*AMMONIA[c] --> 1*AMP[c]+1*PPI[c]+1*ASN[c]+1*PROTO N[c]	MGA-0424
5-FORMYL- THF-CYCLO- LIGASE-RXN	1*ATP[c]+1*5-FORMYL- THF[c]+1*PROTON[c] <--> 1*Pi[c]+1*ADP[c]+1*5-10-METHENYL- THF[c]	MGA-1310
ADENYLOSU CCINATE- SYNTHASE- RXN	1*GTP[c]+1*IMP[c]+1*L-ASPARTATE[c] - -> 1*GDP[c]+1*Pi[c]+1*ADENYLOSUCC[c]+ 2*PROTON[c]	MONOMER97N-473
CTPSYN-RXN	1*WATER[c]+1*GLN[c]+1*UTP[c]+1*ATP [c] --> 1*GLT[c]+1*CTP[c]+1*Pi[c]+1*ADP[c]+3* PROTON[c]	MGA-0953
6.3.5.7-RXN	1*ATP[c]+1*GLUTAMYL-TRNA- GLN[c]+1*GLN[c] --> 1*ADP[c]+1*Pi[c]+1*GLUTAMINYL-	MGA-0413

Name	Reaction	Locus*
	TRNA-GLN[c]+1*GLT[c]	
GMP-SYN-GLUT-RXN	1*ATP[c]+1*GLN[c]+1*WATER[c]+1*XANTHOSINE-5-PHOSPHATE[c] --> 1*AMP[c]+1*PPI[c]+1*GMP[c]+1*GLT[c]+3*PROTON[c]	MGA-0650
RXN490-3617	1*ATP[c]+1*L-aspartyl-tRNAAsn[c]+1*GLN[c] --> 1*ADP[c]+1*Pi[c]+1*Charged-ASN-tRNAs[c]+1*GLT[c]	MGA-0413
PYRUVATE-CARBOXYLASE-RXN	1*ATP[c]+1*PYRUVATE[c]+1*HCO3[c] --> 1*ADP[c]+1*OXALACETIC_ACID[c]+1*Pi[c]+2*PROTON[c]	MONOMER97N-316
DNA-LIGASE-NAD+-RXN	1*NAD[c]+1*DEOXYNUCLEOTIDESM[c]+1*Deoxynucleotides[c] --> 1*AMP[c]+1*NICOTINAMIDE_NUCLEOTIDE[c]+1*Deoxynucleotides[c]	MGA-0569
TRANS-RXN7TV-12	1*WATER[c]+1*ATP[c]+1*CO-2[e] --> 1*Pi[c]+1*PROTON[c]+1*ADP[c]+1*CO-2[c]	MGA-0353, MGA-0351
RXN-9591	1*Acyl-Phosphates[c]+1*GLYCEROL-3P[c] --> 1*Pi[c]+1*ACYL-SN-GLYCEROL-3P[c]	MGA-0008
RXN-9590	1*Pi[c]+1*ACYL-ACP[c] --> 1*ACP[c]+1*Acyl-Phosphates[c]	MGA-0181
TRANS-RXN7TV-13	1*DGTP[e] --> 1*DGTP[c]	MONOMER7TV-14
TRANS-RXN7TV-17	1*PROTON[e]+1*ADENINE[e] <--> 1*PROTON[c]+1*ADENINE[c]	MONOMER7TV-18
TRANS-RXN7TV-1717	1*PROTON[e]+1*2-KETOGLUTARATE[e] <--> 1*PROTON[c]+1*2-KETOGLUTARATE[c]	MONOMER7TV-6
TRANS-RXN7TV-1719	1*PROTON[c]+1*ACET[c] --> 1*PROTON[e]+1*ACET[e]	MONOMER7TV-0
TRANS-RXN7TV-18	1*PROTON[e]+1*CYTOSINE[e] --> 1*PROTON[c]+1*CYTOSINE[c]	MONOMER7TV-19
TRANS-RXN7TV-19	1*PHOSPHO-ENOL-PYRUVATE[c]+1*MANNOSSE[e] --> 1*PYRUVATE[c]+1*MANNOSSE-6P[c]	MONOMER7TV-20
TRANS-RXN7TV-2	1*CO-A[e] --> 1*CO-A[c]	MONOMER7TV-3
3.6.3.7-RXN	1*WATER[c]+1*ATP[c]+1*NA[c] --> 1*ADP[c]+1*Pi[c]+1*NA[e]	
TRANS-RXN7TV-22	1*PROTON[e]+1*THIAMINE[e] --> 1*PROTON[c]+1*THIAMINE[c]	MONOMER7TV-23
TRANS-	1*AMMONIUM[e] <--> 1*AMMONIUM[c]	MGA-0171, MONOMER7TV-

Name	Reaction	Locus*
RXN7TV-23		24
TRANS-RXN7TV-25	1*PHOSPHO-ENOL-PYRUVATE[c]+1*FRU[e] --> 1*PYRUVATE[c]+1*FRU1P[c]	MONOMER7TV-26
TRANS-RXN7TV-258	1*ZN-2[e] <--> 1*ZN-2[c]	MGA-0171
TRANS-RXN7TV-27	1*PROTON[e]+1*DIHYDROFOLATE[e] --> 1*PROTON[c]+1*DIHYDROFOLATE[c]	MONOMER7TV-28
TRANS-RXN7TV-28	1*PROTON[e]+1*THYMIDINE[e] --> 1*PROTON[c]+1*THYMIDINE[c]	MONOMER7TV-98,MONOMER7TV-29
TRANS-RXN7TV-304	1*PROTON[e]+1*ARG[e] --> 1*PROTON[c]+1*ARG[c]	MGA-1188,MGA-0963,MGA-0287
TRANS-RXN7TV-310	1*PROTON[e]+1*ASN[e] --> 1*PROTON[c]+1*ASN[c]	MGA-1188,MGA-0963,MGA-0287
TRANS-RXN7TV-313	1*PROTON[e]+1*GLT[e] --> 1*PROTON[c]+1*GLT[c]	MGA-1188,MGA-0963,MGA-0287
TRANS-RXN7TV-315	1*PROTON[e]+1*HIS[e] --> 1*PROTON[c]+1*HIS[c]	MGA-1188,MGA-0963,MGA-0287
3.6.3.19-RXN	1*ATP[c]+1*WATER[c]+1*MALTOSE[e] -> 1*ADP[c]+1*Pi[c]+1*MALTOSE[c]	
TRANS-RXN7TV-317	1*PROTON[e]+1*ILE[e] --> 1*PROTON[c]+1*ILE[c]	MGA-1188,MGA-0963,MGA-0287
TRANS-RXN7TV-320	1*PROTON[e]+1*LEU[e] --> 1*PROTON[c]+1*LEU[c]	MGA-1188,MGA-0963,MGA-0287
TRANS-RXN7TV-323	1*PROTON[e]+1*LYS[e] --> 1*PROTON[c]+1*LYS[c]	MGA-1188,MGA-0963,MGA-0287
TRANS-RXN7TV-325	1*PROTON[e]+1*MET[e] --> 1*PROTON[c]+1*MET[c]	MGA-1188,MGA-0963,MGA-0287
TRANS-RXN7TV-327	1*PROTON[e]+1*PHE[e] --> 1*PROTON[c]+1*PHE[c]	MGA-1188,MGA-0963,MGA-0287
TRANS-RXN7TV-329	1*PROTON[e]+1*PRO[e] --> 1*PROTON[c]+1*PRO[c]	MGA-1188,MGA-0963,MGA-0287
TRANS-RXN7TV-331	1*PROTON[e]+1*SER[e] --> 1*PROTON[c]+1*SER[c]	MGA-1188,MGA-0963,MGA-0287
TRANS-RXN7TV-333	1*PROTON[e]+1*TRP[e] --> 1*PROTON[c]+1*TRP[c]	MGA-1188,MGA-0963,MGA-0287
TRANS-RXN7TV-335	1*PROTON[e]+1*VAL[e] --> 1*PROTON[c]+1*VAL[c]	MGA-1188,MGA-0963,MGA-0287
TRANS-RXN7TV-338	1*PROTON[e]+1*TYR[e] --> 1*PROTON[c]+1*TYR[c]	MGA-1188,MGA-0963,MGA-0287
TRANS-RXN7TV-8750	1*GMP[e] --> 1*GMP[c]	
TRANS-RXN7TV-53	1*NIACINE[e] --> 1*NIACINE[c]	MGA-1188
TRANS-	1*PYRIDOXAL[e] --> 1*PYRIDOXAL[c]	MONOMER7TV-57

Name	Reaction	Locus*
RXN7TV-56		
TRANS-RXN7TV-60	1*GTP[e] --> 1*GTP[c]	MONOMER7TV-61
TRANS-RXN7TV-62	1*PROTON[e]+1*SULFATE[e] --> 1*PROTON[c]+1*SULFATE[c]	MONOMER7TV-64
TRANS-RXN7TV-63	1*CA-2[e] <--> 1*CA-2[c]	MGA-0171
TRANS-RXN7TV-65	1*PROTON[e]+1*PROPIONATE[e] <--> 1*PROTON[c]+1*PROPIONATE[c]	MONOMER7TV-66
TRANS-RXN7TV-7	1*DATP[e] --> 1*DATP[c]	MONOMER7TV-8
TRANS-RXN7TV-77	1*PROTON[e]+1*URACIL[e] --> 1*PROTON[c]+1*URACIL[c]	MONOMER7TV-78
TRANS-RXN7TV-8	1*PHOSPHO-ENOL-PYRUVATE[c]+1*CPD-1142[e] --> 1*PYRUVATE[c]+1*CPD-1181[c]	MONOMER7TV-9
TRANS-RXN7TV-82	1*PROTON[e]+1*GUANINE[e] --> 1*GUANINE[c]+1*PROTON[c]	MONOMER7TV-84
TRANS-RXN7TV-8749	1*UMP[e] --> 1*UMP[c]	
TRANS-RXN7TV-9	1*L-LACTATE[c] <--> 1*L-LACTATE[e]	G7TV-11
TRANS-RXN7TV-96	1*PROTON[e]+1*Deoxy-Ribonucleosides[e] --> 1*PROTON[c]+1*Deoxy-Ribonucleosides[c]	MONOMER7TV-98
TRANS-RXN7TV-3950	1*PROTON[e]+1*Amino-Acids-20[e] --> 1*PROTON[c]+1*Amino-Acids-20[c]	MGA-0287,MGA-0963,MGA-1188
TRANS-RXN7TV-3966	1*PROTON[e]+1*GLYCEROL[e] --> 1*PROTON[c]+1*GLYCEROL[c]	MGA-0641
TRANS-RXN7TV-21	1*WATER[c]+1*ATP[c]+1*LIPID[e] --> 1*Pi[c]+1*ADP[c]+1*LIPID[c]	MGA-0625A,MGA-0626
TRANS-RXN7TV-24	1*WATER[c]+1*ATP[c]+1*Multidrug[e] --> 1*Pi[c]+1*ADP[c]+1*Multidrug[c]	MGA-0625A,MGA-0626,MGA-0806,MGA-1287,,MGA-1140,,MGA-1138
TRANS-RXN7TV-36	1*WATER[c]+1*ATP[c]+1*Cations[e] --> 1*Pi[c]+1*ADP[c]+1*Cations[c]	MGA-1061
TRANS-RXN7TV-3933	1*WATER[c]+1*ATP[c]+1*SPERMIDINE[e] --> 1*Pi[c]+1*ADP[c]+1*SPERMIDINE[c]	MGA-0131,MGA-0132,MGA-0132
TRANS-RXN7TV-3939	1*WATER[c]+1*ATP[c]+1*NI-2[e] --> 1*Pi[c]+1*ADP[c]+1*NI-2[c]	MGA-1061,MGA-0224,MGA-0220,MGA-0218,MGA-0223,MGA-0221,MGA-0230,MGA-0232,MGA-0234,MGA-0235
TRANS-	1*WATER[c]+1*ATP[c]+1*OLIGOPEPTID	MGA-0224,MGA-

Name	Reaction	Locus*
RXN7TV-3942	E[e] --> 1*Pi[c]+1*ADP[c]+1*OLIGOPEPTIDE[c]	0220,MGA-0218,MGA-0223,MGA-0221,MGA-0230,MGA-0232, MGA-0234,MGA-0235,MGA-0237
TRANS-RXN7TV-8748	1*CMP[e] --> 1*CMP[c]	
TRANS-RXN7TV-3945	1*WATER[c]+1*ATP[c]+1*DIPEPTIDES[e] --> 1*Pi[c]+1*ADP[c]+1*DIPEPTIDES[c]	MGA-0224,MGA-0220,MGA-0218,MGA-0223,MGA-0221,MGA-0230,MGA-0232, MGA-0234,MGA-0235
TRANS-RXN7TV-3969	1*WATER[c]+1*ATP[c]+1*GLYCEROL-3P[e] --> 1*Pi[c]+1*ADP[c]+1*GLYCEROL-3P[c]	MGA-0682, MGA-0680, MGA-0677
TRANS-RXN7TV-3989	1*WATER[c]+1*ATP[c]+1*PUTRESCINE[e] --> 1*Pi[c]+1*ADP[c]+1*PUTRESCINE[c]	MGA-0132, MGA-0134
TRANS-RXN7TV-4008	1*WATER[c]+1*ATP[c]+1*Pi[e] --> 2*Pi[c]+1*ADP[c]	MGA-0689, MGA-0687
TRANS-RXN7TV-43	1*WATER[c]+1*ATP[c]+1*Sugar[e] --> 1*Pi[c]+1*ADP[c]+1*Sugar[c]	MGA-1078, MGA-1077, MGA-1076
TRANS-RXN7TV-3953	1*PHOSPHO-ENOL-PYRUVATE[c]+1*GLC[e] --> 1*PYRUVATE[c]+1*GLC-6-P[c]	MGA-0289
TRANS-RXN7TV-3984	1*PHOSPHO-ENOL-PYRUVATE[c]+1*MANNITOL[e] --> 1*PYRUVATE[c]+1*MANNITOL-1P[c]	MGA-1283
TRANS-RXN7TV-16	1*Cations[e] --> 1*Cations[c]	MGA-0171
TRANS-RXN7TV-31	1*Pi[e] --> 1*Pi[c]	MGA-0694
TRANS-RXN7TV-3930	1*PROTON[e]+1*K[e] --> 1*PROTON[c]+1*K[c]	MGA-0085
TRANS-RXN7TV-8747	1*AMP[e] --> 1*AMP[c]	
ATP_maintenance_requirement	1*WATER[c]+1*ATP[c] --> 1*Pi[c]+1*PROTON[c]+1*ADP[c]	
ammonia_conversion_spontaneous	1*PROTON[c]+1*AMMONIA[c] --> 1*AMMONIUM[c]	
DEOXYADENPHOSPHOR-RXN	1*Pi[c]+1*DEOXYADENOSINE[c] --> 1*DEOXY-RIBOSE-1P[c]+1*ADENINE[c]	MGA-0364
DEOXYGUA	1*Pi[c]+1*DEOXYGUANOSINE[c] <-->	MGA-0364

Name	Reaction	Locus*
NPHOSPHOR-RXN	1*DEOXY-RIBOSE-1P[c]+1*GUANINE[c]	
DEOXYINOPHOSPHOR-RXN	1*Pi[c]+1*DEOXYINOSINE[c] <--> 1*DEOXY-RIBOSE-1P[c]+1*HYPOXANTHINE[c]	MGA-0364
GCVMULTI-RXN	1*NAD[c]+1*THF[c]+1*GLY[c] <--> 1*NADH[c]+1*CARBON-DIOXIDE[c]+1*METHYLENE-THF[c]+1*AMMONIA[c]+1*PROTON[c]	MGA-0161
RXN-6321	1*WATER[c]+1*5-10-METHENYL-THF[c] --> 1*5-FORMYL-THF[c]+3*PROTON[c]	MGA-1146
RXN-9386	1*ATP[c]+1*GLT[c]+1*GLN-tRNAs[c] --> 1*PPI[c]+1*AMP[c]+1*GLUTAMYL-TRNA-GLN[c]	MGA-0594
URA-PHOSPH-RXN	1*DEOXYURIDINE[c]+1*Pi[c] --> 1*URACIL[c]+1*DEOXY-RIBOSE-1P[c]	MGA-0362
1.1.1.34-RXN	1*3-HYDROXY-3-METHYL-GLUTARYL-COA[c]+2*NADPH[c]+2*PROTON[c] --> 1*MEVALONATE[c]+1*CO-A[c]+2*NADP[c]	MONOMER97N-281
2.3.1.15-RXN	1*Fatty-Acyl-CoA[c]+1*GLYCEROL-3P[c] --> 1*CO-A[c]+1*ACYL-SN-GLYCEROL-3P[c]	
6.2.1.3-RXN	1*ATP[c]+1*CO-A[c]+1*Fatty-Acids[c] <--> 1*AMP[c]+1*PPI[c]+1*Fatty-Acyl-CoA[c]	
ATPSYN-RXN	1*ATP[c]+1*WATER[c]+3*PROTON[c] <--> 1*ADP[c]+1*Pi[c]+4*PROTON[e]	MGA-1168,MGA-1164,MGA-1167,MGA-1170,MGA-1172,MGA-1174,MGA-1177,MGA-1179,MGA-0488,MGA-0491
NAD-SYNTH-GLN-RXN	1*ATP[c]+1*DEAMIDO-NAD[c]+1*GLN[c]+1*WATER[c] --> 1*PROTON[c]+1*GLT[c]+1*AMP[c]+1*PPI[c]+1*NAD[c]	

#### A3.4. Exchanges fluxes

**Table S8. Exchange fluxes for nutrients and secretion in the *M. gallisepticum* model.** The name, upper and lower boundary for each exchange fluxes is presented.

Nutrient			
name	reaction	low boundary	up boundary
2-KETOGLUTARATE-Ex-	1*2-KETOGLUTARATE[e]	-1000	1000



Flux	<-->		
CYTOSINE-Ex-Flux	1*CYTOSINE[e] <-->	-1000	1000
GLC-Ex-Flux	1*GLC[e] <-->	-16.53	-16.53
DIHYDROFOLATE-Ex-Flux	1*DIHYDROFOLATE[e] <-->	-1000	1000
GLYCEROL-Ex-Flux	1*GLYCEROL[e] <-->	-1000	1000
GLYCEROL-3P-Ex-Flux	1*GLYCEROL-3P[e] <-->	-1000	1000
WATER-Ex-Flux	1*WATER[e] <-->	-1000	1000
FE-2-Ex-Flux	1*FE-2[e] <-->	-1000	1000
FE-3-Ex-Flux	1*FE-3[e] <-->	-1000	1000
MG-2-Ex-Flux	1*MG-2[e] <-->	-1000	1000
MN-2-Ex-Flux	1*MN-2[e] <-->	-1000	1000
CPD-3-Ex-Flux	1*CPD-3[e] <-->	-1000	1000
NI-2-Ex-Flux	1*NI-2[e] <-->	-1000	1000
NIACINE-Ex-Flux	1*NIACINE[e] <-->	-1000	1000
Pi-Ex-Flux	1*Pi[e] <-->	-1000	1000
K-Ex-Flux	1*K[e] <-->	-1000	1000
PUTRESCINE-Ex-Flux	1*PUTRESCINE[e] <-->	-1000	1000
RIBOFLAVIN-Ex-Flux	1*RIBOFLAVIN[e] <-->	-1000	1000
SPERMIDINE-Ex-Flux	1*SPERMIDINE[e] <-->	-1000	1000
THIAMINE-Ex-Flux	1*THIAMINE[e] <-->	-1000	1000
ADENINE-Ex-Flux	1*ADENINE[e] <-->	-1000	1000
THYMIDINE-Ex-Flux	1*THYMIDINE[e] <-->	-1000	1000
URACIL-Ex-Flux	1*URACIL[e] <-->	-1000	1000
ZN-2-Ex-Flux	1*ZN-2[e] <-->	-1000	1000
CYTIDINE-Ex-Flux	1*CYTIDINE[c] <-->	-1000	1000
PYRIDOXAL-Ex-Flux	1*PYRIDOXAL[e] <-->	-1000	1000
CHOLINE-Ex-Flux	1*CHOLINE[e] <-->	-1000	1000
SULFATE-Ex-Flux	1*SULFATE[e] <-->	-1000	1000
Fatty-Acids-Ex-Flux	1*Fatty-Acids[e] <-->	-1000	1000
Triacylglycerols-Ex-Flux	1*Triacylglycerols[e] <-->	-1000	1000
CHOLESTEROL-Ex-Flux	1*CHOLESTEROL[e] <-->	-1000	1000
AMMONIUM-Ex-Flux	1*AMMONIUM[e] <-->	-1000	1000
Cholesterol-esters-Ex-Flux	1*Cholesterol-esters[e] <-->	-1000	1000
AMP-Ex-Flux	1*AMP[e] <-->	-1000	1000
CMP-Ex-Flux	1*CMP[e] <-->	-1000	1000
UMP-Ex-Flux	1*UMP[e] <-->	-1000	1000
GMP-Ex-Flux	1*GMP[e] <-->	-1000	1000
OXYGEN-MOLECULE-Ex-Flux	1*OXYGEN-MOLECULE[c] <-->	-46	1000
CL-Ex-Flux	1*CL[c] <-->	-1000	1000

GLN-Ex-Flux	1*GLN[c] <-->	-1000	1000
CA-2-Ex-Flux	1*CA-2[e] <-->	-1000	1000
CYS-Ex-Flux	1*CYS[c] <-->	-1000	1000
THR-Ex-Flux	1*THR[c] <-->	-1000	1000
L-ALPHA-ALANINE-Ex-Flux	1*L-ALPHA-ALANINE[c] <-->	-1000	1000
ARG-Ex-Flux	1*ARG[e] <-->	-1000	1000
ASN-Ex-Flux	1*ASN[e] <-->	-1000	1000
L-ASPARTATE-Ex-Flux	1*L-ASPARTATE[c] <-->	-1000	1000
GLT-Ex-Flux	1*GLT[e] <-->	-1000	1000
GLY-Ex-Flux	1*GLY[c] <-->	-1000	1000
HIS-Ex-Flux	1*HIS[e] <-->	-1000	1000
ILE-Ex-Flux	1*ILE[e] <-->	-1000	1000
CARBON-DIOXIDE-Ex-Flux	1*CARBON-DIOXIDE[c] <-->	-1000	1000
LEU-Ex-Flux	1*LEU[e] <-->	-1000	1000
LYS-Ex-Flux	1*LYS[e] <-->	-1000	1000
MET-Ex-Flux	1*MET[e] <-->	-1000	1000
PHE-Ex-Flux	1*PHE[e] <-->	-1000	1000
PRO-Ex-Flux	1*PRO[e] <-->	-1000	1000
SER-Ex-Flux	1*SER[e] <-->	-1000	1000
TRP-Ex-Flux	1*TRP[e] <-->	-1000	1000
TYR-Ex-Flux	1*TYR[e] <-->	-1000	1000
VAL-Ex-Flux	1*VAL[e] <-->	-1000	1000
Ceramides-Ex-Flux	1*Ceramides[e] <-->	-1000	1000
CO-2-Ex-Flux	1*CO-2[e] <-->	-1000	1000
NA-Ex-Flux	1*NA-[e] <-->	-1000	1000
CO-A-Ex-Flux	1*CO-A[e] <-->	-1000	1000
CU-2-Ex-Flux	1*CU-2[e] <-->	-1000	1000

Secretion			
name	reaction	low boundary	up boundary
L-LACTATE-Ex-Flux	1*L-LACTATE[e] <-->	10.29	10.29
ACET-Ex-Flux	1*ACET[e] <-->	0	1000
HYDROGEN-PEROXIDE-Ex-Flux	1*HYDROGEN-PEROXIDE[c] <-->	0	1000
BIOMASS-Ex-Flux	1*BIOMASS[c] <-->	0	1000
HCO3-Ex-Flux	1*HCO3[c] <-->	0	1000
MAL-Ex-Flux	1*MAL[c] <-->	0	1000

PROTON-Ex-Flux	PROTON[e] <-->	0	1000
----------------	----------------	---	------

### A3.5. Biomass reaction

**Table S9. Reactants of Biomass reactions for *M. gallisepticum* model.** The name and stoichiometric coefficients for each species are given.

Name	Stoichiometric coefficients
GTP	0.06313
CTP	0.03898
UTP	0.06872
dATP	0.03180
dGTP	0.01474
dCTP	0.01474
dTTP	0.03166
Ca	0.00412
Chloride	0.00609
Co2+	0.00406
Cu2+	0.00406
Fe2+	0.00914
Fe3+	0.00437
K	0.90830
Mg	0.13079
Mn2+	0.00406
Molybdate	0.00406
Ammonium	0.01523
Sulfate	0.00508
Zn2+	0.00406
10-Formyltetrahydrofolate	0.00051
S-Adenosyl-L-methionine	0.00029
Coenzyme A	0.00074
FAD	0.00029
5,10-Methylenetetrahydrofolate	0.00029
NAD	0.02083
NADP	0.00116
Putrescine	0.04501
Pyridoxal 5'-phosphate	0.00029
Riboflavin	0.00029
Spermidine	0.00900
Tetrahydrofolate	0.00029

Name	Stoichiometric coefficients
Thiamine diphosphate	0.00029
cardiolipin	0.03583
a 1,2-diacylglycerol-3-phosphate	0.01271
a phosphatidyl-choline	0.03205
a sphingomyelin	0.01316
an L-1-Phosphatidyl-glycerol	0.01367
cholesterol	0.08056
a cholesterol ester	0.00497
a triacylglycerol	0.01522
charged-ALA-trnas	0.32989
charged-ARG-trnas	0.23855
charged-ASN-trnas	0.18293
charged-ASP-trnas	0.18293
Charged-CYS-tRNAs	0.07008
Charged-GLN-tRNAs	0.32173
Charged-GLT-tRNAs	0.32185
Charged-GLY-tRNAs	0.50466
Charged-HIS-tRNAs	0.10098
Charged-ILE-tRNAs	0.33360
Charged-LEU-tRNAs	0.42815
Charged-LYS-tRNAs	0.39935
Charged-MET-tRNAs	0.14004
Charged-PHE-tRNAs	0.21741
Charged-PRO-tRNAs	0.19850
Charged-SER-tRNAs	0.26722
Charged-THR-tRNAs	0.23027
Charged-TRP-tRNAs	0.06711
Charged-TYR-tRNAs	0.13695
Charged-VAL-tRNAs	0.37908
N-Formyl-L-methionyl-tRNA <sup>fmet</sup>	0.00705
ATP	73.2236
water	68.0887

**Table S10. Products of Biomass reactions for *M. gallisepticum* model.** The name and stoichiometric coefficients for each species are given.

Name	Stoichiometric coefficients
ALA-trnas	0.32989
ARG-trnas	0.23855
ASN-trnas	0.18293

Name	Stoichiometric coefficients
ASP-trnas	0.18293
CYS-tRNAs	0.07008
GLN-tRNAs	0.32173
GLT-tRNAs	0.32185
GLY-tRNAs	0.50466
HIS-tRNAs	0.10098
ILE-tRNAs	0.33360
LEU-tRNAs	0.42815
LYS-tRNAs	0.39935
MET-tRNAs	0.14004
PHE-tRNAs	0.21741
PRO-tRNAs	0.19850
SER-tRNAs	0.26722
THR-tRNAs	0.23027
TRP-tRNAs	0.06711
TYR-tRNAs	0.13695
VAL-tRNAs	0.37908
MET-tRNAs	0.00705
formate	0.00705
biomass	1
ADP	73.1400
PI	73.1215
PPI	0.3463
Protons	73.1400

### A3.6. Experimentally measured fluxes

Table S11. Measured fluxes for *M. gallisepticum* model.

Flux name	Low boundary	Up boundary
ATP_maintenance_requirement	8.4	1000
GLC-Ex-Flux	-16.53	-16.53
L-LACTATE-Ex-Flux	10.29	10.29

## **APPENDIX 4. GAFBA v1.1 USER MANUAL**

### **A4.1. Introduction**

Metabolic engineering requires a high-quality genome scale metabolic networks to get results near to the physiological behavior. Many of the available metabolic models are incomplete because of lack of information.

GAFBA v1.1 is a tool design to help in the curation of genome scale metabolic models. The software guides the user through the curation process and aids in the determination of metabolites participating in unaccounted for reactions. With this tool, it is possible to quickly identify the key metabolites to focus on for detailed curation, reducing overall curation time. The software is based on a genetic algorithm approach that identifies problematic metabolites.

The tool has an user-friendly interface that receives all the information and generate files that contain the flux distribution, and the list of metabolites which mass balance constraint was unenforced.

### **A4.2. Development.**

GAFBA v1.1 software is a project from Dr. Srivastava research's lab at University of Connecticut 2013. The software platform was developed in Common Lisp and compiled using the LispWorks 6.0.1 Professional Edition compiler. The software is freely available under the BSD Open Source License. The software package carries out

linear programming by calling the GNU Linear Programming Kit<sup>1</sup>. The software is available for Windows, OS X, and Linux.

### **A4.3. Getting Started**

In order to use you only have to click on the executable file named GAFBA v1.1. For using GAFBA v1.1 you will need to have:

1. A SBML file that has the metabolic network representation.
2. A biomass reaction
3. Experimental conditions: media composition, measured fluxes, genotype of the bacteria.
4. A desired objective function
5. Desired genetic algorithm (GA) parameters.

### **A4.4. Quick tour through GAFBA v1.1**

GAFBA v1.1 graphic user interface is divided into three main parts as it is shown in Figure S4. The first one receives the information corresponding to the SBML file name, model name, and the location of the glpsol executable. The second is a tabulated panel where the information of biomass reaction, objective function, exchange fluxes, measured fluxes, medium composition, knockout reaction, GA parameters, and frequency analysis are received. The last part corresponds to the option buttons to start GAFBA

---

<sup>1</sup> <http://www.gnu.org/software/glpk/>

v1.1, to load a pre-existing input file and to save the information submitted to GAFBA v1.1 through the GUI in an input file, and the “about button” which has the information about the copyrights of GAFBA v1.1.

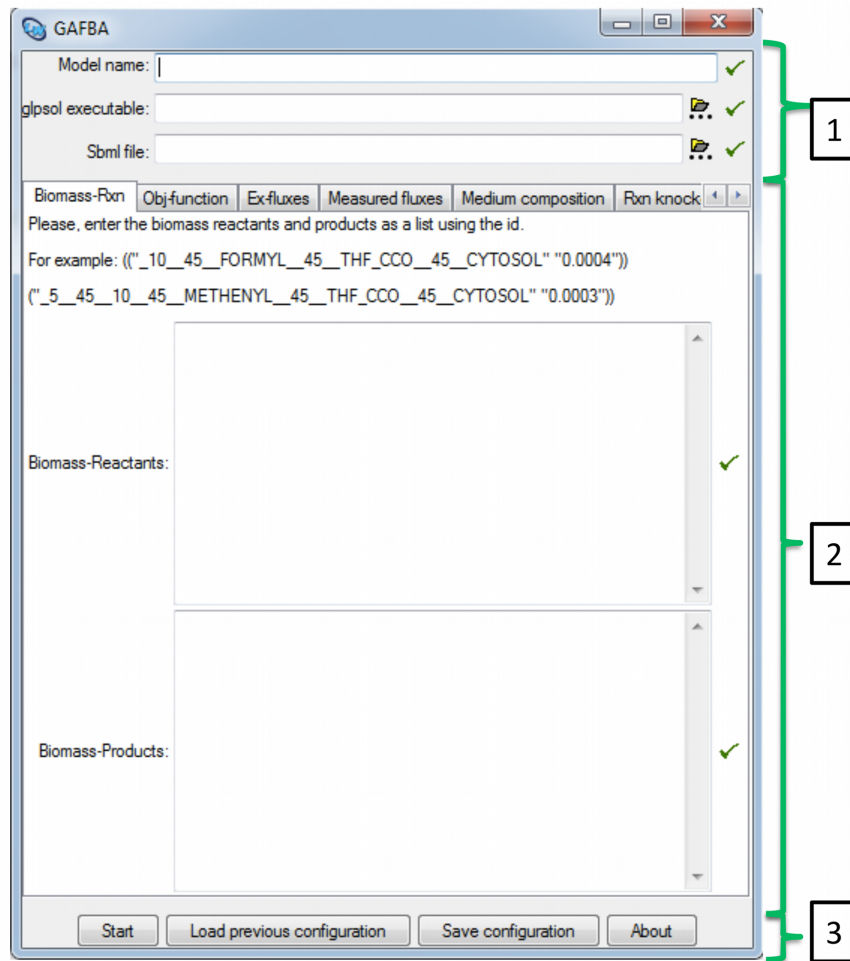


**Figure S4. GAFBA v1.1 structure.** The three main part of the interface are labeled with the corresponding number.

When GAFBA v1.1 starts to run a log file with the actual status of the program is written. In this log file, you can find any problem that can occur during the simulation.



When, GAFBA v1.1 reaches the termination criteria, it will generate the output files and a termination message is shown.

#### **A4.5. Creating the model**

**Defining a model name, loading network file and location of glpsol executable.** In the first panel, the user can define the desired name for the model. It is necessary click the check button after enter the name. Then the location of the glpsol executable has to be specified by searching it through the folder button. Finally, a SBML file is required to be specified in the second panel by selecting the folder button. A window will appear, as it is showed at Figure S5, in this window, you can search for the desired file and then click on the check button.

The SBML file is a representation format, based on XML, for communicating and storing computational models of the biological process [256]. It may be generated from the Pathway Tools bioinformatics suite [66] after a Pathway/Genome Database (PGDB) has been generated with PathoLogic [257] or from an existing PGDB.

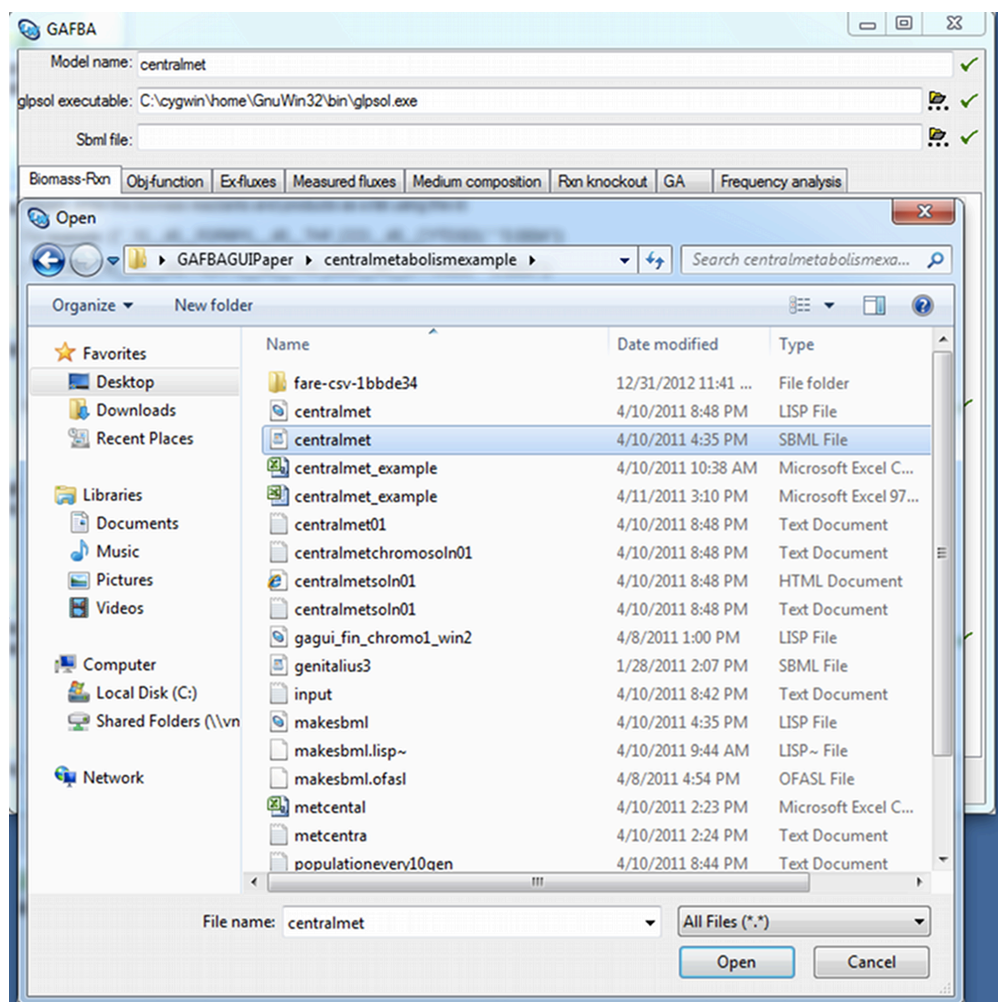


**Figure S5. Choosing a SBML file**

**Submitting Biomass Reaction.** The biomass reaction accounts for all the key cofactors and biosynthetic precursors to produce a 1 gDW of bacteria biomass [128]. All these metabolites have to be given in a relative amount. Thus, the user additional to specify the species id of the metabolite, it is also necessary to enter the stoichiometry coefficient. A special format has to be followed, similar to the one show on Figure S6.

The structure for defined any metabolite should be: “species id” and the stoichiometry coefficient has to be specified between quotes “2.3”. Then, they are joined by a parenthesis (“species id” “2.3”) and all the reactants/products components are joined with an additional parenthesis ((“species id” “2.3”) (“species id” “1.3”)), remember to click on the check button at the right part of the window.

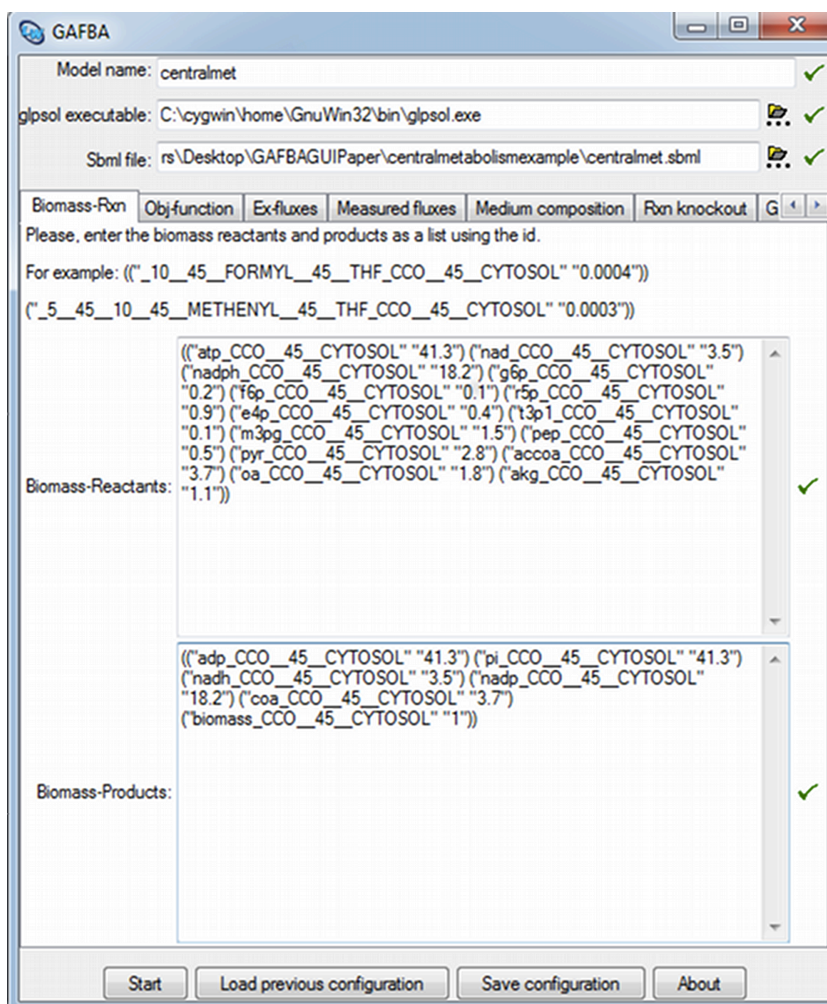


**Figure S6. Creating a biomass reaction.**

The biomass composition may be getting experimentally for cell growing at the exponential phase or from literature review, Thiele *et al.* [3] explain more about the procedure.

**Submitting Objective function.** In order to get the flux distribution with linear programming, it is required to choose an objective function and a case of optimization: maximization or minimization. GAFBA v1.1 has three options to define the objective function: predefined, choose a reaction present in the SBML file, or create a new objective function as it is shown in Figure S7. Each of them is explained below.

- Predefined objective functions.

Biomass. Biomass is one of the most-used objective functions in FBA. It is hypothesized that the bacteria have evolved for optimization of the specific growth rate under several conditions [3,44].

ATP. This function is related with the efficient of energy use by the bacteria. Minimization of ATP production rate means to reduce the energy consumed during the cell growth, thereby conserving. Maximization of ATP means direct the bacteria growth to produce as much energy as it can do [26].

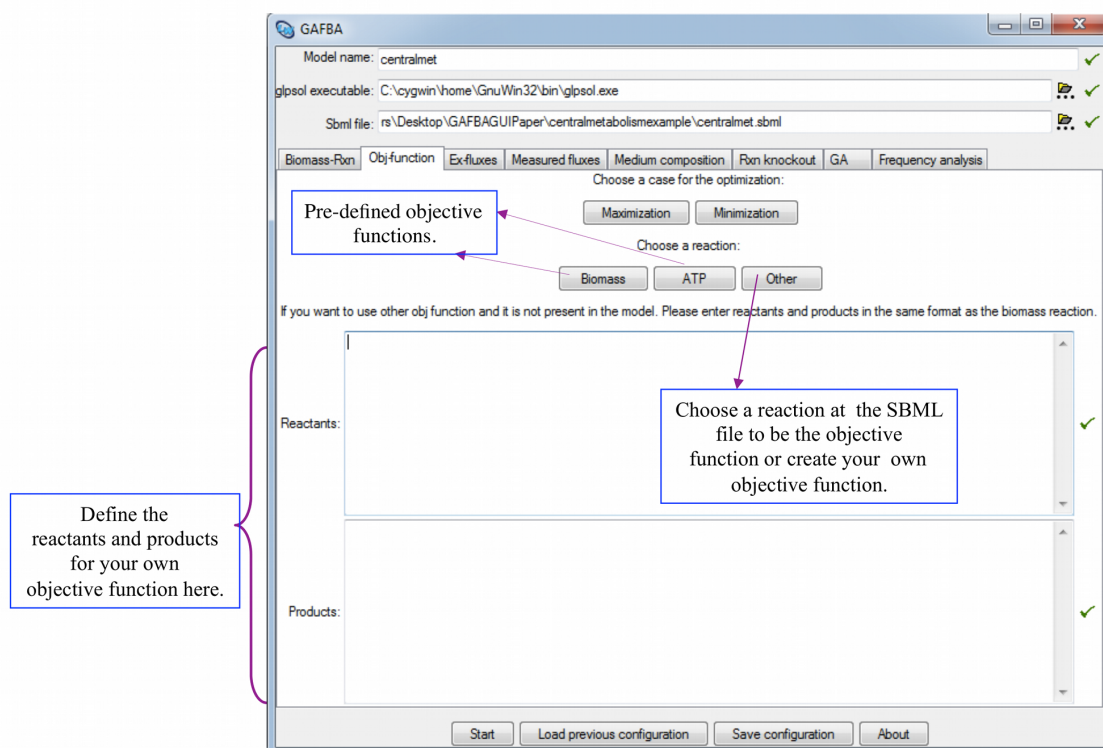


**Figure S7. Choose an objective function**

- Existing reaction in the model as an objective function. If the desired objective function is one present on the SBML file. The user should click on other button. It will appear a window (Figure S8) asking if you need to create a reaction, the user should select No. Then a new window will pop up asking about the name of the reaction. The user should type the name of the reaction as appear in the SBML file.

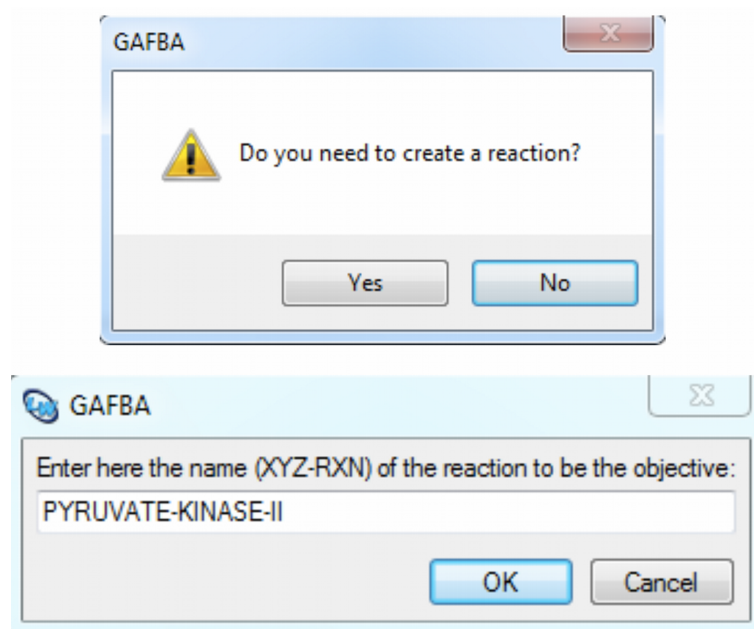


**Figure S8. Existing reaction in the model**

- Creating a new reaction to be the objective function. If the user wants to create a different objective function should select other button and when the program asks if you need to create a reaction, the user should select yes (Figure S9). Then, the name for the new reaction has to be specified following a special format: name\_of\_reaction\_r or name\_of\_reaction\_i. The name of the reaction must not have any space, instead use low dash (\_). At the end of the name, you should use r if the reaction is reversible, or i for irreversible reaction.

The reactants and products for the new reaction have to be entered through the interface window as it shows in Figure S10. It is required to use the same format as

the components of the biomass reaction and also click on the check button at the right part of the window.

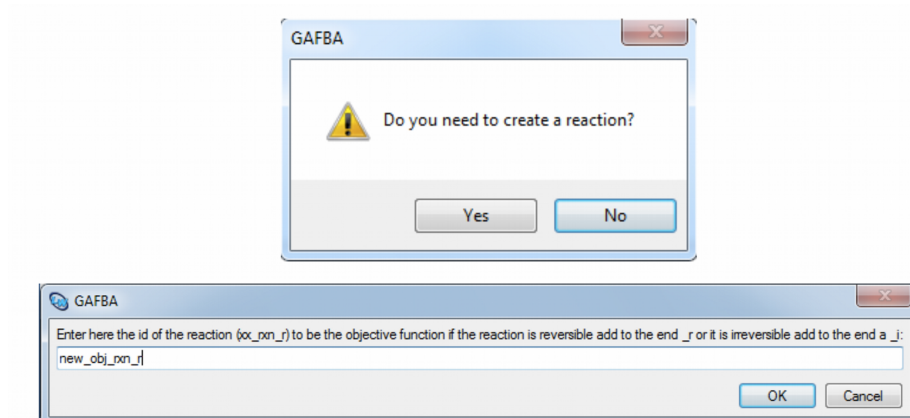


**Figure S9. Create a new reaction**

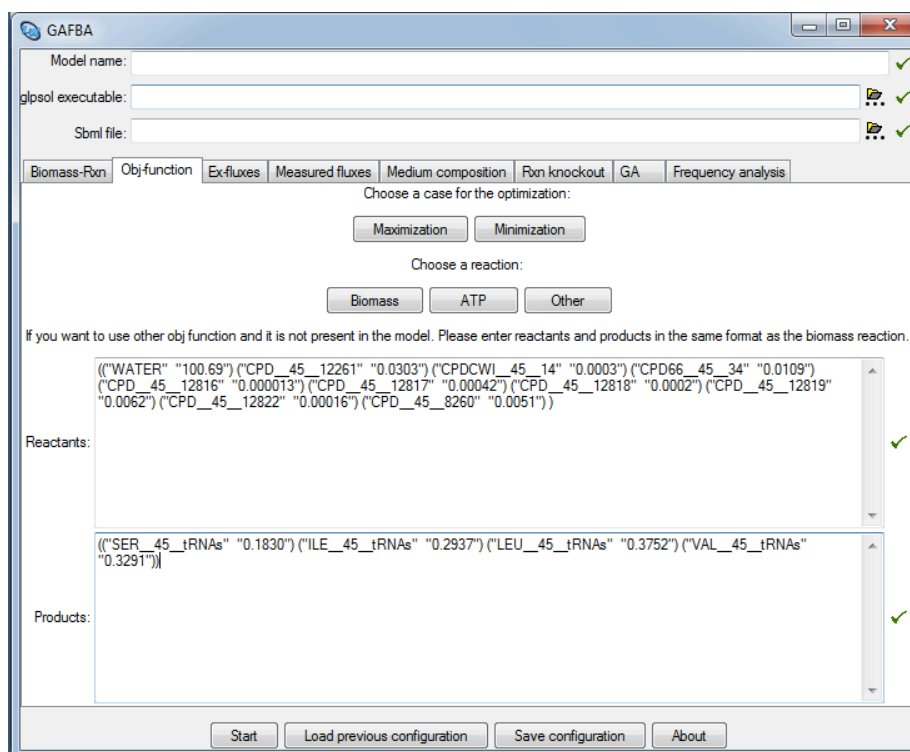


**Figure S10. Defining reactants and products of the new reaction.**

**Submitting exchange fluxes.** The exchange fluxes are the metabolites capable of leaving the cell like byproducts and the metabolites taken in from the media to guarantee the growth of the bacteria. In this part of the software, you should list all of them (secreted fluxes and uptake fluxes). At the Ex-fluxes tab, the user can decide to add or not add the exchange fluxes by clicking on yes or no. It is important to add exchange fluxes to permit the interchange of components between the bacteria and the media.

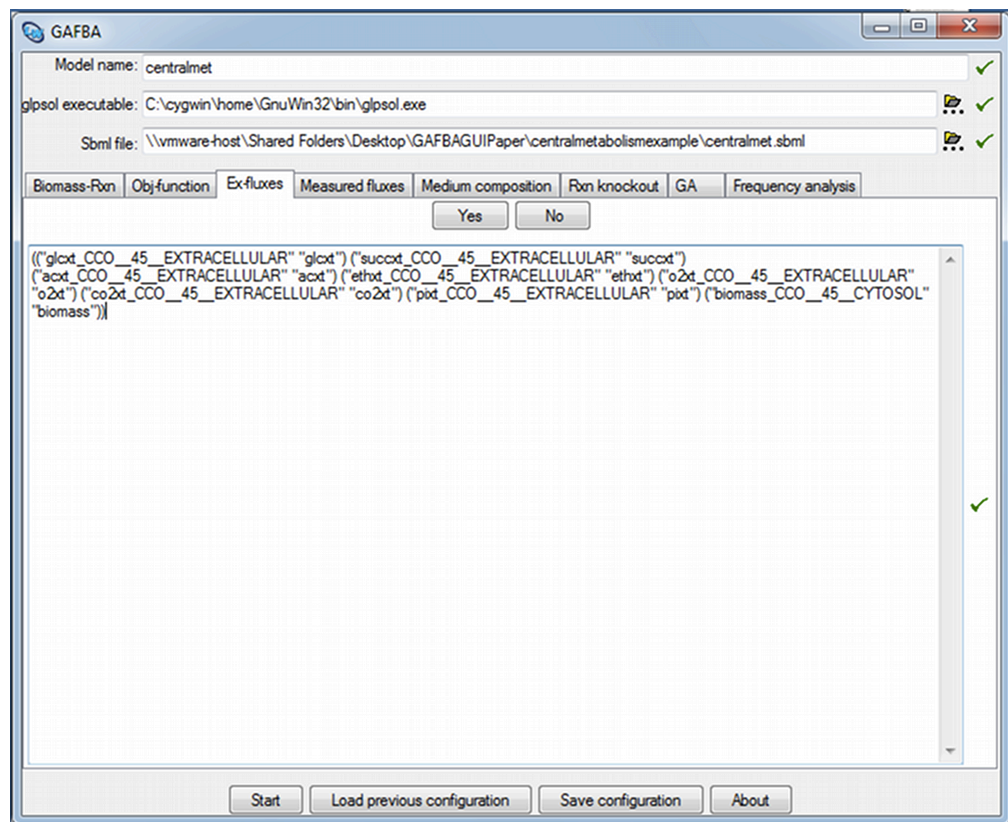


**Figure S11. Defining the exchange fluxes.**



The id and the name for each of the metabolites to be interchange have to be specified between quotation marks and parenthesis as showed in Figure S11. For example: (("id" "name") ("id" "name")). It is required to click on the check button at the right side of the panel to submit the information to GAFBA v1.1.

**Declaring experimental measured fluxes.** The measured fluxes are constraints used in flux balance analysis (FBA) to reflect previous known conditions and fluxes experimentally measured [258]. It is important that each of the metabolites with a measured flux was already defined in the exchange fluxes section.

The software permits to declare the fluxes or not. If no measured fluxes are entered, FBA will generate a flux distribution that probably is not going to be reflect the real behavior of the bacteria. The format to submit the measured fluxes is as follows (Figure S12):

((("species id Exchange FLUX" "lower flux value" "upper flux value")

("species id Exchange FLUX" "lower flux value" "upper flux value"))

Remember to click on the check button after finish to enter all the experimental measured fluxes.

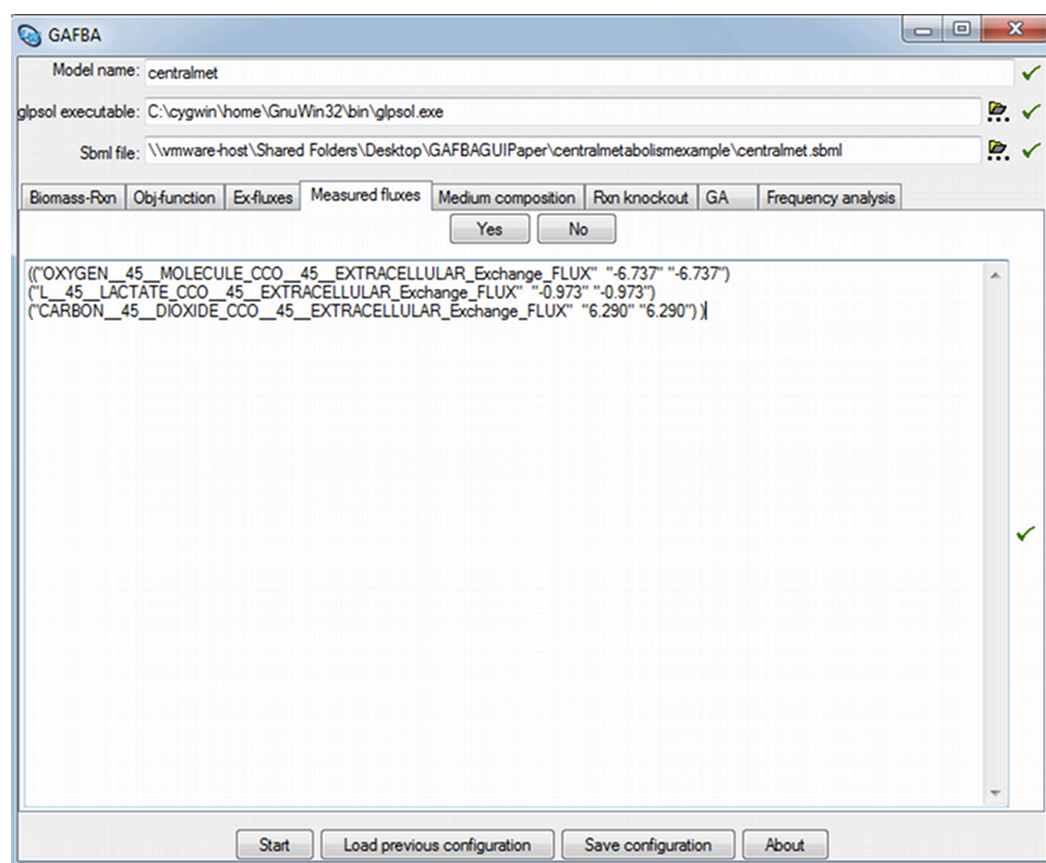


**Figure S12. Measured fluxes.**

**Submitting medium composition.** The media composition represents the constraints imposed to the cells by the environment around them. The growth of the bacteria depends on the presence or absence of certain components [259]. If a metabolite defined in the exchange fluxes is present at the medium composition, it means that the metabolite can go in and go out freely (lower boundary of -1000 and upper boundary of 1000). On the contrary, if the metabolite is presented at the exchange fluxes but not at the

medium composition, the metabolite just can go out the bacteria (secretion) lower boundary of 0 and upper boundary of 1000.

In order to declare the medium composition, first the yes button has to be pressed, then the medium composition has to be enter following the format, finally the user has to click on the check button on the right. The format is shown on Figure S13. It should be used the id of the reaction responsible for the interchange of the metabolite to/from outside from/to inside.

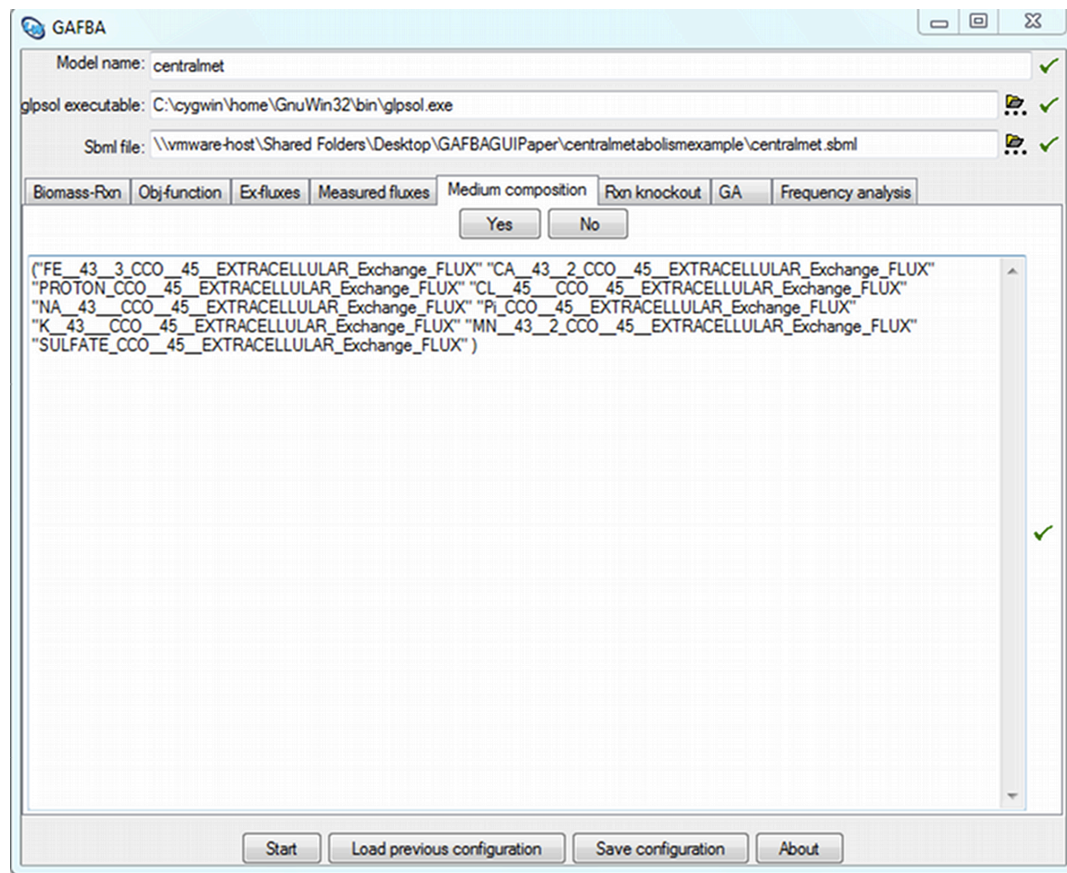


**Figure S13. Medium composition.**

**Submitting knockouts.** Some reactions are knocked out because of gene regulation under different environmental conditions or because of the genotype of the bacteria. In this part of the interface, the user can enter such as reactions. The user can decide to do/not do the knockouts by clicking on yes/or no button. If yes button was pressed the name of the reactions have to be declared on quotes and parenthesis as it is shown on Figure S14. Then the green check button on the right side has to be clicked on.

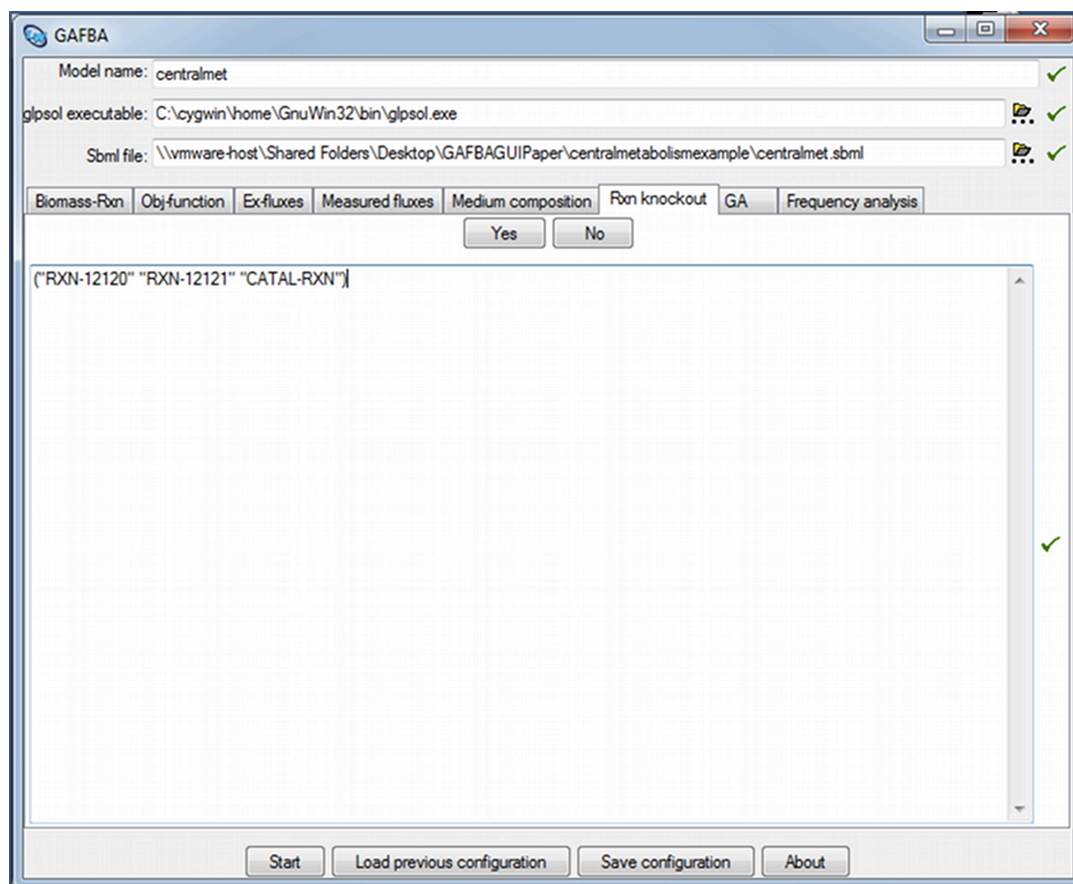


**Figure S14. Regulatory constraints.**

**Genetic algorithm preferences.** At the GA tab, GAFBA v1.1 permits to run just a FBA simulation by clicking on no button or a GAFBA v1.1 simulation by clicking on yes button. The user can define the values for probability of crossover (pc), number of point crossover (npc), probability of mutation (pm), elite fraction (ef), population size (ps), number of generations (ng), number of simulation (ns), bottom re-seed fraction (brsf), frequency of bottom re-seed (fbrs), and the condition for the initial population (ip) under this tab as it is shown on Figure S15.

The screenshot shows the GAFBA application window with the 'GA' tab selected. The window contains the following fields and controls:

- Model name:** centralmet
- glpsol executable:** C:\cygwin\home\GnuWin32\bin\glpsol.exe
- Sbml file:** \\vmware-host\Shared Folders\Desktop\GAFBAGUIPaper\centralmetabolismexample\centralmet.sbml
- Tabs:** Biomass-Rxn, Obj-function, Ex-fluxes, Measured fluxes, Medium composition, Rxn knockout, GA (selected), Frequency analysis
- Buttons:** Yes, No
- Probability crossover:** 0.7
- Number of point crossover:** 2
- Probability mutation:** 0.01
- Elite fraction:** 0.2
- Population size:** 30
- Number of generations:** 2000
- Number of simulations:** 1
- Do you want to do bottom-reseed?** (Yes, No buttons)
- Bottom-reseed fraction:** 0.2
- Frequency of bottom re-seed:** 100
- Initial population:** (Random, Customize buttons)
- Bottom Buttons:** Start, Load previous configuration, Save configuration, About

**Figure S15. Genetic algorithm preferences.**

For the number of n-point crossover, many studies suggested that when the population size is less than 50, it is good to have more than two-point crossover [260-262].

The condition of the initial population represents the way of GAFBA v1.1 has to generate the first population to be used for the GA part. It can be random or using a previous population (customize). When customize button is clicked on, a new window appears asking for the file that contains the desired initial population. Customize population is useful when the user wants to re-use a previous generated population after make some changes but not metabolites had been added/removed. In all the other cases, the population needs to be re-initialized randomly.

Bottom re-seed replaces chromosomes of the bottom part of the population with new randomly generated chromosomes. The user can decide of do/not do it, by selecting yes or no. Also, it needs to define the bottom fraction of the population to be replaced, and the frequency which this process will be repeated. This scheme is useful when the user observed that the population was rapidly becoming uniform [261]. For example, if the user observed that after 2000 generation with a population size of 30 and elite fraction of 0.2, more than the top six chromosomes are the same, it will be useful to do re-seeding.

The number of generation is the limit of runs of GAFBA v1.1 desired. The number of simulations is the times that the user wants to run a model before make any change, for example: a run of GAFBA v1.1 with four simulations and 2000 generations means that the software is going to make a total of 8000 runs of GAFBA v1.1 before the program stop, as it is shown on Figure 15, where the complete structure of GAFBA v1.1 is presented.

If the user does not enter any value for the parameters, and the software is going to run GAFBA v1.1, predefined values are going to be used:  $pc=0.7$ ,  $npc=2$ ,  $pm=0.01$ ,  $ef=0.2$ ,  $ns=1$ ,  $gn=200$ ,  $ps=30$ ,  $brsf=0.2$ ,  $fbrs=100$ , and  $ip=$  random.

#### **A4.6. Saving input information in a file.**

GAFBA v1.1 permits save the information submitted through the interface by clicking on the save configuration button. A window will appear asking for the name of the file to save the information. The file is saved in the same folder as the GAFBA v1.1 executable. The format of the file is explaining on the section number A4.9.

#### A4.7. Load a previous input file.

GAFBA v1.1 has the possibility to load a previous configuration by clicking on the load button. A window will open, as it is shown in Figure S16, it asks about the name of the file. The file can be searched through this window.

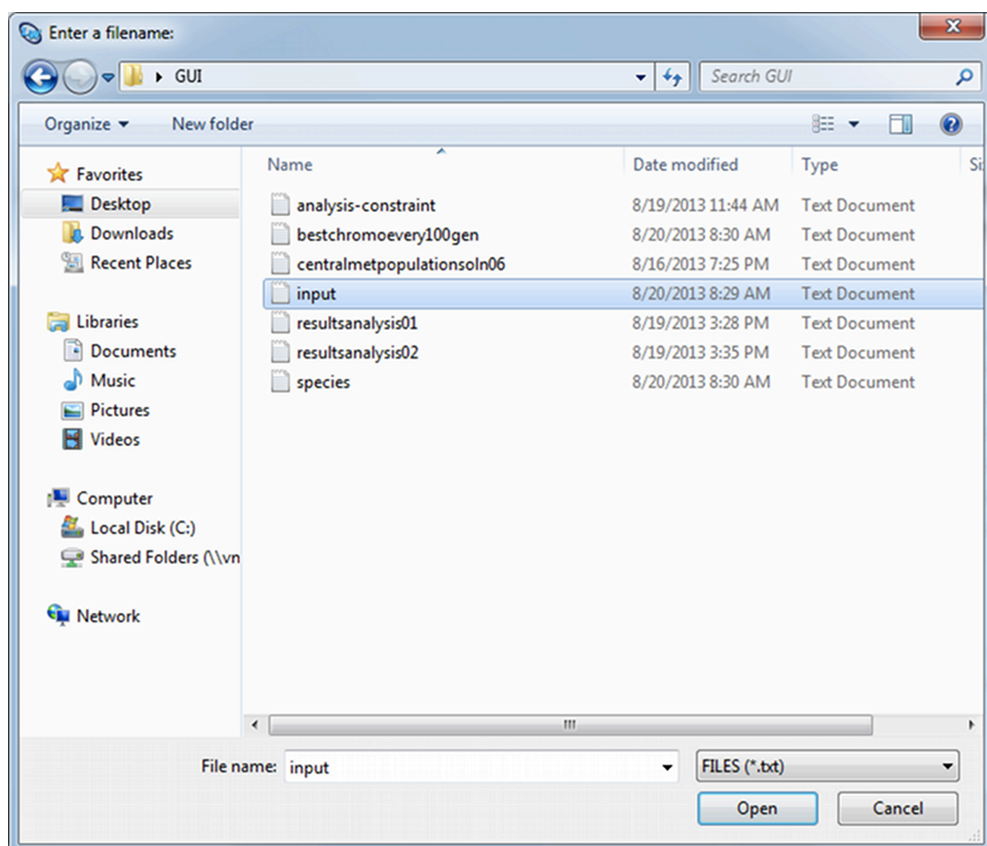


**Figure S16. Loading a saved input file.**



#### **A4.8. Start GAFBA.**

After the required information is entered through the interface or through a previous file, the start button can be clicked. GAFBA v1.1 starts to run and the status of the simulation is going to be printed out in a .log file. When, GAFBA v1.1 is done with the simulation, a message will appear letting know that the process has finished.

#### **A4.9. Results files.**

GAFBA v1.1 generates five output files that contain the best solution to the FBA problem, the best model of the bacteria, the last population, the record of the best chromosome each one hundred generations and the file with the list of problematic metabolites. Each of these files is explained in the following sections.

- **Model file.** This is the input file for running the linear programming solver glpsol. You can find here the variables associated with each of the reactions. There are two kinds of variables  $b_n$  and  $V_n$  where  $n$  is an integer, the first one refers to exchange fluxes and the second one are the rest of reactions (transport reactions, internal reactions, spontaneous reactions).

Model file also has the objective function, the upper and the lower boundaries for the fluxes and the mass balance for each metabolite in the model. The name of the file is: modelname#.txt, the number refers to the simulation number.

- **Flux distribution file.** The flux distribution file is the one with the name in this format `modelnamesoln#.txt`, the number refers to the simulation number. It has the final result for each of the fluxes present in the metabolic network, the result for the objective function and the final status of the model. It is required that in front of the word “Status” always appears OPTIMAL. If the status is different than OPTIMAL, it is necessary to run GAFBA v1.1 for more generation. The value for the objective function is shown in front of the word “Objective:”. The flux for each the reactions is at the middle of the document, in this part you will find a column with a sequence of numbers, then a column with the variables names and the fourth column under the activity title is the flux value for the reaction in  $\text{mmol gDW}^{-1} \text{ h}^{-1}$ . An example of the flux distribution file is shown on Figure S17.

```

Problem:    genitalius
Rows:       1109
Columns:    395
Non-zeros:  1869
Status:     OPTIMAL
Objective:  Biomass = 156.4686901 (MAXimum)

```

No.	Column name	St	Activity	Lower bound	Upper bound
Marginal					
-----					
1	b_19	B	-20.4645		
2	V16_R	B	0.777649		
3	V296	B	15.8002		
4	b_45	B	0		
5	b_71	B	0		
6	V89	B	142.121		
7	V157_R	B	1000		
8	b_28	B	0		
9	V228	B	0.0453759		
10	V15_R	B	0		
11	b_54	B	0		
12	V295	B	0		
13	V88	B	0		
14	b_37	B	1000		
15	V156	B	0		
16	b_63	B	0		
17	V227	B	0		
18	V14_R	B	0		

**Figure S17. FBA solution file**

- **Problematic metabolites file.** The problematic metabolites are listed on the file with the name resultsanalysis#.txt . This file has the number of mass balance constraints kept, the number of mass balance leaving open, the value of the objective function and the list of the metabolites which mass balances were not fulfilled.

It is desired that the number of mass balance constraints dropped are similar to zero.

The user should review this file carefully, since the metabolites listed in here require some adjusted to the reaction or addition of new reaction to complete the mass balance. Since at the beginning of the process many metabolites are dropped. It is advisable to run the model for at least 14000 generations for models with more than 1000 metabolites or 8000 generations for models with less than 1000 metabolites before to review the problematic metabolites file.

- **Population file.** This is the file label as modelnamepopulationsoln#.txt. It has the last population used in GAFBA v1.1 after each simulation. The population is formed by n chromosome, n is defined by the user with the population size parameter. This file is useful when it is wanted to start the program with a customize population, usually when some changes had been made to the model but not metabolites had been added/removed. Thus, when a new simulation is going to start, in the genetic algorithm preferences tab should be chosen customize population and then search for this file.
- **Best chromosome recorded file.** This file keeps tracking the best chromosome each one hundred generations. The name of the file is: modelnamebestchromo#.txt, where again the number refers to the simulation number. It gives an advantage to the user to review the progress of the model.

#### **A4.10. Possible solutions to fill gaps**

The potential solutions for adjust the model are five: 1) change the directionality of a reaction, 2) add an exchange flux for the metabolite, 3) add a transport or intracellular reaction, 4) remove a reaction or metabolite from the model, and 5) no change. The decision taken has to be based on literature survey or information from related species. More information about this topic and examples are available in Bautista *et al.* [192]

#### **A.4.11. Running a new simulation**

There are two kinds of modes for restarting the program, and they depends on the changes made to the model.

1. Enter again all the information through the interface and use a random population: it is applied when the user added/removed a metabolite from the previous model.

2. Enter the information through a saved file, or through the interface and use a customize population: it is implemented when the changes to the model were on the directionality of reactions, added/removed exchange fluxes, or transport reactions, or intracellular reactions, or not change was done to the model.

#### **A.4.12. Input file**

GAFBA v1.1 automatically creates the input file by clicking on save button after enter the information through the interface. The format used to write the input file is based on LISP programming language. The file can be modified, but you always should keep in mind the specified format for each part.

#### **A.4.13. Frequency analysis**

After, some simulation had been carried; a frequency analysis could be done by selecting the frequency analysis tab in the GAFBA v1.1 GUI, which is shown in Figure S18. It will need to provide with the population (modelnamepopulationsoln#.txt), and the file with the model (modelname#.txt), where the number symbol refers to the simulation number to be studied (n). Furthermore, it is required to specify the number of top chromosomes to be analyzed (y). Usually this number should be near to the elite chromosomes. For example, if the elite fraction was 0.2 and the population size was 30 the elite chromosomes are 6. Thus, a good value for y should be 10. After enter all the information through the gui for the frequency analysis, the Results button could be pressed it, and a file with the name analysis-constraint.txt is created that have the metabolites with mass balance constraints that were presented in all the y chromosomes.

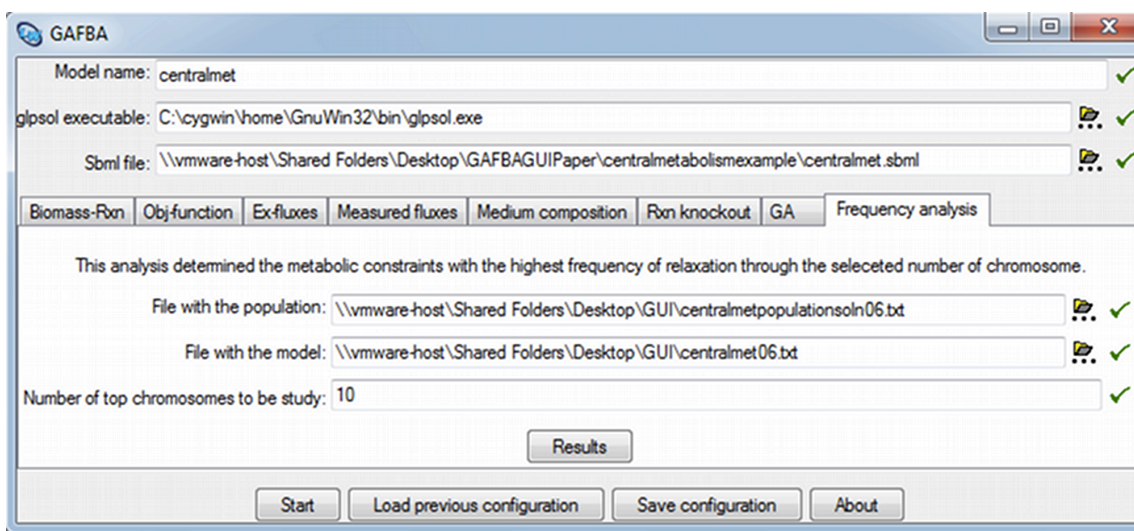


**Figure S18. Frequency analysis input information.**

The rationale behind the frequency analysis is as a follow, when minimizing the number of relaxed constraints, the GA generated a population of models represented by chromosomes indicating which metabolic constraints had to be relaxed. It is possible to determine the frequency with which a metabolic constraint is relaxed across the population of chromosomes. The metabolic constraints with the highest frequency of relaxation were likely the most pathologic to the generation of a feasible metabolic model. As a further point of reference, as populations evolved, frequencies should be tracked across generations. Doing this provided further information regarding how critical a particular metabolic constraint is to the viability of the model.

The process begins by randomly selecting the final populations of two different simulations  $n$  and  $n+x$ , from GAFBA v1.1 for comparison. Each simulation consisted of evolving model populations for the desired generations. Constraints that were

consistently relaxed in the top  $y$  chromosomes of each of the final populations were selected. Relaxed metabolic constraints that arose in both in the top  $y$  chromosomes of each population were considered the most pathological metabolites. Therefore, they were the first metabolites to be analyzed. The algorithm representation of the frequency analysis is presented in Figure 11. More information about this methodology can be found in Bautista *et al.* [127].



## APPENDIX 5. ADDITIONAL EXPERIMENTAL METHODS

**Metabolites uptake and secretion rates calculation.** The glucose uptake rate, iron uptake rate, and glutamic acid uptake rate were calculated by solving the dynamic mass balance [23,24]:

$$\frac{d(V \cdot [S])}{dt} = -q_s \cdot V \cdot X_t \quad \text{Eq. (1)}$$

where  $V$  (L) is the culture volume,  $[S]$  (mM) is the metabolite concentration in the media,  $q_s$  (mmol/gDW\*h) is the glucose uptake, or iron uptake rate, or glutamic acid uptake rate, and  $X_t$  (gDW/L) is the biomass concentration at time=  $t$  (hr).

Oxygen uptake rate was calculated using the Equation 2. The equation is slightly different to Equation 1, because an additional term for diffusion of oxygen into the system is included [23,24]

$$\frac{d(V \cdot [O_2])}{dt} = k_l a \cdot (O_2^{sat} - [O_2]) - q_{O_2} \cdot V \cdot X_t \quad \text{Eq. (2)}$$

where  $V$  (L) is the culture volume,  $[O_2]$  is concentration of oxygen in the medium,  $O_2^{sat}$  is the saturation oxygen concentration at time =  $t$ , and  $k_l a$  is the mass transfer parameter estimated by using the absorption dynamic method [263,264]. The  $k_l a$  was determined to be  $52.2 \text{ h}^{-1}$ . Since, the response time of the electrode was calculated to be 18 s, not correction was applied to the model.

Lactate secretion rate, and catechol siderophores secretion rate were calculated by solving the following equation [23,24],

$$\frac{d(V \cdot [P])}{dt} = q_p \cdot V \cdot X_t \quad \text{Eq. (3)}$$

The terms in Equation 3 are similar to those in Equation 1, however because is secretion rate, the first term is positive.

Carbon dioxide uptake rate was calculated using Equation 4 [265,266],

$$\frac{d(V \cdot [CO_2])}{dt} = k_l a \cdot (CO_2^{sat} - [CO_2]) + q_{CO_2} \cdot V \cdot X_t - \frac{d(V \cdot [HCO_3^-])}{dt} \quad \text{Eq. (4)}$$

The first term represents the diffusion of carbon dioxide from the medium to the surrounding atmosphere, the second terms is the carbon dioxide produced by the cell, and the third term is the chemical transformation of carbon dioxide into/from the hydrogen carbonate buffer.

The  $k_l a$  for carbon dioxide was calculated using the correlation from equation 5. It could be applied because the mass transfer parameter for oxygen and carbon dioxide involve the same interfacial area, the same solvent properties, and the same agitation variables [267,268]. Thus,  $k_l a$  for carbon dioxide was  $46.46 \text{ h}^{-1}$ .

$$\frac{k_l a^{CO_2}}{k_l a^{O_2}} = 0.89 \quad \text{Eq. (5)}$$

The third term of Equation 4 was determined using the following equation [265],

$$\begin{aligned} & \frac{d(V \cdot [HCO_3^-])}{dt} \\ &= \frac{K_{CO_2}}{f} \left( \ln 10 \cdot 10^{pH(t)} \cdot V \cdot [CO_2(t)] \cdot \frac{dpH(t)}{dt} + 10^{pH(t)} \cdot \frac{d(V \cdot [CO_2])}{dt} \right) \end{aligned} \quad \text{Eq. (6)}$$

where  $K_{CO_2}$  is the mass action constant for carbon dioxide in water at 37°C with a value of  $4.21 \cdot 10^{-7} \text{ mol l}^{-1}$  [265],  $f$  is the individual hydrogen carbonate activity which was calculated using the semi-empirical Debye-Hückel equation [269], and it has a value of 0.88. The calculation of the hydrogen carbonate activity are shown in Table S12 and Table S13.

**Table S12. Calculation of Hydrogen carbonate activity for iron-reduced media.** \* Debye-Hückel Equation because ionic strength is less than 0.1

Salt/Buffer	Mass concentration (g l <sup>-1</sup> )	Molar Mass Mi (g mol <sup>-1</sup> )	Molar concentration ci (mol l <sup>-1</sup> )	Ion	Molar concentration ci (mol l <sup>-1</sup> ) <sup>2</sup>	Charge zi (-)	Product ci*zi <sup>2</sup>
MgSO4	0.01	120.366	8.30799E-05	Mg+2	8.30799E-05	2	0.00033232
MnSO4	0.001	151	6.62252E-06	Mn+2	6.62252E-06	2	2.64901E-05
KH2PO4	0.68	136.09	0.004996693	K+	0.015008174	1	0.015008174
K2HPO4	0.872	174.2	0.005005741	H2PO4-	0.004996693	-1	0.004996693
FeSO4			0.00000224	HPO4-2	0.005005741	-2	0.020022962
				Fe+2	0.00000224	2	0.00000896
				SO4-2	9.19425E-05	-2	0.00036777
						Summation	0.04076337
						Ionic strength (I)	0.020381685
						A	0.47
						B	33150000
						a <sub>o</sub> HCO <sub>3</sub> <sup>-</sup>	0.000000054
						I <sup>1/2</sup>	0.142764438
						*log f	-0.053441608
						f	0.884216046

**Table S13. Calculation of Hydrogen carbonate activity for iron-replete media.** \* Debye-Hückel Equation because ionic strength is less than 0.1

Salt/Buffer	Mass concentration ion (g l <sup>-1</sup> )	Molar Mass Mi (g mol <sup>-1</sup> )	Molar concentration ci (mol l <sup>-1</sup> )	Ion	Molar concentration ci (mol l <sup>-1</sup> ) <sup>2</sup>	Charge zi (-)	Product ci*zi <sup>2</sup>
MgSO4	0.01	120.366	8.30799E-05	Mg+2	8.30799E-05	2	0.00033232
MnSO4	0.001	151	6.62252E-06	Mn+2	6.62252E-06	2	2.64901E-05
KH2PO4	0.68	136.09	0.004996693	K+	0.015008174	1	0.015008174
K2HPO4	0.872	174.2	0.005005741	H2PO4-	0.004996693	-1	0.004996693
FeSO4			0.00002	HPO4-2	0.005005741	-2	0.020022962
				Fe+2	0.00002	2	0.00008
				SO4-2	0.000109702	-2	0.00043881
						Summation	0.04090545
						Ionic strength (I)	0.020452725
						A	0.47
						B	33150000
						a <sub>o</sub> HCO <sub>3</sub> <sup>-</sup>	0.000000054
						I <sup>1/2</sup>	0.143013023
						log f	-0.053515695
						f	0.884065218

## APPENDIX 6. TRIPLICATED EXPERIMENTAL DATA

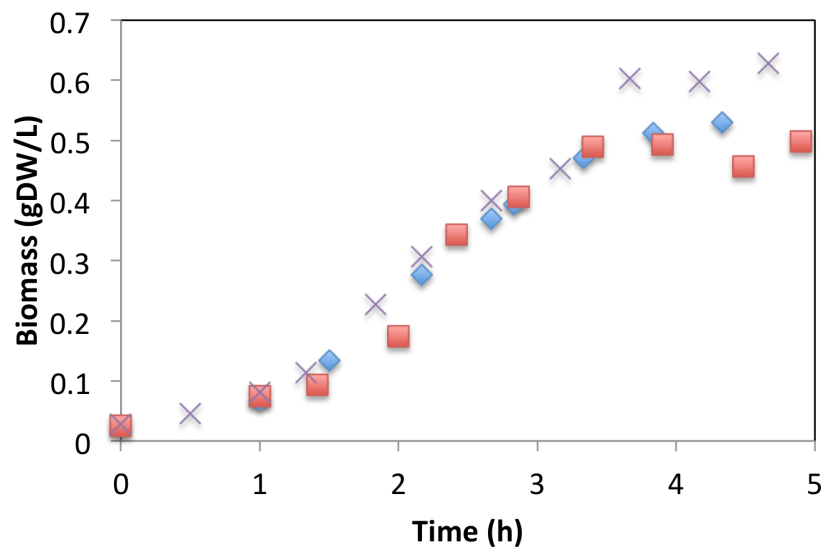


**Figure S19. Levels of biomass under iron-reduced conditions (IRDM) for triplicated experiments.** IRDM1 (red squares), IRDM2 (blue diamonds), IRDM3 (purple stars).

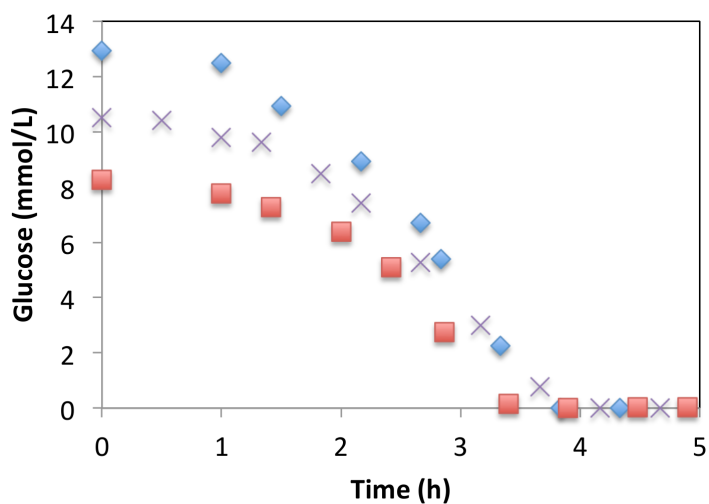


**Figure S20. Levels of glucose under iron-reduced conditions (IRDM) for triplicated experiments.** IRDM1 (red squares), IRDM2 (blue diamonds), IRDM3 (purple stars).

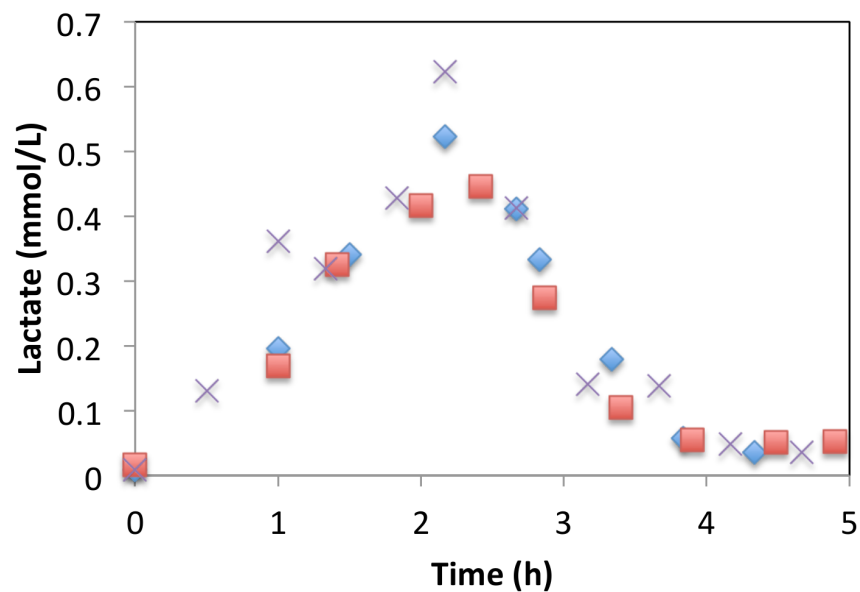


**Figure S21. Levels of lactate under iron-reduced conditions (IRDM) for triplicated experiments.** IRDM1 (red squares), IRDM2 (blue diamonds), IRDM3 (purple stars).

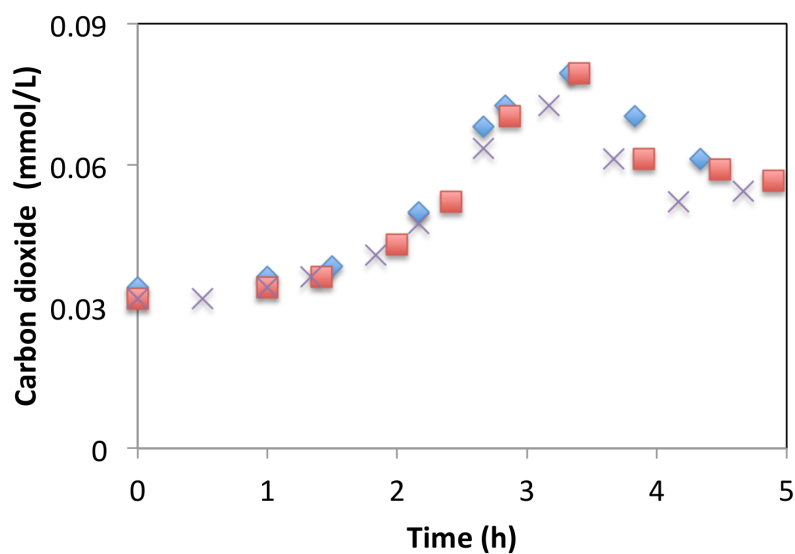


**Figure S22. Levels of carbon dioxide under iron-reduced conditions (IRDM) for triplicated experiments.** IRDM1 (red squares), IRDM2 (blue diamonds), IRDM3 (purple stars).

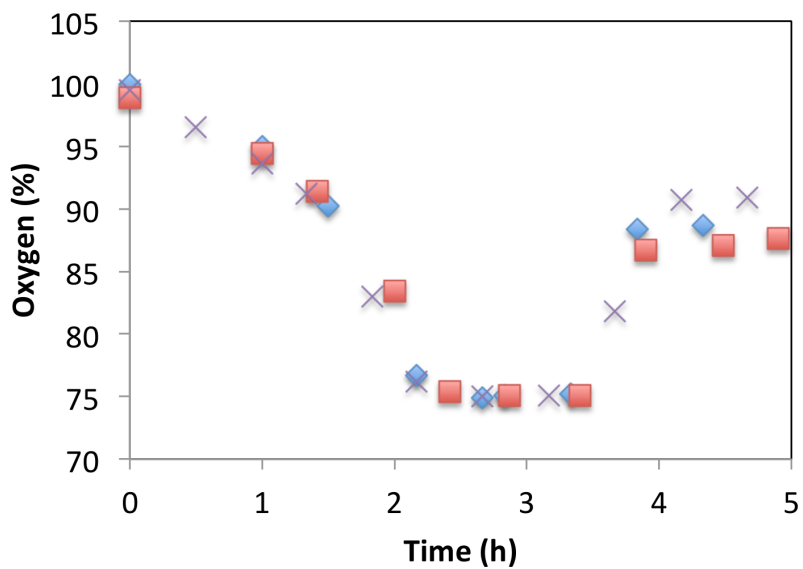


**Figure S23. Levels of oxygen under iron-reduced conditions (IRDM) for triplicated experiments.** IRDM1 (red squares), IRDM2 (blue diamonds), IRDM3 (purple stars).

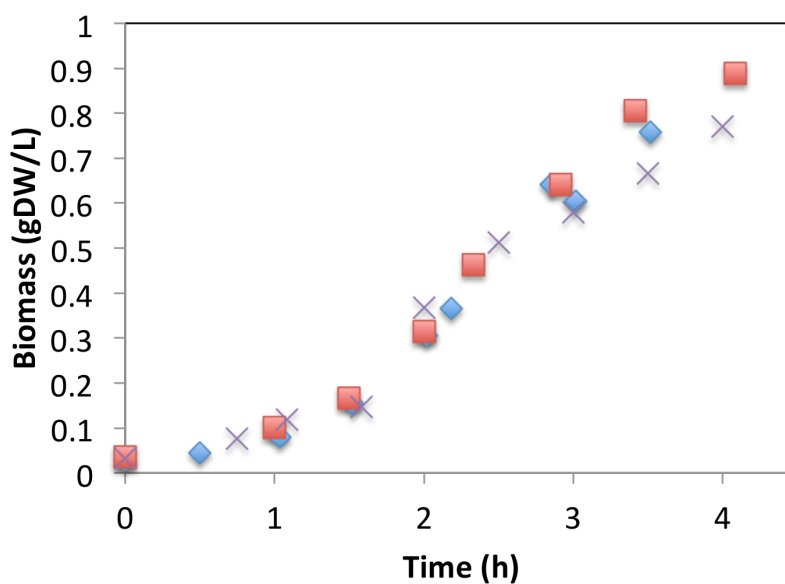


**Figure S24. Levels of biomass under iron-replete conditions (IRM) for triplicated experiments.** IRM1 (red squares), IRM2 (blue diamonds), IRM3 (purple stars).



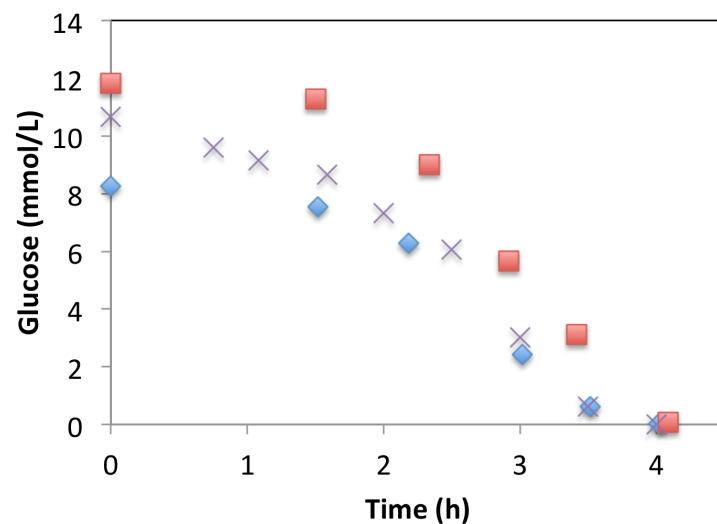


**Figure S25. Levels of glucose under iron-replete conditions (IRM) for triplicated experiments.** IRM1 (red squares), IRM2 (blue diamonds), IRM3 (purple stars).

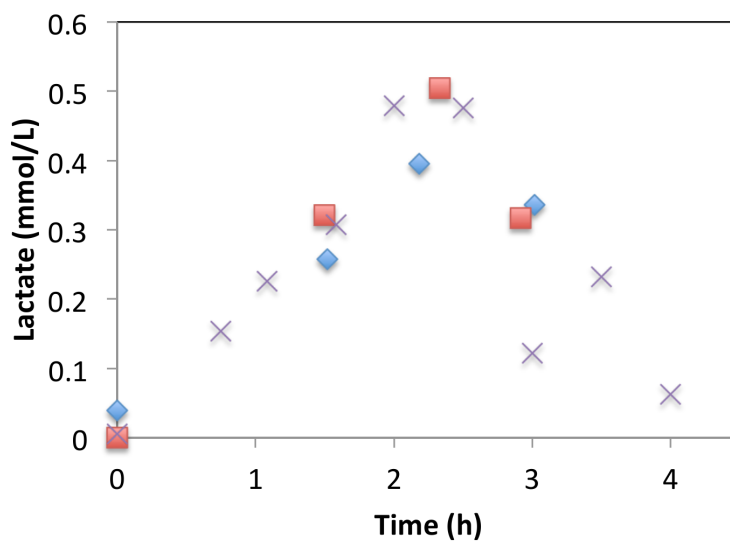


**Figure S26. Levels of lactate under iron-replete conditions (IRM) for triplicated experiments.** IRM1 (red squares), IRM2 (blue diamonds), IRM3 (purple stars).

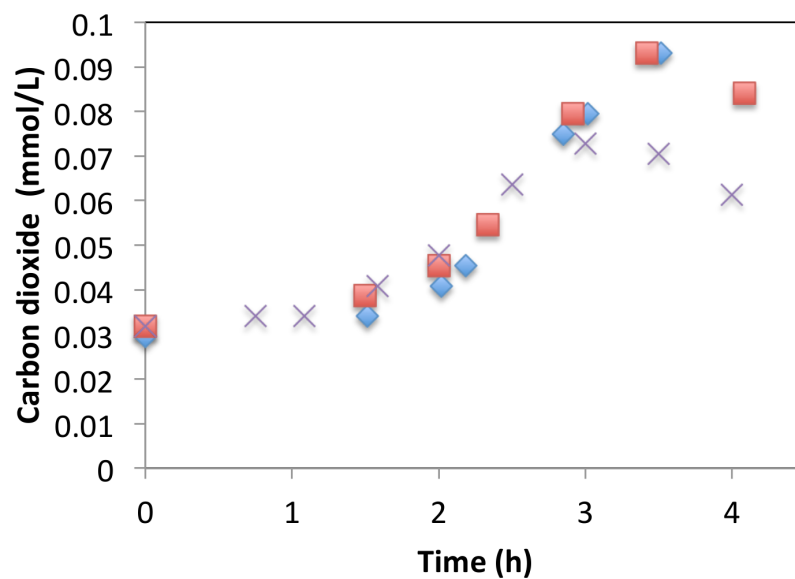


**Figure S27. Levels of carbon dioxide under iron-replete conditions (IRM) for triplicated experiments.** IRM1 (red squares), IRM2 (blue diamonds), IRM3 (purple stars).

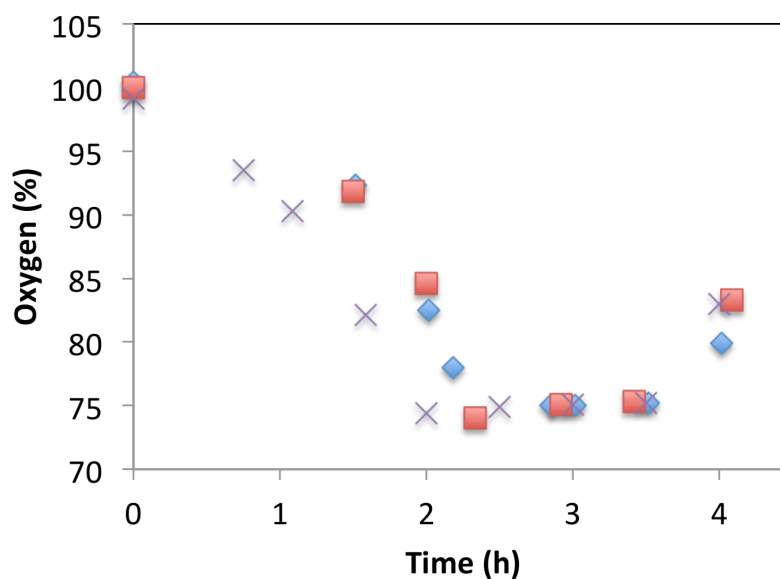


**Figure S28. Levels of oxygen under iron-replete conditions (IRM) for triplicated experiments.** IRM1 (red squares), IRM2 (blue diamonds), IRM3 (purple stars).

## APPENDIX 7. SUPPLEMENTARY FIGURES



**Figure S29. Biosynthesis pathway of petrobactin and protocatechaute.** Metabolites are in red. Reactants or products of the reactions in yellow are acyl carrier proteins. The name of the enzyme that catalyzed each reaction is in yellow next to reaction. The genes associated to each enzyme are in purple, and also the E.C. number for each enzyme has been displayed.

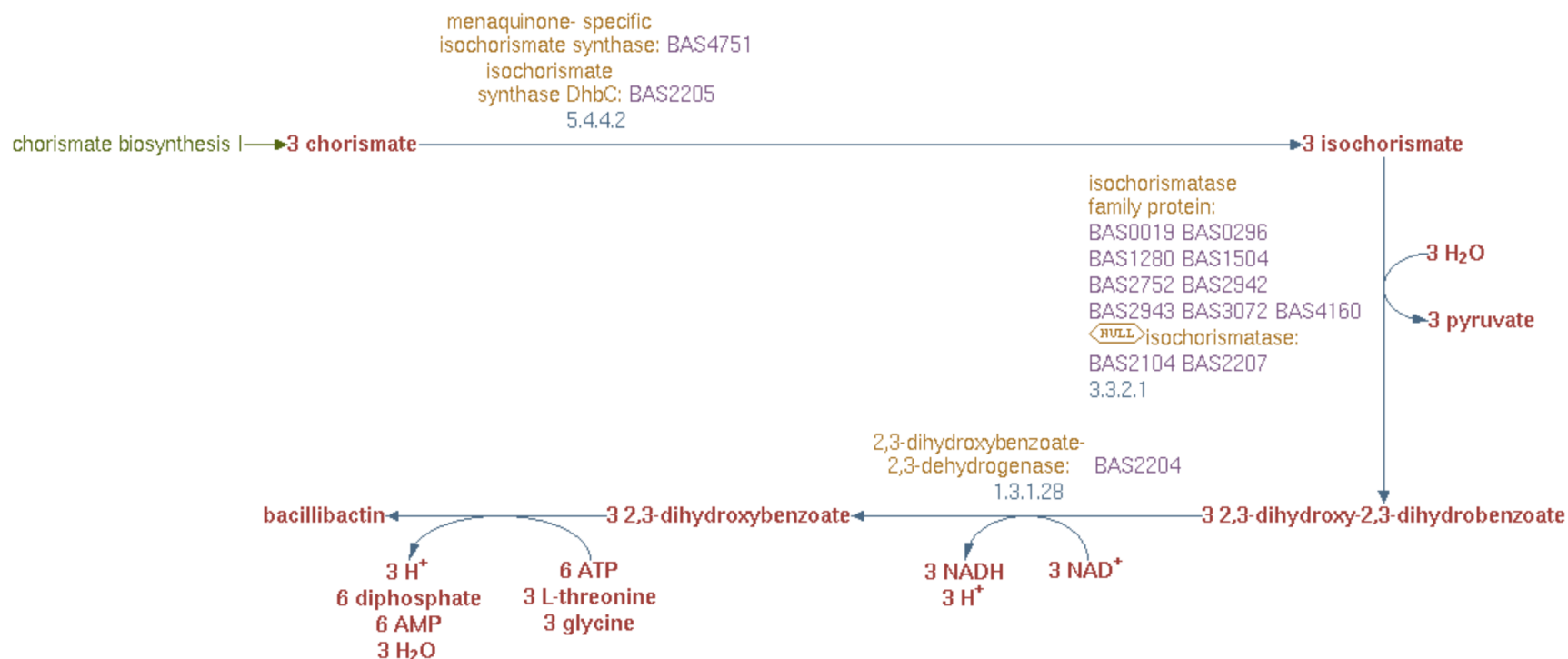


**Figure S30. Biosynthesis pathway of bacillibactin.** Metabolites are in red. The name of the enzyme that catalyzed each reaction is in yellow. The genes associated to each enzyme are in purple, and also the E.C. number for each enzyme has been displayed.

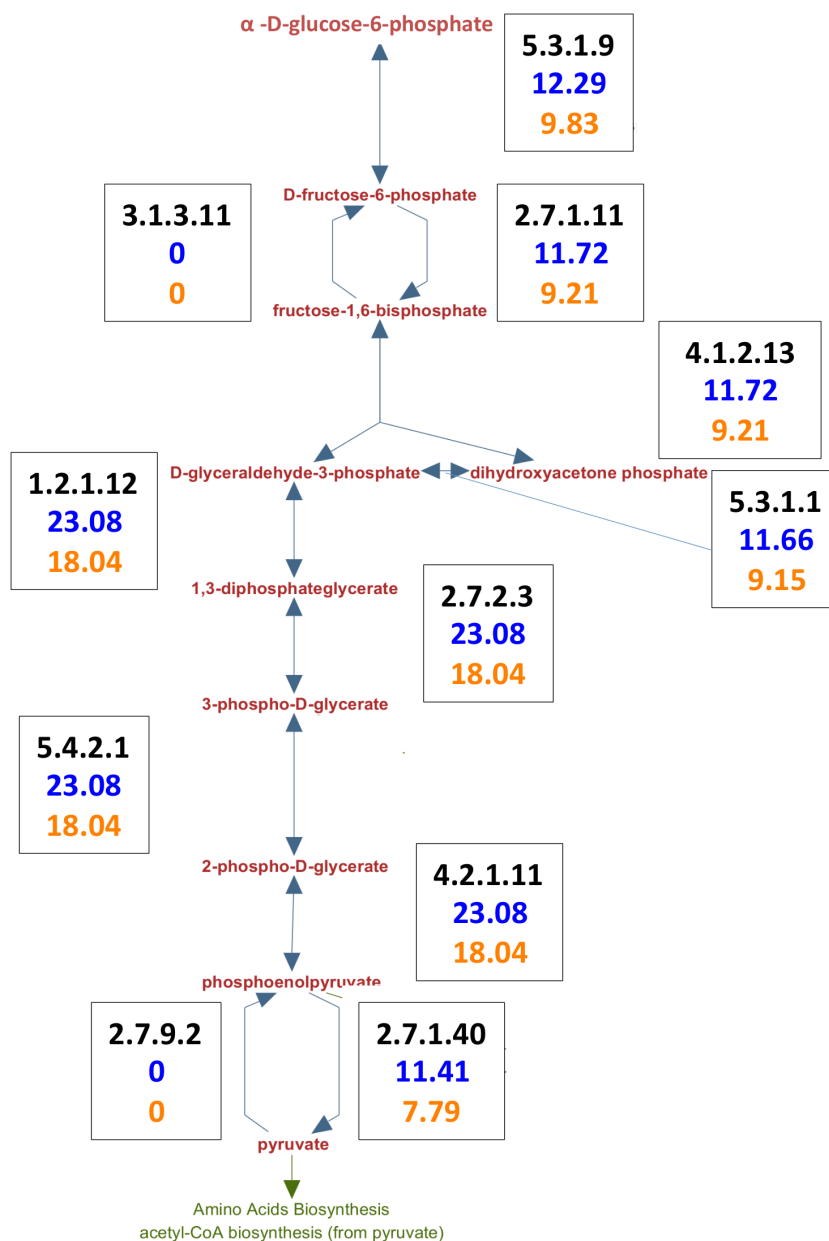


**Figure S31. Comparison of the glycolysis pathway under iron-poor/rich at Phase I.** The words in red represent the metabolites. Rectangular boxes have at the top line the E.C. number for each reaction, the blue numbers correspond to the fluxes value at iron-poor conditions, and the numbers in orange are the fluxes value at iron-rich conditions.

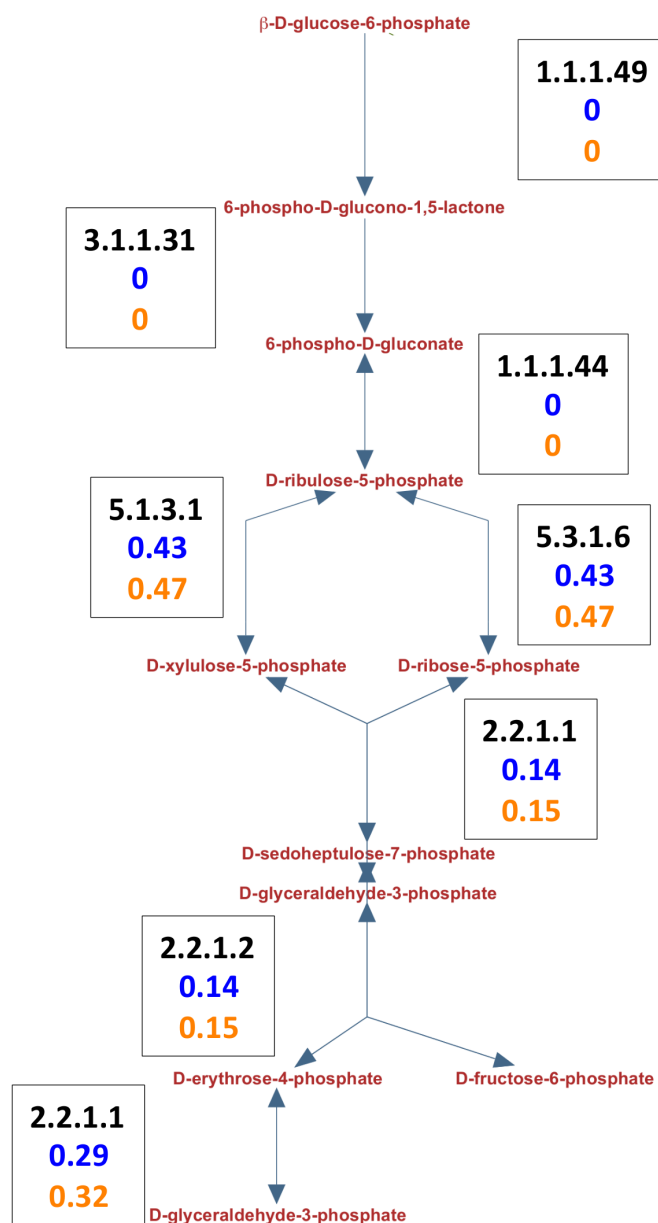


**Figure S32. Comparison of the pentose phosphate pathway under iron-poor and iron-rich conditions at Phase I.** The words in red represent metabolites. Rectangular boxes have at the top line the E.C. number for each reaction, the blue numbers correspond to the fluxes value at iron-poor conditions, and the numbers in orange are the fluxes value at iron-rich conditions.

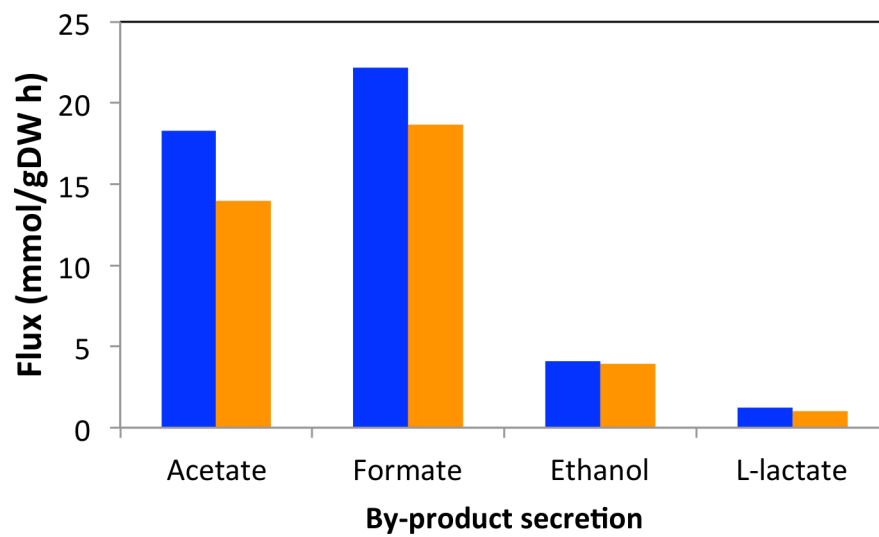


**Figure S33. Comparison of the by-product secretion in *B. anthracis* under iron-poor/rich conditions at Phase I.** The blue columns are iron-poor conditions, and orange columns are iron-rich conditions.

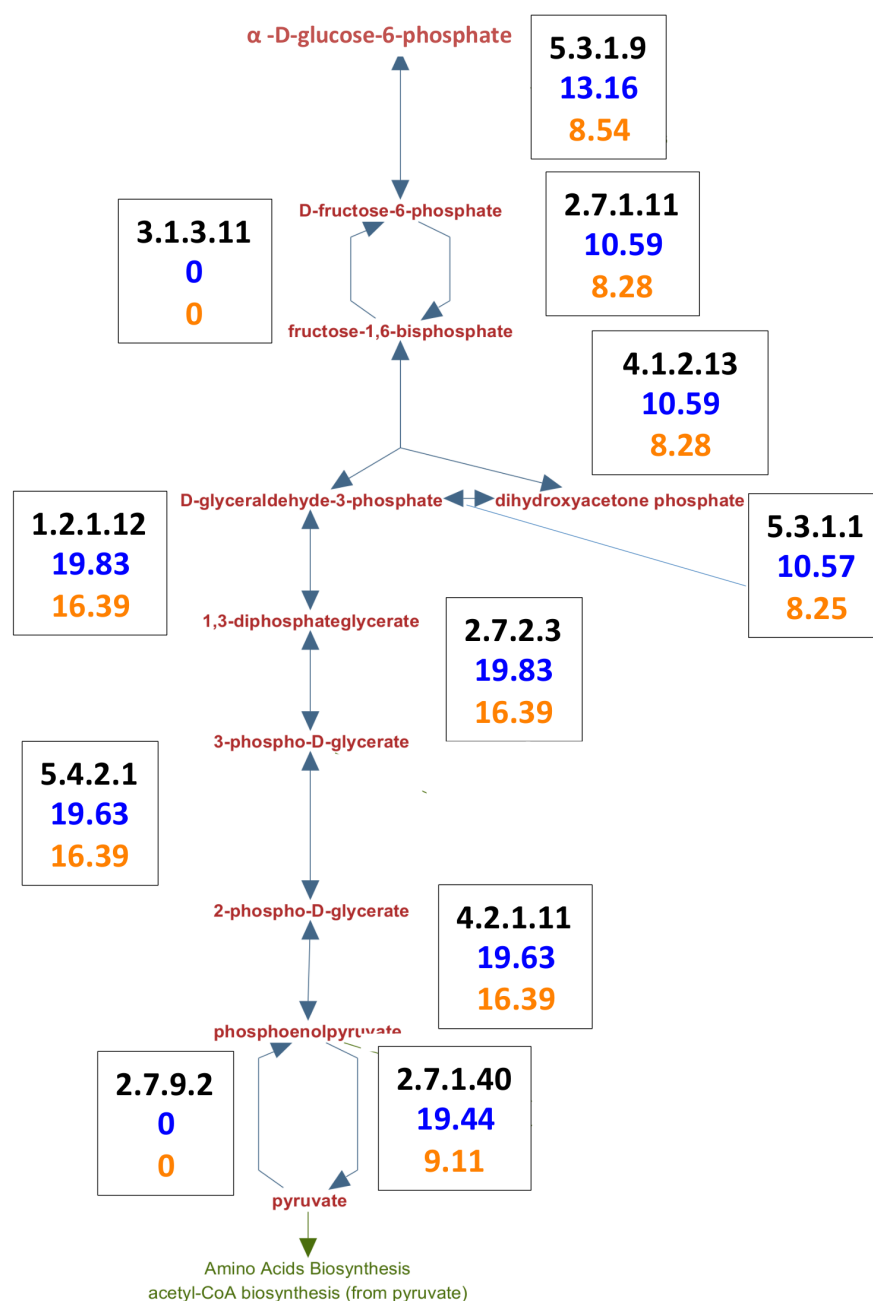


**Figure S34. Comparison of the glycolytic pathway under iron-poor/rich conditions at Phase II.** The words in red represent metabolites. Rectangular boxes have at the top line the E.C. number for each reaction, the blue numbers correspond to the fluxes value at iron-poor conditions, and the numbers in orange are the fluxes value at iron-rich conditions.



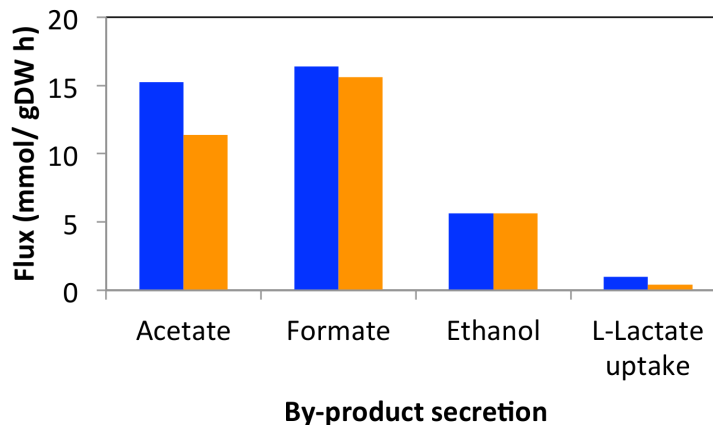


**Figure S35. Comparison of the by-product secretion and L-lactate uptake in *B. anthracis* under iron poor/rich conditions at Phase I.** The blue columns are iron-poor conditions, and orange columns are iron-rich conditions.

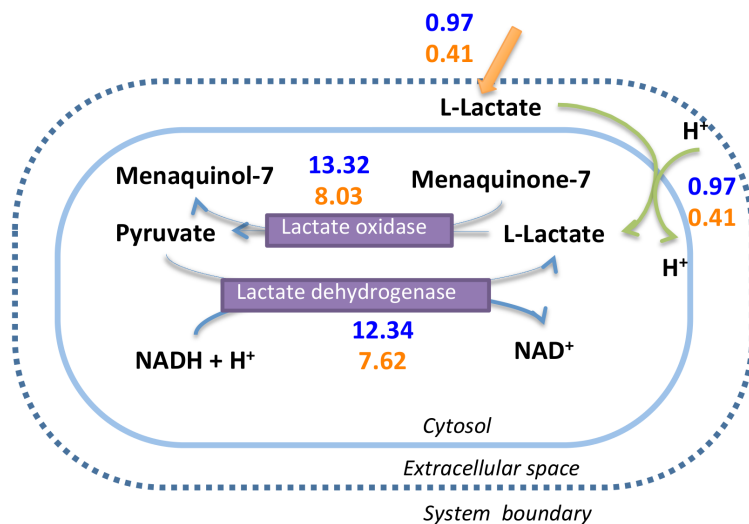


**Figure S36. Lactate metabolism at Phase II.** The metabolites are in black. The exchange flux of lactate is the yellow arrow, transport reactions are the green arrows, and intracellular reactions are the blue arrows. The purple boxes have the enzyme's name that catalyzed each reaction. The values for each flux are next to each reaction. Top value for iron-poor conditions and bottom value for iron-rich conditions.

## APPENDIX 8. GENOME-SCALE METABOLIC MODEL FOR *BACILLUS*

### *ANTHRACIS* STERNE

#### A8.1. Extracellular metabolites

**Table S14. Metabolites in the extracellular space for *B. anthracis*.** The name, id, and formula for each species are provided.

Species name	Species id
SER[e]	L-serine C3H7NO3
TRP[e]	L-tryptophan C11H12N2O2
CARBON-DIOXIDE[e]	CO2 CO2
CA-2[e]	Ca2+ Ca
RIBOSE[e]	D-ribose C5H10O5
ARSENATE[e]	arsenate HO4As
OXYGEN-MOLECULE[e]	oxygen O2
CU-2[e]	Cu2+ Cu
INOSINE[e]	inosine C10H12N4O5
L-ORNITHINE[e]	L-ornithine C5H13N2O2
GLUCONATE[e]	D-gluconate C6H11O7
ACET[e]	acetate C2H3O2
NITRATE[e]	nitrate NO3
NITRITE[e]	nitrite NO2
AMMONIUM[e]	ammonium H4N
TYR[e]	L-tyrosine C9H11NO3
GLYCEROL[e]	glycerol C3H8O3
CYTIDINE[e]	cytidine C9H13N3O5
ARG[e]	L-arginine C6H15N4O2
Nucleosides[e]	a nucleoside
CIT[e]	citrate C6H5O7
L-ASPARTATE[e]	L-aspartate C4H6NO4
GLN[e]	L-glutamine C5H10N2O3
THIAMINE[e]	thiamin C12H17N4OS
LYS[e]	L-lysine C6H15N2O2
PHE[e]	L-phenylalanine C9H11NO2
CL-[e]	chloride Cl
DEOXYADENOSINE[e]	deoxyadenosine C10H13N5O3
HIS[e]	L-histidine C6H9N3O2

Species name	Species id
CPD-4422[e]	chromate HO4Cr
FE-3[e]	Fe3+ Fe
CPD-1106[e]	2-aminoethylphosphonate C2H8NO3P
CPDCWI-18[e]	Ferric-protocatechuate
-3-4-DIHYDROXYBENZOATE[e]	protocatechuate C7H5O4
THR[e]	L-threonine C4H9NO3
L-LACTATE[e]	(S)-lactate C3H5O3
ETOH[e]	ethanol C2H6O
FORMATE[e]	formate CHO2
BETAINE[e]	glycine betaine C5H11NO2
FE-2[e]	Fe2+ Fe
PRO[e]	L-proline C5H9NO2
ALPHA-GLUCOSE[e]	alpha-D-glucose C6H12O6
-4-AMINO-BUTYRATE[e]	4-aminobutyrate C4H9NO2
CO-2[e]	Co2+ Co
SPERMIDINE[e]	spermidine C7H22N3
BENZOATE[e]	benzoate C7H5O2
CPDCWI-7[e]	ferric-petrobactin
Amino-Acids-20[e]	a standard alpha amino acid
CD-2[e]	Cd2+ Cd
WATER[e]	H2O H2O
GLT[e]	L-glutamate C5H8NO4
GUANOSINE[e]	guanosine C10H13N5O5
CPDCWI-6[e]	ferric-bacillibactin
URACIL[e]	uracil C4H4N2O2
PHOSPHONATE[e]	phosphonate HO3P
ILE[e]	L-isoleucine C6H13NO2
L-ALPHA-ALANINE[e]	L-alanine C3H7NO2
Pi[e]	phosphate HO4P
MO-2[e]	Mo2+ Mo
DEOXYCYTIDINE[e]	deoxycytidine C9H13N3O4
-2-KETOGLUTARATE[e]	2-oxoglutarate C5H4O5
PROTON[e]	H+ H
CYS[e]	L-cysteine C3H7NO2S
CPD-12541[e]	N-acetyl-alpha-D-glucosamine C8H15NO6
SUCROSE[e]	sucrose C12H22O11
CPD-763[e]	arsenite H2O3As

Species name	Species id
SUC[e]	succinate C4H4O4
XANTHINE[e]	xanthine C5H4N4O2
CPD-10353[e]	(R)-acetoin C4H8O2
GLYCEROL-3P[e]	sn-glycerol-3-phosphate C3H7O6P
XANTHOSINE[e]	xanthosine C10H12N4O6
LEU[e]	L-leucine C6H13NO2
MN-2[e]	Mn2+ Mn
ADENOSINE[e]	adenosine C10H13N5O4
K-[e]	K+ K
MG-2[e]	Mg2+ Mg
TREHALOSE[e]	trehalose C12H22O11
ASN[e]	L-asparagine C4H8N2O3
OXALATE[e]	oxalate C2O4
MET[e]	L-methionine C5H11NO2S
UREA[e]	urea CH4N2O
CPD-9984[e]	bacillibactin C39H42N6O18
SULFATE[e]	sulfate O4S
CELLOBIOSE[e]	cellobiose C12H22O11
PUTRESCINE[e]	putrescine C4H14N2
Fructose[e]	Fructose C6H12O6
VAL[e]	L-valine C5H11NO2
HOMO-SER[e]	L-homoserine C4H9NO3
NA-[e]	Na+ Na
CPD-9985[e]	petrobactin C34H51N6O11
ZN-2[e]	Zn2+ Zn

## A8.2. Intracellular metabolites

**Table S15. Metabolites in the cytosol space for *B. anthracis*.** The name, id, and formula for each species are provided.

Species name	Species id
-3-Ketopimeloyl-ACP-methyl-esters[c]	a 3-oxo-pimelyl-[acp] methyl ester
TRANS-D2-ENOYL-ACP[c]	a trans-delta2-enoyl-acyl-[acp]
Saturated-Fatty-Acyl-ACPs[c]	a 2,3,4-saturated fatty acyl-[acp]
ITP[c]	ITP C10H11N4O14P3
-4-FUMARYL-ACETOACETATE[c]	4-fumaryl-acetoacetate C8H6O6

Species name	Species id
CPD-237[c]	indole-3-acetamide C10H10N2O
OXALATE[c]	oxalate C2O4
tRNA-pseudouridine-38-40[c]	a tRNA pseudouridine38-40
PROPIONATE[c]	propionate C3H5O2
CPD-448[c]	beta-D-glucose 1-phosphate C6H11O9P
R-3-hydroxy-cis-vaccenoyl-ACPs[c]	a {R}-3-hydroxy-cis-vaccenoyl-[acp]
PROTEIN-LIPOYLLYSINE[c]	a [glycine-cleavage complex H protein] N6-{lipoyl}lysine
-3-HYDROXY-L-KYNURENINE[c]	3-hydroxy-L-kynurenine C10H12N2O4
L-1-phosphatidyl-inositols[c]	an L-1-phosphatidyl-inositol
BCCP-dimers[c]	a biotinylated [BCCP dimer]
ILE-tRNAs[c]	tRNAile
CYTOSINE[c]	cytosine C4H5N3O
NITRITE[c]	nitrite NO2
Bromide[c]	a bromide
CPD-1106[c]	2-aminoethylphosphonate C2H8NO3P
Aldehydes[c]	an aldehyde
THZ[c]	4-methyl-5-{beta-hydroxyethyl}thiazole C6H9NOS
Enoylglutaryl-ACP-methyl-esters[c]	an enoylglutaryl-[acp] methyl ester
Oxo-glutarate-dehydro-suc-DH-lipoyl[c]	a [2-oxoglutarate dehydrogenase E2 protein] N6-{S-succinyldihydrolipoyl}lysine
L-GLUTAMATE-5-P[c]	L-glutamate-5-phosphate C5H8NO7P
ThiI-L-cysteine[c]	a [ThiI sulfur-carrier protein]-L-cysteine
H2CO3[c]	carbonic acid CH2O3
Cytochromes-C-Reduced[c]	a reduced cytochrome c
Charged-TRP-tRNAs[c]	L-tryptophanyl-tRNAtrp
UMP[c]	uridine-5'-phosphate C9H11N2O9P
CPD-4211[c]	dimethylallyl diphosphate C5H9O7P2
GLYCERATE[c]	D-glycerate C3H5O4
BUTYRIC-ACID[c]	n-butanoate C4H7O2
D-HEXOSE-6-PHOSPHATE[c]	D-hexose 6-phosphate C6H11O9P
Pyruvate-dehydrogenase-acetylDHlipoyl[c]	a [pyruvate dehydrogenase E2 protein] N6-{S-acetyldihydrolipoyl}lysine
CPD0-2113[c]	1-octadecanoyl-sn-glycerol 3-phosphate C21H41O7P
IDP[c]	IDP C10H11N4O11P2
SUC-COA[c]	succinyl-CoA C25H35N7O19P3S
PAPS[c]	phosphoadenosine-5'-phosphosulfate

Species name	Species id
	C10H11N5O13P2S
L-CYSTEATE[c]	{R}-cysteate C3H6NO5S
L-LACTATE[c]	{S}-lactate C3H5O3
cis-delta5-lignoceroyl-ACPs[c]	a cis-delta5-C24 1-[acp]
PYRIDOXINE[c]	pyridoxine C8H11NO3
NA-[c]	Na+ Na
Charged-PHE-tRNAs[c]	L-phenylalanyl-tRNAphe
PHOSPHO-ENOL-PYRUVATE[c]	phosphoenolpyruvate C3H2O6P
OXALACETIC-ACID[c]	oxaloacetate C4H2O5
P-RIBOSYL-4-SUCCCARB-AMINOIMIDAZOLE[c]	5'-phosphoribosyl-4-{N-succinocarboxamide}-5-aminoimidazole C13H15N4O12P
DIHYDROXPENTANEDIONE[c]	4,5-dihydroxy-2,3-pentanedione C5H8O4
GUANOSINE[c]	guanosine C10H13N5O5
CPD-9011[c]	streptothricin F C19H37N8O8
GLYCERALD[c]	D-glyceraldehyde C3H6O3
cis-delta11-3-oxo-melissoyl-ACPs[c]	a cis-delta11-3-oxo-C30 1-[acp]
CPD-9923[c]	{1R,6R}-6-hydroxy-2-succinylcyclohexa-2,4-diene-1-carboxylate C11H10O6
CPD0-2117[c]	trans-hexadec-2-enoyl-CoA C37H60N7O17P3S
CPD-9012[c]	Nbeta-acetylstreptothricin F C21H38N8O9
R-3-hydroxybehenoyl-ACPs[c]	a {R}-3-hydroxybehenoyl-[acp]
Protein-L-methionine-R-S-oxides[c]	a protein-L-methionine-{R}-S-oxide
CPD-578[c]	urea-1-carboxylate C2H3N2O3
CPD-13043[c]	7-carboxy-7-deazaguanine C7H5N4O3
VAL[c]	L-valine C5H11NO2
-4-GUANIDO-BUTYRAMIDE[c]	4-guanidinobutyramide C5H13N4O
-3-Hydroxyglutaryl-ACP-methyl-ester[c]	a 3-hydroxyglutaryl-[acp] methyl ester
CPD-9924[c]	2-succinyl-5-enolpyruvyl-6-hydroxy-3-cyclohexene-1-carboxylate C14H13O9
CPD-7888[c]	triacontanal C30H60O
DIHYDROSIROHYDROCHLORIN[c]	precorrin-2 C42H41N4O16
cis-delta7-3-hydroxycerotoyl-ACPs[c]	a cis-delta7-3-hydroxyC26 1-[acp]
Ubiquinols[c]	a ubiquinol
CPD-9925[c]	1,4-dihydroxy-2-naphthoyl-CoA C32H38N7O19P3S
Octanoylated-domains[c]	an octanoylated protein lipoyl-domain
UDP-ACETYL-CARBOXYVINYL-	UDP-N-acetylglucosamine-enolpyruvate

Species name	Species id
GLUCOSAMINE[c]	C20H26N3O19P2
CPD-444[c]	S-methyl-5-thio-alpha-D-ribose 1-phosphate C6H11O7PS
Primary-Alcohols[c]	a primary alcohol
N-ACETYL-D-MANNOSAMINE[c]	N-acetyl-beta-D-mannosamine C8H15NO6
CPD-3708[c]	guanosine 3'-monophosphate C10H12N5O8P
GLY-tRNAs[c]	tRNAgly
Protein-3-phospho-L-histidines[c]	a protein-Npi-phospho-L-histidine
CPD-8624[c]	peptidylproline {omega = 180}
CPD-12261[c]	a peptidoglycan with D,D cross-links {meso-diaminopimelate containing} C203H318N28O87P2
ACETYL-GLU[c]	N-acetyl-L-glutamate C7H9NO5
CPD-3709[c]	guanosine 2',3'-cyclic monophosphate C10H11N5O7P
CPD-9718[c]	menaquinone-7 C46H64O2
Charged-VAL-tRNAs[c]	L-valyl-tRNAval
Acceptor[c]	an oxidized electron acceptor
CPD-8625[c]	peptidylproline {omega = 0}
PPI[c]	diphosphate HO7P2
DIHYDRONEOPTERIN-P3[c]	7,8-dihydroneopterin triphosphate C9H12N5O13P3
Butanoyl-ACPs[c]	a butyryl-[acp]
Nucleoside-Triphosphates[c]	a nucleoside triphosphate
cis-delta19-3-hydroxyC38-ACPs[c]	a cis-delta19-3-hydroxyC38 1-[acp]
-5-P-RIBOSYL-N-FORMYLGLYCINEAMIDE[c]	5'-phosphoribosyl-N-formylglycineamide C8H13N2O9P
Oxidized-flavodoxins[c]	an oxidized flavodoxin C17H19N4O9P
-2-Hexadecenoyl-ACPs[c]	a trans hexadecenoyl-[acp]
ANTHRANILATE[c]	anthranilate C7H6NO2
P-HYDROXY-PHENYLPYRUVATE[c]	4-hydroxyphenylpyruvate C9H7O4
CPD66-45[c]	dipalmitoyl-L-1-phosphatidyl-inositol C41H78O13P
D-SERINE[c]	D-serine C3H7NO3
HOMO-SER[c]	L-homoserine C4H9NO3
SER-tRNAs[c]	tRNAser
DIHYDROXY-BUTANONE-P[c]	1-deoxy-L-glycero-tetralose 4-phosphate C4H7O6P
GLUCONATE[c]	D-gluconate C6H11O7

Species name	Species id
MET-tRNAs[c]	tRNAmet
CPD-7880[c]	dodecanal C12H24O
PALMITATE[c]	palmitate C16H31O2
MALONATE-S-ALD[c]	malonate semialdehyde C3H3O3
D-GLT[c]	D-glutamate C5H8NO4
CPD-7881[c]	dotriacontanal C32H64O
Hexanoyl-ACPs[c]	a hexanoyl-[acp]
Monocarboxylic-Acid-Amides[c]	a monocarboxylic-acid-amide
PHE[c]	L-phenylalanine C9H11NO2
-10-FORMYL-THF[c]	10-formyl-tetrahydrofolate C20H21N7O7
Apo-AsbD-Proteins[c]	an apo-AsbD protein
CPD-7882[c]	eicosanal C20H40O
FAD[c]	FAD C27H31N9O15P2
CPD0-2224[c]	{S}-3-hydroxyoctanoyl-CoA C29H46N7O18P3S
ISOBUTYRYL-COA[c]	isobutyryl-CoA C25H38N7O17P3S
-3-oxo-decanoyl-ACPs[c]	a 3-oxo-decanoyl-[acp]
Protein-Histidines[c]	a [protein]-L-histidine
CPD-7883[c]	hexacosanal C26H52O
R-3-hydroxyhexanoyl-ACPs[c]	an {R}-3-hydroxyhexanoyl-[acp]
CPD-7845[c]	1-docosanol C22H46O
Beta-3-hydroxybutyryl-ACPs[c]	an {R}-3-hydroxybutanoyl-[acp]
CPD-7884[c]	octacosanal C28H56O
DTDP-DEOH-DEOXY-GLUCOSE[c]	dTDP-4-dehydro-6-deoxy-alpha-D-glucose C16H22N2O15P2
-5-DEHYDROGLUCONATE[c]	5-dehydro-D-gluconate C6H9O7
Nucleosides[c]	a nucleoside
Palmitoleoyl-ACPs[c]	a palmitoleoyl-[acp]
COPROPORPHYRINOGEN-III[c]	coproporphyrinogen III C36H40N4O8
D-ALA-D-ALA[c]	D-alanyl-D-alanine C6H12N2O3
CPD-7885[c]	tetracosanal C24H48O
AMINO-HYDROXYMETHYL-METHYL- PYR-P[c]	4-amino-2-methyl-5- phosphomethylpyrimidine C6H8N3O4P
OXYGEN-MOLECULE[c]	oxygen O2
-5-FORMYL-THF[c]	5-formyl-tetrahydrofolate C20H21N7O7
R-3-hydroxystearoyl-ACPs[c]	a {R}-3-hydroxystearoyl-[acp]
NADPH[c]	NADPH C21H26N7O17P3
CPD-7886[c]	tetradecanal C14H28O



Species name	Species id
SIROHEME[c]	siroheme C42H36N4O16Fe
FUM[c]	fumarate C4H2O4
HEME-O[c]	heme o C49H56N4O5Fe
CPD-8999[c]	5-{methylthio}-2,3-dioxopentyl phosphate C6H9O6PS
Cis-Delta5-dodecenoyl-ACPs[c]	a cis-delta5-dodecenoyl-[acp]
GLUCOSAMINE-1P[c]	D-glucosamine 1-phosphate C6H13NO8P
CPD-7887[c]	tetratriacontanal C34H68O
-2-PG[c]	2-phospho-D-glycerate C3H4O7P
SO3[c]	sulfite O3S
Protein-L-methionine[c]	a [protein]-L-methionine
LL-DIAMINOPIMELATE[c]	L,L-diaminopimelate C7H14N2O4
Monocarboxylates[c]	a monocarboxylate
AGMATHINE[c]	agmatine C5H16N4
CPD-3706[c]	3'-adenosine monophosphate C10H12N5O7P
CPD0-2330[c]	phosphatidylglycerol (dihexadec-9-enoyl, n- C16 1) C38H70O10P
PYRUVATE[c]	pyruvate C3H3O3
Decanoyl-ACPs[c]	a decanoyl-[acp]
CPD-3707[c]	adenosine 2'3'-cyclic monophosphate C10H11N5O6P
N-acetyl-D-glucosamine[c]	N-acetyl-D-glucosamine C8H15NO6
Pi[c]	phosphate HO4P
CPD-3746[c]	methanesulfonate CH3O3S
N2-SUCCINYLGUTAMATE[c]	N2-succinylglutamate C9H10NO7
CPD-9717[c]	ubiquinone-7 C44H66O4
CPD0-1699[c]	6-carboxy-5,6,7,8-tetrahydropterin C7H8N5O3
Charged-LEU-tRNAs[c]	L-leucyl-tRNA <sup>leu</sup>
FADH2[c]	FADH2 C27H33N9O15P2
CHORISMATE[c]	chorismate C10H8O6
SHIKIMATE-5P[c]	shikimate-3-phosphate C7H8O8P
L-BETA-ASPARTYL-P[c]	L-aspartyl-4-phosphate C4H6NO7P
ACETYL-COA[c]	acetyl-CoA C23H34N7O17P3S
CPD-62[c]	2,3-dihydroxybenzoyl-AMP C17H17N5O10P
SHIKIMATE[c]	shikimate C7H9O5
HOMO-CYS[c]	L-homocysteine C4H9NO2S

Species name	Species id
N2-SUCCINYLORNITHINE[c]	N2-succinyl-L-ornithine C9H15N2O5
TARTRONATE-S-ALD[c]	tartronate semialdehyde C3H3O4
ASN-tRNAs[c]	tRNAasn
DUTP[c]	dUTP C9H11N2O14P3
Donor-H2[c]	a reduced electron acceptor
CPD-7671[c]	methanethiol CH4S
IMIDAZOLE-ACETOL-P[c]	imidazole acetol-phosphate C6H7N2O5P
PYRIDOXAL-PHOSPHATE[c]	pyridoxal 5'-phosphate C8H8NO6P
CPD-20[c]	3-hydroxy-5- oxohexanoyl-CoA C27H40N7O19P3S
Secondary-Alcohols[c]	a secondary alcohol
CL-[c]	chloride Cl
FRUCTOSE-6P[c]	D-fructose-6-phosphate C6H11O9P
XANTHINE[c]	xanthine C5H4N4O2
CPD-12824[c]	cardiolipin {tetrahexadecanoyl, n-C16 0} C73H140O17P2
CPD-12117[c]	demethylmenaquinol-7 C45H64O2
LAUROYLCOA-CPD[c]	lauroyl-CoA C33H54N7O17P3S
FMN[c]	FMN C17H18N4O9P
CPD-201[c]	4-hydroxybenzoyl-CoA C28H36N7O18P3S
UDP-GALACTOSE[c]	UDP-D-galactose C15H22N2O17P2
ARG-tRNAs[c]	tRNAarg
Charged-ARG-tRNAs[c]	L-arginyl-tRNAarg
FORMYL-L-METHIONYL-PEPTIDE[c]	formyl-L-methionyl peptide
THIAMINE[c]	thiamin C12H17N4OS
TETRA-H-BIOPTERIN[c]	tetrahydrobiopterin C9H15N5O3
COBINAMIDE[c]	cobinamide C48H72N11O8Co
BETAINE[c]	glycine betaine C5H11NO2
UDP-MANNACA[c]	UDP-N-acetyl-beta-D-mannosaminouronate C17H22N3O18P2
ACETYL-P[c]	acetylphosphate C2H3O5P
CPD-12822[c]	phosphatidylglycerol {dioctadecanoyl, n- C18 0} C42H82O10P
D-SEDOHEPTULOSE-7-P[c]	D-sedoheptulose-7-phosphate C7H13O10P
CPD-6321[c]	[procollagen] trans 4-hydroxy-L-proline
UTP[c]	UTP C9H11N2O15P3
THIAMINE-P[c]	thiamin phosphate C12H16N4O4PS
CHLORAMPHENICOL-3-ACETATE[c]	chloramphenicol 3-acetate

Species name	Species id
	C13H14N2O6Cl2
MALONYL-COA[c]	malonyl-CoA C24H33N7O19P3S
R-3-hydroxyarachidoyl-ACPs[c]	a {R}-3-hydroxyarachidoyl-[acp]
CPD-10815[c]	methylphosphate CH3O4P
ADENOSYL-HOMO-CYS[c]	S-adenosyl-L-homocysteine C14H20N6O5S
-34-DHB-AsbD-Proteins[c]	a 3,4-DHB-AsbD protein
BETA-D-FRUCTOSE[c]	beta-D-fructofuranose C6H12O6
Reduced-flavodoxins[c]	a reduced flavodoxin C17H21N4O9P
PHOSPHORIBULOSYL-FORMIMINO-AICAR-P[c]	phosphoribuloseformimino-AICAR-P C15H21N5O15P2
DUDP[c]	dUDP C9H11N2O11P2
ETOH[c]	ethanol C2H6O
GLC-6-P[c]	beta-D-glucose-6-phosphate C6H11O9P
Charged-HIS-tRNAs[c]	L-histidyl-tRNAhis
CPD-12820[c]	phosphatidylglycerophosphate {dioctadecanoyl, n-C18 0} C42H81O13P2
-3-Ketoglutaryl-ACP-methyl-ester[c]	a 3-oxo-glutaryl-[acp] methyl ester
CPD-7100[c]	{2S}-2-isopropyl-3-oxosuccinate C7H8O5
CPD-4841[c]	dipicolinate C7H3NO4
Charged-GLN-tRNAs[c]	L-glutamyl-tRNAgln
MALTOSE[c]	beta-maltose C12H22O11
cis-delta7-cerotoyl-ACPs[c]	a cis-delta7-C26 1-[acp]
CPD-12821[c]	1,2-dipalmitoyl-phosphatidylglycerol-phosphate C38H73O13P2
CPD-11671[c]	5-hydroxytryptophol C10H11NO2
L-HISTIDINOL-P[c]	L-histidinol-phosphate C6H11N3O4P
SPERMIDINE[c]	spermidine C7H22N3
Protein-L-Methionine-S-Oxides[c]	a protein-L-methionine-{S}-S-oxide
DI-H-OROTATE[c]	{S}-dihydroorotate C5H5N2O4
Cyclic-2-3-Ribonucleoside-Monophosphates[c]	a nucleoside 2',3'-cyclic phosphate
Charged-ASP-tRNAs[c]	L-aspartyl-tRNAasp
-2-ACETO-2-HYDROXY-BUTYRATE[c]	2-aceto-2-hydroxy-butanoate C6H9O4
CPDN-384[c]	2-hydroxychromene-2-carboxylate C10H7O4
CPD-245[c]	3-carboxy-cis,cis-muconate C7H3O6
cis-delta15-3-oxo-gheddoyl-ACPs[c]	a cis-delta15-3-oxo-C34 1-[acp]
LYS[c]	L-lysine C6H15N2O2

Species name	Species id
CPD-246[c]	{2Z}-5-oxohex-2-enedioate C6H4O5
CPDN-385[c]	trans-O-hydroxybenzylidenepyruvate C10H7O4
CPD0-2108[c]	trans-oct-2-enoyl-CoA C29H44N7O17P3S
-2-METHYL-BUTYRYL-COA[c]	I
NADH[c]	NADH C21H27N7O14P2
cis-delta21-3-hydroxyC40-ACPs[c]	a cis-delta21-3-hydroxyC40 1-[acp]
HISTIDINAL[c]	histidinal C6H10N3O
CARBAMYUL-L-ASPARTATE[c]	N-carbamoyl-L-aspartate C5H6N2O5
UDP[c]	UDP C9H11N2O12P2
Primary-Amines[c]	a primary amine
METHYLENE-THF[c]	5,10-methylenetetrahydrofolate C20H21N7O6
DIHYDROPTERIN-CH2OH-PP[c]	6-hydroxymethyl-dihydropterin diphosphate C7H8N5O8P2
O-SUCCINYL-L-HOMOSERINE[c]	O-succinyl-L-homoserine C8H12NO6
PALMITYL-COA[c]	palmitoyl-CoA C37H62N7O17P3S
CPD-763[c]	arsenite H2O3As
CPD-1136[c]	cis-2-methylnaconitate C7H5O6
DETHIOBIOTIN[c]	dethiobiotin C10H17N2O3
CIS-ACONITATE[c]	cis-aconitate C6H3O6
L-GLUTAMATE-GAMMA-SEMIALDEHYDE[c]	L-glutamate gamma-semialdehyde C5H9NO3
SUCC-S-ALD[c]	succinate semialdehyde C4H5O3
CPD-8742[c]	{3E}-2-oxohex-3-enedioate C6H4O5
Cytochromes-C-Oxidized[c]	an oxidized cytochrome c
Pyruvate-dehydrogenase-dihydrolipoate[c]	a [pyruvate dehydrogenase E2 protein] N6- {dihydrolipoyl}lysine
HOMOGENITISATE[c]	homogentisate C8H7O4
CPD-371[c]	octanal C8H16O
-2K-4CH3-PENTANOATE[c]	4-methyl-2-oxopentanoate C6H9O3
N3-ACETYLGENTAMICIN-C[c]	N3'-acetylgentamicin C
-4-AMINO-4-DEOXYCHORISMATE[c]	4-amino-4-deoxychorismate C10H10NO5
N-ACETYL-GLUTAMYL-P[c]	N-acetylglutamyl-phosphate C7H9NO8P
CPD-12258[c]	UDP-N-acetylmuramoyl-L-alanyl-gamma- D-glutamyl-L-lysyl-D-alanine C37H57N8O25P2
Trans-D3-cis-D7-tetradecenoyl-ACPs[c]	a trans-delta3-cis-delta7-tetradecenoyl-[acp]
B-KETOACYL-ACP[c]	a 3-oxoacyl-[acp]

Species name	Species id
CANAVANINOSUCCINATE[c]	canavaninosuccinate C9H15N4O7
Protein-L-glutamine[c]	a [protein]-L-glutamine
CPD-8260[c]	1,2-dipalmitoyl-phosphatidylglycerol C38H74O10P
cis-delta17-3-hydroxyC36-ACPs[c]	a cis-delta17-3-hydroxyC36 1-[acp]
UDP-AAGM-DIAMINOHEPTANEDIOATE[c]	UDP-N-acetylmuramoyl-L-alanyl-D-glutamyl-meso-2,6-diaminopimelate C35H51N7O26P2
Stearoyl-ACPs[c]	a stearoyl-[acp]
-2-KETO-3-METHYL-VALERATE[c]	2-keto-3-methyl-valerate C6H9O3
CPD-11740[c]	carboxyphosphinopyruvate C4H2O7P
LEU[c]	L-leucine C6H13NO2
-3-DEHYDRO-SHIKIMATE[c]	3-dehydroshikimate C7H7O5
CH33ADO[c]	5'-deoxyadenosine C10H13N5O3
DAMP[c]	dAMP C10H12N5O6P
-4-CYTIDINE-5-DIPHOSPHO-2-C[c]	4-{cytidine 5'-diphospho}-2-C-methyl-D-erythritol C14H23N3O14P2
CPD-335[c]	{R}-3-hydroxybutanoate C4H7O3
BIOPTERIN[c]	dihydrobiopterin C9H13N5O3
-4-IMIDAZOLONE-5-PROPIONATE[c]	4-imidazolone-5-propionate C6H6N2O3
PHOSPHORIBOSYL-FORMIMINO-AICAR-P[c]	1-{5-phosphoribosyl}-5-[5-phosphoribosylamino]methylideneamino]imidazole-4-carboxamide C15H21N5O15P2
L-CANALINE[c]	L-canaline C4H10N2O3
DIOH-ISOVALERATE[c]	2,3-dihydroxy-3-methylbutanoate C5H9O4
LYS-tRNAs[c]	tRNAlys
CO-2[c]	Co2+ Co
NADP[c]	NADP+ C21H25N7O17P3
CPD-11020[c]	5-chloro-4-hydroxy-2-oxopentanoate C5H6O4Cl
L-methionyl-tRNAfmet[c]	L-methionyl-tRNAfmet
CPD0-2107[c]	{S}-3-hydroxydodecanoyl-CoA C33H54N7O18P3S
BIOTIN[c]	biotin C10H15N2O3S
CPD-7879[c]	docosanal C22H44O
L-ORNITHINE[c]	L-ornithine C5H13N2O2
CPD0-2106[c]	3-oxooctanoyl-CoA C29H44N7O18P3S
N-5-PHOSPHORIBOSYL-ANTHRANILATE[c]	N-{5'-phosphoribosyl}-anthranilate C12H13NO9P
-3-oxo-cis-D9-hexadecenoyl-ACPs[c]	a 3-oxo-cis-delta9-hexadecenoyl-[acp]

Species name	Species id
CPD-377[c]	2-keto-D-gluconate C6H9O7
PROTOPORPHYRINOGEN[c]	protoporphyrinogen IX C34H38N4O4
CPD-10284[c]	3-oxo-myristoyl-CoA C35H56N7O18P3S
MO-2[c]	Mo2+ Mo
CPD0-2105[c]	3-oxododecanoyl-CoA C33H52N7O18P3S
PHOSPHATIDYL-MYO-INOSITOL-45-BISPHOSPHA[c]	a 1-phosphatidyl-1D-myo-inositol 4,5-bisphosphate
CPD0-1423[c]	distearoyl phosphatidate C39H75O8P
HOP-2229-ENE[c]	hop-22{29}-ene C30H50
THYMIDINE[c]	thymidine C10H14N2O5
CPD-12295[c]	N-acetylmuramoyl-L-alanyl-D-isoglutaminyl-N-{beta-D-asparaginyl}-L-lysyl-D-alanyl-D-alanine-diphosphoundecaprenyl-N-acetylglucosamine C98H161N11O27P2
ACETALD[c]	acetaldehyde C2H4O
GENTAMICIN-C[c]	gentamicin-C
CPD-1083[c]	{E}-2-methylcrotonoyl-CoA C26H38N7O17P3S
UDP-MANNAC[c]	UDP-N-acetyl-D-mannosamine C17H25N3O17P2
N-6-AMINOHEXANOYL-6-AMINOHEXANOATE[c]	6-aminohexanoate linear dimer C12H24N2O3
CPD0-1422[c]	dipalmitoyl phosphatidate C35H67O8P
BENZOATE[c]	benzoate C7H5O2
-3-SULFINOALANINE[c]	3-sulfinioalanine C3H6NO4S
UREA[c]	urea CH4N2O
P3I[c]	PPPi O10P3
CPD-9955[c]	ubiquinol-7 C44H68O4
-3-hydroxypimeloyl-ACP-methyl-esters[c]	a 3-hydroxypimelyl-[acp] methyl ester
XYLULOSE-5-PHOSPHATE[c]	D-xylulose-5-phosphate C5H9O8P
TRP-tRNAs[c]	tRNA <sup>trp</sup>
RIBOSE[c]	D-ribose C5H10O5
HS[c]	hydrogen sulfide H2S
NIACINAMIDE[c]	nicotinamide C6H6N2O
-1-4-alpha-D-Glucan[c]	a 1,4-alpha-D-glucan
CPD-1086[c]	5-amino-6-{5-phospho-D-ribitylamino}uracil C9H15N4O9P
-4-MALEYL-ACETOACETATE[c]	4-maleyl-acetoacetate C8H6O6
ACET[c]	acetate C2H3O2

Species name	Species id
PHE-tRNAs[c]	tRNA <sup>phe</sup>
-1-PALMITOYLGLYCEROL-3-PHOSPHATE[c]	1-palmitoylglycerol 3-phosphate C19H37O7P
DIMETHYL-D-RIBITYL-LUMAZINE[c]	6,7-dimethyl-8-{1-D-ribityl} lumazine C13H17N4O6
CPD0-2253[c]	{S}-3-hydroxy-stearoyl-CoA C39H66N7O18P3S
Unsulfurated-Sulfur-Acceptors[c]	an unsulfurated sulfur acceptor
HYDROXYMETHYLBILANE[c]	hydroxymethylbilane C40H38N4O17
ANILINE[c]	aniline C6H7N
N-SUCCINYLL-2-6-DIAMINOPIMELATE[c]	N-succinyl-L,L-2,6-diaminopimelate C11H16N2O7
CPD-7871[c]	1-hexacosanol C26H54O
GLN-tRNAs[c]	tRNA <sup>gln</sup>
B-ALANINE[c]	beta-alanine C3H7NO2
DIHYDRO-NEO-PTERIN[c]	7,8-dihydro-D-neopterin C9H13N5O4
-2-METHYLTHIO-N-6-ISOPENTYL-ADENOSINE-37-[c]	2-methylthio-N-6-isopentyl adenosine-37 tRNA
Tetradec-2-enoyl-ACPs[c]	a trans tetradec-2-enoyl-[acp]
ARSENATE[c]	arsenate HO4As
Glycerophosphodiester[c]	a glycerophosphodiester
CPD-7872[c]	1-octacosanol C28H58O
L-CYSTATHIONINE[c]	L-cystathionine C7H14N2O4S
S-ADENOSYLMETHIONINE[c]	S-adenosyl-L-methionine C15H23N6O5S
AMP[c]	AMP C10H12N5O7P
CPD-5881[c]	4alpha-hydroxy-tetrahydrobiopterin C9H15N5O4
D-PROLINE[c]	D-proline C5H9NO2
HEXANOYL-COA[c]	hexanoyl-CoA C27H42N7O17P3S
CD-2[c]	Cd2+ Cd
K-[c]	K+ K
-7-AMINOMETHYL-7-DEAZAGUANINE[c]	preQ1 C7H10N5O
ASP-tRNAs[c]	tRNA <sup>asp</sup>
CPD-7874[c]	1-tetracosanol C24H50O
-3-oxo-stearoyl-ACPs[c]	a 3-oxo-stearoyl-[acp]
-7-CYANO-7-DEAZAGUANINE[c]	preQ0 C7H5N5O
CPD-582[c]	guanylyl molybdenum cofactor C20H22N10O15P2S2Mo
ADENINE[c]	adenine C5H5N5

Species name	Species id
DIHYDROXYACETONE[c]	dihydroxyacetone C3H6O3
CPD-8123[c]	molybdenum cofactor C10H10N5O8PS2Mo
CPD-7875[c]	1-tetradecanol C14H30O
ADP-D-GLUCOSE[c]	ADP-alpha-D-glucose C16H23N5O15P2
CPD-10353[c]	{R}-acetoin C4H8O2
CPD-7876[c]	1-tetratriacontanol C34H70O
SEC-tRNAs[c]	tRNA <sup>sec</sup>
Protein-phospho-L-histidines[c]	a protein N-phospho-L-histidine
CPD-507[c]	6-phospho-beta-D-glucosyl-{1,4}-D-glucose C12H21O14P
Trans-D3-cis-D9-hexadecenoyl-ACPs[c]	a trans-delta3-cis-delta9-hexadecenoyl-[acp]
DTDP-DEOH-DEOXY-MANNOSE[c]	dTDP-4-dehydro-6-deoxy-beta-L-mannose C16H22N2O15P2
DEOXYXYLULOSE-5P[c]	1-deoxy-D-xylulose 5-phosphate C5H9O7P
TYLOSIN[c]	tylosin C47H79NO16
Charged-ILE-tRNAs[c]	L-isoleucyl-tRNA <sup>ile</sup>
COPROPORPHYRINOGEN-I[c]	coproporphyrinogen I C36H40N4O8
CPD-7877[c]	1-triacontanol C30H62O
SUCROSE[c]	sucrose C12H22O11
N1-ACETYLSPERMINE[c]	N1-acetylspermine C12H31N4O
CHLORAMPHENICOL[c]	chloramphenicol C11H12N2O5Cl2
GLYCOCHOLIC-ACID[c]	glycocholate C26H42NO6
PROPANOL[c]	n-propanol C3H8O
-3-SULFINYL-PYRUVATE[c]	3-sulfinyl-pyruvate C3H2O5S
CYS-tRNAs[c]	tRNA <sup>cys</sup>
-3-oxo-petroselinoyl-ACPs[c]	a 3-oxo-petroselinoyl-[acp]
SUCROSE-6P[c]	sucrose-6-phosphate C12H21O14P
GLUTATHIONE[c]	glutathione C10H16N3O6S
CPD-8989[c]	L-methionine-{S}-S-oxide C5H11NO3S
Oxo-glutarate-dehydrogenase-lipoyl[c]	a [2-oxoglutarate dehydrogenase E2 protein] N6-{lipoyl} lysine
TRP[c]	L-tryptophan C11H12N2O2
UDP-GLUCURONATE[c]	UDP-D-glucuronate C15H19N2O18P2
THIAMINE-PYROPHOSPHATE[c]	thiamin diphosphate C12H16N4O7P2S
CPD-19[c]	3-hydroxy-5-oxohexanoate C6H9O4
trans-D2-cis-D17-C36-ACPs[c]	a trans-delta2-cis-delta17-C36 2-[acp]
BUTANOL[c]	n-butanol C4H10O
ETHANAMINE[c]	ethylamine C2H8N



Species name	Species id
XANTHOSINE[c]	xanthosine C10H12N4O6
Pyruvate-dehydrogenase-lipoate[c]	a [pyruvate dehydrogenase E2 protein] N6-{lipoyl}lysine
DEOXY-RIBOSE-1P[c]	deoxyribose-1-phosphate C5H9O7P
SIROHYDROCHLORIN[c]	sirohydrochlorin C42H38N4O16
CPD-11997[c]	N-acetylmuramoyl-pentapeptide-diphospho-decaprenol C82H131N7O23P2
-3-5-ADP[c]	adenosine 3',5'-bisphosphate C10H11N5O10P2
CPD-884[c]	6-aminohexanoate C6H13NO2
HYDROXY-METHYL-BUTENYL-DIP[c]	1-hydroxy-2-methyl-2-{E}-butenyl 4-diphosphate C5H9O8P2
CPD-11994[c]	omega, mono-trans, poly-cis-decaprenyl phosphate C50H81O4P
DELTA1-PIPERIDEINE-2-6-DICARBOXYLATE[c]	{S}-2,3,4,5-tetrahydrodipicolinate C7H7NO4
DEOXY-RIBOSE-5P[c]	2-deoxy-D-ribose-5-phosphate C5H9O7P
CPD-195[c]	octanoate C8H15O2
-2-PHOSPHO-4-CYTIDINE-5-DIPHOSPHO-2-C-MET[c]	2-phospho-4-{cytidine 5'-diphospho}-2-C-methyl-D-erythritol C14H22N3O17P3
CPD-196[c]	octanoyl-CoA C29H46N7O17P3S
-7-8-DIHYDROPTEROATE[c]	7,8-dihydropteroate C14H13N6O3
O-SUCCINYLBENZOATE[c]	o-succinylbenzoate C11H8O5
DEOXYCYTIDINE[c]	deoxycytidine C9H13N3O4
S-3-HYDROXYBUTANOYL-COA[c]	{S}-3-hydroxybutanoyl-CoA C25H38N7O18P3S
UDP-N-ACETYLMURAMATE[c]	UDP-N-acetylmuramate C20H28N3O19P2
trans-delta2-behenoyl-ACPs[c]	a trans-docos-2-enoyl-[acp]
BCAA-dehydrogenase-2MP-DH-lipoyl[c]	an [apo BCAA dehydrogenase E2 protein] N6-{S-[2-methylpropanoyl]dihydrolipoyl}lysine
CPD-602[c]	5-amino-6-{5-phospho-D-ribosylamino}uracil C9H13N4O9P
CPD-12818[c]	phosphatidylethanolamine {dioctadecanoyl, n-C18 0} C41H82NO8P
trans-D2-cis-D15-gheddoyl-ACPs[c]	a trans-delta2-cis-delta15-C34 2-[acp]
D-GLUCOSAMINE-6-P[c]	D-glucosamine-6-phosphate C6H13NO8P
-4-DIMETHYLAMINOPHENYLAZOBENZENE[c]	4-dimethylaminophenylazobenzene C14H15N3
BCAA-dehydrogenase-3MB-DH-lipoyl[c]	a [lipoamide acyltransferase] N6-{S-[3-methylbutanoyl]dihydrolipoyl}lysine

Species name	Species id
CPD-12819[c]	1,2-dipalmitoyl-phosphatidyl-ethanolamine C37H74NO8P
Kanamycins[c]	a kanamycin
GLYCEROPHOSPHOGLYCEROL[c]	glycerophosphoglycerol C6H14O8P
-2-METHYL-3-HYDROXY-BUTYRYL-COA[c]	2-methyl-3-hydroxybutyryl-CoA C26H40N7O18P3S
-3-hydroxy-cis-D9-hexaecenoyl-ACPs[c]	a 3-hydroxy cis delta9-hexadecenoyl-[acp]
CPD-12816[c]	phosphatidylserine {dioctadecanoyl, n-C18 0} C42H81NO10P
METHACRYLYL-COA[c]	methylacrylyl-CoA C25H36N7O17P3S
BCAA-dehydrogenase-2MB-DH-lipoyl[c]	[lipoamide acyltransferase] N6-{S-[2- methylbutanoyl]dihydrolipoyl} lysine
DGMP[c]	dGMP C10H12N5O7P
-3- HYDROHYDROXYPHOSPHORYLPYRU VATE[c]	phosphinopyruvate C3H3O5P
PANTETHEINE-P[c]	4'-phosphopantetheine C11H21N2O7PS
CPD-12817[c]	1,2-dipalmitoyl-phosphatidylserine C38H73NO10P
DIHYDROFOLATE[c]	7,8-dihydrofolate monoglutamate C19H19N7O6
RIBOFLAVIN[c]	riboflavin C17H19N4O6
-3-oxo-behenoyl-ACPs[c]	a 3-oxo-behenoyl-[acp]
-4-PHOSPHONOOXY-THREONINE[c]	4-phospho-hydroxy-L-threonine C4H8NO7P
-2-KETOGLUTARATE[c]	2-oxoglutarate C5H4O5
CPD-12814[c]	CDP-1,2-dioctadecanoylglycerol C48H87N3O15P2
CPD-12815[c]	CDP-1,2-dipalmitoylglycerol C44H79N3O15P2
Glycogens[c]	a glycogen C24H42O21
CARBAMOYL-P[c]	carbamoyl-phosphate CH2NO5P
L-glutamyl-tRNAGln[c]	L-glutamyl-tRNAGln
PORPHOBILINOGEN[c]	porphobilinogen C10H13N2O4
D-6-P-GLUCONO-DELTA-LACTONE[c]	6-phospho-D-glucono-1,5-lactone C6H9O9P
D-Hexoses[c]	a D-hexose C6H12O6
-3-ENOLPYRUVYL-SHIKIMATE-5P[c]	5-enolpyruvyl-shikimate-3-phosphate C10H9O10P
CADAVERINE[c]	cadaverine C5H16N2
Hex-2-enoyl-ACPs[c]	a trans hex-2-enoyl-[acp]
Pimeloyl-ACPs[c]	a pimelyl-[acp]

Species name	Species id
CO-A[c]	coenzyme A C21H32N7O16P3S
CPD-10490[c]	N-ethylglycine C4H9NO2
cis-delta19-C38-ACPs[c]	a cis-delta19-C38 1-[acp]
-2-3-DIHYDROXYBENZOATE[c]	2,3-dihydroxybenzoate C7H5O4
CPD-13357[c]	{R}-2,3-dihydroxy-3-methylbutanoate C5H9O4
trans-D2-cis-D7-cerotoyl-ACPs[c]	a trans-delta2-cis-delta7-C26 2-[acp]
CPD-1121[c]	D-myo-inositol 1,2-cyclic phosphate C6H10O8P
Red-Glutaredoxins[c]	a reduced glutaredoxin
Ox-Glutaredoxins[c]	an oxidized glutaredoxin
Charged-MET-tRNAs[c]	L-methionyl-tRNA <sup>met</sup>
PYRROLINE-HYDROXY-CARBOXYLATE[c]	pyrroline-hydroxy-carboxylate C5H6NO3
Charged-SER-tRNAs[c]	L-seryl-tRNA <sup>ser</sup>
tRNA-with-7-aminomethyl-7-deazaguanine[c]	7-aminomethyl-7-deazaguanine at position 34 of a tRNA containing GUN anticodon
ACETYL SERINE[c]	O-acetyl-L-serine C5H9NO4
CPD-9038[c]	precorrin-1 C41H38N4O16
cis-delta11-3-hydroxymelissoyl-ACPs[c]	a cis-delta11-3-hydroxyC30 1-[acp]
AMINOMETHYLDIHYDROLIPOYL-GCVH[c]	a [glycine-cleavage complex H protein] N6-{aminomethyldihydrolipoyl} lysine
OH-ACYL-ACP[c]	a {3R}-3-hydroxyacyl-[acp]
PHOSPHORIBOSYL-CARBOXY-AMINOIMIDAZOLE[c]	5-amino-1-{5-phospho-D-ribose}imidazole-4-carboxylate C9H11N3O9P
UROCANATE[c]	urocanate C6H5N2O2
ERYTHROSE-4P[c]	D-erythrose-4-phosphate C4H7O7P
GAP[c]	D-glyceraldehyde-3-phosphate C3H5O6P
DIHYDROXYNAPHTHOATE[c]	1,4-dihydroxy-2-naphthoate C11H7O4
DIAMINONONANOATE[c]	7,8-diaminopelargonate C9H21N2O2
-3-P-HYDROXYPYRUVATE[c]	3-phospho-hydroxypyruvate C3H2O7P
-3-KETOBUTYRATE[c]	acetoacetate C4H5O3
THZ-P[c]	4-methyl-5-{2-phosphonooxyethyl}thiazole C6H8NO4PS
FUCULOSE-1P[c]	L-fucose-1-phosphate C6H11O8P
XANTHOSINE-5-PHOSPHATE[c]	XMP C10H11N4O9P
N-ACETYL-AAA-SEMIALDEHYDE[c]	N2-acetyl-alpha-aminoadipate semialdehyde C8H12NO4
ThiI-S-sulfanyleysteine[c]	a [ThiI sulfur-carrier protein]-S-

Species name	Species id
	sulfanyleysteine
SUC[c]	succinate C4H4O4
Sulfurated-Sulfur-Acceptors[c]	S-sulfanyl-[acceptor]
VAL-tRNAs[c]	tRNAval
HIS[c]	L-histidine C6H9N3O2
CPD-469[c]	N-acetyl-L-glutamate 5-semialdehyde C7H10NO4
Charged-ALA-tRNAs[c]	L-alanyl-tRNAala
PROTON[c]	H+ H
Trans-D2-decenoyl-ACPs[c]	a trans-delta2-decenoyl-[acp]
DATP[c]	dATP C10H12N5O12P3
FMNH2[c]	FMNH2 C17H21N4O9P
cis-delta9-montanoyl-ACPs[c]	a cis-delta9-C28 1-[acp]
Kanamycin-3-phosphates[c]	a kanamycin-3-phosphate
CPD-302[c]	D-aspartate C4H6NO4
Alcohols[c]	an alcohol
N-ACETYL-D-GLUCOSAMINE-6-P[c]	N-acetyl-D-glucosamine-6-phosphate C8H14NO9P
GMP[c]	GMP C10H12N5O8P
AMINO-OH-HYDROXYMETHYL- DIHYDROPTERIDINE[c]	6-hydroxymethyl-7,8-dihydropterin C7H9N5O2
INOSINE[c]	inosine C10H12N4O5
TETRADECANOYL-COA[c]	myristoyl-CoA C35H58N7O17P3S
SUPER-OXIDE[c]	superoxide O2
CPD-380[c]	3-sulfofpyruvate C3H2O6S
-3-Oxo-octanoyl-ACPs[c]	a 3-oxo-octanoyl-[acp]
STEAROYL-COA[c]	stearoyl-CoA C39H66N7O17P3S
cis-delta19-3-oxo-C38-ACPs[c]	a cis-delta19-3-oxo-C38 1-[acp]
MAL[c]	{S}-malate C4H4O5
Delta4-hexadecenoyl-ACPs[c]	a delta4-hexadecenoyl-[acp]
PYRIDOXAL[c]	pyridoxal C8H9NO3
-3-HYDROXY-ANTHRANILATE[c]	3-hydroxyanthranilate C7H6NO3
Monoamines[c]	a monoamine
Dodec-2-enoyl-ACPs[c]	a trans dodec-2-enoyl-[acp]
Oxidized-ferredoxins[c]	an oxidized ferredoxin
-25-DIDEHYDRO-D-GLUCONATE[c]	2,5-didehydro-D-gluconate C6H7O7
CPD-5923[c]	5'-deoxy-5'-fluoroadenosine C10H12N5O3F
CPD-7868[c]	1-dotriacontanol C32H66O

Species name	Species id
GUANOSINE-5DP-3DP[c]	ppGpp C10H12N5O17P4
CPD0-2171[c]	{S}-3-hydroxytetradecanoyl-CoA C35H58N7O18P3S
ATP[c]	ATP C10H12N5O13P3
cis-vaccen-2-enoyl-ACPs[c]	a cis-vaccen-2-enoyl-[acp]
INDOLE-ACETATE-AUXIN[c]	indole-3-acetate C10H8NO2
PRO-tRNAs[c]	tRNA <sub>pro</sub>
MANNOSE-1P[c]	alpha-D-mannose 1-phosphate C6H11O9P
CPD-7869[c]	1-eicosanol C20H42O
GLYCOLALDEHYDE[c]	glycolaldehyde C2H4O2
Phospholipid-Cyclopropane-Fatty-Acids[c]	a phospholipid cyclopropane fatty acid
DADP[c]	dADP C10H12N5O9P2
-3OH-4P-OH-ALPHA-KETOBUTYRATE[c]	2-oxo-3-hydroxy-4-phosphobutanoate C4H4O8P
ACETYL-ETCETERA-GLUCOSAMINYLDIPHOSPHOUND[c]	prenyl-P-P-GlcNAc-ManNAc C71H116N2O17P2
CPD-12287[c]	hydrogen bromide Br
STEARIC-ACID[c]	stearate C18H35O2
PROTOPORPHYRIN-IX[c]	protoporphyrin IX C34H32N4O4
Dipeptides-With-Proline-Carboxy[c]	a dipeptide with proline at carboxy terminal
CPDCWI-18[c]	Ferric-protocatechuate
FRUCTOSE-16-DIPHOSPHATE[c]	fructose-1,6-bisphosphate C6H10O12P2
APS[c]	adenosine 5'-phosphosulfate C10H12N5O10PS
L-PHOSPHATIDATE[c]	a 1,2-diacyl-sn-glycerol-3-phosphate
NITRATE[c]	nitrate NO3
NAD[c]	NAD <sup>+</sup> C21H26N7O14P2
Carboxybiotin-BCCP[c]	a carboxylated-biotinylated [BCCP dimer]
CPD-11444[c]	uroporphyrinogen-I C40H44N4O16
GLYCOLLATE[c]	glycolate C2H3O3
-3b-hydroxy-D5-steroids[c]	a 3beta-hydroxy-delta5-steroid
CPD-9421[c]	2-methyl-trans-aconitate C7H5O6
DTDP-RHAMNOSE[c]	dTDP-alpha-L-rhamnose C16H24N2O15P2
MYO-INOSITOL[c]	myo-inositol C6H12O6
DEOXYURIDINE[c]	deoxyuridine C9H12N2O5
-5-PHOSPHORIBOSYL-N-FORMYLGLYCINEAMIDINE[c]	5-phosphoribosyl-N-formylglycineamidine C8H15N3O8P
Charged-THR-tRNAs[c]	L-threonyl-tRNA <sub>thr</sub>

Species name	Species id
DIACYLGLYCEROL[c]	a 1,2-diacylglycerol
LACTALD[c]	L-lactaldehyde C3H6O2
Pimeloyl-ACP-methyl-esters[c]	a pimelyl-[acp] methyl ester
trans-D2-cis-D19-C38-ACPs[c]	a trans-delta2-cis-delta19-C38 2-[acp]
-3-P-SERINE[c]	3-phospho-L-serine C3H6NO6P
-1-2-DIPALMITOYLPHOSPHATIDYLCHOLINE[c]	1,2-dipalmitoyl-phosphatidylcholine C40H80NO8P
NIACINE[c]	nicotinate C6H4NO2
CPD-7046[c]	S2- S
L-PANTOATE[c]	{R}-pantoate C6H11O4
OXIDIZED-GLUTATHIONE[c]	glutathione disulfide C20H30N6O12S2
GLYCEROL-3P[c]	sn-glycerol-3-phosphate C3H7O6P
cis-delta21-3-oxo-C40-ACPs[c]	a cis-delta21-3-oxo-C40 1-[acp]
CPD-9984[c]	bacillibactin C39H42N6O18
Charged-TYR-tRNAs[c]	L-tyrosyl-tRNA <sup>tyr</sup>
CPD-466[c]	{S}-3-amino-2-methylpropanoate C4H9NO2
MET[c]	L-methionine C5H11NO2S
CPDCWI-13[c]	stearoylcardiolipin C81H158O17P2
ADP[c]	ADP C10H12N5O10P2
CPD-9985[c]	petrobactin C34H51N6O11
-5-METHYLTHIOADENOSINE[c]	S-methyl-5'-thioadenosine C11H15N5O3S
CANAVANINE[c]	L-canavanine C5H13N4O3
GERANYL-PP[c]	geranyl diphosphate C10H17O7P2
C1[c]	UDP-N-acetylmuramoyl-L-alanyl-D-glutamyl-meso-2,6-diaminopimelyl-D-alanyl-D-alanine C41H61N9O28P2
D-MYO-INOSITOL-1-MONOPHOSPHATE[c]	1D-myo-inositol -monophosphate C6H11O9P
CPD-12673[c]	5-chloro-5-deoxy-D-ribonate C5H8O5Cl
INDOLE-3-GLYCEROL-P[c]	{1S,2R}-1-C-{indol-3-yl} glycerol 3-phosphate C11H12NO6P
CPD-1301[c]	tetrahydropteroyl tri-L-glutamate C29H37N9O12
cis-delta17-3-oxo-C36-ACPs[c]	a cis-delta17-3-oxo-C36 1-[acp]
trans-D2-cis-D9-montanoyl-ACPs[c]	a trans-delta2-cis-delta9-C28 2-[acp]
CPD-11480[c]	N8,N'8-citryl-bis{spermidine} C20H45N6O5
CPD0-881[c]	N-acetyl-beta-muramate 6-phosphate

Species name	Species id
	C11H17NO11P
-2-3-DIHYDRODIPICOLINATE[c]	{S}-2,3-dihydrodipicolinate C7H5NO4
PHOSPHORYL-CHOLINE[c]	phosphoryl-choline C5H13NO4P
CPD-12708[c]	fluoroacetaldehyde C2H3OF
CPD-1302[c]	5-methyltetrahydropteroyltri-L-glutamate C30H39N9O12
-8-AMINO-7-OXONONANOATE[c]	7-keto-8-aminopelargonate C9H17NO3
C3[c]	UDP-N-acetylmuramoyl-L-alanyl-gamma-D-glutamyl-L-lysyl-D-alanyl-D-alanine C40H62N9O26P2
T2-DECENOYL-COA[c]	trans-delta2-decenoyl-CoA C31H48N7O17P3S
CPD-551[c]	phosphonoacetaldehyde C2H4O4P
PYRIDOXINE-5P[c]	pyridoxine-5'-phosphate C8H10NO6P
-5-HYDROXYINDOLE-ACETALDEHYDE[c]	5-hydroxyindole acetaldehyde C10H9NO2
R-4-PHOSPHOPANTOTHENOYL-L-CYSTEINE[c]	R-4'-phosphopantothenoil-L-cysteine C12H20N2O9PS
CPD-11481[c]	N1-{3,4-dihydroxybenzoyl}-N8,N'8-citryl-bis{spermidine} C27H48N6O8
CPD0-882[c]	1,6-anhydro-N-acetyl-beta-muramate C11H16NO7
GLYCEROL[c]	glycerol C3H8O3
CPD-12709[c]	fluoroacetate C2H2O2F
-3-DEOXY-D-ARABINO-HEPTULOSONATE-7-P[c]	3-deoxy-D-arabino-heptulosonate-7-phosphate C7H10O10P
C4[c]	N-acetylmuramoyl-L-alanyl-gamma-D-glutamyl-L-lysyl-D-alanyl-D-alanine-diphosphoundecaprenol C86H140N7O21P2
-2-HYDROXY-3-KETO-5-METHYLTHIO-1-PHOSPHOP[c]	2-hydroxy-5-{methylthio}-3-oxopent-1-enyl phosphate C6H8O6PS
-3-oxo-D5-steroids[c]	a 3-oxo-delta5-steroid
LIPOYL-AMP[c]	lipoyl-adenylate C18H25N5O8PS2
Charged-LYS-tRNAs[c]	L-lysyl-tRNAlys
PRO[c]	L-proline C5H9NO2
CPD-12706[c]	5-fluoro-5-deoxy-D-ribose-1-phosphate C5H8O7FP
PROCOLLAGEN-L-PROLINE[c]	[procollagen]-L-proline
C5[c]	N-acetylmuramoyl-L-alanyl-D-glutamyl-meso-2,6-diaminopimelyl-D-alanyl-D-alanine-diphosphoundecaprenol

Species name	Species id
	C87H139N7O23P2
CPDCWI-16[c]	storageiron
CPD0-1456[c]	UDP-N-acetylmuramyl-L-Ala C23H33N4O20P2
Peptidoglycan-With-Cleaved-Nac[c]	a peptidoglycan with cleaved N-acetyl- glucosamine
CPD-592[c]	4-guanidinobutyrate C5H11N3O2
C6[c]	N-acetylmuramoyl-L-alanyl-D-glutamyl- meso-2,6-diaminopimelyl-D-alanyl-D- alanine-diphosphoundecaprenyl-N- acetylglucosamine C95H152N8O28P2
INDOLE-ACETALDEHYDE[c]	indole acetaldehyde C10H9NO
N-6-ISOPENTYL-ADENOSINE-37- TRNA[c]	N-6-isopentyl adenosine-37 tRNA
DEOXYGUANOSINE[c]	deoxyguanosine C10H13N5O4
Glutaryl-ACP-methyl-esters[c]	a glutaryl-[acp] methyl ester
CPD-618[c]	{2R,3S}-2-methylisocitrate C7H7O7
CPD0-1082[c]	L-Ala-gamma-D-Glu-DAP-D-Ala C18H30N5O9
METHIONYL-PEPTIDE[c]	methionyl peptide
BIOMASS-CCO-CYTOSOL[c]	biomass
CPD1G-567[c]	arachidoyl-CoA C41H70N7O17P3S
CPDCWI-14[c]	1,2-distearoyl-sn-glycerol C39H76O5
-4-P-PANTOTHENATE[c]	D-4'-phosphopantothenate C9H15NO8P
-3-OXOADIPATE-ENOL-LACTONE[c]	3-oxoadipate enol lactone C6H5O4
-23-DIPHOSPHOGLYCERATE[c]	2,3-diphosphoglycerate C3H3O10P2
SER[c]	L-serine C3H7NO3
ALA-tRNAs[c]	tRNAala
CPD-1771[c]	N-acetyl-L,L-2,6-diaminopimelate C9H15N2O5
ACETYL-D- GLUCOSAMINYLDIPHOSPHO- UNDECAPRE[c]	N-acetyl-alpha-D-glucosaminyl-diphospho- ditrans,octacis-undecaprenol C63H103NO12P2
CPD0-1081[c]	N-acetyl-beta-D-glucosamine {anhydrous}- N-acetylmuramate C19H30N2O12
L-ASPARTATE-SEMIALDEHYDE[c]	L-aspartate-semialdehyde C4H7NO3
Beta-hydroxydecanoyl-ACPs[c]	an {R}-3-hydroxydecanoyl-[acp]
cis-delta9-3-oxo-montanoyl-ACPs[c]	a cis-delta9-3-oxo-C28 1-[acp]
CPD-7867[c]	1-dodecanol C12H26O
CPD-10774[c]	(2R,4S)-2-methyl-2,3,3,4- tetrahydroxytetrahydrofuran C5H10O5



Species name	Species id
PHOSPHONATE[c]	phosphonate HO3P
L-KYNURENINE[c]	kynurenine C10H12N2O3
CPD0-2244[c]	{S}-3-hydroxydecanoyl-CoA C31H50N7O18P3S
CPD0-1080[c]	GlcNAc-1,6-anhMurNAc-L-Ala-gamma-D- Glu-DAP-D-Ala C37H58N7O20
CPD-3724[c]	uridine 3'-monophosphate C9H11N2O9P
S-ADENOSYLMETHIONINAMINE[c]	S-adenosyl-L-methioninamine C14H24N6O3S
AMINO-RIBOSYLAMINO-1H-3H-PYR- DIONE[c]	5-amino-6-{D-ribitylamino}uracil C9H16N4O6
CPD-3725[c]	uridine 2'3'-cyclic monophosphate C9H10N2O8P
URACIL[c]	uracil C4H4N2O2
BCAA-dehydrogenase-lipoyl[c]	an [apo BCAA dehydrogenase E2 protein] N6-{lipoyl} lysine
b-Keto-cis-D5-dodecenoyl-ACPs[c]	a 3-oxo-cis-delta5-dodecenoyl-[acp]
-4-AMINO-BUTYRATE[c]	4-aminobutyrate C4H9NO2
DIHYDROLIPOYL-GCVH[c]	a [glycine-cleavage complex H protein] N6- {dihydrolipoyl} lysine
ALPHA-GLC-6-P[c]	alpha-D-glucose 6-phosphate C6H11O9P
tRNA-uridine-38-40[c]	a tRNA uridine38-40
THREO-DS-ISO-CITRATE[c]	D-threo-isocitrate C6H5O7
CPD-7222[c]	2-trans-dodecenoyl-CoA C33H52N7O17P3S
CPD-10773[c]	{2R,4S}-2-methyl-2,4- dihydroxydihydrofuran-3-one C5H8O4
cis-delta9-3-hydroxymontanoyl-ACPs[c]	a cis-delta9-3-hydroxyC28 1-[acp]
-3-oxo-cis-D7-tetradecenoyl-ACPs[c]	a 3-oxo-cis-delta7-tetradecenoyl-[acp]
RH[c]	an organic molecule
PANTOTHENATE[c]	{R}-pantothenate C9H16NO5
ACETYL-ACP[c]	an acetyl-[acp]
-2-C-METHYL-D-ERYTHRITOL-4- PHOSPHATE[c]	2-C-methyl-D-erythritol-4-phosphate C5H11O7P
Petrosel-2-enoyl-ACPs[c]	a petrosel-2-enoyl-[acp]
Aliphatic-N-Acetyl-Diamines[c]	an aliphatic N-acetyl-diamine
BCCP-monomers[c]	a [biotin-carboxyl-carrier protein monomer]
PROTOHEME[c]	protoheme IX C34H30N4O4Fe
CARBON-DIOXIDE[c]	CO2 CO2
INDOLE-PYRUVATE[c]	indole-3-pyruvate C11H8NO3
ACRYLAMIDE[c]	acrylamide C3H5NO

Species name	Species id
CPD-7224[c]	N-acetyl-L-citrulline C8H14N3O4
-2-METHYL-ACETO-ACETYL-COA[c]	2-methylacetoacetyl-CoA C26H38N7O18P3S
GLT-tRNAs[c]	tRNA <sup>Glu</sup>
TREHALOSE-6P[c]	trehalose 6-phosphate C12H21O14P
-2-KETO-ISOVALERATE[c]	2-oxoisovalerate C5H7O3
GLUTAMATE-1-SEMIALDEHYDE[c]	glutamate-1-semialdehyde C5H9NO3
Reduced-ferredoxins[c]	a reduced ferredoxin
CPD-2961[c]	6-phospho-D-gluconate C6H10O10P
PROPIONYL-COA[c]	propanoyl-CoA C24H36N7O17P3S
DCMP[c]	dCMP C9H12N3O7P
CPD0-1110[c]	beta-D-ribose C5H10O5
Charged-ASN-tRNAs[c]	L-asparaginyl-tRNA <sup>Asn</sup>
CA-2[c]	Ca <sup>2+</sup> Ca
HCO3[c]	bicarbonate CHO3
ADENOSYLCOBINAMIDE[c]	adenosylcobinamide C58H84N16O11Co
-2C-METH-D-ERYTHRITOL- CYCLODIPHOSPHATE[c]	2-C-methyl-D-erythritol-2,4- cyclodiphosphate C5H10O9P2
PHOSPHORIBOSYL-FORMAMIDO- CARBOXAMIDE[c]	phosphoribosyl-formamido-carboxamide C10H13N4O9P
CPD-650[c]	{R}-3-hydroxybutanoyl-CoA C25H38N7O18P3S
DGTP[c]	dGTP C10H12N5O13P3
LIPOIC-ACID[c]	{R}-lipoate C8H13O2S2
TYR[c]	L-tyrosine C9H11NO3
Phospholipid-Olefinic-Fatty-Acids[c]	a phospholipid olefinic fatty acid
Palmitoyl-ACPs[c]	a palmitoyl-[acp]
-4-HYDROXY-L-PROLINE[c]	trans-4-hydroxy-L-proline C5H9NO3
CH3-MALONATE-S-ALD[c]	{S}-methylmalonate-semialdehyde C4H5O3
CPD-690[c]	adenosyl-cobyrinate a,c-diamide C55H68N11O15Co
CPD-12454[c]	malonyl-CoA methyl ester C25H36N7O19P3S
Cis-Delta7-tetradecenoyl-ACPs[c]	a cis-delta7-tetradecenoyl-[acp]
CPD-7652[c]	4-{beta-D-ribofuranosyl}aminobenzene-5'- phosphate C11H14NO7P
GLC[c]	beta-D-glucose C6H12O6
OH-HEXANOYL-COA[c]	S}-3-hydroxyhexanoyl-CoA C27H42N7O18P3S

Species name	Species id
Amino-Acids-20[c]	a standard alpha amino acid
Enoylpimeloyl-ACP-methyl-esters[c]	an enoylpimelyl-[acp] methyl ester
N-FORMIMINO-L-GLUTAMATE[c]	N-formimino-L-glutamate C6H9N2O4
PRECURSOR-Z[c]	cyclic pyranopterin monophosphate C10H11N5O7P
b-Hydroxy-cis-D5-dodecenoyl-ACPs[c]	a 3-hydroxy cis delta5-dodecenoyl-[acp]
NICOTINATE-NUCLEOTIDE[c]	nicotinate D-ribonucleotide C11H12NO9P
UDP-GLUCOSE[c]	UDP-D-glucose C15H22N2O17P2
Oxo-glutarate-dehydrogenase-DH-lipoyl[c]	a [2-oxoglutarate dehydrogenase E2 protein] N6-{dihydrolipoyl}lysine
-3-Prime-Ribonucleoside-Monophosphates[c]	a nucleoside 3'-phosphate
SQUALENE[c]	squalene C30H50
CPD-11654[c]	{5R}-5,6-dihydro-5-{thymidin-7-yl}thymidine {in DNA}
-3-oxo-palmitoyl-ACPs[c]	a 3-oxo-palmitoyl-[acp]
PHOSPHORIBOSYL-ATP[c]	phosphoribosyl-ATP C15H19N5O20P4
ISOVALERYL-COA[c]	isovaleryl-CoA C26H40N7O17P3S
AMINO-HYDROXYMETHYL-METHYLPYRIMIDINE-PP[c]	4-amino-2-methyl-5-diphosphomethylpyrimidine C6H8N3O7P2
DIHYDROXY-ACETONE-PHOSPHATE[c]	dihydroxyacetone phosphate C3H5O6P
QUINOLINATE[c]	quinolinate C7H3NO4
DIHYDRONEOPTERIN-P[c]	7,8-dihydroneopterin 3'-phosphate C9H12N5O7P
GTP[c]	GTP C10H12N5O14P3
CPD-694[c]	cob{I}yrate a,c-diamide C45H56N6O12Co
-1-CARBOXYVINYL-CARBOXYPHOSPHONATE[c]	carboxyphosphoenolpyruvate C4H2O7P
CYS[c]	L-cysteine C3H7NO2S
R-3-hydroxymyristoyl-ACPs[c]	an {3R}-3-hydroxymyristoyl-[acp]
-3-oxo-cis-vaccenoyl-ACPs[c]	a 3-oxo-cis-vaccenoyl-[acp]
R-3-Hydroxypalmitoyl-ACPs[c]	an {R}-3-hydroxypalmitoyl-[acp]
OROTIDINE-5-PHOSPHATE[c]	orotidine-5'-phosphate C10H10N2O11P
TMP[c]	dTMP C10H13N2O8P
DGDP[c]	dGDP C10H12N5O10P2
cis-delta15-gheddoyl-ACPs[c]	a cis-delta15-C34 1-[acp]
CPD-12175[c]	{S}-3-hydroxy-isobutyrate C4H7O3
CPD-7695[c]	N-acetylmuramoyl-L-alanyl-D-glutamyl-L-lysyl-D-alanyl-D-alanine-

Species name	Species id
	diphosphoundecaprenyl-N-acetylglucosamine C94H153N8O26P2
N3-Acetal-deoxystreptamine-antib[c]	an N3'-acetyl-2-deoxystreptamine antibiotic
BCCP-biotin-monomers[c]	a biotinylated [BCCP monomer]
CPD-9646[c]	ditrans,octacis-undecaprenyl phosphate C55H89O4P
cis-delta15-3-hydroxygheddoyl-ACPs[c]	a cis-delta15-3-hydroxyC34 1-[acp]
-3-HYDROXY-3-METHYL-GLUTARYL-COA[c]	{S}-3-hydroxy-3-methylglutaryl-CoA C27H39N7O20P3S
HISTIDINOL[c]	histidinol C6H12N3O
INOSITOL-1-4-5-TRISPHOSPHATE[c]	D-myo-inositol {1,4,5}-trisphosphate C6H9O15P3
Peptidoglycans[c]	a peptidoglycan
CPD-12173[c]	{S}-3-hydroxy-isobutyryl-CoA C25H38N7O18P3S
L-DELTA1-PYRROLINE-5-CARBOXYLATE[c]	{S}-1-pyrroline-5-carboxylate C5H6NO2
IMINOASPARTATE[c]	alpha-iminosuccinate C4H3NO4
CPD-85[c]	1,2-dihydroxy-5-{methylthio}pent-1-en-3-one C6H9O3S
K-HEXANOYL-COA[c]	3-oxohexanoyl-CoA C27H40N7O18P3S
Myristoyl-ACPs[c]	a myristoyl-[acp]
R-3-hydroxylignoceroyl-ACPs[c]	a {R}-3-hydroxylignoceroyl-[acp]
PUTRESCINE[c]	putrescine C4H14N2
GLYOX[c]	glyoxylate C2HO3
OROTATE[c]	orotate C5H3N2O4
CPD-8720[c]	{2Z,4E}-5-hydroxyhexa-2,4-dienedioate C6H4O5
AMINO-OXOBUT[c]	2-amino-3-oxobutanoate C4H6NO3
CMP[c]	CMP C9H12N3O8P
Carboxylates[c]	a carboxylate
MN-2[c]	Mn2+ Mn
GDP[c]	GDP C10H12N5O11P2
THR-tRNAs[c]	tRNA <sup>thr</sup>
FRU1P[c]	fructose-1-phosphate C6H11O9P
CPD-479[c]	2-oxo-4-methylthiobutanoate C5H7O3S
COB-I-ALAMIN[c]	cob {I} alamin C62H88N13O14PCo
GLN[c]	L-glutamine C5H10N2O3
CIT[c]	citrate C6H5O7
-3-Hydroxy-octanoyl-ACPs[c]	an {R}-3-hydroxyoctanoyl-[acp]

Species name	Species id
-2-ALPHA-HYDROXYETHYL-THPP[c]	2- {alpha-hydroxyethyl} thiamine diphosphate C14H20N4O8P2S
CROTONYL-COA[c]	crotonyl-CoA C25H36N7O17P3S
TYR-tRNAs[c]	tRNA <sup>tyr</sup>
cis-delta5-3-hydroxylignoceroyl-ACPs[c]	a cis-delta5-3-hydroxyC24 1-[acp]
Charged-CYS-tRNAs[c]	L-cysteinyI-tRNA <sup>cys</sup>
Alkanesulfonates[c]	an alkanesulfonate
ADENOSYLCOBALAMIN[c]	coenzyme B12 C72H100N18O17PCo
-3-oxo-arachidoyl-ACPs[c]	a 3-oxo-arachidoyl-[acp]
ZN-2[c]	Zn <sup>2+</sup> Zn
-2-DEHYDROPANTOATE[c]	2-dehydropantoate C6H9O4
Crotonyl-ACPs[c]	a crotonyl-[acp]
CPD0-2123[c]	3-oxodecanoyl-CoA C31H48N7O18P3S
ASN[c]	L-asparagine C4H8N2O3
DEOXYINOSINE[c]	deoxyinosine C10H12N4O4
GDP-TP[c]	pppGpp C10H12N5O20P5
CPD-10226[c]	3-amino-3-deoxy-D-fructose 6-phosphate C6H13NO8P
cis-delta5-3-oxo-lignoceroyl-ACPs[c]	a cis-delta5-3-oxo-C24 1-[acp]
-5-AMINO-LEVULINATE[c]	5-amino-levulinate C5H9NO3
DIPEPTIDES[c]	a dipeptide
cis-delta7-3-oxo-cerotoyl-ACPs[c]	a cis-delta7-3-oxo-C26 1-[acp]
CPD-12279[c]	2-iminoacetate C2H2NO2
SPERMINE[c]	spermine C10H30N4
L-ALPHA-ALANINE[c]	L-alanine C3H7NO2
CPD-10227[c]	1-deoxy-1-imino-D-erythrose 4-phosphate C4H9NO6P
CPD0-2121[c]	trans-hex-2-enoyl-CoA C27H40N7O17P3S
GERANYLGERANYL-PP[c]	all-trans-geranyl-geranyl diphosphate C20H33O7P2
GLC-1-P[c]	alpha-D-glucose 1-phosphate C6H11O9P
D-LACTATE[c]	{R}-lactate C3H5O3
L-CITRULLINE[c]	L-citrulline C6H13N3O3
-5-PHOSPHO-RIBOSYL-GLYCINEAMIDE[c]	5-phospho-ribosyl-glycineamide C7H14N2O8P
CPD-316[c]	reduced riboflavin C17H22N4O6
DELTA3-ISOPENTENYL-PP[c]	isopentenyl diphosphate C5H9O7P2
FORMALDEHYDE[c]	formaldehyde CH2O
CPD0-2120[c]	trans-tetradec-2-enoyl-CoA

Species name	Species id
	C35H56N7O17P3S
CPD-10267[c]	decanoyl-CoA C31H50N7O17P3S
CPDCWI-7[c]	ferric-petrobactin
GLT[c]	L-glutamate C5H8NO4
Nucleoside-Diphosphates[c]	a nucleoside diphosphate
-5-10-METHENYL-THF[c]	5,10-methenyltetrahydrofolate C20H20N7O6
D-ERYTHRO-IMIDAZOLE-GLYCEROL-P[c]	D-erythro-imidazole-glycerol-phosphate C6H9N2O6P
CPD-11479[c]	N-citryl-spermidine C13H25N3O6
CPD-470[c]	L-2,4-diaminobutanoate C4H11N2O2
MANNOSE-6P[c]	D-mannose 6-phosphate C6H11O9P
CPDCWI-6[c]	ferric-bacillibactin
CARBOXYPHENYLAMINO-DEOXYRIBULOSE-P[c]	1-{o-carboxyphenylamino}-1'-deoxyribulose-5'-phosphate C12H13NO9P
CARBON-MONOXIDE[c]	carbon monoxide CO
SARCOSINE[c]	sarcosine C3H7NO2
URIDINE[c]	uridine C9H12N2O6
IMP[c]	IMP C10H11N4O8P
DEOXYADENOSINE[c]	deoxyadenosine C10H13N5O3
CPD-1063[c]	5-methylthioribulose-1-phosphate C6H11O7PS
METOH[c]	methanol CH4O
CPD-568[c]	N1-acetylspermidine C9H23N3O
CPD-11477[c]	N1-{3,4-dihydroxybenzoyl}-N8-citryl-spermidine C20H28N3O9
O-PHOSPHO-L-HOMOSERINE[c]	O-phospho-L-homoserine C4H8NO6P
CPD-10262[c]	trans-2,3-stearoyl-CoA C39H64N7O17P3S
L-ARGININO-SUCCINATE[c]	L-arginino-succinate C10H17N4O6
CPD-569[c]	N-acetylputrescine C6H14N2O
CPD-11474[c]	3,4-dihydroxybenzoate-adenylate C17H17N5O10P
Alkyl-Hydro-Peroxides[c]	an organic hydroperoxide
CPD-397[c]	S-methyl-L-methionine C6H14NO2S
MG-2[c]	Mg2+ Mg
HYDROGEN-PEROXIDE[c]	hydrogen peroxide H2O2
N-FORMYLKYNURENINE[c]	N-formylkynurenine C11H14N2O4
CPD-12231[c]	a peptidoglycan dimer {meso-diaminopimelate containing} C135H214N16O49P2

Species name	Species id
Charged-GLY-tRNAs[c]	glycyl-tRNAgly
-6-PYRUVOYL-5678-TETRAHYDROPTERIN[c]	6-pyruvoyl tetrahydropterin C9H11N5O3
CPD-10260[c]	3-oxo-stearoyl-CoA C39H64N7O18P3S
-2-Oxo-carboxylates[c]	a 2-oxo carboxylate
BUTYRYL-COA[c]	butanoyl-CoA C25H38N7O17P3S
GLY[c]	glycine C2H5NO2
ACP[c]	a holo-[acp]
UROPORPHYRINOGEN-III[c]	uroporphyrinogen-III C40H36N4O16
PHOSPHATIDYLCHOLINE[c]	a phosphatidylcholine
DEPHOSPHO-COA[c]	dephospho-CoA C21H33N7O13P2S
Trans-D3-cis-D5-dodecenoyl-ACPs[c]	a trans-delta3-cis-delta5-dodecenoyl-[acp]
CHOLATE[c]	cholate C24H39O5
D-CYSTEINE[c]	D-cysteine C3H7NO2S
CPD-9451[c]	2-isopropylmaleate C7H8O4
CPD0-2232[c]	{S}-3-Hydroxyhexadecanoyl-CoA C37H62N7O18P3S
-3-4-DIHYDROXYBENZOATE[c]	protocatechuate C7H5O4
GUANINE[c]	guanine C5H5N5O
POLYRIBITOL-PHOSPHATE[c]	poly{ribitol phosphate}
Deoxystreptamine-Antib[c]	a 2-deoxystreptamine antibiotic
METHYL-GLYOXAL[c]	methylglyoxal C3H4O2
Octanoyl-ACPs[c]	an octanoyl-[acp]
DEHYDROQUINATE[c]	3-dehydroquinate C7H9O6
Dodecanoyl-ACPs[c]	a dodecanoyl-[acp]
DIHYDRO-DIOH-BENZOATE[c]	2,3-dihydroxy-2,3-dihydrobenzoate C7H7O4
CPD0-2230[c]	Phosphatidylglycerophosphate {dihexadec-9-enoyl, n-C16 1} C38H69O13P2
-3-hydroxy-cis-D7-tetraecenoyl-ACPs[c]	a 3-hydroxy cis delta7-tetradecenoyl-[acp]
-2-OXOBUTANOATE[c]	2-oxobutanoate C4H5O3
CPD-560[c]	S-methyl-5-thio-D-ribose C6H12O4S
UDP-N-ACETYL-D-GLUCOSAMINE[c]	UDP-alpha-N-acetyl-D-glucosamine C17H25N3O17P2
N-ALPHA-ACETYLORNITHINE[c]	N-acetyl-L-ornithine C7H14N2O3
CPD-12302[c]	N-acetylmuramoyl-L-alanyl-D-isoglutaminyl-N-{beta-D-asparatyl}-L-lysyl-D-alanyl-D-alanine-diphosphoundecaprenyl-N-acetylglucosamine C98H159N10O28P2

Species name	Species id
Aliphatic-Alpha-Omega-Diamines[c]	an aliphatic alpha,omega-diamine
FARNESYL-PP[c]	{2E,6E}-farnesyl diphosphate C15H25O7P2
-3-oxo-dodecanoyl-ACPs[c]	a 3-oxo-dodecanoyl-[acp]
PROPIONYL-P[c]	propionyl-P C3H5O5P
CYTIDINE[c]	cytidine C9H13N3O5
CPD66-34[c]	1,2-dipalmitoylglycerol C35H68O5
CPD-12303[c]	N-acetylmuramoyl-L-alanyl-gamma-D-glutamyl-L-lysyl- D-alanyl-diphosphoundecaprenol C83H135N6O20P2
Charged-PRO-tRNAs[c]	L-prolyl-tRNA <sup>Pro</sup>
CPD-10766[c]	7,8-H <sub>2</sub> pterin-6-yl-methyl-4- {beta-D-ribofuranosyl} aminobenzene 5'-phosphate C18H19N6O8P
N2ACETYL-ALPHA-NP[c]	N2acetyl-alpha-amino adipyl-delta-phosphate C8H11NO8P
Orthophosphoric-Monoesters[c]	a phosphate monoester
FORMATE[c]	formate CHO2
cis-delta17-C36-ACPs[c]	a cis-delta17-C36 1-[acp]
Lipoylated-domains[c]	a lipoylated protein lipoyl-domain
HYPOXANTHINE[c]	hypoxanthine C5H4N4O
-1-L-MYO-INOSITOL-1-P[c]	1D-myo-inositol {3}-monophosphate C6H11O9P
N-formyl-L-methionyl-tRNA <sup>fmet</sup> [c]	N-formyl-L-methionyl-tRNA <sup>fmet</sup>
AICAR[c]	aminoimidazole carboxamide ribonucleotide C9H13N4O8P
CPD0-1108[c]	beta-D-ribofuranose C5H10O5
CPD-3711[c]	cytidine-3'-monophosphate C9H12N3O8P
ADENOSINE[c]	adenosine C10H13N5O4
CPD-564[c]	S-ribosyl-L-homocysteine C9H17NO6S
Light[c]	hnu
DTDP-D-GLUCOSE[c]	dTDP-alpha-D-glucose C16H24N2O16P2
SULFATE[c]	sulfate O4S
UNDECAPRENYL-DIPHOSPHATE[c]	di-trans,octa-cis-undecaprenyl diphosphate C55H89O7P2
CPD-822[c]	N2-succinyl-L-glutamate 5-semialdehyde C9H11NO6
HOPAN-22-OL[c]	hopan-22-ol C30H52O
trans-D2-cis-D5-lignoceroyl-ACPs[c]	a trans-delta2-cis-delta5-C24 2-[acp]
CPD0-1148[c]	N,N'-dimethyl-p-phenylenediamine



Species name	Species id
	C8H12N2
-1-KETO-2-METHYLVALERATE[c]	2,3-dihydroxy-3-methylvalerate C6H11O4
Sulfur-Acceptors[c]	a sulfur acceptor
BUTANAL[c]	butanal C4H8O
apo-ACP[c]	an apo-[acp]
L-ASPARTATE[c]	L-aspartate C4H6NO4
PHENYL-PYRUVATE[c]	keto-phenylpyruvate C9H7O3
CPD-13228[c]	trans-2-pentenal C5H8O
CPD-3713[c]	cytidine 2',3'-cyclic monophosphate C9H11N3O7P
-3-oxo-hexanoyl-ACPs[c]	a 3-oxo-hexanoyl-[acp]
ACETOACETYL-COA[c]	acetoacetyl-CoA C25H36N7O18P3S
BUTYL-HYDROPEROXIDE[c]	tertiary butyl hydroperoxide C4H10O2
WATER[c]	H2O H2O
-5-PHOSPHORIBOSYL-5-AMINOIMIDAZOLE[c]	5-amino-1-{5-phospho-D-ribosyl}imidazole C8H13N3O7P
MALTOTETRAOSE[c]	maltotetraose C24H42O21
CPD-13229[c]	trans-2-pentenol C5H10O
Carboxylic-esters[c]	a carboxylic ester
Holo-AsbD-Proteins[c]	a holo-AsbD protein
Ubiquinones[c]	a ubiquinone
MACROCIN[c]	macrocin C46H77NO16
THF[c]	tetrahydrofolate C19H21N7O6
MALONYL-ACP[c]	a malonyl-[acp]
FORMAMIDE[c]	formamide CH3NO
Acetoacetyl-ACPs[c]	an acetoacetyl-[acp]
CPD-7737[c]	2-carboxy-5-oxo-2,5-dihydrofuran-2-acetate C7H4O6
DCTP[c]	dCTP C9H12N3O13P3
GLUTATHIONYLSPERMIDINE[c]	glutathionylspermidine C17H36N6O5S
-2-Octenoyl-ACPs[c]	a trans oct-2-enoyl-[acp]
UDP-AA-GLUTAMATE[c]	UDP-N-acetylmuramoyl-L-alanyl-D-glutamate C28H39N5O23P2
HIS-tRNAs[c]	tRNA <sub>his</sub>
TTP[c]	dTTP C10H13N2O14P3
Charged-GLT-tRNAs[c]	L-glutamyl-tRNA <sub>Glu</sub>
-3-OXOPALMITOYL-COA[c]	3-oxo-palmitoyl-CoA C37H60N7O18P3S
MESO-DIAMINOPIMELATE[c]	meso-diaminopimelate C7H14N2O4
D-ALANINE[c]	D-alanine C3H7NO2

Species name	Species id
-2-ETHYLHEXAN-1-OL[c]	2-ethylhexan-1-ol C8H18O
CU-2[c]	Cu <sup>2+</sup> Cu
Ceramides[c]	a ceramide
CPD-1243[c]	isomaltose C12H22O11
R-3-hydroxydodecanoyl-ACPs[c]	a {R}-3-hydroxydodecanoyl-[acp]
FRU[c]	D-fructose C6H12O6
FE-3[c]	Fe <sup>3+</sup> Fe
-2-D-THREO-HYDROXY-3-CARBOXY-ISOCAPROATE[c]	{2R,3S}-3-isopropylmalate C7H10O5
NITRIC-OXIDE[c]	nitric oxide NO
CPD-6972[c]	4-{2'-carboxyphenyl}-4-oxobutyryl-CoA C32H39N7O20P3S
tRNAs-containing-epoxy-queuosine[c]	epoxyqueuosine at position 34 of a tRNA containing GUN anticodon
CPD-10434[c]	ethanesulfonate C2H5O3S
-4-hydroxybenzoate[c]	4-hydroxybenzoate C7H5O3
FE-2[c]	Fe <sup>2+</sup> Fe
ISOCHORISMATE[c]	isochorismate C10H8O6
DIACYLGLYCEROL-PYROPHOSPHATE[c]	a 1,2-diacyl-sn-glycerol 3-diphosphate
Sphingomyelins[c]	a sphingomyelin
LONG-CHAIN-KETONE[c]	a ketone
CTP[c]	CTP C9H12N3O14P3
RIBULOSE-5P[c]	D-ribulose-5-phosphate C5H9O8P
PHOSPHORIBOSYL-AMP[c]	1-{5-phospho-D-ribosyl}-AMP C15H19N5O14P2
CPD-70[c]	O-D-Alanyl-poly{ribitol phosphate}
CPD-622[c]	{2S,3S}-2-methylcitrate C7H7O7
N-ACETYL-L-2-AMINO-6-OXO-PIMELATE[c]	L-2-acetamido-6-oxoheptanedioate C9H11NO6
CPD-4422[c]	chromate HO4Cr
BUTYRYL-P[c]	butanoyl phosphate C4H7O5P
BILIVERDINE[c]	biliverdin-IX-alpha C33H32N4O6
DCDP[c]	dCDP C9H12N3O10P2
HYDROXYLAMINE[c]	hydroxylamine H3NO
ACRYLATE[c]	acrylate C3H3O2
AMMONIUM[c]	ammonium H4N
ACETYLMALTOSE[c]	acetylmaltose C14H24O12
CPD-30[c]	4-acetamidobutanal C6H11NO2

Species name	Species id
ALL-TRANS-HEPTAPRENYL-DIPHOSPHATE[c]	all-trans-heptaprenyl diphosphate C35H57O7P2
TDP[c]	dTDP C10H13N2O11P2
RIBOSE-5P[c]	D-ribose-5-phosphate C5H9O8P
G3P[c]	3-phospho-D-glycerate C3H4O7P
-2-ACETO-LACTATE[c]	{S}-2-acetolactate C5H7O4
trans-delta2-arachidoyl-ACPs[c]	a trans-eicos-2-enoyl-[acp]
R-3-hydroxypetroselinoyl-ACPs[c]	a {R}-3-hydroxypetroselinoyl-[acp]
PYRIDOXAMINE-5P[c]	pyridoxamine 5'-phosphate C8H12N2O5P
DIAMINO-OH-PHOSPHORIBOSYLAMINO-PYR[c]	2,5-diamino-6-{5-phospho-D- ribosylamino}pyrimidin-4{3H}-one C9H14N5O8P
trans-delta2-lignoceroyl-ACPs[c]	a trans-tetracos-2-enoyl-[acp]
DUMP[c]	dUMP C9H11N2O8P
-5-METHYL-THF[c]	5-methyl-tetrahydrofolate C20H23N7O6
Protein-N5-methyl-L-glutamine[c]	a [protein]-N5-methyl-L-glutamine
DPG[c]	1,3-bisphospho-D-glycerate C3H4O10P2
ALPHA-GLUCOSE[c]	alpha-D-glucose C6H12O6
CPD-12125[c]	menaquinol-7 C46H66O2
RIBOSE-1P[c]	alpha-D-ribose-1-phosphate C5H9O8P
N-ACETYL-D-GLUCOSAMINE-1-P[c]	N-acetyl-alpha-D-glucosamine 1-phosphate C8H14NO9P
S-ADENOSYL-4-METHYLTHIO-2-OXOBUTANOATE[c]	S-adenosyl-4-methylthio-2-oxobutanoate C15H19N5O6S
Octadec-2-enoyl-ACPs[c]	a trans-octadec-2-enoyl-[acp]
L-seryl-SEC-tRNAs[c]	L-seryl-tRNA <sup>sec</sup>
GLC-D-LACTONE[c]	D-glucono-1,5-lactone C6H10O6
CPD-35[c]	4-acetamidobutanoate C6H10NO3
CPD-13337[c]	4-oxalocrotonate C6H4O5
CPD-665[c]	propanal C3H6O
-5-P-BETA-D-RIBOSYL-AMINE[c]	5-phospho-beta-D-ribosyl-amine C5H11NO7P
-3-oxo-myristoyl-ACPs[c]	a 3-oxo-myristoyl-[acp]
ADENYLOSUCC[c]	adenylo-succinate C14H14N5O11P
THR[c]	L-threonine C4H9NO3
BCAA-dehydrogenase-DH-lipoyl[c]	an [apo BCAA dehydrogenase E2 protein] N6-{dihydrolipoyl}lysine
CPD-233[c]	{3S}-3,6-diaminohexanoate C6H15N2O2
P-AMINO-BENZOATE[c]	4-aminobenzoate C7H6NO2

Species name	Species id
CPD-11643[c]	thymidylyl-{3'-5'}-thymidylate {in DNA}
Red-Thioredoxin[c]	a reduced thioredoxin
CDP[c]	CDP C9H12N3O11P2
METHYLAMINE[c]	methylamine CH6N
DEAMIDO-NAD[c]	nicotinate adenine dinucleotide C21H24N6O15P2
Guanine34-in-tRNA-with-GUN- anticodon[c]	guanine at position 34 of a bacterial tRNA
CPD-667[c]	O-acetyl-L-homoserine C6H11NO4
Ox-Thioredoxin[c]	an oxidized thioredoxin
LEU-tRNAs[c]	tRNA <sup>Leu</sup>
ARG[c]	L-arginine C6H15N4O2
CPD-10194[c]	acetylcadaverine C7H17N2O
AMMONIA[c]	ammonia H3N
PREPHENATE[c]	prephenate C10H8O6
-3-CARBOXY-3-HYDROXY- ISOCAPROATE[c]	{2S}-2-isopropylmalate C7H10O5
O-UREIDOHOMOSERINE[c]	O-ureidohomoserine C5H11N3O4
ILE[c]	L-isoleucine C6H13NO2
PRPP[c]	5-phospho-alpha-D-ribose 1-diphosphate C5H8O14P3
L-ERYTHRO-4-HYDROXY- GLUTAMATE[c]	L-erythro-4-hydroxy-glutamate C5H8NO5

### A8.3. Reactions

**Table S16. Reaction of the model for *B. anthracis*.** The name and the locus associated with each reaction are provided.

Name	Reaction	Locus
{OHACYL-COA- DEHYDROG-RXN-CPD0- 2232-NAD--3- OXOPALMITOYL-COA- NADH-PROTON.46.	+1*CPD0- 2232[c]+1*NAD[c]-- >+1*NADH[c]+1*PROTO N[c]+1*-3- OXOPALMITOYL-COA[c]	GCWI-5129 GCWI-5442
1.1.1.145-RXN	+1*NAD[c]+1*-3b- hydroxy-D5-steroids[c]<-- >+1*NADH[c]+1*PROTO N[c]+1*-3-oxo-D5- steroids[c]	GCWI-3255

Name	Reaction	Locus
1.1.1.215-RXN	+1*GLUCONATE[c]+1*NADP[c]<-->+1*CPD-377[c]+1*NADPH[c]+1*PROTON[c]	GCWI-5026
1.14.11.2-RXN	+1*OXYGEN-MOLECULE[c]+1*PROCOLLAGEN-L-PROLINE[c]+1*-2-KETOGLUTARATE[c]>+1*CARBONDIOXIDE[c]+1*CPD-6321[c]+1*SUC[c]	GCWI-4369
1.18.1.2-RXN	+1*NADP[c]+1*PROTON[c]+2*Reduced-ferredoxins[c]<-->+1*NADPH[c]+2*Oxidized-ferredoxins[c]	
1.2.1.2-RXN	+1*FORMATE[c]+1*NAD[c]>+1*CARBONDIOXIDE[c]+1*NADH[c]	GCWI-795 GCWI-3606
1.2.1.25-RXN	+1*COA[c]+1*NAD[c]+1*-2-KETO-ISOVALERATE[c]>+1*CARBONDIOXIDE[c]+1*ISOBUTYRYL-COA[c]+1*NADH[c]	GCWI-4298
1.2.4.4-RXN	+1*BCAA-dehydrogenase-lipoyl[c]+1*-2-KETO-ISOVALERATE[c]>+1*BCAA-dehydrogenase-2MP-DH-lipoyl[c]+1*CARBONDIOXIDE[c]	GCWI-4298 GCWI-4299
1.4.3.19-RXN	+1*GLY[c]+1*OXYGEN-MOLECULE[c]+1*WATER[c]<-->+1*AMMONIA[c]+1*GLYOX[c]+1*HYDROGEN-PEROXIDE[c]+1*PROTON[c]	GCWI-954 GCWI-2885
1.5.1.20-RXN	+1*METHYLENE-THF[c]+1*NADH[c]+1*PROTON[c]>+1*NAD[c]+1*-5-METHYL-THF[c]	GCWI-4388

Name	Reaction	Locus
1.8.4.12-RXN	+1*Protein-L-methionine-R-S-oxides[c]+1*Red-Thioredoxin[c]-->+1*Ox-Thioredoxin[c]+1*Protein-L-methionine[c]+1*WATER[c]	GCWI-1959
1.8.4.8-RXN	+1*PAPS[c]+1*Red-Thioredoxin[c]-->+1*Ox-Thioredoxin[c]+2*PROTON[c]+1*SO3[c]+1*-3-5-ADP[c]	GCWI-1582
1PFRUCTPHOSN-RXN	+1*ATP[c]+1*FRU1P[c]-->+1*ADP[c]+1*FRUCTOSE-16-DIPHOSPHATE[c]+1*PROTON[c]	GCWI-3799
1TRANSKETO-RXN	+1*D-SEDOHEPTULOSE-7-P[c]+1*GAP[c]<-->+1*RIBOSE-5P[c]+1*XYLULOSE-5-PHOSPHATE[c]	GCWI-3420 GCWI-3707
2-DEHYDROPANTOATE-REDUCT-RXN	+1*NADPH[c]+1*PROTON[c]+1*-2-DEHYDROPANTOATE[c]->+1*L-PANTOATE[c]+1*NADP[c]	GCWI-1993 GCWI-4004
2-ISOPROPYLMALATESYN-RXN	+1*ACETYL-COA[c]+1*WATER[c]+1*-2-KETO-ISOVALERATE[c]-->+1*CO-A[c]+1*PROTON[c]+1*-3-CARBOXY-3-HYDROXY-ISOCAPROATE[c]	GCWI-1563
2-METHYLCITRATE-DEHYDRATASE-RXN	+1*CPD-622[c]-->+1*CPD-1136[c]+1*WATER[c]	GCWI-2433
2-METHYLCITRATE-SYNTHASE-RXN	+1*OXALACETIC-ACID[c]+1*PROPYONYL-COA[c]+1*WATER[c]-->+1*CO-A[c]+1*CPD-622[c]+1*PROTON[c]	GCWI-4721
2-OXOGLUTARATE-SYNTHASE-RXN	+1*CO-A[c]+2*Oxidized-ferredoxins[c]+1*-2-	GCWI-3857

Name	Reaction	Locus
	KETOGLUTARATE[c]-->+1*CARBONDIOXIDE[c]+1*PROTON[c]+2*Reduced-ferredoxins[c]+1*SUC-COA[c]	
2.1.1.79-RXN	+1*Phospholipid-Olefinic-Fatty-Acids[c]+1*S-ADENOSYLMETHIONINE[c]-->+1*ADENOSYL-HOMO-CYS[c]+1*PROTON[c]+1*Phospholipid-Cyclopropane-Fatty-Acids[c]	GCWI-3446
2.3.1.157-RXN	+1*ACETYL-COA[c]+1*GLUCOSAMINE-1P[c]-->+1*CO-A[c]+1*N-ACETYL-D-GLUCOSAMINE-1-P[c]+1*PROTON[c]	GCWI-234
2.3.1.168-RXN	+1*BCAA-dehydrogenase-2MP-DH-lipoyl[c]+1*CO-A[c]-->+1*BCAA-dehydrogenase-DH-lipoyl[c]+1*ISOBUTYRYL-COA[c]	GCWI-4297
2.3.1.179-RXN	+1*MALONYL-ACP[c]+1*Palmitoleoyl-ACPs[c]-->+1*ACP[c]+1*CARBONDIOXIDE[c]+1*-3-oxo-cis-vaccenoyl-ACPs[c]	GCWI-3257 GCWI-1940 GCWI-1349 GCWI-1350
2.3.1.180-RXN	+1*ACETYL-COA[c]+1*MALONYL-ACP[c]-->+1*Acetoacetyl-ACPs[c]+1*CARBONDIOXIDE[c]+1*CO-A[c]	
2.3.1.89-RXN	+1*ACETYL-COA[c]+1*DELTA1-PIPERIDEINE-2-6-DICARBOXYLATE[c]+1*WATER[c]-->+1*CO-A[c]+1*N-ACETYL-L-2-AMINO-6-OXO-PIMELATE[c]	GCWI-4123

Name	Reaction	Locus
2.4.1.129-RXN	+1*CPD-7695[c]+1*Peptidoglycans[c]-->+1*Peptidoglycans[c]+1*UNDECAPRENYL-DIPHOSPHATE[c]	GCWI-2429
2.5.1.19-RXN	+1*PHOSPHO-ENOL-PYRUVATE[c]+1*SHIKIMATE-5P[c]-->+1*Pi[c]+1*3-ENOLPYRUVYL-SHIKIMATE-5P[c]	GCWI-2984
2.5.1.64-RXN	+1*ISOCHORISMATE[c]+1*PROTON[c]+1*2-KETOGLUTARATE[c]-->+1*CARBON-DIOXIDE[c]+1*CPD-9924[c]	GCWI-4979
2.6.1.22-RXN	+1*CPD-466[c]+1*2-KETOGLUTARATE[c]<-->+1*CH3-MALONATE-S-ALD[c]+1*GLT[c]	GCWI-531
2.6.1.37-RXN	+1*CPD-1106[c]+1*PYRUVATE[c]->+1*CPD-551[c]+1*L-ALPHA-ALANINE[c]	GCWI-1492
2.7.1.148-RXN	+1*ATP[c]+1*4-CYTIDINE-5-DIPHOSPHO-2-C[c]-->+1*ADP[c]+1*PROTON[c]+1*2-PHOSPHO-4-CYTIDINE-5-DIPHOSPHO-2-C-MET[c]	GCWI-230
2.7.13.3-RXN	+1*ATP[c]+1*Protein-Histidines[c]<-->+1*ADP[c]+1*PROTON[c]+1*Protein-phospho-L-histidines[c]	GCWI-1619 GCWI-783
2.7.3.9-RXN	+1*PHOSPHO-ENOL-PYRUVATE[c]+1*Protein-Histidines[c]<-->+1*PYRUVATE[c]+1*Protein-3-phospho-L-histidines[c]	GCWI-4190
2.7.4.22-RXN	+1*ATP[c]+1*UMP[c]-->+1*ADP[c]+1*UDP[c]	GCWI-1914 GCWI-3909



Name	Reaction	Locus
2.7.7.60-RXN	+1*CTP[c]+1*PROTON[c] +1*-2-C-METHYL-D- ERYTHRITOL-4- PHOSPHATE[c]-- >+1*PPI[c]+1*-4- CYTIDINE-5- DIPHOSPHO-2-C[c]	GCWI-275
2.7.8.23-RXN	+1*PROTON[c]+1*-1- CARBOXYVINYL- CARBOXYPHOSPHONAT E[c]<-->+1*CARBON- DIOXIDE[c]+1*-3- HYDROHYDROXYPHOS PHORYLPYRUVATE[c]	GCWI-2434
2.8.1.6-RXN	+1*DETHIOBIOTIN[c]+2* S- ADENOSYLMETHIONIN E[c]+1*Sulfurated-Sulfur- Acceptors[c]-- >+1*BIOTIN[c]+2*CH33A DO[c]+2*MET[c]+1*PROT ON[c]+1*Unsulfurated- Sulfur-Acceptors[c]	GCWI-4255
2OXOGLUTARATEDEH- RXN	+1*CO- A[c]+1*NAD[c]+1*-2- KETOGLUTARATE[c]-- >+1*CARBON- DIOXIDE[c]+1*NADH[c]+ 1*SUC-COA[c]	GCWI-1429
2OXOGLUTDECARB- RXN	+1*Oxo-glutarate- dehydrogenase- lipoyl[c]+2*PROTON[c]+1 *-2- KETOGLUTARATE[c]-- >+1*CARBON- DIOXIDE[c]+1*Oxo- glutarate-dehydro-suc-DH- lipoyl[c]	GCWI-1429
2PGADEHYDRAT-RXN	+1*-2-PG[c]<-- >+1*PHOSPHO-ENOL- PYRUVATE[c]+1*WATER [c]	GCWI-5234
2TRANSKETO-RXN	+1*ERYTHROSE- 4P[c]+1*XYLULOSE-5- PHOSPHATE[c]<-- >+1*FRUCTOSE-	GCWI-3420 GCWI-3707

Name	Reaction	Locus
	6P[c]+1*GAP[c]	
3-CH3-2- OXOBUTANOATE-OH- CH3-XFER-RXN	+1*METHYLENE- THF[c]+1*WATER[c]+1*- 2-KETO- ISOVALERATE[c]-- >+1*THF[c]+1*-2- DEHYDROPANTOATE[c]	GCWI-1701
3-DEHYDROQUINATE- DEHYDRATASE-RXN	+1*DEHYDROQUINATE[ c]-->+1*WATER[c]+1*-3- DEHYDRO- SHIKIMATE[c]	GCWI-4335
3-DEHYDROQUINATE- SYNTHASE-RXN	+1*-3-DEOXY-D- ARABINO- HEPTULOSONATE-7- P[c]-- >+1*DEHYDROQUINATE [c]+1*Pi[c]	GCWI-1679
3-HYDROXBUTYRYL- COA-DEHYDRATASE- RXN	+1*CPD-650[c]-- >+1*CROTONYL- COA[c]+1*WATER[c]	GCWI-2439 GCWI-1106 GCWI-2616 GCWI-3561 GCWI-4652 GCWI-2616 GCWI-1478 GCWI-2037 GCWI-4490
3-HYDROXY- KYNURENINASE-RXN	+1*WATER[c]+1*-3- HYDROXY-L- KYNURENINE[c]-->+1*L- ALPHA- ALANINE[c]+1*PROTON[ c]+1*-3-HYDROXY- ANTHRANILATE[c]	GCWI-2808
3-HYDROXYBUTYRATE- DEHYDROGENASE-RXN	+1*CPD- 335[c]+1*NAD[c]<-- >+1*NADH[c]+1*PROTO N[c]+1*-3- KETOBUTYRATE[c]	GCWI-4173
3- HYDROXYDECANOYL- ACP-DEHYDR-RXN	+1*OH-ACYL-ACP[c]-- >+1*TRANS-D2-ENOYL- ACP[c]+1*WATER[c]	GCWI-5366 GCWI-2941
3- HYDROXYDECANOYL- ACP-DEHYDR-RXN- BETA- HYDROXYDECANOYL- ACPS--TRANS-D2- DECENOYL-ACPS- WATER.56.	+1*Beta-hydroxydecanoyl- ACPs[c]-->+1*Trans-D2- decanoyl- ACPs[c]+1*WATER[c]	GCWI-5366 GCWI-2941

Name	Reaction	Locus
3-HYDROXYISOBUTYRATE-DEHYDROGENASE-RXN	+1*CPD-12175[c]+1*NAD[c]>+1*CH3-MALONATE-S-ALD[c]+1*NADH[c]+1*PROTON[c]	GCWI-4184 GCWI-4185
3-HYDROXYISOBUTYRYL-COA-HYDROLASE-RXN	+1*CPD-12173[c]+1*WATER[c]>+1*CO-A[c]+1*CPD-12175[c]+1*PROTON[c]	GCWI-2439
3-ISOPROPYLMALDEHYDE-RXN	+1*NAD[c]+1*-2-D-THREO-HYDROXY-3-CARBOXY-ISOCAPROATE[c]>+1*CPD-7100[c]+1*NADH[c]+1*PROTON[c]	GCWI-1564
3-ISOPROPYLMALISOMER-RXN	+1*-3-CARBOXY-3-HYDROXY-ISOCAPROATE[c]>+1*CPD-9451[c]+1*WATER[c]	GCWI-1565 GCWI-1566
3-OXOACYL-ACP-REDUCT-RXN	+1*B-KETOACYL-ACP[c]+1*NADPH[c]+1*PROTON[c]>+1*NADP[c]+1*OH-ACYL-ACP[c]	GCWI-375 GCWI-2066 GCWI-3377 GCWI-3588 GCWI-3869 GCWI-3935 GCWI-4754 GCWI-375 GCWI-3377 GCWI-4754 GCWI-3427 GCWI-2066 GCWI-3588 GCWI-3869 GCWI-3935
3-OXOACYL-ACP-REDUCT-RXN-R-3-HYDROXYARACHIDOYL-ACPS-NADP--3-OXO-ARACHIDOYL-ACPS-NADPH-PROTON.68.	+1*NADPH[c]+1*PROTON[c]+1*-3-oxo-arachidoyl-ACPs[c]>+1*NADP[c]+1*R-3-hydroxyarachidoyl-ACPs[c]	GCWI-375 GCWI-2066 GCWI-3377 GCWI-3588 GCWI-3869 GCWI-3935 GCWI-4754 GCWI-375 GCWI-3377 GCWI-4754 GCWI-3427 GCWI-2066 GCWI-3588 GCWI-3869 GCWI-3935
3-OXOACYL-ACP-SYNTH-BASE-RXN	+1*ACETYL-ACP[c]+1*MALONYL-ACP[c]>+1*ACP[c]+1*Acetoacetyl-ACPs[c]+1*CARBONDIOXIDE[c]	GCWI-3257 GCWI-1940 GCWI-1349 GCWI-1350
3-OXOACYL-ACP-SYNTH-RXN	+1*MALONYL-ACP[c]+1*Saturated-Fatty-	GCWI-3257 GCWI-1940 GCWI-1349 GCWI-1350

Name	Reaction	Locus
	Acyl-ACPs[c]-- >+1*ACP[c]+1*B- KETOACYL- ACP[c]+1*CARBON- DIOXIDE[c]	
3-OXOACYL-ACP- SYNTH-RXN- PALMITOYL-ACPS- MALONYL-ACP--3-OXO- STEAROYL-ACPS- CARBON-DIOXIDE- ACP.67.	+1*MALONYL- ACP[c]+1*Palmitoyl- ACPs[c]-- >+1*ACP[c]+1*CARBON- DIOXIDE[c]+1*-3-oxo- stearoyl-ACPs[c]	GCWI-3257 GCWI-1940 GCWI-1349 GCWI-1350
3-SULFINOALANINE- AMINOTRANSFERASE- RXN	+1*-2- KETOGLUTARATE[c]+1* -3- SULFINOALANINE[c]<-- >+1*GLT[c]+1*-3- SULFINYL-PYRUVATE[c]	GCWI-1706 GCWI-2940
3.1.2.23-RXN	+1*CPD- 201[c]+1*WATER[c]<-- >+1*CO- A[c]+1*PROTON[c]+1*-4- hydroxybenzoate[c]	GCWI-3639 GCWI-4643
3.1.4.10-RXN	+1*L-1-phosphatidyl- inositols[c]<-->+1*CPD- 1121[c]+1*DIACYLGLYC EROL[c]	GCWI-3839
3.1.4.10-RXN-CPD66-45-- CPD66-34-CPD-1121.28.	+1*CPD66-34[c]+1*CPD- 1121[c]<-->+1*CPD66- 45[c]	GCWI-3839
3.1.4.11-RXN	+1*PHOSPHATIDYL- MYO-INOSITOL-45- BISPHOSPHA[c]+1*WAT ER[c]-- >+1*DIACYLGLYCEROL[ c]+1*INOSITOL-1-4-5- TRISPHOSPHATE[c]+1*P ROTON[c]	GCWI-880
3.2.1.10-RXN	+1*CPD- 1243[c]+1*WATER[c]<-- >+2*ALPHA-GLUCOSE[c]	GCWI-4156
3.2.1.17-RXN	+1*Peptidoglycans[c]+1*W ATER[c]<-->+1*N-acetyl- D- glucosamine[c]+1*Peptidogl	GCWI-3485

Name	Reaction	Locus
	ycan-With-Cleaved-Nac[c]	
3.4.13.5-RXN	+1*DIPEPTIDES[c]+1*WATER[c]<-->+1*Amino-Acids-20[c]+1*Amino-Acids-20[c]	GCWI-2562
3.4.13.9-RXN	+1*Dipeptides-With-Proline-Carboxy[c]+1*WATER[c]<-->+1*Amino-Acids-20[c]+1*PRO[c]	GCWI-3960 GCWI-4334 GCWI-4741
3.4.17.14-RXN	+1*C3[c]+1*WATER[c]<-->+1*CPD-12258[c]+1*D-ALANINE[c]	GCWI-1443 GCWI-1631 GCWI-2057 GCWI-2169 GCWI-2592 GCWI-2624 GCWI-2625 GCWI-4642 GCWI-4972 GCWI-5130 GCWI-5489 GCWI-193 GCWI-4218
3.5.1.88-RXN	+1*FORMYL-L-METHIONYL-PEPTIDE[c]+1*WATER[c]<-->+1*FORMATE[c]+1*METHIONYL-PEPTIDE[c]+1*PROTON[c]	GCWI-3951 GCWI-4116
3.6.3.12-RXN	+1*ATP[c]+1*K-[e]+1*WATER[c]<-->+1*ADP[c]+1*K-[c]+1*PROTON[c]+1*Pi[c]	GCWI-961 GCWI-962
3.6.3.27-RXN	+1*ATP[c]+1*Pi[e]+1*WATER[c]<-->+1*ADP[c]+1*PROTON[c]+2*Pi[c]	GCWI-4405 GCWI-4404 GCWI-4403 GCWI-4402 GCWI-920 GCWI-919 GCWI-918
3.6.3.4-RXN	+1*ATP[c]+1*CU-2[c]+1*WATER[c]<-->+1*ADP[c]+1*CU-2[e]+1*PROTON[c]+1*Pi[c]	GCWI-3810
325-BISPHOSPHATE-NUCLEOTIDASE-RXN	+1*WATER[c]+1*-3-5-ADP[c]<-->+1*AMP[c]+1*Pi[c]	GCWI-4734
3PGAREARR-RXN	+1*G3P[c]<-->+1*-2-PG[c]	GCWI-1868 GCWI-2175 GCWI-3826 GCWI-4078 GCWI-4480 GCWI-5091 GCWI-2556 GCWI-5235

Name	Reaction	Locus
		GCWI-3526
4-CARBOXYMUCONOLACTONE-DECARBOXYLASE-RXN	+1*CPD-7737[c]+1*PROTON[c]>+1*CARBONDIOXIDE[c]+1*-3-OXOADIPATE-ENOL-LACTONE[c]	GCWI-2047 GCWI-2879
4-HYDROXYPHENYLPYRUVATE-DIOXYGENASE-RXN	+1*OXYGEN-MOLECULE[c]+1*P-HYDROXY-PHENYLPYRUVATE[c]>+1*CARBONDIOXIDE[c]+1*HOMOGENTISATE[c]	GCWI-427
4.1.1.74-RXN	+1*INDOLE-PYRUVATE[c]+1*PROTON[c]<-->+1*CARBONDIOXIDE[c]+1*INDOLE-ACETALDEHYDE[c]	GCWI-2554
4.2.1.58-RXN	+1*Beta-3-hydroxybutyryl-ACPs[c]>+1*Crotonyl-ACPs[c]+1*WATER[c]	GCWI-2941 GCWI-5366
4.2.1.59-RXN	+1*-3-Hydroxy-octanoyl-ACPs[c]>+1*WATER[c]+1*-2-Octenoyl-ACPs[c]	GCWI-2941 GCWI-5366
4.2.1.61-RXN	+1*R-3-Hydroxypalmitoyl-ACPs[c]>+1*WATER[c]+1*-2-Hexadecenoyl-ACPs[c]	GCWI-2941 GCWI-5366
4.2.3.12-RXN	+1*DIHYDRONEOPTERIN-P3[c]<-->+1*P3I[c]+1*PROTON[c]+1*-6-PYRUVOYL-5678-TETRAHYDROPTERIN[c]	GCWI-1510
4.3.1.17-RXN	+1*SER[c]>+1*AMMONIA[c]+1*PROTON[c]+1*PYRUVATE[c]	GCWI-4278 GCWI-3306 GCWI-4279 GCWI-3307
5-FORMYL-THF-CYCLO-LIGASE-RXN	+1*ADP[c]+1*Pi[c]+1*-5-10-METHENYL-THF[c]>+1*ATP[c]+1*-5-FORMYL-THF[c]	GCWI-4398
5-METHYLTHIORIBOSE-KINASE-RXN	+1*ATP[c]+1*CPD-560[c]>+1*ADP[c]+1*CPD-	GCWI-552 GCWI-4175

Name	Reaction	Locus
	444[c]+1*PROTON[c]	
5.3.1.23-RXN	+1*CPD-444[c]<-->+1*CPD-1063[c]	GCWI-553 GCWI-4174
5.4.2.10-RXN	+1*D-GLUCOSAMINE-6-P[c]<-->+1*GLUCOSAMINE-1P[c]	GCWI-359
5.4.99.17-RXN	+1*SQUALENE[c]<-->+1*HOP-2229-ENE[c]	GCWI-3590
5.5.1.2-RXN	+1*CPD-245[c]+1*PROTON[c]<-->+1*CPD-7737[c]	GCWI-498
6-PHOSPHO-BETA-GLUCOSIDASE-RXN	+1*CPD-507[c]+1*WATER[c]<-->+1*ALPHA-GLC-6-P[c]+1*ALPHA-GLUCOSE[c]	GCWI-5306
6.1.1.13-RXN	+1*ATP[c]+1*D-ALANINE[c]+1*POLYRIBITOL-PHOSPHATE[c]<-->+1*AMP[c]+1*CPD-70[c]+1*PPI[c]+1*PROTON[c]	GCWI-1537 GCWI-1539
6.3.4.16-RXN	+1*AMMONIA[c]+2*ATP[c]+1*CARBONDIOXIDE[c]+1*WATER[c]<-->+2*ADP[c]+1*CARBAMOYL-P[c]+2*PROTON[c]+1*Pi[c]	GCWI-3970 GCWI-3971
6.3.5.7-RXN	+1*ATP[c]+1*GLN[c]+1*L-glutamyl-tRNA <sup>Gln</sup> [c]<-->+1*ADP[c]+1*Charged-GLN-tRNAs[c]+1*GLT[c]+1*Pi[c]	GCWI-526 GCWI-527 GCWI-528
6PFRUCTPHOS-RXN	+1*ATP[c]+1*FRUCTOSE-6P[c]<-->+1*ADP[c]+1*FRUCTOSE-16-DIPHOSPHATE[c]+1*PROTON[c]	GCWI-4726
6PGLUCONOLACT-RXN	+1*D-6-P-GLUCONODELTA-	GCWI-3421

Name	Reaction	Locus
	LACTONE[c]+1*WATER[c]-->+1*CPD-2961[c]+1*PROTON[c]	
ABC-24-RXN	+1*ATP[c]+1*SPERMIDINE[e]+1*WATER[c]<-->+1*ADP[c]+1*PROTON[c]+1*Pi[c]+1*SPERMIDINE[c]	GCWI-1452 GCWI-1453 GCWI-1454 GCWI-1455
ABC-25-RXN	+1*ATP[c]+1*PUTRESCINE[e]+1*WATER[c]-->+1*ADP[c]+1*PROTON[c]+1*PUTRESCINE[c]+1*Pi[c]	GCWI-1452 GCWI-1453 GCWI-1454 GCWI-1455
ABC-26-RXN	+1*ATP[c]+1*PRO[e]+1*WATER[c]-->+1*ADP[c]+1*PRO[c]+1*PROTON[c]+1*Pi[c]	GCWI-2838 GCWI-2837 GCWI-2371 GCWI-2370 GCWI-2839 GCWI-573 GCWI-847 GCWI-574 GCWI-1070 GCWI-2039 GCWI-2040 GCWI-575 GCWI-4291 GCWI-4290 GCWI-4289 GCWI-2043 GCWI-2042 GCWI-2041 GCWI-1072 GCWI-1071 GCWI-846 GCWI-845 GCWI-844 GCWI-843
ABC-34-RXN	+1*ATP[c]+1*GLYCEROL-3P[e]+1*WATER[c]-->+1*ADP[c]+1*GLYCEROL-3P[c]+1*PROTON[c]+1*Pi[c]	GCWI-773 GCWI-774 GCWI-775 GCWI-776
ACETALD-DEHYDROG-RXN	+1*ACETYL-COA[c]+1*NADH[c]+1*PROTON[c]-->+1*ACETALD[c]+1*CO-A[c]+1*NAD[c]	GCWI-2379 GCWI-3587 GCWI-2881 GCWI-1451 GCWI-4498
ACETATE--COA-LIGASE-RXN	+1*ACET[c]+1*ATP[c]+1*CO-A[c]-->+1*ACETYL-COA[c]+1*AMP[c]+1*PPI[c]	GCWI-2618 GCWI-4792 GCWI-4775
ACETATEKIN-RXN	+1*ACETYL-P[c]+1*ADP[c]-->+1*ACET[c]+1*ATP[c]	GCWI-4767
ACETOACETATE--COA-LIGASE-RXN	+1*ATP[c]+1*CO-A[c]+1*-3-KETOBUTYRATE[c]--	GCWI-2618



Name	Reaction	Locus
	>+1*ACETOACETYL-COA[c]+1*AMP[c]+1*PPI[c]	
ACETOLACTATE-DECARBOXYLASE-RXN	+1*PROTON[c]+1*-2-ACETO-LACTATE[c]-->+1*CARBON-DIOXIDE[c]+1*CPD-10353[c]	GCWI-1082
ACETOLACTREDUCTOISOM-RXN	+1*NADPH[c]+1*PROTON[c]+1*-2-ACETO-LACTATE[c]-->+1*DIOH-ISOVALERATE[c]+1*NADP[c]	GCWI-1562 GCWI-1964
ACETOLACTREDUCTOISOM-RXN-CPD-13357-NADP--2-ACETO-LACTATE-NADPH-PROTON.45.	+1*NADPH[c]+1*PROTON[c]+1*-2-ACETO-LACTATE[c]-->+1*CPD-13357[c]+1*NADP[c]	GCWI-1562 GCWI-1964
ACETOLACTSYN-RXN	+1*PROTON[c]+2*PYRUVATE[c]-->+1*CARBON-DIOXIDE[c]+1*-2-ACETO-LACTATE[c]	GCWI-1963 GCWI-1560 GCWI-1561 GCWI-1962 GCWI-1081
ACETOOHBUTREDUCTOISOM-RXN	+1*NADPH[c]+1*PROTON[c]+1*-2-ACETO-2-HYDROXY-BUTYRATE[c]-->+1*NADP[c]+1*-1-KETO-2-METHYLVALERATE[c]	GCWI-1562 GCWI-1964
ACETOOHBUTSYN-RXN	+1*PROTON[c]+1*PYRUVATE[c]+1*-2-OXOBUTANOATE[c]-->+1*CARBON-DIOXIDE[c]+1*-2-ACETO-2-HYDROXY-BUTYRATE[c]	GCWI-1963 GCWI-1560 GCWI-1561 GCWI-1962 GCWI-1081
ACETYL-COA-ACETYLTRANSFER-RXN	+2*ACETYL-COA[c]<-->+1*ACETOACETYL-COA[c]+1*CO-A[c]	GCWI-3656 GCWI-4164 GCWI-5128 GCWI-5443
ACETYL-COA-CARBOXYLTRANSFER-RXN	+1*ACETYL-COA[c]+1*ATP[c]+1*HCO3[c]-->+1*ADP[c]+1*MALONYL-COA[c]+1*PROTON[c]+1*	GCWI-4320 GCWI-2613 GCWI-2614 GCWI-4321 GCWI-4727 GCWI-4728

Name	Reaction	Locus
	Pi[c]	
ACETYLGLUTKIN-RXN	+1*ACETYL- GLU[c]+1*ATP[c]-- >+1*ADP[c]+1*N- ACETYL-GLUTAMYL- P[c]	GCWI-4270
ACETYLMOMOSER-CYS- RXN	+1*CPD-667[c]+1*HS[c]-- >+1*ACET[c]+1*HOMO- CYS[c]+1*PROTON[c]	GCWI-5507
ACETYLMORNDEACET- RXN	+1*N-ALPHA- ACETYLMORNITHINE[c]+1 *WATER[c]-- >+1*ACET[c]+1*L- ORNITHINE[c]	GCWI-688 GCWI-2386
ACETYLMORNTRANSAM- RXN	+1*CPD-469[c]+1*GLT[c]- ->+1*N-ALPHA- ACETYLMORNITHINE[c]+1 *-2-KETOGLUTARATE[c]	GCWI-4269
ACID-PHOSPHATASE- RXN	+1*Orthophosphoric- Monoesters[c]+1*WATER[ c]-- >+1*Alcohols[c]+1*Pi[c]	GCWI-4638
ACID-PHOSPHATASE- RXN-CPD-10815-WATER- -PI-METOH.26.	+1*METOH[c]+1*Pi[c]-- >+1*CPD- 10815[c]+1*WATER[c]	GCWI-4638
ACONITATEDEHYDR- RXN	+1*CIT[c]-->+1*CIS- ACONITATE[c]+1*WATE R[c]	GCWI-3646
ACONITATEHYDR-RXN	+1*CIS- ACONITATE[c]+1*WATE R[c]-->+1*THREO-DS- ISO-CITRATE[c]	GCWI-3646
ACSERLY-RXN	+1*ACETYLSERINE[c]+1 *HS[c]-- >+1*ACET[c]+1*CYS[c]+1 *PROTON[c]	GCWI-4500 GCWI-255 GCWI-1946
ADCLY-RXN	+1*-4-AMINO-4- DEOXYCHORISMATE[c]- - >+1*PROTON[c]+1*PYRU VATE[c]+1*P-AMINO- BENZOATE[c]	GCWI-258
ADENINE-DEAMINASE- RXN	+1*ADENINE[c]+1*WATE R[c]-- >+1*AMMONIA[c]+1*HY	GCWI-3058

Name	Reaction	Locus
	POXANTHINE[c]	
ADENOSYLHOMOCYSTEINE-NUCLEOSIDASE-RXN	+1*ADENOSYL-HOMO-CYS[c]+1*WATER[c]-->+1*ADENINE[c]+1*CPD-564[c]	GCWI-2913 GCWI-2630 GCWI-4501
ADENPHOSPHOR-RXN	+1*ADENOSINE[c]+1*Pi[c]-->+1*ADENINE[c]+1*RIBOSE-1P[c]	GCWI-4228 GCWI-1624 GCWI-4228
ADENPRIBOSYLTRAN-RXN	+1*ADENINE[c]+1*PRPP[c]-->+1*AMP[c]+1*PPI[c]	GCWI-4533
ADENYL-KIN-RXN	+1*AMP[c]+1*ATP[c]<-->+2*ADP[c]	GCWI-321
ADENYLOSUCCINATE-SYNTHASE-RXN	+1*GTP[c]+1*IMP[c]+1*L-ASPARTATE[c]-->+1*ADENYLOSUCC[c]+1*GDP[c]+2*PROTON[c]+1*Pi[c]	GCWI-5572
ADENYLYLSULFKIN-RXN	+1*APS[c]+1*ATP[c]-->+1*ADP[c]+1*PAPS[c]+1*PROTON[c]	GCWI-1584
ADPREDUCT-RXN	+1*ADP[c]+1*Red-Thioredoxin[c]-->+1*DADP[c]+1*Ox-Thioredoxin[c]+1*WATER[c]	GCWI-1519 GCWI-1521 GCWI-1521 GCWI-1519 GCWI-1522
AGMATIN-RXN	+1*AGMATHINE[c]+1*WATER[c]-->+1*PUTRESCINE[c]+1*UREA[c]	GCWI-5468
AICARSYN-RXN	+1*P-RIBOSYL-4-SUCCARB-AMINOIMIDAZOLE[c]-->+1*AICAR[c]+1*FUM[c]	GCWI-498
AICARTRANSFORM-RXN	+1*AICAR[c]+1*-10-FORMYL-THF[c]-->+1*PHOSPHORIBOSYL-FORMAMIDO-CARBOXAMIDE[c]+1*THF[c]	GCWI-506
AIRCARBOXY-RXN	+1*CARBON-DIOXIDE[c]+1*-5-PHOSPHORIBOSYL-5-AMINOIMIDAZOLE[c]-->+1*PHOSPHORIBOSYL-	GCWI-496 GCWI-497

Name	Reaction	Locus
	CARBOXY-AMINOIMIDAZOLE[c]+2*PROTON[c]	
AIRS-RXN	+1*ATP[c]+1*-5-PHOSPHORIBOSYL-N-FORMYLGLYCINEAMIDINE[c]>+1*ADP[c]+1*PROTON[c]+1*Pi[c]+1*-5-PHOSPHORIBOSYL-5-AMINOIMIDAZOLE[c]	GCWI-504
AKBLIG-RXN	+1*AMINO-OXOBUT[c]+1*COA[c]+1*PROTON[c]>+1*ACETYLCOA[c]+1*GLY[c]	GCWI-823
ALANINE--TRNA-LIGASE-RXN	+1*ALA-tRNAs[c]+1*ATP[c]+1*L-ALPHA-ALANINE[c]+1*PROTON[c]>+1*AMP[c]+1*Charged-ALA-tRNAs[c]+1*PPI[c]	GCWI-3653 GCWI-4515
ALANINE-DEHYDROGENASE-RXN	+1*L-ALPHA-ALANINE[c]+1*NAD[c]+1*WATER[c]>+1*AMMONIA[c]+1*NADH[c]+2*PROTON[c]+1*PYRUVATE[c]	GCWI-798 GCWI-4753
ALARACECAT-RXN	+1*L-ALPHA-ALANINE[c]>+1*D-ALANINE[c]	GCWI-439 GCWI-2178
ALCOHOL-DEHYDROGENERIC-RXN	+1*NAD[c]+1*Primary-Alcohols[c]>+1*Aldehydes[c]+1*NADH[c]+1*PROTON[c]	GCWI-379 GCWI-878 GCWI-1005 GCWI-1195 GCWI-2654 GCWI-2708 GCWI-3152 GCWI-3423 GCWI-3425 GCWI-3545 GCWI-4498 GCWI-2357
ALCOHOL-DEHYDROGENERIC-RXN-2-ETHYLHEXAN-1-OL-NAD--CPD-371-NADH-PROTON.43.	+1*CPD-371[c]+1*NADH[c]+1*PROTON[c]>+1*NAD[c]+1*-2-ETHYLHEXAN-1-OL[c]	GCWI-379 GCWI-878 GCWI-1005 GCWI-1195 GCWI-2654 GCWI-2708 GCWI-3152 GCWI-3423 GCWI-3425 GCWI-3545 GCWI-4498 GCWI-2357
ALCOHOL-DEHYDROGENERIC-RXN	+1*CPD-	GCWI-379 GCWI-878

Name	Reaction	Locus
GENERIC-RXN-CPD-13229-NAD--CPD-13228-NADH-PROTON.37.	13228[c]+1*NADH[c]+1*P ROTON[c]<-->+1*CPD- 13229[c]+1*NAD[c]	GCWI-1005 GCWI-1195 GCWI-2654 GCWI-2708 GCWI-3152 GCWI-3423 GCWI-3425 GCWI-3545 GCWI-4498 GCWI-2357
ALCOHOL-DEHYDROG-GENERIC-RXN-CPD-7845-NAD--CPD-7879-NADH-PROTON.35.	+1*CPD- 7879[c]+1*NADH[c]+1*PR OTON[c]<-->+1*CPD- 7845[c]+1*NAD[c]	GCWI-379 GCWI-878 GCWI-1005 GCWI-1195 GCWI-2654 GCWI-2708 GCWI-3152 GCWI-3423 GCWI-3425 GCWI-3545 GCWI-4498 GCWI-2357
ALCOHOL-DEHYDROG-GENERIC-RXN-CPD-7867-NAD--CPD-7880-NADH-PROTON.35.	+1*CPD- 7880[c]+1*NADH[c]+1*PR OTON[c]<-->+1*CPD- 7867[c]+1*NAD[c]	GCWI-379 GCWI-878 GCWI-1005 GCWI-1195 GCWI-2654 GCWI-2708 GCWI-3152 GCWI-3423 GCWI-3425 GCWI-3545 GCWI-4498 GCWI-2357
ALCOHOL-DEHYDROG-GENERIC-RXN-CPD-7868-NAD--CPD-7881-NADH-PROTON.35.	+1*CPD- 7881[c]+1*NADH[c]+1*PR OTON[c]<-->+1*CPD- 7868[c]+1*NAD[c]	GCWI-379 GCWI-878 GCWI-1005 GCWI-1195 GCWI-2654 GCWI-2708 GCWI-3152 GCWI-3423 GCWI-3425 GCWI-3545 GCWI-4498 GCWI-2357
ALCOHOL-DEHYDROG-GENERIC-RXN-CPD-7869-NAD--CPD-7882-NADH-PROTON.35.	+1*CPD- 7882[c]+1*NADH[c]+1*PR OTON[c]<-->+1*CPD- 7869[c]+1*NAD[c]	GCWI-379 GCWI-878 GCWI-1005 GCWI-1195 GCWI-2654 GCWI-2708 GCWI-3152 GCWI-3423 GCWI-3425 GCWI-3545 GCWI-4498 GCWI-2357
ALCOHOL-DEHYDROG-GENERIC-RXN-CPD-7871-NAD--CPD-7883-NADH-PROTON.35.	+1*CPD- 7883[c]+1*NADH[c]+1*PR OTON[c]<-->+1*CPD- 7871[c]+1*NAD[c]	GCWI-379 GCWI-878 GCWI-1005 GCWI-1195 GCWI-2654 GCWI-2708 GCWI-3152 GCWI-3423 GCWI-3425 GCWI-3545 GCWI-4498 GCWI-2357
ALCOHOL-DEHYDROG-GENERIC-RXN-CPD-7872-NAD--CPD-7884-NADH-PROTON.35.	+1*CPD- 7884[c]+1*NADH[c]+1*PR OTON[c]<-->+1*CPD- 7872[c]+1*NAD[c]	GCWI-379 GCWI-878 GCWI-1005 GCWI-1195 GCWI-2654 GCWI-2708 GCWI-3152 GCWI-3423 GCWI-3425 GCWI-3545 GCWI-4498 GCWI-2357
ALCOHOL-DEHYDROG-GENERIC-RXN-CPD-7874-NAD--CPD-7885-NADH-PROTON.35.	+1*CPD- 7885[c]+1*NADH[c]+1*PR OTON[c]<-->+1*CPD- 7874[c]+1*NAD[c]	GCWI-379 GCWI-878 GCWI-1005 GCWI-1195 GCWI-2654 GCWI-2708 GCWI-3152 GCWI-3423

Name	Reaction	Locus
		GCWI-3425 GCWI-3545 GCWI-4498 GCWI-2357
ALCOHOL-DEHYDROG- GENERIC-RXN-CPD- 7875-NAD--CPD-7886- NADH-PROTON.35.	+1*CPD- 7886[c]+1*NADH[c]+1*PR OTON[c]<-->+1*CPD- 7875[c]+1*NAD[c]	GCWI-379 GCWI-878 GCWI-1005 GCWI-1195 GCWI-2654 GCWI-2708 GCWI-3152 GCWI-3423 GCWI-3425 GCWI-3545 GCWI-4498 GCWI-2357
ALCOHOL-DEHYDROG- GENERIC-RXN-CPD- 7876-NAD--CPD-7887- NADH-PROTON.35.	+1*CPD- 7887[c]+1*NADH[c]+1*PR OTON[c]<-->+1*CPD- 7876[c]+1*NAD[c]	GCWI-379 GCWI-878 GCWI-1005 GCWI-1195 GCWI-2654 GCWI-2708 GCWI-3152 GCWI-3423 GCWI-3425 GCWI-3545 GCWI-4498 GCWI-2357
ALCOHOL-DEHYDROG- GENERIC-RXN-CPD- 7877-NAD--CPD-7888- NADH-PROTON.35.	+1*CPD- 7888[c]+1*NADH[c]+1*PR OTON[c]<-->+1*CPD- 7877[c]+1*NAD[c]	GCWI-379 GCWI-878 GCWI-1005 GCWI-1195 GCWI-2654 GCWI-2708 GCWI-3152 GCWI-3423 GCWI-3425 GCWI-3545 GCWI-4498 GCWI-2357
ALCOHOL-DEHYDROG- GENERIC-RXN- PROPANOL-NAD--CPD- 665-NADH-PROTON.34.	+1*CPD- 665[c]+1*NADH[c]+1*PR OTON[c]<-- >+1*NAD[c]+1*PROPAN OL[c]	GCWI-379 GCWI-878 GCWI-1005 GCWI-1195 GCWI-2654 GCWI-2708 GCWI-3152 GCWI-3423 GCWI-3425 GCWI-3545 GCWI-4498 GCWI-2357
ALCOHOL-DEHYDROG- RXN	+1*ACETALD[c]+1*NAD H[c]+1*PROTON[c]-- >+1*ETOH[c]+1*NAD[c]	GCWI-2357 GCWI-4498 GCWI-379 GCWI-878 GCWI-1005 GCWI-1195 GCWI-2654 GCWI-2708 GCWI-3152 GCWI-3423 GCWI-3425 GCWI-3545
ALKANAL- MONOOXYGENASE- FMN-LINKED-RXN	+1*Aldehydes[c]+1*FMNH 2[c]+1*OXYGEN- MOLECULE[c]<-- >+1*Carboxylates[c]+1*FM N[c]+1*Light[c]+2*PROTO N[c]+1*WATER[c]	GCWI-2049 GCWI-2121 GCWI-3424
ALKAPHOSPHA-RXN	+1*Orthophosphoric- Monoesters[c]+1*WATER[ c]-- >+1*Alcohols[c]+1*Pi[c]	GCWI-3029 GCWI-4475
ALKAPHOSPHA-RXN- CPD-10815-WATER-- METOH-PI.26.	+1*METOH[c]+1*Pi[c]-- >+1*CPD- 10815[c]+1*WATER[c]	GCWI-3029 GCWI-4475

Name	Reaction	Locus
AMIDASE-RXN	+1*Monocarboxylic-Acid-Amides[c]+1*WATER[c]<- - >+1*AMMONIA[c]+1*Monocarboxylates[c]+1*PROTON[c]	GCWI-2029 GCWI-2171
AMINOGLYCOSIDE-N3-ACETYLTRANSFERASE-RXN	+1*ACETYL-COA[c]+1*Deoxystreptamine-Antib[c]<-->+1*CO-A[c]+1*N3-Acetal-deoxystreptamine-antib[c]	GCWI-2962
AMINOGLYCOSIDE-N3-ACETYLTRANSFERASE-RXN-GENTAMICIN-C-ACETYL-COA--N3-ACETYL GENTAMICIN-C-CO-A.52.	+1*CO-A[c]+1*N3-ACETYL GENTAMICIN-C[c]<-->+1*ACETYL-COA[c]+1*GENTAMICIN-C[c]	GCWI-2962
AMP-DEPHOSPHORYLATION-RXN	+1*AMP[c]+1*WATER[c]- - >+1*ADENOSINE[c]+1*Pi[c]	GCWI-2585 GCWI-2586 GCWI-2587 GCWI-3179 GCWI-4241
AMPSYN-RXN	+1*ADENYLOSUCC[c]-- >+1*AMP[c]+1*FUM[c]	GCWI-498
ANTHRANSYN-RXN	+1*CHORISMATE[c]+1*GLN[c]-- >+1*ANTHRANILATE[c]+1*GLT[c]+1*PROTON[c]+1*PYRUVATE[c]	GCWI-1409
ARGDECARBOX-RXN	+1*ARG[c]+1*PROTON[c] -- >+1*AGMATHINE[c]+1*CARBON-DIOXIDE[c]	GCWI-4106
ARGINASE-RXN	+1*ARG[c]+1*WATER[c]<-->+1*L-ORNITHINE[c]+1*UREA[c]	GCWI-356
ARGININE--TRNA-LIGASE-RXN	+1*ARG[c]+1*ARG-tRNAs[c]+1*ATP[c]+1*PROTON[c]-- >+1*AMP[c]+1*Charged-ARG-tRNAs[c]+1*PPI[c]	GCWI-2267 GCWI-5463
ARGSUCCINLYA-RXN	+1*L-ARGININO-SUCCINATE[c]<-->+1*ARG[c]+1*FUM[c]	GCWI-3582 GCWI-4759
ARGSUCCINSYN-RXN	+1*ATP[c]+1*L-	GCWI-4760

Name	Reaction	Locus
	ASPARTATE[c]+1*L-CITRULLINE[c]<-->+1*AMP[c]+1*L-ARGININO-SUCCINATE[c]+1*PPI[c]+1*PROTON[c]	
ARYLFORMAMIDASE-RXN	+1*N-FORMYLKYNURENINE[c]+1*WATER[c]<-->+1*FORMATE[c]+1*L-KYNURENINE[c]+3*PROTON[c]	GCWI-2807
ASNSYNA-RXN	+1*AMMONIA[c]+1*ATP[c]+1*L-ASPARTATE[c]<-->+1*AMP[c]+1*ASN[c]+1*PPI[c]	GCWI-1922
ASNSYNB-RXN	+1*ATP[c]+1*GLN[c]+1*L-ASPARTATE[c]+1*WATER[c]<-->+1*AMP[c]+1*ASN[c]+1*GLT[c]+1*PPI[c]+1*PROTON[c]	GCWI-1328 GCWI-1874 GCWI-2341 GCWI-1922
ASPAMINOTRANS-RXN	+1*L-ASPARTATE[c]+1*2-KETOGLUTARATE[c]<-->+1*GLT[c]+1*OXALACETIC-ACID[c]	GCWI-1706 GCWI-2940
ASPARAGHYD-RXN	+1*ASN[c]+1*WATER[c]<-->+1*AMMONIA[c]+1*L-ASPARTATE[c]+1*PROTON[c]	GCWI-1658 GCWI-3156
ASPARAGINE--TRNA-LIGASE-RXN	+1*ASN[c]+1*ASN-tRNAs[c]+1*ATP[c]+1*PROTON[c]<-->+1*AMP[c]+1*Charged-ASN-tRNAs[c]+1*PPI[c]	GCWI-4686
ASPARTASE-RXN	+1*L-ASPARTATE[c]<-->+1*AMMONIA[c]+1*FUUM[c]+1*PROTON[c]	GCWI-813 GCWI-1916 GCWI-3155
ASPARTATE--TRNA-LIGASE-RXN	+1*ASP-tRNAs[c]+1*ATP[c]+1*L-ASPARTATE[c]+1*PROTON[c]<-->+1*AMP[c]+1*Charged-	GCWI-2277 GCWI-4528



Name	Reaction	Locus
	ASP-tRNAs[c]+1*PPI[c]	
ASPARTATE-RACEMASE-RXN	+1*L-ASPARTATE[c]<-->+1*CPD-302[c]	GCWI-2313 GCWI-2701 GCWI-4879
ASPARTATE-SEMIALDEHYDE-DEHYDROGENASE-RXN	+1*L-BETA-ASPARTYL-P[c]+1*NADPH[c]+1*PROTON[c]<-->+1*L-ASPARTATE-SEMIALDEHYDE[c]+1*NADP[c]+1*Pi[c]	GCWI-2511 GCWI-3885
ASPARTATEKIN-RXN	+1*ATP[c]+1*L-ASPARTATE[c]<-->+1*ADP[c]+1*L-BETA-ASPARTYL-P[c]	GCWI-1925 GCWI-3884
ASPCARBTRANS-RXN	+1*CARBAMOYL-P[c]+1*L-ASPARTATE[c]<-->+1*CARBAMYUL-L-ASPARTATE[c]+1*PROTON[c]+1*Pi[c]	GCWI-3973
ASPDECARBOX-RXN	+1*L-ASPARTATE[c]+1*PROTON[c]<-->+1*B-ALANINE[c]+1*CARBONDIOXIDE[c]	GCWI-1703
ATPPHOSPHORIBOSYLTRANS-RXN	+1*ATP[c]+1*PRPP[c]<-->+1*PHOSPHORIBOSYL-ATP[c]+1*PPI[c]	GCWI-1567 GCWI-1568
ATPSYN-RXN	+1*ATP[c]+3*PROTON[c]+1*WATER[c]<-->+1*ADP[c]+4*PROTON[c]+1*Pi[c]	GCWI-1159 GCWI-3410 GCWI-4891 GCWI-5412 GCWI-1813 GCWI-5408 GCWI-5407 GCWI-5406 GCWI-5405 GCWI-5404 GCWI-3278 GCWI-5411 GCWI-5410 GCWI-5409
AZOBENZENE-REDUCTASE-RXN	+1*ANILINE[c]+1*CPD0-1148[c]+2*NADP[c]<-->+2*NADPH[c]+2*PROTON[c]+1*-4-DIMETHYLAMINOPHENYL-AZOBENZENE[c]	GCWI-2017 GCWI-2331 GCWI-2367 GCWI-5511
BETA-PHOSPHOGLUCOMUTASE-RXN	+1*CPD-448[c]<-->+1*GLC-6-P[c]	
BIOTIN-CARBOXYL-RXN	+1*ATP[c]+1*BCCP-dimers[c]+1*HCO3[c]<-->+1*ADP[c]+1*Carboxybio	GCWI-2613 GCWI-4320

Name	Reaction	Locus
	tin- BCCP[c]+1*PROTON[c]+1 *Pi[c]	
BIOTINLIG-RXN	+1*ATP[c]+1*BCCP- monomers[c]+1*BIOTIN[c] -->+1*AMP[c]+1*BCCP- biotin- monomers[c]+1*PPI[c]	GCWI-1699
BISPHOSPHOGLYCERAT E-MUTASE-RXN	+1*DPG[c]<-- >+1*PROTON[c]+1*-23- DIPHOSPHOGLYCERATE [c]	GCWI-2556 GCWI-5235
BRANCHED- CHAINAMINOTRANSFE RILEU-RXN	+1*ILE[c]+1*-2- KETOGLUTARATE[c]<-- >+1*GLT[c]+1*-2-KETO- 3-METHYL- VALERATE[c]	GCWI-1559 GCWI-1961
BRANCHED- CHAINAMINOTRANSFE RLEU-RXN	+1*GLT[c]+1*-2K-4CH3- PENTANOATE[c]-- >+1*LEU[c]+1*-2- KETOGLUTARATE[c]	GCWI-1559 GCWI-1961
BRANCHED- CHAINAMINOTRANSFE RVAL-RXN	+1*VAL[c]+1*-2- KETOGLUTARATE[c]<-- >+1*GLT[c]+1*-2-KETO- ISOVALERATE[c]	GCWI-1559 GCWI-1961
BTUR2-RXN	+1*ATP[c]+1*COBINAMI DE[c]<-- >+1*ADENOSYLCOBINA MIDE[c]+1*P3I[c]	GCWI-1640
BUTYRATE-KINASE- RXN	+1*ADP[c]+1*BUTYRYL- P[c]-- >+1*ATP[c]+1*BUTYRIC- ACID[c]	GCWI-4301
CARBODEHYDRAT-RXN	+1*H2CO3[c]<-- >+1*CARBON- DIOXIDE[c]+1*WATER[c]	GCWI-4918
CARBOXYLESTERASE- RXN	+1*Carboxylic- esters[c]+1*WATER[c]<-- >+1*Alcohols[c]+1*Carbox ylates[c]+1*PROTON[c]	GCWI-2779 GCWI-5207
CARBPSYN-RXN	+2*ATP[c]+1*GLN[c]+1*H CO3[c]+1*WATER[c]-- >+2*ADP[c]+1*CARBAM OYL- P[c]+1*GLT[c]+2*PROTO	GCWI-3970 GCWI-3971

Name	Reaction	Locus
	N[c]+1*Pi[c]	
CARDIOLIPSYN-RXN-CPD-8260--CPD-12824-GLYCEROL.29.	+2*CPD-8260[c]<-->+1*CPD-12824[c]+1*GLYCEROL[c]	GCWI-829 GCWI-1366
CATAL-RXN	+2*HYDROGEN-PEROXIDE[c]<-->+1*OXYGEN-MOLECULE[c]+2*WATER[c]	GCWI-1061 GCWI-1330 GCWI-3056 GCWI-3180
CDPDIGLYSYN-RXN-CTP-CPD0-1422-PROTON-CPD-12815-PPI.36.	+1*CPD0-1422[c]+1*CTP[c]+1*PROTON[c]<-->+1*CPD-12815[c]+1*PPI[c]	GCWI-3906
CDPDIGLYSYN-RXN-CTP-CPD0-1423-PROTON-CPD-12814-PPI.36.	+1*CPD0-1423[c]+1*CTP[c]+1*PROTON[c]<-->+1*CPD-12814[c]+1*PPI[c]	GCWI-3906
CDPKIN-RXN	+1*ATP[c]+1*CDP[c]<-->+1*ADP[c]+1*CTP[c]	GCWI-1677
CDPREDUCT-RXN	+1*CDP[c]+1*Reduced-Thioredoxin[c]<-->+1*DCDP[c]+1*Oxidized-Thioredoxin[c]+1*WATER[c]	GCWI-1521 GCWI-1519 GCWI-1522
CHLORAMPHENICOL-O-ACETYLTRANSFERASE-RXN	+1*ACETYL-COA[c]+1*CHLORAMPHENICOL[c]<-->+1*CHLORAMPHENICOL-3-ACETATE[c]+1*COA[c]	GCWI-2489
CHOLLOYLGLYCINE-HYDROLASE-RXN	+1*GLYCOCHOLIC-ACID[c]+1*WATER[c]<-->+1*CHOLATE[c]+1*GLYCEROL[c]	GCWI-3303 GCWI-3846
CHORISMATE-SYNTHASE-RXN	+1*-3-ENOLPYRUVYL-SHIKIMATE-5P[c]<-->+1*CHORISMATE[c]+1*Pi[c]	GCWI-1678 GCWI-2987
CHORISMATEMUT-RXN	+1*CHORISMATE[c]<-->+1*PREPHENATE[c]	GCWI-2988
CITSYN-RXN	+1*ACETYL-COA[c]+1*OXALACETIC-ACID[c]+1*WATER[c]<-->+1*CIT[c]+1*COA[c]+1*PROTON[c]	GCWI-2432 GCWI-4721

Name	Reaction	Locus
CMPKI-RXN	+1*ATP[c]+1*CMP[c]-->+1*ADP[c]+1*CDP[c]	GCWI-1659
COBALADENOSYLTRANS-RXN	+1*ATP[c]+1*COB-I-ALAMIN[c]<-->+1*ADENOSYLCOBALAMIN[c]+1*P3I[c]	GCWI-1640
CTPSYN-RXN	+1*ATP[c]+1*GLN[c]+1*UTP[c]+1*WATER[c]-->+1*ADP[c]+1*CTP[c]+1*GLT[c]+2*PROTON[c]+1*Pi[c]	GCWI-5437
CYCPHOSDIESTER-RXN	+1*Cyclic-2-3-Ribonucleoside-Monophosphates[c]+1*WATER[c]-->+1*PROTON[c]+1*-3-Prime-Ribonucleoside-Monophosphates[c]	GCWI-4263
CYCPHOSDIESTER-RXN-CPD-3707-WATER--CPD-3706-PROTON.32.	+1*CPD-3707[c]+1*WATER[c]-->+1*CPD-3706[c]+1*PROTON[c]	GCWI-4263
CYCPHOSDIESTER-RXN-CPD-3709-WATER--CPD-3708-PROTON.32.	+1*CPD-3709[c]+1*WATER[c]-->+1*CPD-3708[c]+1*PROTON[c]	GCWI-4263
CYCPHOSDIESTER-RXN-CPD-3713-WATER--CPD-3711-PROTON.32.	+1*CPD-3713[c]+1*WATER[c]-->+1*CPD-3711[c]+1*PROTON[c]	GCWI-4263
CYCPHOSDIESTER-RXN-CPD-3725-WATER--CPD-3724-PROTON.32.	+1*CPD-3725[c]+1*WATER[c]-->+1*CPD-3724[c]+1*PROTON[c]	GCWI-4263
CYSPH-RXN	+1*CYS[c]+1*O-PHOSPHO-L-HOMOSERINE[c]-->+1*L-CYSTATHIONINE[c]+1*Pi[c]	GCWI-4389
CYSTATHIONINE-BETALYASE-RXN	+1*L-CYSTATHIONINE[c]+1*WATER[c]-->+1*AMMONIA[c]+1*HOMO-CYS[c]+1*PROTON[c]+1*	GCWI-5029 GCWI-4390 GCWI-4499

Name	Reaction	Locus
	PYRUVATE[c]	
CYSTEINE--TRNA-LIGASE-RXN	+1*ATP[c]+1*CYS[c]+1*CYST- tRNAs[c]+1*PROTON[c]-- >+1*AMP[c]+1*Charged- CYS-tRNAs[c]+1*PPI[c]	GCWI-279
CYTIDEAM-RXN	+1*DEOXYCYTIDINE[c]+ 1*WATER[c]-- >+1*AMMONIA[c]+1*DE OXYURIDINE[c]	GCWI-2004 GCWI-3664 GCWI-4431
CYTIDEAM2-RXN	+1*CYTIDINE[c]+1*WAT ER[c]-- >+1*AMMONIA[c]+1*URI DINE[c]	GCWI-2004 GCWI-3664 GCWI-4431
CYTIDINEKIN-RXN	+1*CYTIDINE[c]+1*GTP[ c]-- >+1*CMP[c]+1*GDP[c]+1* PROTON[c]	GCWI-4507
CYTIKIN-RXN	+1*ATP[c]+1*CYTIDINE[ c]-- >+1*ADP[c]+1*CMP[c]+1* PROTON[c]	GCWI-4507
D-ALANINE-AMINOTRANSFERASE-RXN	+1*D-ALANINE[c]+1*-2- KETOGLUTARATE[c]<-- >+1*D- GLT[c]+1*PYRUVATE[c]	GCWI-2346 GCWI-5332
D-PPENTOMUT-RXN	+1*DEOXY-RIBOSE- 1P[c]<-->+1*DEOXY- RIBOSE-5P[c]	GCWI-4229
DADPKIN-RXN	+1*ATP[c]+1*DADP[c]-- >+1*ADP[c]+1*DATP[c]	GCWI-1677
DAHPSYN-RXN	+1*ERYTHROSE- 4P[c]+1*PHOSPHO-ENOL- PYRUVATE[c]+1*WATER [c]-->+1*Pi[c]+1*-3- DEOXY-D-ARABINO- HEPTULOSONATE-7-P[c]	GCWI-2988
DALADALALIG-RXN	+1*ATP[c]+2*D- ALANINE[c]-- >+1*ADP[c]+1*D-ALA-D- ALA[c]+1*PROTON[c]+1* Pi[c]	GCWI-431 GCWI-2677
DAPASYN-RXN	+1*S- ADENOSYLMETHIONIN E[c]+1*-8-AMINO-7-	GCWI-4260

Name	Reaction	Locus
	OXONONANOATE[c]-- >+1*DIAMINONONANO ATE[c]+1*S-ADENOSYL- 4-METHYLTHIO-2- OXOBUTANOATE[c]	
DCDPKIN-RXN	+1*ATP[c]+1*DCDP[c]-- >+1*ADP[c]+1*DCTP[c]	GCWI-1677
DCYSDESULF-RXN	+1*D- CYSTEINE[c]+1*WATER[ c]<-- >+1*AMMONIA[c]+1*HS[ c]+1*PROTON[c]+1*PYR UVATE[c]	GCWI-3244
DEOXYADENPHOSPHOR -RXN	+1*DEOXYADENOSINE[c ]+1*Pi[c]<-- >+1*ADENINE[c]+1*DEO XY-RIBOSE-1P[c]	GCWI-1624 GCWI-4228
DEOXYGUANOSINE- KINASE-RXN	+1*ATP[c]+1*DEOXYGU ANOSINE[c]-- >+1*ADP[c]+1*DGMP[c]+ 1*PROTON[c]	GCWI-199 GCWI-200
DEOXYGUANPHOSPHOR -RXN	+1*DEOXYGUANOSINE[ c]+1*Pi[c]<-->+1*DEOXY- RIBOSE- 1P[c]+1*GUANINE[c]	GCWI-1624 GCWI-4228
DEOXYINOPHOSPHOR- RXN	+1*DEOXYINOSINE[c]+1 *Pi[c]<-->+1*DEOXY- RIBOSE- 1P[c]+1*HYPOXANTHINE [c]	GCWI-1624 GCWI-4228
DEOXYRIBOSE-P-ALD- RXN	+1*DEOXY-RIBOSE- 5P[c]-- >+1*ACETALD[c]+1*GAP [c]	GCWI-2001
DEPHOSPHOCOAKIN- RXN	+1*ATP[c]+1*DEPHOSPH O-COA[c]-- >+1*ADP[c]+1*CO- A[c]+1*PROTON[c]	GCWI-4711
DETHIOBIOTIN-SYN- RXN	+1*ATP[c]+1*CARBON- DIOXIDE[c]+1*DIAMINO NONANOATE[c]-- >+1*ADP[c]+1*DETHIOBI OTIN[c]+3*PROTON[c]+1 *Pi[c]	GCWI-4259
DGDPKIN-RXN	+1*ATP[c]+1*DGDP[c]--	GCWI-1677

Name	Reaction	Locus
	>+1*ADP[c]+1*DGTP[c]	
DHBAMPLIG-RXN	+1*ATP[c]+1*PROTON[c] +1*-2-3- DIHYDROXYBENZOATE [c]<-->+1*CPD- 62[c]+1*PPI[c]	GCWI-2450
DHBDEHYD-RXN	+1*DIHYDRO-DIOH- BENZOATE[c]+1*NAD[c]- - >+1*NADH[c]+1*PROTO N[c]+1*-2-3- DIHYDROXYBENZOATE [c]	GCWI-2448
DHSHIKIMATE- DEHYDRO-RXN	+1*-3-DEHYDRO- SHIKIMATE[c]-- >+1*WATER[c]+1*-3-4- DIHYDROXYBENZOATE [c]	GCWI-2090
DIACYLGLYKIN-RXN	+1*ATP[c]+1*DIACYLGL YCEROL[c]<-- >+1*ADP[c]+1*L- PHOSPHATIDATE[c]+1*P ROTON[c]	GCWI-4432
DIACYLGLYKIN-RXN- ATP-CPD66-34--CPD0- 1422-ADP-PROTON.35.	+1*ATP[c]+1*CPD66- 34[c]<-- >+1*ADP[c]+1*CPD0- 1422[c]+1*PROTON[c]	GCWI-4432
DIAMACTRANS-RXN	+1*ACETYL- COA[c]+1*Aliphatic-Alpha- Omega-Diamines[c]<-- >+1*Aliphatic-N-Acetyl- Diamines[c]+1*CO- A[c]+1*PROTON[c]	GCWI-2127 GCWI-5196
DIAMACTRANS-RXN- CADAVERINE-ACETYL- COA--CPD-10194-CO-A- PROTON.45.	+1*CO-A[c]+1*CPD- 10194[c]+1*PROTON[c]<-- >+1*ACETYL- COA[c]+1*CADAVERINE[ c]	GCWI-2127 GCWI-5196
DIAMINOPIMDECARB- RXN	+1*MESO- DIAMINOPIMELATE[c]+1 *PROTON[c]-- >+1*CARBON- DIOXIDE[c]+1*LYS[c]	GCWI-1581
DIAMINOPIMEPIM-RXN	+1*LL- DIAMINOPIMELATE[c]--	GCWI-5059

Name	Reaction	Locus
	>+1*MESO-DIAMINOPIMELATE[c]	
DIHYDRODIPICSYN-RXN	+1*L-ASPARTATE-SEMIALDEHYDE[c]+1*PYRUVATE[c]-->+1*PROTON[c]+2*WATER[c]+1*-2-3-DIHYDRODIPICOLINATE[c]	GCWI-2882 GCWI-3883
DIHYDROFOLATEREDUCT-RXN	+1*DIHYDROFOLATE[c]+1*NADPH[c]+1*PROTON[c]-->+1*NADP[c]+1*THF[c]	GCWI-853 GCWI-2329
DIHYDROFOLATESYNTH-RXN	+1*ATP[c]+1*GLT[c]+1*-7-8-DIHYDROPTEROATE[c]-->+1*ADP[c]+1*DIHYDROFOLATE[c]+1*PROTON[c]+1*Pi[c]	GCWI-4584
DIHYDRONEOPTERIN-MONO-P-DEPHOS-RXN	+1*DIHYDRONEOPTERIN-P[c]+1*WATER[c]-->+1*DIHYDRO-NEOPTERIN[c]+1*Pi[c]	GCWI-3029 GCWI-4475
DIHYDROOROT-RXN	+1*CARBAMYUL-L-ASPARTATE[c]+1*PROTON[c]-->+1*DI-H-OROTATE[c]+1*WATER[c]	GCWI-3972 GCWI-4969
DIHYDROXYISOVALDEHYDRAT-RXN	+1*DIOH-ISOVALERATE[c]-->+1*WATER[c]+1*-2-KETO-ISOVALERATE[c]	GCWI-1965
DIHYDROXYISOVALDEHYDRAT-RXN-CPD-13357--2-KETO-ISOVALERATE-WATER.36.	+1*CPD-13357[c]-->+1*WATER[c]+1*-2-KETO-ISOVALERATE[c]	GCWI-1965
DIHYDROXYMETVALDEHYDRAT-RXN	+1*-1-KETO-2-METHYLVALERATE[c]-->+1*WATER[c]+1*-2-KETO-3-METHYL-VALERATE[c]	GCWI-1965
DIMETHUROPORDEHYDROG-RXN	+1*DIHYDROSIROHYDROCHLORIN[c]+1*NAD[c]-	GCWI-1589 GCWI-2239



Name	Reaction	Locus
	>+1*NADH[c]+2*PROTON[c]+1*SIROHYDROCHLORIN[c]	
DIOHBUTANONEPSYN-RXN	+1*RIBULOSE-5P[c]-->+1*DIHYDROXY-BUTANONE-P[c]+1*FORMATE[c]+1*PROTON[c]	GCWI-4252
DSERDEAM-RXN	+1*D-SERINE[c]-->+1*AMMONIA[c]+1*PROTON[c]+1*PYRUVATE[c]	GCWI-1902
DTDPDEHYDRHAMEPIM-RXN	+1*DTDP-DEOH-DEOXY-GLUCOSE[c]-->+1*DTDP-DEOH-DEOXY-MANNOSE[c]	GCWI-1390
DTDPDEHYRHAMREDUCT-RXN	+1*DTDP-DEOH-DEOXY-MANNOSE[c]+1*NADPH[c]+1*PROTON[c]-->+1*DTDP-RHAMNOSE[c]+1*NADP[c]	GCWI-1392
DTDPGLUCDEHYDRAT-RXN	+1*DTDP-D-GLUCOSE[c]-->+1*DTDP-DEOH-DEOXY-GLUCOSE[c]+1*WATER[c]	GCWI-1391
DTDPGLUCOSEPP-RXN	+1*GLC-1-P[c]+1*PROTON[c]+1*TTP[c]<-->+1*DTDP-D-GLUCOSE[c]+1*PPI[c]	GCWI-1389
DTDPKIN-RXN	+1*ATP[c]+1*TDP[c]-->+1*ADP[c]+1*TTP[c]	GCWI-1677
DTMPKI-RXN	+1*ATP[c]+1*TMP[c]-->+1*ADP[c]+1*TDP[c]	GCWI-215
DUDPKIN-RXN	+1*ATP[c]+1*DUDP[c]-->+1*ADP[c]+1*DUTP[c]	GCWI-1677
DURIDKI-RXN	+1*ATP[c]+1*DEOXYURIDINE[c]-->+1*ADP[c]+1*DUMP[c]+1*PROTON[c]	GCWI-5429
DUTP-PYROP-RXN	+1*DUTP[c]+1*WATER[c]-->+1*DUMP[c]+1*PPI[c]+1*PROTON[c]	GCWI-4053

Name	Reaction	Locus
DXPREDISOM-RXN	+1*DEOXYXYLULOSE-5P[c]+1*NADPH[c]+1*PROTON[c]-->+1*NADP[c]+1*-2-C-METHYL-D-ERYTHRITOL-4-PHOSPHATE[c]	GCWI-3399 GCWI-3905
DXS-RXN	+1*GAP[c]+1*PROTON[c]+1*PYRUVATE[c]-->+1*CARBONDIOXIDE[c]+1*DEOXYXYLULOSE-5P[c]	GCWI-4313
ENOYL-ACP-REDUCT-NADPH-RXN-PALMITOYL-ACPS-NADP--NADPH-2-HEXADECENOYL-ACPS-PROTON.54.	+1*NADPH[c]+1*PROTON[c]+1*-2-Hexadecenoyl-ACPs[c]-->+1*NADP[c]+1*Palmitoyl-ACPs[c]	GCWI-1393
ENOYL-COA-HYDRAT-RXN-CPD0-2107--CPD-7222-WATER.26.	+1*CPD-7222[c]+1*WATER[c]-->+1*CPD0-2107[c]	GCWI-1106 GCWI-2616 GCWI-3561 GCWI-4652 GCWI-2439
ENOYL-COA-HYDRAT-RXN-CPD0-2171--CPD0-2120-WATER.27.	+1*CPD0-2120[c]+1*WATER[c]-->+1*CPD0-2171[c]	GCWI-1106 GCWI-2616 GCWI-3561 GCWI-4652 GCWI-2439
ENOYL-COA-HYDRAT-RXN-CPD0-2224--CPD0-2108-WATER.27.	+1*CPD0-2108[c]+1*WATER[c]-->+1*CPD0-2224[c]	GCWI-1106 GCWI-2616 GCWI-3561 GCWI-4652 GCWI-2439
ENOYL-COA-HYDRAT-RXN-CPD0-2232--CPD0-2117-WATER.27.	+1*CPD0-2117[c]+1*WATER[c]-->+1*CPD0-2232[c]	GCWI-1106 GCWI-2616 GCWI-3561 GCWI-4652 GCWI-2439
ENOYL-COA-HYDRAT-RXN-CPD0-2244--T2-DECENOYL-COA-WATER.33.	+1*T2-DECENOYL-COA[c]+1*WATER[c]-->+1*CPD0-2244[c]	GCWI-1106 GCWI-2616 GCWI-3561 GCWI-4652 GCWI-2439
ENOYL-COA-HYDRAT-RXN-CPD0-2253--CPD-10262-WATER.27.	+1*CPD-10262[c]+1*WATER[c]-->+1*CPD0-2253[c]	GCWI-1106 GCWI-2616 GCWI-3561 GCWI-4652 GCWI-2439
ENOYL-COA-HYDRAT-RXN-OH-HEXANOYL-COA--CPD0-2121-WATER.33.	+1*CPD0-2121[c]+1*WATER[c]-->+1*OH-HEXANOYL-COA[c]	GCWI-1106 GCWI-2616 GCWI-3561 GCWI-4652 GCWI-2439
ENZRXN-161-RXN	+1*BUTANOL[c]+1*NAD[c]<-->+1*BUTANAL[c]+1*NAHDH[c]+1*PROTON[c]	GCWI-2357 GCWI-4498 GCWI-379 GCWI-878 GCWI-1005 GCWI-1195 GCWI-2654 GCWI-2708

Name	Reaction	Locus
		GCWI-3152 GCWI-3423 GCWI-3425 GCWI-3545
F16ALDOLASE-RXN	+1*FRUCTOSE-16-DIPHOSPHATE[c]<-->+1*DIHYDROXY-ACETONE-PHOSPHATE[c]+1*GAP[c]	GCWI-3011 GCWI-2580 GCWI-5434
F16BDEPHOS-RXN	+1*FRUCTOSE-16-DIPHOSPHATE[c]+1*WATER[c]<-->+1*FRUCTOSE-6P[c]+1*Pi[c]	GCWI-5083 GCWI-5432
FABAUNSATDEHYDR-RXN	+1*Beta-hydroxydecanoyl-ACPs[c]<-->+1*Trans-D2-decenoyl-ACPs[c]+1*WATER[c]	GCWI-2941 GCWI-5366
FADSYN-RXN	+1*ATP[c]+1*FMN[c]+2*P ROTON[c]<-->+1*FAD[c]+1*PPI[c]	GCWI-3893
FGAMSYN-RXN	+1*ATP[c]+1*GLN[c]+1* WATER[c]+1*-5-P- RIBOSYL-N- FORMYLGLYCINEAMID E[c]<-->+1*ADP[c]+1*GLT[c]+1* PROTON[c]+1*Pi[c]+1*-5- PHOSPHORIBOSYL-N- FORMYLGLYCINEAMIDI NE[c]	GCWI-502 GCWI-501 GCWI-500
FLAVONADPREDUCT-RXN	+1*NADP[c]+1*Reduced- flavodoxins[c]<-->+1*NADPH[c]+1*Oxidize d- flavodoxins[c]+1*PROTON [c]	GCWI-5050 GCWI-558
FMNREDUCT-RXN	+1*FMN[c]+1*NADH[c]+2 *PROTON[c]<-->+1*FMNH2[c]+1*NAD[c]	GCWI-1778 GCWI-3373 GCWI-5277
FORMAMIDASE-RXN	+1*FORMAMIDE[c]+1*W ATER[c]<-->+1*AMMONIA[c]+1*FO RMATE[c]+1*PROTON[c]	GCWI-4083
FORMATETHFLIG-RXN	+1*ATP[c]+1*FORMATE[ c]+1*THF[c]<-->+1*ADP[c]+1*Pi[c]+1*- 10-FORMYL-THF[c]	GCWI-2205

Name	Reaction	Locus
FORMIMINOGLUTAMASE-RXN	+1*N-FORMIMINO-L-GLUTAMATE[c]+1*WATER[c]-->+1*FORMAMIDE[c]+1*GLT[c]	GCWI-3677
FPPSYN-RXN	+1*DELTA3-ISOPENTENYL-PP[c]+1*GERANYL-PP[c]->+1*FARNESYL-PP[c]+1*PPI[c]	GCWI-4314
FRUCTOKINASE-RXN	+1*ATP[c]+1*BETA-D-FRUCTOSE[c]-->+1*ADP[c]+1*FRUCTOSE-6P[c]+1*PROTON[c]	GCWI-974
FUCPALDOL-RXN	+1*FUCULOSE-1P[c]<-->+1*DIHYDROXY-ACETONE-PHOSPHATE[c]+1*LACTALD[c]	GCWI-554
FUMARYLACETOACETASE-RXN	+1*WATER[c]+1*-4-FUMARYL-ACETOACETATE[c]-->+1*FUM[c]+1*PROTON[c]+1*-3-KETOBUTYRATE[c]	GCWI-428 GCWI-1323
FUMHYDR-RXN	+1*MAL[c]<-->+1*FUM[c]+1*WATER[c]	GCWI-631 GCWI-1886
GABATRANSAM-RXN	+1*-2-KETOGLUTARATE[c]+1*-4-AMINO-BUTYRATE[c]-->+1*GLT[c]+1*SUC-S-ALD[c]	GCWI-531
GAPOXNPHOSPHN-RXN	+1*GAP[c]+1*NAD[c]+1*Pi[c]<-->+1*DPG[c]+1*NADH[c]+1*PROTON[c]	GCWI-4710 GCWI-5238
GART-RXN	+1*-10-FORMYL-THF[c]+1*-5-PHOSPHO-RIBOSYL-GLYCINEAMIDE[c]-->+1*PROTON[c]+1*THF[c]+1*-5-P-RIBOSYL-N-FORMYLGLYCINEAMID	GCWI-505

Name	Reaction	Locus
	E[c]	
GARTRANSFORMYL2-RXN	+1*ATP[c]+1*FORMATE[c]+1*-5-PHOSPHO-RIBOSYL-GLYCINEAMIDE[c]-->+1*ADP[c]+1*PROTON[c]+1*Pi[c]+1*-5-P-RIBOSYL-N-FORMYLGLYCINEAMIDE[c]	GCWI-505
GCVMULTI-RXN	+1*GLY[c]+1*NAD[c]+1*THF[c]-->+1*AMMONIA[c]+1*CARBONDIOXIDE[c]+1*METHYLENE-THF[c]+1*NADH[c]+1*PROTON[c]	GCWI-4362
GCVP-RXN	+1*GLY[c]+1*PROTEIN-LIPOYLLYSINE[c]-->+1*AMINOMETHYLDIHYDROLIPOYL-GCVH[c]+1*CARBONDIOXIDE[c]	GCWI-4362 GCWI-4360 GCWI-4361
GCVT-RXN	+1*AMINOMETHYLDIHYDROLIPOYL-GCVH[c]+1*THF[c]-->+1*AMMONIA[c]+1*DIHYDROLIPOYL-GCVH[c]+1*METHYLENE-THF[c]	GCWI-4362
GDPKIN-RXN	+1*ATP[c]+1*GDP[c]-->+1*ADP[c]+1*GTP[c]	GCWI-1677
GDPREDUCT-RXN	+1*GDP[c]+1*Red-Thioredoxin[c]-->+1*DGDP[c]+1*Ox-Thioredoxin[c]+1*WATER[c]	GCWI-1519 GCWI-1521 GCWI-1521 GCWI-1519 GCWI-1522
GLU6PDEHYDROG-RXN	+1*GLC-6-P[c]+1*NADP[c]-->+1*D-6-P-GLUCONO-DELTA-LACTONE[c]+1*NADPH[c]+1*PROTON[c]	GCWI-975
GLUC1PADENYLTRANS-RXN	+1*ATP[c]+1*GLC-1-P[c]+1*PROTON[c]<--	GCWI-4989

Name	Reaction	Locus
	>+1*ADP-D- GLUCOSE[c]+1*PPI[c]	
GLUC1PURIDYLTRANS- RXN	+1*GLC-1- P[c]+1*PROTON[c]+1*UT P[c]<-->+1*PPI[c]+1*UDP- GLUCOSE[c]	GCWI-5042
GLUCOKIN-RXN	+1*ALPHA- GLUCOSE[c]+1*ATP[c]-- >+1*ADP[c]+1*ALPHA- GLC-6-P[c]+1*PROTON[c]	GCWI-4396
GLUCONOKIN-RXN	+1*ATP[c]+1*GLUCONA TE[c]-- >+1*ADP[c]+1*CPD- 2961[c]+1*PROTON[c]	GCWI-364 GCWI-365 GCWI-3416
GLUCOSAMINE-6-P- DEAMIN-RXN	+1*D-GLUCOSAMINE-6- P[c]+1*WATER[c]-- >+1*AMMONIA[c]+1*FR UCTOSE- 6P[c]+1*PROTON[c]	GCWI-4196
GLURS-RXN	+1*ATP[c]+1*GLT[c]+1*G LT- tRNAs[c]+1*PROTON[c]-- >+1*AMP[c]+1*Charged- GLT-tRNAs[c]+1*PPI[c]	GCWI-277
GLUTAMATE- DEHYDROGENASE-RXN	+1*GLT[c]+1*NAD[c]+1* WATER[c]-- >+1*AMMONIA[c]+1*NA DH[c]+2*PROTON[c]+1*- 2-KETOGLUTARATE[c]	GCWI-1653
GLUTAMATE-N- ACETYLTRANSFERASE- RXN	+1*GLT[c]+1*N-ALPHA- ACETYLORNITHINE[c]-- >+1*ACETYL- GLU[c]+1*L- ORNITHINE[c]	GCWI-4271
GLUTAMATESYN-RXN	+1*GLN[c]+1*NADPH[c]+ 1*PROTON[c]+1*-2- KETOGLUTARATE[c]-- >+2*GLT[c]+1*NADP[c]	GCWI-719
GLUTAMIDOTRANS- RXN	+1*GLN[c]+1*PHOSPHOR IBULOSYL-FORMIMINO- AICAR-P[c]-- >+1*AICAR[c]+1*D- ERYTHRO-IMIDAZOLE- GLYCEROL- P[c]+1*GLT[c]+1*PROTO	GCWI-1571 GCWI-1573

Name	Reaction	Locus
	N[c]	
GLUTAMIN-RXN	+1*GLN[c]+1*WATER[c]- ->+1*AMMONIA[c]+1*GLT[c]+1*PROTON[c]	GCWI-719 GCWI-692 GCWI-3172
GLUTAMINESYN-RXN	+1*AMMONIA[c]+1*ATP[c]+1*GLT[c]-- >+1*ADP[c]+1*GLN[c]+1*Pi[c]	GCWI-3785
GLUTATHIONE-PEROXIDASE-RXN	+2*GLUTATHIONE[c]+1*HYDROGEN-PEROXIDE[c]-- >+1*OXIDIZED-GLUTATHIONE[c]+2*WATER[c]	GCWI-2217
GLUTKIN-RXN	+1*ATP[c]+1*GLT[c]-- >+1*ADP[c]+1*L-GLUTAMATE-5-P[c]	GCWI-3022
GLUTRACE-RXN	+1*GLT[c]-->+1*D-GLT[c]	GCWI-1064 GCWI-4611
GLUTRNAREDUCT-RXN	+1*Charged-GLT-tRNAs[c]+1*NADPH[c]-- >+1*GLT-tRNAs[c]+1*GLUTAMATE-1-SEMIALDEHYDE[c]+1*NADP[c]	GCWI-4593
GLUTSEMIALDEHYDROG-RXN	+1*L-GLUTAMATE-5-P[c]+1*NADPH[c]+1*PROTON[c]-->+1*L-GLUTAMATE-GAMMA-SEMIALDEHYDE[c]+1*NADP[c]+1*Pi[c]	GCWI-3021
GLY3KIN-RXN	+1*ATP[c]+1*GLYCERATE[c]-- >+1*ADP[c]+1*G3P[c]+1*PROTON[c]	
GLYCEROL-KIN-RXN	+1*ATP[c]+1*GLYCEROL[c]-- >+1*ADP[c]+1*GLYCEROL-3P[c]+1*PROTON[c]	GCWI-1216
GLYCERONE-KINASE-RXN	+1*ATP[c]+1*DIHYDROXYACETONE[c]<-- >+1*ADP[c]+1*DIHYDROXY-ACETONE-PHOSPHATE[c]+1*PROT	GCWI-1164

Name	Reaction	Locus
	ON[c]	
GLYCINE--TRNA-LIGASE-RXN	+1*ATP[c]+1*GLY[c]+1*GLY-tRNAs[c]+1*PROTON[c]>+1*AMP[c]+1*Charged-GLY-tRNAs[c]+1*PPI[c]	GCWI-5037
GLYCOGEN-BRANCH-RXN	+1*-1-4-alpha-D-Glucan[c]>+1*Glycogens[c]	GCWI-4990
GLYCOGENSYN-RXN	+1*ADP-D-GLUCOSE[c]>+1*ADP[c]+1*-1-4-alpha-D-Glucan[c]	GCWI-4987
GLYCOLALD-DEHYDROG-RXN	+1*GLYCOLALDEHYDE[c]+1*NAD[c]+1*WATER[c]>+1*GLYCOLLATE[c]+1*NADH[c]+2*PROTON[c]	
GLYCOPHOSPHORYL-RXN	+1*Glycogens[c]+1*Pi[c]>+1*GLC-1-P[c]	GCWI-4986
GLYCPDIESTER-RXN	+1*Glycerophosphodiester[c]+1*WATER[c]>+1*Alcohols[c]+1*GLYCEROL-3P[c]+1*PROTON[c]	GCWI-5472 GCWI-4306 GCWI-797 GCWI-3539 GCWI-2726
GLYCPDIESTER-RXN-GLYCEROPHOSPHOGLYCEROL-WATER--GLYCEROL-GLYCEROL-3P-PROTON.58.	+1*GLYCEROL[c]+1*GLYCEROL-3P[c]+1*PROTON[c]>+1*GLYCEROPHOSPHOGLYCEROL[c]+1*WATER[c]	GCWI-5472 GCWI-4306 GCWI-797 GCWI-3539 GCWI-2726
GLYMALTOPHOSPHORYL-RXN	+1*Glycogens[c]+1*Pi[c]>+1*GLC-1-P[c]+1*MALTOTETRAOSE[c]	GCWI-4986
GLYOHMETRANS-RXN	+1*SER[c]+1*THF[c]>+1*GLY[c]+1*METHYLENE-THF[c]+1*WATER[c]	GCWI-5415
GLYRIBONUCSYN-RXN	+1*ATP[c]+1*GLY[c]+1*-5-P-BETA-D-RIBOSYL-AMINE[c]>+1*ADP[c]+1*PROTON[c]+1*Pi[c]+1*-5-PHOSPHO-RIBOSYL-GLYCINEAMIDE[c]	GCWI-507
GMKALT-RXN	+1*ATP[c]+1*DGMP[c]>+1*ADP[c]+1*DGDP[c]	GCWI-3955



Name	Reaction	Locus
GMP-REDUCT-RXN	+1*GMP[c]+1*NADPH[c]+ 1*PROTON[c]-- >+1*AMMONIA[c]+1*IMP [c]+1*NADP[c]	GCWI-5557
GMP-SYN-GLUT-RXN	+1*ATP[c]+1*GLN[c]+1* WATER[c]+1*XANTHOSI NE-5-PHOSPHATE[c]-- >+1*AMP[c]+1*GLT[c]+1* GMP[c]+1*PPI[c]+2*PROT ON[c]	GCWI-470
GMP-SYN-NH3-RXN	+1*AMMONIA[c]+1*ATP[ c]+1*XANTHOSINE-5- PHOSPHATE[c]-- >+1*AMP[c]+1*GMP[c]+1 *PPI[c]+1*PROTON[c]	GCWI-470
GPPSYN-RXN	+1*CPD- 4211[c]+1*DELTA3- ISOPENTENYL-PP[c]-- >+1*GERANYL- PP[c]+1*PPI[c]	GCWI-4314
GSAAMINOTRANS-RXN	+1*GLUTAMATE-1- SEMIALDEHYDE[c]-- >+1*-5-AMINO- LEVULINATE[c]	GCWI-720 GCWI-4588
GSPSYN-RXN	+1*ATP[c]+1*GLUTATHI ONE[c]+1*SPERMIDINE[c ]-- >+1*ADP[c]+1*GLUTATH IONYLSPERMIDINE[c]+1 *PROTON[c]+1*Pi[c]	GCWI-2964
GTP-CYCLOHYDRO-I- RXN	+1*GTP[c]+1*WATER[c]-- >+1*DIHYDRONEOPTERI N- P3[c]+1*FORMATE[c]+1* PROTON[c]	GCWI-1673
GTP-CYCLOHYDRO-II- RXN	+1*GTP[c]+3*WATER[c]-- >+1*DIAMINO-OH- PHOSPHORIBOSYLAMIN O- PYR[c]+1*FORMATE[c]+1 *PPI[c]+2*PROTON[c]	GCWI-4252
GTPPYPHOSKIN-RXN	+1*ATP[c]+1*GTP[c]-- >+1*AMP[c]+1*GDP-TP[c]	GCWI-4532
GUANIDINOBUTANAMI DE-NH3-RXN	+1*WATER[c]+1*-4- GUANIDO-	GCWI-2029 GCWI-2171

Name	Reaction	Locus
	BUTYRAMIDE[c]<-->+1*AMMONIA[c]+1*CPD-592[c]+1*PROTON[c]	
GUANPRIBOSYLTRAN-RXN	+1*GUANINE[c]+1*PRPP[c]<-->+1*GMP[c]+1*PPI[c]	GCWI-251 GCWI-4941 GCWI-1727
GUANYL-KIN-RXN	+1*ATP[c]+1*GMP[c]<-->+1*ADP[c]+1*GDP[c]	GCWI-3955
H2NEOPTERINALDOL-RXN	+1*DIHYDRO-NEOPTERIN[c]<-->+1*AMINO-OH-HYDROXYMETHYL-DIHYDROPTERIDINE[c]+1*GLYCOLALDEHYDE[c]	GCWI-260
H2NEOPTERINP3PYROPHOSPHOHYDRO-RXN	+1*DIHYDRONEOPTERIN-P3[c]+1*WATER[c]<-->+1*DIHYDRONEOPTERIN-P[c]+1*PPI[c]+1*PROTON[c]	GCWI-3029 GCWI-4475
H2PTERIDINEPYROPHOSPHOKIN-RXN	+1*AMINO-OH-HYDROXYMETHYL-DIHYDROPTERIDINE[c]+1*ATP[c]<-->+1*AMP[c]+1*DIHYDROPTERIN-CH2OH-PP[c]+1*PROTON[c]	GCWI-261
H2PTEROATESYNTH-RXN	+1*DIHYDROPTERIN-CH2OH-PP[c]+1*P-AMINO-BENZOATE[c]<-->+1*PPI[c]+1*-7-8-DIHYDROPTEROATE[c]	GCWI-259
HEME-OXYGENASE-DECYCLIZING-RXN	+3*Donor-H2[c]+3*OXYGEN-MOLECULE[c]+1*PROTOHEME[c]+2*PROTON[c]<-->+3*Acceptor[c]+1*BILIVERDINE[c]+1*CARBON-MONOXIDE[c]+1*FE-2[c]+3*WATER[c]	GCWI-4669
HEMEOSYN-RXN	+1*FARNESYL-PP[c]+1*PROTOHEME[c]+1*WATER[c]<-->+1*HEME-O[c]+1*PPI[c]	GCWI-4089
HEMN-RXN	+1*COPROPORPHYRINOGEN-III[c]+2*S-	GCWI-1089 GCWI-4447

Name	Reaction	Locus
	ADENOSYLMETHIONIN E[c]-->+2*CARBON- DIOXIDE[c]+2*CH33ADO [c]+2*MET[c]+1*PROTOP ORPHYRINOGEN[c]	
HEXOKINASE-RXN	+1*ATP[c]+1*D- Hexoses[c]<-- >+1*ADP[c]+1*D- HEXOSE-6- PHOSPHATE[c]+1*PROT ON[c]	GCWI-4396
HISTALDEHYD-RXN	+1*HISTIDINAL[c]+1*NA D[c]+1*WATER[c]-- >+1*HIS[c]+1*NADH[c]+2 *PROTON[c]	GCWI-1569
HISTAMINOTRANS-RXN	+1*GLT[c]+1*IMIDAZOL E-ACETOL-P[c]-->+1*L- HISTIDINOL-P[c]+1*-2- KETOGLUTARATE[c]	GCWI-1680 GCWI-2986
HISTCYCLOHYD-RXN	+1*PHOSPHORIBOSYL- AMP[c]+1*WATER[c]-- >+1*PHOSPHORIBOSYL- FORMIMINO-AICAR-P[c]	GCWI-1574
HISTIDINE--TRNA- LIGASE-RXN	+1*ATP[c]+1*HIS[c]+1*HI S- tRNAs[c]+1*PROTON[c]-- >+1*AMP[c]+1*Charged- HIS-tRNAs[c]+1*PPI[c]	GCWI-3369 GCWI-4529
HISTIDINE-AMMONIA- LYASE-RXN	+1*HIS[c]-- >+1*AMMONIA[c]+1*PR OTON[c]+1*UROCANATE [c]	GCWI-3680
HISTIDPHOS-RXN	+1*L-HISTIDINOL- P[c]+1*WATER[c]-- >+1*HISTIDINOL[c]+1*Pi [c]	GCWI-1576
HISTOLDEHYD-RXN	+1*HISTIDINOL[c]+1*NA D[c]-- >+1*HISTIDINAL[c]+1*N ADH[c]+1*PROTON[c]	GCWI-1569
HISTPRATPHYD-RXN	+1*PHOSPHORIBOSYL- ATP[c]+1*WATER[c]-- >+1*PHOSPHORIBOSYL- AMP[c]+1*PPI[c]+1*PROT ON[c]	GCWI-1575

Name	Reaction	Locus
HOLO-ACP-SYNTH-RXN	+1*CO-A[c]+1*apo-ACP[c]-->+1*ACP[c]+1*3-5-ADP[c]	GCWI-437 GCWI-2455
HOMOCYSMET-RXN	+1*CPD-1302[c]+1*HOMO-CYS[c]->+1*CPD-1301[c]+1*MET[c]	GCWI-4144
HOMOCYSMETB12-RXN	+1*HOMO-CYS[c]+1*-5-METHYL-THF[c]-->+1*MET[c]+1*THF[c]	GCWI-4387
HOMOCYSTEINE-S-METHYLTRANSFERASE-RXN	+1*HOMO-CYS[c]+1*S-ADENOSYLMETHIONINE[c]-->+1*ADENOSYL-HOMO-CYS[c]+1*MET[c]+1*PROTON[c]	GCWI-4388
HOMOGENTISATE-12-DIOXYGENASE-RXN	+1*HOMOGENTISATE[c]+1*OXYGEN-MOLECULE[c]<-->+1*PROTON[c]+1*-4-MALEYL-ACETOACETATE[c]	GCWI-429
HOMOSERINE-O-ACETYLTRANSFERASE-RXN	+1*ACETYL-COA[c]+1*HOMO-SER[c]->+1*CO-A[c]+1*CPD-667[c]	GCWI-4859
HOMOSERKIN-RXN	+1*ATP[c]+1*HOMO-SER[c]-->+1*ADP[c]+1*O-PHOSPHO-L-HOMOSERINE[c]+1*PROTON[c]	GCWI-2074
HOMSUCTRAN-RXN	+1*HOMO-SER[c]+1*SUC-COA[c]-->+1*CO-A[c]+1*O-SUCCINYL-L-HOMOSERINE[c]	GCWI-5506
HYDROXYLAMINE-REDUCTASE-RXN	+1*FADH2[c]+1*HYDROXYLAMINE[c]-->+1*AMMONIA[c]+1*FAD[c]+1*WATER[c]	GCWI-3482
HYDROXYMETHYLGLUTARYL-COA-LYASE-RXN	+1*-3-HYDROXY-3-METHYL-GLUTARYL-COA[c]-->+1*ACETYL-COA[c]+1*-3-KETOBUTYRATE[c]	GCWI-2615

Name	Reaction	Locus
HYDROXYPYRROLINED EH-RXN	+1*NAD[c]+1*PYRROLIN E-HYDROXY- CARBOXYLATE[c]+2*W ATER[c]<-->+1*L- ERYTHRO-4-HYDROXY- GLUTAMATE[c]+1*NAD H[c]+1*PROTON[c]	GCWI-516
HYPOXANPRIBOSYLTR AN-RXN	+1*HYPOXANTHINE[c]+ 1*PRPP[c]-- >+1*IMP[c]+1*PPI[c]	GCWI-251 GCWI-4941 GCWI-1727
IGPSYN-RXN	+1*CARBOXYPHENYLA MINO- DEOXYRIBULOSE- P[c]+1*PROTON[c]-- >+1*CARBON- DIOXIDE[c]+1*INDOLE- 3-GLYCEROL- P[c]+1*WATER[c]	GCWI-1412
IMIDAZOLONEPROPION ASE-RXN	+1*PROTON[c]+1*WATE R[c]+1*-4- IMIDAZOLONE-5- PROPIONATE[c]-->+1*N- FORMIMINO-L- GLUTAMATE[c]	GCWI-3678
IMIDPHOSDEHYD-RXN	+1*D-ERYTHRO- IMIDAZOLE-GLYCEROL- P[c]-->+1*IMIDAZOLE- ACETOL- P[c]+1*WATER[c]	GCWI-1570
IMP-DEHYDROG-RXN	+1*IMP[c]+1*NAD[c]+1* WATER[c]-- >+1*NADH[c]+1*PROTO N[c]+1*XANTHOSINE-5- PHOSPHATE[c]	GCWI-192
IMPCYCLOHYDROLASE- RXN	+1*PHOSPHORIBOSYL- FORMAMIDO- CARBOXAMIDE[c]<-- >+1*IMP[c]+1*WATER[c]	GCWI-506
INOPHOSPHOR-RXN	+1*INOSINE[c]+1*Pi[c]-- >+1*HYPOXANTHINE[c] +1*RIBOSE-1P[c]	GCWI-4228 GCWI-1624 GCWI-4228
INORGPYROPHOSPHAT- RXN	+1*PPI[c]+1*WATER[c]-- >+1*PROTON[c]+2*Pi[c]	GCWI-2876 GCWI-5260
IPPISOM-RXN	+1*DELTA3- ISOPENTENYL-PP[c]<--	GCWI-1661

Name	Reaction	Locus
	>+1*CPD-4211[c]	
ISOCHORMAT-RXN	+1*ISOCHORISMATE[c]+ 1*WATER[c]-- >+1*DIHYDRO-DIOH- BENZOATE[c]+1*PYRUV ATE[c]	GCWI-201 GCWI-517 GCWI-1532 GCWI-1754 GCWI-2992 GCWI-3182 GCWI-3183 GCWI-3311 GCWI-4391 GCWI-2350 GCWI-2451
ISOCHORSYN-RXN	+1*CHORISMATE[c]-- >+1*ISOCHORISMATE[c]	GCWI-4980 GCWI-2449
ISOCIT-CLEAV-RXN	+1*THREO-DS-ISO- CITRATE[c]-- >+1*GLYOX[c]+1*SUC[c]	GCWI-1306
ISOCITDEH-RXN	+1*NADP[c]+1*THREO- DS-ISO-CITRATE[c]-- >+1*CARBON- DIOXIDE[c]+1*NADPH[c] +1*-2- KETOGLUTARATE[c]	GCWI-4720
ISOLEUCINE--TRNA- LIGASE-RXN	+1*ATP[c]+1*ILE[c]+1*IL E- tRNAs[c]+1*PROTON[c]-- >+1*AMP[c]+1*Charged- ILE-tRNAs[c]+1*PPI[c]	GCWI-2273 GCWI-3979
ISOVALERYLCOA- DHLIPOAMIDE-RXN	+1*BCAA-dehydrogenase- 3MB-DH-lipoyl[c]+1*CO- A[c]-->+1*BCAA- dehydrogenase-DH- lipoyl[c]+1*ISOVALERYL- COA[c]	GCWI-4297
KANAMYCIN-KINASE- RXN	+1*ATP[c]+1*Kanamycins[ c]<-- >+1*ADP[c]+1*Kanamycin -3- phosphates[c]+1*PROTON[ c]	GCWI-3134 GCWI-4827
KETOACYLCOATHIOL- RXN-BUTYRYL-COA- ACETYL-COA--K- HEXANOYL-COA-CO- A.44.	+1*CO-A[c]+1*K- HEXANOYL-COA[c]-- >+1*ACETYL- COA[c]+1*BUTYRYL- COA[c]	GCWI-5128
KETOACYLCOATHIOL- RXN-CPD-10267- ACETYL-COA--CPD0- 2105-CO-A.37.	+1*CO-A[c]+1*CPD0- 2105[c]-->+1*ACETYL- COA[c]+1*CPD-10267[c]	GCWI-5128
KETOACYLCOATHIOL-	+1*CO-A[c]+1*CPD0-	GCWI-5128

Name	Reaction	Locus
RXN-CPD-196-ACETYL-COA--CPD0-2123-CO-A.35.	2123[c]-->+1*ACETYL-COA[c]+1*CPD-196[c]	
KETOACYLCOATHIOL-RXN-HEXANOYL-COA-ACETYL-COA--CPD0-2106-CO-A.40.	+1*CO-A[c]+1*CPD0-2106[c]-->+1*ACETYL-COA[c]+1*HEXANOYL-COA[c]	GCWI-5128
KETOACYLCOATHIOL-RXN-LAUROYLCOA-CPD-ACETYL-COA--CPD-10284-CO-A.42.	+1*CO-A[c]+1*CPD-10284[c]-->+1*ACETYL-COA[c]+1*LAUROYLCOA-CPD[c]	GCWI-5128
KETOACYLCOATHIOL-RXN-PALMITYL-COA-ACETYL-COA--CPD-10260-CO-A.40.	+1*CO-A[c]+1*CPD-10260[c]-->+1*ACETYL-COA[c]+1*PALMITYL-COA[c]	GCWI-5128
KETOACYLCOATHIOL-RXN-TETRADECANOYL-COA-ACETYL-COA--3-OXOPALMITOYL-COA-CO-A.54.	+1*CO-A[c]+1*-3-OXOPALMITOYL-COA[c]-->+1*ACETYL-COA[c]+1*TETRADECANOYL-COA[c]	GCWI-5128
KETOISOCAPROATE-RXN	+1*BCAA-dehydrogenase-lipoyl[c]+1*-2K-4CH3-PENTANOATE[c]-->+1*BCAA-dehydrogenase-3MB-DH-lipoyl[c]+1*CARBON-DIOXIDE[c]	GCWI-4298 GCWI-4299
KYNURENINASE-RXN	+1*L-KYNURENINE[c]+1*WATER[c]-->+1*ANTHRANILATE[c]+1*L-ALPHA-ALANINE[c]+1*PROTON[c]	GCWI-2808
L-ASPARTATE-OXID-RXN	+1*L-ASPARTATE[c]+1*OXYGEN-MOLECULE[c]-->+1*HYDROGEN-PEROXIDE[c]+1*IMINOASPARTATE[c]+1*PROTON[c]	GCWI-4557
L-GLN-FRUCT-6-P-AMINOTRANS-RXN	+1*FRUCTOSE-6P[c]+1*GLN[c]-->+1*D-GLUCOSAMINE-6-P[c]+1*GLT[c]	GCWI-361

Name	Reaction	Locus
L-LACTATE-DEHYDROGENASE-RXN	+1*L-LACTATE[c]+1*NAD[c]<- ->+1*NADH[c]+1*PROTON[c]+1*PYRUVATE[c]	GCWI-2031 GCWI-4991 GCWI-5121
L-LACTDEHYDROGMN-RXN	+1*CPD-9718[c]+1*L-LACTATE[c]<->+1*CPD-12125[c]+1*PYRUVATE[c]	
LACTALDDEHYDROG-RXN	+1*LACTALD[c]+1*NAD[c]+1*WATER[c]<->+1*L-LACTATE[c]+1*NADH[c]+2*PROTON[c]	GCWI-2379 GCWI-3587 GCWI-2881 GCWI-1451
LEUCINE--TRNA-LIGASE-RXN	+1*ATP[c]+1*LEU[c]+1*LEU-tRNAs[c]+1*PROTON[c]<->+1*AMP[c]+1*Charged-LEU-tRNAs[c]+1*PPI[c]	GCWI-4866
LEUCINE-DEHYDROGENASE-RXN	+1*LEU[c]+1*NAD[c]+1*WATER[c]<->+1*AMMONIA[c]+1*NADH[c]+2*PROTON[c]+1*2K-4CH3-PENTANOATE[c]	GCWI-4302
LUMAZINESYN-RXN	+1*AMINO-RIBOSYLAMINO-1H-3H-PYRIDIONE[c]+1*DIHYDROXY-BUTANONE-P[c]<->+1*DIMETHYL-D-RIBITYL-LUMAZINE[c]+1*PROTON[c]+1*Pi[c]+2*WATER[c]	GCWI-4253
LYSDECARBOX-RXN	+1*LYS[c]+1*PROTON[c]<->+1*CADAVERINE[c]+1*CARBON-DIOXIDE[c]	GCWI-214 GCWI-4106
LYSINE--TRNA-LIGASE-RXN	+1*ATP[c]+1*LYS[c]+1*LYS-tRNAs[c]+1*PROTON[c]<->+1*AMP[c]+1*Charged-LYS-tRNAs[c]+1*PPI[c]	GCWI-264
LYSINE-23-AMINOMUTASE-RXN	+1*LYS[c]<->+1*CPD-233[c]	GCWI-2389
MACROCIN-O-METHYLTRANSFERASE-	+1*MACROCIN[c]+1*S-ADENOSYLMETHIONIN	GCWI-1383



Name	Reaction	Locus
RXN	E[c]<-->+1*ADENOSYL-HOMO-CYS[c]+1*PROTON[c]+1*TYLOSIN[c]	
MALATE-DEH-RXN	+1*MAL[c]+1*NAD[c]<-->+1*NADH[c]+1*OXALACETIC-ACID[c]+1*PROTON[c]	GCWI-4719 GCWI-786 GCWI-1917 GCWI-3163 GCWI-4719 GCWI-4730
MALATE-DEHYDROGENASE-ACCEPTOR-RXN-MAL-CPD-9717--OXALACETIC-ACID-CPD-9955.39.	+1*CPD-9717[c]+1*MAL[c]<-->+1*CPD-9955[c]+1*OXALACETIC-ACID[c]	GCWI-786 GCWI-1917 GCWI-3163 GCWI-4719 GCWI-4730 GCWI-3002
MALIC-NAD-RXN	+1*MAL[c]+1*NAD[c]<-->+1*CARBONDIOXIDE[c]+1*NADH[c]+1*PYRUVATE[c]	GCWI-786 GCWI-1917 GCWI-3163 GCWI-4730
MALIC-NADP-RXN	+1*MAL[c]+1*NADP[c]<-->+1*CARBONDIOXIDE[c]+1*NADPH[c]+1*PYRUVATE[c]	GCWI-786 GCWI-1917 GCWI-3163 GCWI-4719 GCWI-4730
MALONYL-COA-ACP-TRANSACYL-RXN	+1*ACP[c]+1*MALONYL-COA[c]+1*PROTON[c]<-->+1*CO-A[c]+1*MALONYL-ACP[c]	GCWI-3936
MALSYN-RXN	+1*ACETYL-COA[c]+1*GLYOX[c]+1*WATER[c]<-->+1*CO-A[c]+1*MAL[c]+1*PROTON[c]	GCWI-1305
MALTACETYLTRAN-RXN	+1*ACETYL-COA[c]+1*MALTOSE[c]<- ->+1*ACETYLMALTOSE[c]+1*CO-A[c]	GCWI-3394
MBCOA-DHLIPOAMIDE-RXN	+1*BCAA-dehydrogenase-2MB-DH-lipoyl[c]+1*CO-A[c]<-->+1*BCAA-dehydrogenase-DH-lipoyl[c]+1*-2-METHYLBUTYRYL-COA[c]	GCWI-4297
METHENYLTHFCYCLOHYDRO-RXN	+1*WATER[c]+1*-5-10-METHENYL-THF[c]<--	GCWI-4317

Name	Reaction	Locus
	>+1*PROTON[c]+1*-10-FORMYL-THF[c]	
METHGLYSYN-RXN	+1*DIHYDROXY-ACETONE-PHOSPHATE[c]<-->+1*METHYL-GLYOXAL[c]+1*Pi[c]	GCWI-1695
METHIONINE--TRNA-LIGASE-RXN	+1*ATP[c]+1*MET[c]+1*MET-tRNAs[c]+1*PROTON[c]<-->+1*AMP[c]+1*Charged-MET-tRNAs[c]+1*PPI[c]	GCWI-223 GCWI-5154
METHIONINE-GAMMA-LYASE-RXN	+1*MET[c]+1*WATER[c]->+1*AMMONIA[c]+1*CPD-7671[c]+1*PROTON[c]+1*-2-OXOBUTANOATE[c]	GCWI-4785
METHIONYL-TRNA-FORMYLTRANSFERASE-RXN	+1*L-methionyl-tRNA <sup>fmet</sup> [c]+1*-10-FORMYL-THF[c]<-->+1*N-formyl-L-methionyl-tRNA <sup>fmet</sup> [c]+1*THF[c]	GCWI-3950
METHYLACETOACETYL COATHIOL-RXN	+1*CO-A[c]+1*-2-METHYL-ACETO-ACETYL-COA[c]<-->+1*ACETYL-COA[c]+1*PROPIONYL-COA[c]	GCWI-3656 GCWI-4164 GCWI-5128 GCWI-5443
METHYLACYLYLCOA-HYDROXY-RXN	+1*METHACRYLYL-COA[c]+1*WATER[c]<-->+1*CPD-12173[c]	GCWI-1106 GCWI-2616 GCWI-3561 GCWI-4652 GCWI-2439
METHYLENETHFDEHYDROG-NADP-RXN	+1*METHYLENE-THF[c]+1*NADP[c]<-->+1*NADPH[c]+1*-5-10-METHENYL-THF[c]	GCWI-4317
METHYLISOCITRATE-LYASE-RXN	+1*CPD-618[c]<-->+1*PYRUVATE[c]+1*SUC[c]	GCWI-2434
METHYLTHIOADENOSINE-NUCLEOSIDASE-RXN	+1*WATER[c]+1*-5-METHYLTHIOADENOSINE[c]<-->+1*ADENINE[c]+1*CPD-560[c]	GCWI-2913
METHYLVALERATE-	+1*BCAA-dehydrogenase-	GCWI-2827 GCWI-4113

Name	Reaction	Locus
RXN	lipoyl[c]+1*-2-KETO-3-METHYL-VALERATE[c]-->+1*BCAA-dehydrogenase-2MB-DH-lipoyl[c]+1*CARBON-DIOXIDE[c]	GCWI-4297
MMUM-RXN	+1*CPD-397[c]+1*HOMO-CYS[c]-->+2*MET[c]+1*PROTON[c]	GCWI-4388
MYO-INOSITOL-1OR-4-MONOPHOSPHATASE-RXN	+1*WATER[c]+1*-1-L-MYO-INOSITOL-1-P[c]-->+1*MYO-INOSITOL[c]+1*Pi[c]	GCWI-4102
N-ACETYLDIAMINOPIMELATE-DEACETYLASE-RXN	+1*CPD-1771[c]+1*WATER[c]-->+1*ACET[c]+1*LL-DIAMINOPIMELATE[c]	GCWI-4122
N-ACETYLGLUTPREDUCT-RXN	+1*NADPH[c]+1*N-ACETYL-GLUTAMYL-P[c]+1*PROTON[c]-->+1*CPD-469[c]+1*NADP[c]+1*Pi[c]	GCWI-4272
N-ACETYLTRANSFER-RXN	+1*ACETYL-COA[c]+1*GLT[c]-->+1*ACETYL-GLU[c]+1*CO-A[c]+1*PROTON[c]	GCWI-1049
NACGLCTTRANS-RXN	+1*C5[c]+1*UDP-N-ACETYL-D-GLUCOSAMINE[c]<-->+1*C6[c]+1*PROTON[c]+1*UDP[c]	GCWI-3994 GCWI-4386
NAD-KIN-RXN	+1*ATP[c]+1*NAD[c]-->+1*ADP[c]+1*NADP[c]+1*PROTON[c]	GCWI-1374 GCWI-4772
NAD-SYNTH-GLN-RXN	+1*ATP[c]+1*DEAMIDO-NAD[c]+1*GLN[c]+1*WATER[c]-->+1*AMP[c]+1*GLT[c]+1*NAD[c]+1*PPI[c]+1*PROTON[c]	GCWI-2102
NAD-SYNTH-NH3-RXN	+1*AMMONIA[c]+1*ATP[c]+1*DEAMIDO-NAD[c]-->+1*AMP[c]+1*NAD[c]+1	GCWI-2102

Name	Reaction	Locus
	*PPI[c]	
NADH-DEHYDROG-A-RXN	+1*CPD-9718[c]+1*NADH[c]+1*PROTON[c]<-->+1*CPD-12125[c]+1*NAD[c]	GCWI-5390 GCWI-5391 GCWI-5393 GCWI-5394 GCWI-5395 GCWI-5396 GCWI-5397 GCWI-5398 GCWI-5399 GCWI-5400 GCWI-2138 GCWI-2211 GCWI-3525
NADPH-DEHYDROGENASE-FLAVIN-RXN	+1*CPD-316[c]+1*NADP[c]<-->+1*NADPH[c]+2*PROTON[c]+1*RIBOFLAVIN[c]	GCWI-1778 GCWI-3373
NAG1P-URIDYLTRANS-RXN	+1*N-ACETYL-D-GLUCOSAMINE-1-P[c]+1*PROTON[c]+1*UTP[c]<-->+1*PPI[c]+1*UDP-N-ACETYL-D-GLUCOSAMINE[c]	GCWI-234
NAG6PDEACET-RXN	+1*N-ACETYL-D-GLUCOSAMINE-6-P[c]+1*WATER[c]<-->+1*ACET[c]+1*D-GLUCOSAMINE-6-P[c]	GCWI-4197
NAPHTHOATE-SYN-RXN	+1*CPD-6972[c]+1*PROTON[c]<-->+1*CPD-9925[c]+1*WATER[c]	GCWI-4977
NICONUCADENYLYLTRAN-RXN	+1*ATP[c]+1*NICOTINATE-NUCLEOTIDE[c]+1*PROTON[c]<-->+1*DEAMIDONAD[c]+1*PPI[c]	GCWI-4461
NICOTINAMID-RXN	+1*NIACINAMIDE[c]+1*WATER[c]<-->+1*AMMONIA[c]+1*NIACINE[c]+1*PROTON[c]	GCWI-2029 GCWI-2171
NICOTINATEPRIBOSYLTRANS-RXN	+1*NIACINE[c]+1*PROTON[c]+1*PRPP[c]<-->+1*NICOTINATE-NUCLEOTIDE[c]+1*PPI[c]	GCWI-802 GCWI-4815
NITRIC-OXIDE-SYNTHASE-RXN	+2*ARG[c]+3*NADPH[c]+4*OXYGEN-MOLECULE[c]+1*PROTON[c]<-->+2*L-CITRULLINE[c]+3*NADP[c]	GCWI-5547

Name	Reaction	Locus
	c]+2*NITRIC- OXIDE[c]+4*WATER[c]	
NUCLEOSIDE- TRIPHOSPHATASE-RXN	+1*Nucleoside- Triphosphates[c]+1*WATE R[c]-->+1*Nucleoside- Diphosphates[c]+1*PROTO N[c]+1*Pi[c]	GCWI-4608
O- ACETYLHOMOSERINE- THIOL-LYASE-RXN	+1*CPD-667[c]+1*CPD- 7671[c]-- >+1*ACET[c]+1*MET[c]+ 1*PROTON[c]	GCWI-5507
O- SUCCHOMOSERLYASE- RXN	+1*CYS[c]+1*O- SUCCINYL-L- HOMOSERINE[c]-->+1*L- CYSTATHIONINE[c]+1*P ROTON[c]+1*SUC[c]	GCWI-4389
O- SUCCINYLBENZOATE- COA-LIG-RXN	+1*ATP[c]+1*CO- A[c]+1*O- SUCCINYLBENZOATE[c] -->+1*AMP[c]+1*CPD- 6972[c]+1*PPI[c]	GCWI-4976
O- SUCCINYLBENZOATE- COA-SYN-RXN	+1*CPD-9923[c]-->+1*O- SUCCINYLBENZOATE[c] +1*WATER[c]	GCWI-4979
OHACYL-COA- DEHYDROG-RXN-CPD0- 2107-NAD--CPD0-2105- NADH-PROTON.37.	+1*CPD0- 2107[c]+1*NAD[c]-- >+1*CPD0- 2105[c]+1*NADH[c]+1*PR OTON[c]	GCWI-5129 GCWI-5442
OHACYL-COA- DEHYDROG-RXN-CPD0- 2171-NAD--CPD-10284- NADH-PROTON.37.	+1*CPD0- 2171[c]+1*NAD[c]-- >+1*CPD- 10284[c]+1*NADH[c]+1*P ROTON[c]	GCWI-5129 GCWI-5442
OHACYL-COA- DEHYDROG-RXN-CPD0- 2224-NAD--CPD0-2106- NADH-PROTON.37.	+1*CPD0- 2224[c]+1*NAD[c]-- >+1*CPD0- 2106[c]+1*NADH[c]+1*PR OTON[c]	GCWI-5129 GCWI-5442
OHACYL-COA- DEHYDROG-RXN-CPD0- 2244-NAD--CPD0-2123- NADH-PROTON.37.	+1*CPD0- 2244[c]+1*NAD[c]-- >+1*CPD0- 2123[c]+1*NADH[c]+1*PR OTON[c]	GCWI-5129 GCWI-5442
OHACYL-COA-	+1*CPD0-	GCWI-5129 GCWI-5442

Name	Reaction	Locus
DEHYDROG-RXN-CPD0-2253-NAD--CPD-10260-NADH-PROTON.37.	2253[c]+1*NAD[c]-->+1*CPD-10260[c]+1*NADH[c]+1*PROTON[c]	
OHACYL-COA-DEHYDROG-RXN-OH-HEXANOYL-COA-NAD--K-HEXANOYL-COA-NADH-PROTON.48.	+1*NAD[c]+1*OH-HEXANOYL-COA[c]-->+1*K-HEXANOYL-COA[c]+1*NADH[c]+1*PROTON[c]	GCWI-5129 GCWI-5442
OHMETHYLBILANESYN-RXN	+4*PORPHOBILINOGEN[c]+1*WATER[c]-->+4*AMMONIA[c]+1*HYDROXYMETHYLBILANE[c]+4*PROTON[c]	GCWI-4591
ORNCARBAMTRANSFER-RXN	+1*CARBAMOYL-P[c]+1*L-ORNITHINE[c]<-->+1*L-CITRULLINE[c]+1*PROTON[c]+1*Pi[c]	GCWI-4268
ORNITHINE--OXO-ACID-AMINOTRANSFERASE-RXN	+1*L-ORNITHINE[c]+1*-2-Oxo-carboxylates[c]<-->+1*Amino-Acids-20[c]+1*L-GLUTAMATE-GAMMA-SEMIALDEHYDE[c]	GCWI-1325
ORNITHINE-CYCLODEAMINASE-RXN	+1*L-ORNITHINE[c]-->+1*AMMONIUM[c]+1*PRO[c]	GCWI-1112
ORNITHINE-GLU-AMINOTRANSFORASE-RXN	+1*L-ORNITHINE[c]+1*-2-KETOGLUTARATE[c]<-->+1*GLT[c]+1*L-GLUTAMATE-GAMMA-SEMIALDEHYDE[c]	GCWI-1325
OROPRIBTRANS-RXN	+1*OROTATE[c]+1*PRPP[c]-->+1*OROTIDINE-5-PHOSPHATE[c]+1*PPI[c]	GCWI-3966
OROTPDECARB-RXN	+1*OROTIDINE-5-PHOSPHATE[c]+1*PROTON[c]-->+1*CARBONDIOXIDE[c]+1*UMP[c]	GCWI-3967
P-PANTOCYSDECARB-RXN	+1*PROTON[c]+1*R-4-PHOSPHOPANTOTHENYL-L-CYSTEINE[c]-->+1*CARBONDIOXIDE[c]+1*PANTETH	GCWI-3953

Name	Reaction	Locus
	EINE-P[c]	
P-PANTOCYSLIG-RXN	+1*CTP[c]+1*CYS[c]+1*-4-P-PANTOTHENATE[c]-->+1*CMP[c]+1*PPI[c]+1*P ROTON[c]+1*R-4- PHOSPHOPANTOTHENO YL-L-CYSTEINE[c]	GCWI-3953
PABASYN-RXN	+1*CHORISMATE[c]+1*G LN[c]-->+1*GLT[c]+1*-4- AMINO-4- DEOXYCHORISMATE[c]	GCWI-195 GCWI-256 GCWI-257 GCWI-1410
PANTEPADENYLYLTRA N-RXN	+1*ATP[c]+1*PANTETHE INE-P[c]+1*PROTON[c]-- >+1*DEPHOSPHO- COA[c]+1*PPI[c]	GCWI-4073
PANTOATE-BETA- ALANINE-LIG-RXN	+1*ATP[c]+1*B- ALANINE[c]+1*L- PANTOATE[c]-- >+1*AMP[c]+1*PANTOT HENATE[c]+1*PPI[c]+1*P ROTON[c]	GCWI-1702
PANTOTHENATE-KIN- RXN	+1*ATP[c]+1*PANTOTHE NATE[c]-- >+1*ADP[c]+1*PROTON[c ]+1*-4-P- PANTOTHENATE[c]	GCWI-253 GCWI-2942
PEPCARBOXYKIN-RXN	+1*ATP[c]+1*OXALACET IC-ACID[c]-- >+1*ADP[c]+1*CARBON- DIOXIDE[c]+1*PHOSPHO -ENOL-PYRUVATE[c]	GCWI-4890
PEPDEPHOS-RXN	+1*ADP[c]+1*PHOSPHO- ENOL- PYRUVATE[c]+1*PROTO N[c]-- >+1*ATP[c]+1*PYRUVAT E[c]	GCWI-3375 GCWI-4725
PEPSYNTH-RXN	+1*ATP[c]+1*PYRUVATE [c]+1*WATER[c]-- >+1*AMP[c]+1*PHOSPHO -ENOL- PYRUVATE[c]+2*PROTO N[c]+1*Pi[c]	GCWI-3139
PEPTIDYLPROLYL- ISOMERASE-RXN	+1*CPD-8624[c]<-- >+1*CPD-8625[c]	GCWI-4204 GCWI-1229 GCWI-1338 GCWI-2422

Name	Reaction	Locus
PGLUCISOM-RXN	+1*GLC-6-P[c]<-- >+1*FRUCTOSE-6P[c]	GCWI-5020
PGLYCDEHYDROG-RXN	+1*G3P[c]+1*NAD[c]-- >+1*NADH[c]+1*PROTON[c]+1*-3-P-HYDROXYPYRUVATE[c]	GCWI-3317
PGPPHOSPHA-RXN-CPD-12820-WATER--CPD-12822-PI.30.	+1*CPD-12820[c]+1*WATER[c]-- >+1*CPD-12822[c]+1*Pi[c]	
PGPPHOSPHA-RXN-CPD-12821-WATER--CPD-8260-PI.29.	+1*CPD-12821[c]+1*WATER[c]-- >+1*CPD-8260[c]+1*Pi[c]	
PGPPHOSPHA-RXN-CPD0-2230-WATER--CPD0-2330-PI.30.	+1*CPD0-2230[c]+1*WATER[c]-- >+1*CPD0-2330[c]+1*Pi[c]	
PHENYLALANINE--TRNA-LIGASE-RXN	+1*ATP[c]+1*PHE[c]+1*PHE-tRNAs[c]+1*PROTON[c]-- >+1*AMP[c]+1*Charged-PHE-tRNAs[c]+1*PPI[c]	GCWI-4687 GCWI-4688
PHENYLALANINE-4-MONOOXYGENASE-RXN	+1*OXYGEN-MOLECULE[c]+1*PHE[c] +1*TETRA-H-BIOPTERIN[c]-->+1*CPD-5881[c]+1*TYR[c]	GCWI-4484
PHOSACETYLTRANS-RXN	+1*ACETYL-COA[c]+1*Pi[c]-- >+1*ACETYL-P[c]+1*COA[c]	GCWI-5487
PHOSGLYPHOS-RXN	+1*ATP[c]+1*G3P[c]<-- >+1*ADP[c]+1*DPG[c]	GCWI-5237
PHOSMANMUT-RXN	+1*MANNOS-6P[c]-- >+1*MANNOS-1P[c]	GCWI-5043
PHOSNACMURPENTATRANS-RXN	+1*C1[c]+1*CPD-9646[c]-- >+1*C5[c]+1*UMP[c]	GCWI-3997
PHOSPHAGLYPSYN-RXN-CPD-12814-GLYCEROL-3P--CMP-CPD-12820-PROTON.44.	+1*CPD-12814[c]+1*GLYCEROL-3P[c]<-- >+1*CMP[c]+1*CPD-12820[c]+1*PROTON[c]	GCWI-3865
PHOSPHAGLYPSYN-RXN-CPD-12815-GLYCEROL-3P--CMP-CPD-12821-PROTON.44.	+1*CPD-12815[c]+1*GLYCEROL-3P[c]-- >+1*CMP[c]+1*CPD-12821[c]+1*PROTON[c]	GCWI-3865



Name	Reaction	Locus
PHOSPHASERDECARB-RXN-CPD-12816-PROTON--CPD-12818-CARBON-DIOXIDE.43.	+1*CPD-12816[c]+1*PROTON[c]-->+1*CARBON-DIOXIDE[c]+1*CPD-12818[c]	GCWI-4466
PHOSPHASERDECARB-RXN-CPD-12817-PROTON--CPD-12819-CARBON-DIOXIDE.43.	+1*CPD-12817[c]+1*PROTON[c]-->+1*CARBON-DIOXIDE[c]+1*CPD-12819[c]	GCWI-4466
PHOSPHASERSYN-RXN-CPD-12814-SER--CMP-CPD-12816-PROTON.36.	+1*CPD-12814[c]+1*SER[c]-->+1*CMP[c]+1*CPD-12816[c]+1*PROTON[c]	GCWI-1158 GCWI-1578
PHOSPHASERSYN-RXN-CPD-12815-SER--CMP-CPD-12817-PROTON.36.	+1*CPD-12815[c]+1*SER[c]-->+1*CMP[c]+1*CPD-12817[c]+1*PROTON[c]	GCWI-1158 GCWI-1578
PHOSPHATE-BUTYRYLTRANSFERASE-RXN	+1*BUTYRYL-COA[c]+1*Pi[c]-->+1*BUTYRYL-P[c]+1*CO-A[c]	GCWI-4303
PHOSPHOGLUCMUT-RXN	+1*GLC-1-P[c]<-->+1*ALPHA-GLC-6-P[c]	GCWI-5043
PHOSPHOLIPASE-C-RXN	+1*PHOSPHATIDYLCHOLINE[c]+1*WATER[c]-->+1*DIACYLGLYCEROL[c]+1*PHOSPHORYLCHOLINE[c]+1*PROTON[c]	GCWI-880
PHOSPHOLIPASE-C-RXN-1-2-DIPALMITOYLPHOSPHATIDYLCHOLINE-WATER-PHOSPHORYLCHOLINE-CPD66-34-PROTON.77.	+1*WATER[c]+1*-1-2-DIPALMITOYLPHOSPHATIDYLCHOLINE[c]-->+1*CPD66-34[c]+1*PHOSPHORYLCHOLINE[c]+1*PROTON[c]	GCWI-880
PHOSPHONOACETALDEHYDE-HYDROLASE-RXN	+1*CPD-551[c]+1*WATER[c]-->+1*ACETALD[c]+1*PROTON[c]+1*Pi[c]	GCWI-1491
PNKIN-RXN	+1*ATP[c]+1*PYRIDOXINE[c]-->+1*ADP[c]+1*PROTON[c]+1*PYRIDOXINE-5P[c]	GCWI-5515

Name	Reaction	Locus
PORPHOBILSYNTH-RXN	+2*-5-AMINO- LEVULINATE[c]-- >+1*PORPHOBILINOGEN [c]+1*PROTON[c]+2*WA TER[c]	GCWI-4589
PPENTOMUT-RXN	+1*RIBOSE-1P[c]-- >+1*RIBOSE-5P[c]	GCWI-4229
PPGPPSYN-RXN	+1*GUANOSINE-5DP- 3DP[c]+1*WATER[c]-- >+1*GDP[c]+1*PPI[c]+1*P ROTON[c]	GCWI-4532
PRAISOM-RXN	+1*N-5- PHOSPHORIBOSYL- ANTHRANILATE[c]-- >+1*CARBOXYPHENYL AMINO- DEOXYRIBULOSE-P[c]	GCWI-1413
PREPHENATEDEHYDRA T-RXN	+1*PREPHENATE[c]+1*P ROTON[c]-- >+1*CARBON- DIOXIDE[c]+1*PHENYL- PYRUVATE[c]+1*WATER [c]	GCWI-4561
PREPHENATEDEHYDRO G-RXN	+1*NAD[c]+1*PREPHENA TE[c]-->+1*CARBON- DIOXIDE[c]+1*NADH[c]+ 1*P-HYDROXY- PHENYLPYRUVATE[c]	GCWI-2985
PRIBFAICARPISOM-RXN	+1*PHOSPHORIBOSYL- FORMIMINO-AICAR-P[c]- - >+1*PHOSPHORIBULOS YL-FORMIMINO-AICAR- P[c]	GCWI-1572
PRODISULFREDUCT-A- RXN	+2*GLUTATHIONE[c]+1* Ox-Glutaredoxins[c]<-- >+1*OXIDIZED- GLUTATHIONE[c]+1*Red -Glutaredoxins[c]	
PROLINE--TRNA- LIGASE-RXN	+1*ATP[c]+1*PRO[c]+1*P ROTON[c]+1*PRO- tRNAs[c]-- >+1*AMP[c]+1*Charged- PRO-tRNAs[c]+1*PPI[c]	GCWI-603 GCWI-3903
PROLINE-RACEMASE-	+1*PRO[c]-->+1*D-	GCWI-1111 GCWI-2884

Name	Reaction	Locus
RXN	PROLINE[c]	
PROTOHEMEFERROCHE LAT-RXN	+1*FE- 2[c]+1*PROTOPORPHYRI N-IX[c]-- >+1*PROTOHEME[c]+2*P ROTON[c]	GCWI-1255 GCWI-1329
PROTOPORGENOXI-RXN	+3*OXYGEN- MOLECULE[c]+1*PROTO PORPHYRINOGEN[c]-- >+3*HYDROGEN- PEROXIDE[c]+1*PROTOP ORPHYRIN-IX[c]	GCWI-1256 GCWI-2497
PRPPAMIDOTRANS-RXN	+1*GLN[c]+1*PRPP[c]+1* WATER[c]-- >+1*GLT[c]+1*PPI[c]+1* 5-P-BETA-D-RIBOSYL- AMINE[c]	GCWI-503
PRPPSYN-RXN	+1*ATP[c]+1*RIBOSE- 5P[c]-- >+1*AMP[c]+1*PROTON[ c]+1*PRPP[c]	GCWI-235
PRTRANS-RXN	+1*ANTHRANILATE[c]+1 *PRPP[c]-->+1*N-5- PHOSPHORIBOSYL- ANTHRANILATE[c]+1*PP I[c]	GCWI-1410 GCWI-1411
PSERTRANSAM-RXN	+1*GLT[c]+1*-3-P- HYDROXYPYRUVATE[c] -->+1*-2- KETOGLUTARATE[c]+1* -3-P-SERINE[c]	GCWI-3318
PSERTRANSAMPYR- RXN	+1*GLT[c]+1*-3OH-4P- OH-ALPHA- KETO BUTYRATE[c]-- >+1*-2- KETOGLUTARATE[c]+1* -4-PHOSPHONOOXY- THREONINE[c]	GCWI-3318
PYRIDOXKIN-RXN	+1*ATP[c]+1*PYRIDOXA L[c]-- >+1*ADP[c]+1*PROTON[c ]+1*PYRIDOXAL- PHOSPHATE[c]	GCWI-5515
PYRIMSYN3-RXN	+1*AMINO- HYDROXY METHYL-	GCWI-958 GCWI-5515

Name	Reaction	Locus
	METHYL-PYR- P[c]+1*ATP[c]-- >+1*ADP[c]+1*AMINO- HYDROXYMETHYL- METHYLPYRIMIDINE- PP[c]	
PYRROLINECARBDEHY DROG-RXN	+1*L-DELTA1- PYRROLINE-5- CARBOXYLATE[c]+1*NA D[c]+2*WATER[c]-- >+1*GLT[c]+1*NADH[c]+ 1*PROTON[c]	GCWI-516
PYRUFLAVREDUCT- RXN	+1*CO-A[c]+1*Oxidized- ferredoxins[c]+1*PYRUVATE[c]-->+1*ACETYL- COA[c]+1*CARBON- DIOXIDE[c]+1*PROTON[c ]+1*Reduced-ferredoxins[c]	GCWI-3858
PYRUVATE- CARBOXYLASE-RXN	+1*ATP[c]+1*HCO3[c]+1* PYRUVATE[c]-- >+1*ADP[c]+1*OXALACE TIC- ACID[c]+1*PROTON[c]+1 *Pi[c]	GCWI-4091
PYRUVDEH-RXN	+1*CO- A[c]+1*NAD[c]+1*PYRU VATE[c]-->+1*ACETYL- COA[c]+1*CARBON- DIOXIDE[c]+1*NADH[c]	GCWI-4113
PYRUVFORMLY-RXN	+1*CO- A[c]+1*PYRUVATE[c]-- >+1*ACETYL- COA[c]+1*FORMATE[c]	GCWI-702
QUINOLINATE-SYNTHA- RXN	+1*DIHYDROXY- ACETONE- PHOSPHATE[c]+1*IMINO ASPARTATE[c]-- >+1*Pi[c]+1*QUINOLINA TE[c]+2*WATER[c]	GCWI-4555
QUINOPRIBOTRANS- RXN	+2*PROTON[c]+1*PRPP[c ]+1*QUINOLINATE[c]-- >+1*CARBON- DIOXIDE[c]+1*NICOTIN ATE- NUCLEOTIDE[c]+1*PPI[c]	GCWI-4556

Name	Reaction	Locus
R101-RXN	+1*GLT[c]+1*L- ASPARTATE- SEMIALDEHYDE[c]-- >+1*CPD-470[c]+1*-2- KETOGLUTARATE[c]	GCWI-3308
R11-RXN	+1*ACET[c]+1*BUTYRYL -COA[c]-->+1*ACETYL- COA[c]+1*BUTYRIC- ACID[c]	GCWI-2385 GCWI-2384
R145-RXN	+1*CPD-1063[c]-- >+1*CPD- 8999[c]+1*WATER[c]	GCWI-4180
R147-RXN	+1*CPD- 85[c]+1*OXYGEN- MOLECULE[c]-- >+1*CPD- 479[c]+1*FORMATE[c]+1 *PROTON[c]	GCWI-4181
R15-RXN	+1*CPD- 479[c]+1*GLT[c]<-- >+1*MET[c]+1*-2- KETOGLUTARATE[c]	GCWI-5024
R222-RXN	+1*CPD- 371[c]+1*NAD[c]+1*WAT ER[c]<-->+1*CPD- 195[c]+1*NADH[c]+2*PR OTON[c]	GCWI-2379 GCWI-2379 GCWI-3587 GCWI-2881 GCWI-1451
R223-RXN	+1*ATP[c]+1*CO- A[c]+1*CPD-195[c]-- >+1*AMP[c]+1*CPD- 196[c]+1*PPI[c]	GCWI-2036 GCWI-2087 GCWI-3657 GCWI-3659
R311-RXN	+1*ACRYLAMIDE[c]+1* WATER[c]<-- >+1*ACRYLATE[c]+1*A MMONIA[c]+1*PROTON[ c]	GCWI-2029 GCWI-2171
R344-RXN	+1*ATP[c]+1*CPD- 694[c]<-->+1*CPD- 690[c]+1*P3I[c]	GCWI-1640
R4-RXN	+1*Alkyl-Hydro- Peroxides[c]+1*NADH[c]+ 1*PROTON[c]-- >+1*Alcohols[c]+1*NAD[c ]+1*WATER[c]	GCWI-550 GCWI-551
R4-RXN-BUTANOL-NAD-	+1*BUTYL-	GCWI-550 GCWI-551

Name	Reaction	Locus
WATER--BUTYL-HYDROPEROXIDE-NADH-PROTON.51.	HYDROPEROXIDE[c]+1*NADH[c]+1*PROTON[c]>+1*BUTANOL[c]+1*NA D[c]+1*WATER[c]	
R8-RXN	+1*ACETYL-COA[c]+1*CPD-19[c]>+1*ACET[c]+1*CPD- 20[c]	GCWI-2384
R82-RXN	+1*CPD-8999[c]>+1*PROTON[c]+1*-2-HYDROXY-3-KETO-5-METHYLTHIO-1-PHOSPHOP[c]	GCWI-4178
R83-RXN	+1*WATER[c]+1*-2-HYDROXY-3-KETO-5-METHYLTHIO-1-PHOSPHOP[c]>+1*CPD- 85[c]+1*Pi[c]	GCWI-4179
RIB5PISOM-RXN	+1*RIBOSE-5P[c]<-->+1*RIBULOSE-5P[c]	GCWI-2843 GCWI-5417
RIBOFLAVIN-SYN-RXN	+2*DIMETHYL-D-RIBITYL-LUMAZINE[c]+1*PROTON[c]>+1*AMINO-RIBOSYLAMINO-1H-3H-PYR-DIONE[c]+1*RIBOFLAVIN[c]	GCWI-4251
RIBOFLAVINKIN-RXN	+1*ATP[c]+1*RIBOFLAVIN[c]>+1*ADP[c]+1*FMN[c]+1*PROTON[c]	GCWI-3893
RIBOFLAVINSYNDEAM-RXN	+1*DIAMINO-OH-PHOSPHORIBOSYLAMINO-PYR[c]+1*WATER[c]>+1*AMMONIA[c]+1*CPD- 602[c]	GCWI-4250
RIBOFLAVINSYNREDUC-RXN	+1*CPD-602[c]+1*NADPH[c]+1*PROTON[c]>+1*CPD- 1086[c]+1*NADP[c]	GCWI-4250
RIBOKIN-RXN	+1*ATP[c]+1*RIBOSE[c]>+1*ADP[c]+1*PROTON[c]+1*RIBOSE-5P[c]	GCWI-869
RIBOPHOSPHAT-RXN	+1*CPD-	

Name	Reaction	Locus
	1086[c]+1*WATER[c]-- >+1*AMINO- RIBOSYLAMINO-1H-3H- PYR-DIONE[c]+1*Pi[c]	
RIBOSYLHOMOCYSTEIN ASE-RXN	+1*CPD-564[c]-- >+1*DIHYDROXPENTA NEDIONE[c]+1*HOMO- CYS[c]	GCWI-4916
RIBULP3EPIM-RXN	+1*RIBULOSE-5P[c]<-- >+1*XYLULOSE-5- PHOSPHATE[c]	GCWI-3944
RXN-0	+1*ACETYL- COA[c]+1*PUTRESCINE[c] <-->+1*CO-A[c]+1*CPD- 569[c]+2*PROTON[c]	GCWI-2733 GCWI-3297
RXN-10	+1*ATP[c]+1*L- ASPARTATE[c]+1*O- UREIDOHOMOSERINE[c] <-- >+1*AMP[c]+1*CANAVA NINOSUCCINATE[c]+1*P PI[c]+1*PROTON[c]	GCWI-4760
RXN-10009	+1*CPD- 7652[c]+1*DIHYDROPT RIN-CH2OH-PP[c]<-- >+1*CPD- 10766[c]+1*PPI[c]+2*PRO TON[c]	GCWI-259
RXN-10015	+1*DIHYDROXPENTAN EDIONE[c]-->+1*CPD- 10773[c]	
RXN-10017	+1*CPD- 10773[c]+1*WATER[c]-- >+1*CPD-10774[c]	
RXN-10642	+1*CPD-11444[c]<-- >+4*CARBON- DIOXIDE[c]+1*COPROPO RPHYRINOGEN- I[c]+4*PROTON[c]	GCWI-1254
RXN-10654	+1*Cis-Delta5-dodecenoyl- ACPs[c]+1*MALONYL- ACP[c]-- >+1*ACP[c]+1*CARBON- DIOXIDE[c]+1*-3-oxo-cis- D7-tetradecenoyl-ACPs[c]	GCWI-3257 GCWI-1940 GCWI-1349 GCWI-1350

Name	Reaction	Locus
RXN-10655	+1*NADPH[c]+1*PROTO N[c]+1*-3-oxo-cis-D7- tetradecenoyl-ACPs[c]-- >+1*NADP[c]+1*-3- hydroxy-cis-D7- tetraecenoyl-ACPs[c]	GCWI-3935 GCWI-3869 GCWI-3588 GCWI-2066 GCWI-3427
RXN-10657	+1*NADPH[c]+1*PROTO N[c]+1*Trans-D3-cis-D7- tetradecenoyl-ACPs[c]-- >+1*Cis-Delta7- tetradecenoyl- ACPs[c]+1*NADP[c]	GCWI-1393
RXN-10658	+1*Cis-Delta7- tetradecenoyl- ACPs[c]+1*MALONYL- ACP[c]-- >+1*ACP[c]+1*CARBON- DIOXIDE[c]+1*-3-oxo-cis- D9-hexadecenoyl-ACPs[c]	GCWI-3257 GCWI-1940 GCWI-1349 GCWI-1350
RXN-10659	+1*NADPH[c]+1*PROTO N[c]+1*-3-oxo-cis-D9- hexadecenoyl-ACPs[c]-- >+1*NADP[c]+1*-3- hydroxy-cis-D9- hexaecenoyl-ACPs[c]	GCWI-3427 GCWI-2066 GCWI-3588 GCWI-3869 GCWI-3935
RXN-10661	+1*NADPH[c]+1*PROTO N[c]+1*Trans-D3-cis-D9- hexadecenoyl-ACPs[c]-- >+1*NADP[c]+1*Palmitole oyl-ACPs[c]	GCWI-1393
RXN-10674	+1*Apo-AsbD- Proteins[c]+1*CO-A[c]-- >+1*Holo-AsbD- Proteins[c]+1*-3-5-ADP[c]	
RXN-10675	+1*ATP[c]+1*PROTON[c] +1*-3-4- DIHYDROXYBENZOATE [c]-->+1*CPD- 11474[c]+1*PPI[c]	GCWI-2090
RXN-10676	+1*CPD-11474[c]+1*Holo- AsbD-Proteins[c]-- >+1*AMP[c]+1*PROTON[ c]+1*-34-DHB-AsbD- Proteins[c]	GCWI-2087
RXN-10677	+1*CPD-11479[c]+1*-34-	GCWI-2089



Name	Reaction	Locus
	DHB-AsbD-Proteins[c]-->+1*CPD-11477[c]+1*Holo-AsbD-Proteins[c]+1*PROTON[c]	
RXN-10678	+1*ATP[c]+1*CPD-11477[c]+1*SPERMIDINE[c]-->+1*AMP[c]+1*CPD-11481[c]+1*PPI[c]+1*PROTON[c]	GCWI-2086
RXN-10679	+1*CPD-11481[c]+1*-34-DHB-AsbD-Proteins[c]-->+1*CPD-9985[c]+1*Holo-AsbD-Proteins[c]+1*PROTON[c]	GCWI-2089
RXN-10680	+1*ATP[c]+1*CIT[c]+1*SPERMIDINE[c]-->+1*AMP[c]+1*CPD-11479[c]+1*PPI[c]+1*PROTON[c]	GCWI-2085
RXN-10681	+1*ATP[c]+1*CPD-11479[c]+1*SPERMIDINE[c]-->+1*AMP[c]+1*CPD-11480[c]+1*PPI[c]+1*PROTON[c]	GCWI-2086
RXN-10682	+1*CPD-11480[c]+1*-34-DHB-AsbD-Proteins[c]-->+1*CPD-11481[c]+1*Holo-AsbD-Proteins[c]+1*PROTON[c]	GCWI-2089
RXN-10781	+1*NADH[c]+1*PROTON[c]+1*-5-HYDROXYINDOLE-ACETALDEHYDE[c]<-->+1*CPD-11671[c]+1*NAD[c]	GCWI-2357 GCWI-4498
RXN-10814	+1*PHE[c]+1*-2-KETOGLUTARATE[c]<-->+1*GLT[c]+1*PHENYL-PYRUVATE[c]	GCWI-1706 GCWI-2940
RXN-10827	+1*-1-CARBOXYVINYL-CARBOXYPHOSPHONATE[c]<-->+1*CPD-11740[c]	GCWI-2434
RXN-11028	+1*C1[c]+1*CPD-11994[c]<-->+1*CPD-11997[c]+1*UMP[c]	GCWI-3997

Name	Reaction	Locus
RXN-11051	+1*CPD-11654[c]+2*PROTON[c]<-->+1*CPD-11643[c]	GCWI-4341
RXN-11213	+1*CH3-MALONATE-S-ALD[c]+1*CO-A[c]+1*NAD[c]+1*WATER[c]<-->+1*HCO3[c]+1*NADH[c]+1*PROPIONYL-COA[c]+1*PROTON[c]	GCWI-2437 GCWI-2577
RXN-11277	+1*DIACYLGLYCEROL-PYROPHOSPHATE[c]+1*WATER[c]<-->+1*L-PHOSPHATIDATE[c]+1*PROTON[c]+1*Pi[c]	GCWI-1456 GCWI-2398 GCWI-2572 GCWI-4885 GCWI-5119
RXN-11302	+1*CPD-12231[c]+2*WATER[c]<-->+1*CPD-12261[c]+2*D-ALANINE[c]+1*UNDECAPRENYL-DIPHOSPHATE[c]	GCWI-3999
RXN-11322	+1*GAP[c]+1*GLN[c]+1*RIBOSE-5P[c]<-->+1*GLT[c]+1*PROTON[c]+1*PYRIDOXAL-PHOSPHATE[c]+1*Pi[c]+3*WATER[c]	GCWI-194
RXN-11329	+1*CPD-12287[c]+1*HYDROGEN-PEROXIDE[c]+1*PROTON[c]+1*RH[c]<-->+1*Bromide[c]+2*WATER[c]	GCWI-3181
RXN-11338	+1*AMMONIUM[c]+1*ATP[c]+1*CPD-12302[c]<-->+1*AMP[c]+1*CPD-12295[c]+1*PPI[c]+1*PROTON[c]	GCWI-1922
RXN-11347	+1*CPD-12258[c]+1*CPD-9646[c]<-->+1*CPD-12303[c]+1*UMP[c]	GCWI-3997
RXN-11458	+3*DELTA3-ISOPENTENYL-PP[c]+1*GERANYLGERANYL-PP[c]<-->+1*ALL-	GCWI-1674 GCWI-1676

Name	Reaction	Locus
	TRANS-HEPTAPRENYL-DIPHOSPHATE[c]+3*PPI[c]	
RXN-11475	+1*MALONYL-COA[c]+1*S-ADENOSYLMETHIONINE[c]-->+1*ADENOSYL-HOMO-CYS[c]+1*CPD-12454[c]	GCWI-4256
RXN-11476	+1*NADPH[c]+1*PROTON[c]+1*-3-Ketoglutaryl-ACP-methyl-ester[c]-->+1*NADP[c]+1*-3-Hydroxyglutaryl-ACP-methyl-ester[c]	GCWI-3427 GCWI-2066 GCWI-3588 GCWI-3869 GCWI-3935
RXN-11478	+1*Enoylglutaryl-ACP-methyl-esters[c]+1*NADPH[c]+1*PROTON[c]-->+1*Glutaryl-ACP-methyl-esters[c]+1*NADP[c]	GCWI-1393
RXN-11479	+1*Glutaryl-ACP-methyl-esters[c]+1*MALONYL-ACP[c]-->+1*ACP[c]+1*CARBONDIOXIDE[c]+1*-3-Ketopimeloyl-ACP-methyl-esters[c]	GCWI-3257 GCWI-1940 GCWI-1349 GCWI-1350
RXN-11480	+1*NADPH[c]+1*PROTON[c]+1*-3-Ketopimeloyl-ACP-methyl-esters[c]-->+1*NADP[c]+1*-3-hydroxypimeloyl-ACP-methyl-esters[c]	GCWI-3427 GCWI-2066 GCWI-3588 GCWI-3869 GCWI-3935
RXN-11482	+1*Enoylpimeloyl-ACP-methyl-esters[c]+1*NADPH[c]+1*PROTON[c]-->+1*NADP[c]+1*Pimeloyl-ACP-methyl-esters[c]	GCWI-1393
RXN-11483	+1*Pimeloyl-ACP-methyl-esters[c]+1*WATER[c]-->+1*METOH[c]+1*PROTON[c]+1*Pimeloyl-ACPs[c]	GCWI-4257
RXN-11484	+1*L-ALPHA-	GCWI-4258

Name	Reaction	Locus
	ALANINE[c]+1*PROTON[c]+1*Pimeloyl-ACPs[c]>+1*ACP[c]+1*CARBONDIOXIDE[c]+1*-8-AMINO-7-OXONONANOATE[c]	
RXN-11503	+1*ATP[c]+1*FRU[c]<-->+1*ADP[c]+1*FRUCTOSE-6P[c]+1*PROTON[c]	GCWI-974
RXN-11662	+1*ACETOACETYL-COA[c]+1*NADH[c]+1*PROTON[c]>+1*NAD[c]+1*S-3-HYDROXYBUTANOYL-COA[c]	GCWI-5129 GCWI-5129 GCWI-5442
RXN-11667	+1*S-3-HYDROXYBUTANOYL-COA[c]>+1*CROTONYL-COA[c]+1*WATER[c]	GCWI-2616 GCWI-2439 GCWI-1106 GCWI-2616 GCWI-3561 GCWI-4652
RXN-11717	+1*CPD-12673[c]<-->+1*CPD-11020[c]+1*WATER[c]	GCWI-1965
RXN-11737	+1*L-CYSTEATE[c]+1*-2-KETOGLUTARATE[c]<-->+1*CPD-380[c]+1*GLT[c]	GCWI-1706 GCWI-2940
RXN-11743	+1*CPD-5923[c]+1*Pi[c]>+1*ADENINE[c]+1*CPD-12706[c]	GCWI-1624 GCWI-4228
RXN-11746	+1*CPD-12708[c]+1*NAD[c]+1*WATER[c]>+1*CPD-12709[c]+1*NADH[c]+2*PROTON[c]	GCWI-2379 GCWI-3587 GCWI-2881 GCWI-1451
RXN-11752	+1*ACETYL-COA[c]+1*CPD-9011[c]<-->+1*CO-A[c]+1*CPD-9012[c]+1*PROTON[c]	GCWI-3200
RXN-11847	+1*CPD-12117[c]+1*S-ADENOSYLMETHIONINE[c]>+1*ADENOSYL-HOMO-CYS[c]+1*CPD-12125[c]+1*PROTON[c]	GCWI-1675
RXN-12093	+1*AMMONIA[c]+1*ATP[	GCWI-1509

Name	Reaction	Locus
	c]+1*CPD-13043[c]<-->+1*ADP[c]+1*Pi[c]+1*WATER[c]+1*-7-CYANO-7-DEAZAGUANINE[c]	
RXN-12121	+2*HYDROGEN-PEROXIDE[c]<-->+1*OXYGEN-MOLECULE[c]+2*WATER[c]	GCWI-1061 GCWI-1330 GCWI-3056 GCWI-3180
RXN-12352	+1*OXYGEN-MOLECULE[c]+2*Ubiquinol[c]<-->+2*Ubiquinones[c]+2*WATER[c]	GCWI-5324 GCWI-4920 GCWI-4121 GCWI-2051 GCWI-5323 GCWI-4919 GCWI-2050
RXN-12354	+1*CPD-13337[c]<-->+1*CPD-8742[c]	GCWI-5476
RXN-12444	+1*FMN[c]+1*NADPH[c]+2*PROTON[c]<-->+1*FMNH2[c]+1*NADP[c]	GCWI-1778 GCWI-3373
RXN-12448	+1*NAD[c]+1*Secondary-Alcohols[c]<-->+1*LONG-CHAIN-KETONE[c]+1*NADH[c]+1*PROTON[c]	GCWI-2357 GCWI-379 GCWI-878 GCWI-1005 GCWI-1195 GCWI-2654 GCWI-2708 GCWI-3152 GCWI-3423 GCWI-3425 GCWI-3545 GCWI-4498
RXN-12508	+1*Pyruvate-dehydrogenase-lipoate[c]+1*-2-ALPHA-HYDROXYETHYL-THPP[c]<-->+1*Pyruvate-dehydrogenase-acetylDHlipoyl[c]+1*THIAMINE-PYROPHOSPHATE[c]	GCWI-4114 GCWI-4115
RXN-12583	+1*PROTON[c]+1*PYRUVATE[c]+1*THIAMINE-PYROPHOSPHATE[c]<-->+1*CARBON-DIOXIDE[c]+1*-2-ALPHA-HYDROXYETHYL-THPP[c]	GCWI-4114 GCWI-4115
RXN-12588	+1*CYS[c]+1*PROTON[c]+1*Sulfur-Acceptors[c]<-->	GCWI-4558

Name	Reaction	Locus
	>+1*L-ALPHA-ALANINE[c]+1*Sulfurated-Sulfur-Acceptors[c]	
RXN-12614	+1*GLY[c]+1*OXYGEN-MOLECULE[c]<-->+1*CPD-12279[c]+1*HYDROGEN-PEROXIDE[c]+1*PROTON[c]	GCWI-954 GCWI-2885
RXN-1381-PALMITYL-COA-GLYCEROL-3P--1-PALMITOYLGLYCEROL-3-PHOSPHATE-CO-A.63.	+1*GLYCEROL-3P[c]+1*PALMITYL-COA[c]<-->+1*CO-A[c]+1*1-PALMITOYLGLYCEROL-3-PHOSPHATE[c]	GCWI-2538 GCWI-3637 GCWI-3937
RXN-1381-STEAROYL-COA-GLYCEROL-3P--CPD0-2113-CO-A.41.	+1*GLYCEROL-3P[c]+1*STEAROYL-COA[c]<-->+1*CO-A[c]+1*CPD0-2113[c]	GCWI-2538 GCWI-3637 GCWI-3937
RXN-1623-STEAROYL-COA-CPD0-2113--CPD0-1423-CO-A.39.	+1*CPD0-2113[c]+1*STEAROYL-COA[c]<-->+1*CO-A[c]+1*CPD0-1423[c]	GCWI-408 GCWI-2332
RXN-22	+1*CANA VANINOSUCCINATE[c]<-->+1*CANA VANINE[c]+1*FUM[c]	GCWI-3582 GCWI-4759
RXN-2901	+1*B-ALANINE[c]+1*-2-KETOGLUTARATE[c]<-->+1*GLT[c]+1*MALONATE-S-ALD[c]	GCWI-531
RXN-34	+1*CANA VANINE[c]+1*WATER[c]<-->+1*L-CANALINE[c]+1*PROTON[c]+1*UREA[c]	GCWI-356
RXN-37	+1*CPD-30[c]+1*NAD[c]+1*WATER[c]<-->+1*CPD-35[c]+1*NADH[c]+2*PROTON[c]	GCWI-2379 GCWI-3587 GCWI-2881 GCWI-1451
RXN-3962	+1*N-6-AMINOHEXANOYL-6-AMINOHEXANOATE[c]+1*WATER[c]<-->+2*CPD-884[c]	GCWI-3340

Name	Reaction	Locus
RXN-4822	+1*GLT[c]+1*N-ACETYL-L-2-AMINO-6-OXO-PIMELATE[c]-->+1*CPD-1771[c]+1*-2-KETOGLUTARATE[c]	
RXN-4961	+1*SQUALENE[c]+1*WATER[c]<-->+1*HOPAN-22-OL[c]	GCWI-3590
RXN-5041	+1*NAD[c]+1*-2-3-DIHYDRODIPICOLINATE[c]-->+1*CPD-4841[c]+1*NADH[c]+1*PROTON[c]	GCWI-3886 GCWI-3887
RXN-5061	+1*METHYLENE-THF[c]+2*PROTON[c]+2*Reduced-ferredoxins[c]-->+2*Oxidized-ferredoxins[c]+1*-5-METHYL-THF[c]	GCWI-4388
RXN-5076	+1*PROTON[e]+1*XANTHINE[e]-->+1*PROTON[c]+1*XANTHINE[c]	GCWI-1728
RXN-5183	+1*N2ACETYL-ALPHA-NP[c]+1*NADPH[c]+1*PROTON[c]<-->+1*NADP[c]+1*N-ACETYL-AAA-SEMIALDEHYDE[c]+1*Pi[c]	GCWI-4272
RXN-5901	+1*ACETOACETYL-COA[c]+1*NADPH[c]+1*PROTON[c]-->+1*CPD-650[c]+1*NADP[c]	GCWI-5442 GCWI-1482
RXN-6182	+1*FRUCTOSE-6P[c]<-->+1*ALPHA-GLC-6-P[c]	GCWI-5020
RXN-7101	+2*BCCP-biotin-monomers[c]-->+1*BCCP-dimers[c]	
RXN-721	+1*CPD-667[c]+1*CYS[c]-->+1*ACET[c]+1*L-CYSTATHIONINE[c]+1*PROTON[c]	GCWI-4389
RXN-7607	+1*IMP[c]+1*WATER[c]-->+1*INOSINE[c]+1*Pi[c]	GCWI-2585 GCWI-2586 GCWI-2587 GCWI-3179

Name	Reaction	Locus
		GCWI-4241
RXN-7609	+1*GMP[c]+1*WATER[c]- ->+1*GUANOSINE[c]+1*Pi[c]	GCWI-2585 GCWI-2586 GCWI-2587 GCWI-3179 GCWI-4241
RXN-7716	+1*NAD[c]+1*Oxo-glutarate-dehydrogenase-DH-lipoyl[c]-->+1*NADH[c]+1*Oxo-glutarate-dehydrogenase-lipoyl[c]+1*PROTON[c]	GCWI-1429 GCWI-2826 GCWI-4112 GCWI-4300
RXN-7719	+1*BCAA-dehydrogenase-DH-lipoyl[c]+1*NAD[c]-->+1*BCAA-dehydrogenase-lipoyl[c]+1*NADH[c]+1*PROTON[c]	GCWI-2826 GCWI-4112 GCWI-4300
RXN-7800	+1*CPD-7100[c]+1*PROTON[c]-->+1*CARBONDIOXIDE[c]+1*-2K-4CH3-PENTANOATE[c]	
RXN-7908	+1*CPD-5881[c]-->+1*BIOPTERIN[c]+1*WATER[c]	GCWI-4485
RXN-7913	+1*ATP[c]+1*DCMP[c]-->+1*ADP[c]+1*DCDP[c]	GCWI-1659
RXN-7933	+1*CPD-7224[c]+1*WATER[c]-->+1*ACET[c]+1*L-CITRULLINE[c]	GCWI-688 GCWI-2386
RXN-7958	+1*ATP[c]+1*PROPIONATE[c]<-->+1*ADP[c]+1*PROPYL-P[c]	GCWI-4767
RXN-821	+1*FAD[c]+1*PRO[c]-->+1*FADH2[c]+1*L-DELTA1-PYRROLINE-5-CARBOXYLATE[c]+1*PROTON[c]	GCWI-5131
RXN-8340	+1*GTP[c]<-->+1*PPI[c]+1*PRECURSOR-Z[c]	GCWI-405 GCWI-4849 GCWI-3599 GCWI-2233
RXN-8391	+1*Delta4-hexadecenoyl-ACPs[c]+1*MALONYL-ACP[c]--	GCWI-3257 GCWI-1940 GCWI-1349 GCWI-1350



Name	Reaction	Locus
	>+1*ACP[c]+1*CARBON-DIOXIDE[c]+1*-3-oxo-petroselinoyl-ACPs[c]	
RXN-8529	+1*CPD-8720[c]-->+1*CPD-246[c]	GCWI-3434 GCWI-5476
RXN-8629	+1*DIHYDROLIPOYL-GCVH[c]+1*NAD[c]-->+1*NADH[c]+1*PROTEIN-LIPOYLLYSINE[c]+1*PROTON[c]	GCWI-4362 GCWI-2826 GCWI-4112 GCWI-4300
RXN-8631	+1*FRU1P[c]<-->+1*DIHYDROXY-ACETONE-PHOSPHATE[c]+1*GLYCERALD[c]	GCWI-2580 GCWI-5434
RXN-8654	+1*ATP[c]+1*LIPOIC-ACID[c]+1*PROTON[c]-->+1*LIPOYL-AMP[c]+1*PPI[c]	GCWI-1272 GCWI-4343 GCWI-5486
RXN-8668	+1*Protein-L-Methionine-S-Oxides[c]+1*Red-Thioredoxin[c]-->+1*Ox-Thioredoxin[c]+1*Protein-L-methionine[c]+1*WATER[c]	GCWI-5539 GCWI-1959
RXN-8669	+1*CPD-8989[c]+1*Red-Thioredoxin[c]-->+1*MET[c]+1*Ox-Thioredoxin[c]+1*WATER[c]	GCWI-1959 GCWI-5539
RXN-8672	+1*D-ALANINE[c]+1*OXYGEN-MOLECULE[c]+1*WATER[c]<-->+1*AMMONIA[c]+1*HYDROGEN-PEROXIDE[c]+1*PROTON[c]+1*PYRUVATE[c]	GCWI-954 GCWI-2885
RXN-8673	+1*OXYGEN-MOLECULE[c]+1*SARCOSINE[c]+1*WATER[c]<-->+1*GLYOX[c]+1*HYDR	GCWI-954 GCWI-2885

Name	Reaction	Locus
	OGEN- PEROXIDE[c]+1*METHY LAMINE[c]	
RXN-8674	+1*CPD- 10490[c]+1*OXYGEN- MOLECULE[c]+1*WATE R[c]<-- >+1*ETHANAMINE[c]+1* GLYOX[c]+1*HYDROGE N-PEROXIDE[c]	GCWI-954 GCWI-2885
RXN-8675	+1*CPD-9038[c]+1*S- ADENOSYLMETHIONIN E[c]<-->+1*ADENOSYL- HOMO- CYS[c]+1*DIHYDROSIRO HYDROCHLORIN[c]	GCWI-1587 GCWI-2241
RXN-8975	+1*C3[c]+1*CPD- 9646[c]<-- >+1*C4[c]+1*UMP[c]	GCWI-3997
RXN-8976	+1*C4[c]+1*UDP-N- ACETYL-D- GLUCOSAMINE[c]<-- >+1*CPD- 7695[c]+1*PROTON[c]+1* UDP[c]	GCWI-3994 GCWI-4386
RXN-8979	+1*CPD-622[c]<-- >+1*CPD- 9421[c]+1*WATER[c]	GCWI-2433
RXN-8991	+1*CPD- 9451[c]+1*WATER[c]<-- >+1*-2-D-THREO- HYDROXY-3-CARBOXY- ISOCAPROATE[c]	GCWI-1565 GCWI-1566
RXN-8999	+8*DELTA3- ISOPENTENYL- PP[c]+1*FARNESYL- PP[c]<-- >+8*PPI[c]+1*UNDECAP RENYL-DIPHOSPHATE[c]	GCWI-3907
RXN-9190	+1*ALL-TRANS- HEPTAPRENYL- DIPHOSPHATE[c]+1*DIH YDROXYNAPHTHOATE[ c]+1*PROTON[c]<-- >+1*CARBON-	GCWI-3201

Name	Reaction	Locus
	DIOXIDE[c]+1*CPD-12117[c]+1*PPI[c]	
RXN-9310	+1*CPD-9924[c]-->+1*CPD-9923[c]+1*PYRUVATE[c]	GCWI-4978
RXN-9311	+1*CPD-9925[c]+1*WATER[c]-->+1*CO-A[c]+1*DIHYDROXYNAPHTHOATE[c]+1*PROTON[c]	
RXN-9374	+6*ATP[c]+3*GLY[c]+3*THR[c]+3*-2-3-DIHYDROXYBENZOATE[c]-->+6*AMP[c]+1*CPD-9984[c]+6*PPI[c]+3*PROTON[c]+3*WATER[c]	
RXN-9386	+1*ATP[c]+1*GLN-tRNAs[c]+1*GLT[c]-->+1*AMP[c]+1*L-glutamyl-tRNAGln[c]+1*PPI[c]	GCWI-277
RXN-9514	+1*Acetoacetyl-ACPs[c]+1*NADPH[c]+1*PROTON[c]-->+1*Beta-3-hydroxybutyryl-ACPs[c]+1*NADP[c]	GCWI-3427 GCWI-2066 GCWI-3588 GCWI-3869 GCWI-3935
RXN-9516	+1*Butanoyl-ACPs[c]+1*MALONYL-ACP[c]-->+1*ACP[c]+1*CARBONDIOXIDE[c]+1*-3-oxo-hexanoyl-ACPs[c]	GCWI-3257 GCWI-1940 GCWI-1349 GCWI-1350
RXN-9518	+1*NADPH[c]+1*PROTON[c]+1*-3-oxo-hexanoyl-ACPs[c]-->+1*NADP[c]+1*R-3-hydroxyhexanoyl-ACPs[c]	GCWI-3935 GCWI-3869 GCWI-3588 GCWI-2066 GCWI-3427 GCWI-3427 GCWI-2066 GCWI-3588 GCWI-3869 GCWI-3935 GCWI-375 GCWI-3377 GCWI-4754 GCWI-375 GCWI-2066 GCWI-3377 GCWI-3588 GCWI-3869 GCWI-3935 GCWI-4754
RXN-9520	+1*R-3-hydroxyhexanoyl-ACPs[c]-->+1*Hex-2-	GCWI-2941 GCWI-5366

Name	Reaction	Locus
	enoyl- ACPs[c]+1*WATER[c]	
RXN-9521	+1*Hex-2-enoyl- ACPs[c]+1*NADPH[c]+1* PROTON[c]-- >+1*Hexanoyl- ACPs[c]+1*NADP[c]	GCWI-1393
RXN-9523	+1*Hexanoyl- ACPs[c]+1*MALONYL- ACP[c]-- >+1*ACP[c]+1*CARBON- DIOXIDE[c]+1*-3-Oxo- octanoyl-ACPs[c]	GCWI-3257 GCWI-1940 GCWI-1349 GCWI-1350
RXN-9524	+1*NADPH[c]+1*PROTO N[c]+1*-3-Oxo-octanoyl- ACPs[c]-- >+1*NADP[c]+1*-3- Hydroxy-octanoyl-ACPs[c]	GCWI-3935 GCWI-3869 GCWI-3588 GCWI-2066 GCWI-3427 GCWI-3427 GCWI-2066 GCWI-3588 GCWI-3869 GCWI-3935 GCWI-375 GCWI-3377 GCWI-4754 GCWI-375 GCWI-2066 GCWI-3377 GCWI-3588 GCWI-3869 GCWI-3935 GCWI-4754
RXN-9526	+1*NADPH[c]+1*PROTO N[c]+1*-2-Octenoyl- ACPs[c]-- >+1*NADP[c]+1*Octanoyl- ACPs[c]	GCWI-1393
RXN-9527	+1*MALONYL- ACP[c]+1*Octanoyl- ACPs[c]-- >+1*ACP[c]+1*CARBON- DIOXIDE[c]+1*-3-oxo- decanoyl-ACPs[c]	GCWI-3257 GCWI-1940 GCWI-1349 GCWI-1350
RXN-9528	+1*NADPH[c]+1*PROTO N[c]+1*-3-oxo-decanoyl- ACPs[c]-->+1*Beta- hydroxydecanoyl- ACPs[c]+1*NADP[c]	GCWI-3427 GCWI-3427 GCWI-2066 GCWI-3588 GCWI-3869 GCWI-3935 GCWI-375 GCWI-3377 GCWI-4754 GCWI-375 GCWI-2066 GCWI-3377 GCWI-3588 GCWI-3869 GCWI-3935 GCWI-4754
RXN-9530	+1*NADPH[c]+1*PROTO N[c]+1*Trans-D2-decenoyl- ACPs[c]-->+1*Decanoyl-	GCWI-1393

Name	Reaction	Locus
	ACPs[c]+1*NADP[c]	
RXN-9531	+1*Decanoyl- ACPs[c]+1*MALONYL- ACP[c]-- >+1*ACP[c]+1*CARBON- DIOXIDE[c]+1*-3-oxo- dodecanoyl-ACPs[c]	GCWI-3257 GCWI-1940 GCWI-1349 GCWI-1350
RXN-9532	+1*NADPH[c]+1*PROTO N[c]+1*-3-oxo-dodecanoyl- ACPs[c]-- >+1*NADP[c]+1*R-3- hydroxydodecanoyl- ACPs[c]	GCWI-3427 GCWI-2066 GCWI-3588 GCWI-3869 GCWI-3935 GCWI-375 GCWI-3377 GCWI-4754 GCWI-375 GCWI-2066 GCWI-3377 GCWI-3588 GCWI-3869 GCWI-3935 GCWI-4754
RXN-9533	+1*R-3- hydroxydodecanoyl- ACPs[c]-->+1*Dodec-2- enoyl- ACPs[c]+1*WATER[c]	GCWI-2941 GCWI-5366
RXN-9534	+1*Dodec-2-enoyl- ACPs[c]+1*NADPH[c]+1* PROTON[c]-- >+1*Dodecanoyl- ACPs[c]+1*NADP[c]	GCWI-1393
RXN-9535	+1*Dodecanoyl- ACPs[c]+1*MALONYL- ACP[c]-- >+1*ACP[c]+1*CARBON- DIOXIDE[c]+1*-3-oxo- myristoyl-ACPs[c]	GCWI-3257 GCWI-1940 GCWI-1349 GCWI-1350
RXN-9536	+1*NADPH[c]+1*PROTO N[c]+1*-3-oxo-myristoyl- ACPs[c]-- >+1*NADP[c]+1*R-3- hydroxymyristoyl-ACPs[c]	GCWI-3935 GCWI-3869 GCWI-3588 GCWI-2066 GCWI-3427 GCWI-3427 GCWI-2066 GCWI-3588 GCWI-3869 GCWI-3935 GCWI-375 GCWI-3377 GCWI-4754 GCWI-375 GCWI-2066 GCWI-3377 GCWI-3588 GCWI-3869 GCWI-3935 GCWI-4754
RXN-9537	+1*R-3-hydroxymyristoyl- ACPs[c]-->+1*Tetradec-2- enoyl- ACPs[c]+1*WATER[c]	GCWI-2941 GCWI-5366

Name	Reaction	Locus
RXN-9538	+1*NADPH[c]+1*PROTO N[c]+1*Tetradec-2-enoyl- ACPs[c]-->+1*Myristoyl- ACPs[c]+1*NADP[c]	GCWI-1393
RXN-9539	+1*MALONYL- ACP[c]+1*Myristoyl- ACPs[c]-- >+1*ACP[c]+1*CARBON- DIOXIDE[c]+1*-3-oxo- palmitoyl-ACPs[c]	GCWI-3257 GCWI-1940 GCWI-1349 GCWI-1350
RXN-9540	+1*NADPH[c]+1*PROTO N[c]+1*-3-oxo-palmitoyl- ACPs[c]-- >+1*NADP[c]+1*R-3- Hydroxypalmitoyl-ACPs[c]	GCWI-3427 GCWI-2066 GCWI-3588 GCWI-3869 GCWI-3935 GCWI-375 GCWI-3377 GCWI-4754 GCWI-375 GCWI-2066 GCWI-3377 GCWI-3588 GCWI-3869 GCWI-3935 GCWI-4754
RXN-9548	+1*Stearoyl- ACPs[c]+1*WATER[c]-- >+1*ACP[c]+1*STEARIC- ACID[c]	
RXN-9549	+1*Palmitoyl- ACPs[c]+1*WATER[c]<-- >+1*ACP[c]+1*PALMITA TE[c]+1*PROTON[c]	
RXN-9552	+1*NADPH[c]+1*PROTO N[c]+1*-3-oxo- petroselinoyl-ACPs[c]-- >+1*NADP[c]+1*R-3- hydroxypetroselinoyl- ACPs[c]	GCWI-3935 GCWI-3869 GCWI-3588 GCWI-2066 GCWI-3427 GCWI-3427 GCWI-2066 GCWI-3588 GCWI-3869 GCWI-3935 GCWI-375 GCWI-3377 GCWI-4754 GCWI-375 GCWI-2066 GCWI-3377 GCWI-3588 GCWI-3869 GCWI-3935 GCWI-4754
RXN-9553	+1*R-3- hydroxypetroselinoyl- ACPs[c]-->+1*Petrosel-2- enoyl- ACPs[c]+1*WATER[c]	GCWI-2941 GCWI-5366
RXN-9556	+1*NADPH[c]+1*PROTO N[c]+1*-3-oxo-cis- vaccenoyl-ACPs[c]-- >+1*NADP[c]+1*R-3-	GCWI-3427 GCWI-3427 GCWI-2066 GCWI-3588 GCWI-3869 GCWI-3935 GCWI-375 GCWI-3377

Name	Reaction	Locus
	hydroxy-cis-vaccenoyl-ACPs[c]	GCWI-4754 GCWI-375 GCWI-2066 GCWI-3377 GCWI-3588 GCWI-3869 GCWI-3935 GCWI-4754
RXN-9557	+1*R-3-hydroxy-cis-vaccenoyl-ACPs[c]-->+1*WATER[c]+1*cis-vaccen-2-enoyl-ACPs[c]	GCWI-2941 GCWI-5366
RXN-9583	+1*CPD-10226[c]+1*RIBOSE-5P[c]<-->+1*CPD-10227[c]+1*D-SEDOHEPTULOSE-7-P[c]	GCWI-3420 GCWI-3707
RXN-9598	+1*Monoamines[c]+1*OXYGEN-MOLECULE[c]+1*WATER[c]<-->+1*Aldehydes[c]+1*HYDROGEN-PEROXIDE[c]+1*Primary-Amines[c]	GCWI-2032 GCWI-2123
RXN-9615	+1*AMMONIUM[e]-->+1*AMMONIUM[c]	GCWI-1331 GCWI-1740 GCWI-1878 GCWI-2399 GCWI-4535
RXN-9633	+1*NADPH[c]+1*PROTON[c]+1*-3-oxo-stearoyl-ACPs[c]-->+1*NADP[c]+1*R-3-hydroxystearoyl-ACPs[c]	GCWI-2066 GCWI-3588 GCWI-3869 GCWI-3935 GCWI-3427 GCWI-2066 GCWI-3588 GCWI-3869 GCWI-3935 GCWI-375 GCWI-3377 GCWI-4754 GCWI-375 GCWI-2066 GCWI-3377 GCWI-3588 GCWI-3869 GCWI-3935 GCWI-4754
RXN-9634	+1*R-3-hydroxystearoyl-ACPs[c]-->+1*Octadec-2-enoyl-ACPs[c]+1*WATER[c]	GCWI-2941 GCWI-5366
RXN-9655	+1*Beta-hydroxydecanoyl-ACPs[c]-->+1*Trans-D2-decenoyl-ACPs[c]+1*WATER[c]	GCWI-2941 GCWI-5366
RXN-9657	+1*Crotonyl-ACPs[c]+1*NADH[c]+1*PROTON[c]-->+1*Butanoyl-	

Name	Reaction	Locus
	ACPs[c]+1*NAD[c]	
RXN-969	+1*GLYCOLLATE[c]+1*OXYGEN-MOLECULE[c]>+1*GLYOX[c]+1*HYDROGEN-PEROXIDE[c]	GCWI-1462 GCWI-3554 GCWI-1463
RXN-9770	+1*CPD-3746[c]+1*NADH[c]+1*OXYGEN-MOLECULE[c]>+1*FORMALDEHYDE[c]+1*NAD[c]+1*SO3[c]+1*WATER[c]	GCWI-2951
RXN-9772	+1*FUM[c]+1*L-ASPARTATE[c]>+1*IMINOASPARTATE[c]+1*PROTON[c]+1*SUC[c]	GCWI-4557
RXN-9787	+1*CYS[c]+1*ThiI-L-cysteine[c]<->+1*L-ALPHA-ALANINE[c]+1*ThiI-S-sulfanylcysteine[c]	GCWI-4523 GCWI-4778 GCWI-5102 GCWI-4558
RXN-982	+1*ARSENATE[c]+1*PROTON[c]+1*Red-Glutaredoxins[c]<->+1*CPD-763[c]+1*Ox-Glutaredoxins[c]+1*WATER[c]	GCWI-3210
RXN-9929	+1*DI-H-OROTATE[c]+1*FUM[c]>+1*OROTATE[c]+1*SUC[c]	GCWI-3968
RXN-9939	+1*ACETYL-COA[c]+1*SPERMINE[c]<->+1*CO-A[c]+1*N1-ACETYLSPERMINE[c]+1*PROTON[c]	GCWI-5196 GCWI-2127
RXN-9952	+1*CPD-2961[c]+1*NADP[c]>+1*CARBONDIOXIDE[c]+1*NADPH[c]+1*RIBULOSE-5P[c]	GCWI-367 GCWI-367 GCWI-3419
RXN-9987	+1*UDP-N-ACETYL-D-GLUCOSAMINE[c]+1*WATER[c]<->+1*N-ACETYL-D-	GCWI-5298 GCWI-5367



Name	Reaction	Locus
	MANNOSAMINE[c]+1*PROTON[c]+1*UDP[c]	
RXN0-1061	+1*ATP[c]+1*WATER[c]-->+1*ADP[c]+1*PROTON[c]+1*Pi[c]	GCWI-4608
RXN0-1132	+1*NAD[c]+1*Pyruvate-dehydrogenase-dihydrolipoate[c]-->+1*NADH[c]+1*PROTON[c]+1*Pyruvate-dehydrogenase-lipoate[c]	GCWI-2826 GCWI-4112 GCWI-4300
RXN0-1133	+1*CO-A[c]+1*Pyruvate-dehydrogenase-acetylDHlipoyl[c]-->+1*ACETYL-COA[c]+1*Pyruvate-dehydrogenase-dihydrolipoate[c]	GCWI-2827
RXN0-1147	+1*Oxo-glutarate-dehydrogenase-DH-lipoyl[c]+1*PROTON[c]+1*SUC-COA[c]<-->+1*CO-A[c]+1*Oxo-glutarate-dehydro-suc-DH-lipoyl[c]	GCWI-1429 GCWI-1428
RXN0-12	+1*ZN-2[e]-->+1*ZN-2[c]	GCWI-2475 GCWI-1740 GCWI-1878 GCWI-2399 GCWI-4535
RXN0-1241	+1*Protein-L-glutamine[c]+1*S-ADENOSYLMETHIONINE[c]<-->+1*ADENOSYL-HOMO-CYS[c]+1*PROTON[c]+1*Protein-N5-methyl-L-glutamine[c]	GCWI-5427
RXN0-1321	+1*Guanine34-in-tRNA-with-GUN-anticodon[c]+1*-7-AMINOMETHYL-7-DEAZAGUANINE[c]-->+1*GUANINE[c]+1*tRNA-with-7-aminomethyl-7-deazaguanine[c]	GCWI-4542
RXN0-1342	+1*S-ADENOSYLMETHIONINE[c]+1*tRNA-with-7-	GCWI-4543

Name	Reaction	Locus
	aminomethyl-7-deazaguanine[c]-- >+1*ADENINE[c]+1*MET [c]+2*PROTON[c]+1*tRN As-containing-epoxy- quenosine[c]	
RXN0-1461	+1*COPROPORPHYRINO GEN-III[c]+1*OXYGEN- MOLECULE[c]+2*PROTO N[c]-->+2*CARBON- DIOXIDE[c]+1*PROTOPO RPHYRINOGEN[c]+2*WA TER[c]	GCWI-1089 GCWI-4447
RXN0-1483	+4*FE-2[c]+1*OXYGEN- MOLECULE[c]+4*PROTO N[c]-->+4*FE- 3[c]+2*WATER[c]	GCWI-5170
RXN0-16	+1*MN- 2[e]+1*PROTON[e]-- >+1*MN- 2[c]+1*PROTON[c]	GCWI-1990 GCWI-1740 GCWI-1878 GCWI-2399 GCWI-4535
RXN0-2142	+1*NADPH[c]+1*PROTO N[c]+1*b-Keto-cis-D5- dodecenoyl-ACPs[c]-- >+1*NADP[c]+1*b- Hydroxy-cis-D5- dodecenoyl-ACPs[c]	GCWI-3935 GCWI-3869 GCWI-3588 GCWI-2066 GCWI-3427
RXN0-2145	+1*NADPH[c]+1*PROTO N[c]+1*Trans-D3-cis-D5- dodecenoyl-ACPs[c]-- >+1*Cis-Delta5- dodecenoyl- ACPs[c]+1*NADP[c]	GCWI-1393
RXN0-2161	+1*ATP[c]+1*PROTON[c] +1*SEC- tRNAs[c]+1*SER[c]<-- >+1*AMP[c]+1*L-seryl- SEC-tRNAs[c]+1*PPI[c]	GCWI-196
RXN0-262	+1*CPD- 8123[c]+1*GTP[c]+1*PRO TON[c]-->+1*CPD- 582[c]+1*PPI[c]	GCWI-4887
RXN0-280	+1*Alkanesulfonates[c]+1* FMNH2[c]+1*OXYGEN- MOLECULE[c]--	GCWI-2951

Name	Reaction	Locus
	>+1*Aldehydes[c]+1*FMN[c]+2*PROTON[c]+1*SO3[c]+1*WATER[c]	
RXN0-280-CPD-10434-FMNH2-OXYGEN-MOLECULE--ACETALD-SO3-FMN-WATER-PROTON.62.	+1*CPD-10434[c]+1*FMNH2[c]+1*OXYGEN-MOLECULE[c]->+1*ACETALD[c]+1*FMN[c]+2*PROTON[c]+1*SO3[c]+1*WATER[c]	GCWI-2951
RXN0-280-CPD-3746-FMNH2-OXYGEN-MOLECULE--FORMALDEHYDE-SO3-FMN-WATER-PROTON.66.	+1*CPD-3746[c]+1*FMNH2[c]+1*OXYGEN-MOLECULE[c]>+1*FMN[c]+1*FORMALDEHYDE[c]+2*PROTON[c]+1*SO3[c]+1*WATER[c]	GCWI-2951
RXN0-302	+1*-2-PHOSPHO-4-CYTIDINE-5-DIPHOSPHO-2-C-MET[c]>+1*CMP[c]+1*-2C-METH-D-ERYTHRITOL-CYCLODIPHOSPHATE[c]	GCWI-276
RXN0-366	+1*GUANOSINE[c]+1*WATER[c]>+1*GUANINE[c]+1*RIBOSE[c]	GCWI-5211 GCWI-2933 GCWI-2480
RXN0-4022	+2*NADPH[c]+3*PROTON[c]+1*-7-CYANO-7-DEAZAGUANINE[c]>+2*NADP[c]+1*-7-AMINOMETHYL-7-DEAZAGUANINE[c]	GCWI-1512
RXN0-4621	+1*ATP[c]+1*CPD0-882[c]+1*WATER[c]>+1*ADP[c]+1*CPD0-881[c]+1*PROTON[c]	GCWI-2536
RXN0-4641	+1*CPD0-881[c]+1*WATER[c]>+1*D-LACTATE[c]+1*N-ACETYL-D-GLUCOSAMINE-6-P[c]	GCWI-1041
RXN0-5055	+1*ACETYL-COA[c]+1*Carboxybiotin-BCCP[c]>+1*BCCP-dimers[c]+1*MALONYL-	GCWI-4320 GCWI-2613 GCWI-2614 GCWI-4321 GCWI-4727 GCWI-4728

Name	Reaction	Locus
	COA[c]	
RXN0-5063	+1*N-6-ISOPENTYL-ADENOSINE-37-TRNA[c]+2*S-ADENOSYLMETHIONINE[c]+1*Sulfurated-Sulfur-Acceptors[c]<-->+1*ADENOSYL-HOMOCYS[c]+1*CH33ADO[c]+1*MET[c]+1*PROTON[c]+1*Unsulfurated-Sulfur-Acceptors[c]+1*-2-METHYLTHIO-N-6-ISOPENTYL-ADENOSINE-37-[c]	GCWI-3856
RXN0-5114	+1*WATER[c]+1*-3-P-SERINE[c]<-->+1*Pi[c]+1*SER[c]	
RXN0-5199	+1*GUANOSINE[c]+1*Pi[c]<-->+1*GUANINE[c]+1*RIBOSE-1P[c]	GCWI-4228 GCWI-1624 GCWI-4228
RXN0-5219	+1*AMMONIA[c]+1*PROTON[c]<-->+1*AMMONIUM[c]	
RXN0-5223-CPD-12822-ATP--CPD-12820-ADP-PROTON.36.	+1*ATP[c]+1*CPD-12822[c]<-->+1*ADP[c]+1*CPD-12820[c]+1*PROTON[c]	GCWI-529
RXN0-5223-CPD-8260-ATP--CPD-12821-ADP-PROTON.35.	+1*ATP[c]+1*CPD-8260[c]<-->+1*ADP[c]+1*CPD-12821[c]+1*PROTON[c]	GCWI-529
RXN0-5223-CPD0-2330-ATP--CPD0-2230-ADP-PROTON.36.	+1*ATP[c]+1*CPD0-2330[c]<-->+1*ADP[c]+1*CPD0-2230[c]+1*PROTON[c]	GCWI-529
RXN0-5224	+1*HCO3[c]+1*PROTON[c]<-->+1*CARBONDIOXIDE[c]+1*WATER[c]	GCWI-4918
RXN0-5225	+1*CPD0-1080[c]+1*WATER[c]<-->+1*CPD0-1081[c]+1*CPD0-1082[c]	GCWI-3727 GCWI-4017 GCWI-336 GCWI-1087 GCWI-1109 GCWI-1656 GCWI-1931 GCWI-1932 GCWI-2520 GCWI-2594

Name	Reaction	Locus
		GCWI-3666 GCWI-3700 GCWI-5334
RXN0-5240	+1*D- ALANINE[c]+1*PYRIDOX AL-PHOSPHATE[c]<-- >+1*PYRIDOXAMINE- 5P[c]+1*PYRUVATE[c]	GCWI-439 GCWI-2178 GCWI-5415
RXN0-5289	+1*GLYCERATE[c]+1*N AD[c]<-- >+1*NADH[c]+1*PROTO N[c]+1*TARTRONATE-S- ALD[c]	GCWI-2436
RXN0-5292	+1*DCMP[c]+1*WATER[c] ]<-- >+1*DEOXYCYTIDINE[c] +1*Pi[c]	GCWI-2585 GCWI-2586 GCWI-2587 GCWI-3179 GCWI-4241
RXN0-5304	+1*CPD0-1110[c]<-- >+1*CPD0-1108[c]	GCWI-870
RXN0-5305	+1*CPD0-1108[c]<-- >+1*RIBOSE[c]	
RXN0-5330	+1*NADH[c]+1*PROTON[ c]+1*Ubiquinones[c]<-- >+1*NAD[c]+1*Ubiquinols [c]	GCWI-5395 GCWI-5397 GCWI-5398 GCWI-5399 GCWI-5400
RXN0-5330-CPD-9717- NADH-PROTON--CPD- 9955-NAD.35.	+1*CPD- 9717[c]+1*NADH[c]+1*PR OTON[c]<-->+1*CPD- 9955[c]+1*NAD[c]	GCWI-5395 GCWI-5397 GCWI-5398 GCWI-5399 GCWI-5400
RXN0-5405	+2*C6[c]<-->+1*CPD- 12231[c]+1*PROTON[c]+1 *UNDECAPRENYL- DIPHOSPHATE[c]	GCWI-1615
RXN0-5408	+1*D-MYO-INOSITOL-1- MONOPHOSPHATE[c]+1* WATER[c]<-->+1*MYO- INOSITOL[c]+1*Pi[c]	GCWI-4102
RXN0-5468	+1*Alkyl-Hydro- Peroxides[c]+1*Red- Thioredoxin[c]<-- >+1*Alcohols[c]+1*Ox- Thioredoxin[c]+1*WATER[ c]	GCWI-4769
RXN0-5507	+1*DIHYDRONEOPTERI N-P3[c]+1*WATER[c]<-- >+1*ACETALD[c]+1*CPD	GCWI-1510

Name	Reaction	Locus
	0- 1699[c]+1*P3I[c]+2*PROTON[c]	
RXN0-6377	+3*NADH[c]+1*NITRITE[c]+5*PROTON[c]-->+1*AMMONIUM[c]+3*NAD[c]+2*WATER[c]	GCWI-1585 GCWI-2242 GCWI-2243
RXN0-6491-CPD-9717-DI-H-OROTATE--CPD-9955-OROTATE.40.	+1*CPD-9717[c]+1*DI-H-OROTATE[c]-->+1*CPD-9955[c]+1*OROTATE[c]	GCWI-3969
RXN0-6554-DI-H-OROTATE-CPD-9718--OROTATE-CPD-12125.41.	+1*CPD-9718[c]+1*DI-H-OROTATE[c]-->+1*CPD-12125[c]+1*OROTATE[c]	GCWI-3969
RXN0-6575	+1*CPD0-1699[c]+1*PROTON[c]+1*S-ADENOSYLMETHIONINE[c]-->+1*AMMONIA[c]+1*CH33ADO[c]+1*CPD-13043[c]+1*MET[c]	GCWI-1511
RXN0-723	+1*CTP[c]+1*Reduced-flavodoxins[c]-->+1*DCTP[c]+1*Oxidized-flavodoxins[c]+1*WATER[c]	GCWI-3636
RXN0-724	+1*Reduced-flavodoxins[c]+1*UTP[c]-->+1*DUTP[c]+1*Oxidized-flavodoxins[c]+1*WATER[c]	GCWI-3636
RXN0-745	+1*ATP[c]+1*Reduced-flavodoxins[c]-->+1*DATP[c]+1*Oxidized-flavodoxins[c]+1*WATER[c]	GCWI-3636
RXN0-746	+1*GTP[c]+1*Reduced-flavodoxins[c]-->+1*DGTP[c]+1*Oxidized-flavodoxins[c]+1*WATER[c]	GCWI-3636
RXN0-882	+1*PROTON[c]+2*Reduced-ferredoxins[c]+1*-2C-METH-D-ERYTHRITOL-CYCLODIPHOSPHATE[c]	GCWI-4412

Name	Reaction	Locus
	-->+1*HYDROXY-METHYL-BUTENYL-DIP[c]+2*Oxidized-ferredoxins[c]+1*WATER[c]	
RXN0-949	+2*CPD-7046[c]+1*Octanoylated-domains[c]+2*S-ADENOSYLMETHIONINE[c]>+2*CH33ADO[c]+1*Lipoylated-domains[c]+2*MET[c]	GCWI-5093
RXN1G-1053	+1*NADPH[c]+1*PROTON[c]+1*cis-delta19-3-oxo-C38-ACPs[c]<-->+1*NADP[c]+1*cis-delta19-3-hydroxyC38-ACPs[c]	GCWI-3935 GCWI-3869 GCWI-3588 GCWI-2066 GCWI-3427
RXN1G-1130	+1*NADH[c]+1*PROTON[c]+1*trans-D2-cis-D19-C38-ACPs[c]<-->+1*NAD[c]+1*cis-delta19-C38-ACPs[c]	GCWI-1393
RXN1G-163	+1*NADPH[c]+1*PROTON[c]+1*cis-delta11-3-oxo-melissoyl-ACPs[c]<-->+1*NADP[c]+1*cis-delta11-3-hydroxymelissoyl-ACPs[c]	GCWI-3935 GCWI-3869 GCWI-3588 GCWI-2066 GCWI-3427
RXN1G-171	+1*NADH[c]+1*PROTON[c]+1*trans-D2-cis-D5-lignoceroyl-ACPs[c]<-->+1*NAD[c]+1*cis-delta5-lignoceroyl-ACPs[c]	GCWI-1393
RXN1G-240	+1*NADPH[c]+1*PROTON[c]+1*cis-delta9-3-oxo-montanoyl-ACPs[c]<-->+1*NADP[c]+1*cis-delta9-3-hydroxymontanoyl-ACPs[c]	GCWI-3935 GCWI-3869 GCWI-3588 GCWI-2066 GCWI-3427
RXN1G-285	+1*NADH[c]+1*PROTON[c]+1*trans-D2-cis-D9-montanoyl-ACPs[c]<-->+1*NAD[c]+1*cis-delta9-	GCWI-1393

Name	Reaction	Locus
	montanoyl-ACPs[c]	
RXN1G-287	+1*NADPH[c]+1*PROTO N[c]+1*cis-delta21-3-oxo- C40-ACPs[c]<-- >+1*NADP[c]+1*cis- delta21-3-hydroxyC40- ACPs[c]	GCWI-3935 GCWI-3869 GCWI-3588 GCWI-2066 GCWI-3427
RXN1G-320	+1*R-3-hydroxyarachidoyl- ACPs[c]<-- >+1*WATER[c]+1*trans- delta2-arachidoyl-ACPs[c]	GCWI-2941 GCWI-5366
RXN1G-358	+1*NADPH[c]+1*PROTO N[c]+1*cis-delta15-3-oxo- gheddoyl-ACPs[c]<-- >+1*NADP[c]+1*cis- delta15-3-hydroxygheddoyl- ACPs[c]	GCWI-3935 GCWI-3869 GCWI-3588 GCWI-2066 GCWI-3427
RXN1G-364	+1*NADPH[c]+1*PROTO N[c]+1*cis-delta7-3-oxo- cerotoyl-ACPs[c]<-- >+1*NADP[c]+1*cis- delta7-3-hydroxycerotoyl- ACPs[c]	GCWI-3935 GCWI-3869 GCWI-3588 GCWI-2066 GCWI-3427
RXN1G-37	+1*NADH[c]+1*PROTON[ c]+1*trans-D2-cis-D7- cerotoyl-ACPs[c]<-- >+1*NAD[c]+1*cis-delta7- cerotoyl-ACPs[c]	GCWI-1393
RXN1G-396	+1*NADH[c]+1*PROTON[ c]+1*trans-D2-cis-D15- gheddoyl-ACPs[c]<-- >+1*NAD[c]+1*cis- delta15-gheddoyl-ACPs[c]	GCWI-1393
RXN1G-460	+1*CPD1G- 567[c]+1*MALONYL- ACP[c]<-->+1*CARBON- DIOXIDE[c]+1*CO- A[c]+1*-3-oxo-behenoyl- ACPs[c]	GCWI-3257 GCWI-1940 GCWI-1349 GCWI-1350
RXN1G-469	+1*NADP[c]+1*R-3- hydroxybehenoyl-ACPs[c]<-- >+1*NADPH[c]+1*PROTO N[c]+1*-3-oxo-behenoyl- ACPs[c]	GCWI-3935 GCWI-3869 GCWI-3588 GCWI-2066 GCWI-3427
RXN1G-479	+1*R-3-hydroxybehenoyl-	GCWI-2941 GCWI-5366



Name	Reaction	Locus
	ACPs[c]-- >+1*WATER[c]+1*trans- delta2-behenoyl-ACPs[c]	
RXN1G-517	+1*R-3-hydroxylignoceroyl- ACPs[c]-- >+1*WATER[c]+1*trans- delta2-lignoceroyl-ACPs[c]	GCWI-2941 GCWI-5366
RXN1G-72	+1*NADPH[c]+1*PROTO N[c]+1*cis-delta5-3-oxo- lignoceroyl-ACPs[c]<-- >+1*NADP[c]+1*cis- delta5-3- hydroxylignoceroyl- ACPs[c]	GCWI-3935 GCWI-3869 GCWI-3588 GCWI-2066 GCWI-3427
RXN1G-881	+1*NADPH[c]+1*PROTO N[c]+1*cis-delta17-3-oxo- C36-ACPs[c]<-- >+1*NADP[c]+1*cis- delta17-3-hydroxyC36- ACPs[c]	GCWI-3935 GCWI-3869 GCWI-3588 GCWI-2066 GCWI-3427
RXN1G-962	+1*NADH[c]+1*PROTON[ c]+1*trans-D2-cis-D17- C36-ACPs[c]<-- >+1*NAD[c]+1*cis- delta17-C36-ACPs[c]	GCWI-1393
RXN490-3641	+1*OXYGEN- MOLECULE[c]+1*PRO[c] +1*-2- KETOGLUTARATE[c]-- >+1*CARBON- DIOXIDE[c]+1*SUC[c]+1* -4-HYDROXY-L- PROLINE[c]	GCWI-4369
RXN66-3	+1*ACETALD[c]+1*NAD[ c]+1*WATER[c]-- >+1*ACET[c]+1*NADH[c] +2*PROTON[c]	GCWI-2379 GCWI-2379 GCWI-3587 GCWI-2881 GCWI-1451
RXNCWI-10	+1*CPDCWI- 7[c]+1*FMNH2[c]+1*OXY GEN-MOLECULE[c]-- >+1*CIT[c]+1*FE- 2[c]+1*FMN[c]+2*SPERM IDINE[c]+2*-3-4- DIHYDROXYBENZOATE [c]	

Name	Reaction	Locus
RXNCWI-100	+1*FE-3[c]-- >+1*CPDCWI-16[c]	
RXNCWI-104	+1*FE-3[e]+3*-3-4- DIHYDROXYBENZOATE [e]-->+1*CPDCWI- 18[e]+6*PROTON[e]	
RXNCWI-105	+1*ATP[c]+1*CPDCWI- 18[e]+1*WATER[c]-- >+1*ADP[c]+1*CPDCWI- 18[c]+1*Pi[c]	
RXNCWI-106	+1*CPDCWI- 18[c]+6*PROTON[c]-- >+1*FE-3[c]+3*-3-4- DIHYDROXYBENZOATE [c]	
RXNCWI-107	+1*ACET[c]+1*PROTON[ c]<-- >+1*ACET[e]+1*PROTON [e]	
RXNCWI-108	+1*ATP[c]+1*CPD- 10353[c]+1*WATER[c]-- >+1*ADP[c]+1*CPD- 10353[e]+1*PROTON[c]+1 *Pi[c]	
RXNCWI-109	+1*L-ALPHA- ALANINE[e]+1*PROTON[ e]-->+1*L-ALPHA- ALANINE[c]+1*PROTON[ c]	GCWI-5138 GCWI-3501 GCWI-3313 GCWI-3227 GCWI-3159 GCWI-3026 GCWI-1063 GCWI-1037 GCWI-896 GCWI-833 GCWI-799 GCWI-687 GCWI-3147 GCWI-3146 GCWI-907 GCWI-3872 GCWI-3873 GCWI-4677 GCWI-3160 GCWI-2162 GCWI-2019 GCWI-1602 GCWI-1023 GCWI-893
RXNCWI-110	+1*CPD-763[c]<-- >+1*CPD-763[e]	
RXNCWI-111	+1*PROTON[e]+1*SUC[e] <-- >+1*PROTON[c]+1*SUC[c ]	
RXNCWI-112	+1*ATP[c]+1*MN- 2[e]+1*WATER[c]-- >+1*ADP[c]+1*MN-	

Name	Reaction	Locus
	2[c]+1*PROTON[c]+1*Pi[c]	
RXNCWI-113	+1*PROTON[e]+1*TYR[e] -- >+1*PROTON[c]+1*TYR[c]	GCWI-5138 GCWI-3501 GCWI-3313 GCWI-3227 GCWI-3159 GCWI-3026 GCWI-1063 GCWI-1037 GCWI-896 GCWI-833 GCWI-799 GCWI-687 GCWI-3147 GCWI-3146 GCWI-907 GCWI-3872 GCWI-3873 GCWI-4677 GCWI-3160 GCWI-2162 GCWI-2019 GCWI-1602 GCWI-1023 GCWI-893
RXNCWI-114	+1*ASN[e]+1*PROTON[e] -- >+1*ASN[c]+1*PROTON[c]	GCWI-5138 GCWI-3501 GCWI-3313 GCWI-3227 GCWI-3159 GCWI-3026 GCWI-1063 GCWI-1037 GCWI-896 GCWI-833 GCWI-799 GCWI-687 GCWI-3147 GCWI-3146 GCWI-907 GCWI-3872 GCWI-3873 GCWI-4677 GCWI-3160 GCWI-2162 GCWI-2019 GCWI-1602 GCWI-1023 GCWI-893
RXNCWI-115	+1*ATP[c]+1*GLN[e]+1* WATER[c]-- >+1*ADP[c]+1*GLN[c]+1* PROTON[c]+1*Pi[c]	GCWI-573 GCWI-847 GCWI-574 GCWI-1070 GCWI-2039 GCWI-2040 GCWI-575 GCWI-4291 GCWI-4290 GCWI-4289 GCWI-2043 GCWI-2042 GCWI-2041 GCWI-1072 GCWI-1071 GCWI-846 GCWI-845 GCWI-844 GCWI-843
RXNCWI-13	+1*PALMITYL- COA[c]+1*-1- PALMITOYLGLYCEROL- 3-PHOSPHATE[c]-- >+1*CO-A[c]+1*CPD0- 1422[c]	GCWI-408 GCWI-2332
RXNCWI-14	+1*CPD- 12125[c]+2*Cytochromes- C- Oxidized[c]+1*PROTON[c]	GCWI-1684

Name	Reaction	Locus
	-->+1*CPD- 9718[c]+2*Cytochromes-C- Reduced[c]+3*PROTON[e]	
RXNCWI-15	+2*Cytochromes-C- Reduced[c]+0.5*OXYGEN- MOLECULE[c]+6*PROTO N[c]-->+2*Cytochromes-C- Oxidized[c]+4*PROTON[e] +1*WATER[c]	GCWI-4085 GCWI-4086 GCWI-4087 GCWI-4088
RXNCWI-16	+1*CPD- 12125[c]+1*NITRATE[c]+ 2*PROTON[c]-->+1*CPD- 9718[c]+1*NITRITE[c]+2* PROTON[e]+1*WATER[c]	GCWI-2225 GCWI-2223 GCWI-2224 GCWI-2226
RXNCWI-17	+1*CPD- 9718[c]+1*GLYCEROL- 3P[c]-->+1*CPD- 12125[c]+1*DIHYDROXY- ACETONE- PHOSPHATE[c]	GCWI-1217
RXNCWI-21	+1*CPD- 12125[c]+0.5*OXYGEN- MOLECULE[c]+2*PROTO N[c]-->+1*CPD- 9718[c]+2*PROTON[e]+1* WATER[c]	GCWI-5324 GCWI-4920 GCWI-4121 GCWI-2051 GCWI-5323 GCWI-4919 GCWI-2050
RXNCWI-22	+1*NADH[c]+2*NITRIC- OXIDE[c]+2*OXYGEN- MOLECULE[c]-- >+1*NAD[c]+2*NITRATE[ c]+1*PROTON[c]	GCWI-1609
RXNCWI-23	+1*NADPH[c]+2*NITRIC- OXIDE[c]+2*OXYGEN- MOLECULE[c]-- >+1*NADP[c]+2*NITRAT E[c]+1*PROTON[c]	GCWI-1609
RXNCWI-24	+1*NADPH[c]+1*PROTO N[c]+1*-2-3- DIHYDRODIPICOLINATE [c]-->+1*DELTA1- PIPERIDEINE-2-6- DICARBOXYLATE[c]+1* NADP[c]	GCWI-1694
RXNCWI-25	+1*NADH[c]+1*PROTON[ c]+1*-2-3-	GCWI-1694

Name	Reaction	Locus
	DIHYDRODIPICOLINATE [c]-->+1*DELTA1- PIPERIDEINE-2-6- DICARBOXYLATE[c]+1* NAD[c]	
RXNCWI-26	+1*GLC[c]+1*NADP[c]-- >+1*GLC-D- LACTONE[c]+1*NADPH[c] ]+1*PROTON[c]	GCWI-4843
RXNCWI-27	+1*GLC[c]+1*NAD[c]-- >+1*GLC-D- LACTONE[c]+1*NADH[c] +1*PROTON[c]	GCWI-4843
RXNCWI-29	+1*DIHYDROXY- ACETONE- PHOSPHATE[c]+1*NADH [c]+1*PROTON[c]-- >+1*GLYCEROL- 3P[c]+1*NAD[c]	GCWI-1667
RXNCWI-30	+1*L-ASPARTATE- SEMIALDEHYDE[c]+1*N ADPH[c]+1*PROTON[c]-- >+1*HOMO- SER[c]+1*NADP[c]	GCWI-2072 GCWI-2675 GCWI-5505
RXNCWI-31	+1*L-ASPARTATE- SEMIALDEHYDE[c]+1*N ADH[c]+1*PROTON[c]-- >+1*HOMO- SER[c]+1*NAD[c]	GCWI-2072 GCWI-2675 GCWI-5505
RXNCWI-32	+1*HYDROXY-METHYL- BUTENYL- DIP[c]+1*NADPH[c]+1*P ROTON[c]-->+1*DELTA3- ISOPENTENYL- PP[c]+1*NADP[c]+1*WAT ER[c]	GCWI-4421
RXNCWI-33	+1*HYDROXY-METHYL- BUTENYL- DIP[c]+1*NADH[c]+1*PR OTON[c]-->+1*DELTA3- ISOPENTENYL- PP[c]+1*NAD[c]+1*WATE R[c]	GCWI-4421
RXNCWI-35	+1*L-DELTA1- PYRROLINE-5-	GCWI-399 GCWI-3023 GCWI-3161 GCWI-4277

Name	Reaction	Locus
	CARBOXYLATE[c]+1*NA DPH[c]+2*PROTON[c]-- >+1*NADP[c]+1*PRO[c]	
RXNCWI-36	+1*L-DELTA1- PYRROLINE-5- CARBOXYLATE[c]+1*NA DP[c]+2*WATER[c]-- >+1*GLT[c]+1*NADPH[c] +1*PROTON[c]	GCWI-516
RXNCWI-38	+1*HYDROXY-METHYL- BUTENYL- DIP[c]+1*NADPH[c]+1*P ROTON[c]-->+1*CPD- 4211[c]+1*NADP[c]+1*W ATER[c]	GCWI-4421
RXNCWI-39	+1*HYDROXY-METHYL- BUTENYL- DIP[c]+1*NADH[c]+1*PR OTON[c]-->+1*CPD- 4211[c]+1*NAD[c]+1*WA TER[c]	GCWI-4421
RXNCWI-41	+1*PROTON[e]+1*TRP[e]- - >+1*PROTON[c]+1*TRP[c] ]	GCWI-3872 GCWI-3873 GCWI-4677 GCWI-3160 GCWI-2162 GCWI-2019 GCWI-1602 GCWI-1023 GCWI-893 GCWI-5138 GCWI-3501 GCWI-3313 GCWI-3227 GCWI-3159 GCWI-3026 GCWI-1063 GCWI-1037 GCWI-896 GCWI-833 GCWI-799 GCWI-687 GCWI-3147 GCWI-3146 GCWI-907
RXNCWI-42	+1*PROTON[e]+1*VAL[e] -- >+1*PROTON[c]+1*VAL[ c]	GCWI-3872 GCWI-3873 GCWI-4677 GCWI-3160 GCWI-2162 GCWI-2019 GCWI-1602 GCWI-1023 GCWI-893 GCWI-5138 GCWI-3501 GCWI-3313 GCWI-3227 GCWI-3159 GCWI-3026 GCWI-1063 GCWI-1037 GCWI-896 GCWI-833 GCWI-799 GCWI-687 GCWI-3147 GCWI-3146 GCWI-907

Name	Reaction	Locus
RXNCWI-43	+1*CA-2[e]+1*CIT[e]-- >+1*CA-2[c]+1*CIT[c]	GCWI-785
RXNCWI-44	+1*ATP[c]+1*CA- 2[c]+1*WATER[c]-- >+1*ADP[c]+1*CA- 2[e]+1*Pi[c]	
RXNCWI-45	+1*L- ASPARTATE[e]+1*PROT ON[e]-->+1*L- ASPARTATE[c]+1*PROT ON[c]	GCWI-3872 GCWI-3873 GCWI-4677 GCWI-3160 GCWI-2162 GCWI-2019 GCWI-1602 GCWI-1023 GCWI-893 GCWI-5138 GCWI-3501 GCWI-3313 GCWI-3227 GCWI-3159 GCWI-3026 GCWI-1063 GCWI-1037 GCWI-896 GCWI-833 GCWI-799 GCWI-687 GCWI-3147 GCWI-3146 GCWI-907
RXNCWI-46	+1*PHE[e]+1*PROTON[e]- - >+1*PHE[c]+1*PROTON[c] ]	GCWI-3872 GCWI-3873 GCWI-4677 GCWI-3160 GCWI-2162 GCWI-2019 GCWI-1602 GCWI-1023 GCWI-893 GCWI-5138 GCWI-3501 GCWI-3313 GCWI-3227 GCWI-3159 GCWI-3026 GCWI-1063 GCWI-1037 GCWI-896 GCWI-833 GCWI-799 GCWI-687 GCWI-3147 GCWI-3146 GCWI-907
RXNCWI-47	+1*ATP[c]+1*CO- A[c]+1*STEARIC- ACID[c]-- >+1*AMP[c]+1*PPI[c]+1* STEAROYL-COA[c]	GCWI-2036 GCWI-2087 GCWI-3657 GCWI-1090 GCWI-1274 GCWI-4654
RXNCWI-48	+2*CPD- 12822[c]+2*PROTON[c]<-- >+1*CPDCWI- 13[c]+1*GLYCEROL[c]	
RXNCWI-49	+1*ATP[c]+1*CPDCWI- 14[c]<-- >+1*ADP[c]+1*CPD0- 1423[c]+1*PROTON[c]	GCWI-4432
RXNCWI-50	+1*ATP[c]+1*CO- A[c]+1*PALMITATE[c]--	GCWI-2036 GCWI-2087 GCWI-3657 GCWI-1090

Name	Reaction	Locus
	>+1*AMP[c]+1*PALMITYL-COA[c]+1*PPI[c]	GCWI-1274 GCWI-4654
RXNCWI-53	+1*ATP[c]+1*FE-3[e]+1*WATER[c]-->+1*ADP[c]+1*FE-3[c]+1*PROTON[c]+1*Pi[c]	
RXNCWI-54	+1*ATP[c]+1*CYS[e]+1*WATER[c]-->+1*ADP[c]+1*CYS[c]+1*PROTON[c]+1*Pi[c]	GCWI-573 GCWI-847 GCWI-574 GCWI-1070 GCWI-2039 GCWI-575 GCWI-2040 GCWI-4291 GCWI-4290 GCWI-4289 GCWI-2043 GCWI-2042 GCWI-2041 GCWI-1072 GCWI-1071 GCWI-846 GCWI-845 GCWI-844 GCWI-843
RXNCWI-57	+1*DGMP[c]+1*WATER[c]-->+1*DEOXYGUANOSINE[c]+1*Pi[c]	GCWI-2585 GCWI-2586 GCWI-2587 GCWI-3179 GCWI-4241
RXNCWI-58	+1*GUANOSINE[c]<-->+1*GUANOSINE[e]	GCWI-2002 GCWI-5335 GCWI-5174 GCWI-5173 GCWI-3020 GCWI-810 GCWI-538 GCWI-400
RXNCWI-59	+1*XANTHOSINE[c]<-->+1*XANTHOSINE[e]	GCWI-2002 GCWI-5335 GCWI-5174 GCWI-5173 GCWI-3020 GCWI-810 GCWI-538 GCWI-400
RXNCWI-60	+1*INOSINE[c]<-->+1*INOSINE[e]	GCWI-2002 GCWI-5335 GCWI-5174 GCWI-5173 GCWI-3020 GCWI-810 GCWI-538 GCWI-400
RXNCWI-61	+1*ADENOSINE[c]<-->+1*ADENOSINE[e]	GCWI-2002 GCWI-5335 GCWI-5174 GCWI-5173 GCWI-3020 GCWI-810 GCWI-538 GCWI-400
RXNCWI-62	+1*ARG[e]+1*ATP[c]+1*WATER[c]-->+1*ADP[c]+1*ARG[c]+1*PROTON[c]+1*Pi[c]	GCWI-573 GCWI-847 GCWI-574 GCWI-1070 GCWI-2039 GCWI-2040 GCWI-575 GCWI-4291 GCWI-4290 GCWI-4289 GCWI-2043 GCWI-2042 GCWI-2041 GCWI-1072 GCWI-1071 GCWI-846



Name	Reaction	Locus
		GCWI-845 GCWI-844 GCWI-843
RXNCWI-63	+1*ARG[e]+1*PROTON[e] -- >+1*ARG[c]+1*PROTON[c]	GCWI-5138 GCWI-3501 GCWI-3313 GCWI-3227 GCWI-3159 GCWI-3026 GCWI-1063 GCWI-1037 GCWI-896 GCWI-833 GCWI-799 GCWI-687 GCWI-3147 GCWI-3146 GCWI-907 GCWI-3872 GCWI-3873 GCWI-4677 GCWI-3160 GCWI-2162 GCWI-2019 GCWI-1602 GCWI-1023 GCWI-893
RXNCWI-64	+1*ATP[c]+1*LEU[e]+1* WATER[c]-- >+1*ADP[c]+1*LEU[c]+1* PROTON[c]+1*Pi[c]	GCWI-573 GCWI-847 GCWI-574 GCWI-1070 GCWI-2039 GCWI-2040 GCWI-575 GCWI-4291 GCWI-4290 GCWI-4289 GCWI-2043 GCWI-2042 GCWI-2041 GCWI-1072 GCWI-1071 GCWI-846 GCWI-845 GCWI-844 GCWI-843
RXNCWI-65	+1*LEU[e]+1*PROTON[e] -- >+1*LEU[c]+1*PROTON[c]	GCWI-5138 GCWI-3501 GCWI-3313 GCWI-3227 GCWI-3159 GCWI-3026 GCWI-1063 GCWI-1037 GCWI-896 GCWI-833 GCWI-799 GCWI-687 GCWI-3147 GCWI-3146 GCWI-907 GCWI-3872 GCWI-3873 GCWI-4677 GCWI-3160 GCWI-2162 GCWI-2019 GCWI-1602 GCWI-1023 GCWI-893
RXNCWI-66	+1*ATP[c]+1*HIS[e]+1*W ATER[c]-- >+1*ADP[c]+1*HIS[c]+1* PROTON[c]+1*Pi[c]	GCWI-573 GCWI-847 GCWI-574 GCWI-1070 GCWI-2039 GCWI-2040 GCWI-575 GCWI-4291 GCWI-4290 GCWI-4289 GCWI-2043 GCWI-2042 GCWI-2041 GCWI-1072 GCWI-1071 GCWI-846 GCWI-845 GCWI-844 GCWI-843

Name	Reaction	Locus
RXNCWI-67	+1*HIS[e]+1*PROTON[e]- - >+1*HIS[c]+1*PROTON[c]	GCWI-5138 GCWI-3501 GCWI-3313 GCWI-3227 GCWI-3159 GCWI-3026 GCWI-1063 GCWI-1037 GCWI-896 GCWI-833 GCWI-799 GCWI-687 GCWI-3147 GCWI-3146 GCWI-907 GCWI-3872 GCWI-3873 GCWI-4677 GCWI-3160 GCWI-2162 GCWI-2019 GCWI-1602 GCWI-1023 GCWI-893
RXNCWI-68	+1*MET[e]+1*PROTON[e] -- >+1*MET[c]+1*PROTON[c]	GCWI-5138 GCWI-3501 GCWI-3313 GCWI-3227 GCWI-3159 GCWI-3026 GCWI-1063 GCWI-1037 GCWI-896 GCWI-833 GCWI-799 GCWI-687 GCWI-3147 GCWI-3146 GCWI-907 GCWI-3872 GCWI-3873 GCWI-4677 GCWI-3160 GCWI-2162 GCWI-2019 GCWI-1602 GCWI-1023 GCWI-893
RXNCWI-69	+1*ATP[c]+1*MET[e]+1* WATER[c]-- >+1*ADP[c]+1*MET[c]+1* PROTON[c]+1*Pi[c]	GCWI-573 GCWI-847 GCWI-574 GCWI-1070 GCWI-2039 GCWI-2040 GCWI-575 GCWI-4291 GCWI-4290 GCWI-4289 GCWI-2043 GCWI-2042 GCWI-2041 GCWI-1072 GCWI-1071 GCWI-846 GCWI-845 GCWI-844 GCWI-843
RXNCWI-7	+1*CPD-9984[e]+1*FE- 3[e]-->+1*CPDCWI- 6[e]+6*PROTON[e]	
RXNCWI-70	+1*ATP[c]+1*THIAMINE[ e]+1*WATER[c]-- >+1*ADP[c]+1*PROTON[c] ]+1*Pi[c]+1*THIAMINE[c]	
RXNCWI-72	+1*PROTON[e]+1*THIAM INE[e]-- >+1*PROTON[c]+1*THIA MINE[c]	GCWI-5138 GCWI-3501 GCWI-3313 GCWI-3227 GCWI-3159 GCWI-3026 GCWI-1063 GCWI-1037 GCWI-896 GCWI-833

Name	Reaction	Locus
		GCWI-799 GCWI-687 GCWI-3147 GCWI-3146 GCWI-907 GCWI-3872 GCWI-3873 GCWI-4677 GCWI-3160 GCWI-2162 GCWI-2019 GCWI-1602 GCWI-1023 GCWI-893
RXNCWI-73	+1*ATP[c]+1*DEOXYADENOSINE[c]-- >+1*ADP[c]+1*DAMP[c]+ 1*PROTON[c]	GCWI-199 GCWI-200
RXNCWI-74	+1*DEOXYADENOSINE[c] ]<-- >+1*DEOXYADENOSINE [e]	GCWI-2002 GCWI-5335 GCWI-5174 GCWI-5173 GCWI-3020 GCWI-810 GCWI-538 GCWI-400
RXNCWI-75	+1*DAMP[c]+1*WATER[c] ]-- >+1*DEOXYADENOSINE [c]+1*Pi[c]	GCWI-2585 GCWI-2586 GCWI-2587 GCWI-3179 GCWI-4241
RXNCWI-76	+1*ATP[c]+1*DAMP[c]-- >+1*ADP[c]+1*DADP[c]	GCWI-321
RXNCWI-77	+1*TMP[c]+1*WATER[c]- - >+1*Pi[c]+1*THYMIDINE [c]	GCWI-2585 GCWI-2586 GCWI-2587 GCWI-3179 GCWI-4241
RXNCWI-78	+1*CMP[c]+1*WATER[c]- - >+1*CYTIDINE[c]+1*Pi[c]	GCWI-2585 GCWI-2586 GCWI-2587 GCWI-3179 GCWI-4241
RXNCWI-79	+1*ITP[c]+1*URIDINE[c]- - >+1*IDP[c]+1*PROTON[c] +1*UMP[c]	GCWI-3037 GCWI-3096 GCWI-4507
RXNCWI-8	+1*CPD-9985[e]+1*FE- 3[e]-->+1*CPDCWI- 7[e]+5*PROTON[e]	
RXNCWI-81	+1*CYTIDINE[c]+1*ITP[c] -- >+1*CMP[c]+1*IDP[c]+1* PROTON[c]	GCWI-4507
RXNCWI-82	+1*CYTOSINE[c]+1*RIBO SE-1P[c]-- >+1*CYTIDINE[c]+1*Pi[c]	GCWI-2003 GCWI-4227
RXNCWI-83	+1*CYTIDINE[e]-- >+1*CYTIDINE[c]	GCWI-2002 GCWI-5335 GCWI-5174 GCWI-5173 GCWI-3020 GCWI-810

Name	Reaction	Locus
		GCWI-538 GCWI-400
RXNCWI-85	+1*ATP[c]+1*DEOXYCYTIDINE[c]-- >+1*ADP[c]+1*DCMP[c]	GCWI-199 GCWI-200
RXNCWI-86	+1*DEOXYCYTIDINE[c]< -- >+1*DEOXYCYTIDINE[e]	GCWI-2002 GCWI-5335 GCWI-5174 GCWI-5173 GCWI-3020 GCWI-810 GCWI-538 GCWI-400
RXNCWI-87	+1*ATP[c]+1*IDP[c]-- >+1*ADP[c]+1*ITP[c]	GCWI-1677
RXNCWI-88	+1*ILE[e]+1*PROTON[e]-- >+1*ILE[c]+1*PROTON[c]	GCWI-5138 GCWI-3501 GCWI-3313 GCWI-3227 GCWI-3159 GCWI-3026 GCWI-1063 GCWI-1037 GCWI-896 GCWI-833 GCWI-799 GCWI-687 GCWI-3147 GCWI-3146 GCWI-907 GCWI-3872 GCWI-3873 GCWI-4677 GCWI-3160 GCWI-2162 GCWI-2019 GCWI-1602 GCWI-1023 GCWI-893
RXNCWI-89	+1*FAD[c]+1*PALMITYL -COA[c]-->+1*CPD0- 2117[c]+1*FADH2[c]	GCWI-2435 GCWI-2612 GCWI-5127 GCWI-5440 GCWI-5441
RXNCWI-9	+1*CPDCWI- 6[c]+3*PROTON[c]+9*WA TER[c]-->+1*FE- 3[c]+3*GLY[c]+3*THR[c]+ 3*-2-3- DIHYDROXYBENZOATE [c]	GCWI-3817 GCWI-3818 GCWI-3816 GCWI-3815 GCWI-3814
RXNCWI-90	+1*FAD[c]+1*TETRADEC ANOYL-COA[c]-- >+1*CPD0- 2120[c]+1*FADH2[c]	GCWI-2435 GCWI-2612 GCWI-5127 GCWI-5440 GCWI-5441
RXNCWI-91	+1*FAD[c]+1*LAUROYL COA-CPD[c]-->+1*CPD- 7222[c]+1*FADH2[c]	GCWI-2435 GCWI-2612 GCWI-5127 GCWI-5440 GCWI-5441
RXNCWI-92	+1*CPD- 10267[c]+1*FAD[c]-- >+1*FADH2[c]+1*T2- DECENOYL-COA[c]	GCWI-2435 GCWI-2612 GCWI-5127 GCWI-5440 GCWI-5441
RXNCWI-93	+1*CPD-196[c]+1*FAD[c]- ->+1*CPD0-	GCWI-2435 GCWI-2612 GCWI-5127 GCWI-5440

Name	Reaction	Locus
	2108[c]+1*FADH2[c]	GCWI-5441
RXNCWI-94	+1*FAD[c]+1*HEXANOYL-COA[c]-->+1*CPD0-2121[c]+1*FADH2[c]	GCWI-2435 GCWI-2612 GCWI-5127 GCWI-5440 GCWI-5441
RXNCWI-95	+1*BUTYRYL-COA[c]+1*FAD[c]-->+1*CROTONYL-COA[c]+1*FADH2[c]	GCWI-2435 GCWI-2612 GCWI-5127 GCWI-5440 GCWI-5441
RXNCWI-96	+1*FAD[c]+1*STEAROYL-COA[c]-->+1*CPD-10262[c]+1*FADH2[c]	GCWI-2435 GCWI-2612 GCWI-5127 GCWI-5440 GCWI-5441
RXNCWI-99	+1*NADPH[c]+1*Octadec-2-enoyl-ACPs[c]+1*PROTON[c]-->+1*NADP[c]+1*Stearoyl-ACPs[c]	GCWI-1393
RXNI-3-MAL-CPD-9718--OXALACETIC-ACID-CPD-12125.40.	+1*CPD-9718[c]+1*MAL[c]-->+1*CPD-12125[c]+1*OXALACETIC-ACID[c]	GCWI-3002 GCWI-3002 GCWI-786 GCWI-1917 GCWI-3163 GCWI-4719 GCWI-4730
RXNN-386	+1*CPDN-384[c]<-->+1*CPDN-385[c]	GCWI-2027
RXNN-404	+1*CPD-237[c]+1*WATER[c]<-->+1*AMMONIA[c]+1*INDOLE-ACETATE-AUXIN[c]+1*PROTON[c]	GCWI-2029 GCWI-2171
RXNQT-4191	+1*THIAMINE-P[c]+1*WATER[c]-->+1*Pi[c]+1*THIAMINE[c]	GCWI-4638
S-ADENMETSYN-RXN	+1*ATP[c]+1*MET[c]+1*WATER[c]-->+1*PPI[c]+1*Pi[c]+1*S-ADENOSYLMETHIONINE[c]	GCWI-4889
SAICARSYN-RXN	+1*ATP[c]+1*L-ASPARTATE[c]+1*PHOSPHORIBOSYL-CARBOXY-AMINOIMIDAZOLE[c]-->+1*ADP[c]+1*PROTON[c]+1*P-RIBOSYL-4-SUCCARB-AMINOIMIDAZOLE[c]+1*	GCWI-499

Name	Reaction	Locus
	Pi[c]	
SAMDECARB-RXN	+1*PROTON[c]+1*S-ADENOSYLMETHIONIN E[c]-->+1*CARBONDIOXIDE[c]+1*S-ADENOSYLMETHIONIN AMINE[c]	GCWI-4709 GCWI-5311
SARCOX-RXN	+1*OXYGEN-MOLECULE[c]+1*SARCO SINE[c]+1*WATER[c]-->+1*FORMALDEHYDE[c]+1*GLY[c]+1*HYDROGEN-PEROXIDE[c]	GCWI-2888 GCWI-2889
SERINE--TRNA-LIGASE-RXN	+1*ATP[c]+1*PROTON[c]+1*SER[c]+1*SER-tRNAs[c]-->+1*AMP[c]+1*Charged-SER-tRNAs[c]+1*PPI[c]	GCWI-196
SERINE-O-ACETTRAN-RXN	+1*ACETYL-COA[c]+1*SER[c]-->+1*ACETYLSERINE[c]+1*CO-A[c]	GCWI-278
SHIKIMATE-5-DEHYDROGENASE-RXN	+1*NADP[c]+1*SHIKIMATE[c]<-->+1*NADPH[c]+1*PROTON[c]+1*-3-DEHYDRO-SHIKIMATE[c]	GCWI-4463
SHIKIMATE-KINASE-RXN	+1*ATP[c]+1*SHIKIMATE[c]-->+1*ADP[c]+1*PROTON[c]+1*SHIKIMATE-5P[c]	GCWI-4368
SIROHEME-FERROCHELAT-RXN	+1*FE-2[c]+1*SIROHYDROCHLORIN[c]-->+2*PROTON[c]+1*SIROHEME[c]	GCWI-1588
SPERMACTRAN-RXN	+1*ACETYL-COA[c]+1*SPERMIDINE[c]<-->+1*CO-A[c]+1*CPD-568[c]+1*PROTON[c]	GCWI-5196 GCWI-2127
SPERMIDINESYN-RXN	+1*PUTRESCINE[c]+1*S-ADENOSYLMETHIONIN AMINE[c]-->+1*PROTON[c]+1*SPERMIDINE[c]+1*-5-	GCWI-5310 GCWI-5469

Name	Reaction	Locus
	METHYLTHIOADENOSINE[c]	
SPHINGOMYELIN-PHOSPHODIESTERASE-RXN	+1*Sphingomyelins[c]+1*WATER[c]<-->+1*Ceramides[c]+1*PHOSPHORYL-CHOLINE[c]+1*PROTON[c]	GCWI-881
SPONTPRO-RXN	+1*L-GLUTAMATE-GAMMA-SEMIALDEHYDE[c]<-->+1*L-DELTA1-PYRROLINE-5-CARBOXYLATE[c]+1*PROTON[c]+1*WATER[c]	
SUCC-FUM-OXRED-RXN	+1*FAD[c]+1*SUC[c]<-->+1*FADH2[c]+1*FUM[c]	GCWI-4644
SUCCCOASYN-RXN	+1*ATP[c]+1*COA[c]+1*SUC[c]<-->+1*ADP[c]+1*Pi[c]+1*SUC-COA[c]	GCWI-3919 GCWI-3920
SUCCDIAMINOPIMDESUCC-RXN	+1*N-SUCCINYLLL-2-6-DIAMINOPIMELATE[c]+1*WATER[c]<-->+1*LL-DIAMINOPIMELATE[c]+1*SUC[c]	GCWI-4831
SUCCGLUALDDEHYD-RXN	+1*CPD-822[c]+1*NAD[c]+1*WATER[c]<-->+1*N2-SUCCINYLGUTAMATE[c]+1*NADH[c]+2*PROTON[c]	GCWI-2379 GCWI-3587 GCWI-2881 GCWI-1451
SUCCINATE-SEMIALDEHYDE-DEHYDROGENASE-RXN	+1*NAD[c]+1*SUC-S-ALD[c]+1*WATER[c]<-->+1*NADH[c]+2*PROTON[c]+1*SUC[c]	GCWI-533
SUCCORNTRANSAM-RXN	+1*N2-SUCCINYLORNITHINE[c]+1*-2-KETOGLUTARATE[c]<-->+1*CPD-822[c]+1*GLT[c]	GCWI-3055
SUCCSEMIALDDEHYDROG-RXN	+1*NADP[c]+1*SUC-S-ALD[c]+1*WATER[c]<-->+1*NADPH[c]+2*PROTON[c]	GCWI-533

Name	Reaction	Locus
	N[c]+1*SUC[c]	
SUCROSE-PHOSPHATASE-RXN	+1*SUCROSE-6P[c]+1*WATER[c]<-->+1*Pi[c]+1*SUCROSE[c]	GCWI-975
SULFATE-ADENYLYLTRANS-RXN	+1*ATP[c]+1*PROTON[c]+1*SULFATE[c]<-->+1*APS[c]+1*PPI[c]	GCWI-1583
SULFITE-REDUCT-RXN	+3*NADPH[c]+5*PROTON[c]+1*SO3[c]<-->+1*HS[c]+3*NADP[c]+3*WATER[c]	GCWI-3232
SUPEROX-DISMUT-RXN	+2*PROTON[c]+2*SUPER-OXIDE[c]<-->+1*HYDROGEN-PEROXIDE[c]+1*OXYGEN-MOLECULE[c]	GCWI-1630 GCWI-5548 GCWI-4408 GCWI-5030
TEICHOICSYN2-RXN	+1*ACETYL-D-GLUCOSAMINYLDIPHOSPHO-UNDECAPRE[c]+1*UDP-MANNAC[c]<-->+1*ACETYL-ETCETERA-GLUCOSAMINYLDIPHOSPHOUND[c]+1*PROTON[c]+1*UDP[c]	GCWI-5521
THI-P-SYN-RXN	+1*AMINO-HYDROXYMETHYL-METHYLPYRIMIDINE-PP[c]+1*PROTON[c]+1*THI-P[c]<-->+1*PPI[c]+1*THIAMINE-P[c]	GCWI-584
THIAMIN-PYROPHOSPHOKINASE-RXN	+1*ATP[c]+1*THIAMINE[c]<-->+1*AMP[c]+1*PROTON[c]+1*THIAMINE-PYROPHOSPHATE[c]	GCWI-3943
THIAZOLSYN3-RXN	+1*ATP[c]+1*THZ[c]<-->+1*ADP[c]+1*PROTON[c]+1*THZ-P[c]	GCWI-583
THIOREDOXIN-REDUCT-NADPH-RXN	+1*NADPH[c]+1*Ox-Thioredoxin[c]+1*PROTON[c]<-->+1*NADP[c]+1*Red-Thioredoxin[c]	GCWI-2822 GCWI-5257



Name	Reaction	Locus
THREDEHYD-RXN	+1*THR[c]-- >+1*AMMONIA[c]+1*PROTON[c]+1*-2-OXOBUTANOATE[c]	GCWI-4278 GCWI-3306 GCWI-4279 GCWI-3307 GCWI-2540 GCWI-1966
THREONINE--TRNA-LIGASE-RXN	+1*ATP[c]+1*PROTON[c] +1*THR[c]+1*THR-tRNAs[c]-- >+1*AMP[c]+1*Charged-THR-tRNAs[c]+1*PPI[c]	GCWI-2466 GCWI-4704
THRESYN-RXN	+1*O-PHOSPHO-L-HOMOSERINE[c]+1*WATER[c]-- >+1*Pi[c]+1*THR[c]	GCWI-2073
THYKI-RXN	+1*ATP[c]+1*THYMIDINE[c]<-- >+1*ADP[c]+1*PROTON[c]+1*TMP[c]	GCWI-5429
THYMIDYLATESYN-RXN	+1*DUMP[c]+1*METHYLENE-THF[c]-- >+1*DIHYDROFOLATE[c]+1*TMP[c]	GCWI-2328
TIGLYLCOA-HYDROXY-RXN	+1*CPD-1083[c]+1*WATER[c]-- >+1*-2-METHYL-3-HYDROXY-BUTYRYL-COA[c]	GCWI-1106 GCWI-2616 GCWI-3561 GCWI-4652 GCWI-2439
TRANS-HEXAPRENYLTRANSFERASE-RXN	+4*DELTA3-ISOPENTENYL-PP[c]+1*FARNESYL-PP[c]-->+1*ALL-TRANS-HEPTAPRENYLDIPHOSPHATE[c]+4*PPI[c]	GCWI-1674 GCWI-1676
TRANS-RXN-1	+1*FORMATE[c]+1*PROTON[c]<-- >+1*FORMATE[e]+1*PROTON[e]	GCWI-3601 GCWI-3808 GCWI-1474
TRANS-RXN-104	+1*L-LACTATE[e]+1*PROTON[e]<-->+1*L-LACTATE[c]+1*PROTON[c]	GCWI-814 GCWI-1417 GCWI-5327
TRANS-RXN-118	+1*NA-[e]+1*PRO[e]-- >+1*NA-[c]+1*PRO[c]	GCWI-1407 GCWI-3673
TRANS-RXN-125	+1*L-ALPHA-	GCWI-842 GCWI-2461

Name	Reaction	Locus
	ALANINE[e]+1*NA-[e]-- >+1*L-ALPHA- ALANINE[c]+1*NA-[c]	GCWI-2880 GCWI-3173 GCWI-3174 GCWI-5164 GCWI-5175 GCWI-5176
TRANS-RXN-132	+1*PROTON[e]+1*URACI L[e]-- >+1*PROTON[c]+1*URAC IL[c]	GCWI-3974
TRANS-RXN-137	+1*NITRITE[e]-- >+1*NITRITE[c]	GCWI-1474
TRANS-RXN-139	+1*CL-[e]-->+1*CL-[c]	GCWI-5508
TRANS-RXN-141	+1*MG-2[e]-->+1*MG-2[c]	GCWI-3188 GCWI-4226 GCWI-2150 GCWI-1740 GCWI-1878 GCWI-2399 GCWI-4535
TRANS-RXN-141A	+1*CO-2[e]-->+1*CO-2[c]	GCWI-3188 GCWI-4226 GCWI-331 GCWI-2704 GCWI-1740 GCWI-1878 GCWI-2399 GCWI-4535
TRANS-RXN-143	+1*K-[e]-->+1*K-[c]	GCWI-1476 GCWI-1553 GCWI-4120 GCWI-724 GCWI-5494 GCWI-5495 GCWI-1740 GCWI-1878 GCWI-2399 GCWI-4535
TRANS-RXN-144	+1*CA- 2[c]+1*PROTON[e]<-- >+1*CA- 2[e]+1*PROTON[c]	GCWI-627
TRANS-RXN-162	+1*GLT[e]+2*PROTON[e] -- >+1*GLT[c]+2*PROTON[c] ]	GCWI-1592 GCWI-1593 GCWI-5315 GCWI-1552
TRANS-RXN-23	+1*PROTON[e]+1*-2- KETOGLUTARATE[e]-- >+1*PROTON[c]+1*-2- KETOGLUTARATE[c]	GCWI-1126 GCWI-2574
TRANS-RXN-57	+1*PROTON[e]+1*-4- AMINO-BUTYRATE[e]-- >+1*PROTON[c]+1*-4- AMINO-BUTYRATE[c]	GCWI-3805
TRANS-RXN-58	+1*LYS[e]+1*PROTON[e]- - >+1*LYS[c]+1*PROTON[c] ]	GCWI-3102 GCWI-5138 GCWI-3501 GCWI-3313 GCWI-3227 GCWI-3159 GCWI-3026 GCWI-1063 GCWI-1037 GCWI-896 GCWI-833 GCWI-799

Name	Reaction	Locus
		GCWI-687 GCWI-3147 GCWI-3146 GCWI-907 GCWI-3872 GCWI-3873 GCWI-4677 GCWI-3160 GCWI-2162 GCWI-2019 GCWI-1602 GCWI-1023 GCWI-893
TRANS-RXN-8	+1*FE-2[e]-->+1*FE-2[c]	GCWI-917 GCWI-4932 GCWI-916 GCWI-915 GCWI-1740 GCWI-1878 GCWI-2399 GCWI-4535
TRANS-RXN0-209	+1*GLUCONATE[e]+1*PROTON[e]-->+1*GLUCONATE[c]+1*PROTON[c]	GCWI-366 GCWI-3417 GCWI-4964
TRANS-RXN0-468	+1*Nucleosides[c]<-->+1*Nucleosides[e]	GCWI-2002 GCWI-5335 GCWI-5174 GCWI-5173 GCWI-3020 GCWI-810 GCWI-538 GCWI-400
TRANS-RXN0-470	+1*Pi[c]<-->+1*Pi[e]	GCWI-1613
TRANS-RXNCWI-1	+1*ATP[c]+1*CD-2[e]+1*WATER[c]-->+1*ADP[c]+1*CD-2[c]+1*PROTON[c]+1*Pi[c]	GCWI-618 GCWI-801
TRANS-RXNCWI-10	+1*CPD-12125[c]+0.5*OXYGEN-MOLECULE[c]+4*PROTON[c]-->+1*CPD-9718[c]+4*PROTON[e]+1*WATER[c]	GCWI-5324 GCWI-4920 GCWI-4121 GCWI-2051 GCWI-5323 GCWI-4919 GCWI-2050
TRANS-RXNCWI-11	+1*CARBON-DIOXIDE[e]<-->+1*CARBON-DIOXIDE[c]	
TRANS-RXNCWI-11058	+1*ATP[c]+1*CO-2[e]+1*WATER[c]-->+1*ADP[c]+1*CO-2[c]+1*PROTON[c]+1*Pi[c]	GCWI-329 GCWI-330
TRANS-RXNCWI-11074	+1*ATP[c]+1*MO-2[e]+1*WATER[c]-->+1*ADP[c]+1*MO-2[c]+1*PROTON[c]+1*Pi[c]	GCWI-402

Name	Reaction	Locus
TRANS-RXNCWI-11079	+1*URACIL[e]+1*XANTH INE[e]-- >+1*URACIL[c]+1*XANT HINE[c]	GCWI-471 GCWI-897 GCWI-969 GCWI-4225 GCWI-4618 GCWI-5496
TRANS-RXNCWI-11087	+1*BENZOATE[e]-- >+1*BENZOATE[c]	GCWI-570
TRANS-RXNCWI-11090	+1*ATP[c]+1*Amino- Acids-20[e]+1*WATER[c]- ->+1*ADP[c]+1*Amino- Acids- 20[c]+1*PROTON[c]+1*Pi[ c]	GCWI-4291 GCWI-4290 GCWI-4289 GCWI-2043 GCWI-2042 GCWI-2041 GCWI-1072 GCWI-1071 GCWI-846 GCWI-845 GCWI-844 GCWI-843 GCWI-2040 GCWI-575 GCWI-1070 GCWI-2039 GCWI-574 GCWI-573 GCWI-847
TRANS-RXNCWI-11105	+1*Amino-Acids- 20[e]+1*PROTON[e]-- >+1*Amino-Acids- 20[c]+1*PROTON[c]	GCWI-3872 GCWI-3873 GCWI-4677 GCWI-3160 GCWI-2162 GCWI-2019 GCWI-1602 GCWI-1023 GCWI-893 GCWI-5138 GCWI-3501 GCWI-3313 GCWI-3227 GCWI-3159 GCWI-3026 GCWI-1063 GCWI-1037 GCWI-896 GCWI-833 GCWI-799 GCWI-687 GCWI-3147 GCWI-3146 GCWI-907
TRANS-RXNCWI-11108	+1*CPD- 12541[e]+1*PHOSPHO- ENOL-PYRUVATE[c]<-- >+1*N-ACETYL-D- GLUCOSAMINE-1- P[c]+1*PYRUVATE[c]	GCWI-693
TRANS-RXNCWI-11113	+1*BETAINE[e]-- >+1*BETAINE[c]	GCWI-760 GCWI-5339
TRANS-RXNCWI-11116	+1*CIT[e]-->+1*CIT[c]	GCWI-768
TRANS-RXNCWI-11128	+1*NA-[e]+1*PROTON[e]- ->+1*NA- [c]+1*PROTON[c]	GCWI-2306 GCWI-1950 GCWI-1485 GCWI-1590 GCWI-1915 GCWI-3585 GCWI-4214 GCWI-1006 GCWI-911 GCWI-1768 GCWI-2301 GCWI-817 GCWI-892
TRANS-RXNCWI-11133	+1*PHOSPHO-ENOL-	GCWI-835

Name	Reaction	Locus
	PYRUVATE[c]+1*TREHALOSE[e]-- >+1*PYRUVATE[c]+1*TR EHALOSE-6P[c]	
TRANS-RXNCWI-11140	+1*PROTON[e]+1*SULFATE[e]-- >+1*PROTON[c]+1*SULFATE[c]	GCWI-858 GCWI-1092
TRANS-RXNCWI-11143	+1*GLYCEROL-3P[e]-- >+1*GLYCEROL-3P[c]	GCWI-865
TRANS-RXNCWI-11187	+1*PHOSPHO-ENOL-PYRUVATE[c]+1*SUCROSE[e]<-- >+1*PYRUVATE[c]+1*SUCROSE-6P[c]	GCWI-1042
TRANS-RXNCWI-11200	+1*GLYCEROL[e]+1*PROTON[e]-- >+1*GLYCEROL[c]+1*PROTON[c]	GCWI-1215
TRANS-RXNCWI-11255	+1*PROTON[e]+1*THR[c] <-- >+1*PROTON[c]+1*THR[e] ]	GCWI-3305 GCWI-3437 GCWI-1999 GCWI-2438
TRANS-RXNCWI-11258	+1*HOMO-SER[c]-- >+1*HOMO-SER[e]	GCWI-1999 GCWI-2438
TRANS-RXNCWI-11266	+1*Amino-Acids-20[e]-- >+1*Amino-Acids-20[c]	GCWI-2521 GCWI-2018
TRANS-RXNCWI-11281	+1*NITRATE[e]-- >+1*NITRATE[c]	GCWI-2236
TRANS-RXNCWI-11288	+1*ARG[e]+1*L-ORNITHINE[c]-- >+1*ARG[c]+1*L-ORNITHINE[e]	GCWI-2372
TRANS-RXNCWI-11297	+1*FORMATE[c]+1*OXALATE[e]-- >+1*FORMATE[e]+1*OXALATE[c]	GCWI-2447 GCWI-2737
TRANS-RXNCWI-11314	+1*ATP[c]+1*BETAINE[e] +1*WATER[c]-- >+1*ADP[c]+1*BETAINE[c] +1*PROTON[c]+1*Pi[c]	GCWI-2838 GCWI-2837 GCWI-2371 GCWI-2370 GCWI-2839
TRANS-RXNCWI-11353	+1*PROTON[e]+1*SER[e]- - >+1*PROTON[c]+1*SER[c] ]	GCWI-3305 GCWI-3437 GCWI-2018 GCWI-2521

Name	Reaction	Locus
TRANS-RXNCWI-11386	+1*ATP[c]+1*PHOSPHONATE[e]+1*WATER[c]>+1*ADP[c]+1*PHOSPHONATE[c]+1*PROTON[c]+1*Pi[c]	GCWI-3709 GCWI-3710 GCWI-3711 GCWI-3712
TRANS-RXNCWI-11389	+1*Fructose[e]+1*PHOSPHO-ENOL-PYRUVATE[c]>+1*FRU1P[c]+1*PYRUVATE[c]	GCWI-3798
TRANS-RXNCWI-11435	+1*ALPHA-GLUCOSE[e]+1*PROTON[e]>+1*ALPHA-GLUCOSE[c]+1*PROTON[c]	GCWI-4844
TRANS-RXNCWI-11456	+1*CPD-4422[e]>+1*CPD-4422[c]	GCWI-5304
TRANS-RXNCWI-11479	+1*ALPHA-GLUCOSE[e]+1*PHOSPHO-ENOL-PYRUVATE[c]>+1*ALPHA-GLC-6-P[c]+1*PYRUVATE[c]	GCWI-5419
TRANS-RXNCWI-11519	+1*ATP[c]+1*RIBOSE[e]+1*WATER[c]>+1*ADP[c]+1*PROTON[c]+1*Pi[c]+1*RIBOSE[c]	GCWI-3006 GCWI-3005 GCWI-3004 GCWI-873 GCWI-872 GCWI-871
TRANS-RXNCWI-11537	+1*CELLOBIOSE[e]+1*PHOSPHO-ENOL-PYRUVATE[c]<>+1*CPD-507[c]+1*PYRUVATE[c]	GCWI-5312 GCWI-5313 GCWI-5314
TRANS-RXNCWI-12	+1*-3-4-DIHYDROXYBENZOATE[c]>+1*-3-4-DIHYDROXYBENZOATE[e]	
TRANS-RXNCWI-13	+1*CPD-9718[c]+1*FADH2[c]+2*PROTON[e]>+1*CPD-12125[c]+1*FAD[c]+2*PROTON[c]	
TRANS-RXNCWI-14	+1*UREA[c]>+1*UREA[e]	
TRANS-RXNCWI-15	+1*ARSENATE[c]<>+1*ARSENATE[e]	
TRANS-RXNCWI-16	+1*ETOH[c]+1*PROTON[c]	

Name	Reaction	Locus
	e]-- >+1*ETOH[e]+1*PROTON[c]	
TRANS-RXNCWI-17	+1*WATER[c]<-- >+1*WATER[e]	
TRANS-RXNCWI-18	+1*OXYGEN-MOLECULE[e]<-- >+1*OXYGEN-MOLECULE[c]	
TRANS-RXNCWI-2	+1*ATP[c]+1*WATER[c]+ 1*ZN-2[e]-- >+1*ADP[c]+1*PROTON[c] ]+1*Pi[c]+1*ZN-2[c]	GCWI-618 GCWI-801
TRANS-RXNCWI-5	+1*CPD-9984[c]-- >+1*CPD-9984[e]	GCWI-2092
TRANS-RXNCWI-6	+1*CPD-9985[c]-- >+1*CPD-9985[e]	
TRANS-RXNCWI-7	+1*ATP[c]+1*CPDCWI- 6[e]+1*WATER[c]-- >+1*ADP[c]+1*CPDCWI- 6[c]+1*Pi[c]	GCWI-3818 GCWI-3817 GCWI-3816 GCWI-3815 GCWI-3814
TRANS-RXNCWI-8	+1*ATP[c]+1*CPDCWI- 7[e]+1*WATER[c]-- >+1*ADP[c]+1*CPDCWI- 7[c]+1*Pi[c]	GCWI-5203 GCWI-5202 GCWI-5201 GCWI-5200 GCWI-4657 GCWI-4656
TRANS-RXNCWU-12494	+1*ATP[c]+1*CPD- 1106[e]+1*WATER[c]-- >+1*ADP[c]+1*CPD- 1106[c]+1*PROTON[c]+1* Pi[c]	
TRANS-RXNCWU-12497	+1*CPD- 1106[e]+1*PROTON[e]-- >+1*CPD- 1106[c]+1*PROTON[c]	
TRANSALDOL-RXN	+1*D-SEDOHEPTULOSE- 7-P[c]+1*GAP[c]<-- >+1*ERYTHROSE- 4P[c]+1*FRUCTOSE-6P[c]	GCWI-874 GCWI-3418
TRE6PHYDRO-RXN	+1*TREHALOSE- 6P[c]+1*WATER[c]<-- >+1*ALPHA-GLC-6- P[c]+1*ALPHA- GLUCOSE[c]	GCWI-836
TRIOSEPIISOMERIZATION-RXN	+1*GAP[c]<-- >+1*DIHYDROXY-	GCWI-5236

Name	Reaction	Locus
	ACETONE- PHOSPHATE[c]	
TRNA-PSEUDOURIDINE- SYNTHASE-I-RXN	+1*tRNA-uridine-38- 40[c]<-->+1*tRNA- pseudouridine-38-40[c]	GCWI-1375 GCWI-332 GCWI-683 GCWI-3894
TRYPSYN-RXN	+1*INDOLE-3- GLYCEROL- P[c]+1*SER[c]<-- >+1*GAP[c]+1*TRP[c]+1* WATER[c]	GCWI-1414 GCWI-1415
TRYPTOPHAN--TRNA- LIGASE-RXN	+1*ATP[c]+1*PROTON[c] +1*TRP[c]+1*TRP- tRNAs[c]-- >+1*AMP[c]+1*Charged- TRP-tRNAs[c]+1*PPI[c]	GCWI-1353 GCWI-3398
TRYPTOPHAN-23- DIOXYGENASE-RXN	+1*OXYGEN- MOLECULE[c]+2*PROTO N[c]+1*TRP[c]-->+1*N- FORMYLKYNURENINE[c ]	GCWI-2806
TYROSINE--TRNA- LIGASE-RXN	+1*ATP[c]+1*PROTON[c] +1*TYR[c]+1*TYR- tRNAs[c]-- >+1*AMP[c]+1*Charged- TYR-tRNAs[c]+1*PPI[c]	GCWI-4788 GCWI-5187
TYROSINE- AMINOTRANSFERASE- RXN	+1*TYR[c]+1*-2- KETOGLUTARATE[c]<-- >+1*GLT[c]+1*P- HYDROXY- PHENYLPYRUVATE[c]	GCWI-1680 GCWI-2986
UDP-NACMUR-ALA-LIG- RXN	+1*ATP[c]+1*L-ALPHA- ALANINE[c]+1*UDP-N- ACETYLMURAMATE[c]-- >+1*ADP[c]+1*CPD0- 1456[c]+1*PROTON[c]+1* Pi[c]	GCWI-4814
UDP-NACMURALA-GLU- LIG-RXN	+1*ATP[c]+1*CPD0- 1456[c]+1*D-GLT[c]-- >+1*ADP[c]+1*PROTON[c ]+1*Pi[c]+1*UDP-AA- GLUTAMATE[c]	GCWI-3996
UDP- NACMURALGLDAPAALI G-RXN	+1*ATP[c]+1*D-ALA-D- ALA[c]+1*UDP-AAGM- DIAMINOHEPTANEDIOA TE[c]--	GCWI-433 GCWI-2276



Name	Reaction	Locus
	>+1*ADP[c]+1*C1[c]+1*P ROTON[c]+1*Pi[c]	
UDP- NACMURALGLDAPLIG- RXN	+1*ATP[c]+1*MESO- DIAMINOPIMELATE[c]+1 *UDP-AA- GLUTAMATE[c]-- >+1*ADP[c]+1*PROTON[c ]+1*Pi[c]+1*UDP-AAGM- DIAMINOHEPTANEDIOA TE[c]	GCWI-3998
UDPGLCNACEPIM-RXN	+1*UDP-N-ACETYL-D- GLUCOSAMINE[c]-- >+1*UDP-MANNAC[c]	GCWI-5298 GCWI-5367
UDPGLUCEPIM-RXN	+1*UDP-GALACTOSE[c]-- >+1*UDP-GLUCOSE[c]	GCWI-481 GCWI-5552 GCWI-5364
UDPKIN-RXN	+1*ATP[c]+1*UDP[c]-- >+1*ADP[c]+1*UTP[c]	GCWI-1677
UDPMANNACADEHYDR OG-RXN	+2*NAD[c]+1*UDP- MANNAC[c]+1*WATER[c ]<-- >+2*NADH[c]+3*PROTO N[c]+1*UDP- MANNACA[c]	GCWI-5370
UDPNACETYLGLUCOSA MENOLPYRTRANS-RXN	+1*PHOSPHO-ENOL- PYRUVATE[c]+1*UDP-N- ACETYL-D- GLUCOSAMINE[c]-- >+1*Pi[c]+1*UDP- ACETYL- CARBOXYVINYL- GLUCOSAMINE[c]	GCWI-5387 GCWI-5433
UDPNACETYLMURAMA TEDEHYDROG-RXN	+1*NADPH[c]+1*PROTO N[c]+1*UDP-ACETYL- CARBOXYVINYL- GLUCOSAMINE[c]-- >+1*NADP[c]+1*UDP-N- ACETYLMURAMATE[c]	GCWI-3993 GCWI-5188
UDPREDUCT-RXN	+1*Red- Thioredoxin[c]+1*UDP[c]-- >+1*DUDP[c]+1*Ox- Thioredoxin[c]+1*WATER[ c]	GCWI-1521 GCWI-1519 GCWI-1522
UGD-RXN	+2*NAD[c]+1*UDP- GLUCOSE[c]+1*WATER[c ]<--	GCWI-5299

Name	Reaction	Locus
	>+2*NADH[c]+3*PROTON[c]+1*UDP-GLUCURONATE[c]	
UNDECAPRENYL-DIPHOSPHATASE-RXN	+1*UNDECAPRENYL-DIPHOSPHATE[c]+1*WATER[c]<-->+1*CPD-9646[c]+1*PROTON[c]+1*Pi[c]	GCWI-488 GCWI-886 GCWI-1548 GCWI-2761
URA-PHOSPH-RXN	+1*DEOXYURIDINE[c]+1*Pi[c]<-->+1*DEOXY-RIBOSE-1P[c]+1*URACIL[c]	GCWI-1624 GCWI-4228
URACIL-PRIBOSYLTRANS-RXN	+1*PRPP[c]+1*URACIL[c]<-->+1*PPI[c]+1*UMP[c]	GCWI-3975 GCWI-5414
UREA-CARBOXYLASE-RXN	+1*ATP[c]+1*CARBONDIOXIDE[c]+1*UREA[c]+1*WATER[c]<-->+1*ADP[c]+1*CPD-578[c]+2*PROTON[c]+1*Pi[c]	GCWI-3121
URIDINEKIN-RXN	+1*ATP[c]+1*URIDINE[c]<-->+1*ADP[c]+1*PROTON[c]+1*UMP[c]	GCWI-3037 GCWI-3096 GCWI-4507
URKI-RXN	+1*GTP[c]+1*URIDINE[c]<-->+1*GDP[c]+1*PROTON[c]+1*UMP[c]	GCWI-3037 GCWI-3096 GCWI-4507
UROCANATE-HYDRATASE-RXN	+1*UROCANATE[c]+1*WATER[c]<-->+1*PROTON[c]+1*-4-IMIDAZOLONE-5-PROPIONATE[c]	GCWI-3679
UROGENDECARBOX-RXN	+4*PROTON[c]+1*UROPORPHYRINOGEN-III[c]<-->+4*CARBONDIOXIDE[c]+1*COPROPORPHYRINOGEN-III[c]	GCWI-1254
UROGENIIISYN-RXN	+1*HYDROXYMETHYLBILANE[c]<-->+1*UROPORPHYRINOGEN-III[c]+1*WATER[c]	GCWI-4590
UROPORIIIMETHYLTRANS-RXN	+1*S-ADENOSYLMETHIONINE[c]+1*UROPORPHYRIN	GCWI-1587 GCWI-2241

Name	Reaction	Locus
	$\text{OGEN-III[c]} \rightarrow +1 \cdot \text{ADENOSYL-HOMO-CYS[c]} + 1 \cdot \text{CPD-9038[c]} + 1 \cdot \text{PROTON[c]}$	
VALINE--TRNA-LIGASE-RXN	$+1 \cdot \text{ATP[c]} + 1 \cdot \text{PROTON[c]} + 1 \cdot \text{VAL[c]} + 1 \cdot \text{VAL-tRNAs[c]} \rightarrow +1 \cdot \text{AMP[c]} + 1 \cdot \text{Charged-VAL-tRNAs[c]} + 1 \cdot \text{PPI[c]}$	GCWI-4585
XANPRIBOSYLTRAN-RXN	$+1 \cdot \text{PRPP[c]} + 1 \cdot \text{XANTHINE[c]} \rightarrow +1 \cdot \text{PPI[c]} + 1 \cdot \text{XANTHOSINE-5-PHOSPHATE[c]}$	GCWI-1727
XANTHOSINEPHOSPHORY-RXN	$+1 \cdot \text{Pi[c]} + 1 \cdot \text{XANTHOSINE[c]} \rightarrow +1 \cdot \text{RIBOSE-1P[c]} + 1 \cdot \text{XANTHINE[c]}$	GCWI-1624 GCWI-4228
XMPXAN-RXN	$+1 \cdot \text{WATER[c]} + 1 \cdot \text{XANTHOSINE-5-PHOSPHATE[c]} \rightarrow +1 \cdot \text{Pi[c]} + 1 \cdot \text{XANTHOSINE[c]}$	GCWI-2585 GCWI-2586 GCWI-2587 GCWI-3179 GCWI-4241
YIAE1-RXN	$+1 \cdot \text{NADPH[c]} + 1 \cdot \text{PROTON[c]} + 1 \cdot \text{-25-DIDEHYDRO-D-GLUCONATE[c]} \rightarrow +1 \cdot \text{NADP[c]} + 1 \cdot \text{-5-DEHYDROGLUCONATE[c]}$	GCWI-5026

#### A8.4. Exchange fluxes

**Table S17. List of exchange fluxes for nutrients and secretion for the model for *B. anthracis*.** The name, reaction, as well as lower and upper boundaries are provided. The boundaries with the variable label refer to experimentally measured fluxes which depend on the condition to be simulated.

Nutrients			
Name	Rxn	Low-boundary	Upper-boundary
ALPHA-GLUCOSE-Exchange-FLUX	$+1 \cdot \text{ALPHA-GLUCOSE[e]} \leftrightarrow$	variable	variable
ARG-Exchange-FLUX	$+1 \cdot \text{ARG[e]} \leftrightarrow$	-1000	1000
CA-2-Exchange-FLUX	$+1 \cdot \text{CA-2[e]} \leftrightarrow$	-1000	1000
CL--Exchange-FLUX	$+1 \cdot \text{CL-[e]} \leftrightarrow$	-1000	1000

CYS-Exchange-FLUX	+1*CYS[e]<-->	-1000	1000
FE-3-Exchange-FLUX	+1*FE-3[e]<-->	variable	variable
GLT-Exchange-FLUX	+1*GLT[e]<-->	variable	variable
HIS-Exchange-FLUX	+1*HIS[e]<-->	-1000	1000
ILE-Exchange-FLUX	+1*ILE[e]<-->	-1000	1000
K--Exchange-FLUX	+1*K-[e]<-->	-1000	1000
L-ASPARTATE-Exchange-FLUX	+1*L-ASPARTATE[e]<-->	-1000	1000
L-LACTATE-Exchange-FLUX	+1*L-LACTATE[e]<-->	variable	variable
LEU-Exchange-FLUX	+1*LEU[e]<-->	-1000	1000
MET-Exchange-FLUX	+1*MET[e]<-->	-1000	1000
MG-2-Exchange-FLUX	+1*MG-2[e]<-->	-1000	1000
MN-2-Exchange-FLUX	+1*MN-2[e]<-->	-1000	1000
NA--Exchange-FLUX	+1*NA-[e]<-->	-1000	1000
OXYGEN-MOLECULE-Exchange-FLUX	+1*OXYGEN-MOLECULE[e]<-->	variable	variable
PHE-Exchange-FLUX	+1*PHE[e]<-->	-1000	1000
Pi-Exchange-FLUX	+1*Pi[e]<-->	-1000	1000
PRO-Exchange-FLUX	+1*PRO[e]<-->	-1000	1000
PROTON-Exchange-FLUX	+1*PROTON[e]<-->	-1000	1000
SER-Exchange-FLUX	+1*SER[e]<-->	-1000	1000
SULFATE-Exchange-FLUX	+1*SULFATE[e]<-->	-1000	1000
THIAMINE-Exchange-FLUX	+1*THIAMINE[e]<-->	-1000	1000
THR-Exchange-FLUX	+1*THR[e]<-->	-1000	0
TRP-Exchange-FLUX	+1*TRP[e]<-->	-1000	1000
VAL-Exchange-FLUX	+1*VAL[e]<-->	-1000	1000
WATER-Exchange-FLUX	+1*WATER[e]<-->	-1000	1000

Secretion			
Name	Rxn	Low-boundary	Upper-boundary
-3-4-DIHYDROXYBENZOATE-Exchange-FLUX	+1*-3-4-DIHYDROXYBENZOATE[e]<-->	variable	variable
ACET-Exchange-FLUX	+1*ACET[e]<-->	0	1000
BIOMASS-CCO-CYTOSOL-Exchange-FLUX	+1*BIOMASS-CCO-CYTOSOL[c]<-->	0	1000

CARBON-DIOXIDE-Exchange-FLUX	+1*CARBON-DIOXIDE[e]<-->	variable	variable
CPD-10353-Exchange-FLUX	+1*CPD-10353[e]<-->	0	1000
CPD-10774-Exchange-FLUX	+1*CPD-10774[c]<-->	0	1000
CPD-763-Exchange-FLUX	+1*CPD-763[e]<-->	0	1000
CPD-9984-Exchange-FLUX	+1*CPD-9984[e]<-->	variable	variable
CPD-9985-Exchange-FLUX	+1*CPD-9985[e]<-->	variable	variable
CPDCWI-16-Exchange-FLUX	+1*CPDCWI-16[c]<-->	0	1000
ETOH-Exchange-FLUX	+1*ETOH[e]<-->	0	1000
FORMATE-Exchange-FLUX	+1*FORMATE[e]<-->	0	1000
L-LACTATE-Exchange-FLUX	+1*L-LACTATE[e]<-->	variable	variable
L-ORNITHINE-Exchange-FLUX	+1*L-ORNITHINE[e]<-->	0	1000
SPERMIDINE-Exchange-FLUX	+1*SPERMIDINE[e]<-->	0	1000

#### A8.5.Biomass for iron-poor media phase I

**Table S18. List of biomass's reactants for *B. anthracis* model under iron-poor conditions Phase I.** The name, reaction, as well as lower and upper boundaries are provides.

	Metabolite	Species name	mmol/gDW
<b>Protein</b>	Glycine	Charged-GLY-tRNAs[c]	0.412078
0.55	L-Alanine	Charged-ALA-tRNAs[c]	0.433604
	L-Valine	Charged-VAL-tRNAs[c]	0.329047
	L-Leucine	Charged-LEU-tRNAs[c]	0.375175
	L-Isoleucine	Charged-ILE-tRNAs[c]	0.293682
	L-Serine	Charged-SER-tRNAs[c]	0.182975
	L-Threonine	Charged-THR-tRNAs[c]	0.239866
	L-Phenylalanine	Charged-PHE-tRNAs[c]	0.162986
	L-Tyrosine	Charged-TYR-	0.132234

	Metabolite	Species name	mmol/gDW
		tRNAs[c]	
	L-Tryptophan	Charged-TRP-tRNAs[c]	0.007688
	L-Cysteine	Charged-CYS-tRNAs[c]	0.010763
	L-Methionine	Charged-MET-tRNAs[c]	0.083031
	L-Lysine	Charged-LYS-tRNAs[c]	0.264468
	L-Arginine	Charged-ARG-tRNAs[c]	0.184512
	L-Histidine	Charged-HIS-tRNAs[c]	0.087643
	L-Aspartate	Charged-ASP-tRNAs[c]	0.209114
	L-Asparagine	Charged-ASN-tRNAs[c]	0.209114
	L-Glutamine	Charged-GLN-tRNAs[c]	0.266005
	L-Glutamate	Charged-GLT-tRNAs[c]	0.266005
	L-Proline	Charged-PRO-tRNAs[c]	0.155298
<b>RNA</b>	AMP (ATP)	ATP[c]	43.610000
0.145	GMP (GTP)	GTP[c]	0.131137
	CMP (CTP)	CTP[c]	0.089431
	UMP (UTP)	UTP[c]	0.096310
<b>DNA</b>	dAMP (dATP)	DATP[c]	0.010802
0.011	dGMP (dGTP)	DGTP[c]	0.006413
	dCMP (dCTP)	DCTP[c]	0.005738
	dTMP (dTTP)	TTP[c]	0.010802
<b>Ions</b>	K	K-[c]	0.700573
0.03185	Mg	MG-2[c]	0.100903
	Fe(+3)	FE-3[c]	0.003422
	NH4	AMMONIUM[c]	0.001285
	SO4	SULFATE[c]	0.000031
	Ca2+	CA-2[c]	0.003179
<b>Cofactors</b>	coa	CO-A[c]	0.000128
0.01715	spermidine	SPERMIDINE[c]	0.000020
	ACP	ACP[c]	0.000273
	L-Ornithine	L-ORNITHINE[c]	0.000046

	Metabolite	Species name	mmol/gDW
	NAD	NAD[c]	0.018220
	NADP	NADP[c]	0.001053
	NADPH	NADPH[c]	0.000237
	menaquinol 7	CPD-12125[c]	0.000150
	10-formyltetrahydrofolate	-10-FORMYL-THF[c]	0.000207
<b>Lipids</b>	cardiolipin (tetrahexadecanoyl)	CPD-12824[c]	0.000740
0.025	cardiolipin (stearoylcardiolipin)	CPDCWI-13[c]	0.000023
	1,2-dipalmitoyl-phosphatidylglycerol	CPD-8260[c]	0.005107
	phosphatidylglycerol (dioctadecanoyl)	CPD-12822[c]	0.000162
	1,2-dipalmitoyl-phosphatidylethanolamine	CPD-12819[c]	0.006196
	phosphatidylethanolamine (dioctadecanoyl)	CPD-12818[c]	0.000196
	1,2-dipalmitoyl-phosphatidylserine	CPD-12817[c]	0.000415
	phosphatidylserine (dioctadecanoyl, n-c18:0)	CPD-12816[c]	0.000013
	1,2-dipalmitoylglycerol	CPD66-34[c]	0.010908
	1,2-distearoyl-sn-glycerol	CPDCWI-14[c]	0.000339
	hexadecanoic/palmitic/palmitate	PALMITATE[c]	0.000572
	octadecanoic/stearic/stearate	STEARIC-ACID[c]	0.000018
<b>Cell wall</b>	a peptidoglycan subunit	CPD-12261[c]	0.030270
0.22			
	water	WATER[c]	39.200000

**Table S19. List of biomass's products for *B. anthracis* model under iron-poor conditions Phase I.** The name, reaction, as well as lower and upper boundaries are provides.

	name	Species name	mmol/gDW
<b>GAM</b>	ADP	ADP[c]	43.500000
	H+	PROTON[c]	43.500000
	Pi	Pi[c]	43.490000
	PPI	PPI[c]	0.458900
	Biomass	BIOMASS-CCO-CYTOSOL[c]	1.000000
<b>tRNAs recycling</b>	Glycine	GLY-tRNAs[c]	0.412078
	L-Alanine	ALA-tRNAs[c]	0.433604

	<b>name</b>	<b>Species name</b>	<b>mmol/gDW</b>
	L-Valine	VAL-tRNAs[c]	0.329047
	L-Leucine	LEU-tRNAs[c]	0.375175
	L-Isoleucine	ILE-tRNAs[c]	0.293682
	L-Serine	SER-tRNAs[c]	0.182975
	L-Threonine	THR-tRNAs[c]	0.239866
	L-Phenylalanine	PHE-tRNAs[c]	0.162986
	L-Tyrosine	TYR-tRNAs[c]	0.132234
	L-Tryptophan	TRP-tRNAs[c]	0.007688
	L-Cysteine	CYS-tRNAs[c]	0.010763
	L-Methionine	MET-tRNAs[c]	0.083031
	L-Lysine	LYS-tRNAs[c]	0.264468
	L-Arginine	ARG-tRNAs[c]	0.184512
	L-Histidine	HIS-tRNAs[c]	0.087643
	L-Aspartate	ASP-tRNAs[c]	0.209114
	L-Asparagine	ASN-tRNAs[c]	0.209114
	L-Glutamine	GLN-tRNAs[c]	0.266005
	L-Glutamate	GLT-tRNAs[c]	0.266005
	L-Proline	PRO-tRNAs[c]	0.155298
	apo-ACP	apo-ACP[c]	0.000273109

#### A8.6. Biomass for iron-rich media phase I

**Table S20. List of biomass's reactants for *B. anthracis* model under iron-rich conditions Phase I.** The name, reaction, as well as lower and upper boundaries are provides.

	<b>name</b>	<b>Species name</b>	<b>mmol/gDW</b>
<b>Protein</b>	Glycine	Charged-GLY-tRNAs[c]	0.412078
0.55	L-Alanine	Charged-ALA-tRNAs[c]	0.433604
	L-Valine	Charged-VAL-tRNAs[c]	0.329047
	L-Leucine	Charged-LEU-tRNAs[c]	0.375175
	L-Isoleucine	Charged-ILE-tRNAs[c]	0.293682
	L-Serine	Charged-SER-tRNAs[c]	0.182975



	<b>name</b>	<b>Species name</b>	<b>mmol/gDW</b>
	L-Threonine	Charged-THR-tRNAs[c]	0.239866
	L-Phenylalanine	Charged-PHE-tRNAs[c]	0.162986
	L-Tyrosine	Charged-TYR-tRNAs[c]	0.132234
	L-Tryptophan	Charged-TRP-tRNAs[c]	0.007688
	L-Cysteine	Charged-CYS-tRNAs[c]	0.010763
	L-Methionine	Charged-MET-tRNAs[c]	0.083031
	L-Lysine	Charged-LYS-tRNAs[c]	0.264468
	L-Arginine	Charged-ARG-tRNAs[c]	0.184512
	L-Histidine	Charged-HIS-tRNAs[c]	0.087643
	L-Aspartate	Charged-ASP-tRNAs[c]	0.209114
	L-Asparagine	Charged-ASN-tRNAs[c]	0.209114
	L-Glutamine	Charged-GLN-tRNAs[c]	0.266005
	L-Glutamate	Charged-GLT-tRNAs[c]	0.266005
	L-Proline	Charged-PRO-tRNAs[c]	0.155298
<b>RNA</b>	AMP (ATP)	ATP[c]	26.610000
0.145	GMP (GTP)	GTP[c]	0.131137
	CMP (CTP)	CTP[c]	0.089431
	UMP (UTP)	UTP[c]	0.096310
<b>DNA</b>	dAMP (dATP)	DATP[c]	0.010802
0.011	dGMP (dGTP)	DGTP[c]	0.006413
	dCMP (dCTP)	DCTP[c]	0.005738
	dTMP (dTTP)	TTP[c]	0.010802
<b>Ions</b>	K	K-[c]	0.700573
0.03185	Mg	MG-2[c]	0.100903
	Fe(+3)	FE-3[c]	0.003422
	NH4	AMMONIUM[c]	0.001285
	SO4	SULFATE[c]	0.000031
	Ca2+	CA-2[c]	0.003179

	name	Species name	mmol/gDW
<b>Cofactors</b>	coa	CO-A[c]	0.000128
0.01715	spermidine	SPERMIDINE[c]	0.000020
	ACP	ACP[c]	0.000273
	L-Ornithine	L-ORNITHINE[c]	0.000046
	NAD	NAD[c]	0.018220
	NADP	NADP[c]	0.001053
	NADPH	NADPH[c]	0.000237
	menaquinol 7	CPD-12125[c]	0.000150
	10-formyltetrahydrofolate	-10-FORMYL-THF[c]	0.000207
<b>Lipids</b>	cardiolipin (tetrahexadecanoyl)	CPD-12824[c]	0.000740
0.025	cardiolipin (stearoylcardiolipin)	CPDCWI-13[c]	0.000023
	1,2-dipalmitoyl-phosphatidylglycerol	CPD-8260[c]	0.005107
	phosphatidylglycerol (dioctadecanoyl)	CPD-12822[c]	0.000162
	1,2-dipalmitoyl-phosphatidylethanolamine	CPD-12819[c]	0.006196
	phosphatidylethanolamine (dioctadecanoyl)	CPD-12818[c]	0.000196
	1,2-dipalmitoyl-phosphatidylserine	CPD-12817[c]	0.000415
	phosphatidylserine (dioctadecanoyl, n-c18:0)	CPD-12816[c]	0.000013
	1,2-dipalmitoylglycerol	CPD66-34[c]	0.010908
	1,2-distearoyl-sn-glycerol	CPDCWI-14[c]	0.000339
	hexadecanoic/palmitic/palmitate	PALMITATE[c]	0.000572
	octadecanoic/stearic/stearate	STEARIC-ACID[c]	0.000018
<b>Cell wall</b>	a peptidoglycan subunit	CPD-12261[c]	0.030270
0.22			
	water	WATER[c]	22.190000

**Table S21. List of biomass's products for *B. anthracis* model under iron-rich conditions Phase I.** The name, reaction, as well as lower and upper boundaries are provides.

	name	Species name	mmol/gDW
<b>GAM</b>	ADP	ADP[c]	26.500000
	H+	PROTON[c]	26.500000
	Pi	Pi[c]	26.490000
	PPI	PPI[c]	0.458900

	name	Species name	mmol/gDW
	Biomass	BIOMASS-CCO-CYTOSOL[c]	1.000000
<b>tRNAs recycling</b>	Glycine	GLY-tRNAs[c]	0.412078
	L-Alanine	ALA-tRNAs[c]	0.433604
	L-Valine	VAL-tRNAs[c]	0.329047
	L-Leucine	LEU-tRNAs[c]	0.375175
	L-Isoleucine	ILE-tRNAs[c]	0.293682
	L-Serine	SER-tRNAs[c]	0.182975
	L-Threonine	THR-tRNAs[c]	0.239866
	L-Phenylalanine	PHE-tRNAs[c]	0.162986
	L-Tyrosine	TYR-tRNAs[c]	0.132234
	L-Tryptophan	TRP-tRNAs[c]	0.007688
	L-Cysteine	CYS-tRNAs[c]	0.010763
	L-Methionine	MET-tRNAs[c]	0.083031
	L-Lysine	LYS-tRNAs[c]	0.264468
	L-Arginine	ARG-tRNAs[c]	0.184512
	L-Histidine	HIS-tRNAs[c]	0.087643
	L-Aspartate	ASP-tRNAs[c]	0.209114
	L-Asparagine	ASN-tRNAs[c]	0.209114
	L-Glutamine	GLN-tRNAs[c]	0.266005
	L-Glutamate	GLT-tRNAs[c]	0.266005
	L-Proline	PRO-tRNAs[c]	0.155298
	apo-ACP	apo-ACP[c]	0.000273109

#### A8.7. Biomass for iron-poor media Phase II

**Table S22. List of biomass's reactants for *B. anthracis* model under iron-poor conditions Phase II.** The name, reaction, as well as lower and upper boundaries are provides.

	name	Species name	mmol/gDW
<b>Protein</b>	Glycine	Charged-GLY-tRNAs[c]	0.412078
0.55	L-Alanine	Charged-ALA-tRNAs[c]	0.433604
	L-Valine	Charged-VAL-tRNAs[c]	0.329047
	L-Leucine	Charged-LEU-tRNAs[c]	0.375175
	L-Isoleucine	Charged-ILE-tRNAs[c]	0.293682

	<b>name</b>	<b>Species name</b>	<b>mmol/gDW</b>
	L-Serine	Charged-SER-tRNAs[c]	0.182975
	L-Threonine	Charged-THR-tRNAs[c]	0.239866
	L-Phenylalanine	Charged-PHE-tRNAs[c]	0.162986
	L-Tyrosine	Charged-TYR-tRNAs[c]	0.132234
	L-Tryptophan	Charged-TRP-tRNAs[c]	0.007688
	L-Cysteine	Charged-CYS-tRNAs[c]	0.010763
	L-Methionine	Charged-MET-tRNAs[c]	0.083031
	L-Lysine	Charged-LYS-tRNAs[c]	0.264468
	L-Arginine	Charged-ARG-tRNAs[c]	0.184512
	L-Histidine	Charged-HIS-tRNAs[c]	0.087643
	L-Aspartate	Charged-ASP-tRNAs[c]	0.209114
	L-Asparagine	Charged-ASN-tRNAs[c]	0.209114
	L-Glutamine	Charged-GLN-tRNAs[c]	0.266005
	L-Glutamate	Charged-GLT-tRNAs[c]	0.266005
	L-Proline	Charged-PRO-tRNAs[c]	0.155298
<b>RNA</b>	AMP (ATP)	ATP[c]	64.310000
0.145	GMP (GTP)	GTP[c]	0.131137
	CMP (CTP)	CTP[c]	0.089431
	UMP (UTP)	UTP[c]	0.096310
<b>DNA</b>	dAMP (dATP)	DATP[c]	0.010802
0.011	dGMP (dGTP)	DGTP[c]	0.006413
	dCMP (dCTP)	DCTP[c]	0.005738
	dTMP (dTTP)	TTP[c]	0.010802
<b>Ions</b>	K	K-[c]	0.700573
0.03185	Mg	MG-2[c]	0.100903
	Fe(+3)	FE-3[c]	0.002030
	NH4	AMMONIUM[c]	0.001285

	name	Species name	mmol/gDW
	SO4	SULFATE[c]	0.000031
	Ca2+	CA-2[c]	0.003179
<b>Cofactors</b>	coa	CO-A[c]	0.000128
0.01715	spermidine	SPERMIDINE[c]	0.000020
	ACP	ACP[c]	0.000273
	L-Ornithine	L-ORNITHINE[c]	0.000046
	NAD	NAD[c]	0.018220
	NADP	NADP[c]	0.001053
	NADPH	NADPH[c]	0.000237
	menaquinol 7	CPD-12125[c]	0.000150
	10-formyltetrahydrofolate	-10-FORMYL-THF[c]	0.000207
<b>Lipids</b>	cardiolipin (tetrahexadecanoyl)	CPD-12824[c]	0.000740
0.025	cardiolipin (stearoylcardiolipin)	CPDCWI-13[c]	0.000023
	1,2-dipalmitoyl-phosphatidylglycerol	CPD-8260[c]	0.005107
	phosphatidylglycerol (dioctadecanoyl)	CPD-12822[c]	0.000162
	1,2-dipalmitoyl-phosphatidylethanolamine	CPD-12819[c]	0.006196
	phosphatidylethanolamine (dioctadecanoyl)	CPD-12818[c]	0.000196
	1,2-dipalmitoyl-phosphatidylserine	CPD-12817[c]	0.000415
	phosphatidylserine (dioctadecanoyl, n-c18:0)	CPD-12816[c]	0.000013
	1,2-dipalmitoylglycerol	CPD66-34[c]	0.010908
	1,2-distearoyl-sn-glycerol	CPDCWI-14[c]	0.000339
	hexadecanoic/palmitic/palmitate	PALMITATE[c]	0.000572
	octadecanoic/stearic/stearate	STEARIC-ACID[c]	0.000018
<b>Cell wall</b>	a peptidoglycan subunit	CPD-12261[c]	0.030270
0.22			
	water	WATER[c]	59.900000

**Table S23. List of biomass's products for *B. anthracis* model under iron-poor conditions Phase II.** The name, reaction, as well as lower and upper boundaries are provides.

	name	Species name	mmol/gDW
<b>GAM</b>	ADP	ADP[c]	64.200000

	name	Species name	mmol/gDW
	H+	PROTON[c]	64.200000
	Pi	Pi[c]	64.190000
	PPI	PPI[c]	0.458900
	Biomass	BIOMASS-CCO-CYTOSOL[c]	1.000000
<b>tRNAs recycling</b>	Glycine	GLY-tRNAs[c]	0.412078
	L-Alanine	ALA-tRNAs[c]	0.433604
	L-Valine	VAL-tRNAs[c]	0.329047
	L-Leucine	LEU-tRNAs[c]	0.375175
	L-Isoleucine	ILE-tRNAs[c]	0.293682
	L-Serine	SER-tRNAs[c]	0.182975
	L-Threonine	THR-tRNAs[c]	0.239866
	L-Phenylalanine	PHE-tRNAs[c]	0.162986
	L-Tyrosine	TYR-tRNAs[c]	0.132234
	L-Tryptophan	TRP-tRNAs[c]	0.007688
	L-Cysteine	CYS-tRNAs[c]	0.010763
	L-Methionine	MET-tRNAs[c]	0.083031
	L-Lysine	LYS-tRNAs[c]	0.264468
	L-Arginine	ARG-tRNAs[c]	0.184512
	L-Histidine	HIS-tRNAs[c]	0.087643
	L-Aspartate	ASP-tRNAs[c]	0.209114
	L-Asparagine	ASN-tRNAs[c]	0.209114
	L-Glutamine	GLN-tRNAs[c]	0.266005
	L-Glutamate	GLT-tRNAs[c]	0.266005
	L-Proline	PRO-tRNAs[c]	0.155298
	apo-ACP	apo-ACP[c]	0.000273109

#### A8.8. Biomass for iron-rich media Phase II

**Table S24. List of biomass's reactants for *B. anthracis* model under iron-rich conditions Phase II.** The name, reaction, as well as lower and upper boundaries are provides.

	name	Species name	mmol/gDW
<b>Protein</b>	Glycine	Charged-GLY-tRNAs[c]	0.412078
0.55	L-Alanine	Charged-ALA-tRNAs[c]	0.433604

	<b>name</b>	<b>Species name</b>	<b>mmol/gD W</b>
	L-Valine	Charged-VAL-tRNAs[c]	0.329047
	L-Leucine	Charged-LEU-tRNAs[c]	0.375175
	L-Isoleucine	Charged-ILE-tRNAs[c]	0.293682
	L-Serine	Charged-SER-tRNAs[c]	0.182975
	L-Threonine	Charged-THR-tRNAs[c]	0.239866
	L-Phenylalanine	Charged-PHE-tRNAs[c]	0.162986
	L-Tyrosine	Charged-TYR-tRNAs[c]	0.132234
	L-Tryptophan	Charged-TRP-tRNAs[c]	0.007688
	L-Cysteine	Charged-CYS-tRNAs[c]	0.010763
	L-Methionine	Charged-MET-tRNAs[c]	0.083031
	L-Lysine	Charged-LYS-tRNAs[c]	0.264468
	L-Arginine	Charged-ARG-tRNAs[c]	0.184512
	L-Histidine	Charged-HIS-tRNAs[c]	0.087643
	L-Aspartate	Charged-ASP-tRNAs[c]	0.209114
	L-Asparagine	Charged-ASN-tRNAs[c]	0.209114
	L-Glutamine	Charged-GLN-tRNAs[c]	0.266005
	L-Glutamate	Charged-GLT-tRNAs[c]	0.266005
	L-Proline	Charged-PRO-tRNAs[c]	0.155298
<b>RNA</b>	AMP (ATP)	ATP[c]	58.610000
0.145	GMP (GTP)	GTP[c]	0.131137
	CMP (CTP)	CTP[c]	0.089431
	UMP (UTP)	UTP[c]	0.096310
<b>DNA</b>	dAMP (dATP)	DATP[c]	0.010802
0.011	dGMP (dGTP)	DGTP[c]	0.006413
	dCMP (dCTP)	DCTP[c]	0.005738

	name	Species name	mmol/gDW
	dTMP (dTTP)	TTP[c]	0.010802
<b>Ions</b>	K	K-[c]	0.700573
0.03185	Mg	MG-2[c]	0.100903
	Fe(+3)	FE-3[c]	0.003422
	NH4	AMMONIUM[c]	0.001285
	SO4	SULFATE[c]	0.000031
	Ca2+	CA-2[c]	0.003179
<b>Cofactors</b>	coa	CO-A[c]	0.000128
0.01715	spermidine	SPERMIDINE[c]	0.000020
	ACP	ACP[c]	0.000273
	L-Ornithine	L-ORNITHINE[c]	0.000046
	NAD	NAD[c]	0.018220
	NADP	NADP[c]	0.001053
	NADPH	NADPH[c]	0.000237
	menaquinol 7	CPD-12125[c]	0.000150
	10-formyltetrahydrofolate	-10-FORMYL-THF[c]	0.000207
<b>Lipids</b>	cardiolipin (tetrahexadecanoyl)	CPD-12824[c]	0.000740
0.025	cardiolipin (stearoylcardiolipin)	CPDCWI-13[c]	0.000023
	1,2-dipalmitoyl-phosphatidylglycerol	CPD-8260[c]	0.005107
	phosphatidylglycerol (dioctadecanoyl)	CPD-12822[c]	0.000162
	1,2-dipalmitoyl-phosphatidylethanolamine	CPD-12819[c]	0.006196
	phosphatidylethanolamine (dioctadecanoyl)	CPD-12818[c]	0.000196
	1,2-dipalmitoyl-phosphatidylserine	CPD-12817[c]	0.000415
	phosphatidylserine (dioctadecanoyl, n-c18:0)	CPD-12816[c]	0.000013
	1,2-dipalmitoylglycerol	CPD66-34[c]	0.010908
	1,2-distearoyl-sn-glycerol	CPDCWI-14[c]	0.000339
	hexadecanoic/palmitic/palmitate	PALMITATE[c]	0.000572
	octadecanoic/stearic/stearate	STEARIC-ACID[c]	0.000018
<b>Cell wall</b>	a peptidoglycan subunit	CPD-12261[c]	0.030270
0.22			
	water	WATER[c]	54.200000



**Table S25. List of biomass's products for *B. anthracis* model under iron-rich conditions Phase II.** The name, reaction, as well as lower and upper boundaries are provides.

	name	Species name	mmol/gDW
<b>GAM</b>	ADP	ADP[c]	58.500000
	H+	PROTON[c]	58.500000
	Pi	Pi[c]	58.490000
	PPI	PPI[c]	0.458900
	Biomass	BIOMASS-CCO-CYTOSOL[c]	1.000000
<b>tRNAs recycling</b>	Glycine	GLY-tRNAs[c]	0.412078
	L-Alanine	ALA-tRNAs[c]	0.433604
	L-Valine	VAL-tRNAs[c]	0.329047
	L-Leucine	LEU-tRNAs[c]	0.375175
	L-Isoleucine	ILE-tRNAs[c]	0.293682
	L-Serine	SER-tRNAs[c]	0.182975
	L-Threonine	THR-tRNAs[c]	0.239866
	L-Phenylalanine	PHE-tRNAs[c]	0.162986
	L-Tyrosine	TYR-tRNAs[c]	0.132234
	L-Tryptophan	TRP-tRNAs[c]	0.007688
	L-Cysteine	CYS-tRNAs[c]	0.010763
	L-Methionine	MET-tRNAs[c]	0.083031
	L-Lysine	LYS-tRNAs[c]	0.264468
	L-Arginine	ARG-tRNAs[c]	0.184512
	L-Histidine	HIS-tRNAs[c]	0.087643
	L-Aspartate	ASP-tRNAs[c]	0.209114
	L-Asparagine	ASN-tRNAs[c]	0.209114
	L-Glutamine	GLN-tRNAs[c]	0.266005
	L-Glutamate	GLT-tRNAs[c]	0.266005
	L-Proline	PRO-tRNAs[c]	0.155298
	apo-ACP	apo-ACP[c]	0.000273109

### A8.9. Additional constraints

**Table S26. List of biomass's products for *B. anthracis* model under iron-rich conditions Phase II.** The name, reaction, as well as lower and upper boundaries are provides.

Reaction name	lower boundary	upper boundary	rationale	model	Ref.
CATAL-RXN	0	0	repressed by aerobic conditions	IRDM1, IRM1, IRDM2, IRM2	[270]
RXN-12121	0	0	repressed by aerobic conditions	IRDM1, IRM1, IRDM2, IRM2	[270]
RXN-12120	0	0	repressed by aerobic conditions	IRDM1, IRM1, IRDM2, IRM2	[270]
RXNI-3-MAL_CPD-9718_OXALACETIC_ACID_CPD-12125.40.	0	0	Doubt about presence in the bacteria, additionally was causing futile cycle.	IRDM1, IRM1, IRDM2, IRM2	[271]
L-LACTDEHYDROGFMN-RXN	0	0	induction when lactate present in the media or H2O2	IRDM1, IRM1	[5,164,165]
RXNCWI-17	0	0	repressed in presence of glucose	IRDM1, IRM1, IRDM2, IRM2	[272]
URA-PHOSPH-RXN	0	0	on only when deoxyribonucleosides are in the media	IRDM1, IRM1, IRDM2, IRM2	[273]
DEOXYADENPHOSPHOR-RXN	0	0	on only when deoxyribonucleosides are in the media	IRDM1, IRM1, IRDM2, IRM2	[273]
DEOXYINOPHOSPHOR-RXN	0	0	on only when deoxyribonucleo	IRDM1, IRM1,	[273]

Reaction name	lower boundary	upper boundary	rationale	model	Ref.
			sides are in the media	IRDM2, IRM2	
RXN-11743	0	0	on only when deoxyribonucleo sides are in the media	IRDM1, IRM1, IRDM2, IRM2	[273]
XANTHOSINEPHOSPHORY-RXN	0	0	on only when deoxyribonucleo sides are in the media	IRDM1, IRM1, IRDM2, IRM2	[273]
DEOXYGUANPHOSPHOR-RXN	0	0	on only when deoxyribonucleo sides are in the media	IRDM1, IRM1, IRDM2, IRM2	[273]
RXN0-5199	0	0	on only when deoxyribonucleo sides are in the media	IRDM1, IRM1, IRDM2, IRM2	[273]
INOPHOSPHOR-RXN	0	0	on only when deoxyribonucleo sides are in the media	IRDM1, IRM1, IRDM2, IRM2	[273]
ADENPHOSPHOR-RXN	0	0	on only when deoxyribonucleo sides are in the media	IRDM1, IRM1, IRDM2, IRM2	[273]
RXN0-366	0	0	on only when deoxyribonucleo sides are in the media	IRDM1, IRM1, IRDM2, IRM2	[273]
RXNCWI-82	0	0	on only when deoxyribonucleo sides are in the media	IRDM1, IRM1, IRDM2, IRM2	[273]
RXNCWI-105	0	0.000472	experimentally measured boundary for the ferric-siderophore transport	IRDM1, IRM1, IRDM2, IRM2	[187]
TRANS-RXNCWI-7	0	0.000964	experimentally measured boundary for the ferric-siderophore	IRDM1, IRM1, IRDM2, IRM2	[187]

Reaction name	lower boundary	upper boundary	rationale	model	Ref.
			transport		
TRANS-RXNCWI-8	0	0.00119	experimentally measured boundary for the ferric-siderophore transport	IRDM1, IRM1, IRDM2, IRM2	[187]
RXNCWI-53	0	0	not ATPase transport for iron, based on the observation that iron concentration were very low	IRDM2	
L-LACTATE-DEHYDROGENASE-RXN	-1000	0	lactate dehydrogenase only for lactate production in phase II	IRDM2, IRM2	[164]

## 10 REFERENCE

1. Reaves ML, Rabinowitz JD (2011) Metabolomics in systems microbiology. *Curr Opin Biotechnol* 22: 17-25.
2. Kell DB (2006) Systems biology, metabolic modelling and metabolomics in drug discovery and development. *Drug Discov Today* 11: 1085-1092.
3. Thiele I, Palsson BO (2010) A protocol for generating a high-quality genome-scale metabolic reconstruction. *Nat Protoc* 5: 93-121.
4. Bergman NH, Anderson EC, Swenson EE, Janes BK, Fisher N, et al. (2007) Transcriptional profiling of *Bacillus anthracis* during infection of host macrophages. *Infect Immun* 75: 3434-3444.
5. Pohl S, Tu WY, Aldridge PD, Gillespie C, Hahne H, et al. (2011) Combined proteomic and transcriptomic analysis of the response of *Bacillus anthracis* to oxidative stress. *PROTEOMICS* 11: 3036-3055.
6. Carlson PE, Jr., Carr KA, Janes BK, Anderson EC, Hanna PC (2009) Transcriptional profiling of *Bacillus anthracis* Sterne (34F2) during iron starvation. *PLoS One* 4: e6988.
7. Daar AS, Thorsteinsdottir H, Martin DK, Smith AC, Nast S, et al. (2002) Top ten biotechnologies for improving health in developing countries. *Nat Genet* 32: 229-232.
8. Jain R, Srivastava R (2009) Metabolic investigation of host/pathogen interaction using MS2-infected *Escherichia coli*. *BMC Syst Biol* 3: 121.
9. Bordbar A, Lewis NE, Schellenberger J, Palsson BO, Jamshidi N (2010) Insight into human alveolar macrophage and *M. tuberculosis* interactions via metabolic reconstructions. *Mol Syst Biol* 6: 422.
10. Yizhak K, Benyamini T, Liebermeister W, Ruppin E, Shlomi T (2010) Integrating quantitative proteomics and metabolomics with a genome-scale metabolic network model. *Bioinformatics* 26: i255-260.
11. Yim H, Haselbeck R, Niu W, Pujol-Baxley C, Burgard A, et al. (2011) Metabolic engineering of *Escherichia coli* for direct production of 1,4-butanediol. *Nat Chem Biol* 7: 445-452.
12. Väremo L, Nookaew I, Nielsen J (2013) Novel insights into obesity and diabetes through genome-scale metabolic modeling. *Frontiers in physiology* 4.
13. Salimi F, Zhuang K, Mahadevan R (2010) Genome-scale metabolic modeling of a clostridial co-culture for consolidated bioprocessing. *Biotechnol J* 5: 726-738.
14. Price ND, Papin JA, Palsson BØ (2002) Determination of redundancy and systems properties of the metabolic network of *Helicobacter pylori* using genome-scale extreme pathway analysis. *Genome research* 12: 760-769.
15. Oberhardt MA, Palsson BO, Papin JA (2009) Applications of genome-scale metabolic reconstructions. *Mol Syst Biol* 5: 320.

16. Baart GJ, Martens DE (2012) Genome-scale metabolic models: reconstruction and analysis. *Neisseria meningitidis*: Springer. pp. 107-126.
17. Edwards JS, Covert M, Palsson B (2002) Metabolic modelling of microbes: the flux-balance approach. *Environ Microbiol* 4: 133-140.
18. Price ND, Papin JA, Schilling CH, Palsson BO (2003) Genome-scale microbial in silico models: the constraints-based approach. *Trends Biotechnol* 21: 162-169.
19. Orth JD, Thiele I, Palsson BO (2010) What is flux balance analysis? *Nat Biotech* 28: 245-248.
20. Papp B, Notebaart RA, Pal C (2011) Systems-biology approaches for predicting genomic evolution. *Nat Rev Genet* 12: 591-602.
21. Stephanopoulos G, Aristidou AA, Nielsen J (1998) *Metabolic Engineering: Principles and Methodologies*: Elsevier Science.
22. Oberhardt MA, Chavali AK, Papin JA (2009) Flux balance analysis: interrogating genome-scale metabolic networks. *Methods Mol Biol* 500: 61-80.
23. Edwards JS (1999) *Functional genomics and the computational analysis of bacterial metabolism*: University of California, San Diego.
24. Knorr AL (2006) *Development of discrimination analysis for systems biology applications*: University of Connecticut. 224 p.
25. Schuetz R, Kuepfer L, Sauer U (2007) Systematic evaluation of objective functions for predicting intracellular fluxes in *Escherichia coli*. *Mol Syst Biol* 3: 119.
26. Knorr AL, Jain R, Srivastava R (2007) Bayesian-based selection of metabolic objective functions. *Bioinformatics* 23: 351-357.
27. Feist AM, Palsson BO (2010) The biomass objective function. *Current Opinion in Microbiology* 13: 344-349.
28. Mitchell M (1998) *An introduction to genetic algorithms*. Cambridge: Massachusetts Institute of Technology Press. 209 p.
29. Man KF, Tang KS, Kwong S (1996) Genetic algorithms: Concepts and applications. *Ieee Transactions on Industrial Electronics* 43: 519-534.
30. Affenzeller M, Wagner S, Winkler S, Beham A (2009) *Genetic Algorithms and Genetic Programming: Modern Concepts and Practical Applications*: Taylor & Francis.
31. Papazisi L, Gorton TS, Kutish G, Markham PF, Browning GF, et al. (2003) The complete genome sequence of the avian pathogen *Mycoplasma gallisepticum* strain R(low). *Microbiology* 149: 2307-2316.
32. Hennigan SL, Driskell JD, Ferguson-Noel N, Dluhy RA, Zhao Y, et al. (2012) Detection and differentiation of avian mycoplasmas by surface-enhanced Raman spectroscopy based on a silver nanorod array. *Appl Environ Microbiol* 78: 1930-1935.
33. Merck DHL (2012) *Mycoplasma gallisepticum* infection in Poultry. In: professionals TMvmfv, editor.

[http://www.merckmanuals.com/vet/poultry/mycoplasmosis/mycoplasma\\_gallisepticum\\_infection\\_in\\_poultry.html](http://www.merckmanuals.com/vet/poultry/mycoplasmosis/mycoplasma_gallisepticum_infection_in_poultry.html): Meck.

34. Winner F, Rosengarten R, Citti C (2000) In vitro cell invasion of *Mycoplasma gallisepticum*. Infect Immun 68: 4238-4244.
35. Vogl G, Plaickner A, Szathmary S, Stipkovits L, Rosengarten R, et al. (2008) *Mycoplasma gallisepticum* invades chicken erythrocytes during infection. Infect Immun 76: 71-77.
36. Vitula F, Peckova L, Bandouchova H, Pohanka M, Novotny L, et al. (2011) *Mycoplasma gallisepticum* infection in the grey partridge *Perdix perdix*: outbreak description, histopathology, biochemistry and antioxidant parameters. BMC Vet Res 7: 34.
37. Sternbach G (2003) The history of anthrax. J Emerg Med 24: 463-467.
38. Spencer RC (2003) *Bacillus anthracis*. J Clin Pathol 56: 182-187.
39. Sweeney DA, Hicks CW, Cui X, Li Y, Eichacker PQ (2011) Anthrax Infection. Am J Respir Crit Care Med.
40. Drysdale M, Heninger S, Hutt J, Chen YH, Lyons CR, et al. (2005) Capsule synthesis by *Bacillus anthracis* is required for dissemination in murine inhalation anthrax. Embo Journal 24: 221-227.
41. Riedel S (2005) Anthrax: a continuing concern in the era of bioterrorism. Proc (Bayl Univ Med Cent) 18: 234-243.
42. (2008) Three Forms Of Anthrax Which Affect People Often! Health Watch Center.
43. Ajikumar PK, Ng JK, Tang YC, Lee JY, Stephanopoulos G, et al. (2007) Carboxyl-terminated dendrimer-coated bioactive interface for protein microarray: high-sensitivity detection of antigen in complex biological samples. Langmuir 23: 5670-5677.
44. Rocha I, Forster J, Nielsen J (2008) Design and application of genome-scale reconstructed metabolic models. Methods Mol Biol 416: 409-431.
45. Feist AM, Herrgard MJ, Thiele I, Reed JL, Palsson BO (2009) Reconstruction of biochemical networks in microorganisms. Nat Rev Microbiol 7: 129-143.
46. DeJongh M, Formsma K, Boillot P, Gould J, Rycenga M, et al. (2007) Toward the automated generation of genome-scale metabolic networks in the SEED. BMC Bioinformatics 8: 139.
47. Satish Kumar V, Dasika MS, Maranas CD (2007) Optimization based automated curation of metabolic reconstructions. BMC Bioinformatics 8: 212.
48. Notebaart RA, Van Enkevort FHJ, Francke C, Siezen RJ, Teusink B (2006) Accelerating the reconstruction of genome-scale metabolic networks. BMC Bioinformatics 7: -.
49. Green ML, Karp PD (2004) A Bayesian method for identifying missing enzymes in predicted metabolic pathway databases. BMC Bioinformatics 5: 76.

50. Kharchenko P, Vitkup D, Church GM (2004) Filling gaps in a metabolic network using expression information. *Bioinformatics* 20 Suppl 1: i178-185.
51. Kharchenko P, Chen L, Freund Y, Vitkup D, Church GM (2006) Identifying metabolic enzymes with multiple types of association evidence. *BMC Bioinformatics* 7: 177.
52. Latendresse M, Krummenacker M, Trupp M, Karp PD (2012) Construction and completion of flux balance models from pathway databases. *Bioinformatics*.
53. Henry CS, DeJongh M, Best AA, Frybarger PM, Linsay B, et al. (2010) High-throughput generation, optimization and analysis of genome-scale metabolic models. *Nat Biotech* 28: 977-982.
54. Caspi R, Foerster H, Fulcher CA, Hopkinson R, Ingraham J, et al. (2006) MetaCyc: a multiorganism database of metabolic pathways and enzymes. *Nucleic Acids Res* 34: D511-516.
55. Levisohn S, Kleven SH (2000) Avian mycoplasmosis (*Mycoplasma gallisepticum*). *Rev Sci Tech* 19: 425-442.
56. Evans JD, Leigh SA, Branton SL, Collier SD, Pharr GT, et al. (2005) *Mycoplasma gallisepticum*: Current and Developing Means to Control the Avian Pathogen. *J appl poult res* 14: 757-763.
57. Tourtellotte ME, Morowitz HJ, Kasimer P (1964) Defined medium for *Mycoplasmas laidlaw* II. *J Bacteriol* 88: 11-15.
58. Suthers PF, Dasika MS, Kumar VS, Denisov G, Glass JI, et al. (2009) A genome-scale metabolic reconstruction of *Mycoplasma genitalium*, iPS189. *PLoS Comput Biol* 5: e1000285.
59. Barile MF, Razin S, editors (1979) *The Mycoplasmas: Cell biology*. San Diego: Academic press. 547 p.
60. Stephanopoulos G (1998) Metabolic engineering. *Biotechnol Bioeng* 58: 119-120.
61. Ibarra RU, Edwards JS, Palsson BO (2002) *Escherichia coli* K-12 undergoes adaptive evolution to achieve in silico predicted optimal growth. *Nature* 420: 186-189.
62. Schilling CH, Edwards JS, Letscher D, Palsson BO (2000) Combining pathway analysis with flux balance analysis for the comprehensive study of metabolic systems. *Biotechnol Bioeng* 71: 286-306.
63. Edwards JS, Ibarra RU, Palsson BO (2001) *In silico* predictions of *Escherichia coli* metabolic capabilities are consistent with experimental data. *Nat Biotechnol* 19: 125-130.
64. Edwards JS, Palsson BO (2000) The *Escherichia coli* MG1655 *in silico* metabolic genotype: its definition, characteristics, and capabilities. *Proc Natl Acad Sci U S A* 97: 5528-5533.
65. Szczepanek SM, Tulman ER, Gorton TS, Liao X, Lu Z, et al. (2010) Comparative genomic analyses of attenuated strains of *Mycoplasma gallisepticum*. *Infect Immun* 78: 1760-1771.



66. Karp PD, Paley S, Romero P (2002) The Pathway Tools software. *Bioinformatics* 18 Suppl 1: S225-232.
67. Holland JH (1992) Adaptation in natural and artificial systems: an introductory analysis with applications to biology, control, and artificial intelligence. Cambridge: Massachusetts Institute of Technology Press. 211 p.
68. Karp PD, Paley SM, Krummenacker M, Latendresse M, Dale JM, et al. (2010) Pathway Tools version 13.0: integrated software for pathway/genome informatics and systems biology. *Brief Bioinform* 11: 40-79.
69. Smith PF, Henrikson CV (1965) Comparative Biosynthesis of Mevalonic Acid by *Mycoplasma*. *J Bacteriol* 89: 146-153.
70. McIvor RS, Kenny GE (1978) Differences in incorporation of nucleic acid bases and nucleosides by various *Mycoplasma* and *Acholeplasma* species. *J Bacteriol* 135: 483-489.
71. Manolukas JT, Barile MF, Chandler DK, Pollack JD (1988) Presence of anaplerotic reactions and transamination, and the absence of the tricarboxylic acid cycle in mollicutes. *J Gen Microbiol* 134: 791-800.
72. Pollack JD, Razin S, Cleverdon RC (1965) Localization of Enzymes in *Mycoplasma*. *J Bacteriol* 90: 617-622.
73. McElwain MC, Pollack JD (1987) Synthesis of deoxyribomononucleotides in Mollicutes: dependence on deoxyribose-1-phosphate and PPi. *J Bacteriol* 169: 3647-3653.
74. Bizarro CV, Schuck DC (2007) Purine and pyrimidine nucleotide metabolism in mollicutes. *Genetics and Molecular Biology* 30: 190-201.
75. Williams MV, Pollack JD (1985) Pyrimidine Deoxyribonucleotide Metabolism in Members of the Class Mollicutes. *Int J Syst Bacteriol* 35: 227-230.
76. Tryon VV, Pollack JD (1985) Distinctions in Mollicutes Purine Metabolism: Pyrophosphate-Dependent Nucleoside Kinase and Dependence on Guanylate Salvage. *Int J Syst Bacteriol* 35: 497-501.
77. McGarrity GJ, Gamon L, Steiner T, Tully J, Kotani H (1985) Uridine phosphorylase activity among the class mollicutes. *Current Microbiology* 12: 107-112.
78. Pollack JD, Williams MV, McElhaney RN (1997) The comparative metabolism of the mollicutes (Mycoplasmas): the utility for taxonomic classification and the relationship of putative gene annotation and phylogeny to enzymatic function in the smallest free-living cells. *Crit Rev Microbiol* 23: 269-354.
79. Cordwell SJ, Basseal DJ, Pollack JD, Humphery-Smith I (1997) Malate/lactate dehydrogenase in mollicutes: evidence for a multienzyme protein. *Gene* 195: 113-120.
80. Desantis D, Tryon VV, Pollack JD (1989) Metabolism of Mollicutes: the Embden--Meyerhof--Parnas Pathway and the Hexose Monophosphate Shunt. *J Gen Microbiol* 135: 683-691.
81. Gill JW (1962) Culture and metabolism of *Mycoplasma gallisepticum*. *J Bacteriol* 83: 213-218.

82. Stover P, Schirch V (1990) Serine hydroxymethyltransferase catalyzes the hydrolysis of 5,10-methenyltetrahydrofolate to 5-formyltetrahydrofolate. *J Biol Chem* 265: 14227-14233.
83. Rottem S, Markowitz O (1979) Membrane lipids of *Mycoplasma gallisepticum*: a disaturated phosphatidylcholine and a phosphatidylglycerol with an unusual positional distribution of fatty acids. *Biochemistry* 18: 2930-2935.
84. Altschul SF, Wootton JC, Gertz EM, Agarwala R, Morgulis A, et al. (2005) Protein database searches using compositionally adjusted substitution matrices. *FEBS Journal* 272: 5101-5109.
85. Altschul SF, Madden TL, Schaffer AA, Zhang J, Zhang Z, et al. (1997) Gapped BLAST and PSI-BLAST: a new generation of protein database search programs. *Nucleic Acids Res* 25: 3389-3402.
86. Klement ML, Ojemyr L, Tagscherer KE, Widmalm G, Wieslander A (2007) A processive lipid glycosyltransferase in the small human pathogen *Mycoplasma pneumoniae*: involvement in host immune response. *Mol Microbiol* 65: 1444-1457.
87. Schiefer HG, Gerhardt U, Brunner H, Krupe M (1974) Studies with lectins on the surface carbohydrate structures of mycoplasma membranes. *J Bacteriol* 120: 81-88.
88. Pollack JD, Myers MA, Dandekar T, Herrmann R (2002) Suspected utility of enzymes with multiple activities in the small genome *Mycoplasma* species: the replacement of the missing "household" nucleoside diphosphate kinase gene and activity by glycolytic kinases. *OMICS* 6: 247-258.
89. Yus E, Maier T, Michalodimitrakis K, van Noort V, Yamada T, et al. (2009) Impact of genome reduction on bacterial metabolism and its regulation. *Science* 326: 1263-1268.
90. Williams MV, Pollack JD (1990) The importance of differences in pyrimidine metabolism of the mollicutes. *Zentralbl Bakteriol Suppl* 20: 163-171.
91. Tourtellotte ME, Jensen RG, Gander GW, Morowitz HJ (1963) Lipid Composition and Synthesis in the Pleuropneumonia-Like Organism *Mycoplasma Gallisepticum*. *J Bacteriol* 86: 370-379.
92. Cluss RG, Somerson NL (1986) Interaction of albumin and phospholipid:cholesterol liposomes in growth of *Mycoplasma spp.* *Appl Environ Microbiol* 51: 281-287.
93. Le Grimellec C, Cardinal J, Giocondi MC, Carriere S (1981) Control of membrane lipids in *Mycoplasma gallisepticum*: effect on lipid order. *J Bacteriol* 146: 155-162.
94. Taylor RR, Mohan K, Miles RJ (1996) Diversity of energy-yielding substrates and metabolism in avian *mycoplasmas*. *Vet Microbiol* 51: 291-304.
95. Macpherson I (1966) *Mycoplasmas* in tissue culture. *J Cell Sci I*: 145-168.
96. Kanehisa M, Goto S, Hattori M, Aoki-Kinoshita KF, Itoh M, et al. (2006) From genomics to chemical genomics: new developments in KEGG. *Nucleic Acids Res* 34: D354-357.

97. Schummer U, Schiefer HG (1983) Electrophysiology of *mycoplasma* membranes. *Yale J Biol Med* 56: 413-418.
98. Shirvan MH, Schuldiner S, Rottem S (1989) Volume regulation in *Mycoplasma gallisepticum*: evidence that Na<sup>+</sup> is extruded via a primary Na<sup>+</sup> pump. *J Bacteriol* 171: 4417-4424.
99. Linker C, Wilson TH (1985) Cell volume regulation in *Mycoplasma gallisepticum*. *J Bacteriol* 163: 1243-1249.
100. Linker C, Wilson TH (1985) Sodium and proton transport in *Mycoplasma gallisepticum*. *J Bacteriol* 163: 1250-1257.
101. Linker C, Wilson TH (1985) Characterization and solubilization of the membrane-bound ATPase of *Mycoplasma gallisepticum*. *J Bacteriol* 163: 1258-1262.
102. Razin S (1967) The cell membrane of *mycoplasma*. *Ann N Y Acad Sci* 143: 115-129.
103. Shirvan MH, Schuldiner S, Rottem S (1989) Role of Na<sup>+</sup> cycle in cell volume regulation of *Mycoplasma gallisepticum*. *J Bacteriol* 171: 4410-4416.
104. Testa CA, Brown MJ (2003) The Methylerythritol Phosphate Pathway and its Significance as a Novel Drug Target. *Current Pharmaceutical Biotechnology* 4: 248-259.
105. Rodríguez-Concepcion M, Boronat A (2002) Elucidation of the Methylerythritol Phosphate Pathway for Isoprenoid Biosynthesis in Bacteria and Plastids. A Metabolic Milestone Achieved through Genomics. *Plant Physiology* 130: 1079-1089.
106. Lange BM, Rujan T, Martin W, Croteau R (2000) Isoprenoid biosynthesis: the evolution of two ancient and distinct pathways across genomes. *Proc Natl Acad Sci U S A* 97: 13172-13177.
107. Eberl M, Altincicek B, Kollas A-K, Sanderbrand S, Bahr U, et al. (2002) Accumulation of a potent  $\gamma\delta$  T-cell stimulator after deletion of the *lytB* gene in *Escherichia coli*. *Immunology* 106: 200-211.
108. Osterman A, Overbeek R (2003) Missing genes in metabolic pathways: a comparative genomics approach. *Curr Opin Chem Biol* 7: 238-251.
109. Eisenreich W, Rohdich F, Bacher A (2001) Deoxyxylulose phosphate pathway to terpenoids. *Trends Plant Sci* 6: 78-84.
110. Rohmer M, Knani M, Simonin P, Sutter B, Sahm H (1993) Isoprenoid biosynthesis in bacteria: a novel pathway for the early steps leading to isopentenyl diphosphate. *Biochem J* 295 ( Pt 2): 517-524.
111. Cunningham FX, Jr., Lafond TP, Gantt E (2000) Evidence of a role for LytB in the nonmevalonate pathway of isoprenoid biosynthesis. *J Bacteriol* 182: 5841-5848.
112. Eisenreich W, Bacher A, Arigoni D, Rohdich F (2004) Biosynthesis of isoprenoids via the non-mevalonate pathway. *Cell Mol Life Sci* 61: 1401-1426.

113. Sangari FJ, Perez-Gil J, Carretero-Paulet L, Garcia-Lobo JM, Rodriguez-Concepcion M (2010) A new family of enzymes catalyzing the first committed step of the methylerythritol 4-phosphate (MEP) pathway for isoprenoid biosynthesis in bacteria. *Proc Natl Acad Sci U S A* 107: 14081-14086.
114. Eberl M, Hintz M, Reichenberg A, Kollas AK, Wiesner J, et al. (2003) Microbial isoprenoid biosynthesis and human gammadelta T cell activation. *FEBS Lett* 544: 4-10.
115. Eberl M, Hintz M, Jamba Z, Beck E, Jomaa H, et al. (2004) *Mycoplasma penetrans* is capable of activating V gamma 9/V delta 2 T cells while other human pathogenic mycoplasmas fail to do so. *Infection and Immunity* 72: 4881-4883.
116. Fabricant CG, Fabricant J, Vandemark PJ (1964) Studies on the Nutrition and Growth Requirements of *Mycoplasma Gallisepticum*. *J Gen Microbiol* 35: 135-144.
117. Fraser CM, Gocayne JD, White O, Adams MD, Clayton RA, et al. (1995) The minimal gene complement of *Mycoplasma genitalium*. *Science* 270: 397-403.
118. Aziz RK, Bartels D, Best AA, DeJongh M, Disz T, et al. (2008) The RAST Server: rapid annotations using subsystems technology. *BMC Genomics* 9: 75.
119. Reed P, Minsker B, Goldberg DE (2000) Designing a competent simple genetic algorithm for search and optimization. *Water Resources Research* 36: 3757-3761.
120. Kallrath J (2000) Mixed integer optimization in the chemical process industry - Experience, potential and future perspectives. *Chemical Engineering Research & Design* 78: 809-822.
121. Engell S, Guéguen H, Zaytoon J, Control IFoA (2003) Analysis and Design of Hybrid Systems 2003 (ADHS 03): A Proceedings Volume from the IFAC Conference, St. Malo, Brittany, France, 16-18 June 2003: Elsevier.
122. Obiol-Pardo C, Rubio-Martinez J, Imperial S (2011) The methylerythritol phosphate (MEP) pathway for isoprenoid biosynthesis as a target for the development of new drugs against tuberculosis. *Curr Med Chem* 18: 1325-1338.
123. Eoh H, Brennan PJ, Crick DC (2009) The *Mycobacterium tuberculosis* MEP (2C-methyl-d-erythritol 4-phosphate) pathway as a new drug target. *Tuberculosis (Edinb)* 89: 1-11.
124. Matsue Y, Mizuno H, Tomita T, Asami T, Nishiyama M, et al. (2010) The herbicide ketocloromazone inhibits 1-deoxy-D-xylulose 5-phosphate synthase in the 2-C-methyl-D-erythritol 4-phosphate pathway and shows antibacterial activity against *Haemophilus influenzae*. *J Antibiot (Tokyo)* 63: 583-588.
125. Singh N, Cheve G, Avery MA, McCurdy CR (2007) Targeting the methyl erythritol phosphate (MEP) pathway for novel antimalarial, antibacterial and

- herbicide drug discovery: inhibition of 1-deoxy-D-xylulose-5-phosphate reductoisomerase (DXR) enzyme. *Curr Pharm Des* 13: 1161-1177.
126. Wiesner J, Borrmann S, Jomaa H (2003) Fosmidomycin for the treatment of malaria. *Parasitol Res* 90 Suppl 2: S71-76.
  127. Bautista EJ, Srivastava R (2013) Leveraging ensemble information of evolving populations in genetic algorithms to identify incomplete metabolic pathways. *Proceeding of the fifteenth annual conference companion on Genetic and evolutionary computation conference companion*. Amsterdam, The Netherlands: ACM. pp. 39-40.
  128. Palsson BO (2006) *Systems Biology*: Cambridge University Press.
  129. Yang K, Ma W, Liang H, Ouyang Q, Tang C, et al. (2007) Dynamic simulations on the arachidonic acid metabolic network. *PLoS Comput Biol* 3: e55.
  130. Kim TY, Sohn SB, Kim YB, Kim WJ, Lee SY (2012) Recent advances in reconstruction and applications of genome-scale metabolic models. *Curr Opin Biotechnol* 23: 617-623.
  131. Cascante M, Boros LG, Comin-Anduix B, de Atauri P, Centelles JJ, et al. (2002) Metabolic control analysis in drug discovery and disease. *Nat Biotechnol* 20: 243-249.
  132. Raman K, Rajagopalan P, Chandra N (2005) Flux balance analysis of mycolic acid pathway: targets for anti-tubercular drugs. *PLoS Comput Biol* 1: e46.
  133. Diaz-Gomez PA, Hougen DF. *Pseudo Random Generation of the Initial Population in Genetic Algorithms: an Experiment*; 2006; University of Oklahoma.
  134. Maaranen H, Miettinen K, Mäkelä MM (2004) Quasi-random initial population for genetic algorithms. *Computers & Mathematics with Applications* 47: 1885-1895.
  135. Maaranen H, Miettinen K, Penttinen A (2007) On initial populations of a genetic algorithm for continuous optimization problems. *Journal of Global Optimization* 37: 405-436.
  136. Pop PC (2012) *Generalized Network Design Problems: Modeling and Optimization*: De Gruyter.
  137. Cendrowski S, MacArthur W, Hanna P (2004) *Bacillus anthracis* requires siderophore biosynthesis for growth in macrophages and mouse virulence. *Molecular Microbiology* 51: 407-417.
  138. Sauer U, Hatzimanikatis V, Hohmann H-P, Manneberg M, Van Loon A, et al. (1996) Physiology and metabolic fluxes of wild-type and riboflavin-producing *Bacillus subtilis*. *Applied and environmental microbiology* 62: 3687-3696.
  139. Durot M, Bourguignon P-Y, Schachter V (2009) Genome-scale models of bacterial metabolism: reconstruction and applications. *FEMS Microbiology Reviews* 33: 164-190.
  140. Bergman NH (2011) *Bacillus anthracis* and Anthrax: Wiley.

141. Turi JL, Yang F, Garrick MD, Piantadosi CA, Ghio AJ (2004) The iron cycle and oxidative stress in the lung. *Free Radic Biol Med* 36: 850-857.
142. Hotta K, Kim CY, Fox DT, Koppisch AT (2010) Siderophore-mediated iron acquisition in *Bacillus anthracis* and related strains. *Microbiology* 156: 1918-1925.
143. Garner BL, Arceneaux JE, Byers BR (2004) Temperature control of a 3,4-dihydroxybenzoate (protocatechuate)-based siderophore in *Bacillus anthracis*. *Curr Microbiol* 49: 89-94.
144. Brown JS, Holden DW (2002) Iron acquisition by Gram-positive bacterial pathogens. *Microbes Infect* 4: 1149-1156.
145. Nobles CL, Maresso AW (2011) The theft of host heme by Gram-positive pathogenic bacteria. *Metallomics* 3: 788-796.
146. Abergel RJ, Wilson MK, Arceneaux JEL, Hoette TM, Strong RK, et al. (2006) Anthrax pathogen evades the mammalian immune system through stealth siderophore production. *Proceedings of the National Academy of Sciences* 103: 18499-18503.
147. Dong J, Iyer S, Ruggiero C, Wolinsky M, Song J. *Bioinformatic Analysis of Iron Acquisition Systems in Bacillus anthracis*; 2008. CSREA Press. pp. 518-526.
148. Koppisch A, Browder C, Moe A, Shelley J, Kinkel B, et al. (2005) Petrobactin is the Primary Siderophore Synthesized by *Bacillus anthracis* Str. Sterne under Conditions of Iron Starvation. *Biomaterials* 18: 577-585.
149. Wilson MK, Abergel RJ, Arceneaux JE, Raymond KN, Byers BR (2010) Temporal production of the two *Bacillus anthracis* siderophores, petrobactin and bacillibactin. *Biomaterials* 23: 129-134.
150. Lee JY, Janes BK, Passalacqua KD, Pfleger BF, Bergman NH, et al. (2007) Biosynthetic analysis of the petrobactin siderophore pathway from *Bacillus anthracis*. *J Bacteriol* 189: 1698-1710.
151. Nusca TD, Kim Y, Maltseva N, Lee JY, Eschenfeldt W, et al. (2012) Functional and structural analysis of the siderophore synthetase AsbB through reconstitution of the petrobactin biosynthetic pathway from *Bacillus anthracis*. *J Biol Chem* 287: 16058-16072.
152. Dixon SD, Janes BK, Bourgis A, Carlson PE, Jr., Hanna PC (2012) Multiple ABC transporters are involved in the acquisition of petrobactin in *Bacillus anthracis*. *Mol Microbiol* 84: 370-382.
153. Cox CD (1994) Deferration of laboratory media and assays for ferric and ferrous ions. *Methods Enzymol* 235: 315-329.
154. Arnow LE (1937) Colorimetric determination of the components of 3,4-dihydroxyphenylalanine-tyrosine mixtures. *Journal of Biological Chemistry* 118: 531-537.
155. Duarte N, Palsson B, Fu P (2004) Integrated analysis of metabolic phenotypes in *Saccharomyces cerevisiae*. *BMC Genomics* 5: 63.

156. Koehler TM, Dai Z, Kaufman-Yarbray M (1994) Regulation of the *Bacillus anthracis* protective antigen gene: CO<sub>2</sub> and a trans-acting element activate transcription from one of two promoters. *Journal of Bacteriology* 176: 586-595.
157. Dai Z, Koehler TM (1997) Regulation of anthrax toxin activator gene (*atxA*) expression in *Bacillus anthracis*: temperature, not CO<sub>2</sub>/bicarbonate, affects *AtxA* synthesis. *Infect Immun* 65: 2576-2582.
158. Kulshreshtha P, Bhatnagar R (2011) Inhibition of anthrax toxins with a bispecific monoclonal antibody that cross reacts with edema factor as well as lethal factor of *Bacillus anthracis*. *Mol Immunol* 48: 1958-1965.
159. Sonenshein AL (2007) Control of key metabolic intersections in *Bacillus subtilis*. *Nat Rev Micro* 5: 917-927.
160. Tobisch S, Zuhlke D, Bernhardt J, Stulke J, Hecker M (1999) Role of CcpA in regulation of the central pathways of carbon catabolism in *Bacillus subtilis*. *J Bacteriol* 181: 6996-7004.
161. Paczia N, Nilgen A, Lehmann T, Gatgens J, Wiechert W, et al. (2012) Extensive exometabolome analysis reveals extended overflow metabolism in various microorganisms. *Microbial Cell Factories* 11: 122.
162. Majewski RA, Domach MM (1990) Simple Constrained-Optimization View of Acetate Overflow in *Escherichia-Coli*. *Biotechnology and Bioengineering* 35: 732-738.
163. Goffin P, Lorquet F, Kleerebezem M, Hols P (2004) Major role of NAD-dependent lactate dehydrogenases in aerobic lactate utilization in *Lactobacillus plantarum* during early stationary phase. *Journal of Bacteriology* 186: 6661-6666.
164. Chai Y, Kolter R, Losick R (2009) A widely conserved gene cluster required for lactate utilization in *Bacillus subtilis* and its involvement in biofilm formation. *J Bacteriol* 191: 2423-2430.
165. Smaldone GT, Antelmann H, Gaballa A, Helmann JD (2012) The FsrA sRNA and FbpB protein mediate the iron-dependent induction of the *Bacillus subtilis* lutABC iron-sulfur-containing oxidases. *J Bacteriol* 194: 2586-2593.
166. Fuller JR, Vitko NP, Perkowski EF, Scott E, Khatri D, et al. (2011) Identification of a Lactate-Quinone Oxidoreductase in *Staphylococcus aureus* that is Essential for Virulence. *Frontiers in cellular and infection microbiology* 1.
167. Garner BL, Center TUoMM (2005) Iron Acquisition Systems in *Bacillus Anthracis*: University of Mississippi Medical Center.
168. Friedman DB, Stauff DL, Pishchany G, Whitwell CW, Torres VJ, et al. (2006) *Staphylococcus aureus* redirects central metabolism to increase iron availability. *PLoS Pathog* 2: e87.
169. Smaldone GT, Revelles O, Gaballa A, Sauer U, Antelmann H, et al. (2012) A global investigation of the *Bacillus subtilis* iron-sparing response identifies major changes in metabolism. *J Bacteriol* 194: 2594-2605.

170. Baichoo N, Wang T, Ye R, Helmann JD (2002) Global analysis of the *Bacillus subtilis* Fur regulon and the iron starvation stimulon. *Mol Microbiol* 45: 1613-1629.
171. Lee JY, Passalacqua KD, Hanna PC, Sherman DH (2011) Regulation of Petrobactin and Bacillibactin Biosynthesis in *Bacillus anthracis* under Iron and Oxygen Variation. *PLoS ONE* 6: e20777.
172. van Schaik W, Prigent J, Fouet A (2007) The stringent response of *Bacillus anthracis* contributes to sporulation but not to virulence. *Microbiology* 153: 4234-4239.
173. Sirard JC, Mock M, Fouet A (1994) The three *Bacillus anthracis* toxin genes are coordinately regulated by bicarbonate and temperature. *Journal of Bacteriology* 176: 5188-5192.
174. Miethke M, Klotz O, Linne U, May JJ, Beckering CL, et al. (2006) Ferri-bacillibactin uptake and hydrolysis in *Bacillus subtilis*. *Molecular Microbiology* 61: 1413-1427.
175. Carlson PE, Jr., Dixon SD, Janes BK, Carr KA, Nusca TD, et al. (2010) Genetic analysis of petrobactin transport in *Bacillus anthracis*. *Mol Microbiol* 75: 900-909.
176. Braun V, Killmann H (1999) Bacterial solutions to the iron-supply problem. *Trends Biochem Sci* 24: 104-109.
177. Crumbliss AL, Harrington JM (2009) Iron sequestration by small molecules: Thermodynamic and kinetic studies of natural siderophores and synthetic model compounds. In: Rudi van E, Colin DH, editors. *Advances in Inorganic Chemistry: Academic Press*. pp. 179-250.
178. Rainnie D, Bragg P (1973) The effect of iron deficiency on respiration and energy-coupling in *Escherichia coli*. *Journal of General Microbiology* 77: 339-349.
179. Masse E, Salvail H, Desnoyers G, Arguin M (2007) Small RNAs controlling iron metabolism. *Curr Opin Microbiol* 10: 140-145.
180. Salvail H, Massé E (2012) Regulating iron storage and metabolism with RNA: an overview of posttranscriptional controls of intracellular iron homeostasis. *Wiley Interdisciplinary Reviews: RNA* 3: 26-36.
181. CDC (2013) Bioterrorism Agents/ Diseases. Centers for disease control and prevention.
182. Toth DJA, Gundlapalli AV, Schell WA, Bulmahn K, Walton TE, et al. (2013) Quantitative Models of the Dose-Response and Time Course of Inhalational Anthrax in Humans. *PLoS Pathog* 9: e1003555.
183. Day TG (2003) The Autumn 2001 Anthrax Attack on the United States Postal Service: The Consequences and Response. *Journal of Contingencies and Crisis Management* 11: 110-117.
184. Goldenberg A, Shmueli G, Caruana RA, Fienberg SE (2002) Early statistical detection of anthrax outbreaks by tracking over-the-counter medication sales. *Proceedings of the National Academy of Sciences* 99: 5237-5240.



185. Passalacqua KD, Bergman NH, Lee JY, Sherman DH, Hanna PC (2007) The global transcriptional responses of *Bacillus anthracis* Sterne (34F2) and a Delta sodA1 mutant to paraquat reveal metal ion homeostasis imbalances during endogenous superoxide stress. *J Bacteriol* 189: 3996-4013.
186. Kim SH, Kim SK, Jung KH, Kim YK, Hwang HC, et al. (2013) Proteomic analysis of the oxidative stress response induced by low-dose hydrogen peroxide in *Bacillus anthracis*. *J Microbiol Biotechnol* 23: 750-758.
187. Zawadzka AM, Abergel RJ, Nichiporuk R, Andersen UN, Raymond KN (2009) Siderophore-Mediated Iron Acquisition Systems in *Bacillus cereus*: Identification of Receptors for Anthrax Virulence-Associated Petrobactin. *Biochemistry* 48: 3645-3657.
188. Gudmundsson S, Thiele I (2010) Computationally efficient flux variability analysis. *BMC Bioinformatics* 11: 489.
189. Puchalka J, Oberhardt MA, Godinho M, Bielecka A, Regenhardt D, et al. (2008) Genome-scale reconstruction and analysis of the *Pseudomonas putida* KT2440 metabolic network facilitates applications in biotechnology. *PLoS Comput Biol* 4: e1000210.
190. Mahadevan R, Schilling CH (2003) The effects of alternate optimal solutions in constraint-based genome-scale metabolic models. *Metabolic Engineering* 5: 264-276.
191. Rivera J, Cordero RJ, Nakouzi AS, Frases S, Nicola A, et al. (2010) *Bacillus anthracis* produces membrane-derived vesicles containing biologically active toxins. *Proc Natl Acad Sci U S A* 107: 19002-19007.
192. Bautista EJ, Zinski J, Szczepanek SM, Johnson EL, Tulman ER, et al. (2013) Semi-automated Curation of Metabolic Models via Flux Balance Analysis: A Case Study with *Mycoplasma gallisepticum*. *PLoS Comput Biol* 9: e1003208.
193. Koch AL, Putnam SL (1971) Sensitive biuret method for determination of protein in an impure system such as whole bacteria. *Analytical Biochemistry* 44: 239-245.
194. Norris JJR, Ribbons DW (1971) METHODS IN MICROBIOLOGY, VOLUME 5B: Elsevier Science.
195. Stuy JH (1958) The nucleic acids of *Bacillus cereus*. *J Bacteriol* 76: 179-184.
196. Lang DR, Lundgren DG (1970) Lipid composition of *Bacillus cereus* during growth and sporulation. *J Bacteriol* 101: 483-489.
197. Sonenshein AL, Hoch JA, Losick R (2002) *Bacillus subtilis* and its closest relatives: ASM Press.
198. Dauner M, Sauer U (2001) Stoichiometric growth model for riboflavin-producing *Bacillus subtilis*. *Biotechnol Bioeng* 76: 132-143.
199. Oh Y-K, Palsson BO, Park SM, Schilling CH, Mahadevan R (2007) Genome-scale Reconstruction of Metabolic Network in *Bacillus subtilis* Based on High-throughput Phenotyping and Gene Essentiality Data. *Journal of Biological Chemistry* 282: 28791-28799.

200. Koga Y, Kusaka I (1970) Involvement of intracellular phospholipase C in autolytic fragmentation of cytoplasmic membranes of *Bacillus cereus*. European Journal of Biochemistry 16: 407-413.
201. Lawrence D, Heitefuss S, Seifert HS (1991) Differentiation of *Bacillus anthracis* from *Bacillus cereus* by gas chromatographic whole-cell fatty acid analysis. Journal of Clinical Microbiology 29: 1508-1512.
202. Fouet A, Mesnage S (2002) *Bacillus anthracis* cell envelope components. Curr Top Microbiol Immunol 271: 87-113.
203. Langer M, Malykhin A, Maeda K, Chakrabarty K, Williamson KS, et al. (2008) *Bacillus anthracis* Peptidoglycan Stimulates an Inflammatory Response in Monocytes through the p38 Mitogen-Activated Protein Kinase Pathway. PLoS ONE 3: e3706.
204. Garufi G, Hendrickx AP, Beerli K, Kern JW, Sharma A, et al. (2012) Synthesis of lipoteichoic acids in *Bacillus anthracis*. J Bacteriol 194: 4312-4321.
205. Choudhury B, Leoff C, Saile E, Wilkins P, Quinn CP, et al. (2006) The Structure of the Major Cell Wall Polysaccharide of *Bacillus anthracis* Is Species-specific. Journal of Biological Chemistry 281: 27932-27941.
206. Anderson I, Sorokin A, Kapatral V, Reznik G, Bhattacharya A, et al. (2005) Comparative genome analysis of *Bacillus cereus* group genomes with *Bacillus subtilis*. FEMS Microbiol Lett 250: 175-184.
207. Molnar J, Pragai B (1971) Attempts to detect the presence of teichoic acid in *Bacillus anthracis*. Acta Microbiol Acad Sci Hung 18: 105-108.
208. Gaballa A, Antelmann H, Aguilar C, Khakh SK, Song KB, et al. (2008) The *Bacillus subtilis* iron-sparing response is mediated by a Fur-regulated small RNA and three small, basic proteins. Proceedings of the National Academy of Sciences of the United States of America 105: 11927-11932.
209. Semsey S, Andersson AMC, Krishna S, Jensen MH, Massé E, et al. (2006) Genetic regulation of fluxes: iron homeostasis of *Escherichia coli*. Nucleic Acids Research 34: 4960-4967.
210. Tannler S, Decasper S, Sauer U (2008) Maintenance metabolism and carbon fluxes in *Bacillus* species. Microb Cell Fact 7: 19.
211. Zou W, Zhou M, Liu L, Jian C (2013) Reconstruction and analysis of the industrial strain *Bacillus megaterium* WSH002 genome-scale *in silico* metabolic model. Journal of biotechnology.
212. Russell JB, Cook GM (1995) Energetics of bacterial growth: balance of anabolic and catabolic reactions. Microbiol Rev 59: 48-62.
213. Wilson MK, Abergel RJ, Raymond KN, Arceneaux JEL, Byers BR (2006) Siderophores of *Bacillus anthracis*, *Bacillus cereus*, and *Bacillus thuringiensis*. Biochemical and Biophysical Research Communications 348: 320-325.
214. Harris WR, Carrano CJ, Raymond KN (1979) Coordination chemistry of microbial iron transport compounds. 16. Isolation, characterization, and

- formation constants of ferric aerobactin. *Journal of the American Chemical Society* 101: 2722-2727.
215. Miethke M, Pierik AJ, Peuckert F, Seubert A, Marahiel MA (2011) Identification and characterization of a novel-type ferric siderophore reductase from a gram-positive extremophile. *J Biol Chem* 286: 2245-2260.
  216. Miethke M, Marahiel MA (2007) Siderophore-based iron acquisition and pathogen control. *Microbiol Mol Biol Rev* 71: 413-451.
  217. Bergeron RJ, Brittenham GM (1994) *The Development of Iron Chelators for Clinical Use*: CRC Press.
  218. Miethke M, Schmidt S, Marahiel MA (2008) The Major Facilitator Superfamily-Type Transporter YmfE and the Multidrug-Efflux Activator Mta Mediate Bacillibactin Secretion in *Bacillus subtilis*. *Journal of Bacteriology* 190: 5143-5152.
  219. Hider RC, Kong X (2010) Chemistry and biology of siderophores. *Nat Prod Rep* 27: 637-657.
  220. Abergel RJ, Zawadzka AM, Hoette TM, Raymond KN (2009) Enzymatic hydrolysis of trilactone siderophores: where chiral recognition occurs in enterobactin and bacillibactin iron transport. *J Am Chem Soc* 131: 12682-12692.
  221. Tu WY, Pohl S, Gray J, Robinson NJ, Harwood CR, et al. (2012) Cellular iron distribution in *Bacillus anthracis*. *Journal of bacteriology* 194: 932-940.
  222. Pieper R, Huang ST, Parmar PP, Clark DJ, Alami H, et al. (2010) Proteomic analysis of iron acquisition, metabolic and regulatory responses of *Yersinia pestis* to iron starvation. *Bmc Microbiology* 10.
  223. Vendeville A, Winzer K, Heurlier K, Tang CM, Hardie KR (2005) Making 'sense' of metabolism: Autoinducer-2, LuxS and pathogenic bacteria. *Nature Reviews Microbiology* 3: 383-396.
  224. Fong KP, Gao L, Demuth DR (2003) luxS and arcB control aerobic growth of *Actinobacillus actinomycetemcomitans* under iron limitation. *Infect Immun* 71: 298-308.
  225. Kim CM, Shin SH (2011) Modulation of Iron-Uptake Systems by a Mutation of luxS Encoding an Autoinducer-2 Synthase in *Vibrio vulnificus*. *Biological and Pharmaceutical Bulletin* 34: 632-637.
  226. Li L, Xu ZF, Zhou Y, Li TT, Sun LL, et al. (2011) Analysis on *Actinobacillus pleuropneumoniae* LuxS regulated genes reveals pleiotropic roles of LuxS/AI-2 on biofilm formation, adhesion ability and iron metabolism. *Microbial Pathogenesis* 50: 293-302.
  227. Reed JL (2012) Shrinking the Metabolic Solution Space Using Experimental Datasets. *PLoS Comput Biol* 8: e1002662.
  228. Santos F, Boele J, Teusink B (2011) Chapter twenty-four - A Practical Guide to Genome-Scale Metabolic Models and Their Analysis. In: Daniel Jameson MV, Hans VW, editors. *Methods in Enzymology*: Academic Press. pp. 509-532.

229. Pereira CS, Thompson JA, Xavier KB (2013) AI-2-mediated signalling in bacteria. *FEMS Microbiol Rev* 37: 156-181.
230. Waters CM, Bassler BL (2005) Quorum sensing: cell-to-cell communication in bacteria. *Annu Rev Cell Dev Biol* 21: 319-346.
231. Frederix M, Downie AJ (2011) Quorum sensing: regulating the regulators. *Adv Microb Physiol* 58: 23-80.
232. James CE, Hasegawa Y, Park Y, Yeung V, Tribble GD, et al. (2006) LuxS involvement in the regulation of genes coding for hemin and iron acquisition systems in *Porphyromonas gingivalis*. *Infect Immun* 74: 3834-3844.
233. Auger S, Krin E, Aymerich S, Gohar M (2006) Autoinducer 2 affects biofilm formation by *Bacillus cereus*. *Appl Environ Microbiol* 72: 937-941.
234. Henke JM, Bassler BL (2004) Three Parallel Quorum-Sensing Systems Regulate Gene Expression in *Vibrio harveyi*. *Journal of Bacteriology* 186: 6902-6914.
235. Doherty N, Holden MTG, Qazi SN, Williams P, Winzer K (2006) Functional Analysis of luxS in *Staphylococcus aureus* Reveals a Role in Metabolism but Not Quorum Sensing. *Journal of Bacteriology* 188: 2885-2897.
236. Zhu J, Dizin E, Hu X, Wavreille A-S, Park J, et al. (2003) S-Ribosylhomocysteinase (LuxS) Is a Mononuclear Iron Protein†. *Biochemistry* 42: 4717-4726.
237. Jones MB, Blaser MJ (2003) Detection of a luxS-signaling molecule in *Bacillus anthracis*. *Infect Immun* 71: 3914-3919.
238. Wang L (2004) Autoinducer-2 (AI-2) mediated quorum sensing in *Escherichia coli*. College Park, Md.: University of Maryland. 169 p.
239. Parveen N, Cornell KA (2011) Methylthioadenosine/S-adenosylhomocysteine nucleosidase, a critical enzyme for bacterial metabolism. *Molecular Microbiology* 79: 7-20.
240. Winzer K, Hardie KR, Burgess N, Doherty N, Kirke D, et al. (2002) LuxS: its role in central metabolism and the in vitro synthesis of 4-hydroxy-5-methyl-3(2H)-furanone. *Microbiology* 148: 909-922.
241. Strachan R, Aranha H, Lodge J, Arceneaux J, Byers B (1982) Teflon chemostat for studies of trace metal metabolism in *Streptococcus mutans* and other bacteria. *Applied and environmental microbiology* 43: 257-260.
242. Yu J, Madsen ML, Carruthers MD, Phillips GJ, Kavanaugh JS, et al. (2013) Analysis of Autoinducer-2 Quorum Sensing in *Yersinia pestis*. *Infection and Immunity*.
243. Learman DR, Yi H, Brown SD, Martin SL, Geesey GG, et al. (2009) Involvement of *Shewanella oneidensis* MR-1 LuxS in biofilm development and sulfur metabolism. *Applied and environmental microbiology* 75: 1301-1307.
244. Chen X, Alonso AP, Allen DK, Reed JL, Shachar-Hill Y (2011) Synergy between <sup>13</sup>C-metabolic flux analysis and flux balance analysis for

- understanding metabolic adaption to anaerobiosis in *E. coli*. *Metabolic Engineering* 13: 38-48.
245. Tang YJ, Martin HG, Myers S, Rodriguez S, Baidoo EEK, et al. (2009) Advances in analysis of microbial metabolic fluxes via <sup>13</sup>C isotopic labeling. *Mass Spectrometry Reviews* 28: 362-375.
  246. Hayflick L (1965) Tissue cultures and *mycoplasmas*. *Tex Rep Biol Med* 23: Suppl 1:285+.
  247. Hudson P, Gorton TS, Papazisi L, Cecchini K, Frasca S, Jr., et al. (2006) Identification of a virulence-associated determinant, dihydrolipoamide dehydrogenase (lpd), in *Mycoplasma gallisepticum* through in vivo screening of transposon mutants. *Infect Immun* 74: 931-939.
  248. Oshima K, Nishida H (2007) Phylogenetic relationships among mycoplasmas based on the whole genomic information. *Journal of Molecular Evolution* 65: 249-258.
  249. Razin S, Argaman M, Avigan J (1963) Chemical Composition of *Mycoplasma* Cells and Membranes. *J Gen Microbiol* 33: 477-487.
  250. Langworthy TA (1983) Lipid tracers of *mycoplasma* phylogeny. *Yale J Biol Med* 56: 385-390.
  251. Beckman BL, Kenny GE (1968) Immunochemical analysis of serologically active lipids of *Mycoplasma pneumoniae*. *J Bacteriol* 96: 1171-1180.
  252. Gross Z, Rottem S (1979) Lipid distribution in *Acholeplasma laidlawii* membrane. A study using the lactoperoxidase-mediated iodination. *Biochim Biophys Acta* 555: 547-552.
  253. Snowden N, Wilson PB, Longson M, Pumphrey RS (1990) Antiphospholipid antibodies and *Mycoplasma pneumoniae* infection. *Postgrad Med J* 66: 356-362.
  254. Arraes FBM, Carvalho MJAd, Maranhão AQ, Brígido MM, Pedrosa FO, et al. (2007) Differential metabolism of *Mycoplasma* species as revealed by their genomes. *Genetics and Molecular Biology* 30: 182-189.
  255. Argaman M, Razin S (1965) Cholesterol and Cholesterol Esters in *Mycoplasma*. *J Gen Microbiol* 38: 153-160.
  256. Hucka M, Finney A, Sauro HM, Bolouri H, Doyle JC, et al. (2003) The systems biology markup language (SBML): a medium for representation and exchange of biochemical network models. *Bioinformatics* 19: 524-531.
  257. Paley SM, Karp PD (2002) Evaluation of computational metabolic-pathway predictions for *Helicobacter pylori*. *Bioinformatics* 18: 715-724.
  258. Terzer M, Maynard ND, Covert MW, Stelling J (2009) Genome-scale metabolic networks. *Wiley Interdiscip Rev Syst Biol Med* 1: 285-297.
  259. Covert MW, Famili I, Palsson BO (2003) Identifying constraints that govern cell behavior: a key to converting conceptual to computational models in biology? *Biotechnol Bioeng* 84: 763-772.
  260. Jong K, Spears W (1991) An analysis of the interacting roles of population size and crossover in genetic algorithms. In: Schwefel H-P, Männer R,

- editors. Parallel Problem Solving from Nature: Springer Berlin Heidelberg. pp. 38-47.
261. Mendes JJdM, Gonçalves JF, Resende MG (2009) A random key based genetic algorithm for the resource constrained project scheduling problem. *Computers & Operations Research* 36: 92-109.
  262. Spears WM, De Jong KA (1990) An analysis of multi-point crossover. DTIC Document.
  263. Garcia-Ochoa F, Gomez E (2009) Bioreactor scale-up and oxygen transfer rate in microbial processes: an overview. *Biotechnol Adv* 27: 153-176.
  264. Sorenson KL (2010) Comparative studies on Oxygen Mass Transfer for the Design and Development of a Single-Use Fermentor: Utah State University.
  265. Frahm B, Blank H-C, Cornand P, Oelßner W, Guth U, et al. (2002) Determination of dissolved CO<sub>2</sub> concentration and CO<sub>2</sub> production rate of mammalian cell suspension culture based on off-gas measurement. *Journal of Biotechnology* 99: 133-148.
  266. Royce PN (1992) Effect of changes in the pH and carbon dioxide evolution rate on the measured respiratory quotient of fermentations. *Biotechnol Bioeng* 40: 1129-1138.
  267. Royce PNC, Thornhill NF (1991) Estimation of dissolved carbon dioxide concentrations in aerobic fermentations. *AIChE Journal* 37: 1680-1686.
  268. Booger FC, Bos P, Kuenen JG, Heijnen JJ, van der Lans RGJM (1990) Oxygen and carbon dioxide mass transfer and the aerobic, autotrophic cultivation of moderate and extreme thermophiles: A case study related to the microbial desulfurization of coal. *Biotechnology and Bioengineering* 35: 1111-1119.
  269. Sparks DL (1999) Soil physical chemistry: Taylor & Francis.
  270. Van der Voort M, Abee T (2009) Transcriptional regulation of metabolic pathways, alternative respiration and enterotoxin genes in anaerobic growth of *Bacillus cereus* ATCC 14579. *Journal of applied microbiology* 107: 795-804.
  271. Henry C, Zinner J, Cohoon M, Stevens R (2009) iBsu1103: a new genome-scale metabolic model of *Bacillus subtilis* based on SEED annotations. *Genome Biology* 10: R69.
  272. Rosenfeld E, Duport C, Zigha A, Schmitt P (2005) Characterization of aerobic and anaerobic vegetative growth of the food-borne pathogen *Bacillus cereus* F4430/73 strain. *Canadian journal of microbiology* 51: 149-158.
  273. Saxild HH, Andersen LN, Hammer K (1996) Dra-nupC-pdp operon of *Bacillus subtilis*: nucleotide sequence, induction by deoxyribonucleosides, and transcriptional regulation by the deoR-encoded DeoR repressor protein. *Journal of bacteriology* 178: 424-434.

